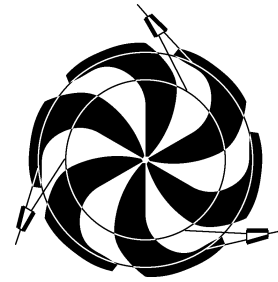


TRIUMF



ANNUAL REPORT SCIENTIFIC ACTIVITIES 2004

ISSN 1492-417X

**CANADA'S NATIONAL LABORATORY
FOR PARTICLE AND NUCLEAR PHYSICS**

OPERATED AS A JOINT VENTURE

MEMBERS:

THE UNIVERSITY OF ALBERTA
THE UNIVERSITY OF BRITISH COLUMBIA
CARLETON UNIVERSITY
SIMON FRASER UNIVERSITY
THE UNIVERSITY OF TORONTO
THE UNIVERSITY OF VICTORIA

ASSOCIATE MEMBERS:

THE UNIVERSITY OF GUELPH
THE UNIVERSITY OF MANITOBA
McMASTER UNIVERSITY
L'UNIVERSITÉ DE MONTRÉAL
QUEEN'S UNIVERSITY
THE UNIVERSITY OF REGINA
SAINT MARY'S UNIVERSITY

UNDER A CONTRIBUTION FROM THE
NATIONAL RESEARCH COUNCIL OF CANADA

OCTOBER 2005

TRIUMF

ISSN 1492-417X

ANNUAL REPORT
SCIENTIFIC ACTIVITIES
2004

Postal Address:

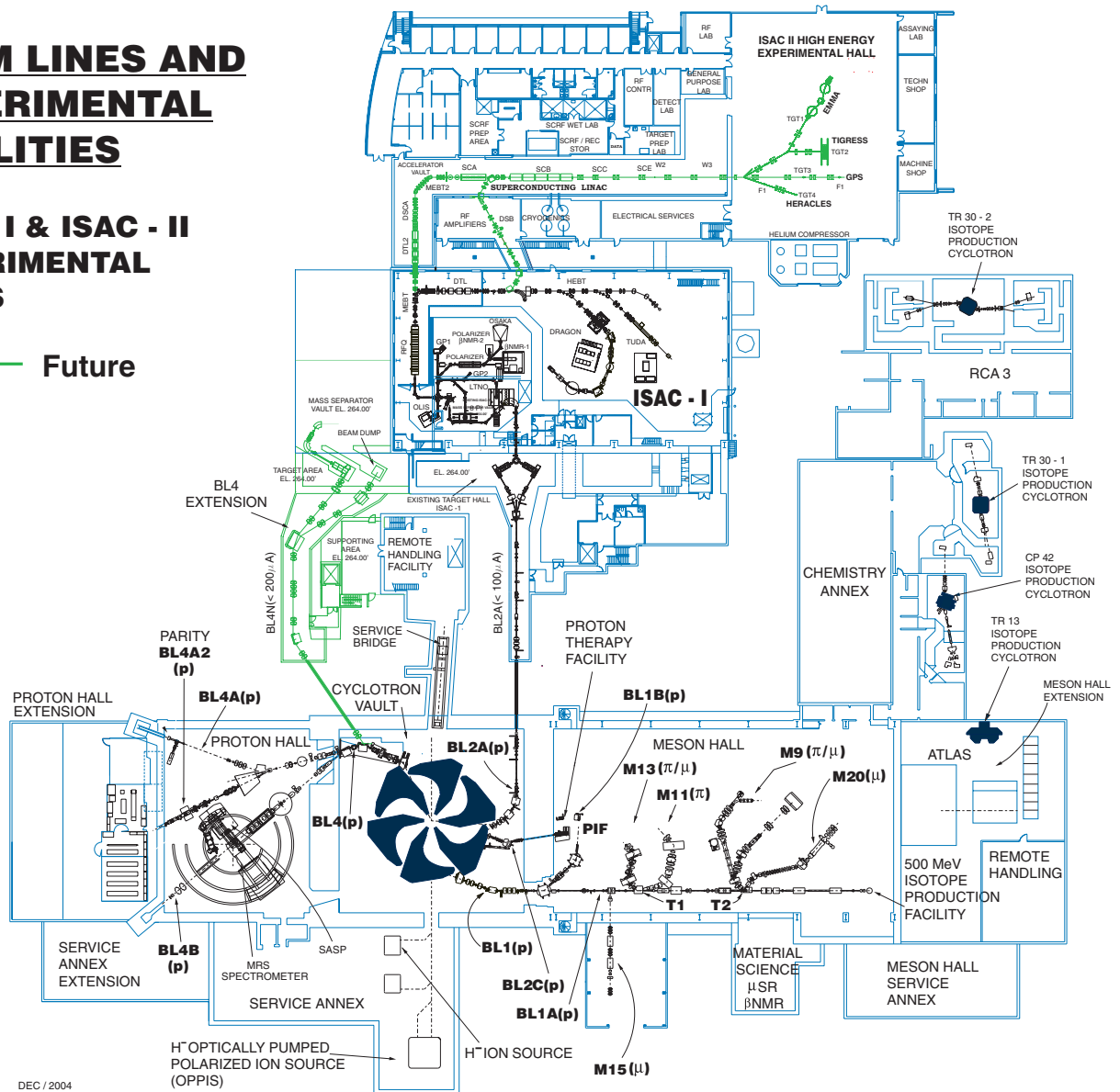
TRIUMF
Publications Office
4004 Wesbrook Mall
Vancouver, BC V6T 2A3
Canada

<http://www.triumf.ca/annrep>

BEAM LINES AND EXPERIMENTAL FACILITIES

ISAC - I & ISAC - II EXPERIMENTAL HALLS

— Future



DEC / 2004

The contributions on individual experiments in this report are outlines intended to demonstrate the extent of scientific activity at TRIUMF during the past year. The outlines are not publications and often contain preliminary results not intended, or not yet ready, for publication. Material from these reports should not be reproduced or quoted without permission from the authors.

FOREWORD

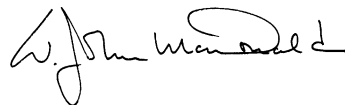
For all of the TRIUMF community, 2004 was a year of satisfaction as a result of the very positive response that the Five Year Plan 2005–2010 received. Prime Minister Martin responded to his copy of the plan in a letter to me dated October 25, 2004. The letter includes the following comment on TRIUMF accomplishments:

“The work undertaken by the TRIUMF laboratory, housed at the University of British Columbia, is a tremendous example of the world-class research facilities Canada has been able to build and operate in the last decade. I am especially pleased at the level of domestic and international cooperation among scientists and researchers which TRIUMF promotes and encourages.”

The Board of Management was impressed with the many TRIUMF supported scientific achievements that were reported in 2004. It was particularly satisfying to congratulate Donald Fleming on his Seaborg Award for pioneering work in muonium chemistry. This is a prestigious US award not often given for work originating outside that country. Also of special note was the publication of first results on the Michel parameters rho and delta from the TWIST experiment.

The success TRIUMF enjoys relies on the dedication and hard work of many groups and individuals and it is important to acknowledge contributions that do not always make the headlines. One example is the vital work of the Safety group. The Board of Management is pleased that TRIUMF continues to have a very good safety record and I wish to acknowledge Lutz Moritz and his staff for their leadership in this regard and for all TRIUMF staff for making sure that safety is practised in all TRIUMF activities. I also wish to encourage continued efforts on the part of staff and visitors to make TRIUMF safety practices as professional and effective as possible.

It was a special pleasure to welcome the University of Toronto as a full member at the June Board meeting which was held in Toronto to mark the occasion. The University of Toronto has a long association with TRIUMF and its researchers have made major contributions to the science program. Its representatives on the Board have also made important contributions and will be of even more help as full voting members. The Joint Venture was further strengthened in December when St. Mary’s University became an associate member.



W. John McDonald
Chair, Board of Management

TRIUMF was established in 1968 as a laboratory operated by the University of Alberta, the University of British Columbia, Simon Fraser University and the University of Victoria under a contribution agreement from the National Research Council of Canada. The initial consortium has been expanded to include Carleton University and the University of Toronto as full members, and the University of Guelph, the University of Manitoba, McMaster University, the Université de Montréal, Queen's University, the University of Regina, and St. Mary's University as associate members. The facility is operated for all Canadian as well as foreign users.

The experimental program is based on a cyclotron which is capable of producing four simultaneous beams of protons, two of which are individually variable in energy from 180–520 MeV, the third from 472–510 MeV, and the fourth between 70 and 110 MeV. The potential for high beam currents – 100 μA at 500 MeV to 300 μA at 400 MeV – qualified this machine as a “meson factory”. The third high intensity beam line feeds the new isotope production facility, ISAC, which started operation in 1998 and qualifies as a second generation radioactive beam facility.

Fields of research include basic science, such as particle physics, nuclear physics, nuclear astrophysics, and condensed matter research, as well as life sciences based primarily on isotope research. There is also a biomedical research facility which uses protons for treatment of ocular melanomae. TRIUMF is providing the Canadian contribution to the Large Hadron Collider at CERN and TRIUMF resources are also available to support the Canadian subatomic program at other laboratories.

The ground for the main facility, located on the UBC campus, was broken in 1970. Assembly of the cyclotron started in 1971. The machine produced its first full-energy beam in 1974 and its full current in 1977.

The laboratory employs approximately 350 staff at the main site in Vancouver and 19 based at the participating universities. The number of university scientists, graduate students and support staff associated with the present scientific program is about 625.

CONTENTS

INTRODUCTION	1
SCIENCE DIVISION	3
Introduction and Overview	3
Particle Physics	5
(Expt. 614) TWIST – the TRIUMF weak interaction symmetry test	5
(ATLAS) The ATLAS Experiment at the LHC	6
(BNL 787/949/KOPIO) Measurement of $K \rightarrow \pi\nu\bar{\nu}$ and other rare decays	9
(HERMES) The HERMES Experiment	14
(J-PARC) T2K long baseline neutrino experiment	19
(SNO) Sudbury Neutrino Observatory	21
(TJNAF 00-006) Measurement of the flavour singlet form factors of the proton (G^0)	21
(TJNAF 02-020) Q_{weak}^p : a search for physics at the TeV scale via a measurement of the proton’s weak charge	29
Nuclear Physics	34
(Expt. 715) Weak interaction symmetries in β^+ decay of optically trapped $^{37,38\text{m}}\text{K}$	34
(Expt. 823) Pure Fermi decay in medium mass nuclei	36
(Expt. 893) The hyperfine field of rubidium in iron	37
(Expt. 909) Isospin symmetry breaking in superallowed Fermi β -decays	41
(Expt. 921) High- K isomers in the neutron-rich Dy-Hf nuclei	43
(Expt. 956) Search for tensor interactions in recoil nucleus singles in decay of polarized ^{80}Rb	44
(Expt. 964) TACTIC – TRIUMF annual chamber for tracking and identification of charged particles ..	47
(Expt. 968) Ortho-para effect of muon catalyzed fusion in liquid deuterium	48
(Expt. 973) Study of coexisting collective phases far from stability: systematic decay spectroscopy of the $N = 90$ isotones	49
(Expt. 984) Fast lifetime measurements with the 8π spectrometer and nuclear structure below $N = 82$	51
(Expt. 985) Half-life and branching-ratio measurement of ^{18}Ne superallowed Fermi β decay	52
(Expt. 989) Astrophysical studies using ^{26}Al ground-state and isomeric beams	53
(Expt. 992) Lifetime of the 4.033 MeV state in ^{19}Ne	54
(Expt. 995) An alternate approach to radioactive beam production for volatile elements	56
(Expt. 1008) A new look at the β -decay of ^{11}Li	57
(LANSCE NPDGamma) Measurement of the parity-violating gamma asymmetry A_γ in the capture of polarized cold neutrons by para-hydrogen, $\bar{n} + p \rightarrow d + \gamma$	58
Molecular and Materials Science	63
(Expt. 782) Non-Fermi liquid behaviour and other novel phenomena in heavy-fermion alloys	63
(Expt. 815, 816, 817, 897 and 913) β -NMR	65
(Expt. 847) Electron-doped high- T_c superconductors	69
(Expt. 917) Correlation between magnetism and transport properties of thermoelectric oxides	71
(Expt. 932) Improving μSR performance	74
(Expt. 938) Muonium formation and ionization in semiconductors and insulators	78
(Expt. 942) Magnetic fluctuations near metal insulator transitions in ruthenate pyrochlores	80
(Expt. 944) Muonium in silicon carbide	81
(Expt. 945) Muoniated radicals formed from carbenes and carbene analogues	82
(Expt. 949) μSR study of magnetic order in high- T_c superconductors under high pressure	85
(Expt. 951) Magnetism and flux line lattice structure of oxychloride superconductors	87
(Expt. 960) Hydrogen (Mu) defects in II-VI chalcogenides	88
(Expt. 998) Muon spin relaxation and dynamic scaling in novel magnetic materials	89
(Expt. 1000) Measurements of the vortex core size in type-II superconductors	90
(Expt. 1001) Mu defect levels in III-V semiconductors	92
(Expt. 1012) Organic free radicals under hydrothermal conditions	93
(Expt. 1013) Superconductivity of β -pyrochlore oxides	95

Life Sciences	97
(Expt. LS0) PET facilities	97
(Expt. LS3) Synthesis of radiopharmaceuticals for positron emission tomography	99
(Expt. LS4) PET targets	99
(Expt. LS8) Radiotracers for the physical and biological sciences	101
(Expt. LS35) Development of ^{18}F labelled nitroimidazole PET imaging agents for tissue hypoxia	101
(Expt. LS39) Positron emission profiling (PEP) for pulp and paper fluid dynamic studies	102
(Expt. LS50) Antisense imaging nucleic acids for Parkinson's disease	102
(Expt. LS51) Auger therapy for prostate cancer	103
(Expt. LS53) Synthesis of $^{99\text{m}}\text{Tc}$ and $^{186,188}\text{Re}$ sugar derivatives	103
(Expt. LS56) Synthesis of radiolabelled nucleotides and oligonucleotides	104
(Expt. LS57) Quantitative imaging with the Concorde microPET [®]	104
(Expt. LS60) The physiological role of copper in marine phytoplankton	105
(Expt. LS63) Non-invasive monitoring of tumour progression in the Shionogi tumour model for prostate cancer	105
(Expt. LS69) <i>In-vivo</i> studies on regulation of dopamine turnover using a Parkinson's disease rat model and a microPET	106
(Expt. LS70) Quantification of high resolution brain imaging	107
Theoretical Program	108
Introduction	108
Nuclear Structure and Reactions	108
Nuclear Astrophysics, Cosmology	110
Lattice QCD	112
Effective Field Theories and Chiral Perturbation Theory	112
Few-Body and Medium Energy Processes	113
Particle Physics	114
Miscellaneous	115
Experimental Facilities	116
Proton and Neutron Irradiation Facilities	116
Proton Therapy Facility	116
Centre for Molecular and Materials Science ($\mu\text{SR} + \beta\text{-NMR}$) User Facility	117
Computing Services	118
Data Acquisition Systems	122
Detector Facility	125
GEANT4	127
Laboratory for Advanced Detector Development (LADD)	128
Scientific Services	129
The DRAGON Facility	131
8π Spectrometer	134
TIGRESS	135
Status of the TITAN System	138
Linear Collider TPC Development	143
TPC R&D for the International Linear Collider	145
CYCLOTRON OPERATIONS DIVISION	149
Introduction	149
Beam Production	150
Winter Shutdown	154
Beam Schedule 105	155
Fall Shutdown	156
Beam Schedule 106	156
Beam Development	157

Cyclotron Beam Development	157
ISIS Beam Dynamics Development	158
BL2A Beam Dynamics Development	158
Probes and Diagnostics Mechanical MRO	159
Cyclotron Diagnostics MRO	159
Beam Line Monitor MRO	159
ISAC Diagnostics	159
HE Probe Refurbishment	159
Radio Frequency Systems	160
RF Operation	160
RF Power Amplifiers	160
Anode HVPS	160
RF Combiners and Coaxial Switch	161
Transmission Line	162
Cyclotron	163
RF Booster	164
Cyclotron Simulations	164
RF Support	165
Radio Frequency Controls	165
Cyclotron Diagnostics	165
Tank Broadband Diagnostics	165
Beam Line Diagnostics	166
Diagnostics MRO	166
Cyclotron Vacuum and Cryogenics	166
Beam Line Vacuum	167
Vacuum and Cryogenic Support	167
ISIS	167
Primary Beam Lines	168
Beam Line 2C	170
Prompt Radiation Hazards	170
Controls	170
Introduction and Summary	170
CCS Facilities	171
Secondary Beam Lines	172
Other Systems	172
Operational Services	172
Remote Handling	172
Magnets and Power Supplies	174
Mechanical Services	174
Electrical Services	174
ISAC DIVISION	177
Introduction	177
ISAC Operations	177
ISAC Ion Sources	187
Operation of the 2.45 GHz ECRIS at ISAC	187
OLIS	188
Charge State Booster (CSB)	190
RIB Development: Resonant Ionization Laser Ion Source	190
ISAC Polarizer	193
ISAC Remote Handling	194
ISAC Controls	194
New Systems	194
Functionality Enhancements	195

Experiment Support	196
System Support	196
Development and QA Support	196
Operation	196
Vacuum	196
ISAC-I	196
ISAC-II	197
ISAC-I RF Systems	197
LEBT Pre-buncher	197
RFQ	198
Bunch Rotator	198
MEBT Rebuncher	198
DTL	198
HEBT High Beta Buncher	199
RF Controls	199
ISAC Diagnostics	199
Cryomodule Alignment Hardware	199
Alpha Acceleration Hardware	199
Stripline FFC	200
Other Activities	200
ISAC-I Conventional Facilities and Infrastructure	200
Mechanical Services	200
ISAC Planning	201
ISAC-I	201
ISAC-II	201
TIGRESS	202
TITAN	202
Actinide Target Test	202
Shutdown Activities	202
Contract Administration	203
Personnel Resources	203
ISAC-II Conventional Facilities and Infrastructure	205
ISAC-II Accelerators	205
Introduction	205
Cavity Testing	205
Medium Beta Cryomodule	205
Cryomodule Testing	206
Alpha Acceleration	208
High Beta Cavities	210
Cryogenics	211
Beam Lines	212
ISAC-II HEBT and Experimental Hall	212
 ACCELERATOR TECHNOLOGY DIVISION	 214
Introduction	214
Beam Dynamics	214
Muon and Electron Acceleration in FFAGs	214
Magnet Lattices	214
Acceleration	215
Electron Model	215
EURISOL Beta Beam	215
Magnets	216
Magnet Measurements	216
Kickers	216

Mechanical Engineering	219
ISAC-I	219
ISAC-II	219
Engineering – Other	221
Engineering – Victoria	222
Engineering – Carleton	223
Planning	224
Shutdown Activities	224
Design Office	225
Machine Shop	225
Building Program	226
Electronics Services	226
Overview	226
Electronics Repair Shop	227
PC Support/Desktop Services	227
Experimental and Target Technical Support	227
High Level Software Support	227
Technical Support	228
Site Communications	228
Electronics Shop	228
Electronics Development	228
ISAC Support	228
CERN	228
Engineering Support	229
Experiment Support	229
Secondary Channel Support	229
New Hardware Designs	229
 CERN COLLABORATION	 230
Introduction	230
Beam Dynamics	230
Beam Optics and Collimation	230
Beam Optics and Stability	230
Controls and Instrumentation	231
LHC Orbit System Components	231
Kicker Magnets	231
 TECHNOLOGY TRANSFER DIVISION	 233
Introduction	233
Technology Transfer	233
Applied Technology Group	233
500 MeV Isotope Production Facility	233
CP42 Facility	233
TR30-1 Facility	233
TR30-2 Facility	235
ATG Development Projects	235
Radioisotope Processing (MDS Nordion)	235
 ADMINISTRATION DIVISION	 237
Introduction	237
Human Resources and Administration	237
Environment Health and Safety	237
Licensing	237

Personnel Dosimetry	238
Interlocks and Monitoring	238
Occupational Health and Safety	238
Administration Computing and Communications	238
Management Information Systems	238
Public Web Services	238
Telephones	239
TRIUMF Outreach Program	239
TRIUMF/ISCBC High School Fellowship	239
Future Directions	239
CONFERENCES, WORKSHOPS AND MEETINGS	240
ORGANIZATION	246
APPENDICES	
A. Publications	250
B. Seminars	267
C. Users Groups	270
D. Experiment Proposals	271
E. Life Sciences Project Proposals	291

INTRODUCTION

This has been an exciting year for TRIUMF. Groundbreaking results are emerging from the scientific program and new facilities are coming on line. In addition, during the year the University of Toronto joined TRIUMF's consortia of universities as a full member and Saint Mary's University joined as an associate member. TRIUMF now has six full member universities and seven associate member universities, representing every region of Canada.

At the core of the ISAC scientific program is the production of intense beams of radioactive nuclei. At ISAC unstable nuclei are produced by nuclear reactions initiated by a 500 MeV proton beam on a thick target. After production, atoms of the unstable nuclei diffuse from the target where they are then directed through an ionizer; the radioactive ions are controlled by electric and magnetic fields. A surface ionizer can produce alkali ions with high efficiency. In particular there is considerable scientific interest in the production of unstable lithium isotopes. ^{11}Li is an isotope that is of considerable interest to many people around the world and since ISAC has developed the most advanced ^{11}Li beam, various international teams are exploiting this capability. For example, during the year this beam has been used to probe the electrical charge distribution of this very exotic nucleus. The Canadian-German scientific team undertaking this work has produced groundbreaking results concerning the fundamental structure of ^{11}Li .

Another unstable isotope, ^8Li , is proving to be an excellent probe to study nanostructures of materials. In collaboration with scientists from BC universities, TRIUMF has developed a special technique, β -NMR, using an intense beam of ^8Li to undertake such investigations. During the year, important new results demonstrated the tremendous power of this technique which will undoubtedly contribute very significantly to the development of this new field of nanostructures.

A surface ionizer produces intense beams of alkali atoms, but to extend the range of species of isotopes other ionizing methods are needed. A particularly good method for producing isotopes, but technically very challenging, is to use high-powered lasers to selectively ionize the short-lived isotopes once they have been produced in the target. During the year, experimenters at TRIUMF used the first laser-ionized, pure isotopic beam. The laser ionization project is over a year ahead of schedule and shows great promise to be the method of choice to produce such beams in the future.

During the year, significant milestones were reached and passed in the construction of the new ISAC-II accelerator. Reaching and passing these milestones is par-

ticularly significant because a new type of technology, involving superconducting accelerating cavities, had to be mastered by the TRIUMF Accelerator Division. It is immensely pleasing that during the year a section of the accelerator was completed and shown to accelerate alpha particles successfully from a radioactive source. The challenge ahead for TRIUMF is to build all the necessary sections required to complete the full ISAC-II accelerator.

Along with facility enhancements, excellent progress has been made in the development of two important ISAC experimental facilities: TIGRESS and TITAN. Both these instruments, when completed, will be world leading so it is perhaps no surprise that large international collaborations are building around them.

The 500 MeV cyclotron has worked well during the year with an actual beam delivery of over 90% of the scheduled delivery. The cyclotron proton beams are not only used to produce isotopes for ISAC, but also to produce intense beams of muons for various experimental purposes. The TWIST experiment to study the decay properties of the muon to high precision had a successful year with the completion of the first phase of the experiment, the results of which are now published. The muon beams are also used for a wide variety of experiments within the molecular and materials science area. The muon spin rotation technique is an excellent method to probe the magnetic nature of materials. A particular highlight of this method is its use in the investigation of the physical parameters that determine the magnetic vortex size in type-II superconductors.

A vital part of TRIUMF's mission is not only to provide support for the subatomic physics program within Canada, but also to support the subatomic physics program based at facilities outside Canada. During the year, TRIUMF provided continued support for the CERN program, the HERMES experiment at DESY, the G^0 and Q_{weak} programs at the Jefferson Laboratory, and the rare kaon decay experiment at Brookhaven National Laboratory.

Canada's contribution to CERN has been substantial over the last 10 years. For the LHC accelerator complex, TRIUMF has been involved in various projects. The largest of these projects has been the design, manufacture, and testing of 52 twin aperture quadrupoles. During the year, the final shipment of the magnets occurred and so now the whole project has been successfully completed. TRIUMF is also responsible for two of the LHC injector kicker magnet systems, and during the year about half of the components needed for this were shipped to CERN. On the detector side, Canada is making substantial contributions to

the ATLAS detector; in particular, the hadronic end-cap calorimeters. Of particular note is the successful in-beam tests of components of this calorimeter system.

During the year, TRIUMF established a collaboration with the Japanese accelerator facility J-PARC to undertake an experiment that will help explain the enigmatic nature of one of the most populous particles in the universe, the neutrino. This experiment follows on from the successful work carried out at the Canadian Sudbury Neutrino Observatory (SNO) – work that TRIUMF has supported for many years.

One of TRIUMF's main successes in the area of technology transfer is the long-standing collaboration with MDS Nordion. Using TRIUMF-run cyclotrons, MDS Nordion produces medical isotopes, which are distributed across North America and internationally. These isotopes are used for medical therapy and diagnostic purposes. Currently, over two and a half million patient procedures are carried out each year with isotopes produced at TRIUMF. The Natural Sciences

and Engineering Research Council (NSERC) recognized this unique collaboration and its achievements by awarding the 2004 University-Commercial Synergy Award to TRIUMF and MDS Nordion. TRIUMF will use the financial portion of the prize to award scholarships to life sciences students involved in TRIUMF-based life sciences research.

Students, undergraduates and postgraduates are our future. As in previous years, TRIUMF was host to many student groups during the year. In particular, a successful Summer Institute was hosted by TRIUMF for young scientists fascinated by the nuclear processes that drive the dynamics of stars. The summer school was planned to coincide with a TRIUMF-hosted international conference on astrophysics, the same subject the students were studying.

TRIUMF has had a very successful year. That TRIUMF is attracting young students and scientists is particularly pleasing to all of us at TRIUMF; our success is their future.



A. Shotter,
Director

SCIENCE DIVISION

INTRODUCTION AND OVERVIEW

In 2004, TRIUMF produced some very exciting new results exploiting past investments in major facilities at ISAC, in the base program, and supporting a carefully selected set of experiments at other high energy laboratories, meanwhile defending its future five-year plan at the government level. It has been a very satisfying year by all accounts, and this Annual Report attempts to capture the highlights of the scientific program.

In ISAC science, a major effort was devoted to the exploitation of the world's most intense ^{11}Li beams, derived from operating Ta foil production targets with up to $60\mu\text{A}$ of proton beam intensity. Experiment 991 used a technology developed by the GSI group to determine the charge radius of the typical halo nucleus of ^{11}Li . This *tour de force* experiment was commissioned on a new dedicated beam line in June, and data-taking on all Li isotopes took place in September and October. By measuring the isotope shift of $2S \rightarrow 3S$ transitions in this series of isotopes, one hopes to follow the redistribution of the 3 protons in the nucleus as more neutrons are added. The 8π group studied the decay of ^{11}Li into ^{10}Be via β -neutron emission. Neutron energy information is obtained by measuring the Doppler-broadened γ -ray lines in the de-excitation of ^{10}Be . This technique has been developed at ISAC and is used to assess the survival probability of the halo neutrons in the decay sequence. This effort provides new information on the nature of the 8.81 MeV state in ^{11}Be leading to a possible excited halo state in ^{10}Be . This information complements the nuclear structure studies undertaken on polarized ^{11}Li by the Osaka group, which also published their spin and parity assignment for several ^{10}Be levels.

The 8π detector proved its versatility in studies of γ -ray spectroscopy of $N = 90$ nuclei searching for coexisting collective phases in ^{156}Ho and also finding new K-isomers in ^{174}Tm . It was also used to get a more precise lifetime measurement of ^{18}Ne , one of the superallowed Fermi decays used to test the conserved vector current hypothesis and extract a value for V_{ud} , the first element of the quark mixing matrix. This program will study several other such transitions in heavier nuclei, and a new branching ratio measurement was made in December on ^{62}Ga using, for the first time, the laser resonant ion source, TRILIS, on-line. This new tool, developed in record time by J. Lassen and his team, will be the main source of radioactive beam at ISAC in the future, providing versatility and selectivity for many isotopes. For the nuclear astrophysics program, a commissioning run of a ^{26}Al beam took place

in July and showed that, with further improvement in yield and ionization efficiency, DRAGON could directly measure the strength of an important but weak resonance in $^{26}\text{Al}(p, \gamma)$ which controls the destruction of ^{26}Al . This came right in time to be showcased at the Nuclei in the Cosmos conference hosted by TRIUMF in Vancouver in July.

Two publications in Physical Review Letters were generated by the β -NMR group. The facility is now well understood and has matured in producing high quality data on their thin samples or their layered structures. A complementary facility for low magnetic field measurements of nuclear quadrupole resonances (β -NQR) is being developed.

In the base program, the highlight has been the announcement of the first results from the TWIST collaboration. Culminating a 12-year effort of attempting the high precision measurement of the Michel parameters governing the decay spectrum from polarized positive muons at rest, the sophisticated blind analysis revealed a factor 3 improvement in the determination of ρ and δ , respectively the first new such measurements in 40 and 20 years. These results help constrain possible modifications of the standard model of weak interactions and every indication is that the ultimate precision envisaged for the experiment is within reach in the next few years. Two Ph.D. theses will be based on these first results.

The rest of the muon program is devoted to muon spin resonance studies (μSR) of material and molecular species. The main theme of the program is to elucidate the interplay between magnetism and superconductivity in many types of high temperature superconductors, either electron or hole doped. Other studies are searching for correlations between magnetism and thermoelectric charge transport properties, linkages between magnetic order and superconductivity under external pressure, magnetic fluctuations and metal to insulator transition, etc. The studies of semi-conductors and the role of hydrogen-like impurities continue using muonium, while the chemistry program is focusing on the studies of muoniated radicals in carbenes and carbene analogues.

In the life sciences, the year was devoted to bringing on-line the two new cameras funded through CFI. A large demand is developing for the microPET animal camera, bringing new user demand for radiotracers. The human program is delayed by the commissioning of the new high resolution camera (which is proving very demanding) and by a delay in the acceptance test

of the patient bed.

Major progress is also reported in the studies of marine phytoplankton related to the regulation of CO₂ in the marine atmosphere interface with the delivery of radiocopper to the UBC group.

For our infrastructure support component of the program, 2004 has seen the completion of major construction commitments towards the ATLAS experiment at CERN, with the effort shifting to installation and commissioning at CERN. Beam tests were also conducted for evaluation of the performance and calibration procedure for the combined end cap calorimeters. Coupled with a major shift towards software support at TRIUMF, this represents a new phase in the program. In anticipation of the development of a major data analysis centre at TRIUMF to support the ATLAS-Canada collaboration in accessing the physics of ATLAS, two new hires were made. This is the start of a major commitment, which will be the centrepiece of the next Five-Year Plan program in Canada.

The T2K experiment moved quickly after the announcement of approval by Japan in December, 2003, and the Canadian team grew to encompass 20 physicists from across Canada. The Canadian contribution to the near detector is being formulated and will likely involve building a TPC type tracker and a water-based fine grain detector.

The KOPIO experiment is still in the R&D phase, pending approval of funding in the US. New technologies are being tested for scintillator manufacturing, and fibre and wire chamber readouts, which have already impacted other experimental programs at TRIUMF – most notably in ISAC (TIGRESS readout electronics,

TACTIC detector, etc.).

HERMES is producing beautiful results on the spin structure of the nucleon and will take data until 2006. The small, but very visible, Canadian team is at the centre of the data analysis effort.

Two experiments at the TJNAF facility in Newport News, VA have benefited from TRIUMF's infrastructure support. The $G\theta$ backward configuration Čerenkov detectors were produced at TRIUMF and delivered to TJNAF after extensive testing at TRIUMF. The first data-taking run in that mode is scheduled for the end of 2005. In the meantime, data from the first phase of the $G\theta$ experiment is being analyzed. The new Q_{weak} experiment relies on TRIUMF to produce the coil of the sector toroidal magnet, and TRIUMF is managing that contract for the collaboration.

Our theory group consists of 4 permanent staff members and 7 research associates. The focus of the group is shifted towards nuclear astrophysics with good interaction with some of the experimentalists. The nuclear structure component is still embryonic and will be further developed with the search for a new staff member approved during the fall. The group also covers QCD studies and physics beyond the standard model to match some of the experimental program as well.

Overall, this was a very satisfying year, and the results presented here support our ambitious plans forwarded to the government for the next five years. This Annual Report helps demonstrate the high quality of our staff and the commitment of our scientists to operate and contribute at the forefront of research in their respective fields. We only hope that our funding masters will agree with this observation.

PARTICLE PHYSICS

Experiment 614

TWIST – the TRIUMF weak interaction symmetry test

(G. Marshall, TRIUMF)

Normal positive muon decay ($\mu^+ \rightarrow e^+ \nu_e \bar{\nu}_\mu$) is an ideal process to investigate the electroweak interaction in the standard model. The reaction involves only leptons, obviating the need for uncertain strong interaction corrections, thus making it a clean probe of the theory’s purely left-handed (V-A) structure. A high-precision determination of the parameters describing the muon decay spectral shape explores physics possibilities beyond the standard model, for example those involving right-handed interactions. The world’s most precise such determination has been the goal of Expt. 614, the TRIUMF weak interaction symmetry test (TWIST). The collaboration has recently completed its first phase by directly measuring the muon decay parameters ρ and δ , improving on the accepted Particle Data Group (PDG) [Eidelman *et al.*, Phys. Lett. **B592**, 1 (2004)] values for the two spectral shape parameters by factors of 2.5 for ρ and 2.9 for δ [Musser *et al.* (Phys. Rev. Lett. **94**, in press) TRI-PP-04-21, hep-ex/0409063; Gaponenko *et al.* (Phys. Rev. D, in press) TRI-PP-04-22, hep-ex/0410045].

The four so-called Michel parameters describe the distribution in energy and angle of positrons from polarized muon decay. The spectrum’s isotropic part has a momentum dependence determined by ρ plus an additional small term proportional to a second parameter, η . The asymmetry is proportional to a third parameter ξ multiplied by the muon polarization, P_μ , while a fourth parameter, δ , determines its momentum dependence. Within the standard model, the parameters are predicted to be $\rho = 3/4$, $\delta = 3/4$, $\xi = 1$, and $\eta = 0$. These values are shown in Table I along with best experimental measurements prior to the new TWIST results.

Beams of positive muons are used by TWIST since they can be produced with high polarization and high stopping density. The high intensity TRIUMF proton beam produces π^+ , some of which decay at rest at the surface of a production target to create a

Table I. Theoretical and measured values of the muon decay parameters.

	SM(V-A)	PDG current value
ρ	3/4	0.7518 ± 0.0026
η	0	-0.007 ± 0.013
δ	3/4	$0.7486 \pm 0.0026 \pm 0.0028$
$P_\mu \xi$	1	$1.0027 \pm 0.0079 \pm 0.0030$

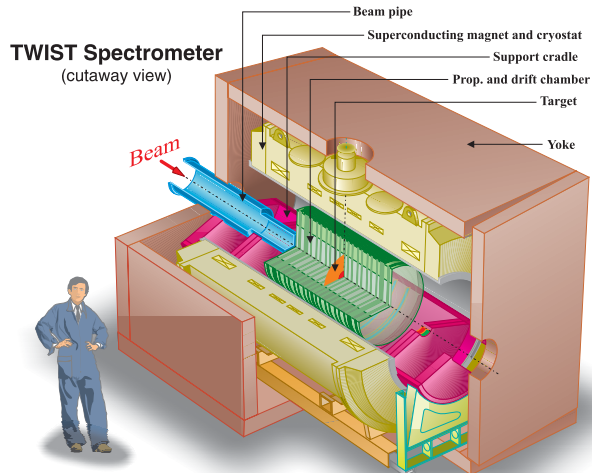


Fig. 1. The TWIST muon-decay spectrometer.

highly polarized “surface” muon beam with momentum 29.6 MeV/c, which is subsequently transported by the M13 beam line into a 2 T superconducting solenoid. A schematic diagram of the TWIST spectrometer is shown in Fig. 1.

Most of the muon beam stops in a thin target, located at the centre of a symmetric array of 56 low mass, high precision planar drift chambers [Henderson *et al.* (Nucl. Instrum. Methods, in press) TRI-PP-04-20, hep-ex/0409066]. Limitations on final errors are dominated by systematic effects since the statistical precision is very high.

The measured momentum and angle distribution of the decay positrons is shown in Fig. 2. The drop in

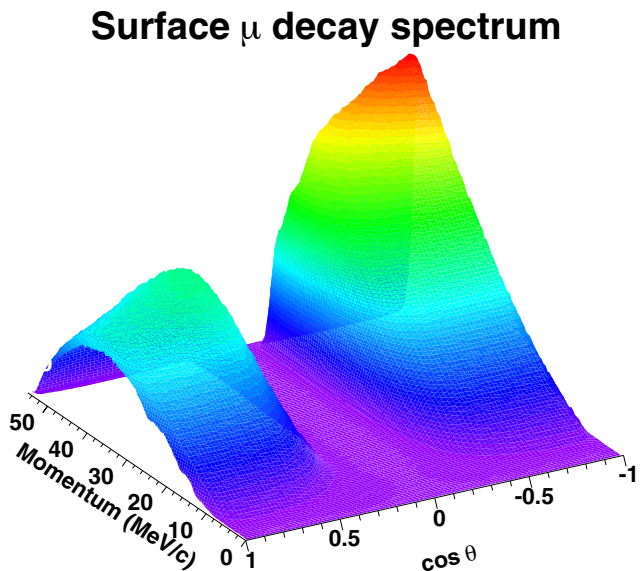


Fig. 2. The observed momentum and angular distribution of positrons from muon decays in the TWIST spectrometer.

acceptance near $|\cos\theta| = 0$ is due to the poor reconstruction efficiency in that region. To extract the muon decay parameters, a two-dimensional fit is made to a fiducial region where the detector acceptance is essentially uniform, utilizing a blind analysis technique. The results are based on 6×10^9 muon decays, spread over sixteen data sets. Four sets were analyzed for both ρ and δ . A fifth set of low polarized muons from pion decays in flight (“cloud” muons) was also analyzed for ρ . The remaining data sets, combined with further MC simulations, were used to estimate the sensitivities to various systematic effects.

TWIST’s new measurement of $\rho = 0.75080 \pm 0.00032(\text{stat}) \pm 0.00097(\text{syst}) \pm 0.00023$ (last uncertainty due to the current PDG error in η) sets an upper limit on the mixing angle $|\zeta| < 0.030$ (90% CL) of the W boson with a possible heavier partner W_2 with right-handed coupling. Combining ρ with the new measurement of $\delta = 0.74964 \pm 0.00066(\text{stat}) \pm 0.00112(\text{syst})$, and the PDG value of $P_\mu\xi\delta/\rho$, an indirect limit is set on $P_\mu\xi$: $0.9960 < P_\mu\xi \leq \xi < 1.0040$ (90% CL). The lower limit $0.9960 < P_\mu\xi$ slightly improves the limit on the mass of the heavier boson, $W_2 \geq 420 \text{ GeV}/c^2$. Finally, an upper limit is found for the muon right-handed coupling probability, $Q_R^\mu < 0.00184$ (90% CL).

In parallel with the major effort to analyze and publish the first data from TWIST, additional new data were taken to establish a direct measurement of $P_\mu\xi$. This was made possible following the replacement of the original Mylar muon stopping target by a very high purity aluminum foil of $71 \mu\text{m}$ thickness, which should minimize muon depolarization in the target after the muon stops. Another source of depolarization is the muon’s passage through the fringe field of the spectrometer solenoid. We are continuing to extend our understanding of the field map in this region, and also of the muon beam characteristics upon which the depolarization depends. An essential tool for the latter is a detector which measures the position and angle of each muon’s track by transverse drift in a very low density gas. This device, known as a TEC (time expansion chamber), operates in the beam line vacuum with DME gas at a pressure of 60 torr, contained in a gas box with entrance and exit windows of $6 \mu\text{m}$ mylar, so as to introduce very little scattering to the low momentum muon beam. The TEC consists of modules (see Fig. 3) to measure tracks in both vertical and horizontal directions, each with up to 24 points, to determine precisely both the location and direction of each muon.

A significant effort is continuing to improve the precision of the analysis software in preparation for final TWIST data, which should become available over the next two years.

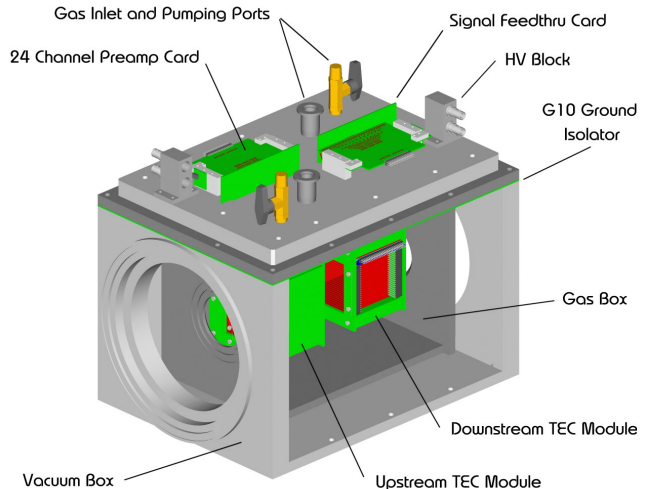


Fig. 3. The TEC, a device which provides characterizations and allows optimization of surface muon beams.

The ATLAS Experiment at the LHC (C. Oram, TRIUMF)

As described in detail in the 1996 Annual Report, ATLAS is building a general purpose pp detector which is designed to exploit the full discovery potential of the Large Hadron Collider (LHC) at CERN. The TRIUMF group is responsible for the management and engineering of the hadronic endcap (HEC) calorimeters, and the feedthroughs for the endcap cryostats. For the HEC, this year has seen the insertion of the two wheels of the second (and final) endcap into their cryostat (see Fig. 4), and the successful cold test of the first endcap. Final engineering for the transport of the 300 ton endcap cryostats from the assembly hall to the ATLAS pit is under way. The team at CERN responsible for the insertion of the wheels into the cryostats and the cryostat transport is led by a TRIUMF staff member.

Physics goals

The present theoretical understanding of elementary particles is in the context of the standard model. It is a remarkably successful model, providing predictions which have been consistently confirmed by experiments for over two decades. Its agreement with experimental results, to enormous accuracy in some cases, makes it the most accurately verified model in science. Of the many elementary particles contained in the standard model, only the Higgs remains to be discovered. The central goal of ATLAS is the search for the Higgs particle.

There are good theoretical reasons to believe that the discovery of the Higgs will at least contain hints of, and more likely direct evidence for, what lies beyond the standard model. If the Higgs is composite, its existence requires as yet unknown ultra-strong forces. If it is elementary, it would be the only spinless particle

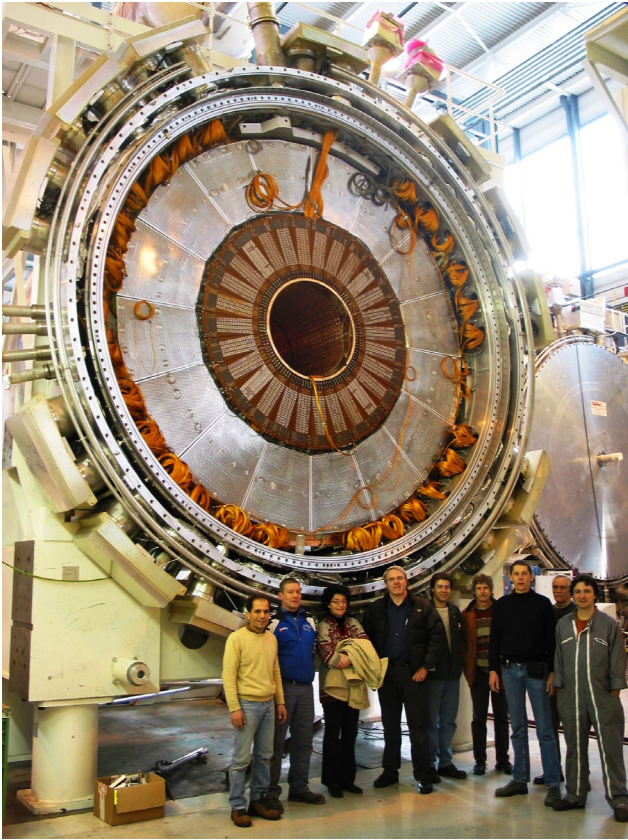


Fig. 4. The second and final cryostat immediately prior to final closure with the cold cover.

to be discovered so far. There is a theoretical “naturalness” problem for the masses of spinless particles. In the standard model, which is a highly nonlinear dynamical system, the elementary particles tend to take on the heaviest of all possible mass scales, which in such a model are at inaccessible energies and inconsistent with other requirements of the model. All other particles discovered thus far have natural mechanisms, such as gauge and chiral symmetries, for protecting their masses so that they can lie in the observable range. For the Higgs particle, there is no such symmetry in the present model. The only theoretical scenarios which leave the Higgs particle light enough to be observed are hypothetical ones, either technicolour or supersymmetry, both radical departures from the present structure of the standard model. If the Higgs is observed at the LHC, one of these scenarios should be seen at the same time.

Particle theory has progressed enormously over the last few decades with many appealing scenarios for physics beyond the standard model. The most likely of these is supersymmetry and the boldest of these is superstring theory. These theories are intimately related and are both radical ideas which promise a new conceptual framework for understanding elementary particles. Though far from being complete theories at present,

there are superstring models which resemble the standard model in their low energy limit. These models have a great appeal as they contain a unification of fundamental forces which includes gravity. They have already had substantial impact on gravitational physics where, for example, in addition to the long sought reconciliation of gravity with quantum mechanics, they have been used to derive a fundamental understanding of black hole thermodynamics. Superstring theory is still in its infancy, but progress has been dramatic and the promise of great things to come has captured the imagination of a substantial fraction of the world’s theoretical particle physicists.

The present theoretical view is that the conventional grand unification of the strong, weak and electromagnetic forces can only work in the supersymmetric extension of the standard model. In that model, the grand unified energy scale is only two decades below the Planck scale, the ultimate energy where space-time itself has quantum fluctuations. It is not out of the realm of imagination that, at energy scales where supersymmetry would be observed, evidence for an ultimate theory of everything, or at least everything that can exist once space-time is formed, is within human grasp.

Experiments at the LHC, where the ATLAS detector will take data, will probe the energy region where the Higgs particle and possibly supersymmetry or other structures will be visible. This will be the first experimental probe in many years of an energy region where fundamentally new physics is expected to occur. There is every reason to believe that the results will be among the most dramatic ever.

Basic ATLAS design considerations

The most prominent issue for the LHC is the quest for the origin of the spontaneous symmetry-breaking mechanism in the electroweak sector of the standard model. This is related to one of the most fundamental questions of physics: What is the origin of the different particle masses? New direct experimental insight is required to answer this question.

One of the possible manifestations of the spontaneous symmetry-breaking mechanism could be the existence of a standard model Higgs boson (H), or of a family of Higgs particles (H^\pm , h , H and A) when considering the minimal supersymmetric extension of the standard model (MSSM). The Higgs search is therefore used as a first benchmark for the detector optimization. For the SM Higgs, the detector has to be sensitive to the following processes ($\ell = e$ or μ) in order to cover the full mass range above the discovery limit set by the final LEP operation in the fall of 2000:

$H \rightarrow b\bar{b}$ from WH , ZH and $t\bar{t}H$ using a ℓ^\pm and b -tagging,
mass range $80 < m_H < 100$ GeV;

$H \rightarrow \gamma\gamma$
mass range $90 < m_H < 150$ GeV;

$H \rightarrow WW^* \rightarrow \ell^\pm\nu\ell^\pm\nu$
mass range $150 < m_H < 200$ GeV;

$H \rightarrow ZZ^* \rightarrow 4\ell^\pm$
mass range $130 \text{ GeV} < m_H < 2m_Z$;

$H \rightarrow ZZ \rightarrow 4\ell^\pm, 2\ell^\pm + 2\nu$
mass range $m_H > 2m_Z$;

$H \rightarrow WW, ZZ \rightarrow \ell^\pm\nu + 2 \text{ jets}, 2\ell^\pm + 2 \text{ jets}$
from WW, ZZ fusion using tagging of forward jets for m_H up to about 1 TeV.

In addition to signatures similar to these, the MSSM Higgs searches also require sensitivity to processes such as:

$$\begin{aligned} A \rightarrow \tau^+\tau^- &\rightarrow e\mu + \nu\text{'s} \\ &\rightarrow \ell^\pm + \text{hadrons} + \nu\text{'s}; \\ H^\pm \rightarrow \tau^\pm\nu &\text{ from } t\bar{t} \rightarrow H^\pm W^\mp b\bar{b} \text{ and} \\ &\rightarrow 2 \text{ jets using a } \ell^\pm \text{ tag and } b\text{-tagging.} \end{aligned}$$

The observable cross sections for most of these processes are small over a large part of the mass range to be explored at the LHC. Hence it is important to operate at high luminosity, and to maximize the detectable rates above backgrounds by high-resolution measurements of electrons, photons, and muons.

Figure 5 shows the estimated signal significance for the standard model Higgs discovery in ATLAS over the presently theoretically favoured region: 100–200 GeV/ c^2 . From 100–190 GeV/ c^2 , the most significant discovery channels are those where the Higgs is produced by vector boson fusion [see Asai *et al.*, *Prospects for the search for a standard model Higgs boson in ATLAS using vector boson fusion*, ATLAS Note SN-ATLAS-2003-24]. While the production cross section is lower in these channels, the ability to cleanly tag the Higgs production using forward jets that enter the endcap calorimeters more than compensates, yielding superior signal to noise. The need to use the endcap calorimeters for this tag puts a premium on obtaining an early robust calibration for the calorimeters over the entire angular range.

Canada's participation in ATLAS

The Canadian group consists of about 35 grant eligible physicists from TRIUMF, University of Alberta, Carleton University, Simon Fraser University, University of British Columbia, Université de Montréal, University of Toronto, University of Victoria, McGill University, and York University. We have been strongly

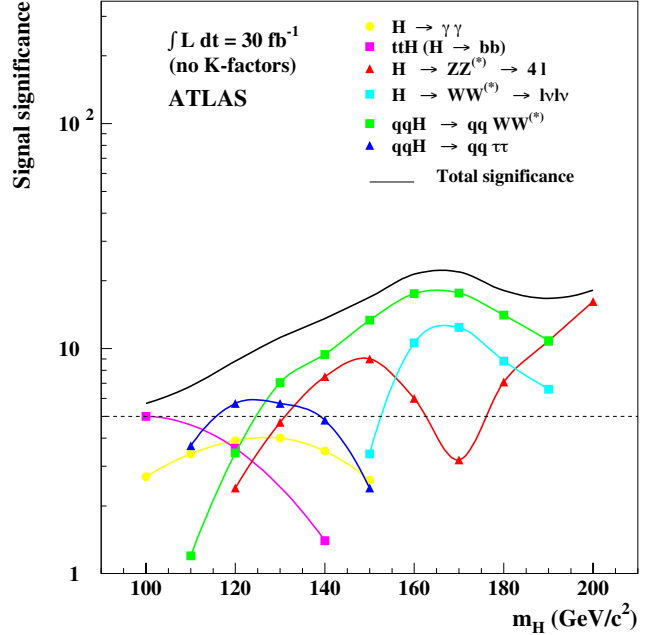


Fig. 5. ATLAS sensitivity for the discovery of a standard model Higgs boson for an integrated luminosity of 30 fb^{-1} . The signal significances are plotted for individual channels, as well as for the combination of all channels.

involved in three construction projects centred around detecting hadrons in the endcap region: the hadronic endcap project, the hadronic portion of the forward calorimeter project, and the pipeline electronics for calorimetry. In addition, as part of our common project contribution, we delivered the cryogenic signal feedthroughs for the two liquid argon endcap cryostats. The calorimeter projects are currently in the final stages of installation. TRIUMF has been directly involved in all of these projects, and is also centrally involved in the detector control system (DCS) for the liquid argon calorimeters. This year Chris Oram was elected to be the ATLAS Collaboration Board (deputy) chair (see the ATLAS organization chart at <http://atlas.web.cern.ch/Atlas/Management/Organization.gif>). This appointment is for four years, and makes him deputy chair in 2005, chair in 2006/7, and then deputy chair again in 2008. He sits *ex officio* on the ATLAS executive board for these four years.

The hadronic endcap project

The hadronic endcap (HEC) calorimeter is a liquid argon sampling calorimeter with copper absorbers [ATLAS Collab., ATLAS Liquid Argon Technical Design Report (1996)]. A concise overview of this design was provided in the 1996 TRIUMF Annual Report. An artist's impression of a module can be seen in Fig. 6. Four detector systems sit in each endcap

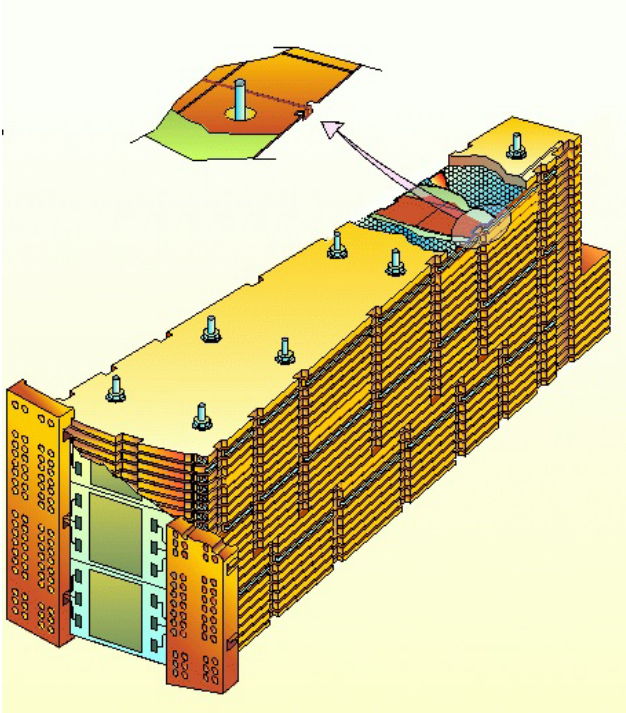


Fig. 6. Artist's impression of a hadronic endcap module.

cryostat: the presampler is closest to the interaction region and is followed by the electromagnetic endcap calorimeter (EMEC) and the HEC. At the inner diameter, the forward calorimeter (FCAL) is installed around the beam pipe.

Hadronic endcap module production and testing

As described in last year's Annual Report, all modules have been manufactured and individually cold tested. This year the first endcap, predominately assembled with Canadian modules, was successfully cold tested, essentially bringing to an end this era of construction and testing of equipment.

ATLAS endcap signal feedthroughs The TRIUMF group contributes to the production of high density cryogenic signal feedthroughs for both endcap cryostats. The feedthroughs are critical to the success of ATLAS. They have been built and tested at the University of Victoria by TRIUMF and Victoria staff. The last shipment to CERN took place in January, 2003. The endcap signal feedthroughs have been installed on the two endcap cryostats between December, 2002 and September, 2003. Cabling and tests were finalized in October, 2003, with no failures out of 96,000 electrical channels. Tasks accomplished in 2004 included finalizing the inventory, the storage of spare parts, and the decommissioning of the feedthrough production equipment. The interfacing of component details and electrical test results with the ATLAS database is nearly complete. Readiness for some repairs is being main-

tained until the endcap cryostats are in operation in the ATLAS cavern. A paper describing the ATLAS LAr signal feedthroughs has been written in collaboration with colleagues from Brookhaven National Laboratory (who produced the barrel signal feedthroughs), and has been accepted for publication in Review of Scientific Instruments.

Test beam measurements of the hadronic endcap modules This year we undertook the joint test of the three calorimeters in the endcap. An engineering run of the test beam set-up was undertaken in February, 2004, with beam runs in the spring and fall of 2004. This test of the EMEC, HEC and FCAL was successful, and preliminary results are in agreement with expectations. In addition, it was a full test of the hardware, electronics and software associated with the calorimeter. As such it was a first test of the complete system, and provided a useful pre-test for the up-coming commissioning and initial data-taking era.

BNL 787/949/KOPIO

Measurement of $K \rightarrow \pi\nu\bar{\nu}$ and other rare decays

(D. Bryman, UBC)

The rare decays of K and B mesons play an important role in the search for the underlying mechanism of flavour dynamics and in particular in the search for the origin of CP violation. Among the many K and B decays, the rare decays $K^+ \rightarrow \pi^+\nu\bar{\nu}$ and $K_L^0 \rightarrow \pi^0\nu\bar{\nu}$ are very special because their branching ratios can be computed to an exceptionally high degree of precision, not matched by any other flavour-changing neutral-current (FCNC) process involving quarks. While the theoretical uncertainties in the branching ratios of other prominent FCNC processes are at the level of 10% or larger, the theoretical uncertainty in $B(K_L^0 \rightarrow \pi^0\nu\bar{\nu})$ is only 1–2%. The non-negligible charm contribution leads to a slightly larger theoretical error in the case of $B(K^+ \rightarrow \pi^+\nu\bar{\nu})$: 8%, which may soon be reduced significantly. Remarkably, the clean access to underlying parameters in $K^+ \rightarrow \pi^+\nu\bar{\nu}$ and $K_L^0 \rightarrow \pi^0\nu\bar{\nu}$, such as for new CP violating phases, remains available in most extensions to the standard model including many examples of supersymmetry.

Although the $K_L^0 \rightarrow \pi^0\nu\bar{\nu}$ reaction is extremely rare with the standard model prediction at $B(K_L^0 \rightarrow \pi^0\nu\bar{\nu}) = (2.9 \pm 0.6) \times 10^{-11}$, the new KOPIO experiment has been designed to observe and study it. KOPIO will have unprecedented sensitivity representing an experimental improvement of a factor of 100,000 over previous measurements. (An experiment is currently under way at KEK aimed to reach $B < 10^{-9}$ which is an order of magnitude above the SM prediction.) With this new technology and remarkable sensi-

tivity, KOPIO has the capability of discovering entirely unanticipated phenomena, of revealing discrepancies in existing theory, or inferring inconsistencies by comparison with B meson experiments. KOPIO builds on the success of the E787/E949 measurements of the decay $K^+ \rightarrow \pi^+ \nu \bar{\nu}$ at BNL.

Results from the E949 measurement of $K^+ \rightarrow \pi^+ \nu \bar{\nu}$

In 2004, E949 reported new results [Anisimovsky *et al.*, Phys. Rev. Lett. **93**, 031801 (2004) TRI-PP-04-07] from data acquired in 2002 using beams, apparatus, and procedures similar to those of E787. Measurements of charged decay products were made in a 1 T magnetic field using an active target, a central drift chamber, and a cylindrical range stack (RS) of scintillator detectors. Photons were detected in a 4π sr calorimeter. Measurement of $K^+ \rightarrow \pi^+ \nu \bar{\nu}$ decay from kaons at rest involved observation of the π^+ in the momentum region $211 < P < 229$ MeV/ c in the absence of other coincident activity. Primary background sources were pions from the two-body decay $K^+ \rightarrow \pi^+ \pi^0 (K_{\pi 2})$, muons from $K^+ \rightarrow \mu^+ \nu (K_{\mu 2})$ and other decays, pions scattered from the beam, and charge exchange reactions followed by $K^0 \rightarrow \pi^+ \ell \nu$, where $\ell = e$ or μ .

Each background source was suppressed by two groups of complementary but independent selection criteria (cuts), and the desired level of background rejection was obtained by adjusting the severity of the cuts. After extensive verification of backgrounds, the total number of background events expected in the signal region was 0.30 ± 0.03 .

Examination of the signal region for the new data set yielded one event with $P = 227.3 \pm 2.7$ MeV/ c , $R = 39.2 \pm 1.2$ cm (range in equivalent cm of scintillator), and $E = 128.9 \pm 3.6$ MeV. The event (2002A) has all the characteristics of a signal event although its high momentum and low apparent time of $\pi \rightarrow \mu$ decay (6.2 ns) indicated a higher probability than the two previously observed (E787) candidate events that it was due to background, particularly $K_{\mu 2}$ decay.

The combined result for the E949 and E787 data is shown in Fig. 7 with the range and kinetic energy of the events surviving all other cuts. The result obtained using a likelihood method described in <http://www.kopio.bnl.gov/> was $B(K^+ \rightarrow \pi^+ \nu \bar{\nu}) = 1.47^{+1.30}_{-0.89} 10^{-10}$ incorporating the three observed events and their associated weights W given in Table II. This result is consistent with the SM expectation although the central value is nearly twice the prediction. The quoted 68% C.L. interval includes statistical and estimated systematic uncertainties. The estimated systematic uncertainties do not significantly affect the confidence levels. The estimated probability that background alone gave rise to the three observed events (or

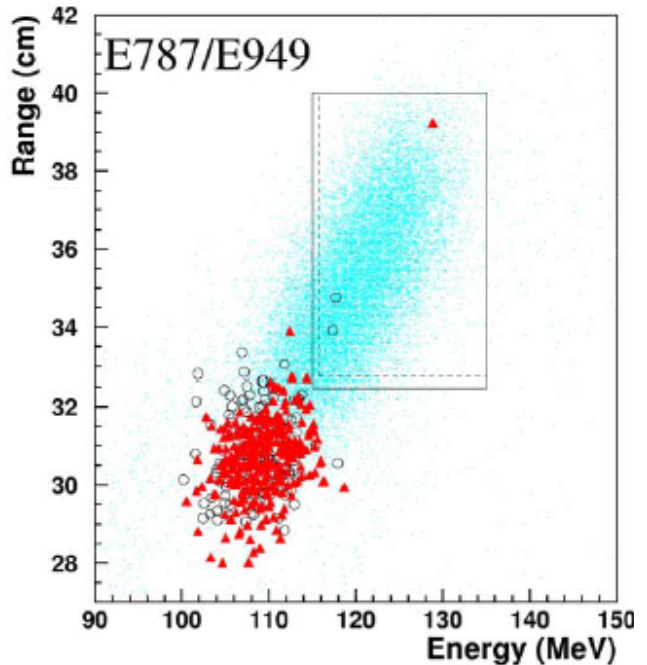


Fig. 7. Range versus energy distribution of events passing all other cuts. The circles represent E787 data and the triangles represent E949 data. The group of events around $E = 108$ MeV was due to the $K^+ \rightarrow \pi^+ \pi^0$ background. The simulated distribution of $K^+ \rightarrow \pi^+ \nu \bar{\nu}$ events is indicated by dots. The solid line (dashed line) box represents the signal region for E949 (E787).

Table II. Numbers of kaons stopped in the target N_K , total acceptance, total numbers of estimated background events for the E949 and E787 data samples, signal-to-background ratio (S/b) and weight (W) for each observed candidate event calculated from a likelihood analysis, and the estimated probability that the background alone gave rise to each event (or any more signal-like event).

	E787	E949	
N_K	5.9×10^{12}	1.8×10^{12}	
Total acceptance	0.0020 ± 0.0002	0.0022 ± 0.0002	
Total background	0.14 ± 0.05	0.30 ± 0.03	
Candidate	1995A	1998C	2002A
S/b	50	7	0.9
W	0.98	0.88	0.48
Background probability	0.006	0.02	0.07

to any more signal-like configuration) was 0.001.

The E787 and E949 data were also used to set a limit on the branching ratio for $K^+ \rightarrow \pi^+ X$ where X is a neutral weakly interacting massless particle. The new result was $B(K^+ \rightarrow \pi^+ X_0) < 0.73 \times 10^{-10}$ (90% C.L.), based on the inclusion of event 2002A, which was observed within 2 standard deviations of the expected pion momentum.

Further analysis of E949 data is being pursued vigorously to study the lower energy phase space region ($P < 205 \text{ MeV}/c$) for $K^+ \rightarrow \pi^+\nu\bar{\nu}$ which became accessible due to the E949 upgrade. The potential exists for doubling the sensitivity of E949. In addition, we are using E949 data to study improvements in photon detection efficiency relevant to KOPIO, to search for several non-SM processes (e.g. $\pi^0 \rightarrow XX$), and to study several important radiative K decays including $K^+ \rightarrow \pi^+\gamma\gamma$, $K^+ \rightarrow \pi^0\mu^+\nu\gamma$, and $K^+ \rightarrow \pi^+\pi^0\gamma$.

History of E949 E949 grew out of the successful precursor experiment, E787, which took data from 1995–98 and improved the sensitivity to $K^+ \rightarrow \pi^+\nu\bar{\nu}$ by four orders of magnitude beyond previous attempts. E787 discovered the first two $K^+ \rightarrow \pi^+\nu\bar{\nu}$ events as well as several other important rare K decays and performed many non-SM searches. E949 was fully operational and poised to collect 10–20 SM-level events when the DOE suspended funding for AGS operations in 2002.

KOPIO

The experimental aspects of measuring $K^+ \rightarrow \pi^0\nu\bar{\nu}$ are challenging. $K_L^0 \rightarrow \pi^0\nu\bar{\nu}$ is a three body decay where only the π^0 is observed. There are many competing decays that also yield π^0 s but with branching ratios that are billions of times larger. Thus, an approach must be developed with these features: an intense source of K mesons, a detector with maximum possible redundancy for observing the kinematically unconstrained decay, a capability for ensuring that the π^0 is the only observable particle emanating from the decay, and multiple handles for identifying small backgrounds. It is with these issues in mind that KOPIO, shown in Fig. 8, has been designed. The beam and detectors for KOPIO employ well-established technologies in novel configurations. New aspects have been

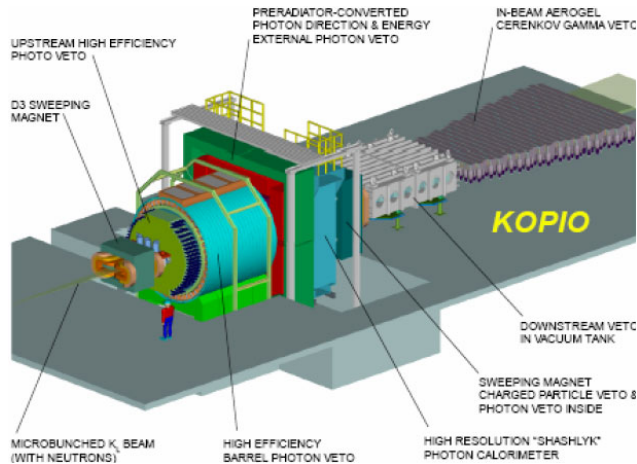


Fig. 8. An engineering perspective of the KOPIO experiment. The apparatus occupies approximately 15 m along the beam line.

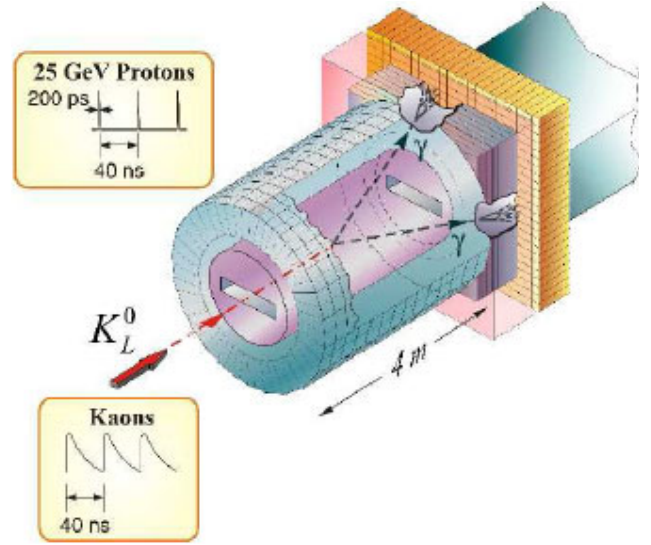


Fig. 9. Schematic of the KOPIO experiment. The time-bunched neutral K meson beam enters from the left. K decays are imaged using the detection of two photons that interact in the preradiator and the calorimeter on the right. The decay region is surrounded by veto detectors.

confirmed in beam measurements, with prototypes, and with simulations.

The concept for KOPIO is shown schematically in Fig. 9. The 24 GeV primary proton beam from the AGS is presented to the production target in 200 ps wide pulses at a rate of 25 MHz. A $360 \mu\text{sr}$ solid angle neutral beam is extracted at 42.5° to produce a “soft” K_L^0 spectrum peaked at $0.65 \text{ GeV}/c$. The low energy, time-structured neutral beam allows determination of the incident K_L^0 momentum using the time-of-flight technique. The vertical acceptance of the beam (4 mrad) is kept much smaller than the horizontal acceptance (90 mrad) so that effective collimation can be applied to severely limit neutron halos and to obtain another constraint on the decay vertex position. Downstream of the final beam collimator is a 4 m long decay region which is surrounded by the main detector. The beam region is evacuated to a level of 10^{-7} torr to suppress neutron-induced pion production. The decay region is surrounded by an efficient charged particle veto detector and Pb/scintillator photon veto detector.

The detection system for $\pi^0 \rightarrow \gamma\gamma$ decay allows a fully constrained reconstruction of the decay vertex, and mass, energy, and momentum measurements in the K_L^0 centre of mass system. This is accomplished by measuring the position of interaction, angle, and energy of each individual photon in a fine grained preradiator (PR) detector followed by an efficient calorimeter.

The PR is a high resolution, high efficiency γ -ray imaging device under development at TRIUMF. Using an array of plastic scintillation counters and dual coor-

dinate drift chambers, the PR will accurately measure positions, energies and angles of photons in the range of 50 to 500 MeV. The resolutions expected are $250 \mu\text{m}$, $\frac{3\%}{\sqrt{E(\text{GeV})}}$, and 25 mrad, for position, energy and angle (at 250 MeV), respectively, based on KOPIO prototype and other measurements and simulations. Efficiency of detection for photons in the preradiator is expected to be 70%.

The goal of the KOPIO experiment is to explore new physics such as CP -violating phases with a sensitivity equivalent to measuring 100 standard model events. The present plan calls for running of the experiment to commence in 2011 with three years of data acquisition. In addition to the $K_L^0 \rightarrow \pi^0 \nu \bar{\nu}$ decay, many other radiative type K decays of significant interest and searches for non-SM processes will also be accessed simultaneously. At the conclusion of the KOPIO experiment, either the SM picture of CPV will be shown to be consistent with present knowledge and the relevant parameters measured accurately, or a new approach to understanding quark mixing and CP violation will have been shown to be required.

The preradiator

The preradiator (PR) is at the heart of the KOPIO signal detection technique designed to efficiently measure the position, angle, time, and energy of photons. The PR will be arranged in four quadrants of modules shown in Figs. 10 and 11. A module consists of eight

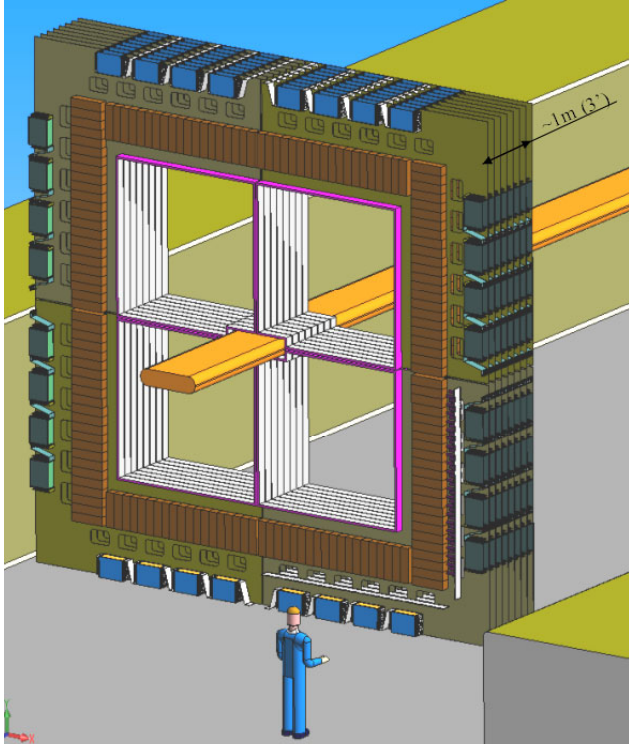


Fig. 10. PR detector composed of 32 modules organized in 4 quadrants of 8 modules surrounding the beam pipe.

$1.5 \text{ m} \times 1.5 \text{ m}$ drift chambers and 9 scintillator sheets.

Preradiator R&D

Drift chambers Several stages of prototype chambers have been constructed to verify the position resolution and develop compatible electronics. A stack of five chambers was used to measure the position resolution of cathode strip arrangements. The resolution for a chamber with 5 mm wide strips was $\sigma = 213 \pm 14 \mu\text{m}$, compatible with the requirements, and anode-wire position resolution $\sigma = 199 \pm 14 \mu\text{m}$ was obtained. There was no drift time dependence to the resolutions indicating that contributions such as misalignment dominated. Further cathode resolution tests accommodating larger angles up to 45° are being carried out and two full length test chambers, with 2 m long anode wires (short strips – see Fig. 12), and with 2 m long cathode strips (short wires), were constructed and have been used for the development of front-end electronics to study efficiency, timing distributions, pulse shape variations, and other parameters. Signal characteristics as a function of position, signal-to-noise ratios, and efficiencies are being studied and modelled.

Prototypes of the KOPIO anode and cathode read-out cards were also manufactured and tested. Each channel is composed of an amplifier and level adaptor.

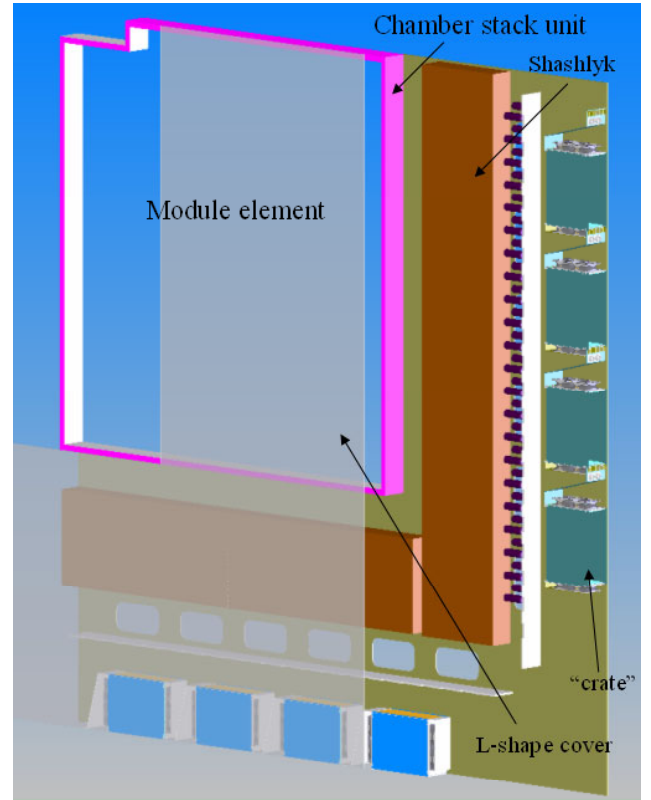


Fig. 11. Module with the chamber stack (pink), Shashlyk (red), and electronic crates (blue).



Fig. 12. 2 m long anode wires with short strips.

For the cathodes, six octal flash ADCs sample the signals and deliver the digital data to their corresponding FPGAs for data processing. The eight channels of each flash ADC are processed in the associated FPGA and sent through a single LVDS output to another FPGA for data merging and data transmission. Self-triggering or an external trigger can be selected in each mode of operation: time window mode, time offset mode, and algorithm mode. Forty prototype cathode readout cards will be assembled and used in the full scale KOPIO PR module prototype set-up. Anode cards consist of front end amplifier-discriminators followed by pipeline TDCs and FPGAs.

Scintillator studies During the past two years we have been perfecting the production of extruded polystyrene scintillator in conjunction with a local company, CELCO Industries (Surrey, BC). The extrusions have dimensions $1\text{ cm} \times 7\text{ cm} \times 2.5\text{ m}$ with six 1 mm holes for WLS fibres. A recent product is shown in Fig. 13. After achieving the dimensional and flatness tolerances and hole extrusion techniques, we studied properties including light output, attenuation, and hole dimensional tolerance. The tests indicate that the amount of the scintillation light from the extruded scintillator was comparable to that of St. Gobain commercial scintillator BC408, though the measured 15 cm attenuation length affected the yield of photo-electrons via WLS readout; the quality of the extruded hole did not have much impact on the photo-electron yield; and MC calculations reasonably describe the WLS readout. To match the precision required for the PR module construction, the extrusions will be machined with tongue and groove on the edges for gluing into $1.5\text{ m} \times 1.5\text{ m}$ sheets using a gluing jig. The first thirty-five satisfactory planks were produced in September.

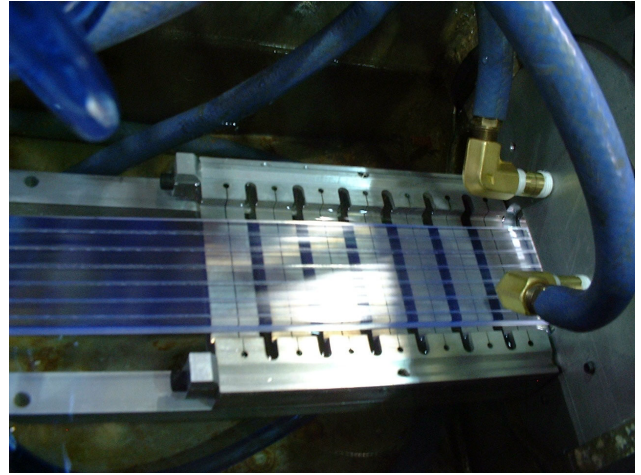


Fig. 13. Scintillator during extrusion process.

After basic tests on the extruded scintillators, the test set-up was modified to accommodate five scintillator pieces, each with six 1 mm diameter holes for WLS fibres which were bundled and read out by a Hamamatsu 3178X photo-multiplier from one end. Using an $X - Y$ readout drift chamber, data were taken simultaneously for the five scintillators and for position dependence across the scintillator. The average number of photo-electrons was 8 p.e./MeV per end with a slight (10%) dependence on the coating/wrapping material. This statistically corresponds to $\sigma_E = \frac{1\%}{\sqrt{E(\text{GeV})}}$ energy resolution and we expect to read out both ends. The observed time resolution of approximately 2 ns corresponds to $\sigma_t = \frac{120\text{ ps}}{\sqrt{E(\text{GeV})}}$ for minimum ionizing particles. Both resolutions conform to KOPIO requirements and are expected to be improved.

KOPIO neutral beam design work at TRIUMF

The neutral K_L^0 beam line is a system of collimators that defines a highly asymmetric beam. During 2004, many studies were made at TRIUMF including investigation of the optimal aspect ratio where a better halo was obtained; minimizing the length of the beam without substantially increasing the neutron halo; reducing the thickness of the photon attenuator to increase the K flux; using a magnetic field in the last collimator to reduce the charged kaon contamination to 10^{-7} of the neutral beam; adding another collimator to limit the entrance aperture just before the decay region to decrease the neutron halo by a factor of 2; and, studies of the material of the collimators which showed that W is best. Our conclusion is that the many aspects of the beam are now well understood.

AGS upgrade work for KOPIO at TRIUMF

The AGS will be upgraded for KOPIO to provide higher beam intensity with a significantly mod-

ified time structure. Three upgrades to the AGS are planned: (1) extraction of a micro-bunched proton beam; (2) increasing the proton intensity by a factor of 1.5 or more to 10^{14} protons (100 T p) per AGS cycle; and (3) constructing a new proton beam line to bring the intense micro-bunched beam to a new K meson production target. The TRIUMF/UBC team was awarded a CFI International Access grant for the Canadian portion of this work, contingent on NSF funding of the KOPIO experiment in the US. In 2004, the CFI provided initial funds for advanced planning to initiate the R&D effort to meet the Canadian responsibilities for items (1) and (2) while the NSF provided funds for items (1)–(3). This work will allow the designs and specifications for these upgrades to be advanced to the point where detailed design, fabrication and placement of contracts can be initiated. Ewart Blackmore (TRIUMF) is coordinating the Canadian AGS upgrade efforts.

25 MHz microbunching cavity The specifications for the 25 MHz microbunching cavity to be provided by TRIUMF include a cavity centre frequency of 24.8694 MHz (67th harmonic of revolution frequency) and a gap voltage of 150 kV. The RHIC 28 MHz cavity design is to be used for reference. The R&D work also involves simulations of the cavity using the HFSS radio frequency design code in order to study the resonant frequency, tuning and coupling to the amplifier. A full-scale 3D model of the 25 MHz cavity will be fabricated for low power rf tests and optimization.

AGS injection kicker Two new kicker modules will be installed in the AGS ring to add to the existing kicker strength in order to provide the 3 mrad deflection required for 2 GeV protons into the AGS. The TRIUMF group has proposed a new design of transmission line kicker to accomplish this task. Detailed specifications have been developed. Proposed prototype work includes computer modelling to gain a good understanding of the performance of the kicker system. In addition, we will design and test a prototype transmission line type kicker.

The HERMES Experiment

(C.A. Miller, S. Yen, TRIUMF)

Introduction

The HERMES experiment was designed to comprehensively study the spin structure of the nucleon. It has been running at the 27.5 GeV HERA electron accelerator at the DESY Laboratory in Hamburg, Germany since 1995, measuring spin asymmetries for deeply inelastic electron scattering (DIS) as well as a wealth of unpolarized observables. The combination of a polarized high energy electron beam in a storage ring with undiluted polarized atomic gas targets is unique in

this field, and has important experimental advantages. Furthermore, the spectrometer detecting the scattered electrons has substantial acceptance and the capability to identify all types of hadrons produced in coincidence.

This was a very productive year of running at HERA while HERMES continued to accumulate data with a transversely polarized hydrogen target. As was explained in some detail in last year’s Annual Report, the asymmetries for the semi-inclusive deep-inelastic events found in these data are sensitive to the previously unmeasured transversity quark distribution. This sensitivity arises through a feature of the fragmentation process described by the Collins function. It acts as a “quark polarimeter” through the appearance of an asymmetry in the distribution of produced pions in the azimuthal angle about the virtual photon direction with respect to the linear polarization of the virtual photon in the lepton scattering plane. Such data from the 2002/03 running years were the basis for a Physics Review Letter, which was published in 2004. Because of the much improved performance of the accelerator, the 2004 running added about three times as much again. Results from these new data will be released in 2005. Running with transverse target polarization will continue until late 2005.

While the new data accumulates, the collaboration continued to complete analyses of the data of previous years, release new preliminary results and publish final ones. Space permits only some highlights to be mentioned here. One publication in Physics Review D was a detailed account of the extraction of quark helicity distributions from the measurements of semi-inclusive deep-inelastic scattering with longitudinally polarized hydrogen and deuterium targets in 1996–2000. The polarizations of the three light flavours of sea quarks are independently determined. This fulfills one of the main original goals of the experiment.

Deeply virtual Compton scattering

One of the dramatic developments of the last decade in the field of nucleon spin physics is the emergence of hard exclusive production of photons and mesons as a new window on nucleon spin structure. New factorization theorems relate observables in such processes to generalized parton distributions (GPDs), which encode both the contribution of parton orbital angular momenta to the nucleon spin, as well as the correlation between the longitudinal momentum of partons and their transverse position. This year, HERMES released new results for the kinematic dependence of beam-charge asymmetries for the hard exclusive deeply virtual Compton scattering (DVCS) process on the hydrogen and deuterium targets. Figure 14 shows their dependence on the momentum transferred

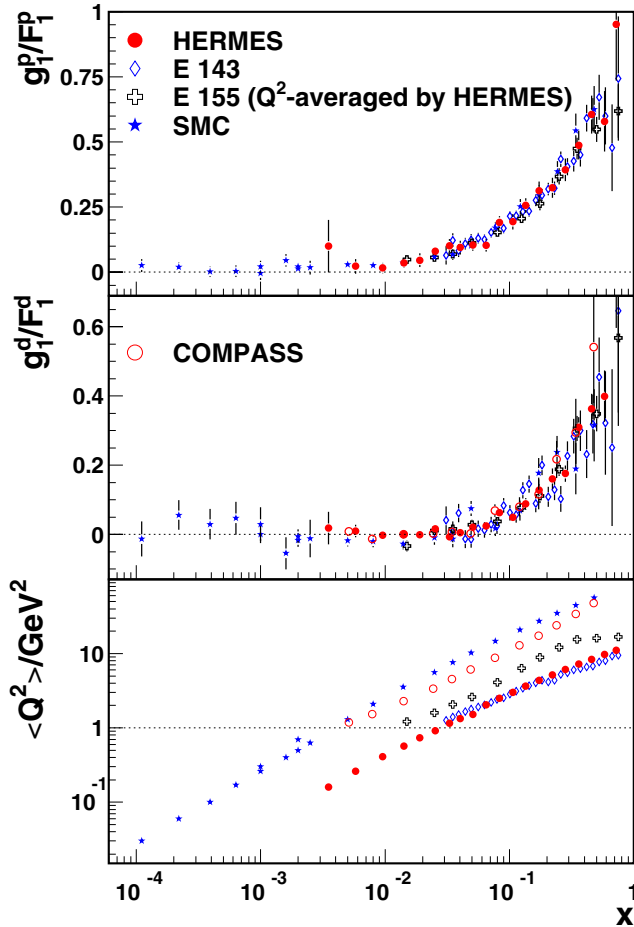


Fig. 14. The virtual-photon asymmetry $g_1(x)/F_1(x)$ for the proton and the deuteron, compared to world data, each at its measured value of Q^2 shown in the lower panel.

to the target nucleon, which remains intact even after one of its quark absorbs a hard virtual photon and then re-emits an energetic real photon. The asymmetries arise from interference with the well-understood Bethe-Heitler process (radiative elastic scattering), giving sensitivity to the DVCS amplitudes. Hence the deuteron asymmetry arises almost entirely from the proton, as the Bethe-Heitler cross section on the neutron is negligible except in the last t -bin. The more precise new deuteron results now confirm the earlier observation on hydrogen of a significant asymmetry at intermediate t -values. These data can be compared to the predictions of various models for GPDs. The asymmetries with respect to transverse target polarization for the events now being recorded from both DVCS and exclusive production of pions will introduce new independent constraints on GPDs.

Interference fragmentation functions

Another new result released this year is the first observation of an asymmetry with respect to longitudinal target polarization in the semi-inclusive production

of $\pi^+\pi^-$ pairs in deep-inelastic scattering. Theoretical predictions of such a possible asymmetry based on an “interference fragmentation function” were motivated by the role it could play as another polarimeter for transverse quark polarization, potentially yielding an independent signal of transversity. An asymmetry did appear in this data, although not with conclusive statistical significance. A larger asymmetry is expected to appear in the data now being recorded with transverse target polarization.

The spin structure function g_1

A primary goal of the HERMES experiment was the precise measurement of the inclusive spin-structure function $g_1(x)$, in deep-inelastic scattering on both hydrogen and deuterium targets. Results for hydrogen were published several years ago. This year, final results for deuterium were also released, together with a reanalysis of the hydrogen data using the refined techniques that have since been developed. These structure functions have been measured in other experiments at both SLAC and CERN. However, the new deuterium data are the most precise available. Furthermore, when all of the available data measured over a significant range in Q^2 representing the hard scale of the process are combined in global analyses, the Q^2 -evolution of the structure functions can be extracted. Due to the coupling of quarks and gluons described by QCD, this evolution constrains the polarization of gluons with respect to the nucleon longitudinal spin orientation. The new results for the ratio $g_1(x)/F_1(x)$ of structure function (closely related to virtual-photon asymmetries) are compared to world data in Fig. 14. This ratio is expected and found to have little dependence on Q^2 . The corresponding values of $g_1(x)$ from HERMES are shown in Fig. 15. The HERMES error bars in these plots cannot be compared directly to those of other experiments, as only the HERMES analysis includes full unfolding of the kinematic smearing due to instrumental resolution and QED radiation, which inflates the diagonal elements of the covariance matrix. However, the compensating interbin correlations represented by the negative off-diagonal elements are accounted for in the calculation of first moments of g_1 , which are shown in Table III. The statistical precision of the HERMES data on the proton is competitive and on the deuteron it is superior.

Fragmentation

Parton distribution functions are not the only observables relevant to understanding confinement in QCD. Equally important are fragmentation functions that describe how an energetic quark ejected from a hadron in a hard collision becomes incorporated into a new hadron together with quarks found in the

Table III. Comparison of the first moments of the structure function g_1 measured by various experiments with that measured by HERMES, in a common measured x -range in each case. The references in the last column appear in Table IV.

Experiment	Q^2 [GeV ²]	x -range	Target	Moment	Our moment in the same x -range	Reference
HERMES	5	0.021–0.9	p	$0.1246 \pm 0.0032 \pm 0.0074$	–	1
E143	5	0.03–0.8	p	$0.117 \pm 0.003 \pm 0.006$	0.1174 ± 0.0027	2
SMC	5	0.03–0.7	p	0.128 ± 0.006	0.1141 ± 0.0026	2(*)
SMC	10	0.003–0.7	p	$0.131 \pm 0.005 \pm 0.006 \pm 0.004$	(**)	3
HERMES	5	0.021–0.9	d	$0.0452 \pm 0.0015 \pm 0.0017$	–	1
E143	5	0.03–0.8	d	$0.043 \pm 0.003 \pm 0.002$	0.0433 ± 0.0013	2
E155	5	0.01–0.9	d	$0.0408 \pm 0.0025 \pm 0.0024$	(**)	4
SMC	5	0.03–0.7	d	0.043 ± 0.007	0.0416 ± 0.0013	2(*)
SMC	10	0.003–0.7	d	$0.037 \pm 0.006 \pm 0.003 \pm 0.003$	(**)	3

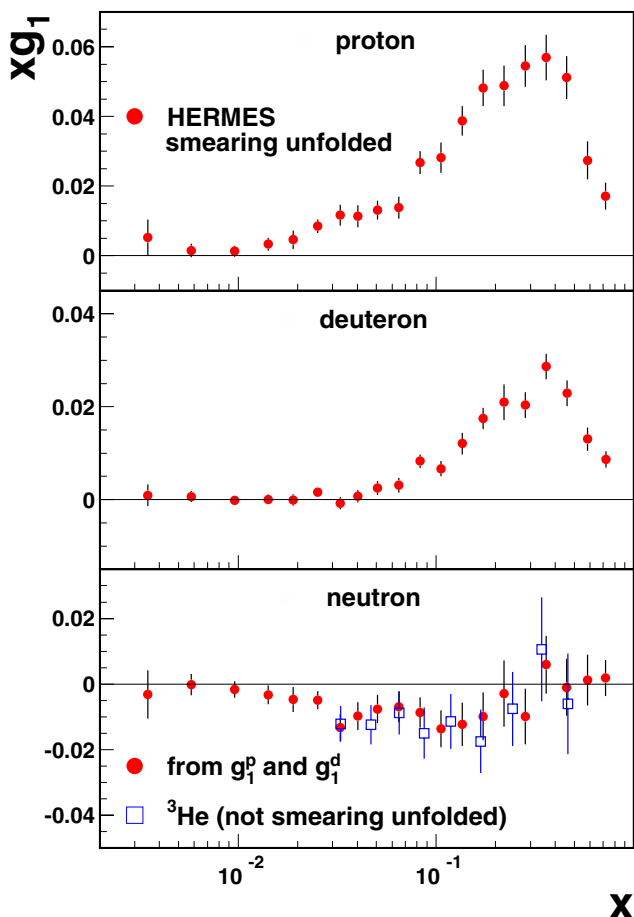


Fig. 15. The spin structure function $g_1(x)$ for the proton and the deuteron.

vacuum. A wealth of information about fragmentation has been extracted from e^+e^- collider data. However, most of these data are not sensitive to the full flavour dependence of fragmentation. Deep-inelastic scattering on both hydrogen and deuterium targets can provide this sensitivity when complete hadron identification is available. HERMES is equipped with a dual-radiator ring-imaging Čerenkov detector that provides this

Table IV. References for the moments shown in Table III.

1	HERMES g_1 paper in preparation
2	E143, Abe <i>et al.</i> , Phys. Rev. D58 , 112003 (1998)
2(*)	Same as above, results calculated by E143 in a smaller x -range than SMC
3	SMC, Adeva <i>et al.</i> , Phys. Rev. D58 , 112001 (1998)
4	E155, Anthony <i>et al.</i> , Phys. Lett. B463 , 339 (1999)
(**)	A comparison value is not calculated because it would mean using our data at $Q^2 < 1$ GeV ²

capability over the full kinematic acceptance. Furthermore, as the HERMES energy regime is lower than collider energies, it is important to compare the results in the two regimes to ensure that they are universal, as expected from factorization theorems.

A fragmentation function represents the number density of hadrons of a particular type that are produced by a struck quark of a particular flavour, expressed as a function of the scaling invariant z . In the target rest frame, z is the hadron energy E_h as a fraction of the energy ν of the virtual photon. The first step towards extracting fragmentation functions is to measure hadron multiplicities for both hydrogen and deuterium targets. New precise multiplicity results for hydrogen were released this year, and are shown as a function of z in Fig. 16. As the contributions from the decay of exclusively produced vector mesons (ρ and ϕ) may not be regarded as a legitimate part of semi-inclusive DIS, results are also shown after their subtraction using simulations tuned to measured exclusive cross sections.

The DIS factorization theorem implies that hadron multiplicities should be independent of x , the momentum fraction of the struck parton in the target. Figure 17 shows the measured multiplicities as a function

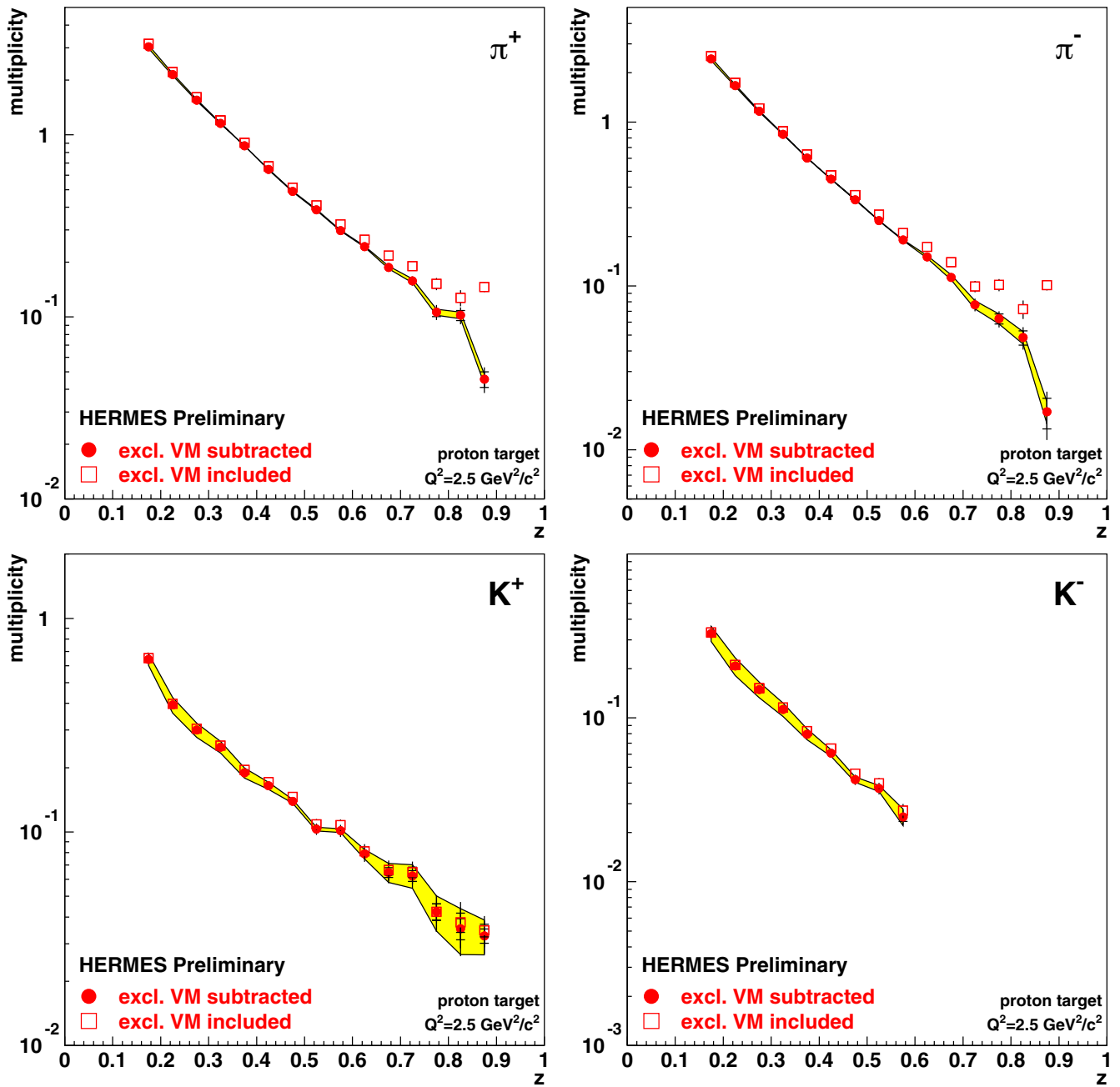


Fig. 16. Hadron multiplicities as a function of z measured by HERMES on the hydrogen target, corrected to 4π acceptance and evolved to a fixed scale $Q^2 = 2.5 \text{ GeV}^2$. The statistical error bars are typically too small to be visible, and the systematic uncertainties are shown as the error bands. Values are shown both with and without subtraction of the simulated contribution from exclusive production of vector mesons.

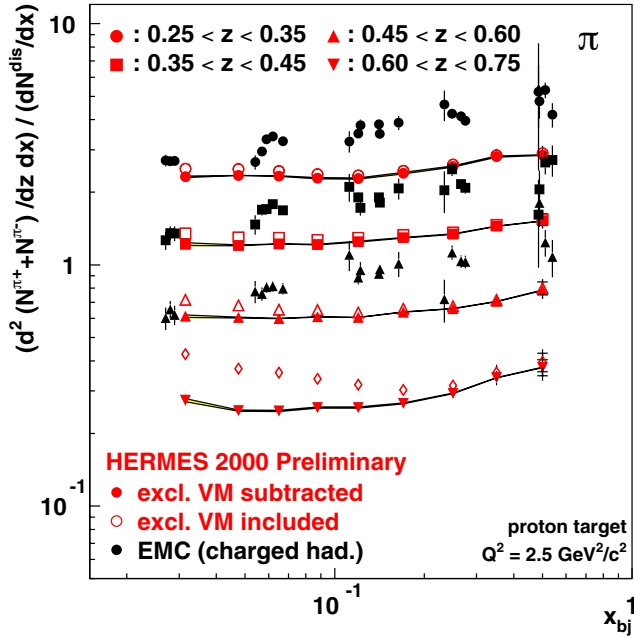


Fig. 17. Charged pion multiplicities as a function of x in four intervals in z , corrected to 4π acceptance and evolved to a fixed scale $Q^2 = 2.5 \text{ GeV}^2$, as measured by HERMES at 27.57 GeV and by the EMC experiment at CERN at 100–280 GeV [Ashman *et al.*, *Z. Phys.* **C52**, 361 (1991)]. (The EMC data includes all charged hadrons.)

of x , for several bins in z . They are compared to results from measurements at higher energy at CERN, the x dependence of which has been a long-standing puzzle. The new HERMES results after subtraction of the exclusive “contamination” show little such dependence. Hence the puzzle may be more experimental than theoretical.

When quark fragmentation occurs in the nuclear environment, it becomes possible to study the sequential stages of this process via the dependence of the effects of the nuclear medium on the nuclear size and the kinematics of the process. The understanding of quark propagation in the nuclear medium is crucial for the interpretation of ultrarelativistic heavy ion collisions. Deeply inelastic scattering (DIS) of charged leptons is an ideal tool for this study, as it provides direct measurement of the kinematic properties of the struck quark. It turns out that the ideal range of energy transfer to the struck quark is 10 to 20 GeV, where the hadron formation length is similar to a typical nuclear size. Hence the HERMES experiment at 27.5 GeV beam energy is well placed to pursue these studies. The usual observable of interest is the multiplicity ratio $R_A(\nu, z)$ – the ratio of the DIS hadron multiplicity measured on a target nucleus to that measured on deuterium. In the absence of nuclear effects on fragmentation, this ratio will be unity. An extensive set of precise data for identified pions and kaons, protons and

antiprotons was published by HERMES the previous year [Airapetian *et al.*, *Phys. Lett.* **B577**, 37 (2003)], giving the dependence of the nuclear ratio on both ν and z . Various theoretical models are able to explain the main features of those data, namely that the ratio decreases as the target mass increases, as ν decreases, or as z increases. These models variously account for energy loss by the energetic struck quark via gluon bremsstrahlung as it propagates through nuclear matter, nuclear absorption of the embryonic colour-singlet “pre-hadron”, and/or absorption of the hadron if it is fully formed within the target. These data revealing the effects of cold nuclear matter of moderate density have constrained interpretations in the context of hot dense nuclear matter of the discovery at RHIC of complete suppression of back-to-back jet pairs in central Au+Au collisions, while two-hadron correlations in the same jet survive. One such interpretation is that fragmentation at RHIC is occurring mostly outside the nucleus, and the jet suppression is due to parton energy loss in the medium [Wang, *Phys. Lett.* **B579**, 299 (2004)]. It was proposed to test this hypothesis by extracting two-hadron attenuation at HERMES. A useful observable here is the super-ratio of the nuclear suppression of two-hadron production to that for one-hadron production:

$$\mathcal{R}_{2h}(z_2) = \frac{\sum_{z_1 > 0.5} N_A^{(2h)}(z_1, z_2)}{\sum_{z > 0.5} N_A^{(1h)}(z)} \cdot \frac{\sum_{z_1 > 0.5} N_D^{(2h)}(z_1, z_2)}{\sum_{z > 0.5} N_D^{(1h)}(z)}.$$

If parton energy loss were dominant, then in terms of the Lund string model of fragmentation, this ratio can be expected to be reduced only moderately below unity via the further energy loss by the lower energy remnant quark after the first string break. Most of the gluon radiation is done by the more energetic leading quark. On the other hand, if nuclear absorption of (pre-)hadrons were dominant, then there would be roughly twice as much absorption suppressing two-hadron production.

HERMES has now released the first such measurements of the two-hadron to one-hadron attenuation super-ratio. The results for nitrogen and krypton targets are shown in Fig. 18 as a function of the z_2 value of the slower of the two hadrons, while the leading hadron is required to have a z_1 value greater than 1/2. The values are indeed only marginally below unity, perhaps somewhat more so for the heavier target. This supports the dominance of energy loss via gluon bremsstrahlung. A recent theoretical calculation of this quantity within such a model is in fair agreement with these nitrogen data [Majumder, nucl-th/0503019]. In this picture, the rise at small values of z_2 can be understood in terms of both small energy loss by the slower quark as well

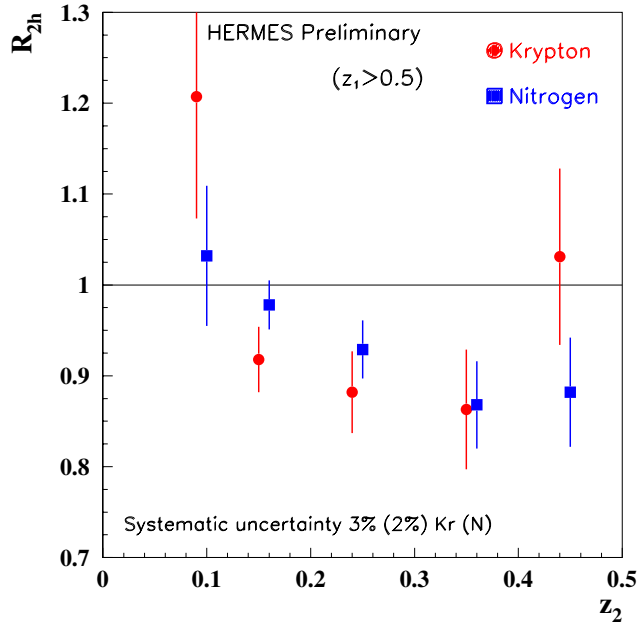


Fig. 18. The super-ratio of the nuclear attenuation of two-hadron production in DIS on nitrogen or krypton to the nuclear attenuation of one-hadron production, as a function of the z_2 value of the slower hadron. The leading hadron is required to have a z_1 value exceeding $1/2$.

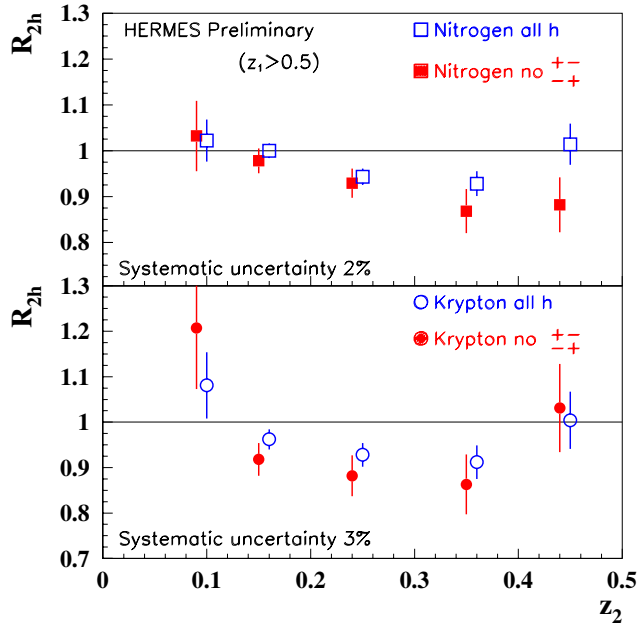


Fig. 19. As in Fig. 18, but additionally the effect of excluding oppositely charged hadrons is shown.

as hadron formation by a radiated gluon. Figure 19 shows the effect of excluding hadron pairs with opposite charge which, in the context of the Lund string model of fragmentation, requires that the two hadrons differ in “rank” by more than unity, i.e. they cannot be separated by only one string-break. (The effect of excluding hadron pairs from decay of exclusively pro-

duced ρ mesons was shown to be negligible by restricting the invariant mass of the pair to not fall near the ρ mass.) The requirement that the slower hadron have a lower rank appears to only slightly suppress two-hadron production. This requirement might be naively expected to increase nuclear absorption of the hadron, as such a hadron will be formed closer to the original interaction point and hence further inside the nucleus. However, detailed model calculations are needed, and can be tested by these data.

The ongoing HERMES program

DESY has promised beam for HERMES until mid-2007. The present running plan is to continue until late 2005 on the transversely-polarized hydrogen target to complete the first measurement of quark transversity in the proton. Meanwhile, HERMES has assembled and is testing a new recoil detector to surround the target cell and detect the recoiling intact target nucleon from hard exclusive processes, in order to guarantee their exclusivity. This detector will be installed in late 2005 and will be the centre-piece for the following two years of running on high density unpolarized targets in 2006/07. This will yield the first really high quality data on asymmetries in both beam spin and charge for DVCS, the process that holds the most promise to shed light on the orbital angular momentum of partons.

HERMES collaborators in 2004: J. Lu, C.A. Miller, S. Yen (TRIUMF), G. Gavrilov (TRIUMF, visiting from DESY), K. Garrow (Alberta/SFU).

J-PARC

T2K long baseline neutrino experiment

(A. Konaka, TRIUMF)

The T2K long baseline neutrino experiment has been approved by the Japanese government, and the neutrino beam line construction started in April, 2004. Sending a beam from the new 1 MW class accelerator at J-PARC (Japan Proton Accelerator Research Complex) to the existing water Čerenkov detector, Super-Kamiokande, it aims at determining the lepton mixing angle θ_{13} and greatly improving the precision on the mixing parameters Δm_{23}^2 and θ_{23} . The commissioning of the J-PARC accelerator is scheduled for 2008 and the first T2K neutrino beam is expected in the beginning of 2009.

The T2K collaboration in Canada consists of accelerator scientists at TRIUMF and physicists and students across Canada from TRIUMF, Alberta, UBC, Carleton, Montreal, Toronto, Victoria, and York University. The Canadian group has been involved in T2K from the very beginning stages of the conceptual design. In particular, we introduced essential design concepts, such as the idea of the $\nu_\mu \rightarrow \nu_e$ analysis and the narrow band off-axis beam, and contributed to the ac-

celerator beam dynamics study, dual abort/extraction kicker design, and the combined function magnet design.

The neutrino beam is produced by a high intensity proton beam hitting the target to produce pions, which decay in the following decay volume to produce neutrinos ($\pi \rightarrow \mu\nu$). The T2K neutrino beam line is the first megawatt beam line. One of its most challenging areas is the target station where a large fraction of the megawatt energy is released. Full remote maintenance is required for the target and the focusing horn magnets. Although the T2K target station is much larger, the structure is very similar to the ISAC target station. The T2K beam line construction group has visited TRIUMF to learn from it, and the TRIUMF experts have contributed to reviewing the conceptual design of the target station. Detailed engineering design of the target station will take place in the next couple of years, and TRIUMF is expected to contribute to the remote handling designs under the new TRIUMF Five-Year Plan. An accelerator contribution, namely the beam damper system in the main ring, is also expected in the Five-Year Plan.

Monitoring the neutrino source is essential in understanding and controlling the neutrino beam. It is done in three places: the primary proton beam monitor, a muon monitor at the beam dump, and a neutrino monitor (on-axis neutrino detector). The Canadian group is in charge of the proton beam profile monitor right in front of the target (target monitor) based on an optical transition radiation (OTR) detector. OTR detectors have been used for electron machines and recently adopted for proton machines at CERN and FNAL. An OTR would likely be the only profile monitor that would work under the extremely high radiation environment in front of the target.

The neutrino oscillations are observed by measuring the neutrino flux in the far detector, Super-Kamiokande, compared with that in an off-axis near detector which is placed in the same direction as the far detector. The off-axis near detector (see Fig. 20)

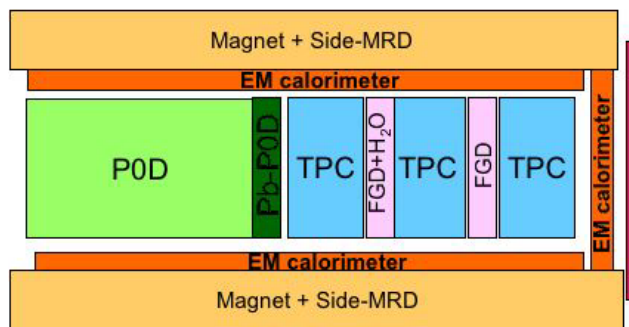


Fig. 20. Conceptual schematics of off-axis near detector.

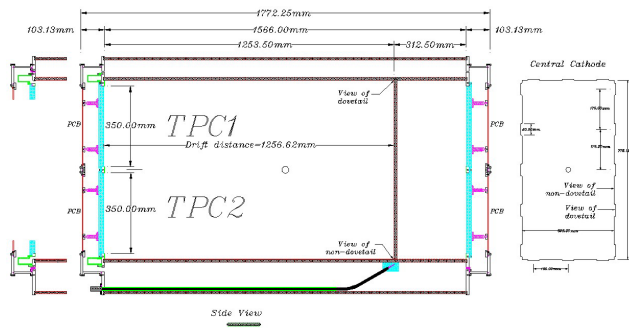


Fig. 21. Prototype design of the TPC.

consists of fine grained calorimeters (FGD, P0D) and time projection chambers (TPC), and an electromagnetic calorimeter (Ecal), which are placed inside the large dipole magnet used for the UA1 experiment at CERN.

The Canadian group is in charge of the TPCs and two FGDs, one based on plastic scintillator and the other based on water-soluble scintillator. There will be three TPCs, each of which is $2.4\text{ m} \times 2.4\text{ m} \times 0.9\text{ m}$ with an electron drift distance of 1.2 m (see Fig. 21). A leading candidate for signal readout is the gas electron multiplier (GEM), which has been studied for linear collider detector R&D.

The FGD (Fig. 22) serves as the neutrino target mass. The required granularity is about $1\text{ cm} \times 1\text{ cm}$ in cross section to be able to detect recoil protons from the quasi-elastic scattering process $\nu_\mu n \rightarrow \mu^- p$.

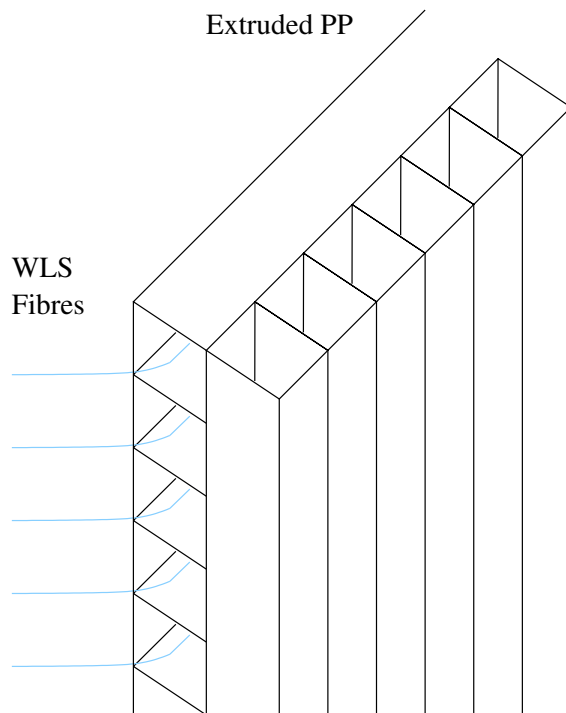


Fig. 22. Schematic view of the water-based FGD.

Because the far detector is water, a scintillator with high water content is desired. We have achieved a water content of 70% with a water-soluble scintillator (Quick-safe A) by adding surfactants. The water-mixed scintillator is contained in polypropylene corrugated plastic sheets with a cell size of 1 cm \times 1 cm and the emitted light is read out by wavelength shifting fibres.

A leading candidate for the FGD photosensor is a multipixel Geiger-mode avalanche photodiode (silicon photomultiplier). R&D for the scintillator and photosensor is under way.

The design of the manipulator for the optical calibration of the 1 kton front detector in the ongoing K2K experiment was completed, and construction begun. The manipulator will be deployed in the coming year.

R&D for the Canadian contributions to the T2K detector, TPC, FGD, and OTR, as well as Canadian participation in K2K, has been funded by NSERC.

Sudbury Neutrino Observatory

(*R. Helmer, TRIUMF*)

As noted in last year's Annual Report, discrete ^3He counters were installed in the heavy water during 2003. Unfortunately, there were several problem strings of counters and it wasn't until the summer (2004) that these were all resolved well enough to begin routine operation. Commissioning continued until late November, at which time a period of running began with the data set open to full analysis. At the end of the year this mode of operation ended and full production running, including a blindness scheme for analysis of the data, is to begin at the start of 2005.

The upgraded glove box, referred to in last year's report, was installed in June. The analysis of the first part of the salt data, also referred to in last year's report, was published [Ahmed *et al.*, Phys. Rev. Lett. **92**, 181301 (2004)]. Meanwhile, analysis has progressed on the full salt data set, with publication expected early in 2005.

Two other papers were published by the collaboration during 2004. In one [Ahmed *et al.*, *ibid.* 102004 (2004)], constraints were placed on nucleon decay into "invisible" modes, e.g. $n \rightarrow 3\nu$. The analysis was based on a search for γ -rays from the de-excitation of the residual nucleus that would result from the disappearance of either a proton or a neutron from ^{16}O . A limit of $\tau_{\text{inv}} > 2 \times 10^{29}$ years was obtained at 90% confidence for either decay mode, an order of magnitude more stringent than previous constraints on invisible proton decay modes and 400 times more stringent than similar neutron modes.

The other published result [Aharmim *et al.*, Phys. Rev. **D70**, 09301 (2004)] concerned a search for electron antineutrinos. These could possibly arise in the

solar flux or from neutron induced fission of naturally occurring elements. It has been suggested that antineutrinos could be produced either by spin flavour precession in the magnetic field of the sun or by decay of a heavier neutrino mass eigenstate into a lighter antineutrino. The signal is distinctive, $\bar{\nu}_e + d \rightarrow e^+ + n + n - 4.03$ MeV, and the triple coincidence permits a search with low background. In the case of $\bar{\nu}_e$ s from nuclear fission, the positron energies from the charged current interaction are below the threshold for detection in an analysis which includes the positron, but it is possible to search for these events nonetheless by looking only at two-neutron coincidences. The latter analysis includes (e^+, n) coincidences, as it is not possible to separate neutron from positron signals on an event by event basis. Hence these signals add to the triple coincidence detection of solar $\bar{\nu}_e$, and in fact are 10 times more likely to be detected than either (n, n) or (e^+, n, n) coincidences. The time coincidence window was set to 150 ms to optimize the sensitivity to 2-fold coincidences in the presence of a background of accidental coincidences. The total background from all sources to these signals was estimated to be $1.7_{-0.5}^{+0.9}$ coincidences.

Two candidate events were observed – one 3-fold and one 2-fold coincidence. Integral limits on the $\bar{\nu}_e$ flux in the energy ranges from 4–14.8 MeV and below 8 MeV were derived from these events, and spectrally independent differential limits were also obtained. The limit from 4–14.8 MeV shows that less than 0.81% of the solar ν_e flux converts to $\bar{\nu}_e$ (90% C.L.), and is comparable to, and consistent with, a similar limit obtained by Super-Kamiokande. The limit obtained for neutron induced fission $\bar{\nu}_e$ s in the energy range 4–8 MeV (2.0×10^6 cm $^{-2}$ s $^{-1}$ at 90% C.L.) is consistent with, but not as constraining as, a similar limit from KamLAND. Similarly, limits on neutrino decay were obtained that were consistent with KamLAND results, but again the SNO results were not as constraining.

The ^8Li source has been sent to TRIUMF for refurbishing before it is used again for calibration. The inside of the spherical source chamber was painted several years ago to enhance the light yield from ^4He scintillation events, and it is feared some of the paint has flaked off.

TJNAF Experiment 00-006

Measurement of the flavour singlet form factors of the proton (G_0)

(*W.T.H. van Oers, Manitoba*)

The structure of the nucleon at low energies in terms of the quark and gluon degrees of freedom is not well understood. The G_0 experiment is to measure two proton ground state matrix elements which

are sensitive to point-like strange quarks and hence to the quark-antiquark sea in the proton. The matrix elements of interest are the elastic scattering vector weak neutral current charge and magnetic form factors, G_E^Z and G_M^Z , respectively. These can be extracted from a set of parity-violating electron-proton scattering measurements. If one assumes a relationship between the proton and neutron structure in that the proton and neutron differ only by the interchange of up and down quarks, i.e., isospin symmetry, the strange quark (as well as the up and down quark) contribution to the charge and magnetic form factors of the nucleon can be determined. This would result from taking appropriate linear combinations of the weak neutral form factors and their electromagnetic counterparts.

Determinations of both the charge and magnetic strange quark form factors are of fundamental interest, as these would constitute the first direct evidence of the quark sea in low energy observables. It is the objective of the $G\theta$ experiment to determine these contributions to the proton form factors at the few per cent level. Observations at high energy suggest that the strange quarks carry about half as much momentum as the up and down quarks in the sea. It is important to determine both the role of the quark sea and the relevance of strange quarks at low energy where there are voids in understanding the theory of the strong interaction (quantum chromo dynamics, QCD). Even if the strange quark contributions do not amount to the level of sensitivity of the experiment, upper limit determinations at this level are as valuable as non-zero results. The matrix elements, G_E^Z and G_M^Z , are also relevant to discussions of the Ellis-Jaffe sum rule and the pion-nucleon sigma term; there is uncertainty in both of these about the strange quark contributions. The $G\theta$ experiment will allow the determination of the strange contributions to the proton charge and magnetic form factors in a much more straightforward manner than is possible with regard to the corresponding observables in the above two deduced relations.

$$A_z = (1/P) \frac{[\sigma^+(\theta) - \sigma^-(\theta)]}{[\sigma^+(\theta) + \sigma^-(\theta)]}$$

where P is the polarization of the incident electron beam and the $+$ and $-$ signs indicate the helicity state. Making pairs of measurements at forward and backward angles will allow the separation of G_E^Z and G_M^Z . Predicted longitudinal analyzing powers range from about $(-3 \text{ to } -35) \times 10^{-6}$; it is planned to measure the longitudinal analyzing powers with statistical uncertainties of $\Delta A/A = 5\%$ and systematic uncertainties related to helicity correlated effects of $\Delta A/A \leq 2.5 \times 10^{-7}$.

The heart of the $G\theta$ detection system is a spectrometer which consists of an eight-sector toroidal magnet, with an array of scintillation detectors located at the focal surface of each octant and, for the backward angle mode, additional arrays of scintillation detectors and a Čerenkov detector located near the magnet cryostat exit window of each octant. In the first phase of the experiment longitudinal analyzing powers have been measured concurrently at several values of the momentum transfer in the range $0.1 \leq Q^2 \leq 1.0 \text{ GeV}^2$. It must be realized that the length of the experiment is in part governed by making rather elaborate control measurements to determine the corrections that have to be made to the measured asymmetries and to assess systematic errors. In the second phase of the experiment each subsequent backward angle analyzing power measurement would require one month of continuous running time. The results of the SAMPLE experiment at the MIT-Bates laboratory have shown the importance of measuring the axial form factor corrections. Therefore, companion measurements of quasi-elastic scattering from deuterium will also be made at the backward angles. With these measurements, the effective axial current of the nucleon will also be determined. This current includes effects from the effective axial coupling of the photon to the nucleon or anapole moment, which are relevant also in other processes, e.g. parity violating Moller scattering and atomic parity violation.

The past year culminated in a very successful data-taking run completing the first phase, forward angle mode, of the $G\theta$ experiment (December, 2003 to May, 2004). Preliminary results have been presented at the Gordon Research Conference on Photonuclear Reactions (Tilton, NH, August 1–6, 2004) and at the DNP Fall Meeting (October 28–30, 2004). Considerable progress has also been made in the design, prototyping, fabrication, testing, and installation of critical components for the second phase, backward angle mode, of the experiment, in particular the cryostat exit detectors, the aerogel Čerenkov detectors, and the support structure for these. The Canadian contributions to these efforts have been significant.

An enumeration of the various Canadian contributions to the $G\theta$ experiment is given below. As well, a brief description of the recently completed $G\theta$ forward angle run is provided, followed by a summary of the progress made in preparing for the second-phase backward angle measurement.

Canadian contributions

The Canadian members of the $G\theta$ collaboration, based at the Universities of Manitoba, Northern British Columbia, and TRIUMF, have made the following contributions:

1. Develop and produce specialized photomultiplier tube bases for the focal plane detector arrays;
2. Design, build, and commission an automated magnetic field measuring (“magnetic verification”) apparatus complete with its own data acquisition system;
3. Prototype and fabricate the cryostat exit detector arrays for the backward angle measurements;
4. Prototype and fabricate (together with the Grenoble group) the aerogel Čerenkov arrays for background rejection in the backward angle measurements;
5. Design the support structure for the aerogel Čerenkov and cryostat exit detector arrays;
6. Coordinate the implementation of TJNAF built beam monitors and control apparatus with TRIUMF built parity electronics.

The forward angle run

The $G\theta$ experiment ran in forward angle mode from December 1, 2003 to May 9, 2004. The run was originally scheduled to begin in mid October, but September’s hurricane Isabel caused a major power outage at Jefferson Lab and delayed the startup by six weeks. The periods in December and January were devoted to engineering runs in preparation for 13 weeks of production running from February 9 to May 9, 2004. University of Manitoba personnel staffed a total of approximately 30 person-weeks of shifts. The experiment accumulated approximately 10 Tbytes of good production data corresponding to 94 Coulombs of beam on the liquid hydrogen target.

To extract the final physics asymmetry, the data must first be corrected for deadtime, helicity correlated beam properties, leakage, and background under the elastic peak.

A blind data analysis is now under way. Preliminary blinded data were presented in August at the Gordon Photonuclear Conference.

An overview of the $G\theta$ equipment is shown in Fig. 23. The 3 GeV electron beam enters from the lower right where it first encounters the $G\theta$ beam monitors. Continuing from right to left, one sees the liquid hydrogen target service module, the eight-sector superconducting magnet system (SMS), and the focal plane detectors mounted in the eight sector “Ferris wheel” structure between the SMS and the green wall. The principle of the forward angle measurement is illustrated in Fig. 24. Longitudinally polarized electrons scatter from the liquid hydrogen target, and the spectrometer accepts recoil protons in the angular range 62° to 78° (corresponding to 15° to 5° electrons). The spectrometer magnet is designed so that protons corresponding to a given momentum transfer (Q^2) are

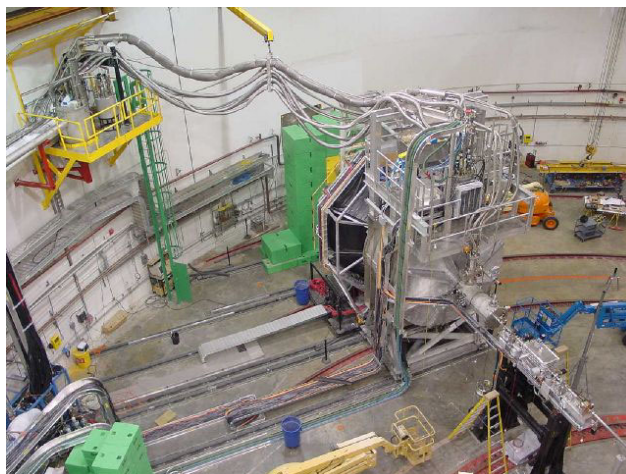


Fig. 23. The $G\theta$ apparatus installed in Hall C at Jefferson Lab. The beam enters from the lower right. From right to left, we see the $G\theta$ beam monitoring girder, the LH_2 target service module, the 8-sector superconducting magnet, the detector Ferris wheel, and the green shielding wall.

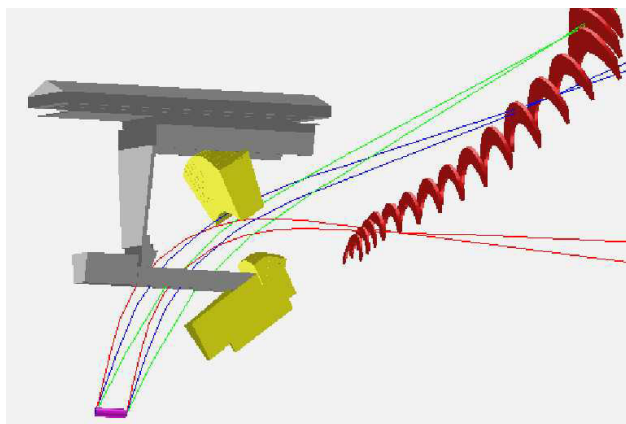


Fig. 24. Principle of the forward angle measurement. The 3 GeV longitudinally polarized electron beam enters the 20 cm liquid hydrogen target from the left. Recoil protons in the angular range 62° to 78° are deflected to the focal plane detectors, which are arranged along contours of constant Q^2 . The magnet sorts the protons by Q^2 , regardless of where in the target they originate. Q^2 from 0.16 to $1.0 (\text{GeV}/c)^2$ can be measured with one magnet setting.

directed to a specific focal plane detector regardless of where in the target they originate. Q^2 from 0.16 to $1.0 (\text{GeV}/c)^2$ can be measured with one magnet setting. The experiment uses a beam time structure with beam bunches 32 ns apart. This is 16 times the usual Jefferson Lab spacing of 2 ns, and permits the protons from elastic scattering to be separated by time of flight from pions and inelastic protons.

Helicity correlated beam properties The helicity of the longitudinally polarized electron beam was selected every 1/30 second. The spin states were chosen in quartets, either $+-+-$ or $-+--$, the first state of

Table V. Helicity correlated beam properties for the February–May production run compared to $G\theta$ specifications. These must be multiplied by the sensitivity to these quantities to give the false signal. In the end, the false asymmetry from helicity correlated beam parameters was <0.01 ppm.

Beam parameter	Achieved	Specification
Charge asymmetry	-0.3 ± 0.3 ppm	1 ppm
x position difference	6 ± 4 nm	20 nm
y position difference	8 ± 4 nm	20 nm
x angle difference	2 ± 0.3 nrad	2 nrad
y angle difference	3 ± 0.5 nrad	2 nrad
Energy difference	58 ± 4 eV	75 eV

the quartet being chosen at random. Ideally, no other beam property would be affected, but in practice small changes in beam properties other than helicity occur. Thanks to good design practices such as cylindrical symmetry, the sensitivity of the experiment to helicity correlated beam properties was very small. Nevertheless, it was necessary to constantly monitor helicity correlated beam properties and to correct for the resultant false asymmetry. Table V shows the helicity correlated beam parameters for the forward angle data. Charge and position feedback were used. The helicity correlated beam properties are all very small and, taken together, produced a false asymmetry <0.01 ppm.

Leakage An unanticipated effect was the leakage of beam from the Hall A and B lasers. Hall A and B beams are 499 MHz, but the Hall C beam is 31 MHz. Unfortunately, the beam current monitors which are used to measure the charge asymmetry measure all the time and respond to the total A+B+C beam, whereas the $G\theta$ time-of-flight cut sees only the 31 MHz beam. This meant that the correction for charge asymmetry was not right. The situation is illustrated in Fig. 25. We were able to measure the effect by looking in a “forbidden region” of the TOF spectrum where the signal could not come from the $G\theta$, 32 ns spaced beam bursts. The leakage was typically 50 nA (c.f. 40 μ A Hall C) with 340 ppm charge asymmetry. Corrections were made for the effects of beam leakage. The leakage correction is estimated to contribute ~ 0.1 ppm systematic uncertainty.

Background The measured asymmetry can be written as a weighted sum of the true elastic asymmetry and the asymmetry of the background.

$$A_{\text{meas}} = \frac{A_{\text{el}} + f_{\text{back}} A_{\text{back}}}{1 + f_{\text{back}}}.$$

To correct for the background, we must know both the background fraction, f , and the asymmetry, A_{back} , under the elastic peak.

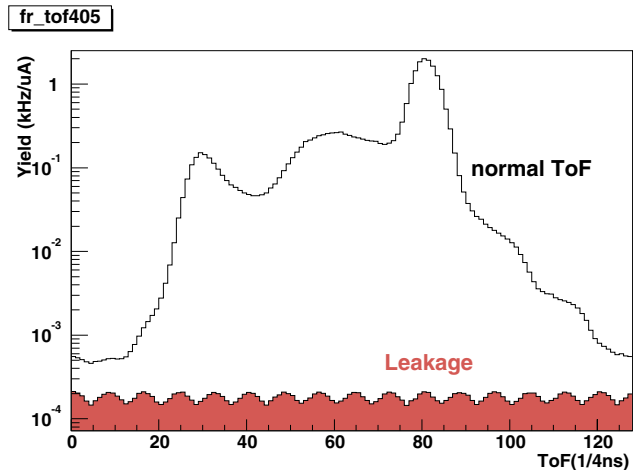


Fig. 25. Contamination of $G\theta$ spectra by leakage beam. Some beam from the Hall A and B lasers was found to be leaking into Hall C. The leakage beam was small, about 50 nA compared to the $G\theta$ 40 μ A main beam, and had the 499 MHz time structure of Halls A and B rather than the 31 MHz Hall C beam.

Following the 2002–2003 engineering run, the target exit window was thinned from 11 mil to 3 mil, which reduced the background under the elastic peak by almost a factor of 2. To better understand the remaining background, an insertable tungsten radiator and insertable dummy entrance and exit windows were provided. Figure 26 shows window backgrounds measured in the 2003–2004 run. In addition to these backgrounds, backgrounds from inelastic LH_2 processes must be taken into account. Using both the measured backgrounds and the results of Monte Carlo simulation, the background fraction can be determined. The fractions were found to vary from about 10% to 40% depending on detector number.

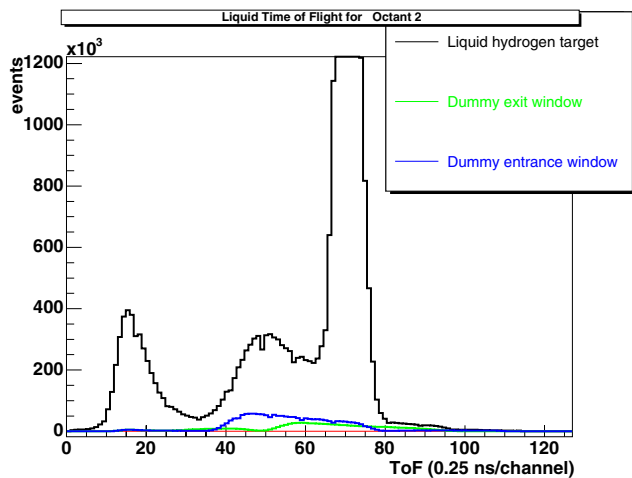


Fig. 26. Estimation of background from entrance and exit windows. The dummy window data have been scaled by charge, thickness and photon flux to match reality in the actual cryogenic cell.

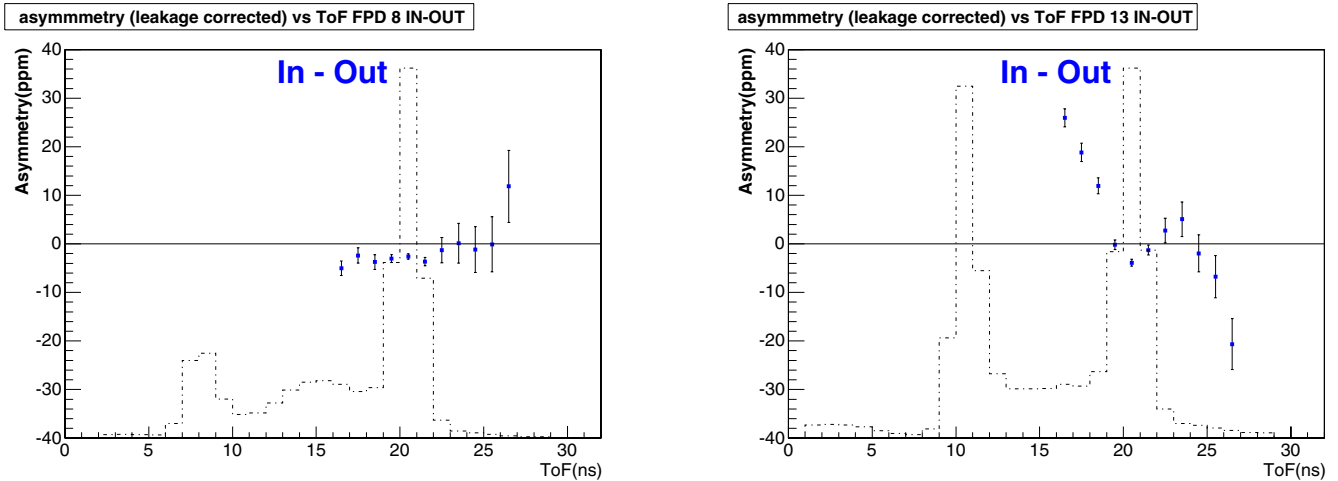


Fig. 27. Estimation of background asymmetry under the peak. The asymmetry is measured on each side of the elastic peak and an interpolation is made. The background correction is more difficult for the higher numbered (higher Q^2) detectors.

Figure 27 shows how the background asymmetry under the peak is estimated by measuring the asymmetry on each side of the peak and interpolating. This method works well for the lower numbered detectors.

Monte Carlo simulations, and investigations of alternative background fitting methods are continuing to make sure that backgrounds are properly understood. The systematic uncertainty in the final result is expected to be dominated by background corrections.

Preliminary data To avoid unintentional bias in the analysis, a blinding factor of from 0.075 to 1.25 has been applied. This is done in such a way as to have the same effect as the wrong beam polarization. Figure 28

shows the data presented at the Gordon Photonuclear Conference in August. The background corrections are still being studied for the highest detector numbers, so these data are not included.

Backward angles

Backward angle running involves detecting electrons at 110° . While at forward angles there was a large variation of Q^2 over the $G\theta$ acceptance, in the backward angle configuration the kinematics are such that there is very little variation of Q^2 with angle. For this reason the experiment plans separate runs at beam energies of 424, 576, and 799 MeV, corresponding to $Q^2 = 0.3, 0.5, \text{ and } 0.8 \text{ (GeV}/c)^2$. This will be done for both LH₂ and LD₂ targets for a total of 6 runs of 700 hours each. The back angle run will use the normal Jefferson Lab 2 ns bunch spacing. We also hope to raise the beam current to $80 \mu\text{A}$.

Now that the forward angle data-taking is complete. The experiment is being reconfigured in backward angle mode. The detector Ferris wheel and spectrometer magnet were turned around in August.

The backward angle running also requires some additional detectors. The cryostat exit detectors (CED) are scintillators that will be used to separate elastic and inelastic electrons. These detectors have been built by Manitoba scientists in collaboration with TRIUMF and are now at Jefferson Lab. To reject pion background (primarily in the LD₂ target run), aerogel Čerenkov detectors have been built by the French and Manitoba/TRIUMF/UNBC collaborators and were delivered to Jefferson Lab in the fall.

Progress for the backward angle run

Cryostat exit detectors For the backward angle second phase of the $G\theta$ experiment, the addition of a second array of scintillation detectors, located near the

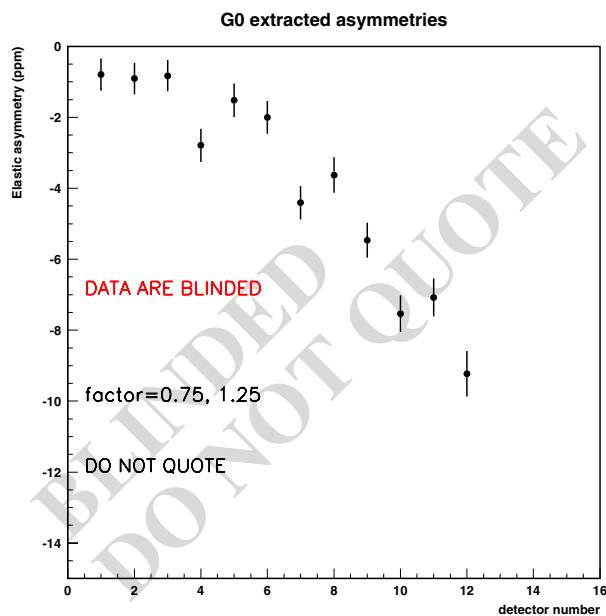


Fig. 28. Preliminary data. The data are not fully corrected and are blinded by an as yet undisclosed factor of 0.75 to 1.25. No data are shown for the highest detectors because the background corrections are not complete.

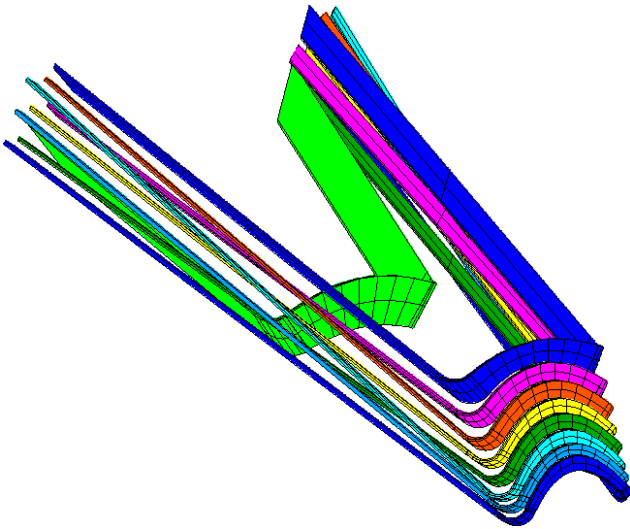


Fig. 29. Layout of a cryostat exit detector (CED) array for a single octant.

spectrometer cryostat exit windows, will be required in order to separate the elastic and inelastically scattered electrons. The geometry of these cryostat exit detector (CED) arrays (see Fig. 29) has been studied in detail and a reference design was completed. With the resident expertise at TRIUMF in producing high quality scintillation detectors and lightguides, the Canadian subgroup was asked to play the lead role in the prototyping and production of the CEDs. A set of prototype CEDs was built at TRIUMF and delivered to the $G\theta$ collaboration for studies with cosmic rays. Results from these studies showed that the reference design and the prototype detectors met the specification requirements for these arrays. Production of a full set of CED prototypes was then completed at TRIUMF to aid in the design of the CED support structure. After finalizing the CED design, construction of the “production” versions of the CED arrays began. Fabrication of the CED scintillators for all 8 octants was completed and delivery was made to TJNAF in late 2001, and fabrication of the special helical-bent lightguides began in 2002. In order to achieve the unique helical bend required in the $G\theta$ backangle geometry, customized bending jigs were designed and constructed at TRIUMF and tested on a first set of prototype CED lightguides. Production of a full set of lightguides for the first CED octant was completed with delivery to TJNAF in 2003, where they underwent further quality-control tests. Production of the lightguides for all 8 octants was completed with delivery to TJNAF in early 2004. Presently, the CED arrays are being assembled and tested on special support frames, which were designed at TRIUMF. These support frames (the mini Ferris wheel) will be mounted onto the existing $G\theta$ detector support structure in 2005. The CEDs will make use of the same types

of photomultiplier tubes and specialized TRIUMF/ $G\theta$ bases as the focal plane detectors.

Aerogel Čerenkov detectors Monte Carlo simulation results have shown that backgrounds from negative pions will be problematic for the second phase backward angle measurements involving the deuterium target. The $G\theta$ Simulation subgroup focused on characterizing this π^- background and provided options regarding the design of an additional set of detectors to reject the background pions. The $G\theta$ Canadian and French (Grenoble) subgroups have been asked to jointly undertake the prototyping and construction of this crucial set of detectors, which will be made up of an array of aerogel Čerenkov counters. Much effort went into the design of this detector array and a conceptual design was evolved into a first prototype at TRIUMF.

In October–November, 2003 a last run was performed with the prototype box to investigate the effect of variations in box geometry and the effect of pulling back the PMTs to a more realistic position for the purpose of magnetic shielding. The final design of the Čerenkov detector was completed, allowing for more realistic shielding of the PMTs and better matching of the acceptance to the distribution of scattered electrons. Four such detectors were built in the TRIUMF Machine Shop.

In addition, newly designed PMT housings were constructed for the 16 PMTs. Tests were also done within a large C-magnet on the requirements and effect of the magnetic shielding.

Three of the four boxes were sent to Jefferson Lab; one was kept at TRIUMF for later tests. The Jefferson Lab boxes were loaded with aerogel tiles, including cut angled pieces at the edges. The retention system consisting of a harp of wire-chamber wires threaded onto an insertable frame was assembled and shown to function properly (see Figs. 30 and 31). A test was also conducted to show that the Čerenkov detectors would fit onto the support frames.

At TRIUMF, further tests are planned in the M11 beam line to calibrate the light output with $\pi/\mu/e$ beams, using the final production detector. Following these tests, this last detector will be delivered to Jefferson Lab.

Backangle support structure Considerable effort has gone into the engineering design of a support structure for the $G\theta$ Čerenkov and CED arrays. Although the Canadian subgroup was initially responsible only for the design of the Čerenkov support structure, it was soon realized that the CED support structure would be closely coupled to the former due to the physical proximity of the two detector subsystems. As such, an integrated design for the two detector subsystems was

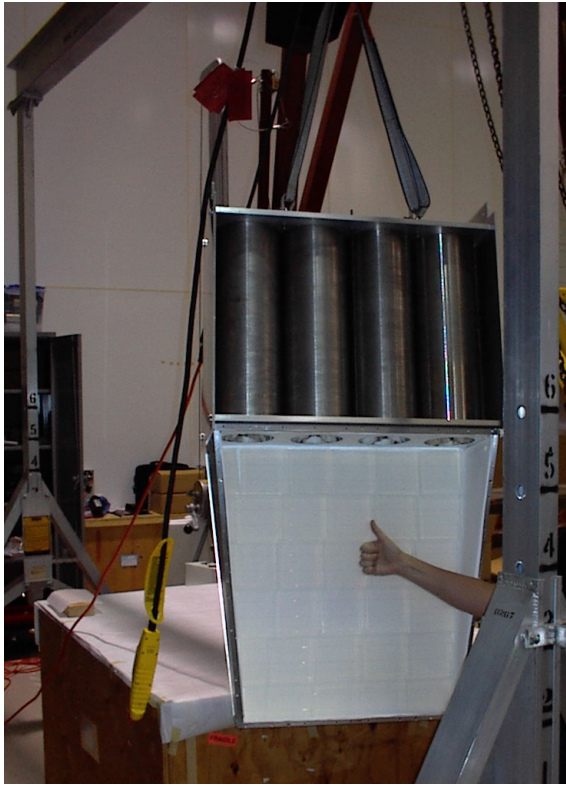


Fig. 30. The new $G\theta$ production version of the aerogel Čerenkov box after arrival at Jefferson Lab. The box is full of aerogel with retainer in place.



Fig. 31. The new boxes and PMT housings after arrival at Jefferson Lab and ready to go.

pursued. The support structure centres around the use of prefabricated aluminum extrusions from Bosch because of their strength, versatility, and relatively low costs. A series of detailed finite-element analysis studies was carried out at TRIUMF, using the program ANSYS, to identify potential problems and to optimize the strength and cost of the support structure. The design consists of a second Ferris wheel type support structure, which will couple to the existing FPD support structure (also a Ferris wheel type design) and to the linear rails on the existing $G\theta$ detector platform. A conceptual illustration of the $G\theta$ backward angle configuration is shown in Fig. 32, with the superconducting magnet, the 3 detector arrays (FPD, CED, Čerenkov) in each of the 8 sectors, and their respective support structures.

In the spring of 2003, the parts for a single octant of the support frame were procured and successfully assembled at TJNAF (see Fig. 33). As various components of the backward angle detectors arrived at TJNAF over the summer of 2003, work began on a “test assembly” of one octant of the backward angle system to validate the overall design and assembly procedure. In particular, the positions of the CED scintillators had to be accurate to ± 2 mm, and the scintillators themselves could only be directly supported by a low-density material. Furthermore, the CED scintillators would have to be glued *in situ* to their respective lightguides and any potential interferences between adjacent detectors would have to be identified and reconciled. An assembly to locate and hold the CED scintillators was designed and built (see Fig. 34). This assembly was constructed from a structural foam material, Rohacell-71, which is light-weight (≈ 71 g/cm³) and is easily machinable. To help complete the test assembly,

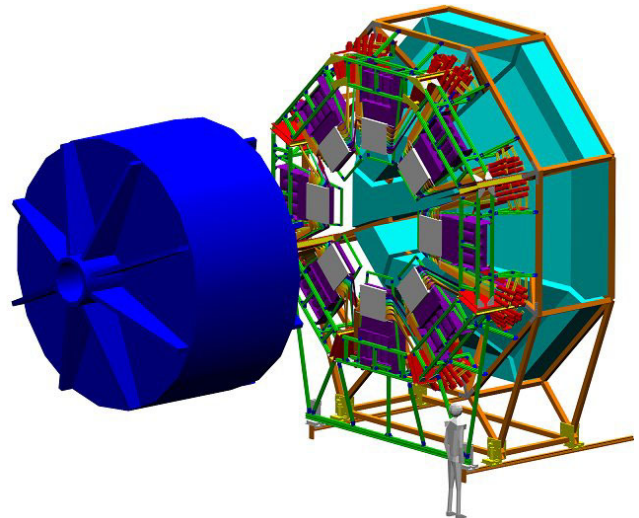


Fig. 32. Conceptual layout of the $G\theta$ backward angle configuration.

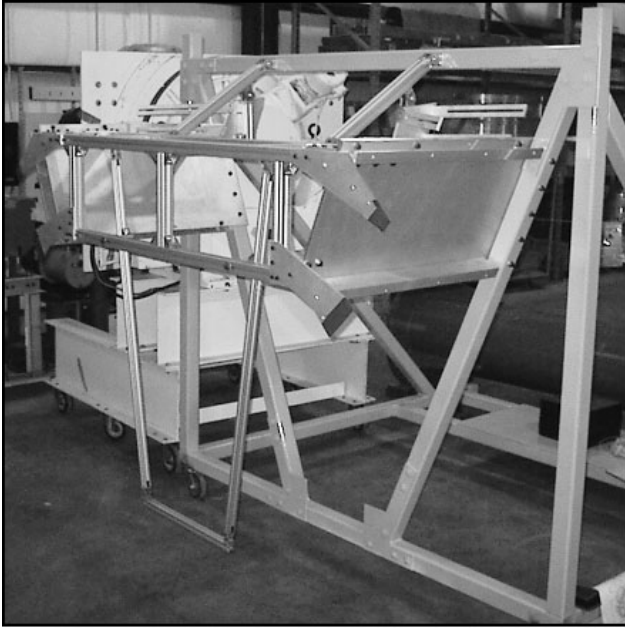


Fig. 33. A single octant of the backangle detector support frame.

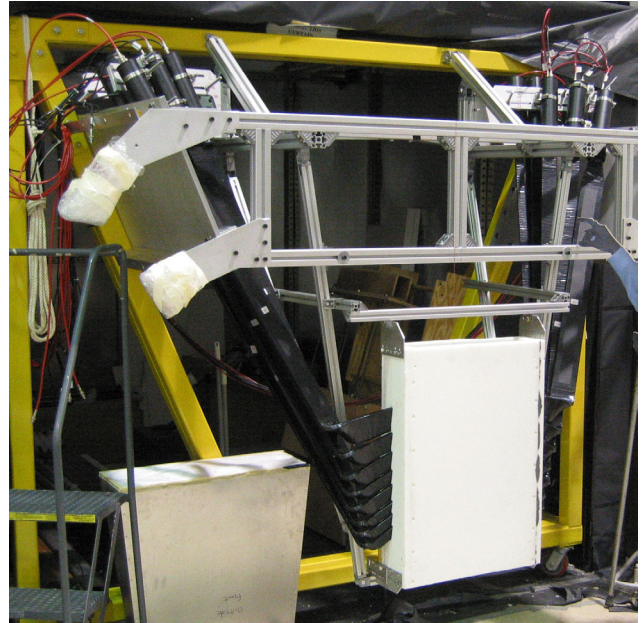


Fig. 35. The first completed octant of CEDs, assembled *in situ* within its octant support frame.

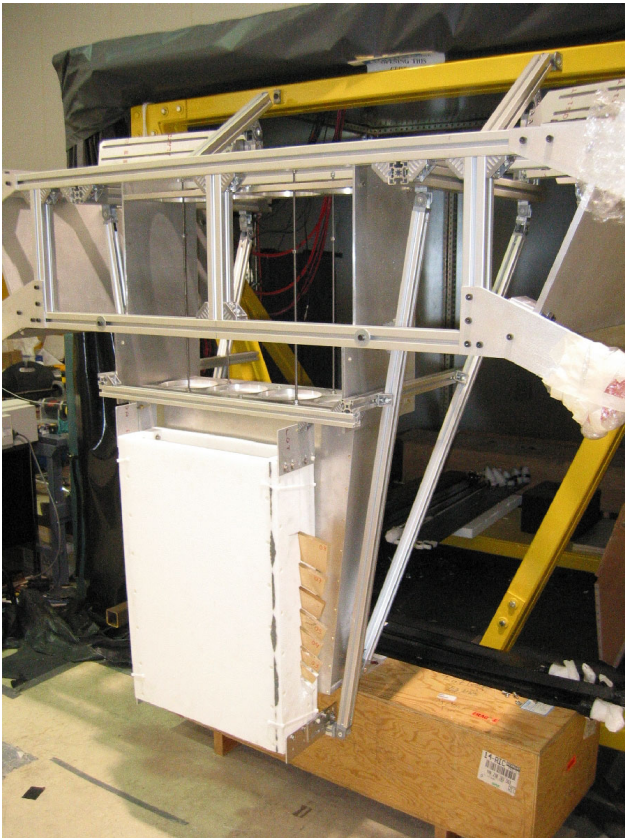


Fig. 34. The Rohacell assembly which both positions and supports the CED scintillators.

both the Canadian and French groups supplied mock-up Čerenkov detectors for test mounting in the support structure frame. Both Čerenkov mock-ups were test fitted and met the nominal mechanical design specifications. In late 2003, the test assembly was completed and the overall support frame design was validated.

In the spring of 2004, procurement of parts for the remaining 7 octants of the support structure began. At the same time, final assembly of the first octant of CEDs also began. By late summer, all parts for the CED octant support frames were delivered to Jefferson Lab, and assembly of the remaining octant support frames was well under way. As well, the first octant of CEDs was successfully assembled (see Fig. 35) and a first set of tests, using cosmic rays, was carried out to quantify the light yield in these detectors. Over the fall, efforts focused on completing the assembly of the remaining octant support frames and assembling the CED arrays *in situ* within these frames. Presently, cosmic ray calibrations of the CED arrays are under way and will continue into early 2005.

Future It is expected that set-up of the backward angle configuration will be completed in the fall, 2005, with a first run possible in late 2005.

Canadian subgroup of the $G0$ collaboration: J. Birchall, W.R. Falk, B. Jasper, Z. Ke, L. Lee, S.A. Page, W.D. Ramsay, G. Rutledge, M.J. Steeds, W.T.H. van Oers (Manitoba); E. Korkmaz, T. Porcelli (UNBC); C.A. Davis (TRIUMF).

TJNAF Experiment 02-020

The Q_{weak} experiment: a search for physics at the TeV scale via a measurement of the proton's weak charge

(S.A. Page, Manitoba)

Introduction

The standard model of electroweak interactions has been confirmed with impressive precision in a variety of experiments, ranging in energies from the eV scale in atomic parity violation to a few hundred GeV in collisions at HERA, LEP, SLC, and the Tevatron.

An essential, but not well tested, prediction of the standard model is the variation of $\sin^2(\theta_W)$ with momentum transfer Q^2 , referred to as the “running of $\sin^2(\theta_W)$ ” (see Fig. 36). Because the radiative corrections which result in the running of $\sin^2(\theta_W)$ can reflect contributions from additional force carriers beyond the standard model, a precision measurement of

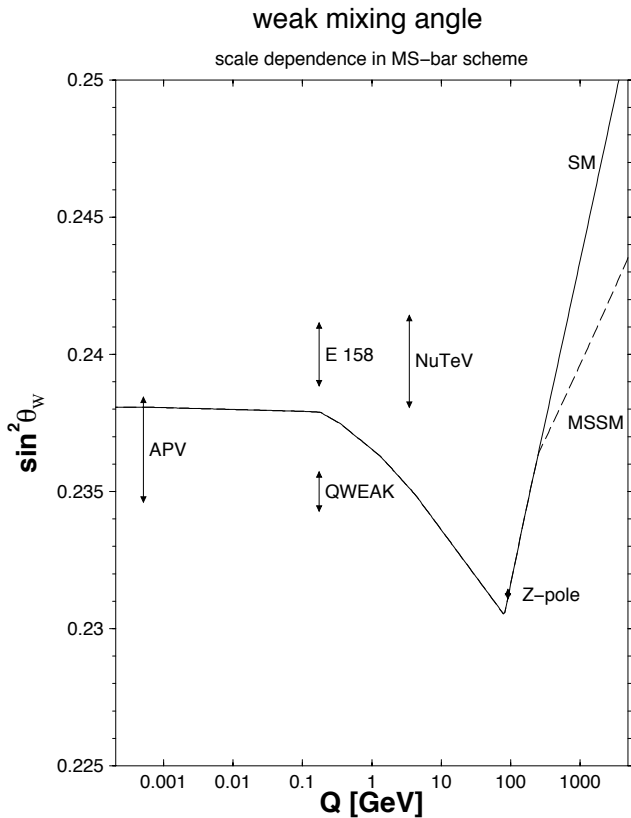


Fig. 36. Calculated running of the weak mixing angle in the standard model [Erlar *et al.*, Phys. Rev. **D68**, 016006 (2003)]. The data points shown are those from the atomic parity violation experiment on Cs (APV), the SLAC experiment (E158), the FNAL (NuTeV) experiment, and from several leptonic and semi-leptonic experiments at the Z^0 pole. Also shown is the anticipated error bar of the Q_{weak} experiment at Jefferson Lab. Møller and deep inelastic scattering experiments at low Q^2 with different extensions to the standard model may follow the upgrade of CEBAF to 12 GeV.

$\sin^2(\theta_W)$ at low energy will provide a surprisingly sensitive test for new physics.

The very precise measurements at the Z^0 pole (at LEP and SLC) set the overall scale of the running of $\sin^2(\theta_W)$. Shown in Fig. 36 are the precise Z^0 pole point and three other measurements which test the running of $\sin^2(\theta_W)$: an atomic parity violation experiment, the SLAC E158 parity violating electron-electron (Møller scattering) experiment and the Fermilab NuTeV neutrino-nucleus scattering experiment. The Jefferson Lab Q_{weak} experiment will have significantly smaller statistical and systematic errors and has a much cleaner theoretical interpretation than the other low Q^2 measurements. It is worth emphasizing that it is extremely useful to have both the SLAC electron measurement and the Jefferson Lab Q_{weak} proton measurement, as the two are affected differently by different extensions to the standard model. This is illustrated in Fig. 37 [Erlar *et al.*, *op. cit.*]. For example, SUSY loops and a 1 TeV Z' would affect both measurements in the same direction, whereas RPV SUSY has effects in opposite directions. Only Q_{weak}^p is sensitive to leptoquarks.

Q_{weak} will measure the parity violating asymmetry in the scattering of longitudinally polarized electrons from protons at very low momentum transfer, $Q^2 = 0.03 (\text{GeV}/c)^2$, and an energy of 1.12 GeV. Under these conditions, the asymmetry arises almost entirely from the proton's weak charge. The results of earlier electron-proton parity violating experiments will be used to constrain the small corrections from hadronic form factors. A 2200 hour measurement employing $180 \mu\text{A}$ of 80% polarized beam on a 0.35 m liquid hydrogen target is expected to determine the proton's weak charge with a 4% combined statistical and

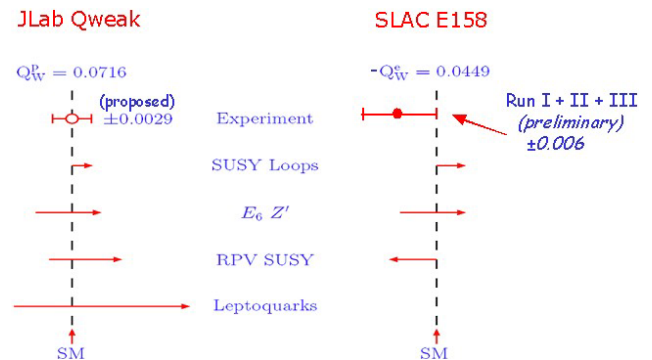


Fig. 37. A comparison of the anticipated error for the Q_{weak} (Q_W^p) experiment and the SLAC E158 (Q_W^e) experiment and the addition of various new physics additions to the standard model that are allowed by fits to existing data at a 95% confidence level. SUSY loops and a 1 TeV Z' would have effects in the same direction for both measurements and could result in evidence for new physics. RPV SUSY has effects in opposite directions. Only Q_W^p is sensitive to leptoquarks, while Q_W^e would serve as a control.

systematic error. A toroidal magnetic field will focus elastically scattered electrons onto a set of eight quartz Čerenkov detectors coupled to photomultiplier tubes, which will be read out in current mode to achieve the high statistical precision required for the measurements. The acceptance averaged asymmetry in the designed experiment is predicted to be -0.3 ppm. This will be measured to $\pm 1.8\%$ statistical and $\pm 1.3\%$ systematic error, leading to the determination of $\sin^2(\theta_W)$ at the 0.3% level. The Canadian group is leading the magnetic spectrometer construction project and are also designing, developing, and fabricating the electronics for the main detector system. Jeff Martin, from the University of Winnipeg, has recently joined the group which now includes members from Winnipeg, Manitoba, UNBC, and TRIUMF. Further responsibilities of the Canadian group are in systematic error evaluations and in beam line monitoring and control apparatus.

The Q_{weak} magnetic spectrometer QTOR

The resistive toroidal magnet with eightfold symmetry has been defined by the magnet working group of physicists and engineers from Jefferson Lab, Louisiana Tech, Manitoba, MIT-Bates, and TRIUMF. The magnet, the coil holders, and the support structure have been designed at MIT-Bates (see Fig. 38). The

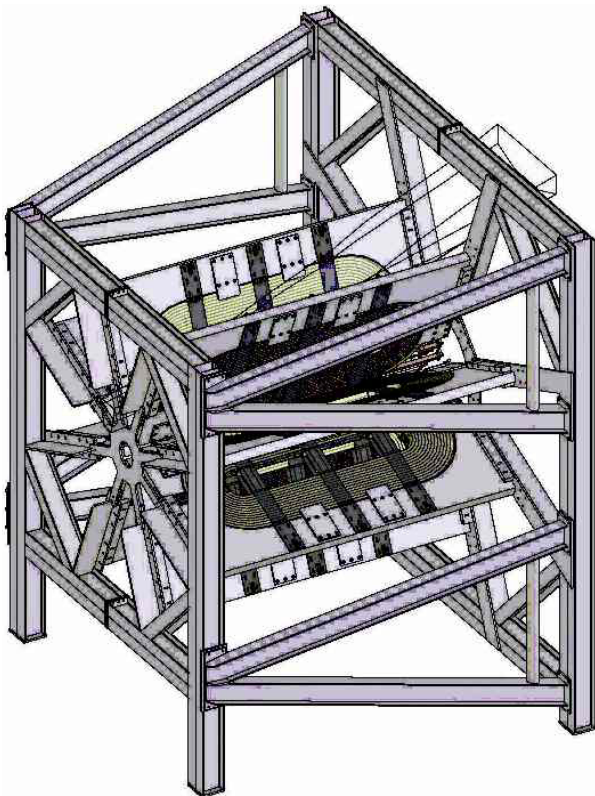


Fig. 38. Three-dimensional view of the Q_{weak} resistive toroidal magnet with its support structure.

copper conductor has been purchased by Jefferson Lab from Phelps-Dodge and delivered to the coil manufacturer. The contract for fabrication of nine coils was awarded to Sigma Phi in Vannes, France. Construction has started and the finished coils are to be delivered to MIT-Bates by the end of July, 2005. The aluminum plate for the coil carriers or holders has been ordered with delivery by March 1, 2005. The current timetable calls for construction of the coil carriers between April 1 and June 30, 2005. A review of the support structure took place in October, 2004. The contract will be awarded in early 2005.

QTOR magnetic field calculations and field mapping

The magnetic field calculation has been updated to reflect information from the latest technical drawings (March, 2004). In this latest design, the coil leads have been modified considerably from the earlier design. The changes result in only very minor differences in the calculated trajectories.

In order to investigate the implications of the latest field calculations and how best to achieve the desired coil placements, sets of ray-trace calculations for a bundle of electron trajectories and absolute field calculations were performed. They were carried out with the coils in their nominal positions and the coils displaced randomly with a normal distribution of $\sigma = 3.5$ mm in the x , y , and z directions, and $\sigma = 4.4$ mrad (0.25°) in rotation. Some sample displacements, in the direction transverse to the bar, are shown in Table VI for sectors 1, 3, 5 and 7. As can be seen, the random coil misalignments generally resulted in unacceptably large displacements of the electron trajectories on the detector bars.

Table VI. Effect of coil misalignment on the position of various rays on the main detector bar. The coil misalignments were chosen randomly from distributions of $\sigma = 3.5$ mm in the x , y , and z directions, and $\sigma = 4.4$ mrad (0.25°) in rotation. Results are shown for octants 1, 3, 5, and 7.

Ray		Transverse displacement on bar (cm)			
$\theta(\text{deg})$	$\phi(\text{deg})$	1	3	5	7
6.00	-10.00	0.025	-0.193	-0.018	0.730
6.00	0.00	0.112	-0.160	-0.153	0.959
6.00	10.00	0.049	-0.139	-0.297	1.238
9.00	-10.00	-1.004	-0.287	0.351	0.222
9.00	0.00	-0.872	-0.149	0.265	0.364
9.00	10.00	-1.162	0.106	0.343	0.384
12.00	-10.00	-0.928	-0.630	0.473	0.060
12.00	0.00	-0.896	-0.318	0.369	-0.033
12.00	10.00	-1.175	-0.094	0.564	-0.378

Since the field at any point depends on the total current distribution of all eight coils, measurements of the absolute field are of limited value in ascertaining coil misalignments. They will, however, still be necessary to verify the overall field strength.

Measurements of the zero-crossings of selected field components in the planes at approximately $Z = \pm 180$ cm would permit determination of the coil positions to about 1.5 mm and rotations to about 1.8 mrad (0.1°). Corrections to the coil positions could then be made, reducing to an acceptable level the asymmetries that would be recorded by the detector bars.

The Q_{weak} current mode electronics

The Q_{weak} experiment detects electrons elastically scattered from the liquid hydrogen target at a laboratory angle of 9° . The experiment will measure the parity-violating difference in scattering cross section for electrons of right-handed and left-handed helicity, expressed as $A_z = (\sigma^+ - \sigma^-)/(\sigma^+ + \sigma^-)$ where σ^+ and σ^- refer to the cross sections for electrons of right-handed and left-handed helicity. It is expected that $A_z \simeq -0.3$ ppm, and it is desired to measure this to a statistical precision of 5×10^{-9} in 2200 hours. To do this requires a count rate of ~ 800 MHz in each of the 8 octants. This is too high for conventional pulse counting techniques, so the experiment will operate in current mode. Custom made electronics for this purpose are being designed and built at TRIUMF.

Figure 39 shows a block diagram of the front end electronics. The current signal from the photomultiplier tube goes to a current to voltage preamplifier followed by a VME based digital signal integrator. These parts, shown in blue on the figure, are the sections to be made at TRIUMF.

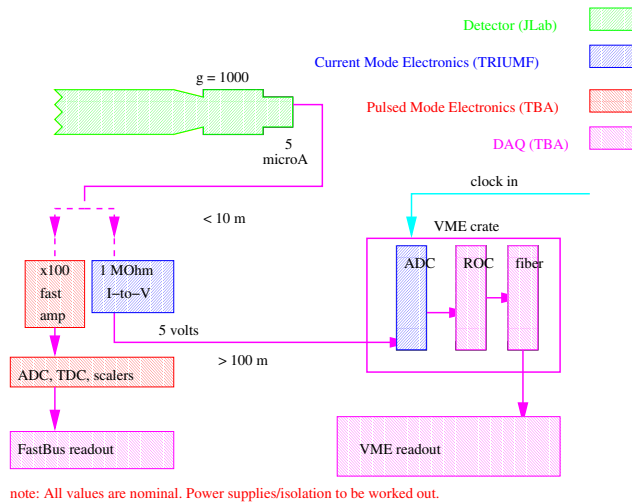


Fig. 39. Q_{weak} front end electronics, showing the division of responsibility for different sections.

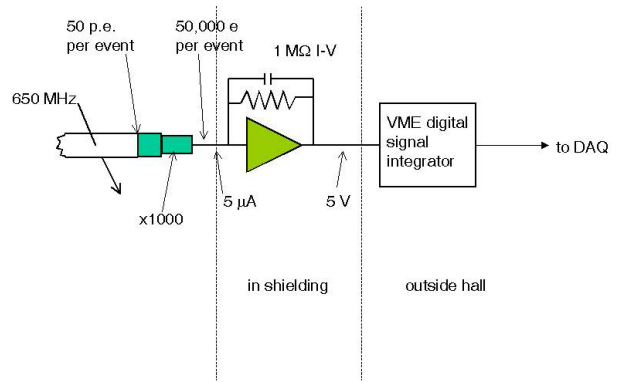


Fig. 40. Nature of the Q_{weak} signals. The charge quantum of the $5 \mu\text{A}$ signal is 50,000 times the electronic charge. The rms shot noise is hence much larger than if the $5 \mu\text{A}$ was from a battery.

The nature of the signal Figure 40 indicates how a $5 \mu\text{A}$ current signal to the TRIUMF electronics is produced from the high count rate at one of the 8 detectors. It is expected that 50 photoelectrons will be released at the photomultiplier tube (PMT) cathode for a typical event. The gain of the photomultiplier is adjusted to yield $5 \mu\text{A}$ at the anode under normal running conditions. In this example, the count rate is 650 MHz; this will require a PMT gain of approximately 1000 (if the count rate is 800 MHz, the current at this gain will be $6.4 \mu\text{A}$). The $5 \mu\text{A}$ signal will be considerably noisier than $5 \mu\text{A}$ from a battery because it is made from large, 50,000 e charge lumps rather than from single electrons. This “shot noise” is given by $i_n^2 = 2QIB [A^2]$, where I is the current, Q the charge quantum, and B the equivalent noise bandwidth.

The analogue section of the electronics will be placed in Hall C near the main detectors, but shielded as much as possible from radiation. We hope to reduce the total dose to the analogue electronics to ~ 1 krad. The VME digital signal integrators will be located outside the hall in the Q_{weak} electronics cage.

The custom VME signal integrators must integrate the signal for a time set by the data acquisition and make the result available on the VME bus. The integration time will depend on the spin flip rate. Two schemes have been considered. In the “120 Hz” scheme, each spin state will last 1/30 s. The current mode electronics will integrate the current over the spin state as four 1/120 s integrals. The scheme would be insensitive to noise at multiples of the 60 Hz ac line frequency; the 4 times over sampling would let us check if significant line noise was being cancelled by the 1/30 s integral. In the “1 kHz” scheme, each spin state will only last 1/250 s and the charge will be digitized as four, 1 ms long, integrals. The argument for the 1 kHz scheme is that it may be difficult to produce a non-boiling liquid hydrogen target to handle 2 kW. Target boiling data

from Hall A indicate that the frequency spectrum of the noise from target boiling is such that bubbling is not seen on a time scale of a few ms.

Method of integration To perform the integration, the VME module divides the integration period, T , into n equal time bins of width Δt and samples the signal at the middle of each bin. The integral is Δt times the sum of the samples.

Analogue bandwidth Integration by this simple method assumes that the sampling rate is high compared to the analogue bandwidth, so that the signal looks like a straight line over one time bin. If this is not the case, either the analogue electronics must be slowed down, or the sampling rate increased. Another important reason to limit the analogue bandwidth is so that signal frequencies higher than half the sampling rate do not “alias” back into the passband. In practice, the digital integrator will have an appropriate sharp cutoff “anti-aliasing” filter built in.

Although, as just explained, we want to restrict the analogue bandwidth, it cannot be made too low. Too low a bandwidth will give too little spread in the individual samples so “least bit” ADC noise will not average out. In addition, the signal we are looking for is a small current signal synchronized with the spin state; an extremely low bandwidth could slow the response to the extent that the electronics would not follow the real signal. Looked at in the time domain, the signal risetime should be fast enough compared to the dead time between spin states that the current is steady on its new value before integration begins.

Noise budget Table VII summarizes the main sources of noise under different running modes. The main noise source during data-taking is shot noise due to the random arrival of electrons at the detectors (i.e. counting statistics). This noise is reduced during beam OFF tests when the charge quantum of the $5\ \mu\text{A}$ signal is smaller. The numbers in Table VI assume $Q = 50,000\ e$ for beam ON, $Q = 1000\ e$ for LED tests, and $Q = e$ for battery tests. If other sources of noise are small compared to shot noise, then the time to achieve a given statistical precision is proportional to the charge quantum. Beam OFF tests in particular, for which the charge quantum is small, benefit greatly from low electronic noise.

Preamp noise cannot be lower than the thermal noise (Johnson noise) in the $1\ \text{M}\Omega$ feedback resistor. This white noise, with a density $e_R = 127\ \text{nV}/\sqrt{\text{Hz}}$ at room temperature, appears added to the output voltage. The input resistor also contributes noise, the size of which depends on the capacitance of the input cable. Pspice simulations at TRIUMF indicate around $400\ \text{nV}/\sqrt{\text{Hz}}$. Since the amplifier noise for a modern

preamp is several factors of ten below this, we assume the resistor noise dominates. As a fraction of $5\ \text{V}$, this is $0.7\ \text{ppm}$ for a $1/120\ \text{s}$ integration or $2\ \text{ppm}$ for a $1/1000\ \text{s}$ integration.

For the VME based digital signal integrator being designed at TRIUMF, the noise will depend on details of the design, but will be effectively one or two least significant bits on a 20 bit number. Internally, the integrators will use 16 or 18 bit ADCs (probably 18 bits) with typically $0.5\ \text{LSB}$ rms noise that is further reduced by averaging 500 to 1000 samples over the integration period.

Dithering In order for the averaging of ADC “least count” noise to work, the raw signal must be spread over sufficient bins in the input ADC. For example, if the input signal was so quiet that it sat in one bin of the ADC, an artificial noise, or “dithering” would have to be added so that the average of many samples could be taken to determine where in the bin the signal was sitting. The analogue signal will be quieter in the $120\ \text{Hz}$ scheme as, due to the slower sampling rate, the bandwidth has to be more limited than in the $1000\ \text{Hz}$ scheme. Table VIII summarizes the situation for the worst case of $1/120\ \text{s}$ integration times (assuming an equivalent analogue noise bandwidth of $15.7\ \text{kHz}$ ($f_{3db} = 10\ \text{kHz}$), and a 16 bit ADC operating at half-scale. One sees that there is only a potential problem if beam OFF tests are made with a battery. Only the shot noise contribution is shown. A move to higher bandwidth or 18 bit ADCs, will further reduce any problem. Table IX shows the improvement when the analogue bandwidth is increased to a value appropriate for the $1000\ \text{Hz}$ scheme. One can see from the last column that high frequency operation, combined with an 18 bit ADC will ensure that even a quiet signal is spread over sufficient bins.

Required modules In addition to handling the signals from the main detectors, we plan to use TRIUMF electronics for a variety of other instrumentation, for example, luminosity monitors and beam line monitors. Some of these deliver voltage signals and will only need digital integrators while others will need both I-V preamplifiers and digital integrators. Initially, we plan to build 28 dual I-V preamplifiers and 14 octal integrators. This will be adequate to handle the main electronics and essential beam line instrumentation. Depending on funding, it may be possible to supply more modules to upgrade other beam line monitors and to provide spares.

Schedule The following schedule has been adopted:

- 2005 – Preliminary design ready for preamplifiers and integrators. Prototype preamplifier built and tested for radiation hardness.

- 2006 – Prototype VME integrator built and tested.
- 2006 – Design finalized and required modules built
- 2007 – Install and commission detectors and electronics.

List of Q_{weak} collaborators: M.J. Ramsey-Musolf, Caltech; D. Armstrong, T. Averett, J.M. Finn, K.H. Grimm, College of William and Mary; T. Smith, Dartmouth College; C. Keppel, Hampton University; P. Bosted, A. Bruell, R.D. Carlini, S. Chattopadhyay, R. Ent, D.J. Gaskell, A. Lung, D. Mack, S. Majewski, D. Meekins, H. Mkrtchyan, M. Poelker, J. Roche, G.R. Smith, S. Wood, C. Zorn, Jefferson Lab; J.D. Bowman, G. Mitchell, S. Penttila, W.S. Wilburn, Los Alamos

National Lab; T. Forest, K. Johnston, N. Simicevic, S. Wells, Louisiana Technical University; J.A. Dunne, Mississippi State University; T. Botto, K. Dow, M. Farkhondeh, W. Franklin, M. Khol, S. Kowalski, Y. Prok, E. Tsentalovich, T. Zwart, MIT; Y. Liang, A.K. Opper, Ohio University; C.A. Davis, J. Doornbos, TRIUMF; J. Erler, Universidad Nacional Autonoma de Mexico; R. Jones, K. Joo, University of Connecticut; J. Birchall, W.R. Falk, M. Gericke, L. Lee, S.A. Page, W.D. Ramsay, W.T.H. van Oers, University of Manitoba; S. Covrig, F.W. Hersman, M. Holtrop, H. Zhu, University of New Hampshire; E. Korkmaz, T. Porcelli, University of Northern BC; J. Martin, University of Winnipeg; J. Mammei, R. Mammei, N. Morgan, M. Pitt, R. Suleiman, Virginia Polytechnic Institute. Experiment status: in preparation.

Table VII. Noise contributions from different sources.

Condition	Noise on 1/120 s integral (ppm)	Noise on 1/1000 s integral (ppm)
Beam ON shot noise	430	1240
Shot noise during LED tests	61	175
Shot noise during battery tests	1.9	5.5
Preamplifier noise	0.7	2.0
Digital integrator noise	1–2	1–2

Table VIII. Number of front end ADC bins covered by the analogue signal for an equivalent noise bandwidth of 15.7 kHz ($f_{3db} = 10$ kHz), appropriate for 8.3 ms integration times. The calculation assumes a 16 bit ADC operating at half of full scale. The last column shows the FWHM with an 18 bit ADC.

Condition	Q (e)	rms noise (mV)	Bins (σ)	Bins (FWHM)	18 bit bins (FWHM)
Beam ON	50,000	36	240	557	2228
LED test	1,000	5	33	79	316
Battery test	1	0.16	1	2.3	9.2

Table IX. Number of front end ADC bins covered by the analogue signal for an equivalent noise bandwidth of 130 kHz ($f_{3db} = 83$ kHz), appropriate for 1.0 ms integration times. As in Table VIII, a 16 bit ADC operating at half scale is assumed. The last column shows the FWHM with an 18 bit ADC.

Condition	Q (e)	rms noise (mV)	Bins (σ)	Bins (FWHM)	18 bit bins (FWHM)
Beam ON	50,000	104	684	1607	6428
LED test	1,000	15	97	227	968
Battery test	1	0.46	3	7	28

NUCLEAR PHYSICS

Experiment 715

Weak interaction symmetries in β^+ decay of optically trapped $^{37,38}\text{K}$

(*J.A. Behr, M.R. Pearson, TRIUMF; K.P. Jackson, TRIUMF/SFU*)

We update our progress in testing the standard model using optically trapped ^{38}K and ^{37}K . The pure Fermi β^+ decay of ^{38}K is a sensitive probe of scalar contributions to the weak interaction, while the decay of polarized ^{37}K can be used to search for right-handed currents and time-reversal symmetry violating interactions. The background and experimental set-ups for these experiments have been described elsewhere (Expt. 715, TRIUMF 2002 Annual Report), so we provide here only a brief report on recent progress. Our tensor interaction experiment, Expt. 956, is described elsewhere in this Annual Report.

Scalar search status

Our result for the β - ν correlation parameter $\tilde{a} = 0.9981 \pm 0.0030^{+0.0032}_{-0.0037}$ is an improvement over previous results in the literature. It is therefore the best limit on general scalar interactions coupling to the first generation. It is now in press [Gorelov *et al.*, Phys. Rev. Lett. (in press)].

Scalar interactions can generally be divided into those that couple only to standard model left-handed ν s and those that couple to right-handed ν s. Recent theoretical progress has pointed out that indirect limits from the pseudoscalar decay $\pi \rightarrow e\nu$ constrain most of the parameter space at a better level than our experiment, but scalars coupling to particular combinations of left- and right-handed ν s are left unconstrained [Campbell and Maybury, Nucl. Phys. B (in press)].

We usually place this in the context of other physics by quoting a sensitivity to scalars with mass to coupling ratios compared to the ratio of the W mass to the electroweak coupling. This requires a form factor g_S relating the quark-lepton scalar interaction to the nucleon- and nucleus-lepton interactions, defined by the equation $\langle p|\bar{u}d|n\rangle = g_S(q^2)\bar{u}_p u_n$. Although there are now lattice gauge calculations for this quantity at zero momentum transfer, to compare such numbers to particle searches can require this form factor as a function of momentum transfer. The scaling is thought to be well-understood [Pospelov, private communication], but the details are best left up to constraints on particular models of particular particle interactions, rather than attempting to cite general limits.

Future: extraction of Fierz interference term The present publication was for data with $E_\beta > 2.5$ MeV, half the Q-value. Experimentally, this avoids a number

of complications, including backscattered β s and singles backgrounds in the β detector from the 2.17 MeV γ -ray from decay of the ^{38}K ground state.

There is great value in extending the experiment to lower E_β , because the Fierz interference term b depends on m/E_β . This term is linearly dependent on scalar interactions that couple to left-handed ν s, so isolating it from \tilde{a} is useful. The limits from the Q-dependence of the superallowed ft values are very stringent, but these do require isospin mixing corrections to be relatively correct across different major shells, a stricter requirement than needed for V_{ud} . So it is worthwhile to search for this effect within one experiment. Based on an analysis of the TOF spectra, our statistical error on b in the present data set is about four times the recent limits of Towner and Hardy. Systematic error analysis is proceeding, along with an extension of the angular distribution reconstruction to lower energies as a systematic check.

ISAC is now producing five times as much ^{38}K as when we took this data. A larger MCP would gather a higher fraction of β -Ar $^{+1}$ recoils (currently 89% for $T_\beta > 2.58$ MeV), which would reduce one source of several systematic errors. We are considering whether an upgrade of the experiment might be worth pursuing.

Polarized measurements

Our result for the neutrino asymmetry in the decay of polarized ^{37}K is $B_\nu = -0.771 \pm 0.020 \pm 0.011$, consistent with the standard model prediction $B_\nu = -0.7692$. The largest error is from knowledge of the displacement of the trap position for the two different polarizations. We could measure this better in the future by taking more snapshots of the cloud expansion with the MOT light.

This is the only measurement of a ν asymmetry other than in neutron decay, and has achieved similar accuracy. This constrains a W_R boson coupling to right-handed ν s to have mass >170 GeV/ c^2 (90% confidence), a result which is not yet competitive with the world average of other β -decay experiments. D. Melconian is completing his SFU Ph.D. and a publication on this topic.

Data were taken under a variety of exploratory experimental conditions, and about 2/3 of the data set was compromised by a combination of poor overlap of the optical pumping beam with the cold atom cloud and imperfect alignment of the magnetic field with the optical pumping axis. We are working experimentally to correct these deficiencies. The present method used (switching off the MOT and optically pumping the atoms on millisecond timescales) can be projected to produce better than 0.5% errors if we pursue it with

modest upgrades. It would be preferable to do these experiments in a trap environment, and we describe these efforts in the next section.

CFORT We are working to develop a circularly-polarized far-off resonance trap (CFORT) which promises extremely high polarizations because only the $M_F = F$ state is trapped and all others are repelled. It is expected that we can achieve $>99.9\%$ polarization. This type of trap was developed and loaded efficiently with Rb atoms by JILA [Miller *et al.*, Phys. Rev. **A66**, 023406 (2002)].

As a first step, we have recently succeeded in loading ^{39}K atoms into a far off-resonance dipole force trap (FORT) using linearly polarized light. We have loaded $\approx 4\%$ of the MOT atoms into the FORT, and achieved FORT lifetimes between 1 and 2 s. This is the M.Sc. thesis data of E. Prime. Work is progressing to improve the loading efficiency and to cool the atoms within the FORT. Light for the MOT for this set-up comes from the 899-21 ring (the MOPA chip has died). The MOT light must be carefully tuned in frequency and power to minimize the temperature of the atoms in order to successfully load the FORT. The FORT uses 700 mW of light from the MBR-110 ring, after first order diffraction in an acousto-optic modulator.

We show the FORT lifetime as a function of detuning from resonance in Fig. 41. The lifetimes are consistent with expected heating from real absorption of photons near the resonance. At larger detunings, another effect is dominating that is not understood. This could be some combination of heating from pointing effects, power, and frequency instability of the FORT laser, or resonant photoassisted dimer formation. Note that the trap has very short lifetimes and trapping efficiency in between the D1 and D2 resonances.

The eventual goal is to use circularly polarized light for the FORT. An intermediate goal would be to optically pump within the FORT environment to polarize the atoms, to produce a better-controlled polarized cloud localization.

MBR-110 upgrade The commercial upgrade to the fully frequency-locked system is incomplete, due to unreliable commercial electronics and etalon hardware and poor support from the company. In the 899-21, the lock to the ring mode is maintained by one (“thick”) etalon with 10 GHz free spectral range, and the mode of that etalon is selected by a 200 GHz (“thin”) etalon. In the MBR both functions are combined in a single 200 GHz etalon with narrow finesse. This is a very finicky system, and after a great deal of struggle with hardware and electronics, the lock to one cavity mode is made difficult for potassium because it lies close to an oxygen molecular resonance. Complete nitrogen purging of the laser cavity is necessary to obtain an

etalon lock (in the 899-21 this merely decreases the power, and the lock is robust over an order of magnitude of output power). It is possible this will be satisfactorily resolved soon.

Potassium $5P_{1/2}$ lifetime We have measured the natural decay lifetime of the $5P_{1/2}$ state in potassium by pulsed excitation using our 405 nm narrow diode laser, followed by non-resonant photoionization to monitor the state population. The result for the lifetime is $\tau = 137.6 \pm 1.3$ ns, an improvement compared to previous results in the literature. If we were to measure the $5P_{3/2}$ lifetime with similar accuracy, a detailed comparison and test of the oscillator strength anomaly could be made, and this is one small test of detailed many-body calculations in alkali atoms of use for atomic parity violation. In reality, we pursued this as a test of experimental methods to be used in francium. Our probe of the excited-state population using non-resonant photoionization has a number of problems, including subtle coherent effects induced by this active probe, and we do not intend to use this method in the future. A paper on the lifetime has been submitted.

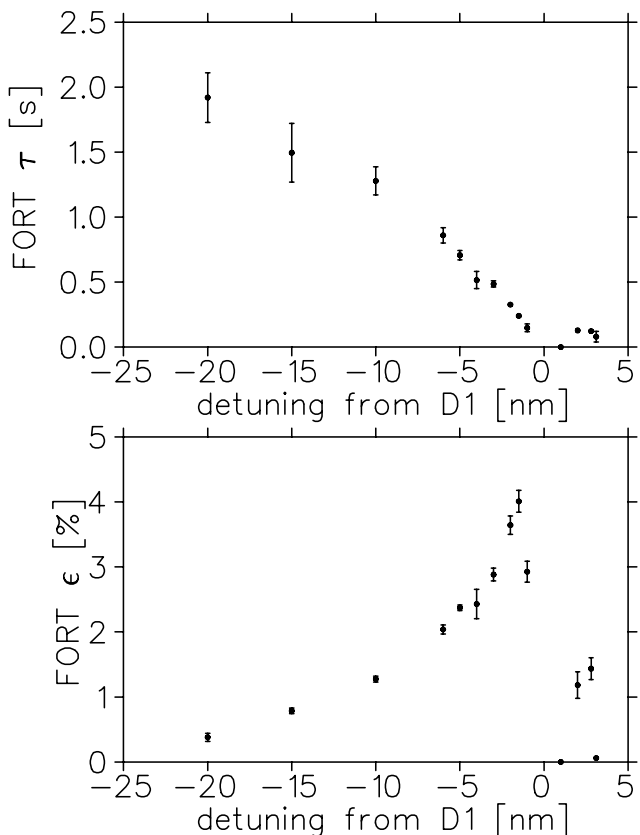


Fig. 41. FORT lifetime τ and loading efficiency ϵ as a function of detuning from the D1 resonance.

Experiment 823

Pure Fermi decay in medium mass nuclei

(*G.C. Ball, TRIUMF*)

Precise measurements of the intensities for superallowed Fermi $0^+ \rightarrow 0^+$ β decays have provided a demanding test of the CVC hypothesis at the level of 3×10^{-4} and also led to a result in disagreement with unitarity (at the 98% confidence level) for the CKM matrix. Since this would have profound implications for the minimal standard model, it is essential to address possible “trivial” explanations for this apparent non-unitarity, such as uncertainties in the theoretical isospin symmetry-breaking correction. Uncertainties in the calculated Coulomb corrections can be studied by extending the precision β -decay measurements to heavier ($A \geq 62$, $T_z = 0$) odd-odd nuclei where these corrections are predicted to be much larger [Towner and Hardy, *Phys. Rev.* **C66**, 035501 (2002)]. The primary goal of the Expt. 823 experimental program is to measure the half-lives and branching ratios for the superallowed β -decay of these radioactive nuclei produced at ISAC. The early measurements focused on ^{74}Rb (see TRIUMF 1999–2002 Annual Reports).

High precision decay measurements of the superallowed β -emitter ^{62}Ga

A preliminary measurement of the half-life of ^{62}Ga , the first in the series of ($A \geq 62$, $T_z = 0$) odd-odd superallowed β -emitters was carried out in the spring of 2003. The long-lived (9.74 m) isobar ^{62}Cu was a significant contaminant that limited the precision of this measurement. A preliminary analysis of these data was reported previously (see TRIUMF 2003 Annual Report). The final result, 116.01 ± 0.19 ms, is statistically consistent with all previous measurements [Canchel *et al.*, *Eur. Phys. J.* (in press)] and references therein; and the world average is 116.17 ± 0.04 ms. Approval has been obtained to substantially improve the precision of the present measurement to the required precision of 0.05% once the TRIUMF resonant ionization laser ion source (TRILIS) is fully operational.

Non-analogue Fermi and Gamow-Teller branches in the superallowed β -decay of ^{62}Ga have been investigated recently at ISAC using the 8π spectrometer. Since the Q_{EC} value for this decay is large, there are a large number of excited 1^+ states in the daughter nucleus predicted to be populated through GT transitions. These transitions, together with non-analogue Fermi (F) branches must be taken into account to determine the partial half-life of the superallowed transition. However, their individual intensities are very

small and many of them cannot be detected with high-resolution gamma spectroscopy. In a previous study [Piechaczek *et al.*, *Phys. Rev.* **C67**, 051305(R) (2003)] of the superallowed β -emitter ^{74}Rb we have shown that this problem can be overcome with the help of theory. It is not necessary to reconstruct the GT strength function of the decay, only the total amount of non-superallowed feeding must be determined. The low-lying levels in ^{62}Zn act as collector states for a large fraction of the non-superallowed feeding and by observing their de-excitation, the larger part of their feeding can be determined. The remaining component, which directly feeds the ^{62}Zn ground state, can be estimated from shell-model calculations provided they reproduce well the relative feeding to excited levels in ^{62}Zn . In previous studies of the β -decay of ^{62}Ga [Hyman *et al.*, *Phys. Rev.* **C68**, 015501 (2003)] it was only possible to observe the γ -decay of the first excited 2^+ level in ^{62}Zn .

A beam of ~ 1600 ^{62}Ga ions/s was produced during the first beam development run with TRILIS (see ISAC Ion Source Development, TRIUMF 2003–2004 Annual Reports for details). A production target of 24 g/cm^2 ZrC was bombarded with 500 MeV protons at an intensity of $35 \mu\text{A}$. TRILIS used an ionization scheme that required frequency tripling of the titanium sapphire laser light. Although the laser-ionized ^{62}Ga beam intensity was only increased by a factor of two over that obtained with a surface source in the previous high-precision lifetime measurement, the isobaric contaminant ^{62}Cu was reduced by a factor of ~ 20 . The activity was implanted into the 8π collector tape that was moved every 14 s to prevent the build-up of longer-lived contaminants. The β particles were detected by the SCEPTAR array and recorded cycle by cycle using multichannel scalers. In addition, prescaled β singles, and $\beta - \gamma$ coincidence events were recorded event by event. Portions of the coincident γ -ray spectra obtained when the beam was on and one second after the beam was turned off, but before the tape was moved, are shown in Fig. 42. The peaks observed at 851 and 954 keV correspond to the decay of the first and second 2^+ levels in ^{62}Zn , respectively. The γ -ray at 1387 keV is attributed to the $0_2^+ \rightarrow 2_1^+$ transition. From a preliminary analysis of these data it was possible to observe the decay of the lowest five known 2^+ levels in addition to the feeding of several 1^+ levels up to ~ 5 –6 MeV excitation in ^{62}Zn . As a result, from these data it should be possible to determine the superallowed branching ratio with the required precision of $< 0.1\%$.

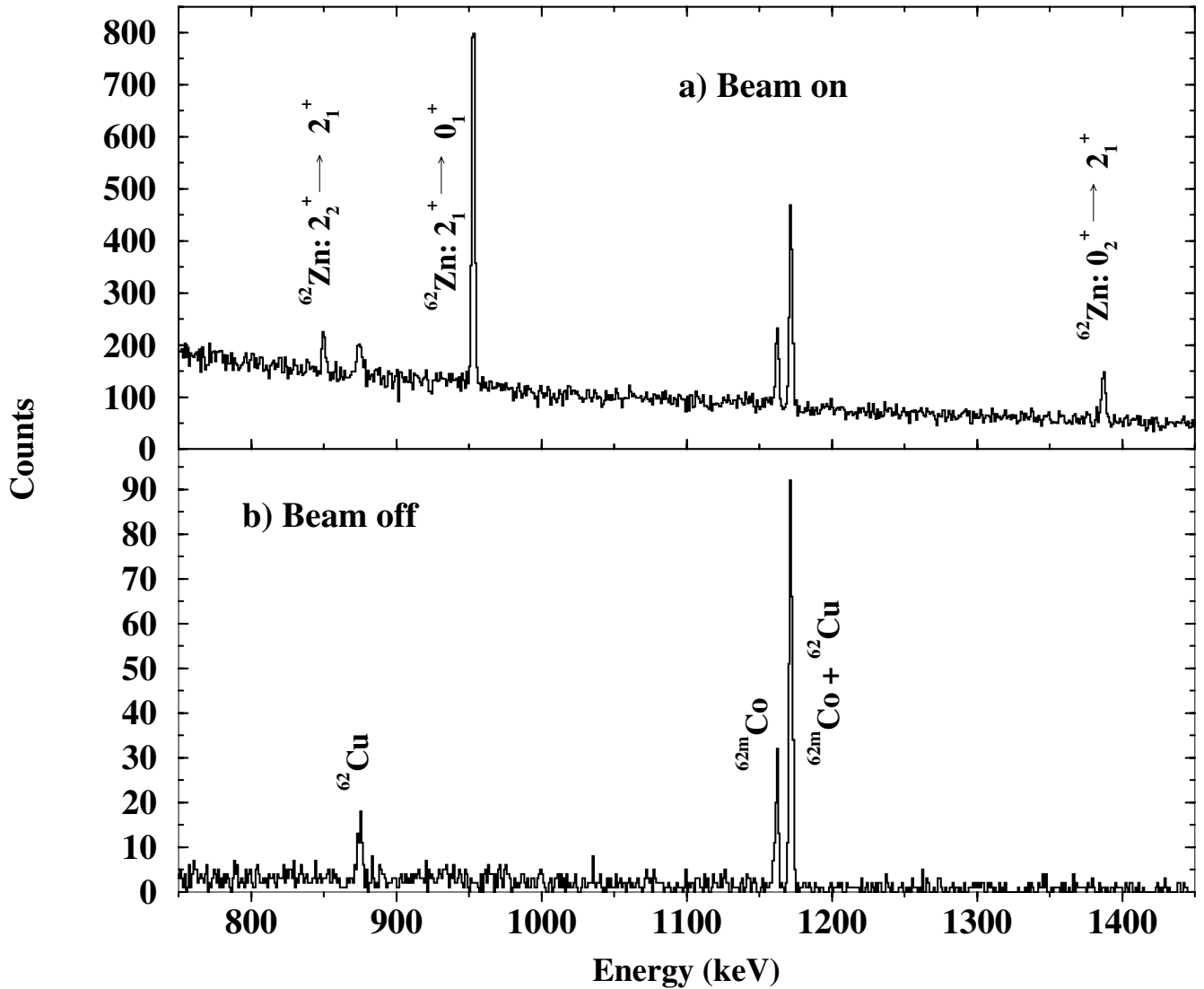


Fig. 42. Portions of the coincident γ -ray spectra obtained in the β -decay of ^{62}Ga : a) during the time in the cycle when the beam was on and b) one second after the beam was turned off. Known transitions in ^{62}Zn as well as peaks resulting from the decay of long-lived isobaric contaminants in the mass 62 beam are identified.

Experiment 893

The hyperfine field of rubidium in iron

(*P.P.J. Delheij, TRIUMF*)

Introduction

The goal of this experiment is the measurement of the hyperfine field for dilute Rb implanted in Fe. The latest theoretical calculations for the elements from Rb to Xe were able to reproduce the experimental values at the few per cent level [Cottenier and Haas, *Phys. Rev.* **B62**, 461 (2000)]. The only exception is Rb for which a discrepancy of a factor ~ 5 exists. The NMRON (nuclear magnetic resonance with oriented nuclei) technique can deliver reliable experimental values for the hyperfine field with errors at the 10^{-3} level or bet-

ter. A beam of ^{79}Rb , the most suitable isotope for this measurement, can be produced at TRIUMF-ISAC with sufficient intensity. Leading up to a measurement with Rb, considerable effort was spent on NMRON development. Test measurements with ^{57}Co and ^{60}Co followed. In view of the beam schedule, an exploratory experiment with ^{22}Na was brought forward and encouraged by the EEC. With this measurement a new mass region was entered for NMRON, being the first one below the element manganese. In addition a new technique was developed by applying NMRON in zero external magnetic field. This avoids the uncertainty from the extrapolation if the zero field resonance frequency must be derived from the field dependence of measurements in non-zero fields. Another new development was the observation of the beta asymmetry through the mea-

surement of the positron annihilation gammas. This provides, independently, the sign of the hyperfine interaction. In such a situation, the simultaneous relaxation of the polarization and the alignment in the sample can be compared.

For these measurements the geometry consisted of a 0.25 mm thick and 10 mm diameter sample disk in the horizontal plane, soldered with Wood's metal on the vertical cold finger that is attached to the dilution refrigerator. A magnetic field up to 1.5 T can be applied horizontally in the east-west direction. So, the cold finger reaches the centre of the magnet through the split. HP-Ge detectors were located east, west and north at a distance of 100 mm from the centre of the sample. A two loop NMR coil with a diameter of 20 mm and a separation of 20 mm between the loops (the axis of the loops is aligned along the north-south direction) produced the rf field for the NMRON measurements.

NMRON development

At the start of 2004 there were indications that the NMRON efficiency at 300 MHz was a factor 10 lower than the 50% we had measured several times for $^{60}\text{CoFe}$ at 166 MHz. A mockup of our NMR probe assembly showed 1) a rather small variation of the signal from the pickup loop as a function of the relative orientation of the transmitter coil and the pickup loop, and 2) a poor agreement of the frequency dependence of the observed and the calculated impedance. Then, it was suggested to remove the pickup loop and split the damping resistance, which is mounted in series with the transmitter coil, in such a way that it would include a 50 Ω resistor. The voltage drop over this resistor was brought out of the cryostat as a measure of the rf current in the transmitter coil and consequently the rf magnetic field amplitude.

Tests with Co sources

After implementing the new NMR arrangement, it was tested with new sources of $^{57}\text{CoFe}$ at 295 MHz and $^{57}\text{CoNi}$ at 123 MHz.

Thereafter, the cold beam line was connected to the cryostat. The test with $^{57}\text{CoFe}$ was repeated and our old $^{60}\text{CoFe}$ was measured. The purpose of these tests was to demonstrate the performance of the LTNO system at ISAC by reproducing previously measured parameters like the resonance frequency and especially the NMRON efficiency. For these long lived sources NMRON efficiencies varied from 50% to 70%. By increasing the rf amplitude the off-resonance anisotropy decreased but the destroyed fraction increased. This can be explained by the larger amplitude depolarizing the nuclei near the surface on-resonance as well as off-resonance. At the same time the larger rf amplitude reaches further into the sample destroying on-

resonance a larger fraction of the Co orientation. It implies that the diffusion depth of our thick samples is limited to about 1 μm , the penetration depth of the rf field at these frequencies. This was accomplished by a short diffusion time when the samples spend only approximately 5 min on the temperature trajectory $600^\circ\text{C} \rightarrow 800^\circ\text{C} \rightarrow 600^\circ\text{C}$.

Furthermore, the spin-lattice relaxation time was measured for $^{60}\text{CoFe}$ in an external magnetic field of 0.2 T, 0.8 T, and 1.4 T. For $^{57}\text{CoFe}$ it was measured in a field of 0.2 T, 0.4 T and 0.6 T. The data in the lowest field are shown in Figs. 43 and 44. This relaxation time is related to the spin dynamics, which is sensitive to the sample structure. The good agreement with values in the literature gives confidence that the quality of our sample preparation procedure is adequate.

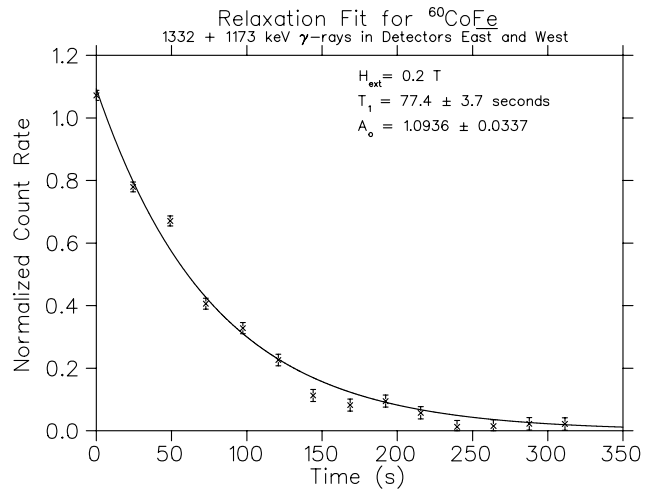


Fig. 43. Relaxation curve of $^{60}\text{CoFe}$. At time = 0 the frequency modulation of the rf field is turned off.

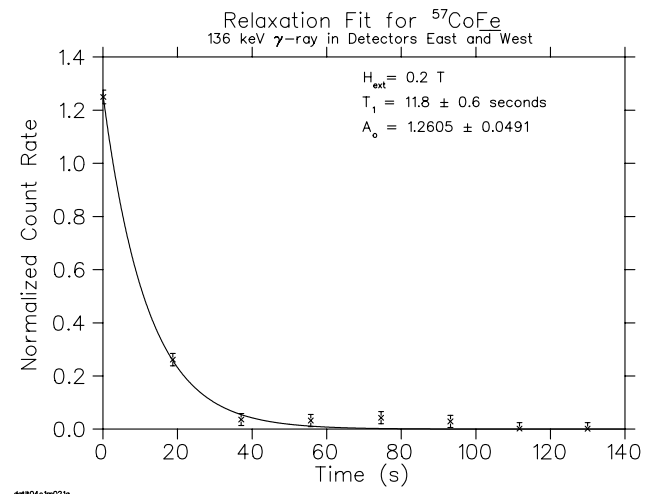


Fig. 44. Relaxation curve of $^{57}\text{CoFe}$. At time = 0 the frequency modulation of the rf field is turned off.

The experiment with $^{22}\text{NaFe}$

At this stage it was considered to explore the low mass region and provide accurate and reliable NMRON data to achieve a comparison with theoretical calculations of the hyperfine field at the same level as in the Rb-Xe region. This is appropriate at ISAC because several astrophysics experiments require beam development efforts near mass 20. In this mass region particularly for dilute oxygen in Fe there exist large discrepancies between the values of the hyperfine field from different experimental techniques. Theoretical calculations give a hyperfine field with the opposite sign, see for example the review in Severijns *et al.* [Hyp. Int. **60**, 889 (1990)]. But no NMRON measurements have been reported previously for impurities with a lower mass than manganese. To explore the feasibility in this mass region an experiment with long-lived $^{22}\text{NaFe}$ was considered. ^{22}Na , with a lifetime of 2.7 years, is available copiously at the ISAC facility and the required resources to produce a sample are fairly limited. A challenge was the rather low expected anisotropy (the nuclear magnetic moment is $+1.746(3)$ n.m.) of 1% to 2% for the 1274 keV gamma transition. Therefore, we explored with $^{57}\text{CoFe}$ whether accuracies at the 10^{-3} level could be obtained for the γ -ray peak areas during a NMRON scan. When this turned out favourably, the pilot measurement with $^{22}\text{NaFe}$ was submitted to the EEC and it received a positive judgement. Subsequently, these measurements were carried out over the summer. One of our standard Fe disks, polished and annealed as usual, was mounted in the ISAC collection station. Then this sample was cooled in the low temperature nuclear orientation set-up at ISAC to a temperature near 8 mK.

In view of the long relaxation time, 16 runs of 15 min duration were taken at each frequency leading to approximately 24 hours for a complete rf scan. At all magnetic fields a scan stepping up in frequency and a scan stepping down in frequency were taken. For each frequency in the plots frequency modulation with a range of $\pm 1/2$, the frequency step size was applied. The modulation consisted of ramping up the frequency with a sawtooth pattern at a repetition rate of 15 Hz. Resonance frequencies were determined in external magnetic fields of 0.2 T, 0.4 T, 0.6 T and 1.4 T. Scans for the lowest and highest magnetic field are plotted in Figs. 45 and 46. These graphs show that, as expected, the intensity change for the 1274 keV γ -ray has the same sign for the detectors along the external magnetic field and the detector perpendicular to the magnetic field shows a resonance amplitude with the opposite sign.

In contrast, for the 511 keV gammas, the east and west detectors, parallel and antiparallel to the magnetic field, show resonance amplitudes with opposite

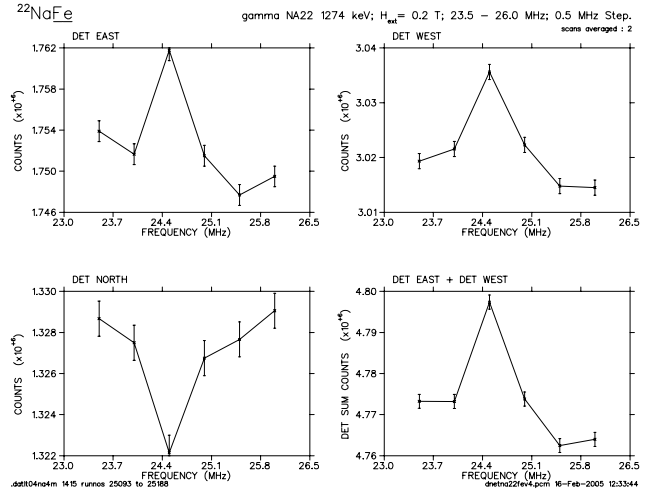


Fig. 45a. NMRON resonance in the anisotropy of the 1274 keV gamma transition with $H_{\text{ext}} = -0.2$ T.

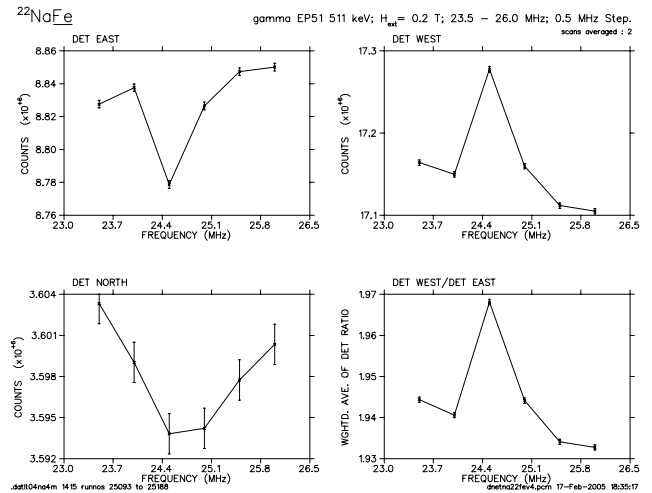


Fig. 45b. NMRON resonance in the asymmetry of the 511 keV gammas, that originate from the annihilation of positrons coming from the beta decay, with $H_{\text{ext}} = -0.2$ T.

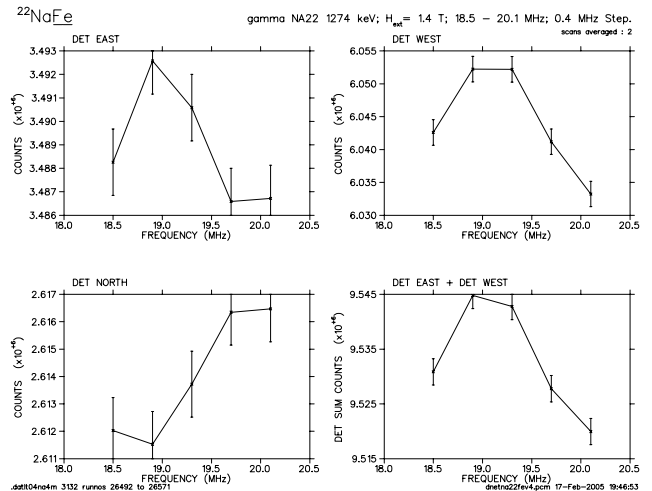


Fig. 46a. NMRON resonance in the anisotropy of the 1274 keV gamma transition with $H_{\text{ext}} = -1.4$ T.

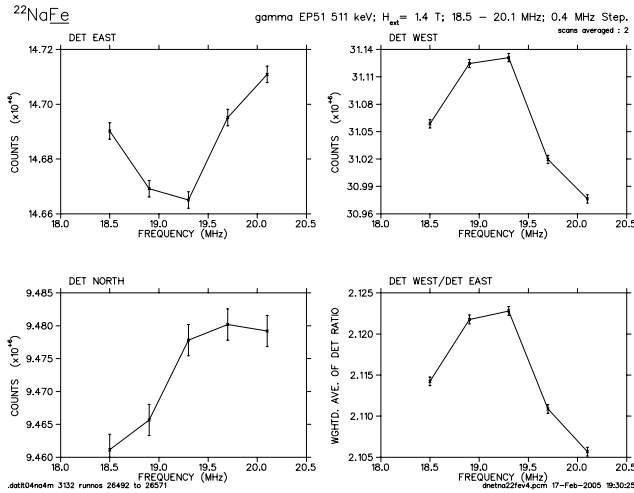


Fig. 46b. NMRON resonance in the asymmetry of the 511 keV gammas, that originate from the annihilation of positrons coming from the beta decay, with $H_{\text{ext}} = -1.4$ T.

sign. For the north detector, perpendicular to the magnetic field, the amplitude is an order of magnitude smaller. This can be understood if it is realized that the positrons, which are emitted asymmetrically from this polarized sample, meet only a substantial material mass at the cryostat wall. Therefore, the cryostat wall in front of the Ge detectors serves as a converter of positrons propagating towards a particular detector. As a consequence the rate of the 511 keV gammas reflects the positron asymmetry. To our knowledge this effect has never been applied in LTNO or NMRON experiments. A lowering of the resonance frequency versus increasing external magnetic field implies a negative sign for the hyperfine interaction. The data at 1.4 T show a negative frequency shift which also determines the negative sign for the hyperfine field. It should be noted that the width is approximately a factor 1.5 larger and the amplitude a factor 2 smaller in comparison with the resonance data at 0.2 T. These factors were considerably smaller than could be expected for this ratio of 7 in the external magnetic fields.

The direction of our external magnetic field was calibrated against the magnetic field of the TRIUMF main cyclotron. This provides, through the positron asymmetry, an independent measurement of the sign of the hyperfine interaction for NaFe .

NMRON scans were also taken without an external magnetic field applied to the sample as is shown in Fig. 47. We have observed in the past that, without an external magnetic field, the nuclear spins are confined to the plane of the Fe disk. This provides an oriented nuclear spin ensemble with a rather uncommon character. There is no axial symmetry. With this nuclear orientation it was nevertheless possible to observe an NMRON resonance. In this geometry all three

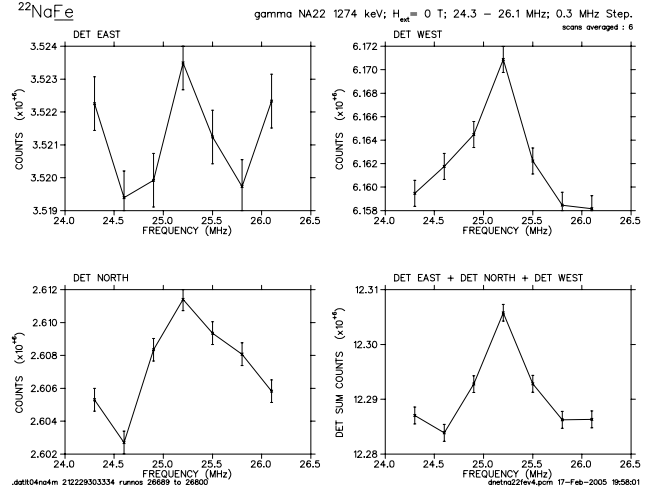


Fig. 47. NMRON resonance in the anisotropy of the 1274 keV gamma transition without an external magnetic field, $H_{\text{ext}} = 0$ T.

Ge detectors occupy equivalent positions for the angular distribution.

In this way the hyperfine field can be determined without errors from an extrapolation versus the magnetic field requiring an estimate of the external field that saturates the magnetization and also the estimate of the demagnetizing factor. Our data gave a resonance frequency of 25.200 ± 0.013 MHz. With a magnetic moment of 1.746 ± 0.003 n.m., this leads to a measured magnetic field of -5.67 ± 0.01 T where the size of the error is determined by the uncertainty in the magnetic moment. After applying the correction for the Lorentz field, which is $1/3 \times$ the saturation magnetization in Fe (which is 2.196 T) under the assumption of a spherical cavity for the impurity atom, the result is a value of 6.40 ± 0.01 T. This value is consistent with the result -5.8 ± 0.5 from a previous integral LTNO experiment with ^{24}Na [Vanderpoorten *et al.*, Hyp. Int. **75**, 331 (1992)] which had a considerably larger uncertainty. Furthermore, the relaxation time was determined in an external field of 0.2 T as shown in Fig. 48a for the gammas and Fig. 48b for the positrons. Within the errors there is no significant difference in relaxation times of the dipolar nuclear orientation component (positrons) and quadrupolar orientation component (gammas).

The experiment with $^{79}\text{RbFe}$ and $^{79}\text{KrFe}$

In the fall, NMRON was attempted with $^{79}\text{RbFe}$. The anisotropy for the intensity ratio of the 688 keV and 622 keV gamma transitions turned out a factor two smaller than we had observed previously. In this context it was not so surprising that the NMR linewidth was a factor 10 larger than expected and consequently the amplitude, by the same factor, smaller. About 30 hrs of beam time was available to get to the result shown in Fig. 49, leaving no opportunity to confirm

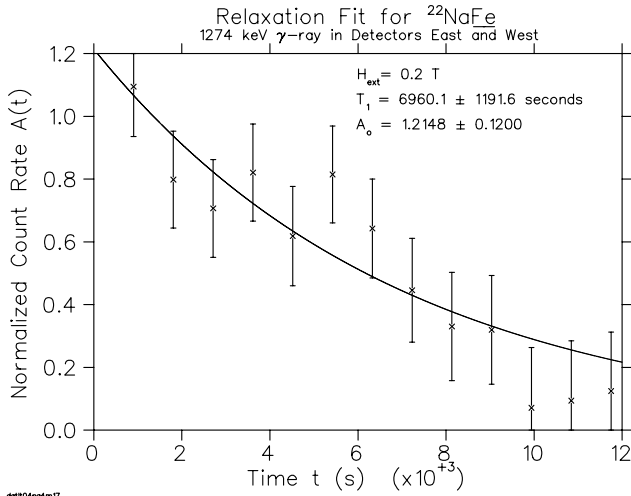


Fig. 48a. Relaxation curve from the 1274 keV transition for $^{22}\text{NaFe}$. Shown is the normalized rate, averaged for DET_{east} and DET_{west}. At time = 0 the frequency modulation of the rf field is turned off.

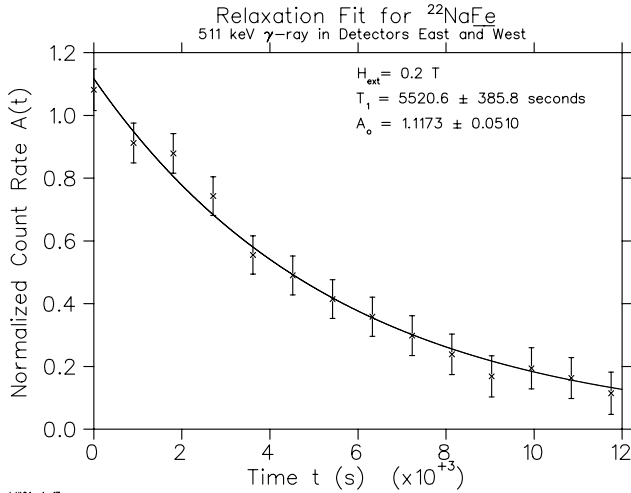


Fig. 48b. Relaxation curve from the annihilation gammas for $^{22}\text{NaFe}$. Shown is the normalized ratio of DET_{west}/DET_{east}. At time = 0 the frequency modulation of the rf field is turned off.

it with a different external field. In view of the reduced integral anisotropy (while the temperature was certainly not worse than previously) a reasonable conclusion was that the sample surface had been damaged in the last stages of the mounting procedure.

Plans were made for a procedure such that the surface could be inspected with XPS and/or auger electron spectroscopy to prevent a repeat of this occurrence.

After the ^{79}Rb had decayed, the intensity of the 511 keV gamma from the positron decay of ^{79}Kr was measured. The intensity was sufficient to observe the asymmetry on cooldown but too low to obtain NM-RON results. The results are listed in Table X for two measurements with a magnetic field of -0.2T

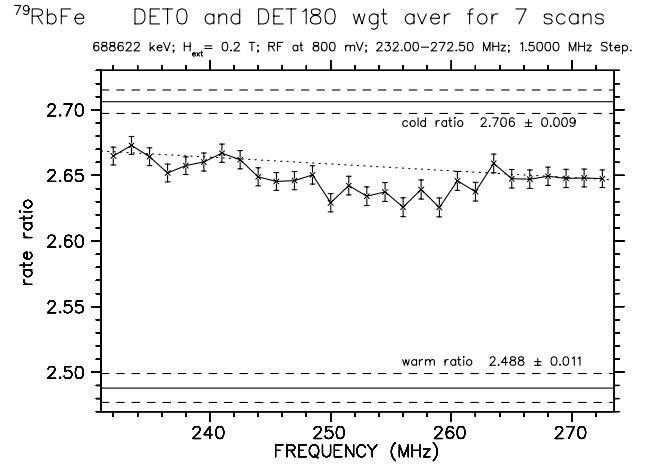


Fig. 49. The measured intensity ratio for the 688 keV and 622 keV transitions is shown versus rf frequency. The dotted line is a least squares fit to the data points at the three highest and three lowest frequencies. Also the cold and warm ratio without rf field are shown.

Table X. Change of the positron decay asymmetry on cool down of the sample for two values of the external magnetic field.

H_{ext}	Warm	Cold	Delta
-0.2T	2.548(7)	2.504(7)	+0.044(10)
$+0.8\text{T}$	3.243(14)	3.319(14)	-0.078(20)

and $+0.8\text{T}$. The first field was the same as used for the measurement on ^{22}Na that is shown in Fig. 45. Since the sign of the magnetic moment ($+1.124(10)$) is the same too, it is straightforward to derive that the sign of the hyperfine field for $^{79}\text{KrFe}$ is negative confirming the result from a previous measurement [Severijns *et al.*, Hyp. Int. **43**, 415 (1988)].

Summary

With $^{22}\text{NaFe}$ a beam implanted sample was produced that extended the mass range and frequency range for NM-RON considerably. For mass 79, a not yet convincing NM-RON result was obtained. The observation of NM-RON without an external magnetic field and the measurement of the beta asymmetry through converted positrons were methods (to our knowledge) not applied previously.

Experiment 909

Isospin symmetry breaking in superallowed Fermi β -decays

(G.F Grinyer, Guelph)

Precision measurements of the ft values for superallowed $0^+ \rightarrow 0^+$ Fermi β -decays between isobaric analogue states provide demanding tests of the standard model description of electroweak interactions. To date, superallowed ft values have been determined at the $\pm 0.1\%$ level for nine nuclei between ^{10}C and

^{54}Co . Once corrected for small radiative and isospin symmetry-breaking effects, their consistency has confirmed the conserved vector current (CVC) hypothesis at the level of 3×10^{-4} . From these studies, the Cabibbo-Kobayashi-Maskawa (CKM) matrix element, V_{ud} , can be derived by comparing the β -decay data with pure leptonic muon decay. Combining the results from superallowed Fermi beta decay studies with the present knowledge of V_{us} and V_{ub} , indicates a violation of CKM unitarity at the 98% confidence level [Towner and Hardy, Phys. Rev. **C66**, 035501 (2002)]. Although recent measurements indicate the accepted value of V_{us} may be the cause of this discrepancy, these results are still under intense scrutiny and must be confirmed by independent measurements.

Should this discrepancy be firmly established, it would indicate the need for new physics, either in terms of explicit quark effects in nuclear structure or an extension of the minimal electroweak standard model. Before a definitive conclusion can be reached, all uncertainties contributing to the unitarity test must be carefully scrutinized and, if possible, reduced. For V_{ud} , the dominant uncertainties are those associated with theoretical corrections to the ft values, and the search for systematic effects has focused on the nuclear-structure dependent δ_C corrections that account for the breaking of isospin symmetry by charge-dependent forces in the nucleus.

Experiment 909 involves a series of measurements with the 8π spectrometer and the scintillating electron positron tagging array (SCEPTAR) aimed at constraining the above-mentioned isospin symmetry-breaking corrections in superallowed Fermi β -decays. This program will take advantage of the unique beams of radioactive ions available at ISAC to study particular decays in which the predicted δ_C corrections show the greatest model sensitivity. An initial focus of Expt. 909 will be on lifetime and branching ratio measurements for ^{34}Ar , with the aim of establishing the superallowed ft value at the $\pm 0.1\%$ level. The first objective will be to improve the current half-life precision by approximately one order of magnitude. These measurements will be carried out by collecting samples of ^{34}Ar at the centre of the 8π and following their decay for ~ 30 half-lives by time-stamping γ -rays emitted from excited states in the daughter ^{34}Cl populated in Gamow-Teller decay branches of ^{34}Ar .

In anticipation of ^{34}Ar beams from the ISAC ECR ion source in spring, 2005, tests of the experimental techniques to be employed in Expt. 909 were carried out with radioactive ^{26}Na beams. This isotope was chosen because: i) high yields were available from ISAC surface ion sources, ii) the half-life (~ 1.07 s) is similar to ^{34}Ar , iii) the daughter ^{26}Mg is stable, and iv)

$\sim 99\%$ of ^{26}Na β -decays are followed by an 1809 keV γ -ray transition in ^{26}Mg , facilitating tests of the γ -ray lifetime technique to be employed for ^{34}Ar . The first requirement was to determine a precise value for the ^{26}Na lifetime. To this end, a ^{26}Na beam was delivered in 2002 to the fast tape system at the ISAC general purpose station (GPS) and its lifetime determined to high precision by the well-established β counting technique with a 4π gas proportional counter. The analysis of these data (a sample of which is shown in Fig. 50) is now complete, and the ^{26}Na half-life has been established as $T_{1/2} = 1.07128 \pm 0.00013 \pm 0.00021$ s, where the first error is statistical and the second systematic.

The second requirement for measurements of precision partial lifetimes is the beta branching ratios to the excited states in the daughter nucleus. In August, 2002, a beam of ^{26}Na at $\sim 10^5$ s $^{-1}$ was delivered to the 8π from a Ta target coupled to a surface ionization source. From the data obtained, a total of 84 γ -rays from 20 excited states in ^{26}Mg were identified (see Fig. 51) with energies between 240 keV and 7.370 MeV and intensities ranging from 0.99 to below 10^{-5} per β -decay. This extends previous work in which 20 γ -rays from 11 populated levels were identified. Combining the precision lifetime measurement from the beta counter at GPS, with the beta branching ratios from the 8π γ -ray spectrometer, and the previously known Q -value allowed a calculation of the ft values for each of 20 excited states in ^{26}Mg . These data in addition to the precision lifetime measurement are reported in a recent publication [Grinyer *et al.*, Phys. Rev. C (in press)].

In April, a beam of ^{26}Na was delivered to the 8π spectrometer to test the methodology and techniques for a γ -ray lifetime measurement of ^{26}Na which will

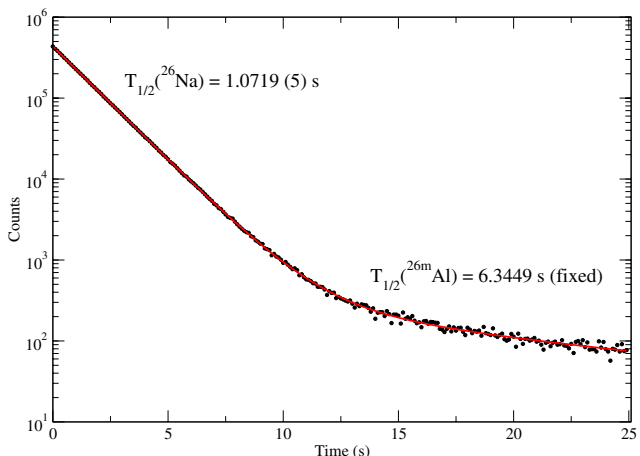


Fig. 50. Decay curve from a single run of β counting ^{26}Na samples with the 4π gas proportional counter at the ISAC GPS. The second (longer lived) decay component results from a small $^{26\text{m}}\text{Al}$ contamination of the beam. A total of 24 runs of similar precision were obtained which yielded an overall statistical precision of $\pm 0.03\%$.

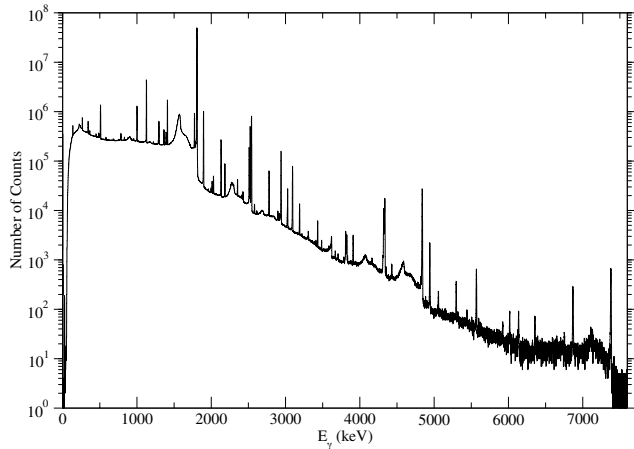


Fig. 51. γ -ray singles spectrum from ^{26}Na decay recorded with the 8π spectrometer at ISAC. In this experiment, the 8π spectrometer was sensitive to beta branching ratios of 2×10^{-5} .

later be employed for ^{34}Ar . These data are currently being analyzed for a comparison with the precise ^{26}Na half-life result determined through β counting. This comparison will provide fundamental insight into systematic effects such as detector pile-up corrections that have not allowed previous γ -ray lifetime measurements to achieve the level of precision ($\sim 0.05\%$) necessary for distinguishing between the model dependencies of the isospin symmetry breaking corrections described above.

Another key detector that will be employed for the measurements described is SCEPTAR, an array of 20 plastic scintillators which is situated at the centre of the 8π spectrometer. A commissioning run for SCEPTAR using a beam of ^{26}Na took place in June, 2003. Although SCEPTAR will not be essential in the ^{34}Ar lifetime measurement, β - γ coincidences will provide a crucial normalization necessary to perform the ^{34}Ar superallowed β branching ratio determination. In another experimental program (Expt. 985 led by M.B. Smith) which aimed to measure the lifetime and superallowed β branching ratio in ^{18}Ne , SCEPTAR provided an invaluable tool in the identification of small beam contamination components of ^{18}F and ^{17}F during a June, 2004 experiment.

Following measurement of the ^{34}Ar lifetime and branching ratio, subsequent measurements with the 8π and SCEPTAR will focus on an improved determination of these quantities in several other superallowed nuclei. Large, and model-dependent, isospin symmetry-breaking corrections are also predicted for the $A \geq 62$ odd-odd $N = Z$ nuclei. A program of precision lifetime measurements (Expts. 823 and 1028) for these nuclei with the 4π gas proportional counter at GPS is being led by G.C. Ball of TRIUMF. Future experiments with the 8π spectrometer and SCEPTAR

will provide branching ratio measurements for these short-lived isotopes. Weak non-analogue Fermi decay branches that provide direct and absolute information on one component of the isospin symmetry breaking will also be measured. The first such measurement with the 8π was performed in December with a beam of $\sim 1600 \text{ s}^{-1}$, ^{62}Ga delivered by the TRIUMF resonant ionization laser ion source (TRILIS). Several γ -ray transitions following weak Gamow-Teller and non-analogue Fermi branches were identified. These data should allow for a determination of the superallowed branching ratio at the $< 0.1\%$ level. With the continuing development of ion source technology at ISAC, these superallowed and non-analogue Fermi β -decay branching ratio studies will be extended to include $^{26\text{m}}\text{Al}$, $^{38\text{m}}\text{K}$, ^{66}As , ^{70}Br , and ^{74}Rb .

Experiment 921

High- K isomers in the neutron-rich Dy-Hf nuclei

(*R.S. Chakrawarthy, TRIUMF; P.M. Walker, Surrey*)

The detection and study of high- K isomers is an active area of current nuclear structure research. In particular, one of the goals of a future study involving neutron-rich nuclei in the Dy-Hf region is to search for the possible existence of an “island” of β -decaying high- K isomers. The close proximity of high- K states to the Fermi surface in neutron-rich $A = 170$ – 190 nuclei makes this region very attractive to search for high- K isomers [Walker and Dracoulis, *Hyp. Int.* **135**, 83 (2001)]. In two sets of experiments several of the known high- K isomers in the Dy-Hf region, with half-lives ranging from a few ms to several minutes, could be accessed [Smith *et al.*, *Nucl. Phys.* **A746**, 617 (2004)]. We report here the discovery of a new isomer in the neutron-rich nucleus ^{174}Tm . The $A = 174$ isobaric beam was implanted onto a moveable tape transport facility, with beam-on/beam-off cycling times of 2 s/2 s, 3 s/3 s (“short”), 10 s/10 s and 100 s/50 s. In the short cycling times γ -ray transitions with energies of 100.3 and 152.1 keV were observed, which are known to be present in the ground-state β -decay of ^{174}Er ($t_{1/2} = 3.3 \text{ min}$) [Becker *et al.*, *Nucl. Phys.* **A522**, 557 (1991); Chasteler *et al.*, *Z. Phys.* **A332**, 239 (1989)].

In the present experiment we found no evidence for the production of ^{174}Er . A new half-life of 2.29(1) s was deduced from γ -time matrices gated by the 100 and 152 keV γ -ray transitions (Fig. 52). A “short” time-gated singles spectrum, obtained by subtracting out the long-lived β decays, shows prominently only the Tm K X-rays and the 100 and 152 keV γ -ray transitions (Fig. 53). Based on the singles and the coincidence data, a new isomer in ^{174}Tm with a half-life

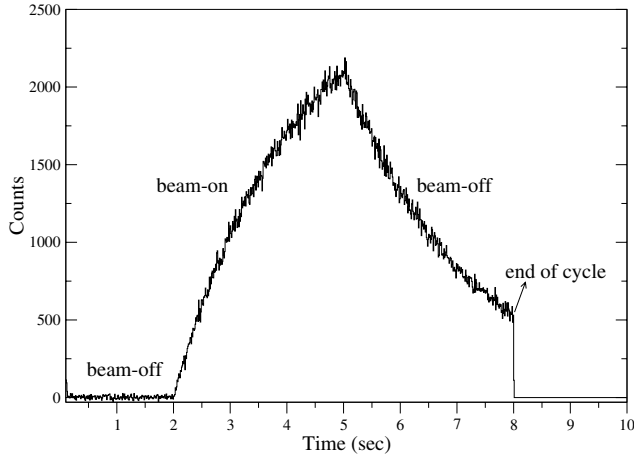


Fig. 52. Time spectrum gated by the 100.3 keV γ -ray transition. The beam-off/beam-on/beam-off tape-cycling times correspond to 2 s–3 s–3 s.

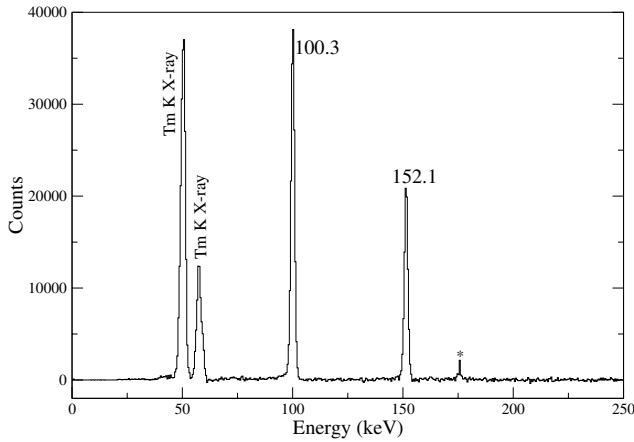


Fig. 53. Singles spectrum in the “short” cycling time of 2 s–3 s–3 s corresponding to the beam-off/beam-on/beam-off periods. The dominant component due to the longer lived ^{174}Tm β -decay ($T_{1/2} = 5.4$ min) has been subtracted. The peak marked by the asterisk is a remnant of the subtraction procedure.

of 2.29(1) s is established unambiguously. From the coincidence data the K -conversion coefficients for the 100 and 152 keV γ -ray transitions were deduced to be 3.1(1) and 1.13(6) respectively, suggesting mainly M1 multipolarity with an E2 admixture. The new data are in close agreement with the theoretically expected values of 2.69 and 0.82 for M1 multipolarity, respectively, but differ from the values 1.7(3) and 0.54(6), respectively, reported by Becker *et al.* [Nucl. Phys. **A522**, 557 (1991)].

A careful analysis of the singles spectrum (Fig. 53) did not yield any new γ -ray transitions that could be candidate γ -ray transitions between the isomer and the known states. These data suggest the possibility of the existence of very low-energy and highly-converted transitions in the decay of the isomer and the excited states. Furthermore, if the origin of isomerism is presumed

to be partly due to K -hindrance (in line with several known examples in this mass region) then this level could possibly have a high K value. Based on systematics and Nilsson model calculations of the single-particle levels in ^{174}Tm , the isomer is tentatively assigned to have a $K^\pi = (8^-)\pi 7/2^- [523] \otimes \nu 9/2^+ [624]$ Nilsson configuration, while the other excited states may be based on $K^\pi = ((4/5)^+)\pi 1/2^+ [411] \otimes \nu 9/2^+ [624]$ configurations. The levels involved in the isomer decay may have spins greater than the low values suggested from the previous works. The present interpretation would be consistent with the earlier data only if the decay through the 100 and 152 keV transitions originates from a high-spin β -decaying isomer in ^{174}Er instead of the ground-state β -decay of ^{174}Er . The preceding results have been reported at the ENAM04 conference [Chakrawarthy *et al.*, Proc. ENAM04, Pine Mountain, USA (Eur. Phys. J. A, in press)]. Preparations for an experiment to detect the low energy/highly-converted transitions, using a Si detector-array, are in progress.

Experiment 921 is a collaboration of scientists from TRIUMF, University of Surrey, Colorado School of Mines, Lawrence Livermore National Laboratory, Louisiana State University, McMaster University, Saint Mary’s University and University of Guelph.

Experiment 956

Search for tensor interactions in recoil nucleus singles in decay of polarized ^{80}Rb

(J.A. Behr, M.R. Pearson, TRIUMF; K.P. Jackson, TRIUMF/SFU)

Scientific motivation

The recoiling daughter nuclei from the β decay of polarized nuclei have spin asymmetry $A_{\text{recoil}} \approx 5/8 (A_\beta + B_\nu)$ [Treiman, Phys. Rev. **110**, 448 (1958)], in the limit $Q_\beta \gg m_\beta$. This vanishes in the allowed approximation for pure Gamow-Teller decays, making it a very attractive experimental observable because knowledge of the nuclear polarization at 1 to 10% level is sufficient to be competitive. Our novel capability of measuring the recoil nuclei from laser-polarized cold atoms allows this observable to be measured now.

Right-handed currents do not contribute, so A_{recoil} is uniquely sensitive to lepton-nucleon tensor interactions. A renormalizable interaction that Lorentz transforms like a tensor can be generated by the exchange of spin-0 leptoquarks [Herczeg, Prog. in Part. and Nucl. Phys. **46/2**, 413 (2001)].

“Recoil-order” corrections beyond the allowed approximation do produce a nonzero A_{recoil} within the standard model. These produce corrections to the β asymmetry A_β for ^{80}Rb of order 0.01, and we expect similar effects on A_{recoil} , so the result will depend on

calculation of the nuclear structure-dependent weak magnetism and first-class induced tensor terms (b and d in Holstein's notation). Our knowledge of these could be tested by measuring the momentum dependence of the recoil asymmetry. We are negotiating for theory support.

The PIBETA collaboration has reported hints of a finite tensor interaction [Frlež, Phys. Rev. Lett. **93**, 181804 (2004)] in $\pi \rightarrow \nu e \gamma$ decay, though at a level considerably smaller than that reported at Dubna [Bolotov *et al.*, Phys. Lett. **B243**, 308 (1991)]. Experiment 956 would become competitive with other nuclear β -decay measurements if it achieves 0.01 accuracy in the recoil asymmetry [Herczeg, Phys. Rev. **D49**, 247 (1994)], while ~ 0.001 level is needed to reach similar sensitivity to the tensor interaction indicated by the π decay experiments. Since the recoil asymmetry vanishes, the degree and knowledge of polarization achieved in Expt. 715 is already sufficient for Expt. 956.

“Resolution” of nucleon form factor question

To interpret β decay results in terms of quark-lepton interactions, the form factor $g_T(0)$ defined by: $\langle p | \bar{u} \sigma_{\mu\lambda} d | n \rangle = g_T(q^2) \bar{u}_p \sigma_{\mu\lambda} u_n$ is needed, and there has been controversy over this quantity [Herczeg, *op. cit.*]. This situation is now in good shape both theoretically and experimentally, because the quantity is related by simple isospin rotation to the “transverse spin” function of the nucleon. This is the last of the nucleon spin functions to be measured, is a source of intense theoretical and experimental (at HERMES) effort, and should be known at the 20% level or better soon [Pospelov, private communication]. This would be more than good enough to allow comparison of a nonzero tensor in nuclear β decay to π decay.

Experiment

In the Expt. 956 apparatus (Fig. 54) the TRINAT β telescope is replaced with a 7.5×7.5 cm NaI(Tl) detector. An electric field collects much of the angular distribution from charged recoils into a microchannel plate (MCP). The NaI detector tests the experimental practicality of γ -recoil coincidences. It also serves as a β detector for polarization diagnostics, since β -recoil coincidences in this geometry are proportional to the neutrino asymmetry B_ν . The NaI detects 617 keV γ s from the 22% β branch to the first excited 2^+ state of ^{80}Rb . The intent is to measure the “singles” asymmetry for decays to the 2^+ state separately via the γ -ray coincidence. The angular distribution of γ 's with respect to the spin direction is given by $W(\theta_\gamma) = 1 - 0.25 P_2(\cos\theta)$, so there is no recoil asymmetry induced. That allows measurement of a correction to the total asymmetry to deduce the singles asymmetry for the $1^+ \rightarrow 0^+$ transition, which has

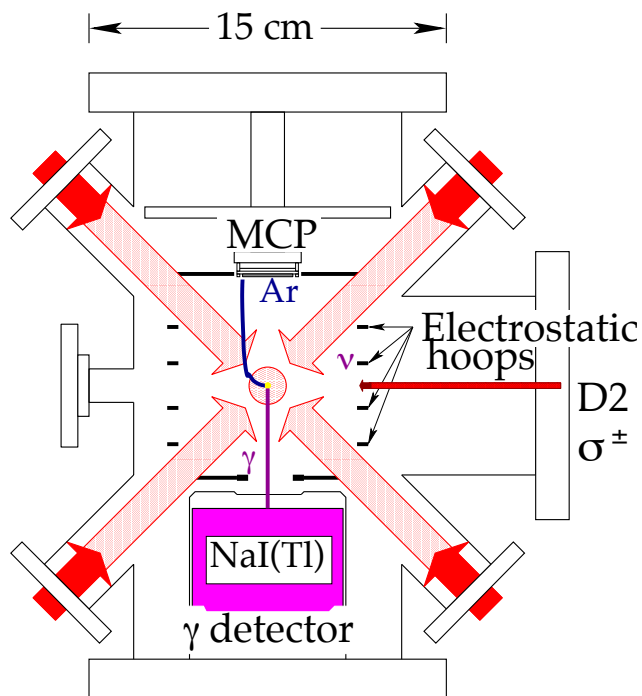


Fig. 54. TRINAT apparatus as modified for Expt. 956. A NaI(Tl) detector for γ -rays replaces the main β^+ telescope. D2 light is used to optically pump ^{80}Rb .

only two recoil-order form factors (b , weak magnetism, and d , induced first-class tensor). That simplifies the nuclear structure corrections needed.

The recoil order effects are expected to enter at ~ 0.01 level. To reach 0.001 level it will be necessary to measure the momentum-dependence of the recoil asymmetry. This could be done by detecting atomic shakeoff electrons in coincidence with recoils to provide a bias-free TOF trigger.

Another possibility would be a measurement of ^{47}K decay, a much better case for recoil- γ experiments. The β^- decay always produces a measureable charged recoil, increasing count rates and recoil/ β ratios by $6\times$ over β^+ decay. The 81% $\frac{1}{2}^+ \rightarrow \frac{1}{2}^+$ transition will also only have two form factors, and always produces a γ . A complication will be isospin mixing of this final state with the analogue state, which would produce a nonzero Fermi matrix element and a nonzero A_{recoil} that is constant with recoil momentum. The plan would be to measure both isospin mixing – an interesting observable in its own right – and tensor interaction effects.

Data-taking An ^{80}Rb beam of $6 \times 10^7/\text{s}$ from a Ta target was delivered for several days, enough to make a large start towards the first goal of 0.01 in the integrated singles measurement. This was a thin target optimized for ^{11}Li production. Yields adequate for the final experiment have been produced by 20 μA on 44 g/cm^2 Ta ($2 \times 10^9/\text{s}$) and 40 μA on 22 g/cm^2 Nb

($3 \times 10^{10}/\text{s}$) in the past, and unpolarized tests were handled by TRINAT data acquisition in 1999 at one hundred times the present count rate. It is also possible to do an experiment in ^{82}Rb , which has similar Gamow-Teller decay branches and ten times greater yields, although the 1.26 minute half-life and the existence of a 6.5 hour isomer will make backgrounds larger.

Nuclear and atomic level diagrams are shown in Fig. 55. The β decay scheme is a relatively simple Gamow-Teller decay. The atom structure has narrow hyperfine splitting, and we trapped it with one 899-21 ring laser. We also use transitions at similar wavelength for the optical pumping.

Our usual atomic physics probe of the polarization is to optically pump with circularly polarized light to the $P_{1/2}$ state. The fluorescence will vanish once the atoms are fully polarized, because the total angular momentum of the initial and final states is the same and the atom no longer absorbs photons. We do not have a 795 nm D1 laser for rb, so for ^{80}Rb we use the $P_{3/2}$ state with the light tuned on resonance for $F = 3/2$ to $F' = 3/2$. Since we pump at about 5 times saturation intensity, there will always be 10–20% of the initial fluorescence by off-resonant excitation of the $F = 3/2$ to $F' = 5/2$ transition.

Signals in nuclear detectors We show in Fig. 56 a NaI spectrum in coincidence with the Kr^{+1} recoils. The low-energy bremsstrahlung tail is reasonably well-correlated with the β^+ direction, providing some on-line diagnostics for polarization with reasonable statistics; however, this will require a full Monte Carlo GEANT simulation to quantify. The 617 keV gamma can be seen as a shoulder on the 511 keV gamma; coincidences with the MCP would let us measure the recoil asymmetry as a function of momentum.

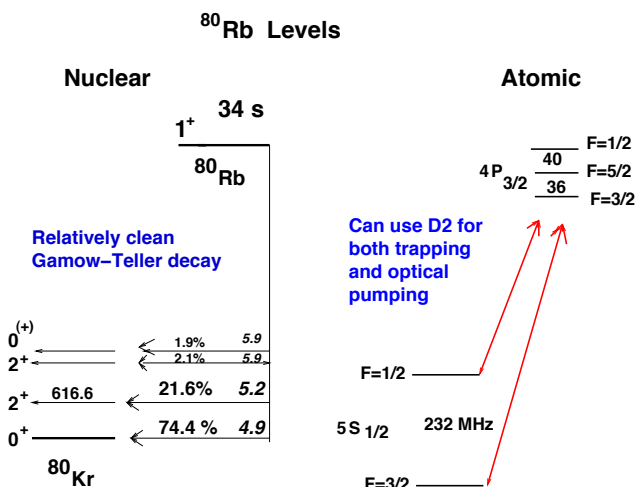


Fig. 55. ^{80}Rb nuclear and atomic level schemes.

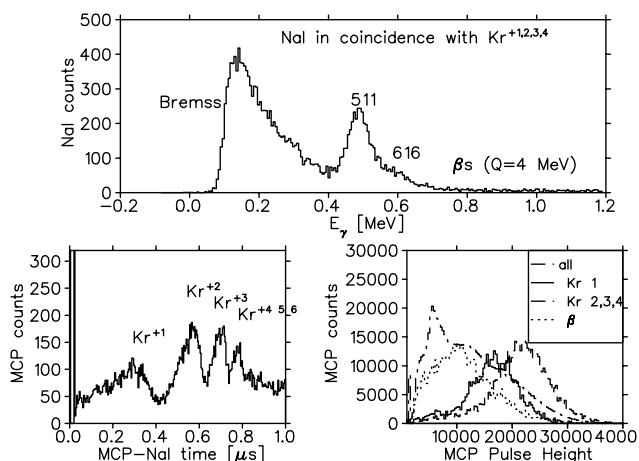


Fig. 56. NaI energy spectrum, time-of-flight spectrum from NaI-MCP coincidences, and singles pulse height spectrum in the MCP for various types of events. See text.

Also shown is a typical TOF spectrum of the recoils in coincidence with all MCP events. The various ion charge states produced in the β^+ decay are separated by the electric field. The third part of the figure shows the MCP pulse heights for the various types of events, as determined with the NaI coincidences. High pulse heights are dominated by Kr ion recoils, so a cut on pulse heights can suppress backgrounds from β s and γ s.

Polarization and trap motion systematic Our analysis of ^{37}K data was made very difficult by this effect. In Expt. 715, we switched off the MOT quadrupole coils as well as the trap laser light, with 2 ms off/on duty cycle. We optically pumped during the cloud expansion to polarize the atoms. The atom cloud expands from 2 to 4 mm FWHM in this time. We can measure this in all 3 dimensions by photoionizing a small fraction of the atoms with a pulsed 355 nm laser and measuring their position and TOF information with the MCP. The analysis is complicated by the small number of trapped atoms, and a systematic error is introduced.

For Expt. 956 such a systematic error would go directly into the asymmetry and not be suppressed by the vanishing observable. So we chose to minimize it by switching the MOT off for 20 μs , which does not allow the atoms to expand. We must leave the MOT 10 G/cm quadrupole field on to do this, and optically pump in the presence of this field. We have achieved 80% polarization in ^{37}K in the past by this method, which would be adequate for the vanishing observable in Expt. 956.

We successfully measured the trap motion systematic. The trap shifted by 0.51 ± 0.02 mm between σ^+ and σ^- optical pumping light. This produces a false $\Delta A_{\text{recoil}} = 0.0100 \pm 0.0004$.

The polarization achieved, however, was only 0.55 ± 0.11 , as measured by asymmetries of β -MCP coincidences using the NaI and the additional CaF detectors. The earlier ^{37}K 80% polarization was achieved in the horizontal plane of the MOT quadrupole field, so displacing the atoms horizontally by unbalancing the MOT beams produces a local B field that points toward the origin. The mistake we made was to optically pump instead along the 30° axis determined by the CaF detectors. In the future we will either pump horizontally (sacrificing accuracy in the CaF detector asymmetries, which are not essential to Expt. 956) or we can optically pump with the MOT off as in Expt. 715.

Data were taken that would determine A_{recoil} to 0.01 statistical error. Analysis is proceeding to quantify systematic errors from the background in the MCP, as well as a subtle effect caused by saturation of the position-determining resistive anode data.

Future In December we received EEC approval for shifts to complete data-taking for this experiment. This experiment constitutes the main component of the M.Sc. for students R. Pitcairn and D. Roberge, UBC.

Experiment 964

TACTIC – TRIUMF annular chamber for tracking and identification of charged particles
(*G. Ruprecht for the TACTIC collaboration*)

TACTIC is a cylindrical ionization chamber for the detection of ejectiles from nuclear reactions. It allows the three-dimensional reconstruction of particle tracks by means of a two-dimensional anode array combined with a time-of-flight measurement of the drift electrons. For more details see the TACTIC Web site: <http://tactic.triumf.ca>.

One key element of TACTIC is a gas electron multiplier (GEM) foil [Sauli and Sharma, *Ann. Rev. Nucl. Part. Sc.* **49**, 341 (1999); Sharma and Sauli, *Nucl. Instrum. Methods* **A350**, 470 (1994)] which acts as a preamplifier inside the chamber and therefore provides low-noise signals requiring only one further stage of amplification. In order to determine the operational parameters of this relatively new device a planar test chamber including a 5 MeV α particle source has been assembled. Different gas mixtures have been applied and the signals were measured with the results shown in Fig. 57. It was found that a 90% helium–10% CO_2 gas mixture (as required in the $^8\text{Li}(\alpha, n)^{11}\text{B}$ experiment, see below) is very well suited to achieve a high gain.

The test chamber has a drift volume of about $20 \times 20 \times 2 \text{ cm}^3$ and an active GEM area of $8 \times 8 \text{ cm}^2$, covering 16 active anode strips with 5 mm width each.

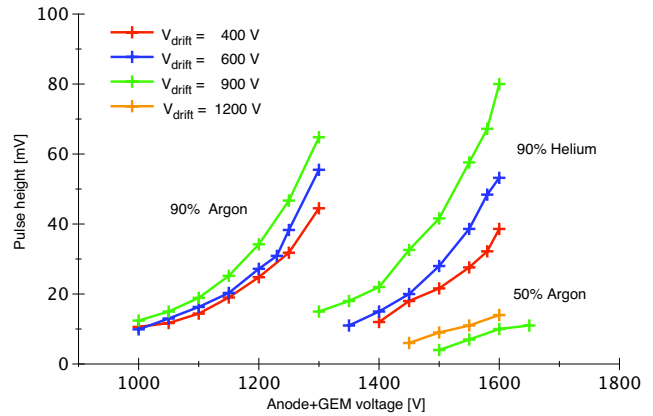


Fig. 57. Pulse heights vs. GEM+anode voltage. The GEM voltage is a factor of 3.3 smaller.

Measuring the time differences between the signals on 4 consecutive strips, we have been able to gain a projected image of the particle tracks, as can be seen in Fig. 58. The source was 5 cm before the first strip but due to a missing trigger the tracks are normalized to the first strip.

In a second phase a gas handling system has been set up. This allows a continuous regulation of the pressure down to 100 mbar while keeping the He- CO_2 mixture at a constant ratio (below 100 mbar the oxygen contamination becomes too high and quenches the signals) and the flow rate at $200 \text{ cm}^3/\text{min}$. This enabled the dependence of the GEM gain on the pressure and the applied GEM voltage to be determined.

The geometry for the planar as well as for the cylindrical chamber has been entered in the particle simulation program GEANT4 which allows a better separation of geometrical side effects from the actual physics. The simulated spectra are in good agreement with the test chamber measurements. Particle track simulation

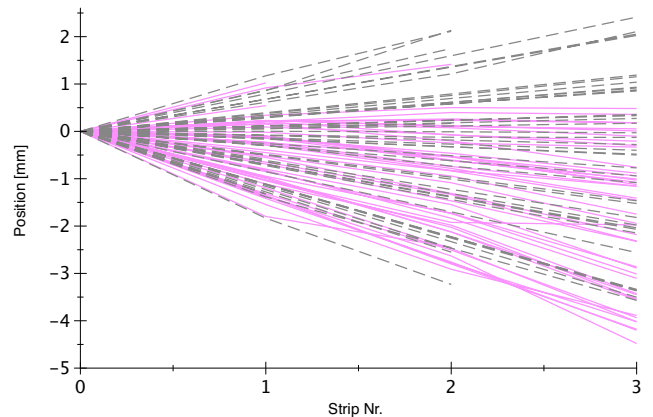


Fig. 58. Electron drift times w.r.t. the first strip, converted to distances assuming a drift velocity of $12 \text{ mm}/\mu\text{s}$. The electrons are released along the tracks of the α 's. The dashed lines stem from a GEANT4 simulation, the solid, purple lines from the measurement.

for the cylindrical chamber is and will be an indispensable tool for the design of the prototype chamber. The process will involve modifying the low energy stopping algorithm of GEANT4 to give accurate ranges for heavy ions, an effort which will result in a contribution to GEANT4 development.

For a precise calculation of the electrical drift field and fringe effects of the chamber end-caps, we are using the FEMLAB code which can model the field of the chamber in 3 dimensions. A two dimensional code, GARFIELD, has been used to model the field in the target region to investigate the beam ionization problem; electrons produced in the target region can drift into the tracking region of the chamber. It was found that a cylindrical ring of guard wires at slightly higher potential than the cathode wires would eliminate the unwanted electrons.

For the data acquisition we will use a 48 channel flash-ADC VME board. The pulses will be sampled with a rate of 10–100 MHz and the required time and charge information will be extracted in real time by a user-defined algorithm in the on-board firmware. For the collection, storage, and on-line analysis of the data we will use the TRIUMF DAQ packages, MIDAS and ROME (see <http://midas.triumf.ca>).

TACTIC is useful in particular for experiments with gas targets and low-energy ejectiles that cannot penetrate a gas cell window, or for experiments with a high number of background particles that cannot be separated by conventional methods. The first planned experiment is the measurement of the ${}^8\text{Li}(\alpha, n){}^{11}\text{B}$ reaction. Since helium can be used very well as a detector gas in combination with a GEM, no separation foil between target and detection region is necessary and the low-energy ${}^{11}\text{B}$ recoils can easily pass out of the target through the cathode wires and into the drift region to be tracked.

Other planned experiments are to measure the proton elastic scattering length on ${}^7\text{Be}$ which can be used to pin down the $S_{17}(0)$ value of the ${}^7\text{Be}(p, \gamma){}^8\text{B}$ reaction, and to measure the cross section of ${}^{12}\text{C}+{}^{12}\text{C}$ fusion reactions which play an important role in many stellar environments.

The TACTIC collaboration: P. Amaudruz, L. Buchmann, D. Gigliotti, T. Kirchner, R. Openshaw, M. Pavan, J. Pearson, G. Ruprecht, P. Walden (TRIUMF), S. Fox, B. Fulton, A. Laird (University of York, UK).

Experiment 968

Ortho-para effect of muon catalyzed fusion in liquid deuterium

(H. Imao, N. Kawamura, K. Nagamine, KEK)

The ortho-para state of the hydrogen isotope affects resonant molecular formation in muon catalyzed fusion (μCF). Controlling the ortho-para composition is a key technique to enhancing the cycling rate of μCF . In addition, μCF experiments with ortho-para controlled deuterium provide helpful information in order to understand muonic-atomic and muonic-molecular processes. The aim of the present work is to comprehensively understand the nature of condensed-matter effects and ortho-para dependent phenomena on μCF in pure deuterium ($dd\text{-}\mu\text{CF}$). In $dd\text{-}\mu\text{CF}$, there have been some unsolved problems concerning the condensed-matter effects. An understanding of the unexpectedly high resonant molecular formation rates for solids, observed in several experiments, has not yet been achieved. Also, the ortho-para effect for solids observed by Toyoda *et al.* [Phys. Rev. Lett. **90**, 243401 (2003)] has not yet been explained by the recent theory [Adamczak and Faifman, Phys. Rev. **A64**, 052705 (2001)]. To understand these unexpected μCF phenomena in the solid phase, experiments with liquid deuterium are a key because the μCF phenomena can be observed without specific solid-state effects. We observed the dependence of $dd\text{-}\mu\text{CF}$ phenomena on the ortho-para composition in solid, liquid and gaseous deuterium.

The main observable quantity in our experiment was a fusion neutron emitted from the $d-d$ fusion reaction, which has a monochromatic energy of 2.5 MeV. Our experiments were performed at M9B using a backward decay 52 MeV/ c μ^- beam. A schematic of our experimental set-up is shown in Fig. 59. To detect 2.5 MeV fusion neutrons, four NE-213 liquid scintillators (N1–N4) were placed perpendicular to the incoming μ^- beam axis. NE-213 was chosen for its pulse shape discrimination properties. Muon-decay electrons were also detected by four pairs of plastic scintillators (E1–E8) placed around the target. The time spectra

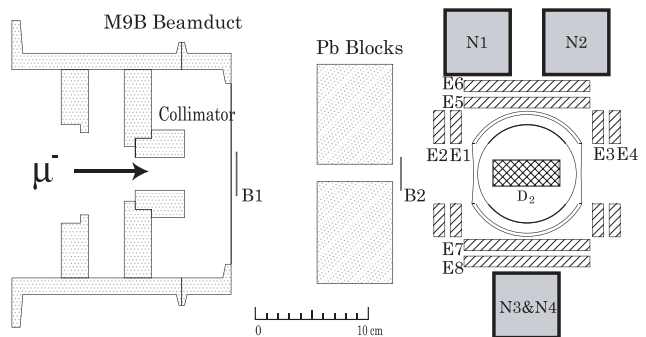


Fig. 59. Experimental set-up for solid and liquid deuterium.

of muon-decay electrons provided information about the distribution of muons stopping around the target. In addition, the number of electrons from the target was used to normalize the muon stopping number. The preparation of ortho-para controlled targets and the measurements of the ortho-para composition were essential procedures. The ortho-rich deuterium was prepared by employing a paramagnetic conversion method. In order to determine the ortho-para composition of deuterium, a rotational Raman spectroscopy method was employed for the first time in μ CF. The compact Raman laser system was installed near the experimental area for *in situ* measurements. In the present study, both ortho targets and normal targets were successfully produced.

Table XI provides our results for the $dd\mu$ resonant molecular formation rate $\tilde{\lambda}_{\frac{3}{2}}$, the $d\mu$ hyperfine transition rate, $\tilde{\lambda}_{\frac{3}{2}\frac{1}{2}}$, and the non-resonant molecular formation rate, $\tilde{\lambda}_{\frac{1}{2}}$, for normal and ortho deuterium in solid and liquid phases. The decrease in the resonant molecular formation rates and in the hyperfine transition rates with ortho-rich deuterium has been observed in these phases. On the other hand, the non-resonant molecular formation rate is independent of the ortho-para state of deuterium within experimental errors. The ortho-para effect on the rates for $\tilde{\lambda}_{\frac{3}{2}}$ and $\tilde{\lambda}_{\frac{3}{2}\frac{1}{2}}$ in the solid phase is qualitatively consistent with that in Toyoda's experiment. It is worth noting that the decrease in ortho was observed even in the liquid phase, although the better resonant condition for the molecular formation process in ortho deuterium was predicted by the theory for gas. Our lower resonant molecular formation rate in liquid ortho deuterium cannot be described only by the non-thermalization effect of

Table XI. Results of the ortho-para effect on the resonant molecular formation rate, $\tilde{\lambda}_{\frac{3}{2}}$, the hyperfine transition rate, $\tilde{\lambda}_{\frac{3}{2}\frac{1}{2}}$, and the non-resonant molecular formation rate, $\tilde{\lambda}_{\frac{1}{2}}$.

T (K)	O (%)	$\tilde{\lambda}_{\frac{3}{2}}$ (μs^{-1})	$\tilde{\lambda}_{\frac{3}{2}\frac{1}{2}}$ (μs^{-1})	$\tilde{\lambda}_{\frac{1}{2}}$ (μs^{-1})
5.5	67 (2)	2.35(5)	31.6(4)	0.044(fix)
	99 (1)	1.98(5)	28.3(4)	0.043(2)
11.7	67 (2)	2.61(9)	32.0(8)	0.040(3)
	99 (1)	2.15(8)	30.1(8)	0.041(3)
18.2	67 (2)	2.46(5)	33.2(4)	0.043(2)
	99 (1)	2.11(5)	30.8(4)	0.045(2)
18.8	67 (2)	2.70(6)	32.4(4)	0.044(2)
	99 (1)	2.32(5)	30.2(4)	0.045(2)
21.2	67 (2)	2.91(8)	33.0(6)	0.048(3)
	99 (1)	2.34(7)	29.1(6)	0.046(3)
23.2	67 (2)	2.86(6)	32.6(4)	0.047(2)
	99 (1)	2.38(5)	29.8(4)	0.048(2)

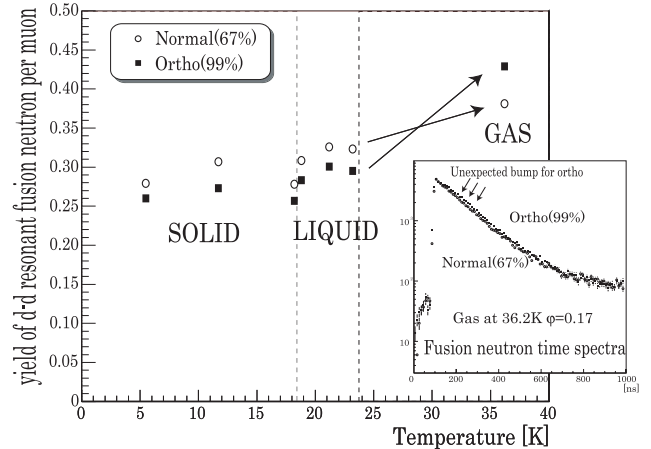


Fig. 60. The temperature dependence of the yield of fusion neutrons via resonant molecular formation.

$d\mu$ in normal deuterium, because the experimental rates in liquid deuterium are not higher than those of the conventional theory which assumes the rapid thermalization of $d\mu$. While in the gaseous phase, the yield of the resonant fusion neutron from an ortho-rich target is significantly enhanced (Fig. 60). The ortho-para effect without condensed matter effects was observed in the gas phase. However, the neutron time spectra with gaseous ortho targets were quite strange. The unexpected bump structure was found only in neutron time spectra with gaseous ortho deuterium. The cause of this structure is not yet determined. A detailed analysis is in progress. Our experimental results will provide a breakthrough in the understanding of condensed-matter effects in $dd\text{-}\mu\text{CF}$.

Experiment 973

Study of coexisting collective phases far from stability: systematic decay spectroscopy of the $N = 90$ isotones

(W.D. Kulp, J.L. Wood, Georgia Tech.)

The structure of nuclei far from stability is primarily addressed using the shell model, the pairing model, and collective models. Collective models such as the model of Bohr and Mottelson [*Nuclear Structure Vol. II* (World Scientific, Singapore, 1998)], the dynamic pairing plus quadrupole model [Kumar, Nucl. Phys. **A231**, 189 (1974)], and the interacting boson model [Arima and Iachello, Phys. Rev. Lett. **35**, 1069 (1975)] have been explored extensively, but all of these models rely on parameters determined systematically from data on nuclei near stability. Further from stability, the collective structure of nuclei will be more difficult to understand as the systematic trends become less clear.

It is the goal of this experiment to map the evolution of structural trends, not only to recognize nuclear structure far from stability, but also to provide data constraining the collective models near stabil-

ity and help to discriminate between models. One of the richest regions for comparing collective models is found at $N = 90$, where the shape of the nucleus changes from nearly spherical to well deformed very abruptly as the neutron number increases from $N = 88$ to $N = 92$. In the $N = 90$ transitional region, this investigation targets the doubly-even isotones, ^{146}Ba , ^{148}Ce , ^{150}Nd , ^{152}Sm , ^{154}Gd , ^{156}Dy , ^{158}Er , and ^{160}Yb for detailed $\gamma - \gamma$, $\gamma - e^-$, and $e^- - e^-$ coincidence spectroscopy using the 8π γ -ray spectrometer and the PACES conversion-electron detector array.

A study of the β decay of ^{156}Ho to ^{156}Dy was the first stage in Expt. 973 and was the first pairing of the 8π spectrometer with the PACES array. The focus of this run was to identify excited states in ^{156}Dy populated in the decay of three isomers ^{156g}Ho ($J^\pi = 4$, $T_{1/2} = 56$ m), $^{156m_1}\text{Ho}$ ($J^\pi = 1$, $T_{1/2} = 9.5$ s), and $^{156m_2}\text{Ho}$ ($J^\pi = 9^+$, $T_{1/2} = 7.8$ m). Nearly 750 Gb of γ -ray and conversion-electron data were recorded in an 11 day experiment. The ^{156}Ho beam was extracted from a tantalum target and implanted onto a moving

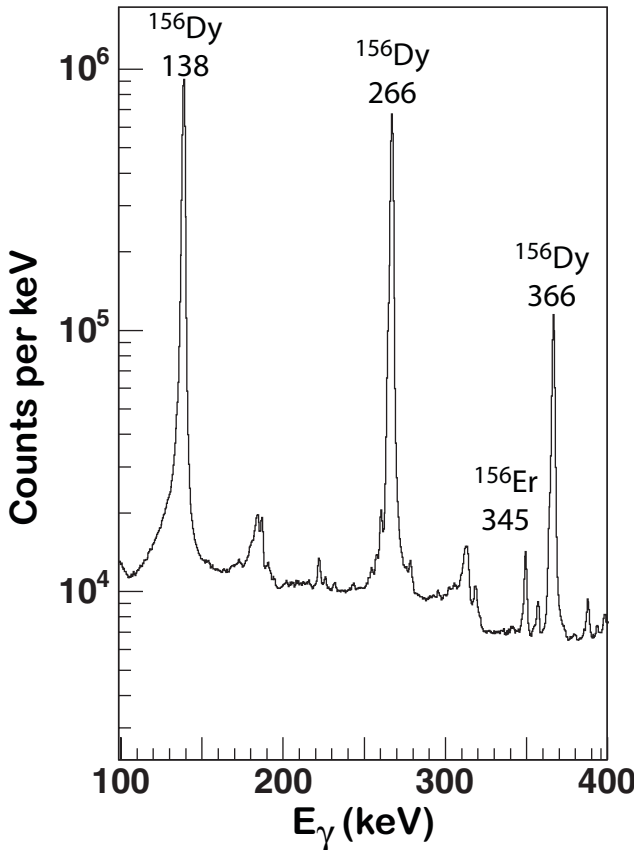


Fig. 61. γ -ray spectra from the 115 minute tape cycle reveal transitions in the ground-state band of ^{156}Dy : 138 keV ($2^+ \rightarrow 0^+$), 266 keV ($4^+ \rightarrow 2^+$), and 366 keV ($6^+ \rightarrow 4^+$) consistent with the decay of the ^{156g}Ho ($J^\pi = 4$, $T_{1/2} = 56$ m) isomer. Additional labelled transitions are associated with decays from other $A = 156$ nuclides.

tape at the centre of the 8π spectrometer. Tape move cycles of 115 minutes, 10 minutes, and 10 seconds were used to focus on the decay of the ^{156g}Ho , $^{156m_2}\text{Ho}$, and $^{156m_1}\text{Ho}$ isomers, respectively.

Preliminary spectra reveal γ -ray and conversion-electron transitions in ^{156}Dy associated with the decays of ^{156g}Ho and $^{156m_2}\text{Ho}$. Data from the 115 minute tape cycles clearly show the 138 keV ($2^+ \rightarrow 0^+$), 266 keV ($4^+ \rightarrow 2^+$), and 366 keV ($6^+ \rightarrow 4^+$) γ -ray transitions associated with the decay of ^{156g}Ho (as illustrated in Fig. 61). A spectrum from the 10 minute tape cycle (Fig. 62) shows enhanced $^{156m_2}\text{Ho}$ decay transitions, including the 445 keV ($8^+ \rightarrow 6^+$) γ -ray. However, other contaminating lines from other short-lived activities in the $A = 156$ chain complicate the spectrum shown in Fig. 62 and elucidation of the full decay scheme requires detailed coincidence spectroscopy.

Of particular interest in this study is the placement of weak, low-energy transitions for identification of band structures and the measurement of $E0$ transitions for interpretation of the nature of the bands. The 675 keV $E0$ transition from the first excited 0^+ to the 0^+ ground state, shown in Fig. 63, is observed in the decay of ^{156g}Ho . Thus far only an internal transition from the $^{156m_1}\text{Ho}$ isomer is observed with the strong decays from short-lived isobars (cf. Fig. 64), but weak decay branches may be found in further analysis with the fine tuning of timing and coincidence gates on $\gamma - \gamma$, $\gamma - e^-$, and $e^- - e^-$ coincidence events. It will be such

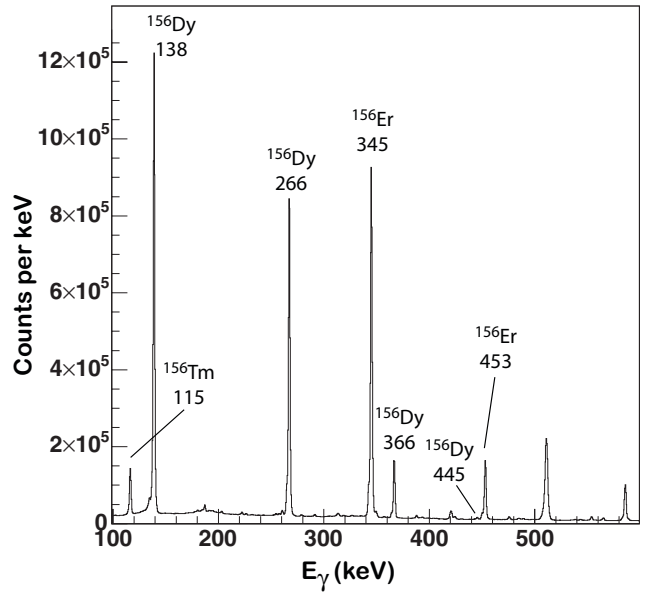


Fig. 62. The 138 keV ($2^+ \rightarrow 0^+$), 266 keV ($4^+ \rightarrow 2^+$), 366 keV ($6^+ \rightarrow 4^+$) and 445 keV ($8^+ \rightarrow 6^+$) γ -ray transitions in ^{156}Dy are highlighted using a 10 minute tape cycle, indicating the presence of the high-spin isomer $^{156m_2}\text{Ho}$ ($J^\pi = 9^+$, $T_{1/2} = 7.8$ m). Additional labelled transitions are associated with decays from other $A = 156$ nuclides.

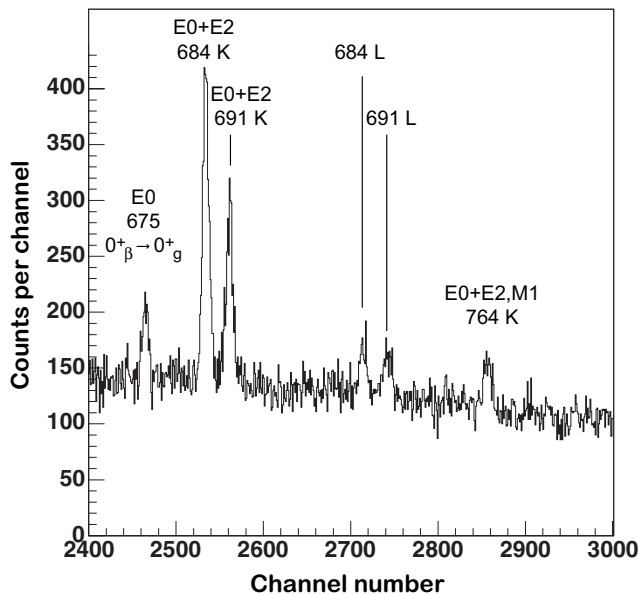


Fig. 63. The conversion electron associated with the 675 keV $E0$ transition ($0_2^+ \rightarrow 0_1^+$) observed in the decay of ^{156g}Ho to ^{156}Dy (90 minute tape cycle).

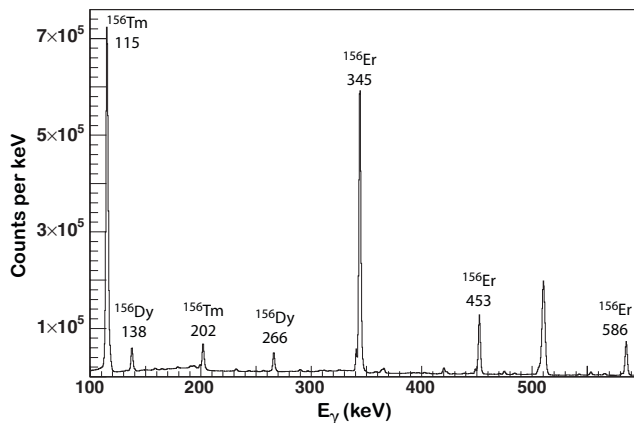


Fig. 64. While the 138 keV ($2^+ \rightarrow 0^+$) and 266 keV ($4^+ \rightarrow 2^+$) γ -ray transitions in ^{156}Dy are visible in the 10 second tape cycle, transitions associated with decays from other $A = 156$ nuclides dominate the spectrum.

detailed $\gamma - \gamma$, $\gamma - e^-$, and $e^- - e^-$ coincidence data of nuclides further from stability using the 8π spectrometer and PACES which will help discriminate between models and understand the physics of this transition region.

Experiment 973 is a collaboration of scientists from Georgia Tech., Colorado School of Mines, Lawrence Livermore National Laboratory, Louisiana State University, McMaster University, Oregon State University, Saint Mary's University, Simon Fraser University, TRIUMF, University of Guelph, University of Surrey, University of Toronto, and University of Vienna.

Experiment 984

Fast lifetime measurements with the 8π spectrometer and nuclear structure below $N = 82$ (P.E. Garrett, Guelph)

Lifetimes of nuclear levels provide crucial information on nuclear structure. Since the transition rates are determined by matrix elements of the well understood electromagnetic operator, they provide sensitive information on the charge distribution. Under the experimental program, an array of 10 BaF_2 detectors, the world's fastest scintillator, will be implemented into the 8π spectrometer to enable lifetime measurements. Experience has shown that time-delayed measurements following β decay have provided a wealth of critical level lifetimes in exotic nuclei over a wide range of nuclei in all regions of the nuclei chart. Of particular importance are studies of odd- A to locate single-particle states, and side-bands or isomeric quasi-particle states in even-even ones, that are strongly populated in beta decay but very weakly in Coulomb-excitation studies. Consequently a wide range of applications is envisaged for this timing array, with the flexibility guaranteed by a simultaneous measurement of $\beta(t) - \gamma(t) - \gamma(t)$ and $\gamma(t) - \gamma(t) - \gamma(t)$ coincidences with the Ge and BaF_2 detectors.

The array of 10 BaF_2 detectors will be mounted in available open positions on the 8π spectrometer. For standard 8π spectroscopy experiments, the time difference between the β particle detected in the plastic scintillators of SCEPTAR and the γ -ray detected in a BaF_2 detector will be used to measure lifetimes down to the sub-100 ps range. The particular decay path of the γ -ray cascade will be chosen by the high-resolution Ge detectors of the 8π . For experiments aimed at the shortest lifetimes, down to the 10 ps level, the time signal from the SCEPTAR array will be replaced with that from a single fast-plastic scintillator, mounted immediately behind the beam spot of the moving tape collector, coupled directly to a fast photomultiplier tube. These very fast lifetimes may also be measured by recording the time difference between two BaF_2 detectors, provided that the decay path can be isolated sufficiently.

As a proof of principle, a test experiment was performed in June using 4 BaF_2 detectors borrowed from the University of Surrey. A beam of ^{26}Na was delivered to the 8π spectrometer. The trigger logic was set up such that both BaF_2 -SCEPTAR coincidences and BaF_2 - BaF_2 coincidences could be recorded. The spectrum shows the timing of a single crystal with respect to any one of the four BaF crystals in the array. The rightmost peak in Fig. 65 is the "self timing" peak, where the same detector acts as both the start and stop for the TAC. The width of this peak indicates the

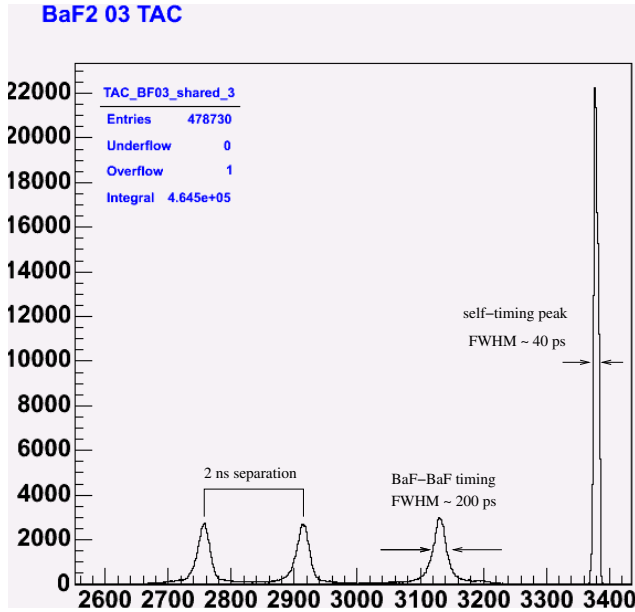


Fig. 65. Results from a test experiment using the 8π spectrometer and four borrowed BaF₂ detectors. The timing FWHM for BaF₂-BaF₂ coincidences was ≈ 200 ps.

amount of jitter contributed by the trigger logic for the system. The FWHM was determined to be 40 ps, which is much less than the timing resolution of the detectors themselves. The remaining peaks in this spectrum correspond to coincidences with the three other detectors, with selected delays of 3, 6 and 8 ns (respectively, left to right of the self-timing peak) for the stop pulse. The FWHM resolution for timing between separate BaF₂ crystals was ≈ 200 ps. Provided sufficient statistics, a precision of a few ps on the centroid position can be readily achieved.

With the addition of an array of BaF₂ detectors, the 8π spectrometer and its associated equipment will be a world-unique facility for the study of β decay in that γ -ray singles, $\gamma\gamma$ coincidences, conversion electrons, β tagging, and lifetimes can be measured simultaneously for all proposed experiments. Equipment is currently being acquired, and it is expected that the first elements of the array will be in place in the fall, 2005.

Experiment 985

Half-life and branching-ratio measurement of ^{18}Ne superallowed Fermi β decay

(M.B. Smith, TRIUMF)

Precision measurements of ft values for superallowed Fermi β decays between isobaric analogue states provide stringent tests of the electroweak standard model. Currently ft values have been measured to a precision of $\pm 0.1\%$ or better for nine superallowed transitions in nuclei between ^{10}C and ^{54}Co , confirming the conserved vector current (CVC) hypothesis

at the level of 3×10^{-4} . These data, together with the Fermi coupling constant G_F obtained from muon-decay experiments, also provide the most accurate value for the up-down quark mixing matrix element, V_{ud} , of the Cabibbo-Kobayashi-Maskawa (CKM) matrix. Combining the V_{ud} measurement with the recommended values of V_{us} and V_{ub} from the Particle Data Group [Eidelman *et al.*, Phys. Lett. **B592**, 1 (2004)] leads to the well-known result that the sum of the squares of the three matrix elements fails to meet unity by more than two standard deviations [Hardy and Towner, Phys. Rev. Lett. (in press)]. Unitarity of the CKM matrix is a strict requirement of the standard model and the failure of this test, should the result be firmly established, would imply the need for important new physics.

A definitive conclusion on CKM unitarity can only be reached after the elimination of “trivial” explanations for the current discrepancy. For nuclear β -decay, the role of the theoretical corrections which must be applied to the experimental results has come under considerable recent scrutiny, particularly for the isospin-symmetry-breaking (Coulomb) term δ_C . The theoretical calculations can best be tested by measuring the ft values (by determining the half-lives, branching ratios and Q -values) for decays with particularly large predicted Coulomb terms or for cases where the predictions differ significantly. An example is the superallowed decay of ^{18}Ne , for which a large δ_C correction, relative to other decays with $A < 30$, has been calculated [Towner and Hardy, Phys. Rev. **C66**, 035501 (2002)]. The objective of Expt. 985 is to precisely determine the ^{18}Ne half-life and superallowed branching ratio. First beams were taken during 2004 and a precision measurement of the half-life was performed.

The technique of precisely measuring lifetimes by detecting γ -rays using the 8π spectrometer, an array of 20 Compton-suppressed HPGe detectors, is being pioneered at ISAC and has been investigated in great detail for the β decay of ^{26}Na (Expt. 909). The current measurement is the first to use this technique for a superallowed Fermi β decay. Beams of ^{18}Ne were extracted during the first development run of ISAC’s electron cyclotron resonance (ECR) ion source and $\sim 4 \times 10^5$ ions/s were delivered to the 8π spectrometer for approximately 90 hours. The 30 keV beam was collected using a Mylar-backed aluminum tape, of thickness 40 μm , moving through the centre of the array. Samples were implanted for approximately four half lives and the subsequent decay was measured for ~ 24 half lives before the tape was moved and the cycle repeated.

Time-stamped singles γ -ray events were recorded during the entire implantation and decay cycle for 15

runs, each run typically lasting three hours. The half-life was determined by selecting events correlated with the 1042 keV γ -ray, which follows the superallowed decay of ^{18}Ne and connects the analogue 0^+ state in ^{18}F to the 1^+ ground state. Dead-time-corrected decay curves associated with these data were fitted using a maximum-likelihood χ^2 -minimization technique developed for Expt. 909 [Grinyer *et al.*, Phys. Rev. C, in press]. Experimental conditions were changed between runs in order to investigate systematic uncertainties. The 8π data acquisition system provides software-selectable pile-up and/or Compton suppression and variable (measured event by event) or fixed dead-time. These settings were varied throughout the experiment and systematic errors were also investigated by varying the shaping times of the amplifiers and thresholds of the constant-fraction discriminators. No systematic effects were found at the level of the statistical errors.

The preliminary value of the half-life of ^{18}Ne , obtained from a weighted average of the 15 runs, is 1.6676 ± 0.0016 s. This result agrees with three of the four previous half-life measurements and is five times more accurate than the currently-accepted value (1.672 ± 0.008 s) based on these determinations. After finalizing the half-life result, a publication will be submitted during 2005.

Experiment 989

Astrophysical studies using ^{26}Al ground-state and isomeric beams

(C. Ruiz, TRIUMF: for the DRAGON collaboration)

Motivation

Recent advances in space-based γ -ray astronomy have led to the mapping out of the galactic ^{26}Al distribution. The ground state of ^{26}Al is a β^+ emitter decaying to the first excited state of ^{26}Mg with a half-life of 717,000 years. This decay is then characterized by the decay of the first excited state of ^{26}Mg with a single γ -ray at 1809 keV. Because of its relatively long half-life, ^{26}Al persists in the interstellar medium long after the particular stellar cataclysm which has produced it has subsided or ended, allowing us to observe it. However, 717,000 years is a short time on the galactic star-formation timescale. The ^{26}Al distribution is then a useful indicator of the history of nucleosynthesis averaged over the last million years.

Concentrations of ^{26}Al in the galactic plane and spiral arms indicate a young, high-mass star origin of its nucleosynthesis. Candidates for this production are: core-collapse supernovae, AGB stars and classical binary-system novae. Hydrodynamic and reaction network models of supernovae and novae have produced intriguing results. The supernovae models show that

100% of the measured ^{26}Al in the galaxy can result from nucleosynthesis in the pre-collapse hydrogen-rich shell of such a star. The largest uncertainties in this model are the galactic supernova rate, the model complexity, and the nuclear reaction rates involved in the production and destruction of ^{26}Al . For novae, there is a similar uncertainty. It is still of great debate whether novae can produce a significant fraction of the galactic ^{26}Al or not. Present models say they can, however, the uncertainty in the low-temperature reaction rate of $^{26}\text{gAl}(p, \gamma)^{27}\text{Si}$ gives rise to a factor 2 uncertainty in the amount of ^{26}Al produced. The models require that this uncertainty be reduced in order to make better predictions on the nova contribution to the galactic ^{26}Al abundance that future space based γ -ray missions such as INTEGRAL will study.

At present the uncertainty in the $^{26}\text{gAl}(p, \gamma)^{27}\text{Si}$ reaction rate at nova temperatures is dominated by a single isolated resonance at $E_{\text{cm}} = 188$ keV. There has only been one direct measurement of the resonance strength of this state which has to date remained unpublished. Such a dominating resonance is required to be experimentally measured at least twice by different methods to ensure confidence in this parameter's insertion into hydrodynamic models. The previous measurement was made at Caltech in 1989 using a "traditional" (p, γ) method of impinging a low energy proton beam onto a purified radioactive ^{26}Al target and observing the γ -rays resulting from reactions using a germanium detector.

The development of intense ^{26}Al beams at TRIUMF-ISAC has provided us with the opportunity to measure the 188 keV resonance in $^{26}\text{gAl}(p, \gamma)^{27}\text{Si}$ at the DRAGON recoil separator using inverse kinematics.

Experiment

This year, DRAGON performed test studies for the $^{26}\text{Al}(p, \gamma)^{27}\text{Si}$ reaction in order to determine the feasibility of measurement of the 188 keV resonance strength. A silicon carbide target at ISAC provided an accelerated ^{26}Al beam with currents reaching a maximum of 3×10^8 particles per second, and an average of 0.7×10^8 particles per second.

The level of ^{26}Na and $^{26\text{m}}\text{Al}$ contaminants in the beam were monitored using a diagnostic set-up at the separator mass slits, the point where unreacted beam is deposited. Two diametrically arranged sodium iodide detectors were used to detect annihilation γ -rays from β^+ decay of the 6 second lifetime decay of the ^{26}Al isomeric state, while a high purity germanium detector was used to detect the decay of the ^{26}Na via the 1809 keV γ -ray from the first excited state of ^{26}Mg . In this way, contamination levels of $0.4 \pm 0.07\%$ for ^{26}Na and $0.004 \pm 0.0007\%$ for $^{26\text{m}}\text{Al}$ were determined.

DRAGON's ionization chamber was used to detect particles at the end of the separator in an attempt to separate "leaky" unreacted beam particles from true recoils using $\Delta E - E$ information from the separate anode segments in the chamber. Particles were detected in coincidence with γ -ray signals from the BGO array surrounding DRAGON's windowless gas target.

Runs were taken primarily at a higher beam energy in order to see the "strong" resonance at $E_{\text{cm}} = 363$ keV. 5×10^{12} ions were received on target for this energy, and 117 ^{27}Si recoils were detected in coincidence with cascade γ -rays. The ion chamber anode information showed that at this energy, leaky beam and true recoils are just separable using the $\Delta E - E$ method (Fig. 66). ^{27}Si recoils are easily identified, however, using the time of flight round the separator between a coincident prompt γ -ray and particle detected in the ion chamber (Fig. 67). By extrapolation it was determined that recoils from the 188 keV resonance would not be separable using the $\Delta E - E$ method. A local time-of-flight system in conjunction with the separator time of flight would be necessary. Runs taken on the 188 keV resonance yielded no recoil particles because only 2×10^{13} ions were incident on target, insufficient to produce any recoils due to the low yield of 4×10^{-14} reactions per incoming ion.

The conclusions of this running period were that:

- A local time-of-flight method would be preferable in the attempt to separate recoils and leaky beam.

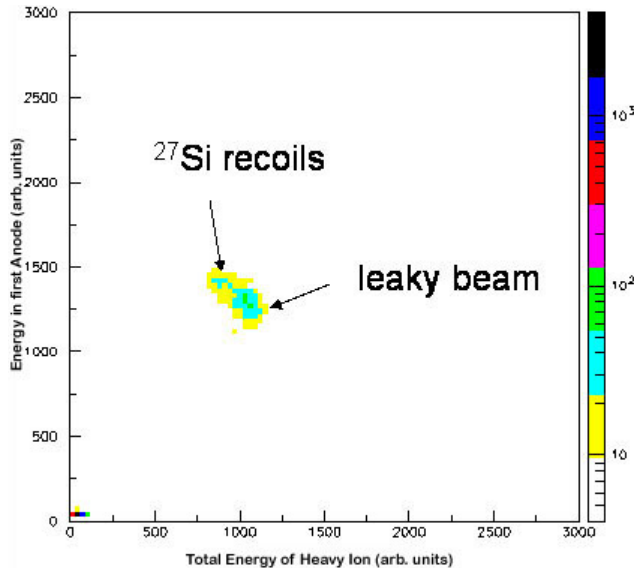


Fig. 66. Ion chamber total pulse height versus anode 1 pulse height for the $^{26}\text{gAl}(p,\gamma)^{27}\text{Si}$ reaction, showing ^{27}Si recoils and "leaky" beam.

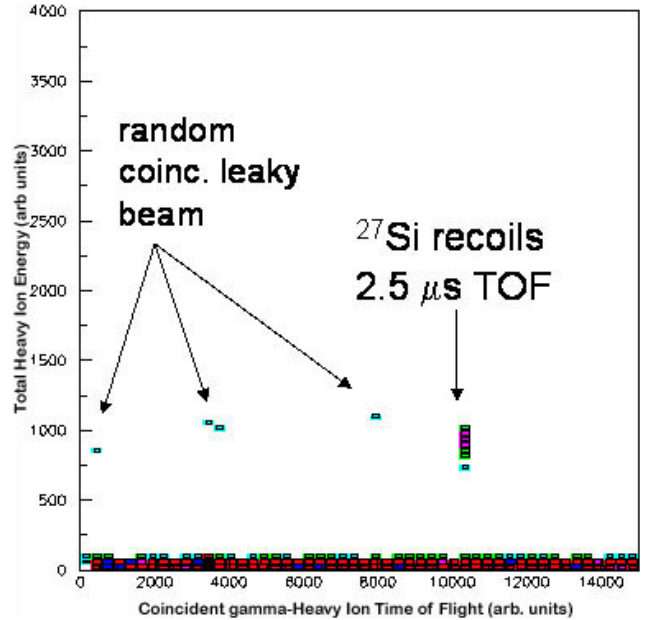


Fig. 67. Heavy ion - γ coincident separator time of flight for the $^{26}\text{gAl}(p,\gamma)^{27}\text{Si}$ reaction, showing ^{27}Si recoils and randomly coincident "leaky" beam.

- Insufficient beam intensity sustained for a reasonable duration was obtained, leading to the conclusion that a high-power silicon carbide target in combination with the TRIUMF resonant ionization laser ion source would be required to provide order of magnitude higher beam intensities.

With the improvements listed above due to be operational at ISAC over the coming year, DRAGON will attempt to make the direct measurement of the 188 keV resonance strength of the $^{26}\text{Al}(p,\gamma)^{27}\text{Si}$ in the period of running in 2005.

Experiment 992 Lifetime of the 4.033 MeV state in ^{19}Ne (G.C. Ball, B. Davids, TRIUMF)

Novae are thermonuclear runaways resulting from the accretion of hydrogen- and helium-rich material onto the surfaces of white dwarfs in binary systems. X-ray bursts result from a similar accretion process on neutron stars, during which the temperature and density are sufficiently high to initiate breakout from the hot CNO cycles into the rp process, dramatically increasing the luminosity of outbursts and synthesizing nuclei up to masses of 100 u. Several reactions have been suggested as pathways for this breakout, but only two are currently thought to be possibilities: $^{15}\text{O}(\alpha,\gamma)^{19}\text{Ne}$ and $^{18}\text{Ne}(\alpha,p)^{21}\text{Na}$. In astrophysical environments the $^{15}\text{O}(\alpha,\gamma)^{19}\text{Ne}$ reaction proceeds predominantly through resonances lying just above the $^{15}\text{O} + \alpha$ threshold at 3.529 MeV in ^{19}Ne . The reaction

rate in novae is determined by the resonance strength of the 4.033 MeV $3/2^+$ state. This state may also make the largest contribution to the reaction rate at the higher peak temperatures reached in X-ray bursts.

Direct measurements of the low energy cross section, which require high-intensity radioactive ^{15}O beams, are planned at TRIUMF. Until such beams are available, the best information on the reaction rate will come from indirect measurements of the decay properties of the relevant resonances. These states lie beneath the proton and neutron separation energies, and can therefore decay only by α and γ emission. By populating these states and observing the subsequent α - and γ -decays, one can deduce the branching ratio $B_\alpha \equiv \Gamma_\alpha / (\Gamma_\alpha + \Gamma_\gamma)$. If Γ_γ is also known, one can then calculate the resonance strength and thereby the contribution of each state to the astrophysical rate of the $^{15}\text{O}(\alpha, \gamma)^{19}\text{Ne}$ reaction. In a recent experiment at the KVI, the α branching ratios have been measured. However, experimental data on the radiative widths of these states are sparse. An effort to measure the lifetime of the 4.033 MeV state by the Doppler shift attenuation method (DSAM) resulted in an upper limit. A complementary measurement of the Coulomb excitation to this state at intermediate beam energies resulted in an upper limit on the radiative width, corresponding to a lower limit on the lifetime. The 95% confidence level allowed region for the lifetime, and therefore the reaction rate, spans two orders of magnitude. TRIUMF Expt. 992 aims to measure the lifetime of this state using the DSAM, populating it via the $^3\text{He}(^{20}\text{Ne}, \alpha)^{19}\text{Ne}$ reaction at a ^{20}Ne beam energy of 34 MeV. A measurement of this lifetime will definitively settle the question of whether this reaction plays any role in novae, and substantially reduce the uncertainty on the reaction rate in X-ray bursts.

Preparations for the lifetime measurement are proceeding along several lines simultaneously. Implantation of Al, Zr, and Au foils with ^3He is being carried out at the Université de Montréal. Si surface barrier detectors have been ordered and will soon arrive. A

schematic design for the cold trap and vacuum chamber assembly has been completed, and detailed designs will be completed shortly. Fabrication of the chamber can proceed promptly upon completion of these drawings. Ion optical calculations for the transport of the beam to the experiment at the end of the medium energy beam transport line have been completed and indicate a good beam spot can be achieved without any additional focusing elements. This experiment will be the subject of the master's thesis of a new UBC student, Mythili Subramanian.

EMMA

Ion optical design work has been completed for EMMA, an electromagnetic mass analyzer for ISAC-II at TRIUMF. EMMA is a recoil mass spectrometer that will be used to separate the recoils of nuclear reactions from the beam, and to disperse them according to mass/charge. ISAC-II will provide intense, low-emittance beams of unstable nuclei with masses up to 150 u and maximum energies of at least 6.5 MeV/nucleon. EMMA will be used in many different types of experiments with radioactive beams, especially those involving fusion-evaporation and transfer reactions. As such, it must be both efficient and selective, possessing large acceptances in angle, mass, and energy without sacrificing the necessary beam suppression and mass resolution.

EMMA is based on a symmetric configuration of electric and magnetic dipoles, a proven design that allows for energy dispersion cancellation. (Figure 68 schematically depicts the layout of electromagnetic components.) However, the design represents a significant improvement over existing instruments of this type. In particular, EMMA has the largest energy and angular acceptances of any recoil mass spectrometer, while simultaneously providing high mass resolving power due to the design of its quadrupole lenses and the curvature of its magnetic dipole field boundaries. This combination of large acceptance and high resolution will make EMMA the most advanced instrument of its kind. It will be an

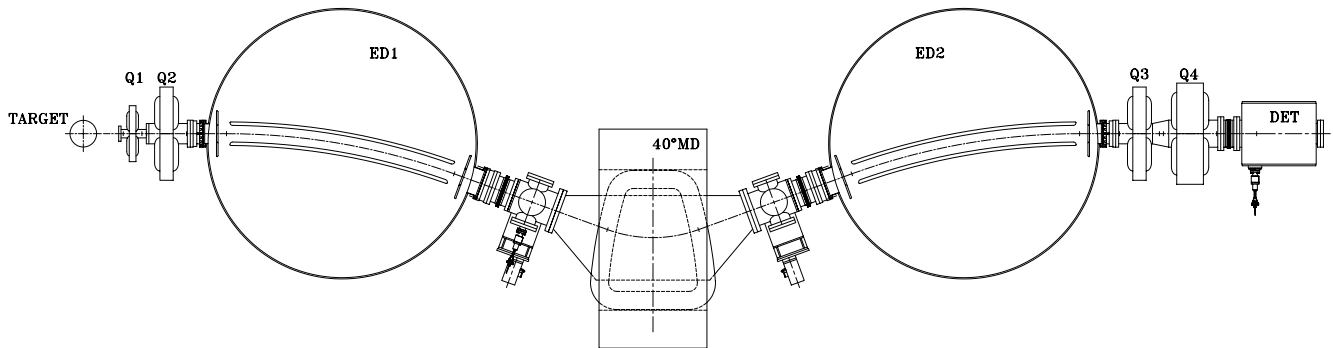


Fig. 68. Schematic view of EMMA, showing the target, quadrupole and dipole magnets, and electric dipoles. The detector box is also indicated.

indispensable part of the ISAC-II experimental facility, and will be used extensively in conjunction with the TIGRESS γ -ray detector array as well as the TUDA charged particle detectors.

The design of EMMA underwent both internal (TRIUMF) and external (NSERC) technical reviews in 2004 in order to ascertain the soundness of its ion optics as well as its suitability for the anticipated users. A paper describing the design has been accepted for publication by Nuclear Instruments and Methods in Physics Research A.

Experiment 995

An alternate approach to radioactive beam production for volatile elements

(*J. D'Auria, S. Lapi, SFU*)

Overview

The goal of this experiment is to demonstrate that certain radioactive beams of volatile elements, which have proven to be difficult to produce using the standard ISOL approach at the ISAC facility, can be produced using low energy protons. If successful, the produced species could be transferred in the gas phase to ISAC (either to OLIS or the on-line system), ionized using an appropriate ion source (ECR or FEBIAD) and the ionized beam accelerated to required energies using the ISAC accelerator. This approach has been successfully demonstrated at the BEAR facility at LBL [Powell *et al.*, Nucl. Instrum. Methods **B204**, 440 (2003)]

and could allow ISAC to have two methods of producing beams, perhaps simultaneously (if OLIS is used). The experiment received approval at low priority in 2003 and initial studies have been performed in 2004.

Background

The proposed method of production is the irradiation of gaseous targets with 13 MeV protons using the TR13 facility. This facility (H^- cyclotron) is located in the TRIUMF accelerator building and is primarily used to produce radioisotopes for medical purposes. Possible beams available with this approach are given in Table XII along with information on target material, reaction and rate of production.

This method of production and transfer was tested in the M.Sc. study of S. Lapi who measured the production and transfer efficiency for ^{14}O [Lapi, *Development of an intense ^{15}O radioactive beam using low energy protons*, M.Sc. thesis, Simon Fraser University (2003)] using the TR13 facility.

Table XIII presents some of the beam requirements of approved ISAC experiments.

Studies in 2004

Approximately 1 Ci of ^{11}C as $CH_4(g)$ was produced in a (p, α) reaction using the TR13. Following chemical manipulations, the active methane was hand delivered to the injection port of the on-line ECR ion source at ISAC, on two occasions. Stable methane had been injected previously into the ECR to study the operation

Table XII. Calculated production rates in a target using 50 μA of 13 MeV protons (TR13).

Isotope	Half-life	Target material	Production reaction	Saturation rate of production
^{11}C	20.3 m	$^{14}N_2$ (g)	$^{14}N(p, \alpha)^{11}C$	$2.4 \times 10^{11}/s$
^{14}O	70.6 s	$^{14}N_2$ (g)	$^{14}N(p, n)^{14}O$	$2 \times 10^{10}/s$
^{15}O	122.2 s	$^{15}N_2$ (g)	$^{15}N(p, n)^{15}O$	$2.1 \times 10^{11}/s$
^{13}N	9.97 m	O_2 (g)	$^{16}O(p, \alpha)^{13}N$	$4.8 \times 10^{10}/s$
^{18}F	1.83 h	Enriched ^{18}O (g)	$^{18}O(p, n)^{18}F$	$5.2 \times 10^{11}/s$
^{17}F	64.5 s	Neon gas	$^{20}Ne(p, \alpha)^{17}F$	$1.5 \times 10^{11}/s$

Table XIII. Beam requirements for ISAC experiments approved or to be presented.

Beam	Experiment #	Optimal intensity	Minimum intensity
^{11}C	new	$10^{8,9}$	
^{14}O	924	10^6	5×10^5
^{15}O	813	10^{11}	10^{10}
^{15}O	900	10^9	10^8
^{13}N	805	10^9	10^8
^{17}F	946	10^9	10^8
^{19}Ne	811	10^8	10^7

of the source for ionizing methane, e.g. the optimal ion was CH_3^+ . A NaI(Tl) gamma detection system was set up at the ISAC collection station (on the mass separator floor), and a stable beam was optimized onto the FC positioned just before this station. The result of these two studies was not completely successful. While there was an indication of ^{11}C possible activity at the collection station (10^4 cps), this represented an overall efficiency of $\sim 0.01\%$. This includes but is not limited to decay losses prior to the observation, losses due to the transfer through a mass transfer value prior to the ECR, the ECR efficiency, beam tuning transmission losses and perhaps others. Apparently most of the activity did not make it into the ion source efficiently but seemed to remain in the gas inlet system prior to the source. While the exact cause of this is not clear, nevertheless, the manipulations with the ECR were useful and may have played a role in the ultimate successful operation of this new system. It should be noted that the tests for Expt. 995 were limited to a narrow one week window during which the ECR was available for such types of tests, in order not to interfere with its use for RB production for experiments.

A series of tests are planned for 2005 at the off-line ECR test system (essentially the same ECR source). Initial studies will use a $^{13}\text{CO}_2$ gaseous source to understand the ionization efficiency of the ECR for CO_2 . In addition a series of gaseous dilutions will be studied which will attempt to mimic the concentrations of ^{11}C in an actual production cell. Following these tests, approval will be sought to perform some low activity tests with an actual ^{11}C production cell in order to fully understand this system prior to seeking time with the on-line system.

Experiment 1008

A new look at the β -decay of ^{11}Li

(F. Sarazin, Colorado School of Mines)

Last year, a measurement of the ^{11}Li yield out of a tantalum target reached a record breaking 44000 ^{11}Li per second, making TRIUMF/ISAC the facility delivering the most intense ^{11}Li beam in the world. Following an already successful measurement of the β -decay of ^{11}Li in August, 2002 [Sarazin *et al.*, Phys. Rev. **C70**, 031302(R) (2004)], the time was right to investigate again the complex decay of ^{11}Li , using the enhanced ^{11}Li yield available and also utilizing the new addition to the 8π : SCEPTAR, an array of 20 plastic scintillators allowing the detection of β - γ coincidences. The experiment took place in October. A beam of about 15000 pps was delivered to the 8π and implanted on an aluminum foil at the centre of the 8π /SCEPTAR arrays. Most of the ^{11}Li β -decay strength is observed to proceed through unbound states in ^{11}Be , which sub-

sequently decay by one-neutron emission to ^{10}Be . This results in the observation of a γ -spectrum dominated by the decay of the excited states in ^{10}Be . These transitions exhibit characteristic Doppler-broadened lineshapes, due to the recoiling effect induced by the neutron emission. The main objective of this measurement was, by means of lineshape analysis, to look for weak branches in the β -delayed one-neutron emission to excited states in ^{10}Be . In particular, good statistics are required to determine the precise lineshape of the 5.96 MeV peak, which is crucial to resolve unanswered questions left from the first experiment. Moreover, some results of the first analysis are in disagreement with results reported recently by Hirayama *et al.* [Phys. Lett. **B611**, in press] on another experiment performed at TRIUMF/ISAC, using a polarized ^{11}Li beam and neutron detectors. About 15 times more data were obtained with an improved signal to background ratio due to the measurement in β - γ coincidences. This ratio was further improved by the rejection of bremsstrahlung events, e.g. high-energy electrons slowing down in the plastic scintillators and emitting one or more γ -rays in the forward direction, firing the nearby germanium detector (see Experimental Facilities: 8π Spectrometer, this Annual Report). The improvement in the lineshape quality is particularly impressive for the 5.96 MeV peak, as can be seen in Fig. 69.

The improved statistics obtained in this experiment also allowed us to look at γ - γ coincidences. The lineshape of the 2.59 MeV and 5.96 MeV peaks results from the decay of a doublet of states (1^- , 2_2^+) in ^{10}Be only 1.7 keV apart. The sharp contribution originates from the decay of the relatively long-lived second 0_2^+ state to the 1^- state in ^{10}Be located at 6.180 MeV. By

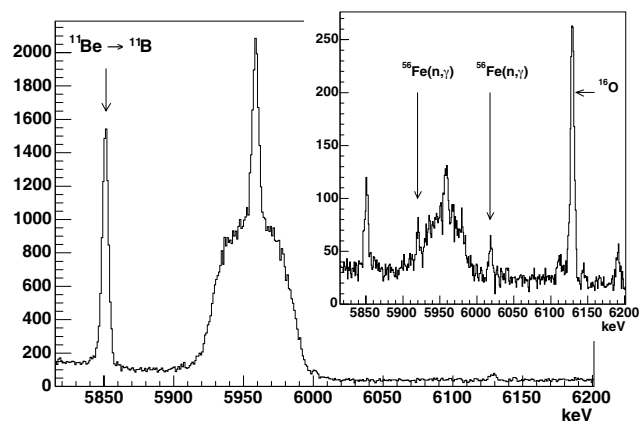


Fig. 69. Compton suppressed γ -spectrum following the β -decay of ^{11}Li . The lineshape of the 5.96 MeV peak obtained in β - γ coincidence with bremsstrahlung correction is shown. The lineshape obtained in the first experiment is shown in the inset. One can see that background γ -ray lines, unrelated to the β -decay of ^{11}Li , have disappeared in the new spectrum.

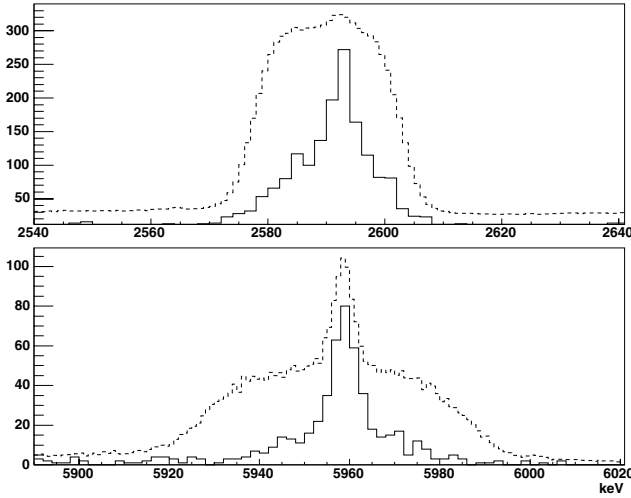


Fig. 70. γ - γ coincidences gated with the 219 keV $0_2^+ \rightarrow 1^-$ transition. The sharp component is singled out by the coincidence (continuous line) and is shown together with the scaled-down original lineshape at 2.59 MeV (top) and 5.96 MeV (bottom).

gating on the 219 keV transition linking both states, it is possible to isolate this sharp contribution, as seen in Fig. 70.

More analysis is in progress to actually fit the various lineshapes with a Monte Carlo simulation developed during the analysis of the first measurement. This will be the main body of the Ph.D. thesis of Caleb Mattoon at the Colorado School of Mines.

LANSCE Experiment NPDGamma Measurement of the parity-violating gamma asymmetry A_γ in the capture of polarized cold neutrons by para-hydrogen, $\bar{n} + p \rightarrow d + \gamma$ (S.A. Page, W.D. Ramsay, Manitoba)

Introduction

The $\bar{n} + p \rightarrow d + \gamma$ experiment had a very successful commissioning run from February to April. All the equipment except the liquid hydrogen target was successfully commissioned during the run. It was intended to install the liquid hydrogen target during the summer of 2004, with another data-taking starting again in the fall, but a site-wide “stop work order” at Los Alamos National Laboratory put all work not related to security or safety on hold and normal activities were very slow to resume. We now expect the liquid hydrogen target to be commissioned in late 2005. A Manitoba M.Sc. student is now completing his thesis on work performed for the 2004 commissioning run.

The $\bar{n}p \rightarrow d\gamma$ collaboration involves 13 institutions, with Canadian collaborators from the University of Manitoba, and infrastructure support from TRIUMF. The authors of this report, S.A. Page and W.D. Ramsay, took responsibility for precision monitoring of the

neutron beam flux, and designed a new current mode beam monitor that was first tested in the fall of 2001 at LANSCE. Three additional beam monitors based on this new design were subsequently constructed and used with great success in the 2004 commissioning run. Canadian participation in $\bar{n} + p \rightarrow d + \gamma$ includes vital infrastructure support from TRIUMF on the design and construction of a computer controlled motion system for the gamma detector array and liquid hydrogen target to be used for calibration of the effective detector alignment *in situ*. This procedure requires that the entire one-tonne detector array be moved accurately in the vertical and horizontal directions by up to ± 5 mm. TRIUMF also designed and built custom VME modules that permit the gain of each of 48 detector channels to be adjusted under computer control. A prototype was tested at Los Alamos in 2003 and 6 more were built at TRIUMF in 2004 and delivered to Los Alamos.

The experiment is designed to measure the very slight up-down asymmetry, A_γ , in the capture of vertically polarized cold neutrons on liquid parahydrogen. If parity is conserved in the reaction, A_γ will be zero. The reason for doing this is that it provides a very clean measure of the weak pion nucleon coupling, f_π^1 . In fact, to a very good approximation, $A_\gamma = -0.11 f_\pi^1$. The value of f_π^1 is somewhat controversial [Wilburn and Bowman, Phys. Rev. **C57**, 3425 (1998)]. The experimental and theoretical situation is summarized in Fig. 71. ^{18}F gamma circular polarization experiments give zero. Haxton interprets the results to indicate $f_\pi^1 = 0 \pm 1.0 \times 10^{-7}$ [Ann. Rev. Nucl. Part. Sci. **35**, 501 (1985)]. The ^{133}Cs anapole moment, on the other hand, gives a non-zero value. Flambaum interprets the result

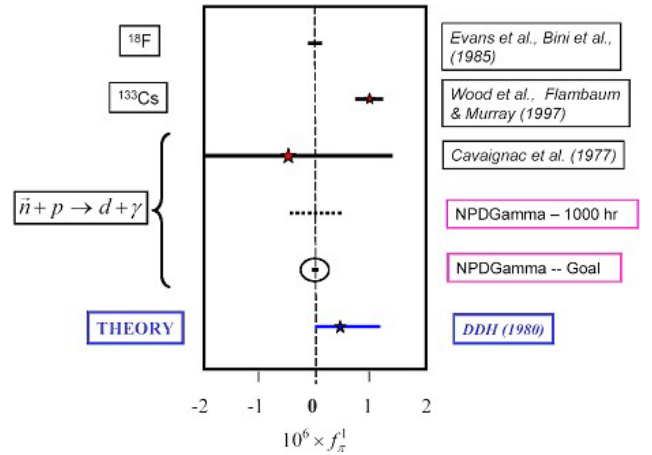


Fig. 71. Experimental and theoretical limits on the weak pion-nucleon coupling f_π^1 . The expected precision of an initial run of the NPDGamma experiment at LANSCE, assuming 1000 hours of data, is shown, as is the statistics-limited final result planned for the experiment.

to give $f_{\pi}^1 = 7 \pm 3 \times 10^{-7}$ [Phys. Rev. **C56**, 1641 (1997)]. Because NPDGamma is based on a simple two-nucleon system without the complex many-body dynamics of the ^{18}F and ^{133}Cs experiments, the LANSCE experiment has a good chance of laying this controversy to rest. The goal of the experiment, as indicated in Fig. 71, is to measure f_{π}^1 to $\pm 0.5 \times 10^{-7}$, which is approximately 1/10 of the mid-range theoretical estimates. The “1000 hour” point in Fig. 71 is based on test run results [Mitchell *et al.*, Nucl. Instrum. Methods **A521**, 468 (2004)] and shows the uncertainty we might reasonably expect to achieve in the first data run with hydrogen at LANSCE, which is expected in 2006.

The NPDGamma experiment

The experiment set-up at LANSCE is shown schematically in Fig. 72. An 800 MeV proton beam pulsed at 20 Hz impinges on a tungsten spallation target; MeV neutrons emerging from the target are cooled in a liquid hydrogen moderator and transported via a supermirror guide to the experimental apparatus, where they emerge from the $(9.5 \times 9.5) \text{ cm}^2$ guide at 21 m from the source. The $m = 3$ supermirror guide enhances the total neutron flux in the desired energy range 0–15 meV with respect to the Maxwellian distribution of neutrons emerging from the moderator. The pulsed nature of the beam enables the energies of the neutrons to be determined from their times of flight, which is an important advantage for diagnosing and reducing many types of systematic error. Neutrons are polarized in the vertical direction by selective transmission through a polarized ^3He gas cell which acts as a spin filter, producing an energy dependent polarization spectrum.

The three beam monitors (marked “Monitor” in

Fig. 72) are ^3He ionization chambers provided by the University of Manitoba collaborators, supported by NSERC. In Fig. 73, two of these monitors are shown mounted for testing at the start of the 2004 commissioning period at Los Alamos. The three monitors measure the neutron beam intensity upstream and downstream of the polarizer cell, and at the end of the beam line. The transmission of the ^3He cell serves as an on-line measurement of its polarization and hence that of the neutron beam, and the transmission through the liquid hydrogen target is an on-line monitor of the orthohydrogen/parahydrogen ratio in the target.

A uniform vertical guide field, $B_o = 1 \text{ mT}$, preserves the neutron beam polarization as it is transported to the liquid hydrogen target, where the incident neutrons are captured to produce the 2.2 MeV γ -rays of interest. Low energy neutrons depolarize rapidly in orthohydrogen, while those below 15 meV retain their polarization in a parahydrogen target; hence, it is important to ensure that the liquid hydrogen target is prepared and maintained with the very low equilibrium orthohydrogen concentration of 0.1%. By placing monitors before and after the target, the ortho-hydrogen concentration can be monitored on-line, since the scattering cross sections for ortho- and para-hydrogen differ by about a factor of 20 in the energy range of interest. Approximately 60% of the beam neutrons will be captured in the target.

The 2.2 MeV γ -rays from neutron capture in the target are detected with an array of 48 ($15 \times 15 \times 15$) cm^3 CsI(Tl) crystals surrounding the target. The detectors are read out in current mode by vacuum photodiodes coupled via low noise current-to-voltage preamplifiers to transient digitizers sampling the diode signals every 10 μs . A resonant radio frequency (rf)

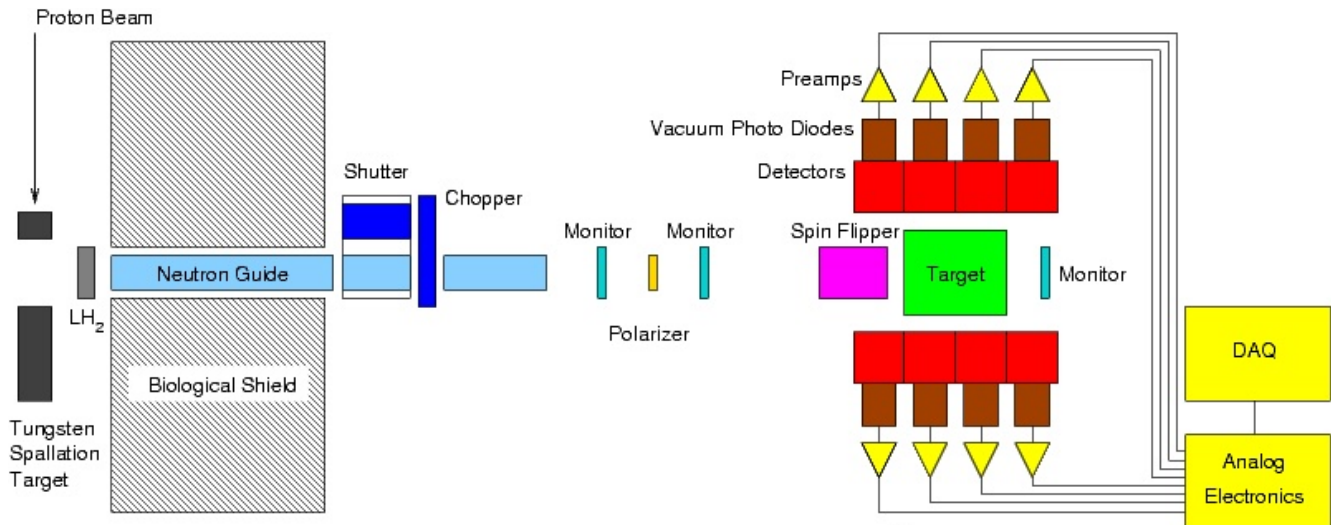


Fig. 72. Schematic of the NPDGamma apparatus on flight path 12 at LANSCE.



Fig. 73. Manitoba ^3He neutron monitors installed on FP12 near the start of the 2004 commissioning run. Later in the run, the monitors were used to measure neutron flux, neutron polarization, and spin flip efficiency.

spin flipper, consisting of a 30 cm diameter by 30 cm long solenoid whose magnetic field amplitude is tailored as a function of time of flight to flip neutron spins of all energies, is located upstream of the target. The spin flipper reverses the direction of the neutron spin on successive beam pulses according to an 8-step [+ - - + - + + -] reversal pattern, which cancels systematic drifts of detector efficiencies and electronic gains to second order. The spin flipper efficiency has been measured in tests runs to be in excess of 98% across a large area as appropriate to the beam size in our experiment.

The statistical uncertainty in the measurement of A_γ is ultimately determined by counting statistics, set by the beam intensity, the detector solid angle, and the counting time. Care has been taken to identify all possible sources of error, to minimize the sensitivity of the apparatus, and to work out a program of ancillary measurements to quantify individual error sources. The overall conclusion of these studies is that it should be possible to measure A_γ to $\pm 0.5 \times 10^{-8}$ with systematic errors no larger than 10% of the statistical error quoted above. Several key features of the experimental design should be noted here, namely:

1. three independent magnetic field reversals can be employed to manipulate the neutron spin and should give identical results for A_γ (^3He cell, rf spin flip, holding field in the experimental area);
2. the pulsed beam allows systematic effects to be isolated by their different time-of-flight dependences;
3. the use of vacuum photodiodes for detector readout reduces the gain sensitivity to magnetic

fields as compared to conventional photomultiplier tubes by 4 orders of magnitude, and the detector gains are essentially independent of bias voltage;

4. the depolarization of the beam above 15 meV allows a number of systematics associated with interaction of polarized neutrons in the target to be isolated;
5. the very small value of the electronic noise compared to counting statistics (1/100) makes it possible to test for instrumental effects with a standard uncertainty of 10^{-9} on a timescale of one day.

Systematic errors arising from interactions of the neutron spin are potentially the most serious for the experiment. Spin dependent effects can lead to either up-down or left-right asymmetries which could leak into the up-down signal from which A_γ is deduced. To limit contributions from left-right asymmetries at or below 5×10^{-10} , we require a means of determining the detector alignment with respect to the neutron spin direction to 20 mrad or better. To accomplish this, TRIUMF, in collaboration with the University of Manitoba, has designed and built a computer controlled detector stand capable of moving the entire 1000 kg CsI array by a few millimetres horizontally and vertically with the target in place. The effective position of each detector can be determined by the γ yield in that detector as a function of the array position. Figure 74 shows the array in place on the TRIUMF/Manitoba motion controller.



Fig. 74. CsI array mounted on the Manitoba/TRIUMF detector motion stand in the NPDGamma cave. The 1000 kg detector can be moved ± 10 mm in x and y under computer control.

Progress toward data-taking

The new FP12 beam line for NPDGamma was completed late in 2003, and the experimental apparatus, exclusive of the liquid hydrogen target, was installed in the new FP12 cave early in 2004 (Fig. 74). We have just completed a very successful first commissioning run, during which the beam line, chopper, beam monitors, magnetic guide field, ^3He polarizer and analyzer cells, rf spin flipper, full CsI detector array and data acquisition systems were exercised. Following a tune up and commissioning of each element of the apparatus, time was devoted to measurements of parity violating asymmetries from solid targets that will contribute to backgrounds in the NPDGamma measurements, e.g. from the aluminum target vessel, and measurements with a boron target were used to confirm that the full array operates at the counting statistics limit. Highlights of the commissioning run are discussed briefly below.

A very important demonstration was that the electronic noise was insignificant compared to counting statistics. Figure 75 compares the electronic noise to the counting statistics. One sees that the detector electronics performed well and that the electronic noise is indeed small.

The neutron guide and frame overlap chopper were also commissioned. Figure 76 shows the measured neutron time-of-flight distribution using the ^3He ionization chamber mounted at the end of the flight path 12 neutron guide. Agreement with the Monte Carlo calculation as normalized to the measured moderator brightness is excellent. Ultimately, the FP12 neutron flux will limit the precision in A_γ that we can obtain in a reasonable amount of running time at LANSCE.

The experimental counting rate asymmetry is given by $\epsilon = P_n A_\gamma$ where P_n is the beam polarization; the performance of the ^3He spin filter cell therefore

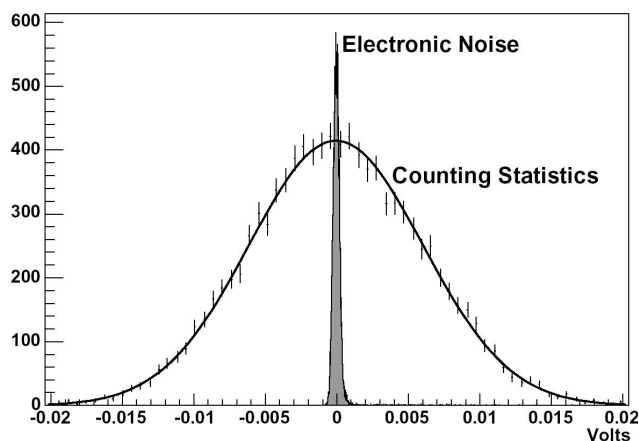


Fig. 75. Performance of the detector electronics during the commissioning run. Electronic noise alone is insignificant compared to counting statistics.

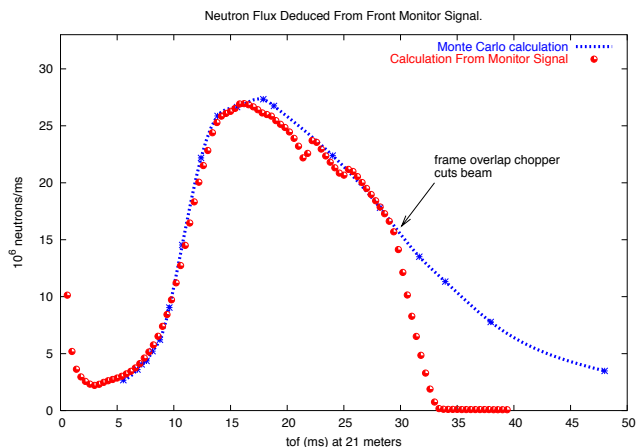


Fig. 76. Neutron time-of-flight distribution at the exit of the neutron guide compared to a Monte Carlo calculation. The large red dots are measured by the first Manitoba monitor and the small blue dots are a Monte Carlo calculation. The measured time-of-flight distribution falls off sharply around 30 ms when the frame overlap chopper enters the beam. The two sharp dips near the peak of the curve are Bragg edges from aluminum in the beam.

has a crucial influence on the statistical precision of the A_γ result. With precision beam monitors located upstream and downstream of the ^3He polarizer cell, the neutron beam polarization can be inferred directly from a comparison of the polarized and unpolarized cell transmissions – this allows for a continuous on-line measurement of the neutron beam polarization during NPDGamma data-taking. An example under commissioning run conditions (the ^3He polarization was not yet fully optimized) is shown in Fig. 77. It is worth noting that, with the spin filter technique, the neutron polarization can be considerably more than the ^3He polarization.

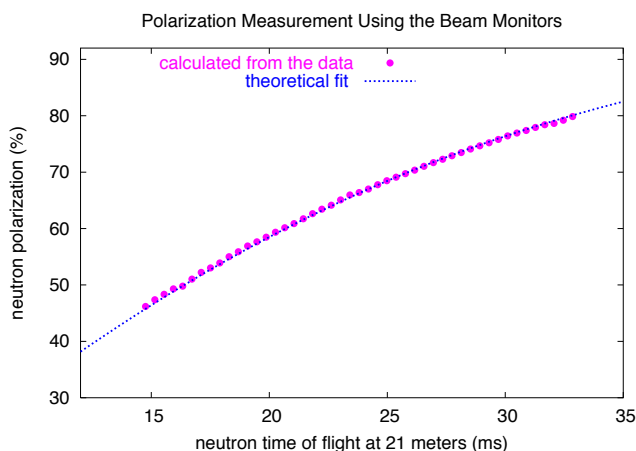


Fig. 77. Polarization measured with the Manitoba beam monitors during the 2004 commissioning run. By measuring the transmission through the ^3He cell with the cell polarized and unpolarized, the absolute neutron polarization can be determined without knowing the ^3He polarization.

During the commissioning run, we repeated our earlier measurements of the parity violating up-down γ asymmetry following neutron capture on ^{35}Cl and confirmed the earlier results to much higher precision in a few hours of integration time. The NPDGamma detector array is such a precise instrument that we were able to use this small parity-violating asymmetry to tune the rf spin flipper, although use of a polarized ^3He analyzer cell and a third beam monitor downstream of the cell is the preferred method. During NPDGamma data-taking, we plan to periodically measure this asymmetry with a Cl target to monitor the consistency of the detector performance.

To study a possible background, we also measured the asymmetry using a solid aluminum target. The CsI detector array performed superbly. The γ -ray asymmetry histogram was Gaussian over at least 4 orders of magnitude, with only very loose cuts on the incident neutron beam intensity. The conclusion from this preliminary analysis is that the parity violating asymmetry following neutron capture on aluminum is small enough that it will result in a negligible background correction with the liquid hydrogen target running.

Summary and future outlook

The NPDGamma experiment has just completed a very successful first commissioning run on flight path 12 at LANSCE. We have demonstrated that the full CsI detector array, instrumented for current mode readout, achieves a statistical error consistent with counting statistics. In late 2005, the liquid hydrogen target will be installed, followed by first data-taking as soon as possible, probably during the 2006 run cycle. We have determined that the physics asymmetry A_γ can be measured at LANSCE with the full NPDGamma apparatus with a statistical error of $\pm 4 \times 10^{-4}$ per beam pulse with 120 μA proton beam on the spallation target – unfortunately this falls short of our original $\pm 1 \times 10^{-4}$ per beam pulse goal that would enable us to measure A_γ to 10% of its predicted value in one calendar year of running time. Our test measurements have shown that expectations of the available neutron flux from the upgraded LANSCE facility were too optimistic by almost a factor of 4, with roughly equal contributions from reduced moderator brightness and reduced production beam current.

In view of the ultimate limit on the statistical accuracy that we can hope to achieve at LANSCE, the NPDGamma collaboration plans to complete commissioning of the apparatus and carry out a first measurement in 2006, which would provide a statistics-limited result for A_γ accurate to a standard uncertainty of 5×10^{-8} or better, improving on existing measurements in the neutron-proton system by a factor of 4, as shown in Fig. 71. In the longer term, the collaboration has carefully considered its options for relocating the experiment to achieve a 10% measurement of A_γ . Oak Ridge National Laboratory (ORNL) is a particularly attractive alternative to LANL by virtue of its two state-of-the-art neutron beam facilities – the upgraded High Flux Isotope Reactor (HFIR) which is currently in operation, and the Spallation Neutron Source (SNS), which is under construction. Both facilities would offer 1–2 orders of magnitude higher beam flux than is presently available at LANSCE. While HFIR management had initially offered to build a new cold neutron beam line to accommodate the NPDGamma experiment in the short term, the US DOE Office of Nuclear Physics has recently indicated a strong preference to relocate NPDGamma at the SNS as a high priority element of the SNS nuclear physics program [DOE Review of the NPDGamma Experiment, Los Alamos National Laboratory, October 5–7, 2004].

Collaborators (spokesman is underlined): M. Gericke, G. Hansen, M.B. Leuschner, B. Losowski, H. Nann, S. Santra, W.M. Snow (Indiana University); J.D. Bowman, G.S. Mitchell, S.I. Penttila, P.-N. Seo, W.S. Wilburn, V.W. Yuan (Los Alamos National Laboratory); R.D. Carlini (Thomas Jefferson National Accelerator Facility); T.E. Chupp, K.P. Coulter (University of Michigan); T.R. Gentile (National Institute of Standards and Technology); T. Case, S.J. Freedman, B. Lauss (University of California, Berkeley); T. Ino, S. Ishimoto, Y. Masuda (KEK National Laboratory, Japan); G.L. Jones (Hamilton College); M. Dabaghyan, F.W. Hersman, H. Zhu (University of New Hampshire); R.C. Gillis, S.A. Page, W.D. Ramsay (University of Manitoba); E.I. Sharapov (Joint Institute for Nuclear Research, Dubna); T.B. Smith (University of Dayton); D. Desai, G.L. Greene, R. Mahurin (University of Tennessee).

Experiment 782**Non-Fermi liquid behaviour and other novel phenomena in heavy-fermion alloys***(D.E. MacLaughlin, California, Riverside)***Penetration depth in time-reversal symmetry-breaking superconductors**

PrOs₄Sb₁₂ is a superconductor ($T_c = 1.85$ K) with a number of extraordinary properties. It is the only known Pr-based heavy-fermion superconductor, the Pr³⁺ ground state is nonmagnetic, a novel ordered phase appears at high fields and low temperatures, there are multiple superconducting phases, and time-reversal symmetry (TRS) is broken in the superconducting state. Our previous μ SR measurements of λ in the vortex state of a powdered sample found evidence for a BCS-like activated dependence at low temperatures, suggesting the absence of gap nodes. But radiofrequency (rf) inductive measurements of the surface penetration depth indicate point nodes in the gap, in disagreement with the μ SR results.

We have carried out new μ SR experiments on oriented PrOs₄Sb₁₂ crystals, and compared μ SR and “surface” penetration-depth measurements (e.g., from rf inductance measurements) in PrOs₄Sb₁₂ and a number of other superconductors. The discrepancy between these measurements noted above is found in TRS-breaking superconductors but not otherwise, and is therefore correlated with TRS breaking.

Time-differential TF- μ SR experiments were carried out at the M15 channel on a mosaic of oriented PrOs₄Sb₁₂ crystals. The crystals were mounted on a thin GaAs backing, which rapidly depolarizes muons in transverse field and minimizes any spurious signal from muons that do not stop in the sample. μ SR asymmetry data were taken for temperatures in the range 0.02–2.5 K and $\mu_0 H$ between 10 mT and 100 mT applied parallel to the $\langle 100 \rangle$ axes of the crystals. The data were fitted with the functional form $G(t) \cos(\omega t + \phi)$, where the frequency ω and phase ϕ describe the average μ^+ precession and the relaxation function $G(t)$ describes the loss of phase coherence due to the distribution of precession frequencies. The relaxation rate associated with $G(t)$ is a measure of the width of this distribution and hence of the width δB of the vortex-lattice field distribution.

Neither of the commonly-used exponential or Gaussian functional forms accurately fit the asymmetry data in the normal state, due to μ^+ coupling to both nuclear and Pr³⁺ moments. Data from both the normal and the superconducting states are well fit, however, by either of two slightly more complex functional forms:

the “power exponential”

$$G(t) = \exp[-(\Lambda t)^K], \quad (1)$$

and the damped Gaussian

$$G(t) = e^{-Wt} \exp(-\frac{1}{2}\sigma^2 t^2). \quad (2)$$

These functions are both phenomenological and have no theoretical motivation. We shall see that the superconducting-state properties obtained from these fits are similar for both functions, which indicates insensitivity to details of the fitting function and justifies *a posteriori* these otherwise arbitrary choices.

Figure 78 gives the temperature dependence of the corrected superconducting-state μ^+ relaxation rates for $\mu_0 H = 10, 20,$ and 100 mT. It can be seen that the qualitative behaviour of the rates is remarkably independent of the fit function. At 10 and 20 mT both Λ_s and σ_s are nearly temperature-independent below ~ 1 K. At the lowest temperatures the rate is field-independent to within a few per cent between 10 mT and 100 mT. In an isotropic superconductor such as cubic PrOs₄Sb₁₂, vortex-lattice disorder is expected to increase the low-field rate; increasing field (increasing vortex density) then decreases the rate as intervortex interactions stabilize the lattice. Thus the field independence of the rate indicates a substantially ordered

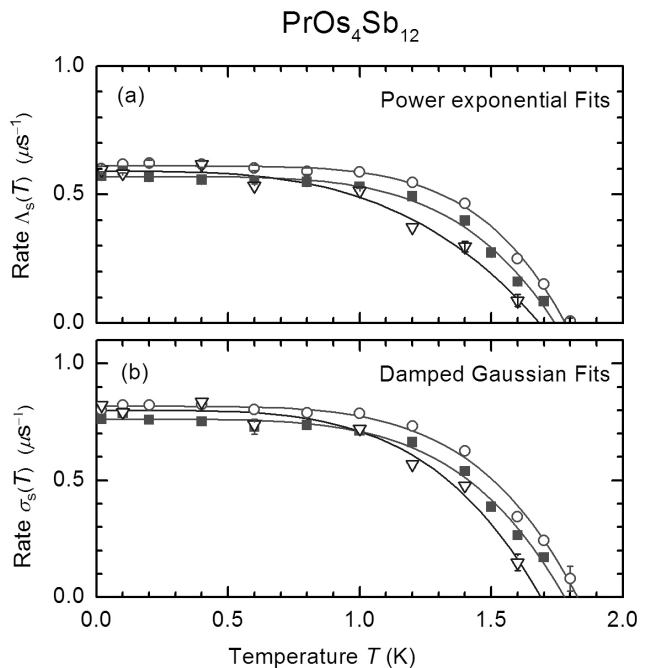


Fig. 78. Temperature dependence of superconducting-state relaxation rates in PrOs₄Sb₁₂, corrected for normal-state relaxation (see text). (a) power exponential rates Λ_s . (b) damped Gaussian rates σ_s . Circles: applied field $\mu_0 H = 10$ mT. Squares: $\mu_0 H = 20$ mT. Triangles: $\mu_0 H = 100$ mT. The curves are guides to the eye.

vortex lattice, in which case the temperature dependence of the rate is controlled solely by the temperature dependence of the vortex-lattice field distribution $P_v(B)$. We can also conclude that the field dependence expected as $H \rightarrow H_{c1}$ plays no role.

The expression

$$\delta B^2(T) = 0.00371 \Phi_0^2 \lambda^{-4}(T), \quad (3)$$

where Φ_0 is the flux quantum, relates the second moment δB^2 of $P_v(B)$ to λ for a triangular vortex lattice in the London limit. The second moment of the corresponding μ^+ frequency distribution is $\delta\omega^2 = \gamma_\mu^2 \delta B^2$, where γ_μ is the μ^+ gyromagnetic ratio. Then the μ SR estimate $\lambda_{\mu\text{SR}}$ of the penetration depth from Eq. (3) is

$$\lambda_{\mu\text{SR}} (\mu\text{m}) = 0.328 / \sqrt{\delta\omega (\mu\text{s}^{-1})}. \quad (4)$$

Now the rms width σ_s of the best-fit Gaussian is not necessarily $\delta\omega$, and replacement of $\delta\omega$ in Eq. (4) by σ_s is not completely justified. Nevertheless σ_s should scale with $\delta\omega$ and, within its range of validity, Eq. (4) should give the correct temperature dependence of $\lambda_{\mu\text{SR}}$. This is because under these circumstances effects of nonzero ξ are restricted to the high-field tail of $P_v(B)$, which is not heavily weighted in a Gaussian fit. $\text{PrOs}_4\text{Sb}_{12}$ is a strongly type-II superconductor (Ginzburg-Landau $\kappa = \lambda/\xi \approx 30$), and this picture should be applicable.

Figure 79(a) compares $\Delta\lambda_{\text{surf}}(T) = \lambda_{\text{surf}}(T) - \lambda_{\text{surf}}(0)$, obtained from rf inductance measurements in the Meissner state, with $\Delta\lambda_{\mu\text{SR}}(T)$ obtained using μ^+ relaxation rates for $\mu_0 H = 10$ mT in Eq. (4). At low temperatures the difference $\Delta\lambda_{\text{surf}}(T) - \Delta\lambda_{\mu\text{SR}}(T)$ increases markedly with increasing temperature; this

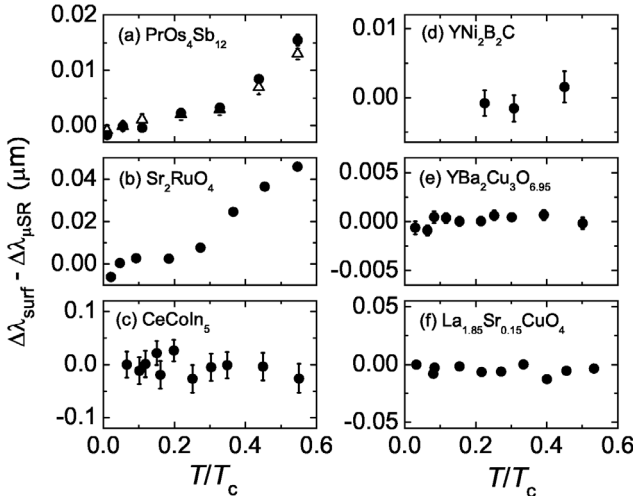


Fig. 79. Dependence of difference $\Delta\lambda_{\text{surf}} - \Delta\lambda_{\mu\text{SR}}$ (see text) on reduced temperature T/T_c in six superconductors. (a) $\text{PrOs}_4\text{Sb}_{12}$ (this work). Triangles: $\lambda_{\mu\text{SR}}$ from Λ_s (Fig. 78(a)). Circles: $\lambda_{\mu\text{SR}}$ from σ_s (Fig. 78(b)). (b) Sr_2RuO_4 . (c) CeCoIn_5 . (d) $\text{YNi}_2\text{B}_2\text{C}$. (e) $\text{YBa}_2\text{Cu}_3\text{O}_{6.95}$. (f) $\text{La}_{1.85}\text{Sr}_{0.15}\text{CuO}_4$.

is the discrepancy between the measurements noted above. It is the same whether $\Lambda_s(T)$ (Fig. 78(a)) or $\sigma_s(T)$ (Fig. 78(b)) is used in Eq. (4); the comparison does not depend on the choice of fitting function. Figure 79(b) gives $\Delta\lambda_{\text{surf}}(T) - \Delta\lambda_{\mu\text{SR}}(T)$ for the TRS-breaking superconductor Sr_2RuO_4 , using data from the literature. Again there is a discrepancy, which is very similar to that in $\text{PrOs}_4\text{Sb}_{12}$. Small-angle neutron diffraction experiments also found a temperature-independent vortex-lattice field distribution in Sr_2RuO_4 at low temperatures.

Figures 79(c)–(f) give $\Delta\lambda_{\text{surf}}(T) - \Delta\lambda_{\mu\text{SR}}(T)$ from literature data for the heavy-fermion compound CeCoIn_5 , the borocarbide $\text{YNi}_2\text{B}_2\text{C}$, and the high- T_c cuprates $\text{YBa}_2\text{Cu}_3\text{O}_{6.95}$ and $\text{La}_{1.85}\text{Sr}_{0.15}\text{CuO}_4$. None of these superconductors exhibit TRS breaking, and none exhibit the temperature dependence of $\Delta\lambda_{\text{surf}} - \Delta\lambda_{\mu\text{SR}}$ seen in Figs. 79(a) and (b). There is a significant difference between $\Delta\lambda_{\text{surf}}(T)$ and $\Delta\lambda_{\mu\text{SR}}(T)$ only for the TRS-breaking superconductors $\text{PrOs}_4\text{Sb}_{12}$ and Sr_2RuO_4 . This is in spite of a wide range of experimental methods and analysis techniques. In Figs. 79(a), (b), (c) and (f) $\Delta\lambda_{\text{surf}}$ was obtained from rf measurements, in (d) from magnetization, and in (e) from microwave impedance; in Figs. 79(a) and (c) $\lambda_{\mu\text{SR}}$ was obtained from Eq. (4), in (b), (e) and (f) from fits to the expected vortex-state field distribution, and in (d) from a generalization of Eq. (4) to low and high fields.

The origin of this discrepancy and its relation to TRS breaking is not clear. Low-field, low-temperature phase transitions between superconducting states have been reported in both $\text{PrOs}_4\text{Sb}_{12}$ and Sr_2RuO_4 , and may be involved in the discrepancy. The TRS-breaking state may couple to rf or microwave fields, necessitating a revised interpretation of the surface measurements. A mechanism of this sort, in which subgap chiral surface states affect the surface penetration depth, has been proposed for Sr_2RuO_4 . A T^2 power law is found for surface measurements even though the bulk energy spectrum is gapped. The theory requires $\lambda \approx \xi$, however, and thus seems inapplicable to $\text{PrOs}_4\text{Sb}_{12}$. It has also been noted that surface scattering breaks pairs in an odd-parity superconductor. To our knowledge the surface penetration depth has not been calculated taking this effect into account, but pair breaking would decrease the gap and therefore increase the temperature dependence of λ . The discrepancy might be related to a breakdown of the relation $\delta B(T) \propto 1/\lambda^2$ due to non-linear/nonlocal effects, or to the spontaneous magnetic field in the vortex state (although the measured field is not large enough to have a significant direct effect on δB).

Sr_2RuO_4 and $\text{PrOs}_4\text{Sb}_{12}$ are both TRS-breaking superconductors but are otherwise very different. Tetragonal Sr_2RuO_4 is an anisotropic transition-metal-oxide superconductor that is weakly type-II for $\mathbf{H} \parallel \mathbf{c}$ ($\kappa_{ab} = 2.3$), whereas cubic $\text{PrOs}_4\text{Sb}_{12}$ is an isotropic strongly type-II heavy-fermion superconductor. The fact that a similar discrepancy between μSR and surface measurements of $\lambda(T)$ is found in such different materials, but not in a variety of non-TRS-breaking superconductors, strongly suggests that TRS breaking is involved.

Experiment 815, 816, 817, 897 and 913

β -NMR

(W.A. MacFarlane, UBC)

The development of β -NMR at ISAC is one of the major efforts at TRIUMF to employ radioactive ion beams in the fields of condensed matter and materials science. These experiments use implanted beta radioactive ions as NMR (nuclear magnetic resonance) probes of local magnetic fields in materials. The beam energies at ISAC are such that 1) the ions penetrate at most a few hundred nanometres (nm) into conventional solids and 2) it is possible to electrostatically decelerate the incident beam (by biasing the target at a high voltage) to vary the implantation depth down to the level of a few nm. Thus many technologically relevant and scientifically interesting phenomena occurring near surfaces and in synthetic thin film heterostructures can be studied with β -NMR. Moreover, there are very few competing depth-resolved probes of such effects. The β -NMR group is pursuing these questions in a variety of materials under several TRIUMF EEC proposals. Some of the recent results in these areas are highlighted below. It should be noted that simultaneously with these measurements, we have been making important technical advances in the instrumentation in order to carry out these measurements with the limited beam time available at ISAC. Some of these are detailed in the last section.

Conventional metals

As part of the initial testing and commissioning of the β -NMR spectrometer at ISAC, we have studied some simple elemental metals, for example silver [Morris *et al.*, Phys. Rev. Lett. **93**, 157601 (2004)]. These measurements are important in establishing the behaviour of the probe in simple materials, for example. There is also fundamental interest in these materials (see Expt. 815 and the new TRIUMF EEC proposal Expt. 1042). As part of this ongoing effort we recently studied a thin film of copper. The behaviour is very similar to that of Au and Ag (reported previously), but the resonances are broader, due to the copper nuclear magnetic dipoles. Similar to Au and Ag, we find a tran-

sition from a cubic interstitial site for the implanted ^8Li at low temperature to a substitutional site at higher temperature. The transition occurs at a slightly lower temperature than for Ag (see Fig. 80).

Palladium is another cubic close packed elemental metal which we have previously used to measure ^8Li spin relaxation. We have now extended these measurements to the resonances, where we find a remarkably large and negative frequency shift (see Fig. 81). This behaviour is distinct from all the other simple metals we have measured so far and is the subject of active investigation (Expt. 1042).

Niobium is an elemental superconducting metal with the body-centred cubic structure which differs from the cubic close packed structure in that there are no interstitial sites of cubic symmetry. Like the other

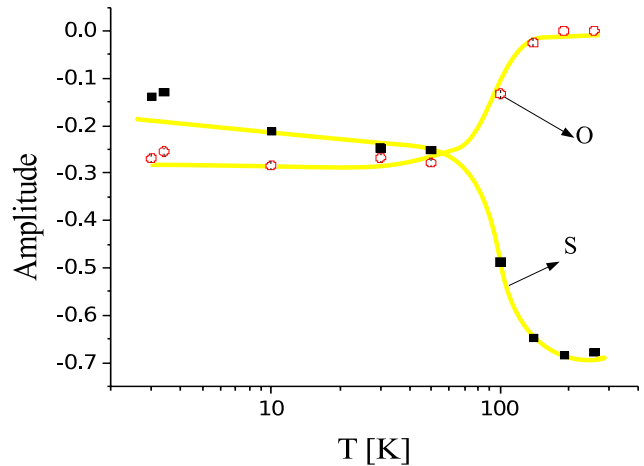


Fig. 80. The resonance amplitudes of the ^8Li implanted in a thin Cu film as a function of temperature reflecting the site transition above 100 K, from the octahedral (O) interstitial site to the substitutional (S) site.

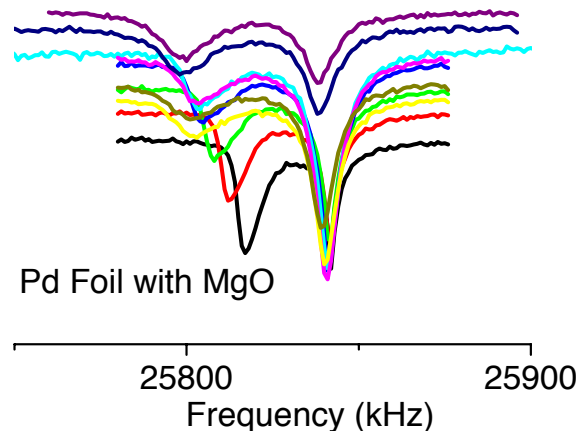


Fig. 81. The resonances of ^8Li implanted in a thin foil of Pd as a function of temperature. The foil was wrapped around a crystalline substrate of MgO and pierced with a pin. Centring the beamspot on the pinhole resulted in the composite spectrum including the MgO resonance at the right of the broader Pd resonance.

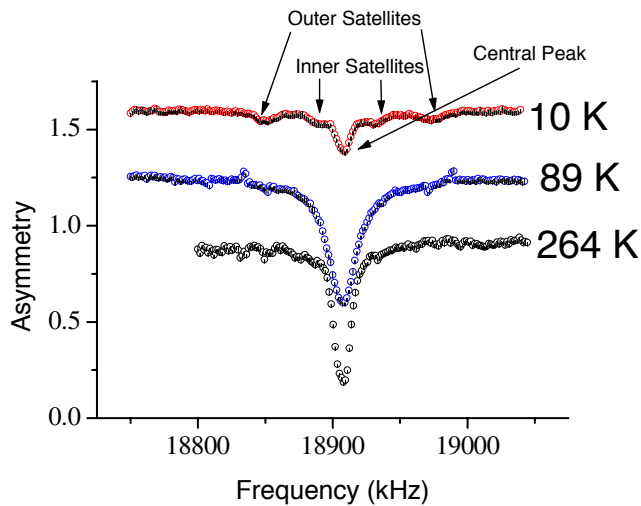


Fig. 82. The resonance of ^8Li implanted in an oriented thin film of niobium on a sapphire substrate.

elemental metals we find that the ^8Li stops in an interstitial site at low temperature, and at higher temperature it moves to a substitutional site. In niobium this situation is dramatically confirmed as the sites differ in symmetry, and, due to the electric quadrupole moment of the ^8Li nucleus, the resonance of the interstitial site is split into quadrupolar satellites (see Fig. 82). This demonstrates the potential to use the quadrupole interaction to identify the ^8Li site.

Magnetic heterostructures

As part of Expt. 815, we have been studying a variety of epitaxial metallic heterostructures of iron and silver on GaAs substrates. These kinds of structures are important as they can exhibit giant magnetoresistance and are for this reason used in magnetic storage applications. The effect is a consequence of the depth-dependent magnetic polarization of the nonmagnetic layer by the ferromagnetic layer. A detailed understanding of this polarization (which would represent a significant advance in the field) requires a depth sensitive magnetic probe such as β -NMR.

We have made preliminary studies on several structures of this type, one of which is shown schematically in Fig. 83. This structure had a thick Ag layer deposited on top of a thin magnetic Fe layer. The Ag is then capped with 20 monolayers (4 nm) of Au to protect it. In order to vary the implantation depth the sample was biased to a series of positive voltages. The implantation energy is thus the beam energy minus this bias voltage. In Fig. 84 the resonances are shown at a temperature of 280 K as a function of the bias voltage. The changes in the resonance as a function of voltage clearly show the depth sensitivity of this technique. In particular, at 25 kV the signal is primarily that of unperturbed Ag. At this bias the stopping energy (about

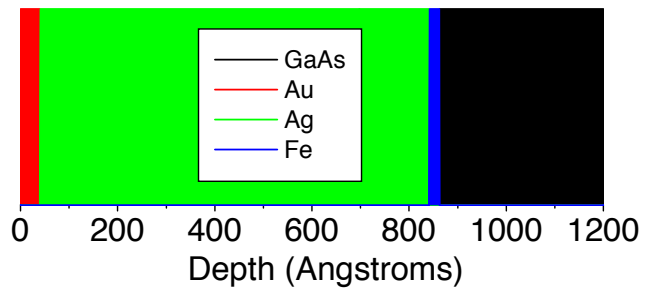


Fig. 83. A schematic of the heterostructure for which a platform bias scan is shown in Fig. 84. The thicknesses are to scale.

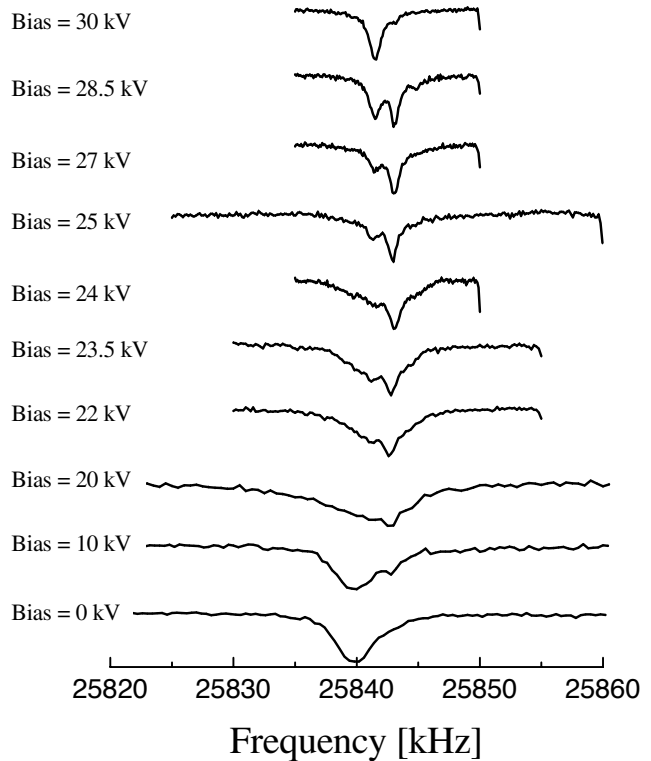


Fig. 84. A bias scan of the ^8Li resonances in the heterostructure of Fig. 83 at 280 K. As the bias goes up the implantation energy goes down. The change in the resonance with bias thus demonstrates the depth resolution of the technique.

600 eV) is such that Li stops mainly in the Ag which is too far from the Fe to be perturbed. At the maximum bias (about 100 eV implantation energy), the signal is nearly that of pure gold, i.e. we are stopping all the probe ions in a 4 nm overlayer! This sample is not the ideal geometry to study the polarizing effects of the Fe film, however, so other samples have been and will be studied. One example is shown in Fig. 85. The structure is analogous to that shown in Fig. 83, except the Ag layer is only 20 nm thick. Measurements were taken at room temperature, in an applied external field of 4.5 T, for a range of implantation energies where most of the ^8Li stops within the Ag layer. The distribution of

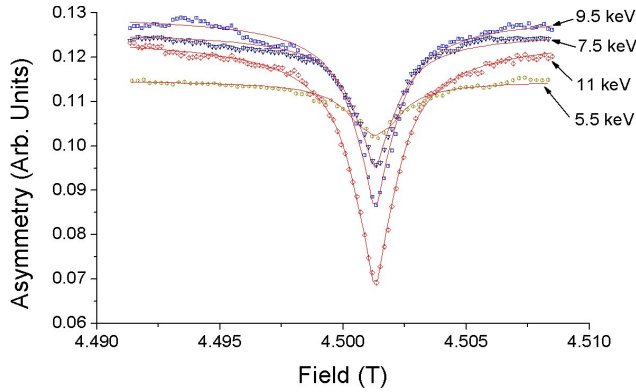


Fig. 85. The resonances as a function of implantation energy in a thin Fe/Ag heterostructure (see text) – courtesy of T.A. Keeler.

magnetic fields in the Ag layer is reflected in the resonance lineshapes in Fig. 85. The hyperfine coupling is predicted to have an oscillating spatial dependence for a perfectly sharp interface, however, roughness at the interface will introduce random phases that will tend to suppress these oscillations upon averaging over a large lateral area determined by the beam spot, several mm in diameter. Using the stopping distribution of ^8Li in the sample, and the form of the hyperfine field decay, it was possible to model the resonance and extract the form of the hyperfine field decay in the Ag layer, which was determined to be a power law $x^{-1.2}$. Detailed analysis is ongoing and will be used to compare with theory and other types of measurements.

Semiconductors

As part of Expt. 816 and Expt. 913 we have been studying high purity crystalline semiconductors. Here the implanted lithium is interesting as an electronically active impurity. Also since these materials are often used as substrates (e.g. for the magnetic heterostructures above) a proper characterization of the β -NMR will be very important for interpreting such measurements correctly.

We have made initial studies of the structure and dynamics associated with $^8\text{Li}^+$ in the semiconductors GaAs, Si and Ge. In GaAs (as previously reported) at low temperatures, the amplitude of the $^8\text{Li}^+$ resonance indicates that a large fraction (at least 70%) of the Li end up in locations with cubic symmetry (such as the tetrahedral interstitial and substitutional sites). The linewidth of the β -NMR $^8\text{Li}^+$ resonance increases dramatically above 150 K, reaches a maximum at about 290 K, and decreases again. This suggests a site-change transition for Li, probably from an interstitial to a substitutional site, at ≈ 150 K, similar to what is found in metals. The picture is similar in germanium, but the line is much narrower at all temperatures, exhibiting only a slight broadening up to room temperature. Additionally, at room temperature there appears a small

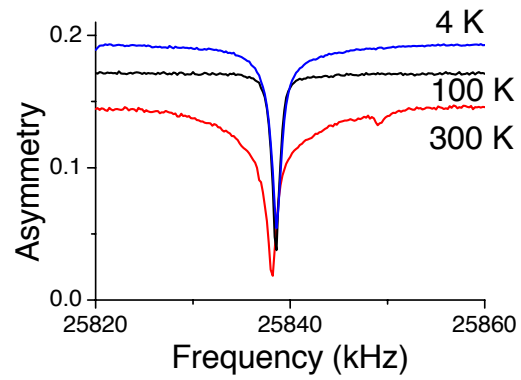


Fig. 86. The resonance of ^8Li implanted in a crystal of Ge as a function of temperature.

satellite line shifted to high frequency from the main resonance (see Fig. 86).

Superconductors

The magnetic field distribution in NbSe_2 was measured using β -detected NMR of ^8Li with a variable implantation energy of 1–30 keV. Figure 87 shows the β -NMR lineshape above and below the superconducting transition temperature ($T_c = 7.0$ K) in a magnetic field of 0.3 T parallel to the hexagonal c -axis. In the normal state at $T = 10$ K a symmetric lineshape is observed with a linewidth attributed to nuclear dipolar

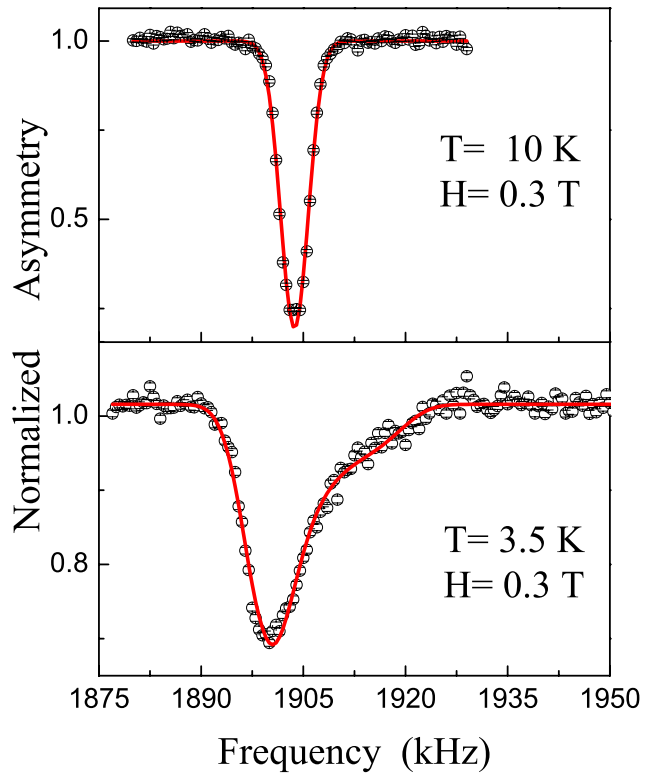


Fig. 87. β -detected nuclear magnetic resonances in NbSe_2 above and below the superconducting transition temperature of 7.0 K.

broadening from the Nb nuclear moments. Surprisingly there is no evidence for a quadrupolar splitting in the resonance even though NbSe₂ is noncubic. At $T = 0.5T_c$ (3.5 K) the characteristic lineshape from a vortex lattice is clearly evident; the peak frequency, from the region between vortices, shifts to a slightly lower frequency and a high frequency develops from the vortex core region. The lineshape was fitted to a modified London model with a Gaussian cutoff function yielding a penetration depth of 272 nm and a coherence length of 12 nm which can be compared with μ SR measurements from deeper inside the material. The dependence on implantation energy has also been studied.

While NbSe₂ is a very well studied conventional superconductor, its transition temperature is quite low. The recent discovery of high temperature “conventional” superconductivity in MgB₂ may provide another important test case. A preliminary room temperature resonance in a thin film of hexagonal MgB₂ on a sapphire substrate is shown in Fig. 88. The resonance is broad but shows no large quadrupolar effects.

β -detected nuclear quadrupole resonance

As previously reported, the first β -detected nuclear quadrupole resonances (β -NQR) of ⁸Li at zero field were observed using the newly developed β -NQR spectrometer [Salman *et al.*, Phys. Rev. **B70**, 104404 (2004)]. The resonances were detected in SrTiO₃, Al₂O₃ and Sr₂RuO₄ single crystals by monitoring the β -decay anisotropy as a function of a small audio frequency magnetic field (see Fig. 89). The resonances show clearly that ⁸Li occupies one site with non-cubic symmetry in SrTiO₃, two in Al₂O₃ and three sites in Sr₂RuO₄.

The resonance amplitude and width are surprisingly large compared to the values expected due to the transition between $2 \rightarrow 1$ spin states of the ⁸Li nuclei. The main reason for the enhanced amplitudes is the effect of small, non-axial electric field gradient, which

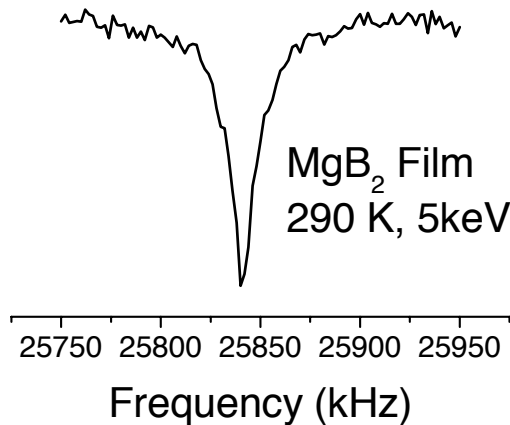


Fig. 88. The resonance lineshape of ⁸Li implanted in a thin film of MgB₂ deposited on a sapphire substrate.

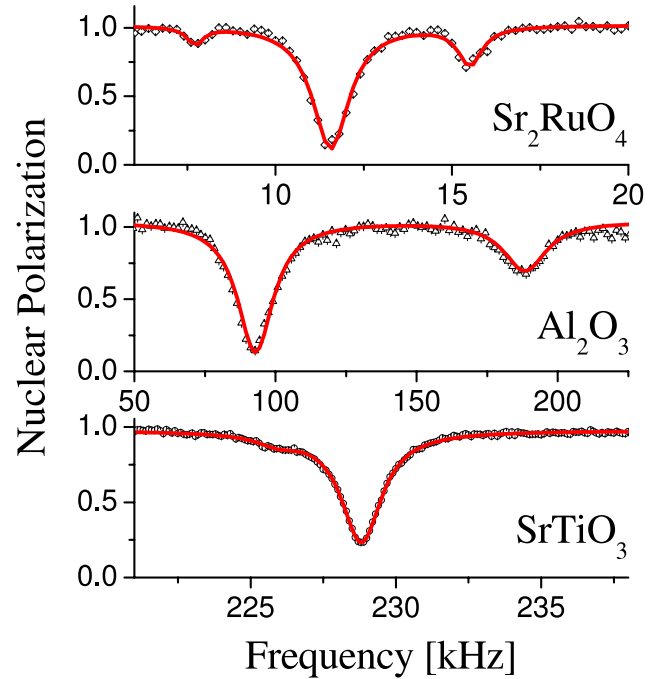


Fig. 89. β -detected nuclear quadrupole resonances in SrTiO₃, Al₂O₃ and Sr₂RuO₄ single crystals.

mixes the ± 2 and the ± 1 states, enabling a larger loss of the polarization compared to that expected with vanishing non-axial electric field gradient (i.e. without mixing of the different spin states).

Zero field μ SR measurements have proven to be very useful in studies of magnetism. Similarly, we expect that zero field β -NQR will provide a very useful addition for studies of magnetism in thin films and nano-structures.

Summary of technical advances

We have in the past several years transformed the polarimeter station into the β -NQR spectrometer, a second instrument capable of measurements in low fields up to about 150 G. This spectrometer is equipped with its own cryostat and pulsed radio-frequency magnetic system, and we are in the process of designing and implementing a deceleration system similar to the high field platform. We are moving towards near-simultaneous operation of the two spectrometers. For polarization monitoring, we have implemented the “neutral beam monitor” which intercepts the neutral ⁸Li atoms that are not reionized in the helium vapour cell at the end of the polarizer. Numerous advances have also been made in the data acquisition software, laser polarizer, detector and rf components of the spectrometer. We have also identified problems with ISAC beam stability as well as advanced our understanding of the beam dynamics near the sample. We have *in situ* capability to monitor the beamspot using a sapphire scintillating crystal and a CCD camera. We iden-

tified a problem with discharge electrons produced in the final Einzel lens in the beam line being accelerated and focused by the high magnetic field in the β -NMR spectrometer. We have recently addressed this problem with a negative ring barrier electrode in consultation with M. Olivo. Technical advances such as these will allow us to make maximal use of the scarce ISAC beam time.

Experiment 847 Electron-doped high- T_c superconductors (*J.E. Sonier, F.D. Callaghan, SFU*)

All high-temperature superconductors have an insulating antiferromagnetic (AF) phase, and have remnants of this magnetism in the superconducting phase. Determining the role magnetism plays remains the most important fundamental issue in the problem of high- T_c superconductivity. It is still unknown whether magnetism competes or cooperates with superconductivity, and whether these two phases coexist microscopically or are spatially separated. The electron-doped cuprates $R_2Ce_xCuO_{4-y}$ ($R \equiv La, Pr, Nd, Eu$ or Sm) present an interesting situation by having rare-earth moments that strongly couple to the Cu spins residing in the superconducting CuO_2 layers. One purpose of Expt. 847 has been to use the extreme sensitivity of the muon to probe the local magnetic properties of these compounds. The other goal has been to investigate the nature of the low-energy quasiparticle excitations in the vortex state, in an effort to directly address the controversial issue of the symmetry of the pairing state in this class of superconductors. This is a nontrivial task, given that there is no established phase diagram for the vortex state of electron-doped cuprates. In fact, the first direct observation of the vortex lattice in the bulk of an electron-doped superconductor was reported on just this past year [Gilardi *et al.*, Phys. Rev. Lett. **93**, 217001 (2004)]. It is worth noting that prior to this, our own sophisticated analysis of Expt. 847 data determined that the vortex lattice has the square symmetry observed in Gilardi *et al.* [*op. cit.*] by neutrons.

Given that the magnetic exchange interactions in electron-doped cuprates are anisotropic, and that accurate analysis of μ SR data in the vortex state must account for all sources of lineshape broadening, it is essential to study single crystals. It is only in recent years that single crystals of reasonable quality have been available in the sizes required for μ SR experiments.

The ground state of the Nd^{3+} ion in $Nd_{2-x}Ce_xCuO_4$ is a Kramer doublet, which is split by the interaction with the Cu spins. Doping with Ce introduces itinerant electrons, which are believed to

predominantly occupy the Cu $d_{x^2-y^2}$ orbitals of the adjacent CuO_2 plane. The Ce doping is expected to reduce the magnitude of the Cu-Nd exchange field at the Nd site, thus decreasing the splitting of the Nd-ground state doublet. To further understand the role of magnetism in NCCO, we performed zero-field μ SR measurements on an as-grown (non-superconducting) and reduced (superconducting) single crystal with near optimal Ce concentration. The single crystal exhibited a fairly sharp superconducting transition at 23 K.

In the as-grown crystal we determined that there are at least two spatially separated regions with different magnetic character. One of the regions is characterized by slow spin fluctuations, occupying an increasing volume fraction as the temperature is reduced below ~ 40 K. Below ~ 6 K, magnetic order is observed (Fig. 90). The other spatial region exhibits fast spin fluctuations down to low temperatures. The temperature dependence of the slow spin-fluctuation volume fraction suggests that the Nd-Nd and Nd-Cu exchange couplings are qualitatively similar to that found in the parent compound Nd_2CuO_4 (in which uniform magnetic order exists). In other words, in a large volume of the sample the exchange couplings are not drastically altered by Ce doping. On the other hand, Ce apparently frustrates magnetic interactions in nearby spatial regions. Thus, the two distinct magnetic regions are most likely due to the disordered spatial distribution of Nd and Ce ions.

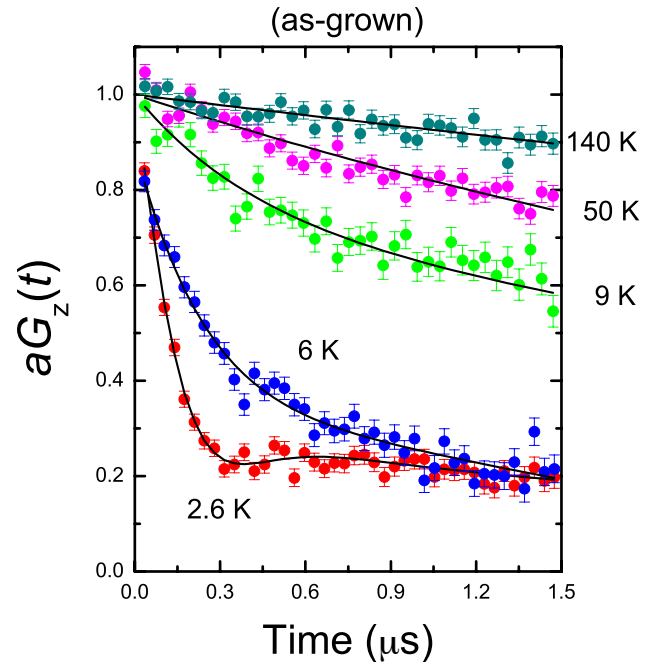


Fig. 90. Temperature dependence of the zero-field μ SR asymmetry spectrum of as-grown $Nd_{2-x}Ce_xCuO_4$.

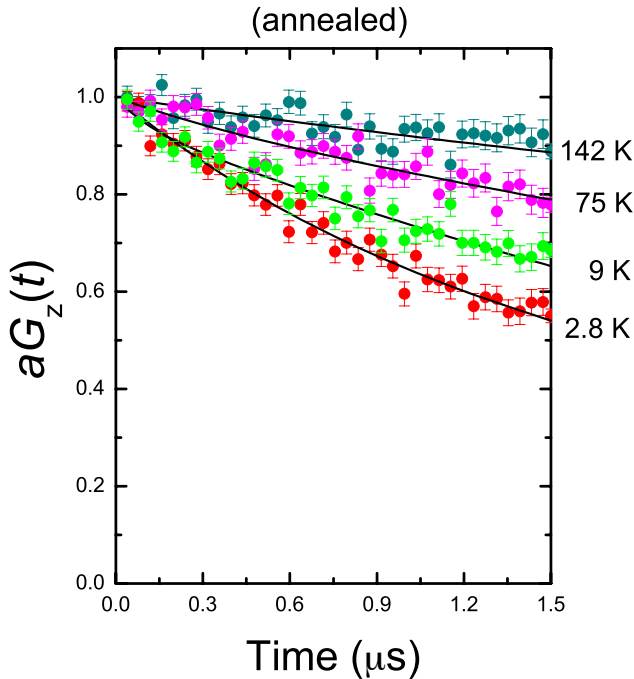


Fig. 91. Temperature dependence of the zero-field μ SR asymmetry spectrum of reduced $\text{Nd}_{2-x}\text{Ce}_x\text{CuO}_4$.

Recently, it has been determined that reduction of highly doped $\text{Nd}_{2-x}\text{Ce}_x\text{CuO}_4$ creates O(1) vacancies in the CuO_2 planes. This is contrary to the widespread belief that the reduction process removes O(3) apical oxygen [Richard *et al.*, Phys. Rev. **B70**, 064513 (2004)]. The O(1) vacancies likely affect long-range AF order. Consistent with this, after annealing the NCCO crystal we observed only fast spin fluctuations throughout the volume of the sample and no magnetic order (Fig. 91).

In transverse-field (TF) μ SR experiments on electron-doped cuprates, the rare-earth paramagnetism produces a large muon-spin depolarization rate, proportional to the strength of the applied field and inverse temperature, $1/T$. In the past, this has prevented accurate measurements of the magnetic penetration depth λ_{ab} in the vortex state. The ultimate goal of Expt. 847 is to determine the limiting low-temperature behaviour of λ_{ab} . In 2004, we carried out TF- μ SR measurements on the reduced single crystal of $\text{Nd}_{2-x}\text{Ce}_x\text{CuO}_4$ at a field of 1 kG. The field strength was chosen as a compromise between the paramagnetic broadening effects and the vortex density. A considerable amount of time has already been devoted to analyzing the data. The need to account for the paramagnetism of the Nd moments makes the task more difficult than comparable studies on hole-doped cuprates. Even so, at low temperatures we determined that the vortices form a square lattice. While a square vortex lattice is consistent with theories based on $d_{x^2-y^2}$

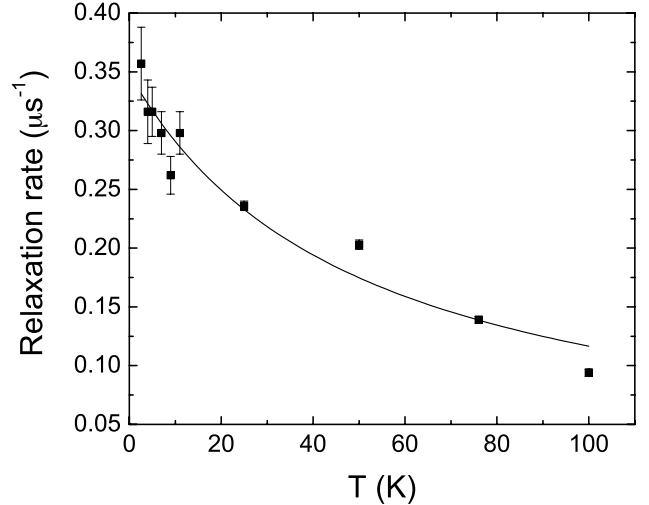


Fig. 92. Temperature dependence of the paramagnetic contribution to the lineshape in $\text{Nd}_{2-x}\text{Ce}_x\text{CuO}_4$ at $H = 1$ kG. The curve is a fit to the data assuming a Curie-Weiss temperature dependence.

superconductivity, it could also arise from strong coupling to the underlying Fermi surface (as is the case in the conventional s -wave superconductor V_3Si) or other sources of anisotropy. Recently, the square vortex lattice at low fields has been confirmed by neutron scattering [Gilardi *et al.*, *op. cit.*]. The neutron study shows that the vortex lattice at ~ 2.5 K is highly disordered in fields below 0.5 kG and above 2 kG. Thus, it seems our choice of 1 kG was ideal. However, the simplest theory function for the magnetic field distribution of a square vortex lattice contains two additional fitting parameters, and there are additional fitting parameters needed to account for the paramagnetism.

In Fig. 92 we plot the relaxation rate of the term which accounts for the paramagnetism. The data are well described by a Curie-Weiss function indicating that we have successfully extracted the paramagnetic contribution to the μ SR lineshape. In Fig. 93 we plot the temperature dependence of the magnetic penetration depth λ determined from our analysis. The data only goes up to $T = 11$ K as the asymmetry of the lineshape decreases at higher temperatures making it more difficult to fit. It can be seen that λ exhibits a steep linear temperature dependence at this field (1 kG). Although the extracted absolute values of λ are very large, a steep linear temperature dependence has recently been observed in the related compound $\text{Sm}_{2-x}\text{Ce}_x\text{CuO}_4$ (SCCO) [Prozorov *et al.*, Phys. Rev. Lett. **93**, 147001 (2004)], the physical cause of which is not yet clear. The behaviour in Fig. 92 may be related to the behaviour in SCCO, and further μ SR experiments to investigate this possibility will be undertaken later this year.

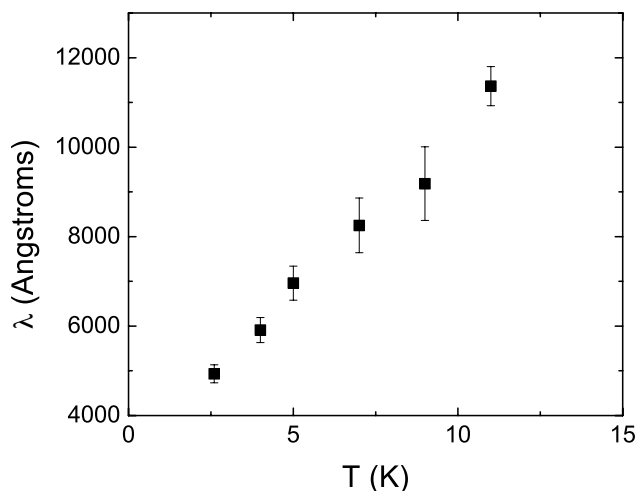


Fig. 93. Temperature dependence of the penetration depth in $\text{Nd}_{2-x}\text{Ce}_x\text{CuO}_4$ at $H = 1$ kOe.

Experiment 917

Correlation between magnetism and transport properties of thermoelectric oxides

(*J. Sugiyama, Toyota CRDL Inc.; J.H. Brewer, UBC/TRIUMF*)

Recently, a homologous series of $A_{n+2}\text{Co}_{n+1}\text{O}_{3n+3}$ ($A = \text{Ca}, \text{Sr}, \text{and Ba}$) was discovered, in which charge carrier transport is restricted mainly to a one-dimensional (1D) CoO_3 chain [Boulahya *et al.*, *J. Solid State Chem.* **142**, 419 (1999)]. Each chain is surrounded by six equally spaced chains forming a triangular lattice in the ab -plane. As seen in Fig. 94, the CoO_3 chain in the $n = 1$ compound consists of alternating face-sharing CoO_6 trigonal prisms and CoO_6 octahedra. As n increases, only the number of CoO_6 octahedra increases so as to build the chain with n CoO_6 octahedra and one CoO_6 trigonal prism.

The $n = 1$ compound, $\text{Ca}_3\text{Co}_2\text{O}_6$, in particular, has attracted much attention for the past eight years [Aasland *et al.*, *Solid State Commun.* **101**, 187 (1997); Kageyama *et al.*, *J. Phys. Soc. Jpn.* **66**, 1607 (1997)]

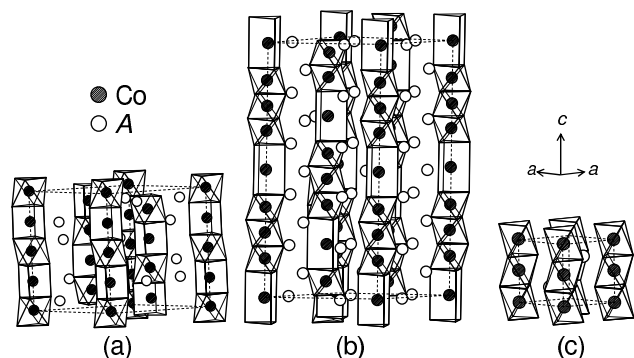


Fig. 94. Structures of the quasi one-dimensional cobalt oxides $A_{n+2}\text{Co}_{n+1}\text{O}_{3n+3}$ ($A = \text{Ca}, \text{Sr}, \text{and Ba}$). (a) $n = 1$, (b) $n = 3$ and (c) $n = \infty$.

because it is considered to be a typical quasi-1D system. It was found that $\text{Ca}_3\text{Co}_2\text{O}_6$ exhibits a transition from a paramagnetic to an antiferromagnetic state below 24 K ($= T_N$), although the magnetic structure is not fully understood even after neutron scattering studies, probably due to the competition between the intra-chain ferromagnetic (F) and inter-chain antiferromagnetic (AF) interactions. The valence state of the Co ions was assigned to be +3; also, the spin configuration of Co^{3+} ions in the CoO_6 octahedron is the low-spin (LS) state with $S = 0$ and in the CoO_6 prism the high-spin (HS) state with $S = 2$. At lower temperatures, magnetization and ^{59}Co -NMR measurements suggested the existence of a ferrimagnetic transition around 10 K [Sampathkumaran *et al.*, *Phys. Rev.* **B70**, 14437 (2004)] which, however, was not seen in the specific heat (C_p) [Hardy *et al.*, *Phys. Rev.* **B68**, 14424 (2003)]. Furthermore, the C_p measurement revealed an indication of either a short-range magnetic order or a gradual change in the spin state of Co ions at higher temperatures (100–200 K).

The other end member, BaCoO_3 ($n = \infty$), crystallizes in the hexagonal perovskite structure, in which the face sharing CoO_6 octahedra form a 1D CoO_3 chain. The chains locate on a corner of the two-dimensional triangular lattice separated by Ba ions [Takeda, *J. Solid State Chem.* **15**, 40 (1975)]. Although a weak ferromagnetic, ferrimagnetic or spin-glass-like behaviour was observed below ~ 100 K in the susceptibility [Yamaura *et al.*, *J. Solid State Chem.* **146**, 96 (1999)], so far there are no reported studies using neutron scattering, NMR or $\mu^+\text{SR}$ on BaCoO_3 .

For the compounds with $2 \leq n < \infty$, there are very limited data on physical properties, except for the structural data. Very recently, Takami *et al.* reported transport and magnetic properties for the compounds with $n = 2-5$ [Takami *et al.*, *Jpn. J. Appl. Phys.* **43**, 8208 (2004)]. According to their susceptibility (χ) measurements, there are no drastic changes in the $\chi(T)$ curve below 300 K for all these compounds, while the slope of χ^{-1} changes at around 180 K for the compounds with $n = 2$ and 3. As n increases from 1, the Co valence increases from +3 and approaches +4 with increasing n up to ∞ ; i.e., BaCoO_3 . Also the ratio between prism and octahedron in the 1D CoO_3 chain reduces from 1/1 for $n = 1$ to 0 for $n = \infty$. Further systematic research on $A_{n+2}\text{Co}_{n+1}\text{O}_{3n+3}$ is therefore needed to provide more significant information concerning the dilution effect of HS Co^{3+} in the 1D chain on magnetism. In particular, muon spin spectroscopy, as it is very sensitive to the local magnetic environment, is expected to yield crucial data in a frustrated low-dimensional system, as was the case for the 2D layered cobaltites.

$n = 1, 2, 3$ and 5 compounds

Figures 95(a)–(c) show the temperature dependences of (a) normalized A_{TF} ($N_{A_{\text{TF}}}$), (b) λ_{TF} , and (c) χ^{-1} in $\text{Ca}_3\text{Co}_2\text{O}_6$ ($n = 1$), $\text{Sr}_4\text{Co}_3\text{O}_9$ ($n = 2$), $\text{Sr}_5\text{Co}_4\text{O}_{12}$ ($n = 3$), and $(\text{Ba}_{0.5}\text{Sr}_{0.5})_7\text{Co}_6\text{O}_{18}$ ($n = 5$). The wTF- μ^+ SR spectrum below ~ 100 K was well fitted in the time domain with a combination of three signals; a slowly relaxing precessing signal caused by the applied field, a slowly non-oscillatory and a fast non-oscillatory background signal, namely:

$$A_0 P(t) = A_{\text{TF}} \exp(-\lambda_{\text{TF}} t) \cos(\omega_{\mu, \text{TF}} t + \phi_{\text{TF}}) + A_{\text{fast}} \exp(-\lambda_{\text{fast}} t) + A_{\text{slow}} \exp(-\lambda_{\text{slow}} t).$$

In order to compare the value of A_{TF} for these samples, $N_{A_{\text{TF}}}$ is defined as $N_{A_{\text{TF}}} \equiv A_{\text{TF}}(T)/A_{\text{TF}, \text{max}}$, in which $A_{\text{TF}, \text{max}}$ is the maximum value of A_{TF} . Since $A_{\text{TF}, \text{max}}$

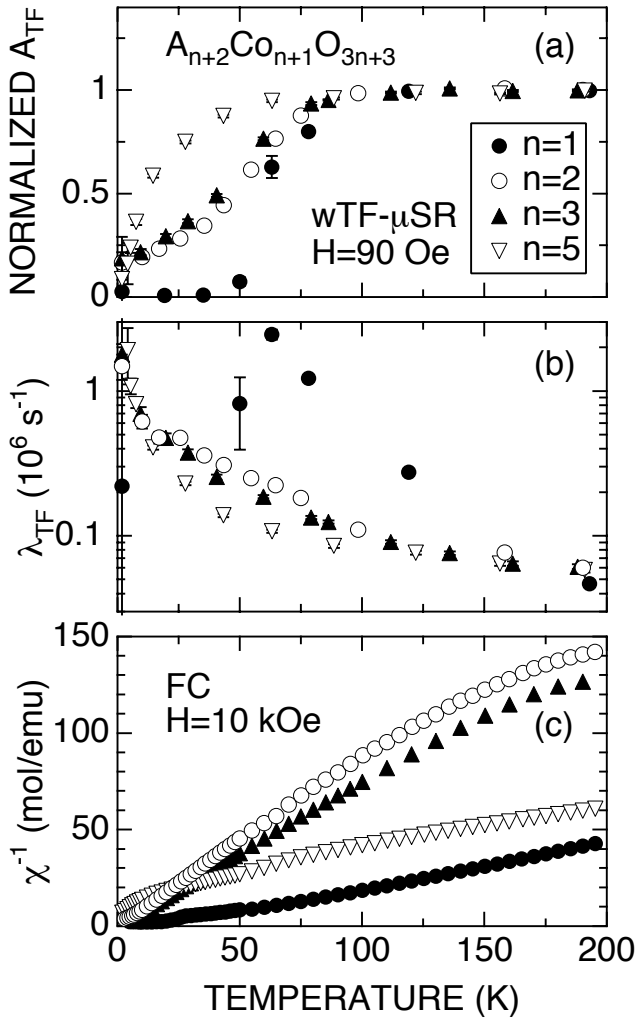


Fig. 95. Temperature dependences of (a) normalized A_{TF} , (b) λ_{TF} , and (c) inverse susceptibility χ^{-1} in $\text{Ca}_3\text{Co}_2\text{O}_6$ ($n = 1$), $\text{Sr}_4\text{Co}_3\text{O}_9$ ($n = 2$), $\text{Sr}_5\text{Co}_4\text{O}_{12}$ ($n = 3$), and $(\text{Ba}_{0.5}\text{Sr}_{0.5})_7\text{Co}_6\text{O}_{18}$ ($n = 5$).

corresponds to A_{TF} for the paramagnetic state, $N_{A_{\text{TF}}}$ is roughly equivalent to the volume fraction of the paramagnetic phase in the sample.

All four samples show the magnetic transition below 100 K; the onset temperatures of the transition (T_c^{on}) are estimated as 100 ± 25 K for $n = 1$, 90 ± 10 K for $n = 2$, 85 ± 10 K for $n = 3$ and 50 ± 10 K for $n = 5$, respectively. The magnitude of T_c^{on} is thus found to decrease with n . It should be noted that there are no marked anomalies in the $\chi^{-1}(T)$ curve measured with $H = 10$ kOe at T_c^{on} for the four compounds. Although $N_{A_{\text{TF}}}$ for the $n = 1$ compound levels off to its minimum value (~ 0) below 30 K, the $N_{A_{\text{TF}}}(T)$ curve for the other three compounds never reaches their minimum even at 1.8 K, indicating that the internal magnetic field is still fluctuating. Indeed, λ_{TF} for the samples with $n = 2, 3$ and 5 increases monotonically with decreasing T , whereas the $\lambda_{\text{TF}}(T)$ curve for $\text{Ca}_3\text{Co}_2\text{O}_6$ ($n = 1$) exhibits a sharp maximum around 55 K.

In spite of the large decrease in A_{TF} below 100 K for the samples with $n = 2, 3$ and 5 , the ZF- μ^+ SR spectra exhibit no oscillations even at 1.8 K, whereas a clear oscillation is observed in $\text{Ca}_3\text{Co}_2\text{O}_6$. Figures 96(a)–(b) show the muon precession frequency $\nu_{\text{AF}} (= \omega_{\mu, \text{AF}}/2\pi)$ and χ^{-1} in $\text{Ca}_3\text{Co}_2\text{O}_6$. The oscillating signal has a finite intensity below 27 K, while the slow exponential relaxed signal disappears below around 30 K. This

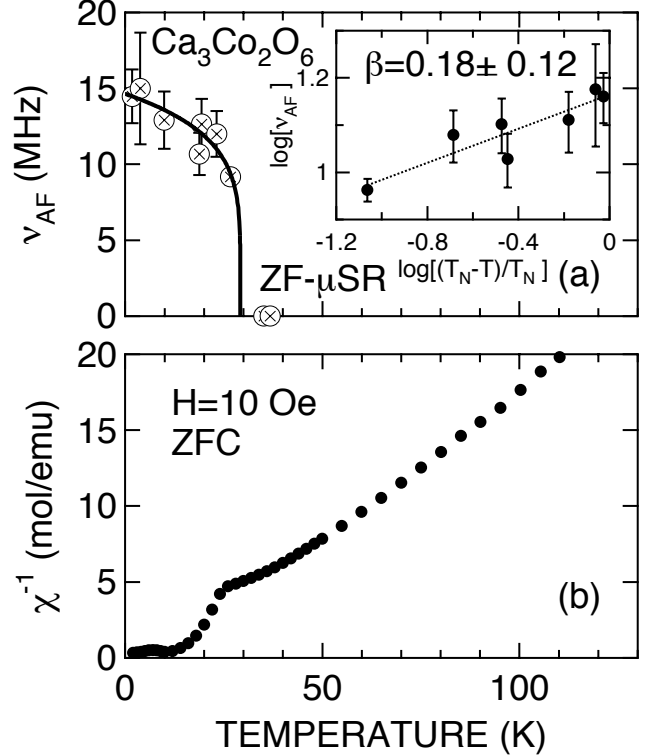


Fig. 96. Temperature dependences of (a) muon precession frequency $\nu_{\text{AF}} 2\pi = \omega_{\mu, \text{AF}}$ and (b) χ^{-1} measured in a zero field cooling mode with $H = 10$ Oe in $\text{Ca}_3\text{Co}_2\text{O}_6$.

means that the magnetic moment fluctuating at high temperatures slows down with decreasing T and then orders below 27 K, and becomes quasi-static (within the experimental time scale). The T dependence of ν_{AF} , which is an order parameter of the transition, is in good agreement with the T dependence of the intensity of the AF magnetic diffraction peak determined by a neutron experiment [Aasland *et al.*, Solid State Commun. **101**, 187 (1997)]. Actually, the $\nu_{\text{AF}}(T)$ curve is well fitted by the following expression:

$$\nu_{\text{AF}}(T) = \nu_{\text{AF}}(0\text{K}) \times \left(\frac{T_{\text{N}} - T}{T_{\text{N}}} \right)^{\beta}.$$

This provides $\nu_{\text{AF}}(0\text{K}) = 14.6 \pm 0.8\text{ MHz}$, $\beta = 0.18 \pm 0.12$, and $T_{\text{N}} = 29 \pm 5\text{ K}$. The critical exponent (β) obtained lies between the predictions for the 2D and 3D Ising models ($\beta = 0.125$ and 0.3125). The value of T_{N} is also in good agreement with the results of χ and neutron diffraction measurements ($T_{\text{N}} = 24\text{ K}$). These results confirm that muons experience the internal magnetic field due to the long-range 2D AF order.

$n = \infty$ compound, BaCoO₃

Figures 97(a)–(e) show the temperature dependences of (a) A_{TF} , (b) λ_{TF} , (c) χ^{-1} , (d) specific heat C_{p} , and (e) its temperature derivative dC_{p}/dT for BaCoO₃ ($n = \infty$). Both A_{TF} and λ_{TF} were obtained by fitting the wTF- μ^+ SR spectra, the same way as the compounds with $n = 1-5$. The $\chi^{-1}(T)$ curve indicates the existence of an AF transition at 14 K ($= T_{\text{N}}$) with $H = 10\text{ kOe}$, but a weak F or ferrimagnetic behaviour below 53 K with $H = 100\text{ Oe}$. Also, the $C_{\text{p}}(T)$ curve shows a sharp maximum at 15 K, indicating the existence of a magnetic transition. However, at around 53 K, there are no clear anomalies in the $C_{\text{p}}(T)$ curve, although the slope (dC_{p}/dT) increases slightly around 50 K with decreasing T . The lack of a clear anomaly around 50 K in the $C_{\text{p}}(T)$ curve suggests that the transition at 53 K is induced by the 1D F order, as in the case for the 1D F order in Ca₃Co₂O₆.

The wTF- μ^+ SR experiment with 90 Oe shows that as T decreases from 100 K, A_{TF} drops suddenly down to ~ 0 at T_{N} , indicating that the whole sample enters into an AF state. Such abrupt change in A_{TF} is very different from those for the other quasi-1D cobalt oxides with $n = 1-5$, which typically show a large transition width of 50–80 K. On the other hand, the $\lambda_{\text{TF}}(T)$ curve exhibits a small increase below $\sim 50\text{ K}$ with decreasing T , probably associated with the complicated magnetism observed in χ with low magnetic fields. As T decreases further from 50 K, λ_{TF} increases rapidly below 17 K, showing typical critical behaviour towards T_{N} .

The ZF- μ^+ SR spectrum at 1.7 K exhibits a clear but complex muon spin oscillation, displayed in

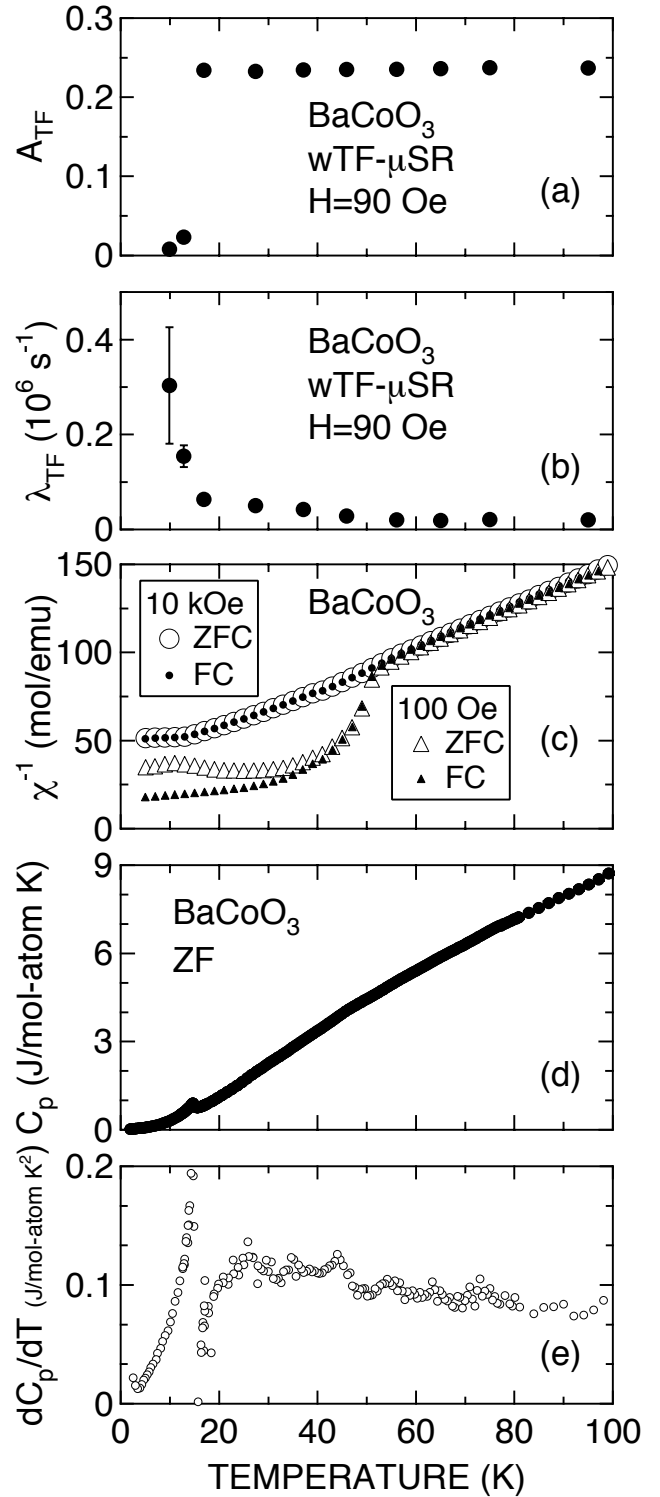


Fig. 97. Temperature dependences of (a) weak transverse field asymmetry A_{TF} , (b) exponential relaxation rate λ_{TF} , (c) inverse susceptibility χ^{-1} , (d) specific heat C_{p} , and (e) its temperature derivative dC_{p}/dT for BaCoO₃ ($n = \infty$). χ was measured with magnetic field $H = 10\text{ kOe}$ and 100 Oe in both zero-field cooling (ZFC) and field cooling (FC) mode.

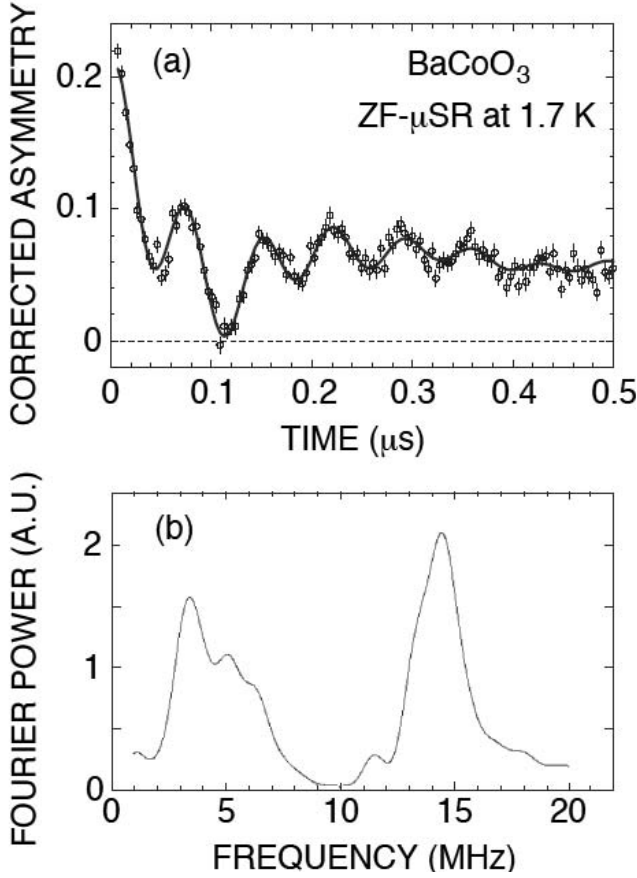


Fig. 98. (a) ZF- μ^+ SR spectrum for BaCoO₃ ($n = \infty$) at 1.7 K and (b) Fourier transform of (a).

Fig. 98(a). The Fourier transform of the ZF- μ^+ SR time spectrum indicates that the ZF- μ^+ SR spectrum has five frequency components ($\nu_\mu = 14.4, 13.5, 6.4, 5.1$ and 3.5 MHz), even though the sample is structurally single phase at room temperature and there is no indication of any structural phase transition down to 77 K in resistivity (ρ) and thermopower (TEP) measurements; nor are there any anomalies in the $\chi(T)$ curve down to 4 K, except around T_N . The ZF-spectra were well fitted by the following equation:

$$A_0 P(t) = \sum_{i=1}^5 A_{AF,i} \exp(-\lambda_{AF,i}t) \cos(\omega_{\mu,i}t + \phi) + \sum_{i=1}^2 A_i \exp(-\lambda_i t),$$

where A_0 is the empirical maximum experimental muon decay asymmetry, $A_{AF,i}$ and $\lambda_{AF,i}$ ($i = 1-5$) are the asymmetries and exponential relaxation rates associated with the five oscillating signals, and A_i and λ_i ($i = 1$ and 2) are the asymmetries and exponential relaxation rates of the two non-oscillating signals (for the muon sites experiencing fluctuating magnetic fields).

Summary

Magnetism of quasi one-dimensional (1D) cobalt oxides $A_{n+2}Co_{n+1}O_{3n+3}$ ($A = Ca, Sr$ and Ba , $n = 1, 2, 3, 5$ and ∞) was investigated by susceptibility (χ) and muon spin rotation and relaxation (μ^+ SR) measurements using polycrystalline samples, at temperatures from 300 K down to 1.8 K. The χ measurement confirmed a systematic change in the charge and spin distribution in the 1D CoO₃ chain with n . The weak transverse field (wTF-) μ^+ SR experiments showed the existence of a magnetic transition in all five samples investigated. The onset temperature of the transition (T_c^{on}) was found to decrease with n ; that is, 100 ± 25 K, 90 ± 10 K, 85 ± 10 K, 50 ± 10 K, and 15 ± 1 K for $n = 1, 2, 3, 5$, and ∞ , respectively. In particular, for the samples with $n = 2-5$, T_c^{on} was detected only by the present μ^+ SR measurements. A muon spin oscillation was clearly observed in both Ca₃Co₂O₆ ($n = 1$) and BaCoO₃ ($n = \infty$), whereas only a fast relaxation is apparent even at 1.8 K in the other three samples ($n = 2, 3$ and 5).

A large negative paramagnetic Curie temperature for the samples with $n = 2$ and 3 indicated that the transition at T_c^{on} is caused by an inter-chain two-dimensional (2D) antiferromagnetic (AF) interaction. Considering the structural similarity among the quasi 1D cobalt oxides, the transitions at T_c^{on} for the samples with $n = 1$ and 5 were therefore most likely due to the appearance of the short-range 2D AF order. This suggested that the 1D ferromagnetic order in the CoO₃ chain of Ca₃Co₂O₆ ($n = 1$) would occur at higher temperatures (~ 200 K) than proposed previously (~ 80 K).

For BaCoO₃ ($n = \infty$), the χ measurement confirmed that $T_c^{\text{on}} = T_N = 15$ K and $T_C = 53$ K, which corresponds to the ferromagnetic (F) transition caused by an intra-chain 1D interaction. Nevertheless, the wTF-asymmetry (A_{TF}) did not exhibit a marked anomaly at T_C , while A_{TF} is very sensitive to the formation of magnetic order. This is likely to be caused by a domain motion in the 1D chain, as in the case for CsCoCl₃. In spite of the fact that the sample is structurally homogeneous, the ZF- μ^+ SR spectrum showed a complex of at least five frequency components below T_N , which require further detailed studies.

Experiment 932

Improving μ^- SR performance

(*J.H. Brewer, UBC/TRIUMF*)

The surface μ^+ beams that now dominate most applications of μ SR can be “spin-rotated” using Wien filters to orient the muon spins perpendicular to their momenta, thus allowing injection of the beam into arbitrarily high magnetic fields parallel to the momenta

but still perpendicular to the spin polarization. Unfortunately, there are no surface μ^- beams, because negative pions stopping in the production target are immediately captured by positive nuclei. All polarized negative muon beams come from “decay channels” in which the π^- decays in flight. Even “backward” muons generally have higher momentum than the surface μ^+ from π^+ decay at rest, so no “spin rotators” exist for negative muon beams.

In 2004 it was discovered that TRIUMF’s M9B superconducting muon channel can be tuned to produce a substantial (roughly 50%) transverse spin polarization in its backward μ^- beam. Although this was not among the new μ^- -SR techniques originally proposed for Expt. 932, it represents a significant advance for transverse field (TF)- μ^- -SR, one of whose disadvantages relative to TF- μ^+ -SR has previously been its limitation to weaker transverse magnetic fields.

We have utilized this new capability to make improved TF- μ^- -SR measurements of several fundamental phenomena. The magnetic field strength was limited to about 2 T in this experiment by our time resolution of ~ 1 ns (which must be a small fraction of the muon precession period) and by the large radius of the cylinder formed by the electron counters (decay electrons have a radius of curvature of about 5 cm at 2 T and may not reach the detectors at higher fields). Neither of these limitations is intrinsic, but the miniaturization required to go to larger fields conflicts with the sample thickness required to stop backward muons, so it would be difficult to work at fields higher than about 5 T.

Relativistic shifts of g_μ in muonic atoms

A lepton bound in a deep Coulomb potential experiences a relativistic shift of its spin precession frequency in a magnetic field. This effect was first calculated by Breit in 1928 assuming pointlike nuclei, and later improved upon by Margeneau and later by Ford *et al.* in papers accompanying the first experimental measurements of such shifts for negative muons. Subsequent measurements of bound μ^- frequency shifts were made by Yamazaki *et al.* in heavier muonic atoms where the finite size of the nucleus is comparable to the mean radius of the muon wavefunction, causing the relativistic shift to level off toward a constant value as a function of atomic number. Since then there have been few measurements or calculations, except for some recent experiments by Mamedov *et al.*, in which Yamazaki’s experimental result for $\text{Cd}\mu^-$ atoms was called into question.

We have now remeasured many of these shifts in a 2 T magnetic field. The “raw” fitted frequencies are given in Table XIV.

Table XIV. Measured frequencies in a constant magnetic field. Only statistical uncertainties are exhibited in this table, to illustrate that the potential accuracy of this technique is much higher than we have achieved in this modest effort.

Sample	Frequency (MHz)
μ^+ in graphite	271.69888 ± 0.00072
μ^+ in Al metal	271.58520 ± 0.00038
μ^- on ^{12}C (graphite)	271.3684 ± 0.0016
μ^- on ^{16}O (H_2O)	271.258 ± 0.010
μ^- on ^{24}Mg (metal)	270.9259 ± 0.0027
μ^- on ^{28}Si	270.6502 ± 0.0069
μ^- on ^{32}S (powder)	270.406 ± 0.008
μ^- on ^{40}Ca (metal)	270.164 ± 0.069
μ^- on Ti (metal)	269.719 ± 0.066
μ^- on Zn (metal)	268.440 ± 0.072
μ^- on Cd (metal)	$265.73^{+0.46}_{-0.57}$
μ^- on Pb (metal)	$264.50^{+0.59}_{-0.62}$

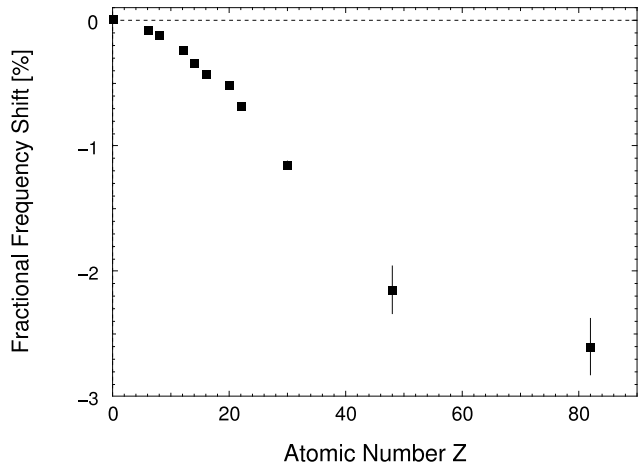


Fig. 99. Fractional shifts of bound μ^- spin precession frequencies in various muonic atoms, relative to the μ^+ precession frequency in vacuum, assuming a μ^+ Knight shift of $+80 \pm 4$ ppm in Al, which was used as a reference.

All samples were measured in a transverse magnetic field of 2 T. Unlike those in Table XIV, the error bars shown in Fig. 99 include all known systematic uncertainties, but not diamagnetic or paramagnetic shifts, hyperfine anomalies or other phenomena. The largest systematic uncertainty arises from the dependence of the field on the position in the magnet combined with the finite range straggling of the beam. This was estimated using positive muons by intentionally moving a graphite sample back and forth several cm along the beam direction, producing a frequency shift on the order of 20 ppm per cm at the point of steepest slope within the sample region. For dense samples, the muon stopping position could be controlled with confidence only to within about 1 cm, so the purely statistical uncertainties shown in Table XIV have been added

in quadrature with a systematic uncertainty of about 0.006 MHz to obtain the net uncertainties shown in Fig. 99.

Further work is required to convert our raw data into corrected magnetogyric ratios that can be critically compared with the predictions of theory. A thorough analysis of these corrections is beyond the scope of this Annual Report. We are therefore not in a position to make a definitive statement about the relativistic shift in $\text{Cd}\mu^-$ where the disagreement between previous measurements is largest. However, such corrections would have to account for more than half the net shift in cadmium to bring it into agreement with the $(0.67 \pm 0.22)\%$ value claimed by Mamedov *et al.*

We invite others to make free use of the improved precision of our measurements.

Hyperfine transition in $^{23}\text{Na}\mu^-$

When a negative muon reaches the $1s$ ground state of a muonic atom with a nucleus of non-zero spin, it experiences a strong hyperfine (HF) interaction with that nucleus; for heavier odd- A nuclei the effective HF magnetic field can be as high as 5×10^{10} T. This HF coupling makes the total spin $F^\pm = I \pm \frac{1}{2}$ an exceedingly good quantum number. If the muonic atom forms initially in the lower HF state (which will be the F^- state as long as the nuclear magnetic moment is positive), it will remain in that state and precess at the corresponding characteristic frequency ω_- in a transverse magnetic field until the muon decays or captures. The upper (F^+) state, however, is subject to radiative or (much more often) Auger transitions to the F^- state, which in heavy elements is $\sim\text{keV}$ lower. (The radiative lifetime is much longer than that of the muon.) This Auger-mediated transition rate, R , was calculated for numerous nuclei by Winston, who also made the first direct measurement of $R_F = 6.1 \pm 0.7 \mu\text{s}^{-1}$ in muonic ^{19}F .

In lighter nuclei, especially those consisting of an odd proton outside a closed shell, the weak capture rate from one HF state is usually much faster than that from the other, reflecting the “ $V - A$ ” character of the weak nuclear current. Precise measurements of these differences offer access to the induced pseudoscalar coupling constant at large q^2 . In addition, they provide a superior method for direct determination of the HF transition rate R , since the rate of “neutrals” (photons and neutrons) from muon capture can actually increase with time if the slow-capturing HF state de-excites to the fast-capturing HF state. (The opposite situation will cause a neutrals rate that decreases more rapidly than the muon decays – which is also easy to interpret, but somehow seems less miraculous.) Such measurements thus inform us simultaneously of R and the differential capture rate.

If the F^+ and F^- capture rates are small or similar, or if R is very slow, it is often easier to measure R independently by observing the decay in time of the asymmetry of muon decay electrons in the F^+ state. As long as $R < \omega_+$ (the characteristic precession frequency of the F^+ state in a transverse magnetic field) it is easy to distinguish this asymmetry from that of the F^- state or various backgrounds; this “ μ^- -SR method” was used by Favart *et al.* in 1970 to measure R_B in muonic ^{10}B and ^{11}B and to set upper limits on R in muonic ^6Li , ^7Li and ^9Be . That experiment established a new standard for μ^- -SR measurements of R ($< 0.02 \mu\text{s}^{-1}$ in muonic Li) and is unlikely to be much improved upon by that method, since spin relaxation by dipolar fields from neighbouring nuclei should have a rate $\sim 0.01 \mu\text{s}^{-1}$. A more recent experiment by Wiaux *et al.* overcame that limitation by directly observing the 320 keV γ -ray from the excited state of ^{11}Be created by nuclear muon capture on ^{11}B , an effect independent of dipolar relaxation. In this way they measured $R = 0.181 \pm 0.017 \mu\text{s}^{-1}$ in muonic ^{11}B .

For $R > \omega_+$ it is sometimes feasible to measure R by a “residual polarization” method where the dephasing of the muon polarization (due to the exponential distribution of HF transition times) is measured as a function of magnetic field. This method was used to determine $R_{\text{Al}} = 41 \pm 9 \mu\text{s}^{-1}$ in muonic ^{27}Al , in embarrassingly good agreement with Winston’s prediction.

When $R \sim \omega_+$, one can use the μ^- -SR method only if ω_+ is increased by applying a stronger magnetic field. For the HF transition rate of muonic ^{23}Na , where Winston predicted $R_{\text{Na}} \approx 14 \mu\text{s}^{-1}$, this requires a transverse magnetic field of ~ 1 T or higher, in which the radius of curvature of 60 MeV/ c muons is ~ 2 m or less, causing deflection of the muon beam relative to its path in weak fields. As a result, the entire experiment must be designed and reconfigured for each target magnetic field, drastically reducing the versatility of the apparatus. This is one reason why no previous μ^- -SR measurements have been made of R_{Na} in muonic ^{23}Na .

In 2002 we made a preliminary measurement in a magnetic field of 0.7 T where a precession signal from the F^+ HF state of muonic ^{23}Na was just detectable for about one full period. That measurement gave a tentative value of $R_{\text{Na}} = 13 \pm 4 \mu\text{s}^{-1}$, consistent with Winston’s prediction.

We have now made a more precise measurement in a transverse magnetic field of 2 T, using the newfound transverse polarization of M9B.

Combining this new value of R_{Na} with our previous preliminary measurement gives a best experimental estimate of $R_{\text{Na}} = 13.7 \pm 2.2 \mu\text{s}^{-1}$. This result is quite consistent with that measured by Gorrings *et al.* in

metallic sodium ($15.1 \pm 1.1 \mu\text{s}^{-1}$) by observing characteristic γ -rays from ^{23}Ne (a product of μ^- nuclear capture), but less so with their previous result in NaF ($8.4 \pm 1.9 \mu\text{s}^{-1}$), and even less with the measurements of Stocki *et al.* who found $R = 38 \pm 9 \mu\text{s}^{-1}$ in Na metal and $R = 28 \pm 5 \mu\text{s}^{-1}$ in NaH using the time dependence of capture neutrons. The latter three numbers disagree significantly with Winston’s prediction of $R_{\text{Na}} \approx 14 \mu\text{s}^{-1}$.

It has been suggested that the HF transition rate may be altered by processes that depend on the chemical environment. One possibility would be delayed refilling of vacant electronic orbitals in insulating materials. A related medium-dependent mechanism might be external Auger.

The fitted frequencies of the F^+ and F^- states can be compared with the μ^+ frequency in aluminum at the same field, namely 271.5852 ± 0.0004 MHz. Correcting for a $+80 \pm 4$ ppm Knight shift in the latter gives a reference frequency of 271.5635 ± 0.0012 MHz. Comparing ω_{\pm} with this reference gives $\omega_+/\omega_{\mu} = 0.1878 \pm 0.0012$ and $\omega_-/\omega_{\mu} = -0.3534 \pm 0.0001$, in good agreement

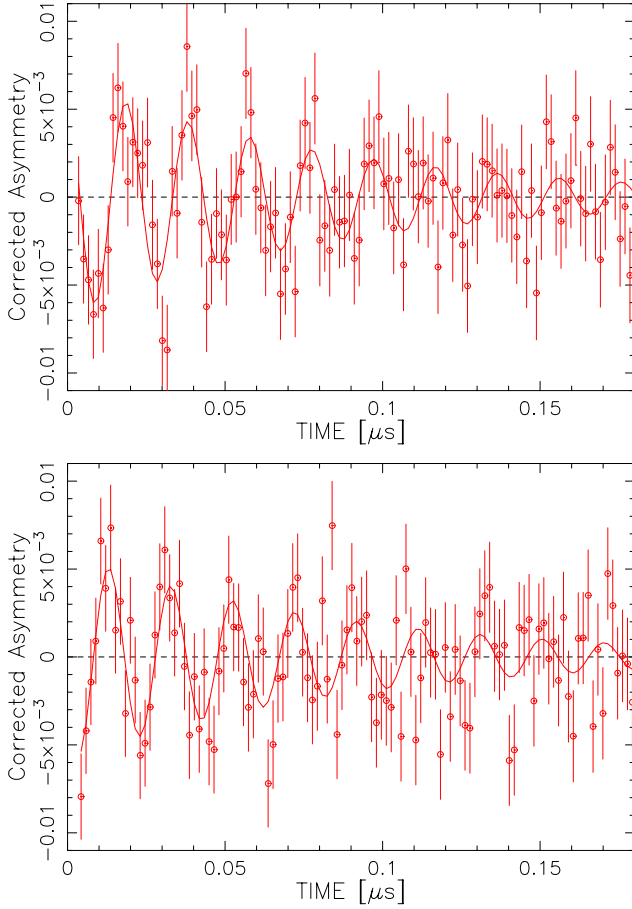


Fig. 100. “Real” (top) and “imaginary” (bottom) parts of the precession signal of the F^+ hyperfine state in muonic ^{23}Na , showing the rapid decay into the F^- state.

with the frequencies predicted by simply combining the spins and magnetic moments of the muon and the nucleus, namely $\omega_+/\omega_{\mu} = 0.18765$ and $\omega_-/\omega_{\mu} = -0.35392$. The F^+ signal disappears within a few hundred ns but is visible in all four histograms; it is displayed in Fig. 100 with two histograms combined at a time to form the “real” (top) or “imaginary” (bottom) parts of the precession signal. This serves to reduce the statistical scatter for display purposes; the global fit to all four histograms simultaneously was used for the final results in Table XV.

Figure 101 shows the much smaller but longer-lived signal from the F^- state. For the figure, the complex asymmetry spectra were transformed into a reference frame rotating at a frequency slightly lower than ω_- and then packed to much coarser bins; this again serves to clearly display a signal that is otherwise (in the lab frame) invisible to the eye.

The signal amplitudes (muon decay asymmetries) can be compared with that of the positive muon in aluminum at the same field, $A_0 = 0.133 \pm 0.001$, to give the products of the residual μ^- polarizations P_{\pm} and the fractional populations f_{\pm} of the two HF states: $f_+P_+ = A_+/A_0 = 0.0638 \pm 0.0083$ and $f_-P_- = A_-/A_0 = 0.0090 \pm 0.0015$. These numbers have not been corrected for the frequency dependence of the observed asymmetry; due to the finite time resolution of the detectors, higher frequency signals suffer an amplitude reduction. The reference asymmetry A_0 is therefore suppressed slightly, so that f_+P_+ and f_-P_- are slightly overestimated. For comparison, the asymmetry

Table XV. Results of fitting μ^- SR spectra in metallic sodium at 2 T. Only the physically relevant parameters are shown and only statistical uncertainties are given. Here τ_{Na} is the muon lifetime in muonic ^{23}Na , A^{\pm} is the muon decay asymmetry in the F^{\pm} HF state of muonic ^{23}Na , R is the $F^+ \rightarrow F^-$ HF transition rate, ω_{\pm} is the precession frequency of the F^{\pm} state, ϕ_i^{\pm} is the apparent initial phase of the precession in the F^{\pm} state and Λ is the spin relaxation rate of the F^- state, presumably caused by a combination of spatial inhomogeneity of the applied field, random fields from nearby magnetic moments and the effect of local electric field gradients on the ^{23}Na electric quadrupole moment. The asymmetric errors in R are returned by the MINOS command in MINUIT.

τ_{Na}	=	$(1.1955 \pm 0.0012) \times 10^{-6}$ s
A^+	=	0.00848 ± 0.0011
R	=	$(13.97^{+2.9}_{-2.4}) \times 10^6$ s $^{-1}$
ω_+	=	$2\pi \times (51.0 \pm 0.3$ MHz)
ϕ_+	=	$-18.6^\circ \pm 11^\circ$
A^-	=	0.0012 ± 0.0002
Λ	=	$(0.024 \pm 0.1) \times 10^6$ s $^{-1}$
ω_-	=	$2\pi \times (-95.9676 \pm 0.015$ MHz)
ϕ_-	=	$-175.4^\circ \pm 13.4^\circ$

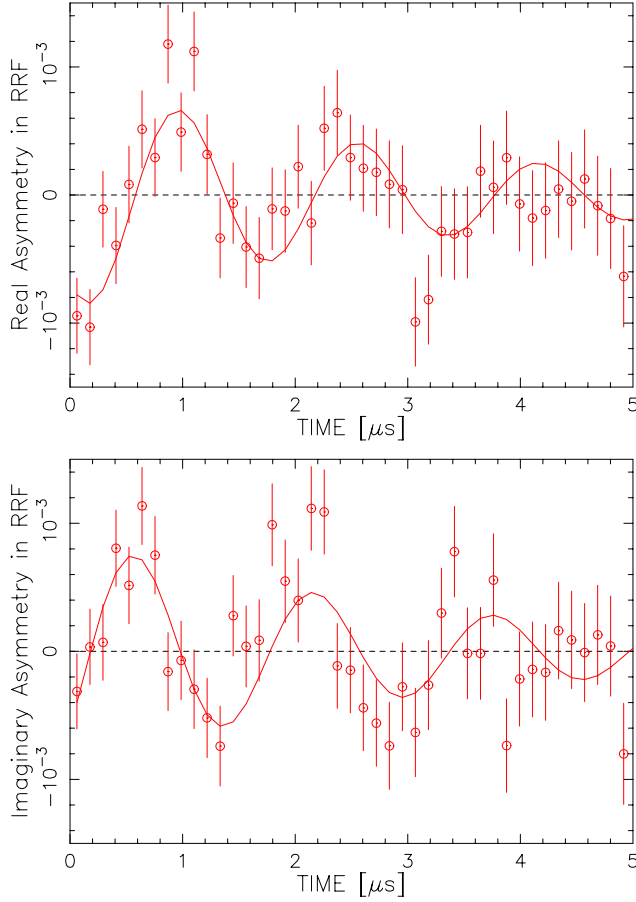


Fig. 101. Precession signal of the F^- hyperfine state in muonic ^{23}Na , viewed in the rotating reference frame at exactly $\Omega_{\text{RRF}} = -95.3$ MHz. The apparent frequency of -0.6676 ± 0.015 MHz is added to Ω_{RRF} to obtain the result shown in Table XV.

in muonic carbon (graphite) at the same field, $A_c = 0.0256 \pm 0.0008$, gives $P_c = A_c/A_0 = 0.1925 \pm 0.0062$, generally regarded as one of the highest residual μ^- polarizations available.

In muonic atoms, negative muons lose polarization due to $\vec{L} \cdot \vec{S}$ couplings in atomic transitions down to the ground state; in the case of nuclei with spin, this is complicated by the HF structure of the atomic levels, which can also lead to partial polarization of the nuclei themselves. This makes the populations and polarizations of the final F^\pm states difficult to predict. If we were to assume the same initial polarization for both states, $P_+ = P_-$, then we could conclude that $(87.6 \pm 11.4)\%$ of muonic ^{23}Na atoms are initially in the F^+ state and $(12.4 \pm 2.1)\%$ are initially in the F^- state. Such experimental values should be useful for an unambiguous interpretation of muon capture results in terms of the effective weak couplings \tilde{g}_a and \tilde{g}_p .

Experiment 938

Muonium formation and ionization in semiconductors and insulators

(V.G. Storchak, Kurchatov Inst.; J.H. Brewer, UBC/TRIUMF)

To date, most muonium studies in semiconductors have been focused on the lowest electronic states without considering the details of how these states are formed: spectroscopic experiments have revealed two quite different types of Mu centres. These centres are characterized by their different muon-electron hyperfine interactions. So-called “normal” muonium has an isotropic hyperfine interaction with a hyperfine frequency A about half of that in the free Mu atom ($A_0 = 4463$ MHz) and is located at the tetrahedral interstitial site; it is therefore denoted Mu_T^0 . “Bond-centred” muonium, with a small anisotropic hyperfine interaction ($A \sim A_0/50$) because of somewhat extended electron distribution, is located near the centre of the relaxed crystal bond and is thus denoted Mu_{BC}^0 . Both centres are associated with quite deep energy levels in the gap.

Experiments in electric fields designed for detailed studies of muonium formation processes in semiconductors have revealed an essential difference between Mu_{BC}^0 and Mu_T^0 : while the former is found to form via the electron capturing initially into a very excited state and then cascading down through the weakly bound (shallow) short-lived hydrogenic effective-mass state (EMS) into a deep ground state, the latter is believed to form directly into a deep state.

No matter how the muonium atom is formed, it may act as a trapping centre or a recombination centre depending on the host material and the temperature range in the same manner as other impurities in a semiconductor. Indeed, Mu (or a filled trap) is typically found at lower temperatures, while a diamagnetic state (which could be an ionized trap or, alternatively, a recombination centre) is observed at higher temperatures. This “general trend” of muonium spectroscopy (high probability of Mu formation at low temperatures along with the absence of muonium at high temperatures) has so far been explained as Mu ionization at elevated temperatures: the muonium atom loses its electron into the conduction band in an activated Arrhenius-like mechanism – a process which suggests that the Mu atom is a trapping centre. Although it is easy to understand such muonium ionization for a shallow Mu centre (either for a long-lived state or a short-lived one), thermal ionization of a deep-level Mu state encounters certain difficulties. Indeed, the binding energy of a shallow Mu state typically amounts to about 10 meV, which is less than the typical Debye energy (several tens of meV), while the typical binding energy

of a deep Mu state significantly exceeds the Debye energy. Under these circumstances, Mu ionization via an activated Arrhenius-like mechanism requires simultaneous absorption of many phonons – a process which is severely suppressed. These features of Mu formation and ionization processes make it hard to consider certain shallow (and the majority of deep) muonium centres as trapping centres.

Deep muonium state in InSb: recombination centre vs. trapping centre

To date, various muonium centres in semiconductors (as well as in the above discussion) have been considered to have their energy levels (either deep or shallow, lying below the conduction band minima either a few tenths or a few hundredths of an eV, respectively) in the forbidden gap. In this case certain Mu centres may be treated as trapping centres. Another situation is realized in narrow-gap semiconductors where deep Mu energy level cannot be accommodated in the gap.

Here we present new results on the deep-level muonium centre in InSb – a semiconductor with an extremely narrow energy gap. We argue that this centre can be better considered as a recombination centre rather than a trapping centre.

Last year our experiments in high magnetic field in both *n*- and *p*-type InSb revealed several signals which were identified as those corresponding to a paramagnetic muonium state and diamagnetic state (probably a bare muon). In last year’s Annual Report we showed the magnetic field dependence of muonium precession frequencies ν_{12} and ν_{34} which correspond to muon spin flipping in states with electron spin “down” and “up”, respectively, along with the diamagnetic

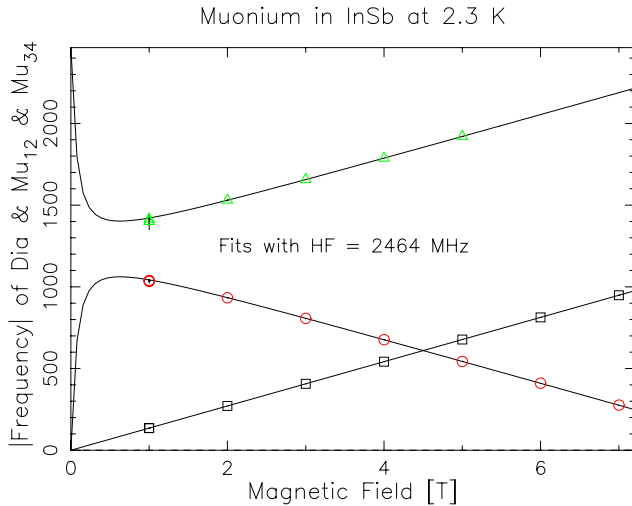


Fig. 102. Magnetic field dependences of two Mu frequencies (ν_{12} : circles and ν_{34} : triangles) and the diamagnetic frequency (squares) in *n*-type (10^{12} cm^{-3}) InSb. Solid lines for Mu frequencies present fit according to isotropic muonium hyperfine interaction.

frequency (Fig. 102). Fitting to a Breit-Rabi Hamiltonian showed that such field dependence of the precession frequencies corresponded to a muonium centre with an isotropic hyperfine interaction $A = 2464(1)$ MHz.

This value for the hyperfine interaction parameter A is characteristic of tetrahedral muonium centre Mu_T^0 observed in other III-V semiconductors GaAs and GaP as well as in elemental group-IV semiconductors Si, Ge and C. The high value of A is taken as evidence for a highly localized Mu centre in InSb; the characteristic radius is expected to be on the order of the Bohr radius. In accordance, the energy level of such centre is expected to lie quite deep below the conduction band minimum, a rough estimate being about 1 eV. Such a high value for the binding energy of a Mu centre does not allow one to accommodate this energy level in the extremely narrow forbidden gap of InSb (0.24 eV at 80 K). No matter how weird it looks, we probably have to admit that this Mu energy level lies in the valence band. It is worth noting that several theoretical attempts to account for the observed high value for the hyperfine frequency A of Mu_T^0 in semiconductors have come to the same conclusion.

No matter where one can accommodate the energy level for such a deep Mu state in a semiconductor (in the forbidden gap or in the valence band), the high value of its binding energy ensures that the ionization of this state is expected to occur only at very high temperature. In contrast to all other deep Mu centres in semiconductors, experiments in InSb show that Mu centre starts to disappear at about 20 K. Figure 103 presents temperature dependence of the relaxation rate of Mu signals in magnetic field 3 T. Above about 60 K we found no Mu signal at all.

Fitting this temperature dependence with an Arrhenius law yields $E_a = 75(15)$ K for the activation

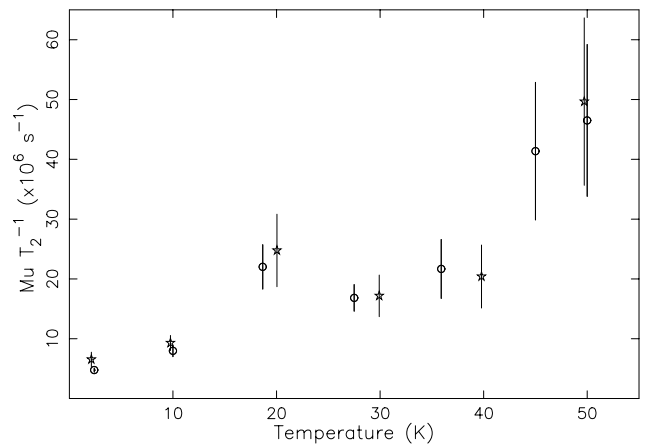


Fig. 103. Temperature dependence of the exponential spin relaxation rate of the Mu signal in *n*-InSb (circles) and *p*-InSb (stars) in a transverse magnetic field of 3 T.

energy. Neither this activation energy nor the temperature range of Mu disappearance in InSb are consistent with thermal ionization of a deep Mu centre. Both the activation energy and the temperature range, on the other hand, might indicate that this centre is formed via initial electron capture into very excited orbit – a process analogous to Mu_{BC}^0 formation in GaAs and GaP. Then thermal ionization of Mu might take place from an intermediate weakly bound highly excited state. The key to distinguishing this scenario from prompt muonium formation is an application of electric field. Unfortunately, our InSb samples do not hold even very weak electric field (probably due to activation of very shallow impurity centres). However, we argue that the possibility of electron capture into (and thus thermal ionization from) some weakly bound excited state of the observed Mu centre in InSb can be ruled out: we found no electron freezeout effect – a characteristic signature of an intermediate weakly bound Mu state.

We further argue that the observed disappearance of Mu signals at low temperatures may be consistent with recombination of the Mu electron with thermally activated holes in InSb: the binding energy of shallow acceptors in InSb amounts to about 100 K. This process, however, requires absorption of energy in the eV range, which is much higher than the Debye energy. Therefore neither acoustic nor optical phonons can be effective here. Then the only energy bath which can deposit this energy for hole capture by the Mu atom is the electron subsystem. We suggest that processes analogous to impact ionization may be responsible for the disappearance of the Mu centre at low temperatures in InSb. Such electron-hole recombination is commonly observed for deep-level defects in semiconductors.

Experiment 942

Magnetic fluctuations near metal insulator transitions in ruthenate pyrochlores

(*S.R. Dunsiger, McMaster; R.F. Kiefl, UBC*)

The nearly free electron model may often successfully describe the band structure of a crystal, the highest band being completely filled for insulators or only partially so for metals. However, many transition metal oxides with partially filled d -electron bands have nonetheless been found to be poor conductors or indeed insulators. The origin of this behaviour is thought to be the Coulomb repulsion between electrons: strong electron-electron correlations. Indeed, an otherwise insulating material may be driven into a metallic state in a controllable way with doping, chemical composition, pressure or magnetic field. Such metal-insulator transitions are widely observed in condensed matter physics. The scientific interest in these materials is based on the fact that near the transition point the metal shows fluctua-

tions of spin, charge and orbital degrees of freedom.

The focus of Expt. 942 is the study of pyrochlores with chemical composition $\text{A}_2\text{B}_2\text{O}_7$ where only the B site is occupied by a magnetic ion, in particular $\text{Y}_{2-x}\text{Bi}_x\text{Ru}_2\text{O}_7$. This system may be driven in a controlled manner from a geometrically frustrated insulator to a Pauli paramagnetic metal with increasing Bi doping. Susceptibility measurements on insulating $\text{Y}_2\text{Ru}_2\text{O}_7$ by Yoshii and Sato [J. Phys. Soc. Jpn. **68**, 3034 (1999)] show evidence of an ordering transition at $T_G \sim 76$ K. Doping with Bi on the Y site increases the lattice constant and the system becomes progressively more metallic as the Bi 6p states mix with 4d states of Ru via the framework oxygen [Cox *et al.*, J. Solid State Chem. **62**, 360 (1986)]. There is a metal-insulator transition at $x = 0.9$. The ordering transition temperature is also progressively suppressed and broadened. From published work [Yoshii and Sato *op. cit.*], T_G is expected to go to zero in $\text{Y}_1\text{Bi}_1\text{Ru}_2\text{O}_7$. It is important to note that, while this Mott-Hubbard system is tuned through a bandwidth controlled metal-insulator transition, the concentration of magnetic Ru ions is not altered. In other words, the magnetic sublattice has not been diluted.

Muon spin relaxation is one of the principal methods we have used to characterize the dynamic behaviour, since it is uniquely sensitive to the low frequency magnetic fluctuations which are often present in these systems. Longitudinal field measurements have provided insight into the ordering transition in this family of compounds. Alternatively, in a transverse field configuration, measurements of the muon spin precession frequency with respect to the applied field probe the contact hyperfine and dipolar fields within these materials and yield information on the local spin susceptibility. Anomalous behaviour has been observed in $(\text{V}_{1-x}\text{Cr}_x)_2\text{O}_3$, the archetypal system undergoing a bandwidth controlled metal-insulator transition [Gossard *et al.*, Phys. Rev. **B3**, 3993 (1991)], where the frequency shift as measured with NMR does not track the bulk susceptibility χ . We have therefore recently undertaken a series of studies of the shift in the muon spin precession frequency as a function of temperature in $\text{Y}_{2-x}\text{Bi}_x\text{Ru}_2\text{O}_7$ to compare the local and bulk susceptibilities.

Transverse field muon spin rotation measurements on sintered powder samples were carried out on the M15 beam line at TRIUMF, using the Belle magnet with high timing insert. The frequency shift measures the real part of the dynamic susceptibility χ' , while the linewidth may be related to the imaginary part χ'' through the fluctuation-dissipation theorem. The frequency shift is then given by $(\nu_{\text{Sample}} - \nu_{\text{CaCO}_3})/\nu_{\text{CaCO}_3}$. Calcium carbonate is used as a refer-

ence material as it induces only negligibly small chemical shifts in the muon spin precession frequency. The temperature variation of the paramagnetic frequency shifts in an applied magnetic field of 40 kOe is shown in Fig. 104 for four Bi concentrations ($x = 0, 0.9, 1.0, 2.0$). Note that a negative frequency shift is observed. Naively one might expect a positive shift in a paramagnetic material. However, in general, in an isotropic system of point magnetic dipoles and assuming axial symmetry, the frequency shift in a polycrystalline paramagnet is solely a measure of the local contact hyperfine field at the muon site, since the dipolar field contributes nothing in an isotropic powder material [Ibers *et al.*, Phys. Rev. **121**, 1620 (1961)]. The sign of the hyperfine coupling may take either positive or negative values. More generally, dipolar fields will also typically contribute, given an anisotropic g tensor.

The measurements of the paramagnetic frequency shifts may be compared with those of the bulk susceptibility, shown in Fig. 105. These data were also collected by field cooling (FC) the samples in an applied magnetic field of 40 kOe. The magnetic history of the samples during the bulk and local probe measurements is thus equivalent. There are several features of interest. As may be seen in Fig. 105, the bulk susceptibility decreases with increasing Bi concentration, despite the fact that the magnetic Ru^{4+} ion concentration has not been altered. Rather, the size of the permanent magnetic moment of the Ru ion is decreasing as the valence electrons become more itinerant in character. Surprisingly, the paramagnetic frequency shifts do not show this same monotonic trend. The magnitude of the shift in $\text{Y}_2\text{Ru}_2\text{O}_7$ is anomalously small. This is unlikely due to an instrumental effect, since the data shown are a combination of two sets taken approximately one week

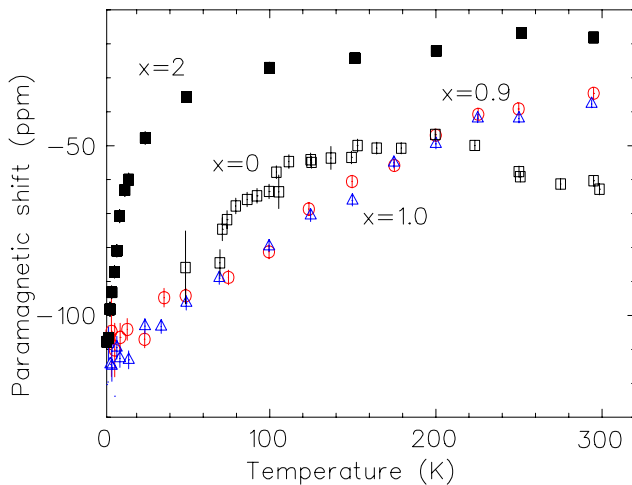


Fig. 104. Temperature dependence of the paramagnetic frequency shift in $\text{Y}_{2-x}\text{Bi}_x\text{Ru}_2\text{O}_7$ in an applied transverse magnetic field of 40 kOe.

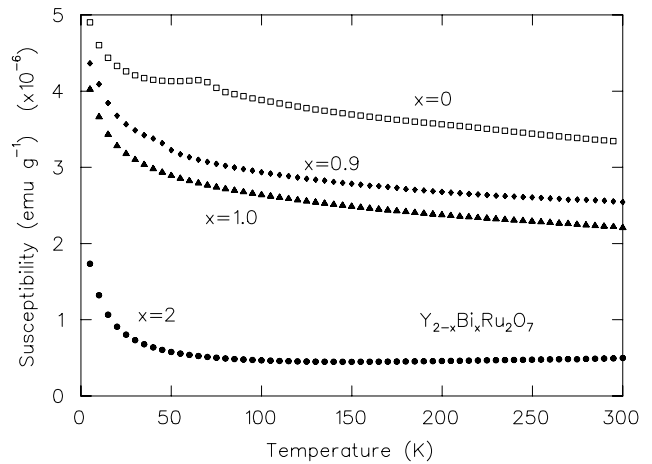


Fig. 105. Temperature dependence of the bulk susceptibility in $\text{Y}_{2-x}\text{Bi}_x\text{Ru}_2\text{O}_7$ in an applied magnetic field of 40 kOe.

apart, the remaining samples being studied in the intervening period.

Another interesting anomaly is observed in $\text{Y}_2\text{Ru}_2\text{O}_7$: the paramagnetic frequency shift undergoes a change in the slope of its temperature dependence. Initially increasing with temperature, the frequency shift starts to decrease again above 200 K. No such effect is observed in measurements of the bulk susceptibility, which decreases monotonically with increasing temperature. This disparity could arise either because of a muon induced effect or temperature dependence in the contact hyperfine and/or dipolar field. One might anticipate such a change in the local field in the neighbourhood of the metal-insulator transition, by analogy with $(\text{V}_{1-x}\text{Cr}_x)_2\text{O}_3$. However, its origin in pure $\text{Y}_2\text{Ru}_2\text{O}_7$ is still under investigation.

Finally, the low temperature upturn in both the bulk susceptibility as well as the magnitude of the frequency shift of all four samples is likely due to paramagnetic impurities.

Currently, we are working to quantify the various contributions to the bulk and local susceptibilities. We would like to compare these results with our existing data on $\text{Y}_2\text{Mo}_2\text{O}_7$. The latter compound is an isostructural geometrically frustrated 4d electron system. A comparison of the two could thus provide insight into the role of the 4d magnetic species on the metal-insulator transition.

Experiment 944 Muonium in silicon carbide

(*R.L. Lichti, Texas Tech; K.H. Chow, Alberta*)

The goal of Expt. 944 has been to investigate the muonium states formed in the three most common structures of SiC, the cubic 3C and the 4H and 6H hexagonal polytypes. We initially focused on the Mu^0

signals observed in the 4H and 6H structures, examining n -type, p -type and high-resistivity samples of each.

Following the initial hyperfine spectroscopy using the HiTime spectrometer, we tentatively identified likely sites for the observed Mu^0 states [Lichti *et al.*, Phys Rev **B70**, 165204 (2004)]. Figure 106 shows a section of the 4H structure with various theoretically predicted sites marked and labelled. Based on the latest predictions and the acceptor behaviour we observe for one of the paramagnetic signals in 4H-SiC, hyperfine values ranging from 3010 to 3030 MHz extrapolated to zero temperature have been assigned to a T_{Si} site which is predicted to be the stable locations for both Mu^0 and Mu^- in 4H-SiC. There are two slightly inequivalent T_{Si} sites in the 6H structure, leading to two signals in this range in the high-resistivity 6H-SiC samples. We have also assigned HF values below 2900 MHz to the AB_{Si} locations near the centre of the 2H-like channels for one signal in each of the 4H and 6H structures. Additionally, a second signal in this region seen only at very low temperatures in n -type 6H-SiC is suggested to be formed via electron capture by a Mu^+ at its predicted stable site, AB_{C} , which should then quite easily switch to T_{Si} at relatively low temperatures.

In the most recent beam time we investigated the dynamics reported earlier for 6H samples. In the high resistivity 6H sample, high frequency spin precession data imply a large dip in amplitude for all of the Mu^0 signals near 150 K and a peak in the associated relaxation rates. Longitudinal relaxation rates also show a peak near 170 K and a second one near 280 K in n -type 6H, as reported previously. Figure 107 shows the

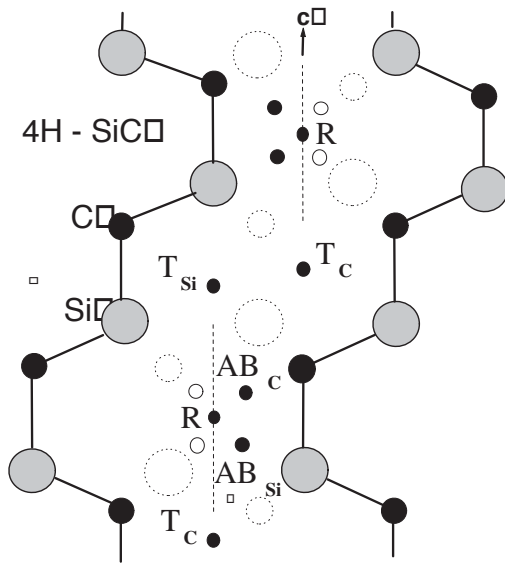


Fig. 106. Possible sites for Mu in the 4H structure of SiC. 6H-SiC will have an additional step in the zig-zag channel and a second type of T_{Si} site, but is otherwise similar.

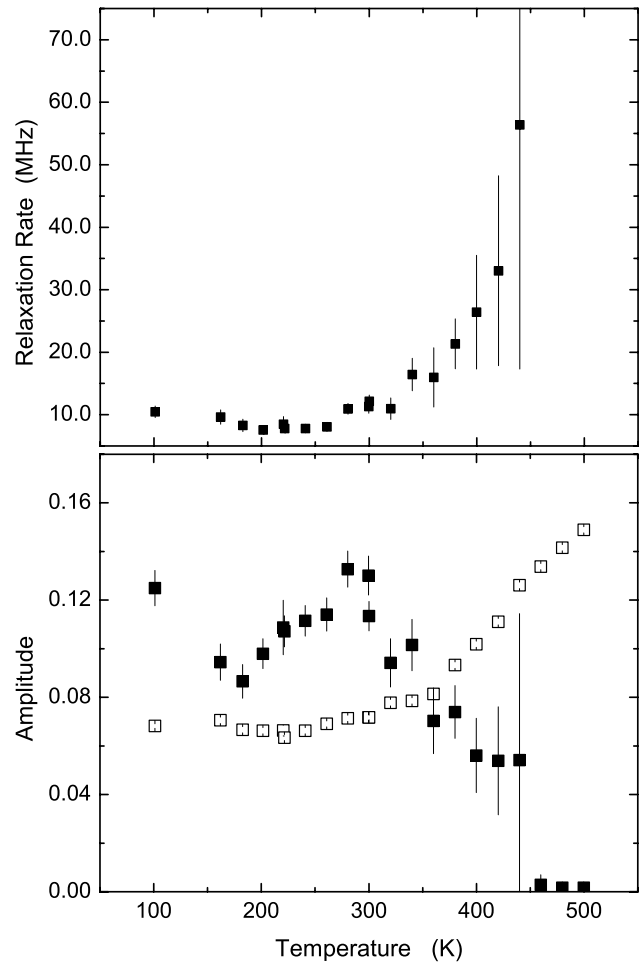


Fig. 107. The composite Mu^0 relaxation rates (top), and the amplitudes for the diamagnetic (open squares) and triplet Mu^0 signals (filled squares) (bottom), in TF- μ SR data for high-resistivity 6H-SiC taken at 15 G.

amplitudes and Mu^0 relaxation rate for low-field data taken to explore the composite Mu^0 dynamics above 300 K. These data suggest at least partial ionization of Mu^0 states above room temperature as suggested from the high-frequency results, but do not distinguish which Mu^0 state is involved (all three showed an increase in relaxation rate on approach to 300 K in the HiTime data). We plan to investigate this region further with rf or microwave driven resonance experiments in the near future in order to separate the dynamics arising from each neutral muonium centre.

Experiment 945 Muoniated radicals formed from carbenes and carbene analogues (P.W. Percival, SFU)

Experiment 945 has its origins in Expt. 883, which concerns muoniated methyl and its derivatives. One method for creating such α -muoniated radicals involves addition of Mu to carbenes (see Fig. 108a). Carbenes

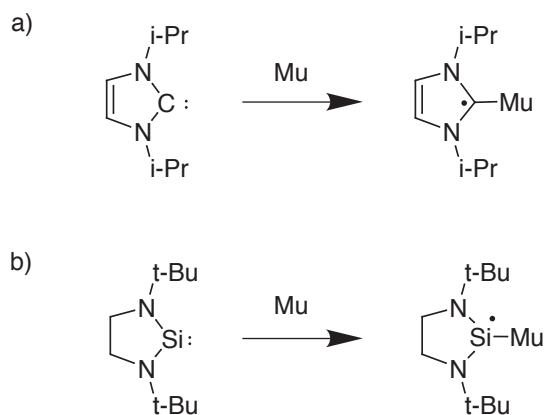


Fig. 108. (a) Muonium adds to a carbene to form a substituted methyl radical. (b) Muonium adds to a silylene to form a silyl radical.

($R_2C:$) are molecules that possess a neutral dicoordinate carbon atom with six valence electrons, which generally results in high reactivity, so that carbenes tend to be considered only as reaction intermediates. However, over the past decade several singlet carbenes have been synthesized and isolated. The addition of a hydrogen atom to a dicoordinate carbon corresponds to a very significant chemical process – the isolated creation of a new chemical bond – and Expt. 945 was conceived to explore this fundamental chemistry.

A preliminary account of our experiments with carbenes was included under Expt. 883 in the 2002 TRIUMF Annual Report; full details have since been published [McKenzie *et al.*, *J. Am. Chem. Soc.* **125**, 11565 (2003); McKenzie, Ph.D. thesis, SFU (2004)]. A new aspect of Expt. 945 is the extension of this novel chemistry to analogous molecules containing other Group 14 elements at the carbene site, such as the silylene depicted in Fig. 108b. Stable molecules containing a divalent silicon atom were synthesized for the first time only a few years ago. Nevertheless, they have been hypothesized as intermediates in many thermal and photochemical reactions of organosilicon compounds, so questions concerning their reactivity are of considerable import. When Expt. 945 was first proposed there was no literature at all on radical reactions of stable silylenes. However, a short communication has since appeared reporting the first ESR spectra of radical adducts of a silylene [Tumanskii *et al.*, *J. Am. Chem. Soc.* **126**, 7786 (2004)]. Relatively large radicals were chosen so that the silyl radical products are stabilized by electron delocalization. Our own experiments complement this work since we employ Mu as an isotopic substitute for H. Instead of creating a carbon-silicon bond at the reaction site, we form a silicon-hydrogen bond. The resulting radicals are short-lived and much closer to the intermediates posited in industrial processes.

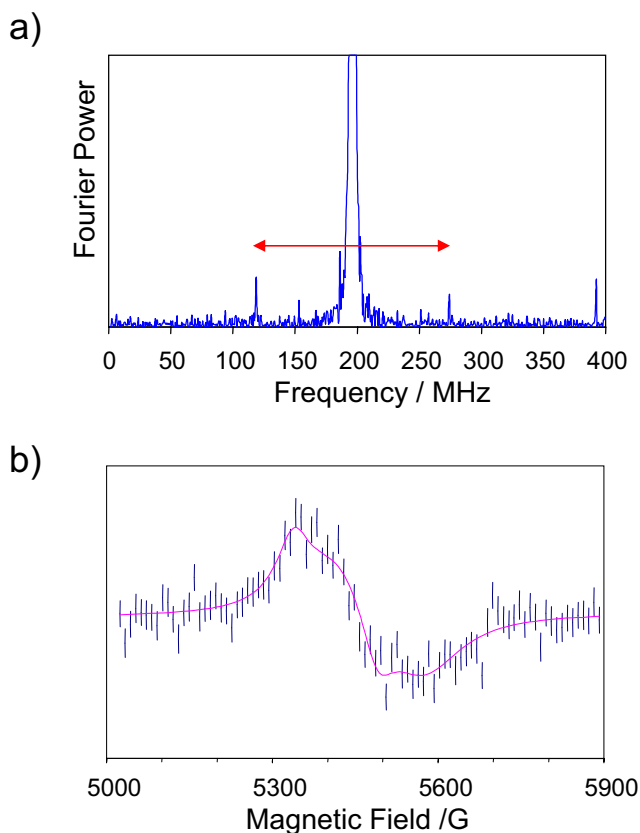


Fig. 109. (a) TF- μ SR and (b) μ LCR spectrum of the silyl radical formed from the reaction of muonium with a stable silylene.

To date we have been successful in detecting one muoniated silyl radical; the transverse-field μ SR and level-crossing spectra are shown in Fig. 109.

The second theme pursued in Expt. 945 during 2004 concerns an investigation of muonium addition to azulene (Fig. 110). Azulene, $C_{10}H_8$, is a polycyclic

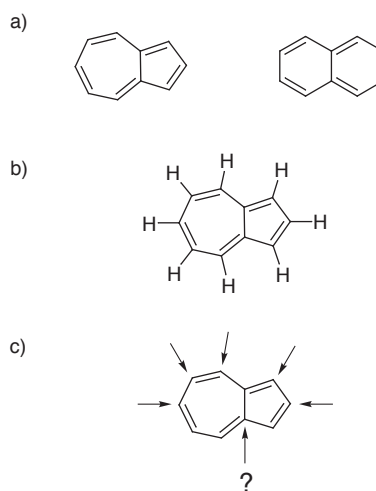


Fig. 110. (a) Azulene is an isomer of naphthalene. (b) The bridgehead carbons do not have attached H atoms. (c) Five of the six chemically distinct carbon sites are expected to be more reactive than the bridgeheads.

aromatic hydrocarbon consisting of fused 5- and 7-membered rings. It is an isomer of naphthalene, to which it rearranges at high temperature. A recent computational study [Alder *et al.*, J. Am. Chem. Soc. **125**, 5375 (2003)] suggests that the mechanism for this reaction involves bond formation at a bridgehead carbon, i.e. at a carbon shared by the two rings. Our own experience (Expt. 749) led us to doubt this hypothesis, so we decided to investigate the reactivity of azulene towards H atom attack by identifying the radical products formed by Mu addition.

Preliminary calculations suggested preferential addition at two sites on the 5-ring. However, μ SR experiments soon showed the situation to be more complicated. It is evident from Fig. 111 that there are *at least* five distinct radical products, each characterized by a pair of precession frequencies. Since this is a power spectrum, the amplitudes are proportional to the yields squared. Thus, the five strongest pairs of lines represent radicals with relative yields of approximately 1:2:2:2:2. Our previous work with pyrene and fluoranthene [Brodovitch *et al.*, Can. J. Chem. **77**, 326 (1999); *ibid.* **81**, 1 (2003)] clearly showed a preference for carbon sites bearing a hydrogen, suggesting that the radical signals in Fig. 111 are the products of Mu addition to the sites indicated by the arrows in Fig. 110c. These have degeneracies 1:2:2:2:1. The deviation of the experimental yields from these ratios could be explained by differential reactivity of the sites, but there is also the possibility that Mu does indeed add to one of the bridgehead carbons.

To resolve this question we need to assign molecular structures to each of the radical signals. This can be done by calculating the structures and properties of the radical isomers. The calculated muon hyperfine constants can be compared with values derived from the μ SR spectrum, and the associated proton hyperfine constants can then be used to predict resonance positions in the μ LCR spectrum. However, this is not trivial, since the spectrum obviously contains many signals (see Fig. 112). Detailed analysis is under way.

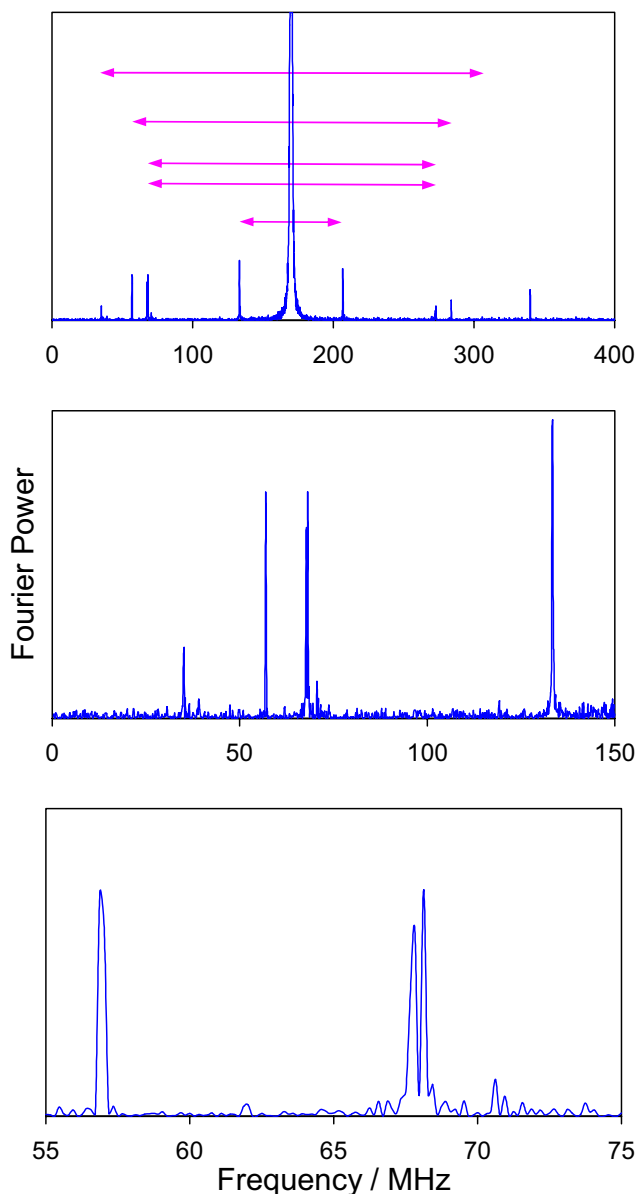


Fig. 111. TF- μ SR spectrum obtained from a solution of azulene in tetrahydrofuran. Each muoniated radical gives rise to a pair of precession frequencies, as indicated in the top panel.

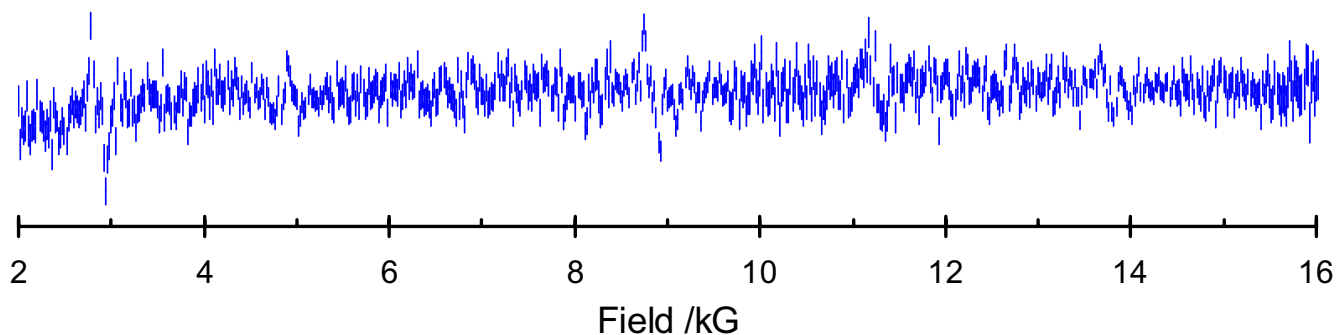


Fig. 112. A synthesis of μ LCR spectra obtained from a solution of azulene in tetrahydrofuran.

Experiment 949

μ SR study of magnetic order in high- T_c superconductors under high pressure

(J. Arai, T. Goko, Tokyo U. Science)

Anomalous suppression of superconducting transition temperature T_c observed in a narrow range of $x \sim 1/8$ for $\text{La}_{2-x}\text{M}_x\text{CuO}_4$ ($M = \text{Ba}, \text{Sr}$), which is called the “1/8 problem”, is one of the most important issues to understand the relation between superconductivity and magnetism in high- T_c cuprates. At the beginning, the 1/8 problem was considered to be particular to La-214 compounds. However, 1/8 anomaly is also observed in Bi-2212 and Y-123, suggesting that the 1/8 problem is a common property of high- T_c superconductors.

Structural instability is inherent in La-214 compounds, which are the most typical system in high- T_c superconductors. The crystal structure is closely related to the electronic state in this system. With decreasing temperature, La-214 compounds undergo a well-known phase transition from a high-temperature tetragonal (HTT) structure to a low-temperature orthorhombic (LTO) structure except for the overdoped region. In addition, $\text{La}_{2-x}\text{Ba}_x\text{CuO}_4$ (LBCO) displays a second transition to a low-temperature tetragonal (LTT) structure around $x = 1/8$ at low temperatures. Because superconductivity is strongly suppressed in LBCO around $x = 0.125$ and slightly suppressed in $\text{La}_{2-x}\text{Sr}_x\text{CuO}_4$ (LSCO) around $x = 0.115$, it is widely believed that the LTT structure plays an important role in suppressing superconductivity around $x \sim 1/8$.

On the other hand, in La-214 compounds around $x \sim 1/8$, magnetic order has been observed by neutron scattering experiments and μ SR experiments. These results indicate the close relation between the suppression of superconductivity and the appearance of magnetic order.

In order to clarify the relation among superconductivity, the magnetic order and the LTT structure, we have performed the zero-field μ SR measurement and the resistivity measurement in LBCO with $x = 0.125$ and 0.135 under high pressure up to ~ 1.5 GPa by using a pressure cell which we have developed. The LTT phase of LBCO with $x = 0.125$ is suppressed by applying pressure up to ~ 0.6 GPa [Katano *et al.*, Phys. Rev. **B48** (1993)]. In La-214 compounds, the carrier concentration hardly depends on pressure [Tanahashi *et al.*, Jpn. J. Appl. Phys. **28** (1989)] in contrast to other high- T_c cuprates. We can control the LTT structure by applying pressure without changing the carrier concentration.

Figures 113 and 114 show the μ SR spectra for LBCO with $x = 0.125$ at $P \sim 0.5$ GPa and 1.5 GPa, respectively. The LTT structure spreads over the

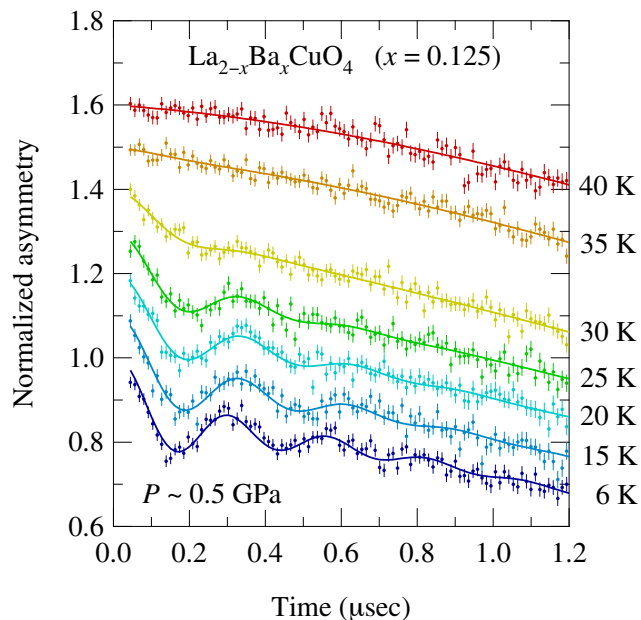


Fig. 113. ZF- μ SR spectra of LBCO with $x = 0.125$ at $P \sim 0.5$ GPa. The spectra are vertically offset for clarity.

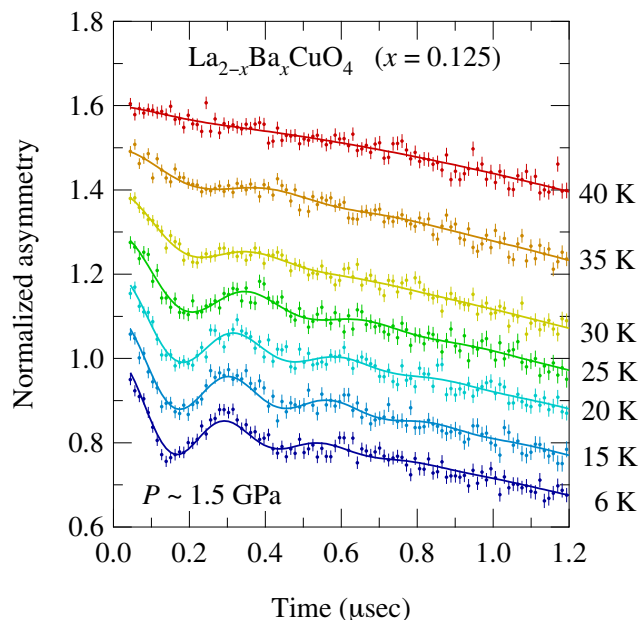


Fig. 114. ZF- μ SR spectra of LBCO with $x = 0.125$ at $P \sim 1.5$ GPa. The spectra are vertically offset for clarity.

sample at ~ 0.5 GPa and vanishes at ~ 1.5 GPa. An oscillation component is observed at low temperatures under both pressures. Since the oscillation component indicates the magnetic order, this result suggests that the LTT structure is dispensable for the appearance of the magnetic order. These spectra include contributions from the sample and the pressure cell. The ratio of the sample signal to the background is typically 1 : 2. The slow relaxation observed over a wide temperature range is due to the pressure cell. Here we define the magnetic ordering temperature T_m as the temperature

where an oscillation component starts to appear in the μ SR spectra. For example, in the case of $P \sim 1.5$ GPa, T_m exists between 35 and 40 K.

The values of T_c and T_m for LBCO with $x = 0.125$ are plotted as a function of pressure in Fig. 115. Here T_c is determined by zero resistivity. With increasing pressure, T_c increases linearly with an initial rate of $dT_c/dP \sim +8.1$ K/GPa. At $P_d \sim 1.1$ GPa, dT_c/dP changes to $+1.9$ K/GPa. It seems that P_d corresponds to the LTT-LTO phase transition pressure, since dT_c/dP is affected by the crystal structure in La-214 compounds, and dT_c/dP observed in the orthorhombic phase of LSCO is $\sim +2$ K/GPa. On the other hand, T_m does not decrease but increases, suggesting that the suppression of T_c has no correlation with T_m in LBCO with $x = 1/8$.

Figures 116 and 117 show the μ SR spectra for LBCO with $x = 0.135$ at ambient pressure and at $P \sim 1.1$ GPa, respectively. The LTT structure spreads over the sample at ambient pressure and vanishes at $P \sim 1.1$ GPa. An oscillation component is observed at low temperatures under both pressures, suggesting that the LTT structure is dispensable for the appearance of the magnetic order also in LBCO with $x = 0.135$. The ratio of the sample signal to the background is typically 1 : 4, because of failure in tuning of muon momentum. The magnetic volume fraction estimated from the amplitude of the oscillation component in the μ SR spectra is reduced from $\sim 100\%$ to $\sim 30\%$ by applying pressure up to 1.1 GPa.

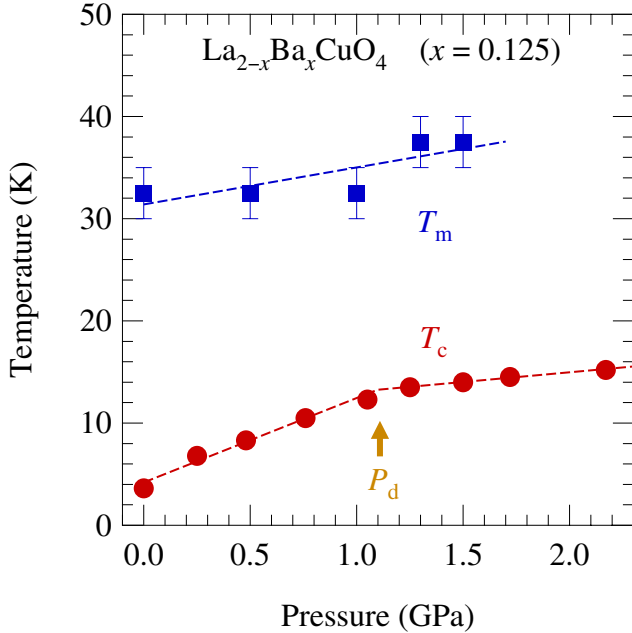


Fig. 115. Pressure dependence of T_m and T_c for LBCO with $x = 0.125$. P_d indicates the LTT-LTO phase transition pressure.

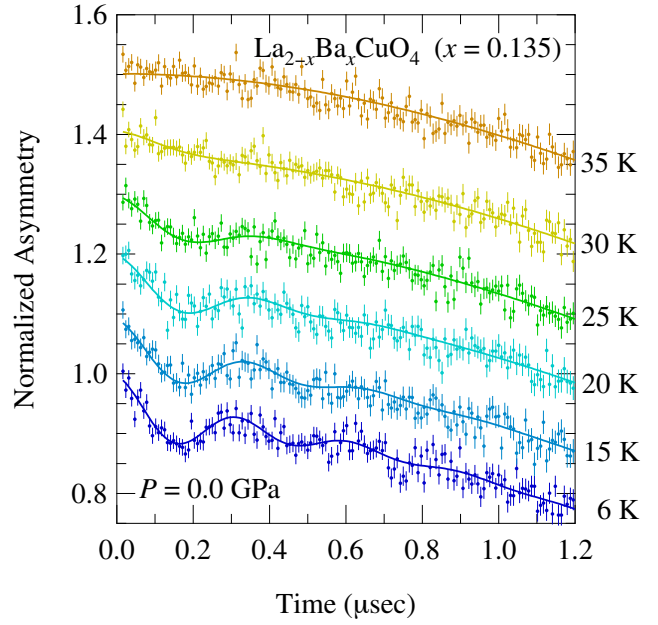


Fig. 116. ZF- μ SR spectra of LBCO with $x = 0.135$ at ambient pressure. The spectra are vertically offset for clarity.

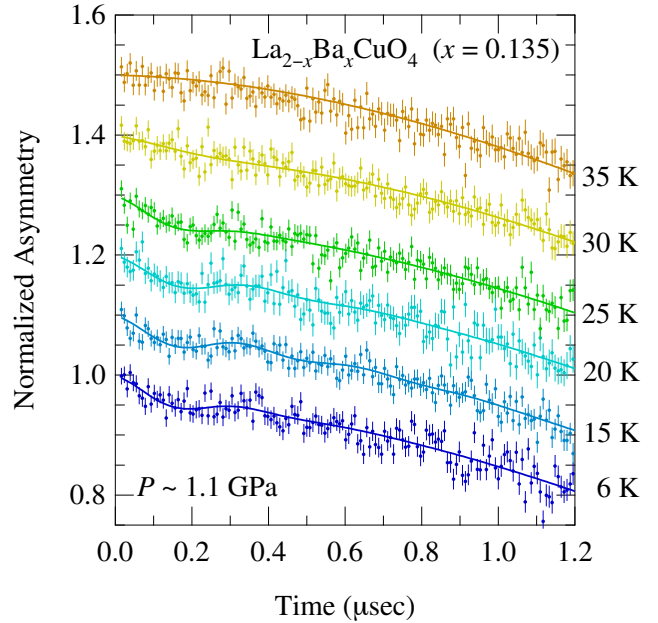


Fig. 117. ZF- μ SR spectra of LBCO with $x = 0.135$ at $P \sim 1.1$ GPa. The spectra are vertically offset for clarity.

For LBCO with $x = 0.135$, T_c drastically increases with increasing pressure, as shown in Fig. 118. At $P_d \sim 1.0$ GPa, T_c reaches ~ 30 K and dT_c/dP changes to $+2.1$ K/GPa which corresponds to the pressure dependence of T_c in the orthorhombic phase. On the other hand, T_m hardly changes. The suppression of T_c therefore has no correlation with T_m . We speculate that the suppression of T_c is closely related to the magnetic volume fraction.

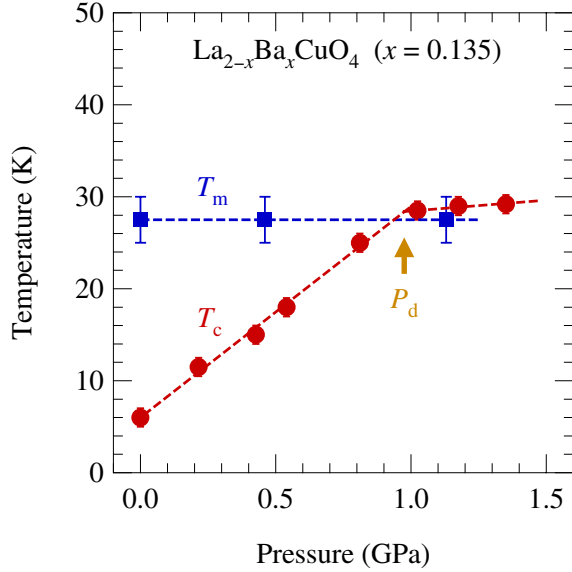


Fig. 118. Pressure dependence of T_m and T_c for LBCO with $x = 0.135$. P_d indicates the LTT-LTO phase transition pressure.

Experiment 951

Magnetism and flux line lattice structure of oxychloride superconductors

(K. Ohishi, R. Kadono, KEK-IMSS)

The $\text{Ca}_{2-x}\text{Na}_x\text{CuO}_2\text{Cl}_2$ (Na-CCOC) compounds used in this study were synthesized under high pressure [Hiroi *et al.*, *Nature* **371**, 139 (1994); *ibid.*, *Physica* **C266**, 191 (1996)]. The samples were characterized by means of magnetization and powder X-ray diffraction. The lattice parameters were determined by using a Rietveld analysis for all samples in order to evaluate the sodium concentration dependence of the lattice parameters. The ZF- μSR measurements were conducted at TRIUMF and at the Muon Science Laboratory, High Energy Accelerator Research Organization (KEK-MSL). We prepared eleven sets of Na-CCOC polycrystalline specimens, $x = 0, 0.0025, 0.005, 0.01, 0.02, 0.05, 0.07, 0.10, 0.12, 0.15,$ and 0.20 , having a dimension of about $100 \sim 250 \text{ mm}^2$ with $\sim 1 \text{ mm}$ thickness. These samples were mounted on a thick silver sample holder (KEK-MSL) or on a thin sheet of mylar film (TRIUMF, where one can obtain background free spectra) and loaded to the ^4He gas flow cryostat. ZF- μSR measurements were mainly performed at temperatures between 2 K and room temperature, and additional measurements were performed at ambient temperature under a transverse field ($\approx 2 \text{ mT}$) to calibrate the instrumental asymmetry. The dynamics of local magnetic fields at the muon sites was investigated by longitudinal field (LF)- μSR measurements [Schenck, *Muon Spin Rotation: Principles and Applications in Solid State Physics* (Adam Hilger, Bristol, 1986)].

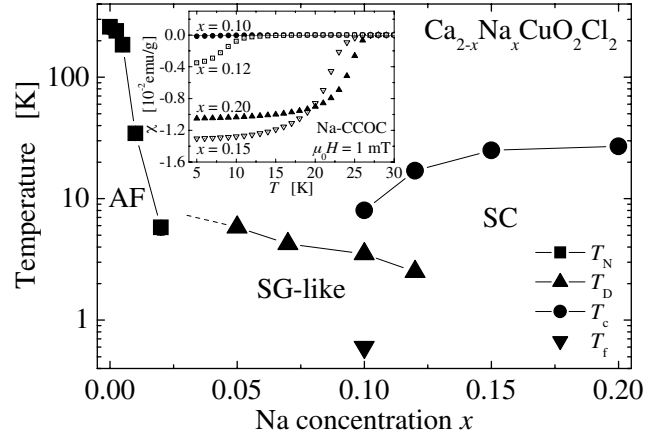


Fig. 119. Magnetic phase diagram of Na-CCOC. The transition temperature for the SG-like state (T_D) is defined as an onset temperature where the spin fluctuation rate becomes lower than 10^9 s^{-1} . The spin freezing temperature (T_f) was determined only for $x = 0.10$. The inset shows the temperature dependence of magnetic susceptibility measured for $x = 0.10, 0.12, 0.15$ and 0.20 in an applied field $\mu_0 H = 1 \text{ mT}$ after field-cooling process.

Figure 119 shows the magnetic phase diagram of Na-CCOC ($0 \leq x \leq 0.20$) determined by μSR measurements. As we reported in last year's Annual Report, we have observed clear muon spin precession signals in the lightly doped samples ($x \leq 0.02$), indicating the appearance of a long range antiferromagnetic (AF) order. While no precession signal was identified in those with $0.05 \leq x \leq 0.12$, evidence was found for a quasi-static spin glass (SG)-like state at lower temperatures. It suggests a general trend that the suppression of long range AF order is strong but incomplete over the relevant range of sodium concentration. In particular, the present result is the first example for a good correspondence between such an inhomogeneous magnetic state and the nanoscale electronic inhomogeneity revealed by STM/STS [Kohsaka *et al.*, *Phys. Rev. Lett.* **93**, 097004 (2004); Hanaguri *et al.*, *Nature* **430**, 1001 (2004)]. ZF- μSR time spectra in the specimen with $x = 0.15$ and 0.20 exhibit the least temperature dependence down to 2 K. Besides the signature of the static nuclear magnetic moments described by the Kubo-Toyabe function, we obtained no evidence for any kind of additional magnetic moments in the specimen with $x = 0.15$ and 0.20 .

In summary, our μSR measurements on Na-CCOC revealed a magnetic phase diagram as a function of carrier doping x , which shares many features in common with other hole-doped cuprates [Niedermayer *et al.*, *Phys. Rev. Lett.* **80**, 3843 (1998)]. The AF order observed in the sample with $0 \leq x \leq 0.02$ is drastically suppressed in those with $x > 0.02$. However, the suppression is incomplete so that a SG-like phase appears over a region $0.05 \leq x \leq 0.12$. The present result

strongly suggests that the inhomogeneous magnetic state commonly found in the underdoped cuprates has an intrinsic origin related to the nanoscale electronic inhomogeneity observed by STM/STS measurements.

Experiment 960

Hydrogen (Mu) defects in II-VI chalcogenides (*R.L. Lichti, Texas Tech; J.M. Gil, Coimbra*)

In this run, we focused our attention on the compound ZnSe, which is the most interesting zinc chalcogenide both from the fundamental and the technological point of view. We had previously identified, in the 2003 run, the existence of two possible Mu states in high transverse field, in two different, nominally undoped, ZnSe single crystals, obtained from Crystec and from Alpha Aesar. In this run, we have pursued the spectroscopic study of these Mu states and the respective interconversion dynamics, together with the study of the missing fraction.

Anisotropy vs. two isotropic states hypothesis

We have performed high-transverse field experiments on two other single crystals from Crystec, oriented 110 and 111, from the same batch as the 100 sample used previously. The results preclude the hypothesis that the two observed lines arise from anisotropy of a single Mu state. The existence of two isotropic Mu states in ZnSe has thus been firmly established. As pointed out previously, the obtained hyperfine interactions are consistent with those calculated theoretically by Van de Walle and Blöchl [Phys. Rev. **B47**, 4244 (1993)], suggesting that the observed states are located in the tetrahedral interstitial sites. Thus, the signal (Mu_{I}) with hyperfine interaction $A_{\text{I}} = 3423.99$ MHz is tentatively assigned the T_{Zn} location and the signal (Mu_{II}) with hyperfine interaction $A_{\text{II}} = 3255.3$ MHz is tentatively assigned the T_{Se} location.

Detailed study of the interconversion of the states

We have performed a detailed temperature scan at a high transverse field (6 T), in order to investigate the thermal stability of both states. A single crystal of ZnSe obtained from Alpha-Aesar, nominally undoped, was used. We have verified the conversion of one of the states (named Mu_{II}) to the other (Mu_{I}) at around 50 K. This conversion is accompanied by a characteristic peak in the phase of the frequency of Mu_{I} (shown in Fig. 120), together with an increase of the relaxation rate of Mu_{II} . Above 50 K, only the Mu_{I} line is seen up to 300 K, with a temperature dependent formation probability (Fig. 121).

Missing fraction

We have also undertaken studies in high longitudinal fields in order to investigate the behaviour of the observed missing fraction. The data are well described

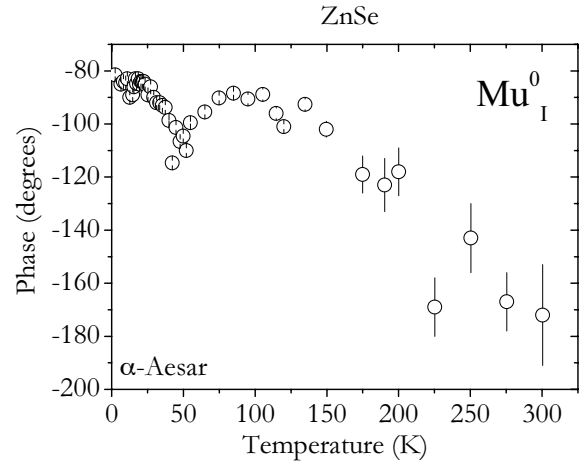


Fig. 120. Phase of the Mu_{I} frequency, peaking at about 50 K.

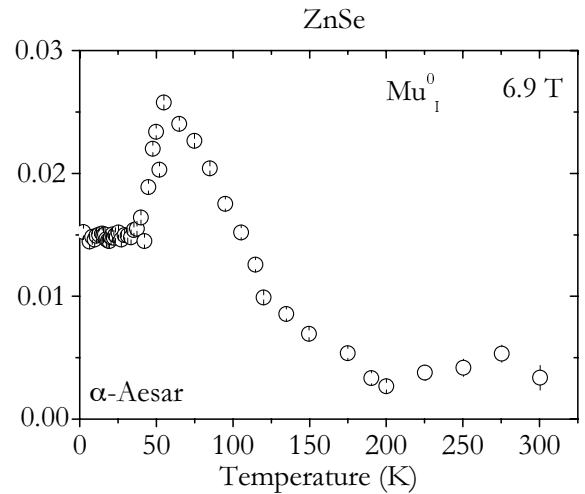


Fig. 121. Asymmetry of the Mu_{I} state as a function of temperature.

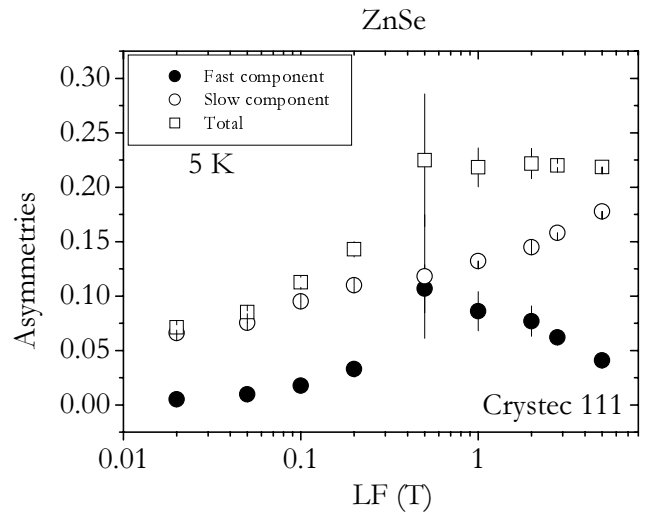


Fig. 122. Asymmetry dependence with longitudinal field for the two components observed in the Crystec 111 ZnSe sample, at 5 K.

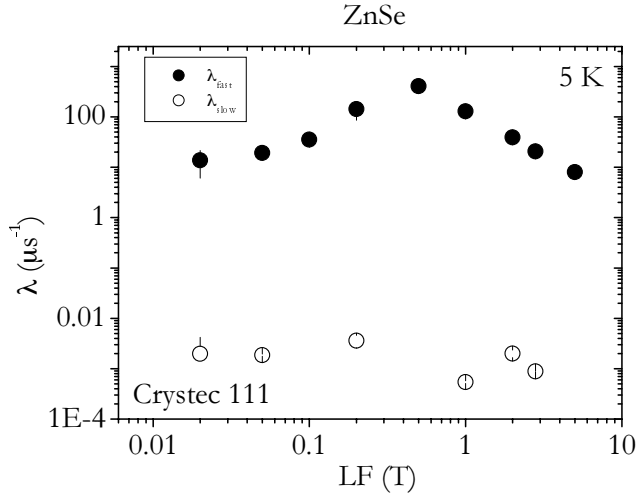


Fig. 123. Relaxation rate dependence with longitudinal field for the two components observed in the Crystec 111 ZnSe sample, at 5 K.

with two-component fits, where an extremely fast relaxation component is superimposed to an almost non-relaxing component. The corresponding asymmetries and relaxation rates at 5 K are depicted in Figs. 122 and 123, respectively. As illustrated in these figures, full asymmetry is recovered at low temperatures, the TF missing fraction corresponding to the fast relaxing component observed in LF.

Experiment 998 Muon spin relaxation and dynamic scaling in novel magnetic materials

(D.E. MacLaughlin, California, Riverside; R.H. Heffner, JAERI-ASRC)

Magnetic materials provide flexible and universal systems in which to study the dynamics of interacting electron spins. Critical behaviour is a well-known example that has been fairly well characterized for simple ferromagnets and antiferromagnets, but less is known about exotic quantum, glassy, and frustrated spin systems, in which spin fluctuations are slowed significantly. We have begun μ SR experiments to study spin dynamics in a number of such systems.

μ SR is a low-frequency probe of spin dynamics and hence is particularly sensitive to slow spin fluctuations. It is therefore ideally suited to studies of long-lived spin correlations in these novel spin systems. Under certain conditions, the muon spin relaxation function $G(t, H)$ can be shown to obey the time-field scaling relation $G(t, H) = G(t/H^y)$, where y is related to the form of the spin correlation function and low-frequency divergences in the fluctuation spectrum. In the case of critical fluctuations near a phase transition, this in turn gives information on the dynamical scaling exponent z .

In 2004, μ SR experiments were carried out to study slow spin dynamics in the non-Fermi-liquid (NFL) heavy-fermion alloy $Ce_{0.2}La_{0.8}RhIn_5$ and geometrically frustrated antiferromagnet $Gd_2Ti_2O_7$. We did not observe time-field scaling in either of these systems, and $Ce_{0.2}La_{0.8}RhIn_5$ showed no evidence at all for slow fluctuations. The results are interesting in their own right, however, as described below. Papers on both these experiments are currently in preparation.

Spin freezing and non-glassy dynamics in $Ce_{0.2}La_{0.8}RhIn_5$

Specific heat and magnetization studies of the $Ce_{1-x}La_xRhIn_5$ alloy series give evidence for the Griffiths-phase theory disorder-driven NFL behaviour of Castro Neto and co-workers. In this picture quantum tunneling of RKKY-coupled local-moment clusters dominate the low-temperature properties of the system. Our zero-field muon spin relaxation (μ SR) experiments on $Ce_{0.2}La_{0.8}RhIn_5$ show that this alloy exhibits disordered spin freezing with a sharp transition at 0.16 K, and thus does not remain a paramagnetic metal, NFL or Fermi-liquid, as $T \rightarrow 0$.

Figure 124 shows the evolution of the zero-field muon spin relaxation from high-temperature Kubo-Toyabe behaviour due to nuclear dipolar fields to faster relaxation as $T \rightarrow 0$. This behaviour is well fit by an exponentially damped Kubo-Toyabe function. The temperature dependence of the exponential rate is given in Fig. 125, where it can be seen that a sudden onset occurs at $T = 0.16$ K. Assuming that this additional relaxation is due to a static distribution of local fields, the frozen moment at $T = 0$ is estimated as $\sim 0.13 \mu_B/Ce$ ion. This is an order of magnitude smaller than found from thermodynamic data, which indicates substantial compensation of the local moments by a Kondo effect with a characteristic temperature considerably higher than the freezing temperature.

That the zero-field relaxation is indeed static is indicated by the behaviour of the longitudinal-field μ SR

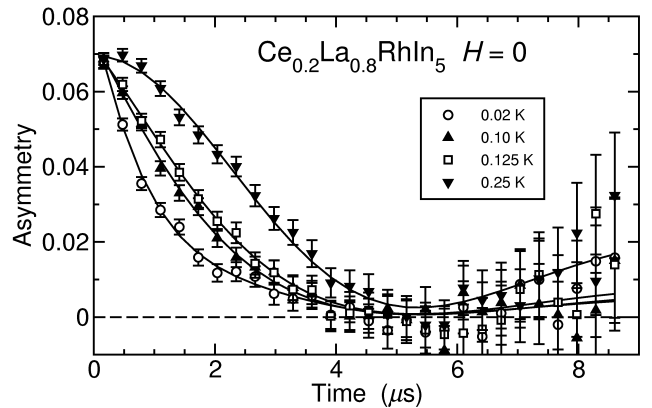


Fig. 124. Zero-field μ SR asymmetry functions in $Ce_{0.2}La_{0.8}RhIn_5$.

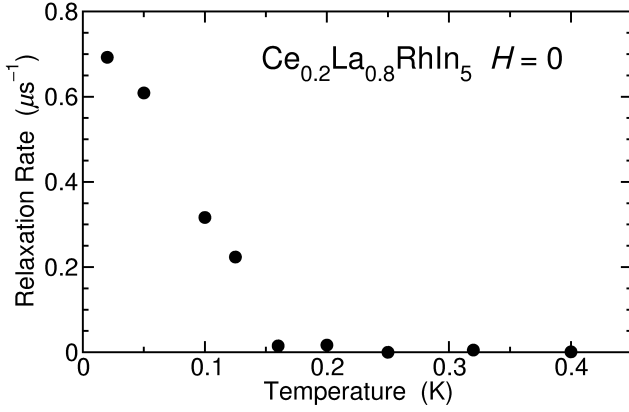


Fig. 125. Temperature dependence of the exponential muon spin relaxation rate in $\text{Ce}_{0.2}\text{La}_{0.8}\text{RhIn}_5$, $H = 0$.

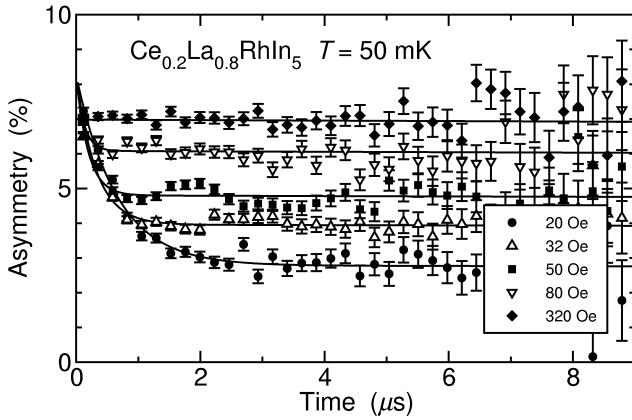


Fig. 126. Longitudinal-field muon spin relaxation functions at $T = 50$ mK in $\text{Ce}_{0.2}\text{La}_{0.8}\text{RhIn}_5$.

shown in Fig. 126, where it can be seen that the relaxation of the long-time component is extremely slow and the applied field decouples the relaxation. No dynamic relaxation is observed at any temperature; the spin freezing is not accompanied by the slow spin fluctuations found in spin glasses above the glass temperature and in a number of disordered NFL systems. This suggests that the freezing process never generates slow spin fluctuations, which seems inconsistent with the Griffiths-phase model.

Field dependence of critical slowing down in the frustrated pyrochlore $\text{Gd}_2\text{Ti}_2\text{O}_7$

In the pyrochlore titanate $\text{Gd}_2\text{Ti}_2\text{O}_7$ the Gd^{3+} local moments occupy corner-shared tetrahedra, leading to geometrical frustration, enormous ground-state degeneracy, and extreme sensitivity to mechanisms that break this degeneracy. $\text{Gd}_2\text{Ti}_2\text{O}_7$ exhibits a magnetic phase transition around 1 K, and a complex field-temperature phase diagram is found below this temperature. The 1 K transition is depressed slightly with field, and at ~ 2.5 T and ~ 0.86 K a pentacritical point is observed.

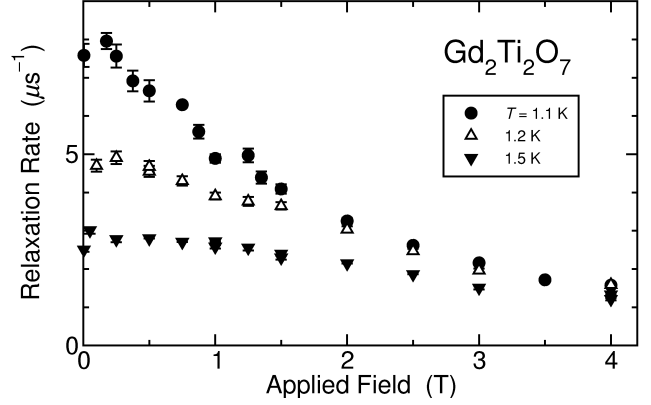


Fig. 127. Field dependence of the longitudinal-field muon spin relaxation rate in $\text{Gd}_2\text{Ti}_2\text{O}_7$.

We have carried out LF- μ SR in $\text{Gd}_2\text{Ti}_2\text{O}_7$ at temperatures just above the phase transition in longitudinal fields of up to 4 T. As can be seen in Fig. 127, at low fields the exponential relaxation rate increases markedly as the freezing temperature is approached from above. Similar behaviour is often observed in the neighbourhood of a magnetic transition, and is interpreted as evidence for critical slowing down of the spin fluctuations. In this case the rate increase is suppressed by applied field. This is surprising if the high- and low-temperature phases are separated by a line of second-order phase transitions, since then there should be critical slowing down at any applied field as the transition line is approached.

Our results suggest that only the zero-field transition is of second order, a situation that is reminiscent of ferromagnetism (which of course has no transition in nonzero field), and that to our knowledge has not been anticipated theoretically. No relaxation-rate anomaly is seen in the neighbourhood of the pentacritical point at ~ 2.5 T even at the lowest temperatures.

Experiment 1000

Measurements of the vortex core size in type-II superconductors

(*J.E. Sonier, F.D. Callaghan, SFU*)

Muon spin rotation (μ SR) has emerged as the leading experimental probe of the effective size of magnetic vortices in type-II superconductors. μ SR data on several different classes of type-II superconductors show that the size of the vortex core can depend quite strongly on temperature and the strength of the external magnetic field. These behaviours are attributable to the quasiparticle excitation spectrum both inside and outside of the vortex cores. Recently, we clearly demonstrated that the vortex-core size in the conventional superconductor V_3Si changes as a function of magnetic field due to the intervortex transfer of quasiparticles [Sonier *et al.*, Phys. Rev. Lett. **93**, 017002 (2004)]. The result confirms a key prediction of recent

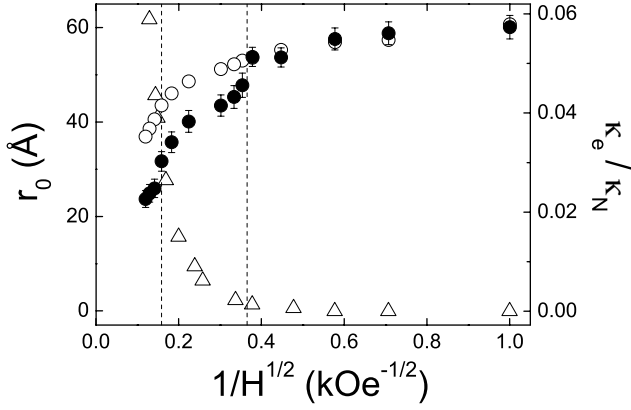


Fig. 128. The magnetic field dependence of the vortex core size r_0 measured by μ SR (solid circles) at $T = 3.8$ K from Sonier *et al.* [*op. cit.*], and the electronic thermal conductivity κ_e/T (open triangles) from Boaknin *et al.* [Phys. Rev. Lett. **90**, 117003 (2003)]. The open circles indicate the reduction of r_0 due only to the superposition of spatial current density profiles from individual vortices, and not the delocalization of vortex bound states. The data are plotted as a function of $1/H^{1/2}$, which is proportional to the inter-vortex spacing. The dashed vertical lines indicate the field range over which the vortex lattice undergoes a continuous hexagonal-square transition.

microscopic theories for strongly interacting vortices (Fig. 128). The effects of vortex-vortex interactions on the magnetic and electronic structure of the vortex state are of crucial importance to the interpretation of experiments on both conventional and exotic superconductors in an applied magnetic field.

The aim of Expt. 1000 is to apply our present understanding of quasiparticle core states in conventional superconductors to the investigation of the vortex-core size in unconventional type-II superconductors – keeping in mind that comparatively little is known about the structure of vortices in many of the exotic superconductors, including high-temperature cuprates. From theoretical considerations, one expects the electronic structure of a vortex to be strongly influenced by anisotropy of the superconducting energy gap, and anisotropy of the Fermi surface. With the discovery of MgB_2 has come particular interest in the effects of multi-band superconductivity (MBSC) on vortex structure. The presence of different superconducting gaps on separate Fermi sheets may lead to abnormally large vortices at low temperatures and magnetic fields. Such multi-band effects appear to be important in a number of type-II superconductors. This includes NbSe_2 , and even the high-temperature superconductor $\text{YBa}_2\text{Cu}_3\text{O}_{7-\delta}$.

In 2004 we carried out transverse-field μ SR measurements on several type-II superconductors. The determination of the vortex-core size from these measurements requires extensive data analysis. A considerable amount of time was spent this past year writing a

more powerful analysis code that takes full advantage of today's high-speed computers. Very recently we have completed our analysis of low-temperature data for the multi-band superconductor NbSe_2 .

The measurements on NbSe_2 were performed in a dilution refrigerator at $T = 20$ mK. Such low temperatures suppress thermal excitations of the electronic vortex core states, which tend to obscure the effects of MBSC on the field-dependence of the core size. The results of our data analysis are presented in Fig. 129. We see that ξ (the Ginzburg-Landau coherence length, which is a measure of the vortex core size) decreases rapidly at low fields before saturating at $H \approx 5$ kOe. The rapid shrinkage at low field is due to the more extended nature of the loosely bound core states associated with the smallest energy gap. This leads to rapid quasiparticle delocalization, as evidenced by the rapid increase in electronic thermal conductivity in the same field range. This behaviour is consistent with recent theoretical calculations of the local density of states in a multi-band superconductor. The rapid suppression of core states associated with the smaller energy gap means that the behaviour of the core size above 5 kOe is determined solely by the larger gap. The observed field-independent behaviour of the core size for $5 \text{ kOe} \leq H \leq 16 \text{ kOe}$ indicates no significant delocalization of core states associated with the large gap in this field range.

We have also established a direct relationship between the vortex core size and the electronic thermal conductivity in both single-band and multi-band type-II superconductors. In the conventional picture of an

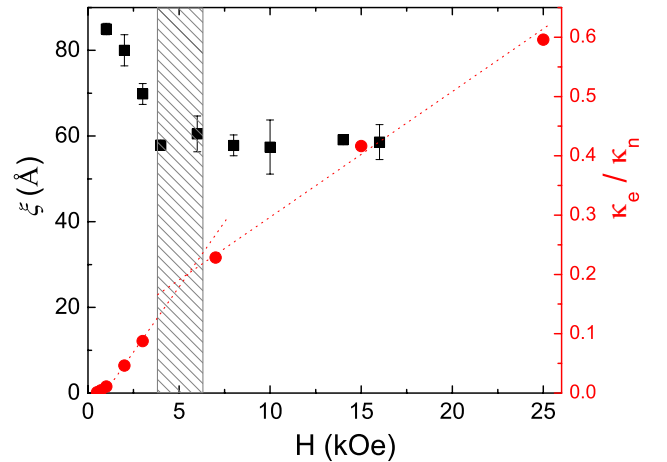


Fig. 129. The magnetic field dependence of the vortex core size ξ measured by μ SR (solid squares) at $T = 20$ mK, and the electronic thermal conductivity κ_e/T (solid circles) from Boaknin *et al.* [*op. cit.*]. The dashed line is a guide for the eye. The shaded region indicates the field range in which the form of the field-dependence of both quantities changes due to the multi-band nature of the superconductivity in this material.

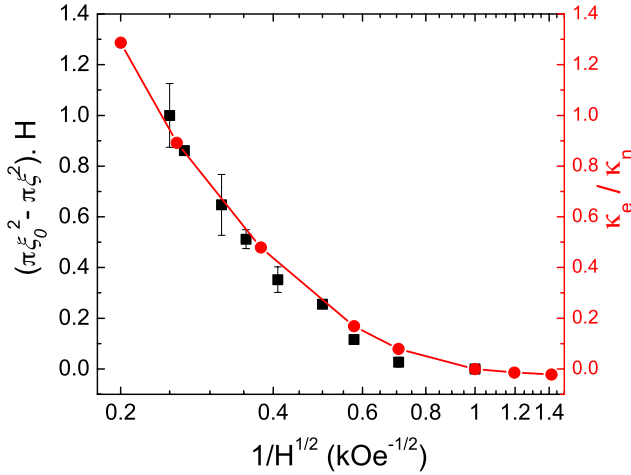


Fig. 130. The total reduction in core area (left axis, solid squares) and the electronic thermal conductivity (right axis, solid circles) for NbSe₂ plotted against $1/\sqrt{H}$ which is proportional to the intervortex spacing.

s-wave type-II superconductor, the density of bound core states is proportional to the vortex core area. Extending this to the scenario of a field-dependent core size, we have shown that the electronic thermal conductivity is directly proportional to the field-induced reduction in core area in the sample ($\sim(\pi\xi_0^2 - \pi\xi^2) \cdot H$, where ξ_0 is the measured low-field value of the coherence length). This is demonstrated in Fig. 130 where we plot both quantities for NbSe₂ against $1/\sqrt{H}$ (which is proportional to the intervortex spacing). For both materials the two data sets show the same field-dependence. This agreement is also observed in V₃Si. Coupled with earlier work [Sonier *et al.*, Phys. Rev. Lett. **82**, 4914 (1999)] that established the effect of core size on the specific heat of NbSe₂, we have now established an intimate relationship between the vortex core size and the thermal properties of *s*-wave type-II superconductors.

Experiment 1001 Mu defect levels in III-V semiconductors (*R.L. Lichti, Texas Tech*)

The main experimental goal of Expt. 1001 is to accurately measure ionization rates for the bond-centred (BC) and tetrahedral (T) muonium species in III-V compounds in order to determine the muonium analogue of the donor and acceptor defect energy levels for hydrogen impurities in these compounds. If both of these defect levels fall within the bandgap, their midpoint locates the primary hydrogen level that has been predicted to be pinned at a universal energy with respect to vacuum, independent of the host material [Van de Walle and Neugebauer, Nature **423**, 625 (2003)]. The purpose of this experiment is to test these predictions and locate that energy as accurately as pos-

sible for materials where the neutral charge state of Mu is observed for both the BC (donor) and T (acceptor) sites. Both Mu⁰ centres are well known to occur in GaAs and GaP; however, previous data did not provide any of the required ionization energies to sufficient accuracy.

During the first week of beam time for this experiment, we have concentrated on obtaining the Mu donor energy level in GaAs and GaP by obtaining the ionization energy for Mu_{BC}⁰. This is best done by extracting the lifetime broadening from the relaxation rate for the hyperfine lines for that species in spin-precession measurements. We used the HiTime apparatus, taking spectra at 5 T with relatively small temperature steps across the region where the spectra for Mu_{BC}⁰ was known to disappear. We chose to apply the field along a $\langle 111 \rangle$ direction where one set of BC hyperfine lines is for a single bond orientation. In fact, for GaAs we were able to use all of the lines even though the field was not precisely aligned.

Figure 131 shows the activated part of the relaxation rates for a semi-insulating GaAs sample, separately extracted for each BC (0°) line and each set of slightly misaligned 70° lines. These data yield an ionization energy of 165 ± 6 meV for Mu_{BC}⁰ in GaAs from an average of the four separate measurements. A similar treatment gives about 150 meV for Mu_{BC}⁰ in GaP, although a final analysis of that data is not yet completed. Figure 132 shows the preliminary analysis for one of the BC hyperfine lines in a semi-insulating sample of GaP. Assuming that the BC site lies lowest in energy for Mu⁰ and the disappearance is due to

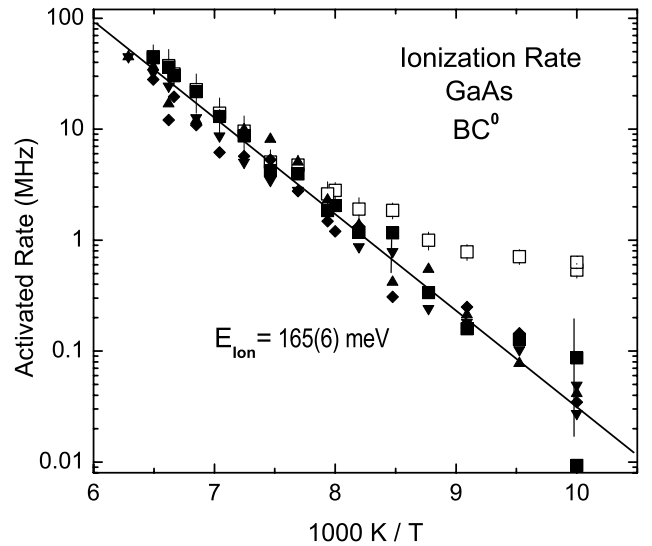


Fig. 131. Ionization rate for Mu_{BC}⁰ in GaAs extracted from the relaxation rates for the various lines in the BC hyperfine spin-precession signals. Open squares are the raw data for one line, filled symbols have the non-lifetime contributions removed.

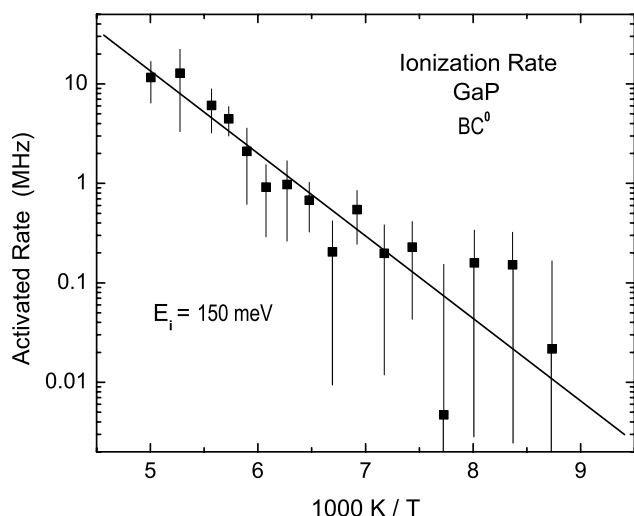


Fig. 132. Preliminary result for the ionization rate of Mu_{BC}^0 in GaP from one of the BC hyperfine lines.

ionization via thermal promotion of an electron to the conduction band, these numbers accurately define the Mu donor level in GaAs and GaP, providing half the information required to experimentally define the hydrogen pinning energy in each case.

The energy for the Mu_{T}^0 transition to Mu^- via “hole ionization” (promotion of an electron from the valence band onto the T-site Mu species) would yield the acceptor energy level as the other half of the necessary experimental information. The initial data imply that, in the semi-insulating GaP sample used for the BC result, the Mu_{T}^0 signal persists to above the upper temperature limit for the HiTime spectrometer. The lower temperature data that were acquired indicate that the atomic muonium centre may be localized at a single T-site in GaP near 100 K, while in GaAs this centre is very mobile at all temperatures. There may also be a second atomic-like Mu^0 signal in GaP in addition to the Mu_{T}^0 spectra previously reported. Specifically, between roughly 15 and 90 K a new and very narrow isotropic Mu^0 signal was observed with a HF constant roughly 250 MHz lower than that reported for Mu_{T}^0 . The origin of this signal is not identified at this point and the nature of this new paramagnetic muonium state in GaP will be pursued in future experiments, in addition to obtaining accurate ionization energies for the standard Mu_{T}^0 centres in both GaAs and GaP.

Experiment 1012

Organic free radicals under hydrothermal conditions

(P.W. Percival, SFU)

Research on organic chemistry under hydrothermal conditions is motivated by many different applications, including geochemical production of fossil fuels, biology of submarine volcanic vents, corrosion in pressur-

ized water nuclear reactors, destruction of chemical weapons and other hazardous materials, and “green” industrial processes. However, fundamental investigations of chemical reactions require the detection and monitoring of intermediates, often transient free radicals, which are difficult to detect under the extremes of pressure and temperature that define near critical and supercritical aqueous systems. In Expt. 842 we demonstrated the ability to study chemistry in aqueous systems up to 400°C and 400 bar, and in last year’s Annual Report we reported the first muon level-crossing spectra of muoniated free radicals under such conditions. Experiment 1012 was specifically designed to capitalize on this success, and to apply the combination of transverse-field μSR and level-crossing spectroscopy to investigate organic free radical chemistry in superheated water. To date we have explored applications in two areas: dehydration of alcohols and the enolization of acetone. The radicals detected, and their means of generation in superheated water, are listed in Fig. 133.

Examples of spectra are shown in Fig. 134 for the 2-propyl radical. The muon hyperfine constant is readily determined from the transverse-field μSR spectrum, being the difference between the two radical precession frequencies, as indicated by the double-headed arrow. The proton hyperfine constants can then be calculated from the μLCR resonance fields. There are three chemically distinct H atoms in 2-propyl, and this gives rise to three resonances, of which two are close enough to overlap. The hyperfine constants are sufficient to confirm the identification of the radicals produced in various chemical systems. For example, 2-propyl was identified as a product of the dehydration of both 2-propanol

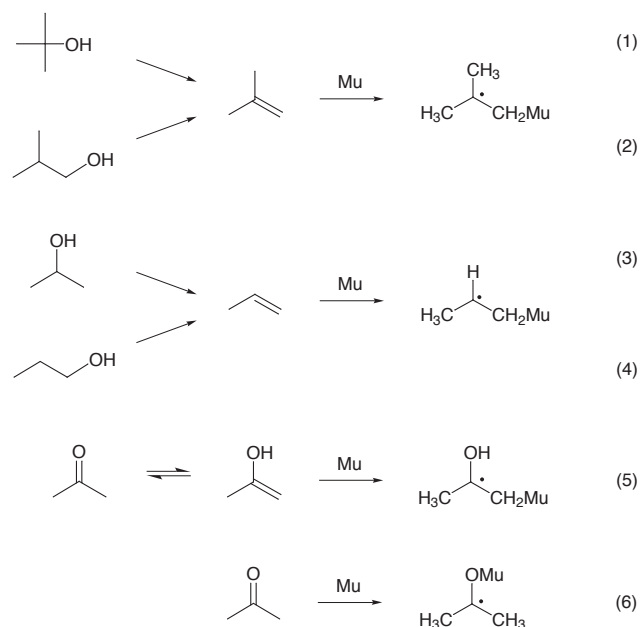


Fig. 133. Generation of muoniated radicals in superheated water.

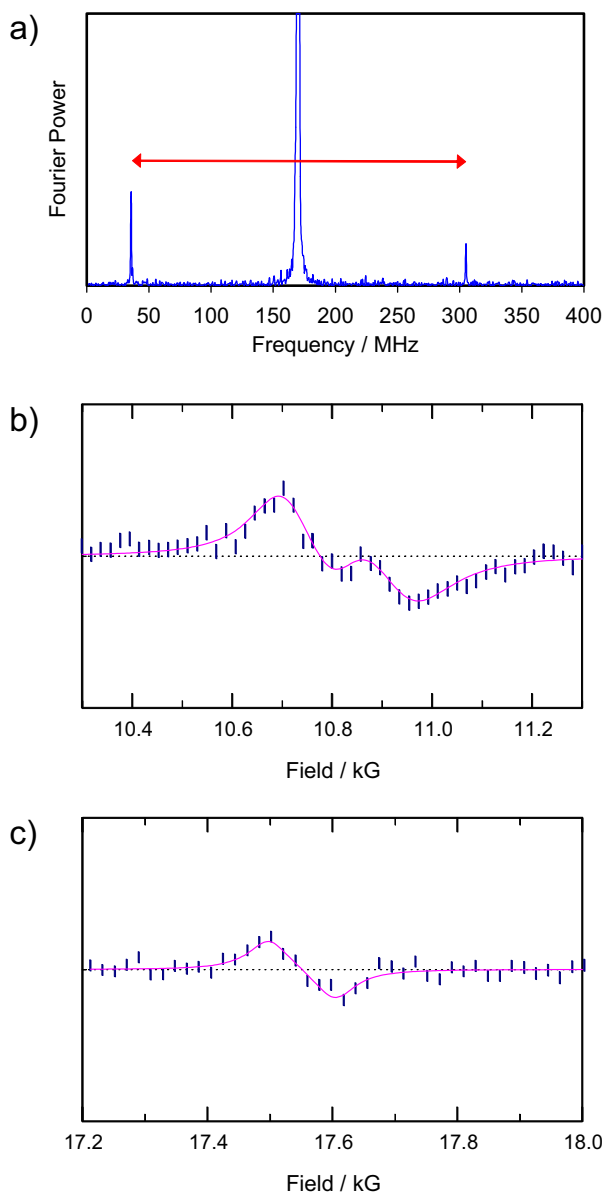


Fig. 134. Muon spectra of the 2-propyl radical in water at 350°C: (a) TF- μ SR spectrum, (b) CH₃ and CH₂Mu resonances from the μ LCR spectrum, and (c) α -H resonance.

and 1-propanol. A summary of muon and proton hyperfine constants, and their assignments, is given in Table XVI.

Sometimes identification of the radical intermediate is sufficient to resolve a particular question, such as the detailed mechanism of a reaction. In other cases the radical may merely play the role of a useful, identifiable “marker”. For example, the *keto-enol* tautomerism of acetone may be investigated by “labelling” the isomeric molecular forms as indicated in reactions (5) and (6) of Fig. 133.

Yet a third class of investigation involves the properties of the muoniated radical itself. By analyzing the temperature dependence of free radical hyperfine con-

stants it is possible to deduce details of intramolecular motion as well as potential interactions with the solvent. We emphasize that there is currently *no other technique available* to study organic free radicals under hydrothermal conditions. The subject of our first detailed study is the *tert*-butyl radical, which we have previously studied at much lower temperatures in organic media [Percival *et al.*, Chem. Phys. **127**, 137 (1988)]. Our new data are summarized in Fig. 135. Consistent with the earlier study, we find that the muon hyperfine constant falls with temperature and that this is matched by an increase in one of the proton hyperfine constants. To aid comparison, a reduced muon hyperfine constant is defined, $A'_\mu = 0.31413A_\mu$, to account for the ratio of proton to muon magnetic moments. It is then possible to calculate an average hyperfine constant for the CH₂Mu group: $(A'_\mu + 2A_p)/3$. As is evident from Fig. 135 this quantity is essentially temperature-independent, indicating that the temperature dependence of the separate muon and proton hyperfine constants is due to the rotational motion of the CH₂Mu group about a C–C bond. The second proton hyperfine constant is also temperature invariant, consistent with its assignment to the CH₃ groups, whose C_3 symmetry results in an average value regardless of the motion. Detailed modelling of the results should provide the potential barrier for CH₂Mu rotation.

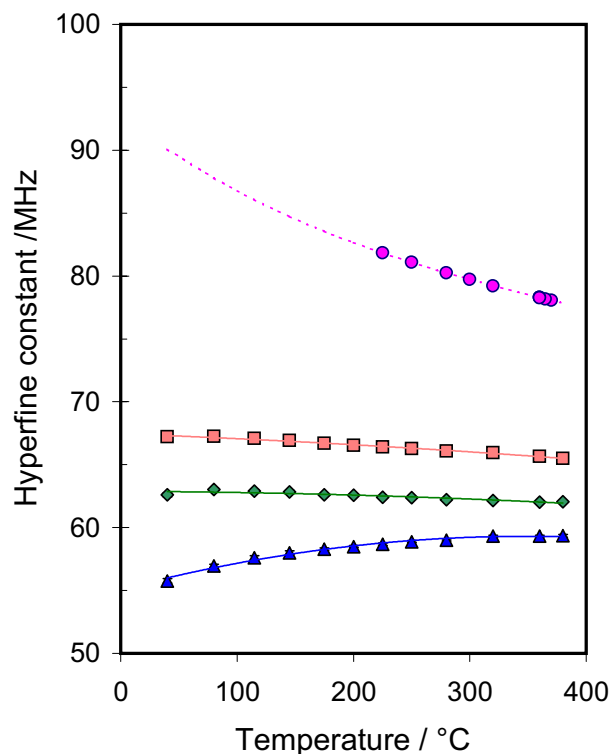


Fig. 135. Hyperfine constants for *tert*-butyl in water: \circ reduced muon constant (from CH₂Mu), \diamond proton constant from CH₃, \triangle proton constant from CH₂Mu, \square average for the CH₂Mu group.

Table XVI. Assignments and hyperfine constants for muoniated radicals detected in aqueous solutions of organic compounds at high temperature.

Sample	Radical	$T/^\circ\text{C}$	P/bar	B_{LCR}/kG	A_μ/MHz	A_p/MHz	Assignment
1 M t-BuOH	$(\text{CH}_3)_2\dot{\text{C}}\text{CH}_2\text{Mu}$	250	250	10.47	258.14	62.4	CH_3
		250	250	10.66	249.95	59.8	CH_2Mu
0.01 M t-BuOH	$(\text{CH}_3)_2\dot{\text{C}}\text{CH}_2\text{Mu}$	350	260	10.03	249.95	62.4	CH_3
		350	260	10.17	249.95	59.8	CH_2Mu
0.7 M i-BuOH	$(\text{CH}_3)_2\dot{\text{C}}\text{CH}_2\text{Mu}$	350	260	10.03	249.95	62.4	CH_3
		350	260	10.18	249.95	59.7	CH_2Mu
1 M 2-PrOH	$\text{CH}_3\dot{\text{C}}\text{HCH}_2\text{Mu}$	350	258	10.76	269.3	68.1	CH_3
		350	258	10.91	269.3	65.4	CH_2Mu
1 M 1-PrOH	$\text{CH}_3\dot{\text{C}}\text{HCH}_2\text{Mu}$	350	251	10.75	269.3	68.2	CH_3
		350	251	10.91	269.3	65.4	CH_2Mu
		350	240	17.55	269.3	-57.7	$\alpha\text{-H}$

Experiment 1013

Superconductivity of β -pyrochlore oxides

(A. Koda, R. Kadono, KEK)

Very recently, it was revealed that KOs_2O_6 , having a β -pyrochlore structure, exhibits a bulk superconductivity below $T_c \simeq 9.6$ K [Yonezawa *et al.*, J. Phys. Cond. Matter **16**, L9 (2004)]. Subsequently, a series of β -pyrochlore superconductors, RbOs_2O_6 ($T_c \simeq 6.3$ K) and CsOs_2O_6 ($T_c \simeq 3.3$ K), were discovered [Yonezawa *et al.*, J. Phys. Soc. Jpn. **73**, 819 (2004); *ibid.*, J. Phys. Soc. Jpn. **73**, 1655 (2004).] In the β -pyrochlore structure, it is notable that the formal oxidation state of the Os ion is $5.5+$ ($5d^{2.5}$). Such a mixed valence state has scarcely been studied in pyrochlore oxides so far, because of difficulty in the crystal synthesis. Another intriguing aspect is that the superconductivity occurs under a geometrically frustrated condition. This is in marked contrast to the case of $\text{Cd}_2\text{Re}_2\text{O}_7$ which has been the only pyrochlore oxide known as a superconductor until the discoveries of β -pyrochlore superconductors; the superconductivity in $\text{Cd}_2\text{Re}_2\text{O}_7$ occurs after a structural phase transition which is presumed to lift the degeneracy due to the geometrical frustration. Thus, there is an interesting possibility that the superconductivity in β -pyrochlore oxides might be realized on the spin-liquid ground state, as predicted for the triangular lattice by Anderson a long time ago. In order to obtain the clue to the pairing mechanism of superconductivity on pyrochlore lattice, we have conducted μSR measurements on KOs_2O_6 under a high transverse field.

In Fig. 136, the temperature dependence of the transverse relaxation rate (σ) of KOs_2O_6 at $B = 2$ T is shown. According to the Gorter-Casimir two-fluid model, the magnetic penetration depth λ is inversely proportional to $\sqrt{1 - (T/T_c)^4}$. From a relation $\sigma \propto \lambda^{-2}$, we obtain $\sigma \propto 1 - (T/T_c)^4$. As shown in Fig. 136,

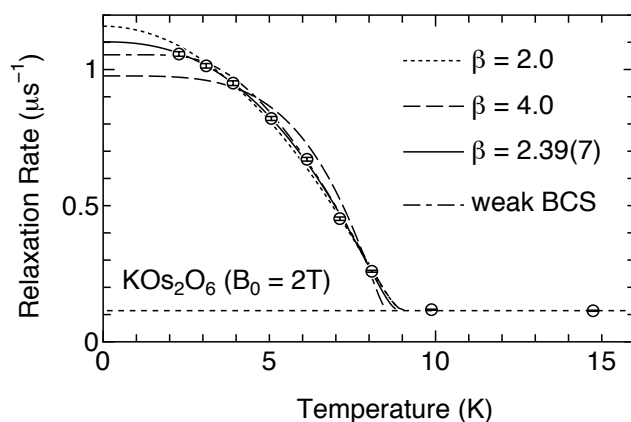


Fig. 136. Temperature dependence of transverse spin relaxation rate (σ) under a field of 2 T. The results of fitting analysis using the relation $\sigma \propto 1 - (T/T_c)^\beta$ are shown, together with the weak-coupling BCS case (dot-dashed curve). The dotted curve is for $\beta = 2$, whereas the dashed curve is for $\beta = 4$. The best fit is obtained when $\beta = 2.39$, which is represented by the solid curve.

our data exhibit significant deviation from this relation. The fitting analysis was then made with an arbitrary power,

$$\sigma = \sigma(T = 0) \left[1 - \left(\frac{T}{T_c} \right)^\beta \right],$$

with T_c as a free parameter. Here, the contribution from the nuclear magnetic moments like ^{39}K and ^{189}Os seen at $T > T_c$ was subtracted by a fixed amount prior to the fitting analysis. While the best fit is obtained when $\beta = 2.39(7)$ and $T_c = 8.91(3)$, the observed temperature dependence is nearly reproduced by $\beta = 2$ and $T_c = 9.07(2)$. The results are shown in Fig. 136 together with the fitting result by the weak-coupling BCS model. As seen in Fig. 136, it is quite difficult to distinguish those power-laws from the fully gapped case (weak BCS) only by analyzing the present data points above 2 K.

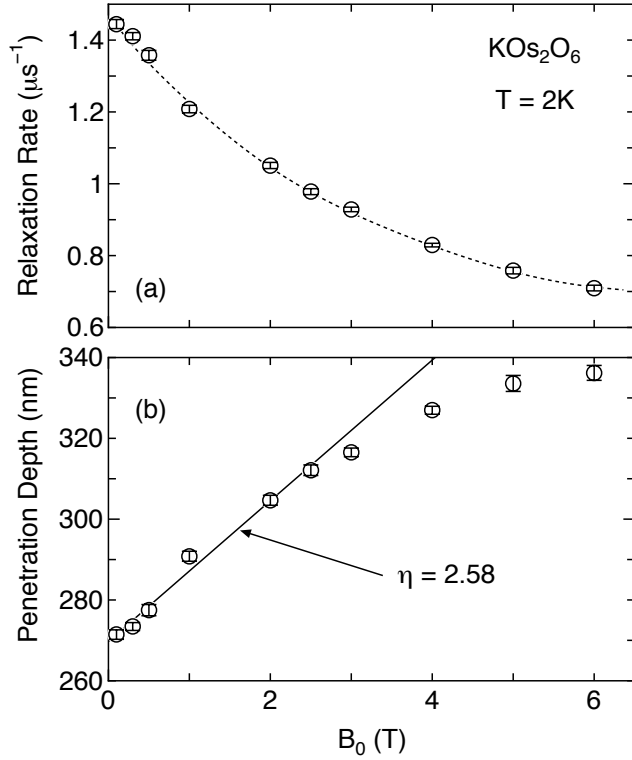


Fig. 137. Field dependence of (a) the transverse relaxation rate at 2 K and (b) the penetration depth (λ) deduced by assuming $B_{c2} = 40$ T. The broken curve in the upper panel is a guide to the eye. λ clearly obeys a linear dependence below $B \simeq 3$ T, whereas it shows a saturating tendency at higher fields. By fitting data below 2.5 T with the relation $\lambda = \lambda_0(1 + \eta(B/B_{c2}))$, we obtain $\eta = 2.58$.

In order to examine the low-lying quasiparticle excitations of KOs_2O_6 , we measured the field dependence of λ at the lowest temperature of 2 K. In Fig. 137(a), the field dependence of σ is shown. Although the exact value of the upper critical field B_{c2} in the present

specimen is unknown, we deduced λ versus the external field by assuming $B_{c2} \simeq 40$ T as suggested by bulk measurements. As shown in Fig. 137(b), the obtained λ is clearly field-dependent, showing a slight negative curvature with respect to the applied field. In particular, an approximately linear tendency is seen below ~ 3 T. Such increase of λ with increasing field indicates the occurrence of quasiparticle excitation due to the Doppler shift (i.e., so-called nonlinear effect) in the flux line lattice state and thereby strongly suggests the presence of low-lying quasi-particle excitations characterized by a small energy scale less than 2 K ($\simeq 0.2$ meV).

It is interesting to note that the observed tendency of saturation for λ against applied field has been reported in the case of $\text{YBa}_2\text{Cu}_3\text{O}_7$, which is explained by a combination of nonlinear and nonlocal effects [Sonier *et al.*, Phys. Rev. Lett. **83**, 4156 (1999); Amin *et al.*, Phys. Rev. Lett. **84**, 5864 (2000)]. However, we cannot exclude the multiple-gap scenario in KOs_2O_6 , as it has been found in MgB_2 [Ohishi *et al.*, J. Phys. Soc. Jpn. **72**, 29 (2003)], with one being a smaller energy gap than the thermal excitation energy at the temperature where the measurements were performed.

In summary, we have investigated the quasiparticle excitation in KOs_2O_6 by measuring the temperature/field dependence of λ . Our result demonstrates that λ increases markedly with applied external field up to 6 T, suggesting the presence of nonlinear and nonlocal effects. In particular, the presence of the nonlinear effect strongly suggests that the superconducting order parameter in KOs_2O_6 has a significant anisotropy or multigapped structure with a small gap energy. It is of particular interest to see whether or not the superconductivity in the other β -pyrochlore oxides is conventional.

LIFE SCIENCES

Experiment LS0

PET facilities

(K.R. Buckley, TRIUMF)

The PET facilities comprise the TR13 13 MeV H⁻ cyclotron, the ECAT 953B/31, HRRT, and microPET tomographs, and ancillary equipment such as counting and data acquisition systems. The HRRT (high resolution research tomograph) has been used for some primate studies over the past year. The patient bed was installed in the spring. The microPET scanner has been used routinely for the past year. The ECAT 953B continues to be the most used scanner despite its advancing age though the number of scans did decrease this year. The TR13 cyclotron continues to reliably produce radioisotopes for the varied projects undertaken by the Life Sciences program.

Personnel

Caroline Williams returned from maternity leave this fall. Due to limited funding from CIHR she is working reduced hours and Shilpa Shah, who had replaced Caroline during her maternity leave, is currently available on an hourly basis.

Siobhan McCormick of the Pacific Parkinsons Research Centre has taken over the routine operation of the microPET scanner to provide consistent scanning support to the varied groups making use of this scanner.

Rabbit line

This fall a new rabbit system controller was installed to replace the old controller that had shown some anomalous errors. Incorporated in this new controller, constructed by the TRIUMF Controls group, are new sensors installed in the 9 manholes between TRIUMF and the hospital. These sensors replace the old method of passive counting of pulses from parallel coils placed around the transfer line (the rabbits have magnets inside) with active sensors that send out a digital id when the rabbit passes. This method allows for better tracking of the rabbit even when a sensor fails since it is known which sensor detected the rabbit. In the old system if one sensor was not detected subsequent sensors were misidentified. The active sensors are constructed of robust parts that (we trust) will operate for many years.

TR13 cyclotron

Usage of the TR13 cyclotron was stable this year in delivered beam and the number of irradiations. The total number of runs was 942 vs. 970 in total last year and delivered beam is 454438 μ A min vs. 430630 μ A min total for 2003.

Unscheduled downtime this year was quite minor. The cryocompressor internal controls continue to function poorly, occasionally turning the compressor off for no reason. This is an inconvenience but does not generally cause downtime. A one-week scheduled shutdown allowed for the installation of a new controller for the rf amplifier restoring automatic operation of the amplifier after nearly 2 years without. This controller was made and installed by the TRIUMF RF group. This extended shutdown was also used to replace seals in the vacuum valve on the injection line that had begun to leak, and to service the mechanical vacuum pumps.

The target selector lid assembly on side 1 of the cyclotron required a complete overhaul in the spring to restore electrical isolation among the 4 sector collimators in front of each target. These collimator mountings gradually build up carbon deposits that need to be removed.

One extraction foil change was required through the year and only the fluoride production target was rebuilt. Four ion source filament changes have been done along with other miscellaneous service items.

At year end all eight target locations are occupied. These consist of

- one ¹⁸O-O₂ gas target (aluminum body)
- one ¹⁸O water target (niobium body)
- one ¹⁶O water target (aluminum body)
- one N₂/H₂ gas target (niobium body)
- one experimental flow through gas target (aluminum body)
- one experimental gas target (tantalum body)
- one experimental gas target for scattering measurements
- one location used for various solid targets.

A number of irradiations took place this year in support of LS8, in particular the production of ⁶⁴Cu for Oceanography. Similar beam to last year was delivered to LS4 in support of target development.

ECAT tomograph

Gantry electronics have been the dominant failures for the camera this year. In the past years replacement of some programmable logic chips in the buckets was sufficient to fix this problem. This past year some errors persisted in some boards even after changing these chips necessitating replacement of these boards. At the beginning of this year CTI gave notice that the supply of ECAT 953 and 951 parts would be discontinued at the end of March, 2004. A significant discount on an assortment of parts for the gantry electronics was negotiated, including 6 position/energy boards that have been the most failure prone item

lately. These parts were all installed in the gantry by the fall. Over the summer we received notice from the Hammersmith PET group that they were decommissioning their ECAT 953B and would sell parts to us. We have placed an order for an assortment of parts and are anxiously awaiting delivery. With receipt of these parts we hope to be able to assemble a test stand to troubleshoot a growing assortment of malfunctioning boards.

We are routinely repairing blocks in-house but have replaced only 1 block this year.

High resolution research tomograph

We are still learning our way around the HRRT scanner and interacting extensively with both CTI and other HRRT users to bring this system into routine use. The scanner has been used for some preliminary investigations with non-human primates. With the very large number of detectors in this camera (120000) the set-up and calibration is quite time consuming and the tools to do these tasks and evaluate the quality of the results are in their infancy (or non-existent). One concern for us and all HRRT users is the stability of the camera calibration but even in determining this we have encountered other obstacles. We experienced several failures of the acquisition disk array which resulted in losing some data for both stability measurements and normalizations. We believe this may have been caused by the combination of SCSI raid card and network card in the acquisition computer as determined by our computer system manager, Kelvin Raywood. The inconsistency of various software programs has also made evaluation of the camera difficult. In November the HRRT project manager visited for a few days and we were able to deal with several issues. The major task we began at that time was a complete detector set-up with a new lower gain on the phototubes. This lower gain appears to have resulted in much better position profiles but the process of the set-up for all 120000 detectors is tedious, taking 3.5 weeks. Fortunately this resulted in improved camera performance.

The patient bed arrived in June and was easily installed. Some difficulties exist with the bed motion control and we are working with CTI and the bed manufacturer to resolve these. The bed was shipped with a head holder but this holder is not adequate so an outstanding item on the to do list is to design an appropriate head holder.

MicroPET

The microPET scanner was used routinely throughout the year. The major difficulty encountered was with the transmission point source behaviour and with software updates. We have been acting as a beta test

site for Concorde which necessitates an investment of time to test and evaluate the software.

The point source mechanism is used in singles mode to generate the blank and transmission scans. Occasionally the reported source position was not accurate and these files were unusable. Attempts by Concorde to fix this were prolonged but an intermediate solution is in place now.

The microPET room underwent some additional modifications to add oxygen service, anesthetic gas withdrawal, and additional cooling. This has made the room much more comfortable.

In some cases microPET scans are scheduled to coincide with tracer deliveries for the ECAT scanner to minimize load on the chemists. Two scans were thus lost this year when the ECAT scans did not proceed and the production of tracer for the microPET alone was not deemed appropriate.

Statistics

Table XVII. TR13 run statistics.

	2004	2003
Total runs conducted	942	970
Total runs lost	6	18
Total beam delivered ($\mu\text{A min}$)	454438	430630
Delivered to – LS 3	310309	294090
– LS 4	63925	63279
– LS 8	78518	55636
– LS 13	0	14066
– LS 24	0	3559
– LS 56	1210	–
– LS 60	18	–
– LS 73	458	–

Table XVIII. ECAT scanning statistics.

	2004	2003
Total scans conducted	257	388
Total scans lost	64	75
Lost to – patient	31	23
– cyclotron	6	18
– chemistry	8	3
– scanner	12	20
– staff sick/away	7	11

Table XIX. HRRT scanning statistics.

	2004	2003
Total scans conducted	36	23
Total scans lost	9	2
Lost to – chemistry	1	2
– scanner	8	0

Table XX. MicroPET scanning statistics.

	2004	2003
Total scans conducted	142	66
Total scans lost	19	10
Lost to – cyclotron	1	1
– subject	12	6
– staff sick/away	0	3
– scanner	4	0
– ECAT	2	0

Experiment LS3

Synthesis of radiopharmaceuticals for positron emission tomography

(S. Jivan, A. Studenov, TRIUMF)

The PET group at TRIUMF continued to produce 2 to 3 radiopharmaceuticals on any given day despite the fact that the CIHR grant was not funded. This absence of funding resulted in the termination of two chemistry staff members.

In collaboration with TRIUMF, the BC Cancer Agency has hired two chemists to set up and routinely produce [F-18]fluorodeoxy glucose. They will use the TR13 cyclotron and PET lab space until their eventual move to the BC Cancer Agency in downtown Vancouver.

Routine production

Table XXI summarizes the total number of deliveries to UBC hospital and other facilities, and the number of development runs.

Of the 355 deliveries sent to UBC, 17% were processed for the microPET scanner only and 9% were shared with ECAT and microPET. 14% of the total were synthesized for the HRRT scanner.

^{13}N deliveries for the Botany Department at UBC were reduced but still continue on demand. An increase in development runs was due to graduate students doing target development and researching new materials for increasing production demands.

We continue to use tetrabutylammonium fluoride, a base source in most of the ^{11}C methyl iodide reactions, to enhance and stabilize yields and lower the amount of precursor used. Most precursors are made in-house by JML Biopharm Inc. except Raclopride which is donated by ASTRA ZENECA AB.

Table XXI. Total number of deliveries for 2003 and 2004.

	2003	2004
UBC	406	355
Others*	75	57
Development runs	177	226

*UBC Botany, Chemical Engineering, PETScan Centre.

New development

Two new tracers, [F-18]FHBG and [F-18]FLT, were successfully developed and routinely produced for microPET scanning. FHBG is used as a reporter probe to image expression of herpes simplex virus type-1 thymidine kinase (HSV1-tk) reporter gene and FLT is used as a marker for cell proliferation in cancer cells. Development continues in upgrading the methyl iodide system and improving yields from targets.

Experiment LS4

PET targets

(T.J. Ruth, TRIUMF)

The development of targets for the production of the neutron deficient isotopes ^{18}F ($T_{1/2} = 109.8$ min), ^{11}C ($T_{1/2} = 20.4$ min), ^{13}N ($T_{1/2} = 10.0$ min) and ^{15}O ($T_{1/2} = 2.05$ min) on the TR13 has been a major task for the TRIUMF PET group during the last several years and has been supporting a number of other projects as indicated in LS8 – Radiotracers.

Progress

Status of high current $^{18}\text{O}_2$ gas target The high current target for the production of ^{18}F -fluoride from ^{18}O - O_2 is presently going through the detailed design stage. The overall internal target dimensions have been specified based on beam size and scatter, gas pressure, stopping power, and heat transfer. The raw niobium has been purchased as has the pressure transducer, ^{18}O - O_2 gas, and the cold trap vessel. The CP42 cyclotron can deliver beam down to an energy of 23 MeV. The initial concept was to irradiate at 20 MeV and, after an analysis of the target parameters required for this energy, it was decided to incorporate a degrader to bring the beam to 20 MeV. Once the detailed target drawings are complete the target will be sent out for machining. The ATG group is currently assembling a wire scanner to be placed in front of the target to allow the beam spot to be measured and controlled.

Status of heat transfer tests Gas target heat transfer is not optimized in most gas target designs nor is it readily predictable when designing a target. Various works have looked at pressure rise behaviour as a means to determine thick target conditions and some have sought an empirical relationship between pressure and power deposition. None have proven to be generally applicable over a broad range of target designs or energies. We have begun some measurements with a heating assembly that can be inserted into a gas target to deposit a known power while observing pressure rise. With these data, heat transfer properties can be measured and ultimately optimized.

^{11}C - CH_4 production

Status of methane production As reported at last year's LSPEC meeting, we discovered that niobium is a very good target chamber material for the production of ^{11}C -methane. This result was published in the Journal of Nuclear Medicine and Biology mid-year along with the observation that an equation of the form $Y = A I e^{-at} \times \text{SF}$ accurately describes the ^{11}C -methane yield from the target where A and a are fitted parameters, t is the length of irradiation, I the beam current (μA) and SF is the saturation factor ($1 - e^{-\lambda t}$). This observation implies that a first order reaction competes for the ^{11}C . Since tantalum exhibits very similar properties to niobium, it is expected to provide similar methane yields. However, a gas target constructed from tantalum provided very good ^{11}C - CO_2 yields but exceptionally poor ^{11}C - CH_4 yields (see Fig. 138). It is not understood why this is.

Interaction of the proton beam with the target chamber walls

Gas targets are the most common form of target used in the production of short-lived radioisotopes for positron emission tomography (PET). Many researchers, however, have reported a non-linear relationship between radioisotope production yield and particle beam current. This lowered yield has been attributed to several factors including the scattering of beam particles into the target body walls, radioactive species becoming trapped in the target body walls, and gas density reduction due to the deposition of heat from the incident ion beam. In this study we investigate the last factor. A 13 MeV proton beam from the TRIUMF TR13 cyclotron was used to measure the energy of scattered protons in a gas target. The average proton energy reaching the target body walls was determined by measuring the ratio of radioactivity of two simultaneously produced radioisotopes in a metal foil lining the wall of the target. The relationship between

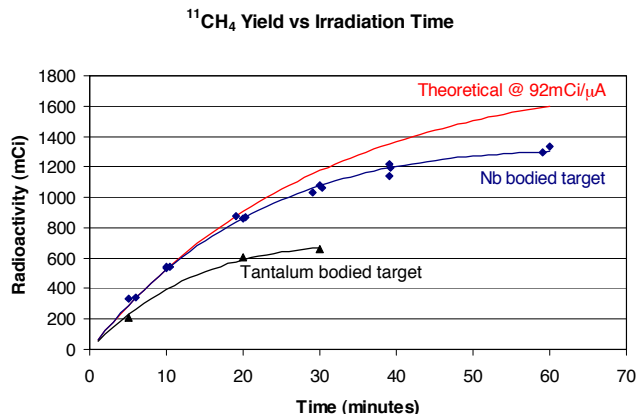


Fig. 138. Tantalum bodied target yields for ^{11}C - CO_2 ($A = 85$; $a = \text{NA}$) and ^{11}C - CH_4 ($A = 41$; $a = 42$) with $I = 20 \mu\text{A}$.

the ratio of radioactivities (production of $^{63}\text{Zn}/^{65}\text{Zn}$ from copper foils) and proton energy was determined using a stacked foil calibration technique. These experiments were compared to theory using a Monte Carlo program (SRIM) to model the interactions of a proton beam within a gas target.

Production of ^{64}Cu

NatNi foils were irradiated with 6.9 MeV protons for the production of ^{64}Cu via the $^{64}\text{Ni}(p, n)$ reaction. This energy was achieved by means of an Al degrader to reduce the incident proton energy of 13 MeV to 6.9 MeV. This reduced proton energy was used to suppress the (p, α) reactions and hence the production of undesirable Co isotopes. Irradiations were nominally 4 hours with a beam intensity of 7–8 μA . After irradiation the short lived copper isotopes ($^{60,61,62}\text{Cu}$) were allowed to decay overnight to reduce radiation exposure to personnel. After this decay time the foils were dissolved in concentrated HCl. An AG1-X8 anion exchange column was used to separate the copper isotopes from the nickel target. The nickel was eluted with 100 ml 0.2 N HCl in 95% ethanol and the copper isotopes were eluted with 25 ml 0.1 N HCl in 75% ethanol. The solution containing the copper isotopes was evaporated and an AG1-X8 anion exchange column preconditioned with HCl was used for further purification. The remaining nickel was eluted with 25 ml concentrated HCl and the copper isotopes were eluted with 20 ml 2 N HCl. Separation using a single column was not satisfactory for this application.

Production of $^{66,68}\text{Ga}$ for sugar labelling

NatZn foils were irradiated with 13 MeV protons for the production of $^{66,68}\text{Ga}$ via the $^{66}\text{Zn}(p, n)$ and $^{68}\text{Zn}(p, n)$ reactions. Typical irradiations were 10–15 min with a beam intensity of 5 μA . After irradiation, the target foil was removed and dissolved in concentrated HCl. The gallium isotopes were extracted from this solution with isopropyl ether. The dissolved zinc target and several copper isotopes ($^{61,64}\text{Cu}$), which are co-produced with the gallium, remained in the acidic aqueous phase. The gallium isotopes were back-extracted with water containing a few drops of HCl. The final aqueous phase was evaporated to a few ml in volume. This production method resulted in approximately 3 mCi of ^{66}Ga and 4 mCi of ^{68}Ga two hours after the end of irradiation.

In 2004 four batches of $^{66,68}\text{Ga}$ were produced for sugar labelling (LS53).

Experiment LS8

Radiotracers for the physical and biological sciences

(*T.J. Ruth, TRIUMF*)

Many of the projects formerly associated with LS8 have been spun off into their own separate Life Sciences projects. For historical reasons, the collaboration with Botany remains the major focus of LS8 and progress in this project is reported below along with an indication of the supply of tracers for other uses within the TRIUMF community as shown in Table XXII.

Increased nitrogen uptake

(*Collaboration with CELLFOR: M.Y. Siddiqi, M. Shariati, W. Li, J. Vidmar*)

Our goal of increasing nitrate uptake in tobacco plants and poplar seedlings by over-expressing the high-affinity NO_3^- transporter gene (AtNRT2.1) was initially unsuccessful. Following upon our discovery that a second family of genes (the NAR2 family) must be co-expressed in order to achieve efficient NO_3^- uptake, we have successfully demonstrated that knock-out mutants of Arabidopsis lacking a functional NAR2 gene fail to absorb nitrate. We have now developed strains of tobacco over-expressing both the AtNRT2.1 gene and the AtNAR2 gene. Using $^{13}\text{NO}_3^-$ to measure nitrate uptake, we have obtained increased nitrate uptake and our preliminary growth measurements indicate increased growth in these lines. This work is now proceeding to the next stage, namely pseudo-agricultural testing in greenhouse studies being conducted by agronomists in Alberta.

$^{13}\text{NO}_3$ influx in the fungus *Aspergillus nidulans*: a structure function study of the NRTA gene sequence and NO_3^- uptake

(*Collaboration with S. Unkles, J. Kinghorn, St. Andrews, Scotland; T. Glass, Y. Siddiqi, W. Ye, UBC*)

With our Scottish collaborators, we have generated clones of *Aspergillus* modified at specific (putatively critical) arginine loci of the nitrate transporter protein. These arg sites are highly conserved in this gene family from fungi to higher plants. Our data have been accepted for publication in the Journal of Biological Chemistry. Replacement of arg 87 or 386 converts the protein from a high-affinity transporter with K_m 's for nitrate uptake around $10\ \mu\text{M}$ to a low-affinity transporter with a K_m around $15\ \text{mM}$. We believe that this positively charged amino acid is critical in the transmembrane uptake of nitrate. We are continuing to probe gene structure/function by replacing putative phosphorylation sites (serine and other amino acid residues) of the *Aspergillus* nitrate transporter. We believe that these phosphorylated amino acid residues are responsible for regulating nitrate uptake. The geneti-

Table XXII. Miscellaneous runs on the TR13 for 2004.

^{88}Y point sources for 8π group (SrCO ₃ target)		
Date	$\mu\text{A min}$	$\mu\text{Ci produced}$
June 4	61	9.2
June 11	300	117
(1 μCi and 2 μCi sources were prepared from the second run for the 8π group)		
^{48}V pins for microPET sources (Ti pin target)		
Date	$\mu\text{A min}$	$\mu\text{Ci produced}$
May 26	304	5×50
June 8	35	5×11

cally modified fungal strains will be tested for nitrate uptake using $^{13}\text{NO}_3^-$.

The role of the NAR2 gene family

During his Ph.D. studies at UBC, Mamoru Okamoto isolated an Arabidopsis mutant disrupted in the NAR2 gene. We have demonstrated that this mutant is unable to grow normally when nitrate is the sole source of N and that $^{13}\text{NO}_3^-$ uptake is dramatically reduced. Thus high-affinity nitrate uptake requires the participation of both the NRT2 and the NAR2 gene families. Using molecular methods we have evidence that the two proteins are associated in the plasma membrane for normal function. This evidence (based on the yeast hybrid method) is being tested at a biochemical level by use of affinity chromatography. We have expressed the NAR2 protein in *E.coli* and have made an affinity resin by conjugating this protein to an immobilized cobalt affinity resin. This will be used to "fish out" the putative NRT2.1 protein. If we can successfully bind NRT2.1 to the resin via its interactions with the bound NAR2 protein, we will have strong support for the molecular evidence that the two proteins interact in the cell membrane.

Experiment LS35

Development of ^{18}F labelled nitroimidazole PET imaging agents for tissue hypoxia

(*M.J. Adam, TRIUMF; D. Yapp, BCCA*)

Hypoxia in cells and tissues is an important component of various pathological states (e.g. ischemia and stroke). Hypoxic tumour cells are extremely important within cancer treatment because they are more likely to survive radiation and chemotherapy, leading to an increase in tumor resistance to treatment. More recent evidence suggests that hypoxia is related to the aggressiveness of disease. Such studies employed a microelectrode, used in many centres, but were limited because of invasiveness and requirement for an accessible tumour.

Derivatives of 2-nitroimidazole are used extensively as hypoxia markers. The 2-nitroimidazoles are not metabolized in oxygenated tissues, but bind to macromolecular proteins after reduction in hypoxic cells. This permits detection by a variety of techniques. For example, the products of such binding for the (pentafluoropropyl)acetamide (EF5) and (trifluoropropyl)acetamide (EF3) derivatives of 2-nitroimidazole can be detected by specific fluorescent antibodies.

The synthesis of ^{18}F -EF5 has now been developed and was achieved by preparing the allyl precursor and fluorinating it with ^{18}F elemental fluorine in trifluoroacetic acid. The radiochemical yield is 17% after HPLC purification.

We have made considerable progress on the use of ^{18}F -EF5 as a PET tracer for imaging hypoxia in malignant tumours. The installation and commissioning of the MicroPET[®] scanner at the UBC hospital sparked a series of studies with animal models for cancer. The logistics involved in performing these experiments (radiotracers from TRIUMF, animals from the BC Cancer Agency, scans at the PET suite in the UBC hospital) have been resolved. We now have funding for two studies in animal tumours.

We intended to submit a clinical trial application (CTA) with Health Canada in 2004 for a pilot study to examine hypoxia in resectable lung cancer tumours. Unfortunately, this was delayed while Health Canada finalized its regulations on the human use of positron emitting radiopharmaceuticals (PERs). Thus, our original plan to carry out human PET imaging was delayed. However, Health Canada has now provided our group with guidance on the combined (labelled and unlabelled) EF5, and Dr. Laskin has taken the lead in preparing a CTA for submission. We anticipate the application will be submitted in the second quarter of 2005. In preparation for this application, all pyrogen and sterility testing has been completed and all QC and production data are available so the Quality Information Summary (QIS) portion of the CTA can be finalized.

The animal studies first described in LS35 have gone well in 2004. We have also successfully obtained funding from the Cancer Research Society to carry out studies in a colorectal cancer model (HT-29); preliminary data and scans from LS35 were used to support this application.

Experiment LS39

Positron emission profiling (PEP) for pulp and paper fluid dynamic studies

(M. Martinez, UBC)

Over the past year, we have attempted to extend the PET technique and measure the activity distribu-

tion in pulp suspension flowing in a tube with a sudden expansion in its area. Three preliminary scans have been conducted and a numerical simulation of the experiment has been developed.

Background

It is widely known that pulp suspensions do not flow until a certain critical shear stress (or yield stress) is exceeded. With traditional papermaking, the suspension is initially fluidized by turbulence created locally from a sudden change in flow area in a device called a "head box". In this case, the fibre network is broken down into smaller flocs and single fibres with weakly correlated velocities. Suspension fluidization is attained by inducing turbulence and is aided by the addition of chemical deflocculants. Characterizing this event is difficult as these suspensions are opaque.

Progress

Over the past 12 months we have built the experimental apparatus, performed three preliminary scans on the microPET, and started developing a numerical algorithm to simulate the experiment.

The flow loop used in the experiments consists of a 30 gallon tank, a 1.5 hp centrifugal pump, two magnetic flow meters, two pressure transducers, a recirculation path, and valves for control. The test section is made of clear polycarbonate and has a 2.75 in. inner diameter and is 46 in. long. The inlet diameter is 0.55 in. forming a 1:5 sudden expansion on one end and a 5:1 sudden contraction on the other. The flow reaches and leaves the test section through 15 ft. lengths of 0.55 in. inner diameter reinforced hose. Both ends of the test section are terminated with a pair of full bore ball valves and a full bore quick disconnect coupling to facilitate placement and removal of the test section into the gantry of the scanner. The test section is mounted to a 30 in. linear stage on both sides of the scanner so that the test section can be moved along its axis. To shield the scanner's detector blocks from events originating outside of the camera, 3/4 in. lead shielding is positioned concentrically with the test section up against the scanner. Three scans were conducted last year.

Experiment LS50

Antisense imaging nucleic acids for Parkinson's disease

(H. Dougan, TRIUMF)

A sizable literature exists demonstrating the antisense action of short DNA sequences on brain messenger RNAs. With the loss of such mRNAs, production of specific proteins is knocked down, leading to observable changes in animal physiology and behavior. We have a specific interest in mRNAs related to Parkinson's disease. We wish to image such mRNAs using radio-tracer DNA molecules. So far, our labelled DNAs have

been unsuccessful in this application. A classical problem with pharmaceuticals is crossing the blood brain barrier (BBB), and this is probably related to our difficulties. We are currently studying two technologies for crossing the BBB. One technology is infusion of the DNA into the brain through a fine capillary. The second technical approach to the BBB problem is transport of the DNA using an antibody directed to the iron transportation mechanism in the BBB.

Experiment LS51

Auger therapy for prostate cancer

(H. Dougan, TRIUMF)

Experiment LS51 examines the possibility of killing prostate cancer cells using an iodoandrogen steroid (EMIVNT labelled with ^{125}I or ^{123}I) brought into proximity with cancer cell DNA by the androgen receptor. The graduate student M. Fedoruk believes that he made the preliminary observation that [^{125}I]EMIVNT results in small but detectable Auger killing of a line of prostate cancer cells in tissue culture. This was presented at 5ISR in Whistler, BC in September. A multidisciplinary group of scientists has formed from the BC Cancer Agency and the Prostate Centre to find the strengths and liabilities of EMIVNT for prostate cancer therapy. At present there is optimism that a drug similar to EMIVNT may be developed for practical cancer therapy.

Experiment LS53

Synthesis of $^{99\text{m}}\text{Tc}$ and $^{186,188}\text{Re}$ sugar derivatives

(M.J. Adam, TRIUMF; C. Orvig, UBC)

An NSERC strategic grant was awarded (October, 2001) (M.J. Adam, PI, \$78,200/year for 3 years) to carry out research on the synthesis of technetium and rhenium labelled carbohydrates for use in nuclear medicine imaging and therapy. An extension to September 30, 2005 was granted. Dr. Adam is collaborating with Dr. Orvig in the UBC Chemistry Dept., AnorMED (M. Abrams, CEO), and MDS Nordion (Brian Abeysekera). Post doctoral fellows (Dr. Simon Bayly and Nathaniel Lim) and two graduate students (Cara Fisher and Charles Ewart) have also been working on this project for approximately three years. Cara Fisher was awarded an NSERC IPS scholarship for two years, starting in September, 2004, with MDS Nordion as the sponsoring company.

Radiolabelled carbohydrates have been of significant interest to nuclear medicine due to the success of 2- ^{18}F -fluoro-2-deoxy-glucose (FDG) as an imaging agent in positron emission tomography (PET). This success has naturally raised the question of whether a single-photon emitting glucose analogue with similar properties to FDG can be developed for use with single-

photon emission computed tomography (SPECT). In fact, just this year another group demonstrated that a glucosamine Tc complex does indeed get taken up into tumours. The mechanism for this uptake is as yet unknown. Because of the relatively short half life of ^{18}F (110 min) its use is limited to facilities that have an accelerator in close proximity to chemistry laboratories and medical facilities. $^{99\text{m}}\text{Tc}$ is the most widely used isotope in SPECT due to the fact that it is a generator produced, commercial isotope which makes it convenient to use and relatively inexpensive. It also has ideal physical properties for imaging. The drawback to this isotope is that it must be attached to the molecule via a chelate or organo-metal conjugate, which may perturb the system being studied. A SPECT analogue based on a widely available isotope such as $^{99\text{m}}\text{Tc}$ would make these agents available to the broader medical community. Among elements of the same series as Tc the isotopes ^{186}Re and ^{188}Re show promise in the development of therapeutic strategies. For a β^- emitting radioelement to be therapeutically useful, a half-life of between 12 hours and 5 days is preferred: moreover, for a 1 MeV β^- particle, the depth of penetration into tissue is approximately 5 mm. Furthermore, if some of the disintegrations are accompanied by 100–300 keV gamma photon, the behaviour of the radioelement can be conveniently followed by using a gamma camera. The nuclear properties of ^{186}Re and ^{188}Re are optimal for these purposes.

For the last three years we have been developing two synthetic approaches to the preparation of sugar-metal derivatives because of the known avidity of glucose to tumours. One approach forms compounds containing a Cp-M-tricarbonyl moiety (M = Tc or Re) and the other forms chelate compounds with *fac*-[M(H₂O)₃(CO)₃]⁺ metal cores. With the first approach several ferrocenyl sugars have been synthesized. Attempts to synthesize the corresponding Cp-M-tricarbonyl products have been successful and we are now employing a single ligand transfer reaction. As a side project we have observed that several of these ferrocenyl sugar conjugates have shown cytotoxicity towards mouse lymphoma cells with IC₅₀ values less than 20 μm . They are now being tested for cytotoxicity towards human breast cancer cells and are being examined for antimalarial activity. The second approach involving sugar-pendent ligands has been even more productive and we have now synthesized and characterized several new glucose and glucosamine Tc-99m and Re-186 complexes. The first of these has been published recently in *Bioconjugate Chemistry* [Bayly *et al.*, **15**, 923 (2004)]. These complexes with Tc and Re radionuclides were formed by using the *fac*-[M(H₂O)₃(CO)₃]⁺ aqueous reagent originally de-

veloped by Alberto and co-workers. Since this first glucosamine compound we have synthesized several pyridinone, diamine and bipyridyl sugar chelate complexes with ^{99m}Tc and ^{186}Re and are now focusing on developing other tridentate and Cp-tricarbonyl ligand compounds. These are expected to be the most stable and thus, more likely to be better candidates as therapy and imaging agents. Several of these chelate ligands have also been complexed with positron emitting Cu-61,64 and Ga-66. Complexes with these isotopes are structurally different than the Tc or Re tricarbonyl derivatives giving us a broader range of agents to evaluate. With this combination of SPECT and PET agents, coupled with the recent findings that similar agents are indeed taken up into tumours, we feel these compounds have significant potential as therapy and imaging in oncology.

Experiment LS56

Synthesis of radiolabelled nucleotides and oligonucleotides

(M.J. Adam, T. Ruth, H. Dougan, TRIUMF; D. Perrin, UBC)

This is a progress report on the development of chemistry for the F-18 labelling of oligonucleotides. One of the strategies that we are pursuing is to develop a general method to label the phosphorous atom directly with nca F-18 fluoride so that there is little structural change to the molecule. Thus, the biological activity of the oligo will be preserved. Model compound systems were developed this year to determine if P(III) and P(V) containing derivatives could be labelled with nca fluoride. We were able to successfully incorporate F-18 into both P(III) and P(V) model compounds. Another approach, undertaken by Dr. Perrin's group in UBC Chemistry, makes use of the fact that fluoride anion reacts readily with boron containing derivatives of oligonucleotides. A grant application to the CIHR to support this work was successful. An abstract to the 2004 Society of Nuclear Medicine meeting was presented and a manuscript on the P-F chemistry was submitted.

Experiment LS57

Quantitative imaging with the Concorde microPET[®]

(V. Sossi, UBC)

Several issues were addressed in relation to the microPET[®]: detector normalization, attenuation correction and scanning protocols.

Normalization

Detector normalization has been identified as one of the major contributors to image non-uniformity. A new component based normalization method in collab-

oration with D. Newport from CTI-Concorde has been developed and tested on phantom and rat data [Camborde *et al.*, Proc. IEEE/MIC, Rome, Italy (2004)]. During the course of this study a direct application of the measured attenuation correction factors was confirmed to be another very important source of image non-uniformity. Image uniformity was found to improve greatly if μ -map images were first segmented into air and tissue and the segmented regions were assigned pre-defined μ -values.

Attenuation correction

Presently, the attenuation correction factors are obtained using a rotating ^{68}Ge point source. These data result in an incorrect attenuation correction, because the effect of photon scatter in the transmission scan is not properly accounted for. Using simple water phantoms, we find a 50% overestimation of the reconstructed linear-attenuation coefficients for water using the reconstruction software and scatter correction (SC) currently provided by the manufacturer. Linear attenuation coefficients without the SC data are underestimated by 25%. These errors have also been found to vary with the size of the object being imaged and spatially over the extent of the object. Currently, we must segment the attenuation maps to obtain reasonable attenuation correction factors (ACFs). However, noise in the reconstructed attenuation map is a significant problem, which causes this segmentation to be difficult and highly user dependent. We are currently investigating scatter correction methods for transmission data.

We have also performed a preliminary investigation of a post-injection transmission protocol using the ^{68}Ge transmission source. It was found that the key step in this procedure was to apply segmentation to the μ -maps obtained from the post-injection transmission scan and to assign pre-defined μ values.

Dead time correction

As part of our collaboration with CTI-Concorde, we have also investigated the dead-time correction currently applied by the microPET[®] acquisition program. During these studies we have identified and resolved an error in this software.

Development and validation of bloodless scanning procedures and analysis

In this study we have investigated the possibility of obtaining an estimate of the BP using only 30 minutes of data [Sossi *et al.*, Proc. 5th Int. Conf. on Neuroreceptor Mapping, Vancouver (2004)].

The practical impact of this study is the fact that we will be able to perform two scans on rats with the same DTBZ delivery, since we produce DTBZ with a typical SA of 5300 Ci/mmol at end of synthesis (EOS).

Preliminary results indicate that specific activities as low as 600 Ci/mmol do not cause significant receptor occupancy.

Impact of measurement uncertainties on the determination of the DVR and BP

This work was prompted by a need to evaluate the feasibility of biological studies on the microPET[®], i.e. to obtain an estimate of the expected accuracy with which parameters related to neuro-receptor studies can be determined on the microPET[®]. We thus investigated the effect of measurement uncertainty on the determination of the distribution volume ratio (DVR) and binding potential (BP) as estimated using the tissue input Logan (DVR_L, BP_L) and the ratio (DVR_r, BP_r) methods for two tracers, with the microPET[®] R4 camera. Parameter coefficients of variation (COV) were estimated from a combination of rat and phantom data. For ¹¹C-dihydrotetrabenazine the COV was 11% for the BP_L and 13.4% for the BP_r when using TACs obtained from individual regions of interest (ROIs) and segmented attenuation correction. The COVs were reduced to 7.5% (BP_L) and 8.6% (BP_r) when the striatal and cerebellar TACs were estimated as averages of 3 and 2 ROIs respectively. Results obtained for ¹¹C-methylphenidate (MP) yielded approximately 30% higher COVs. With measured attenuation correction the COVs were on average 100% higher [Sossi *et al.*, Proc. IEEE/MIC, Rome, Italy (2004); Sossi *et al.* (submitted to Phys. Med. Biol.)]. The practical impact of this study is the fact that we were able to obtain an estimate of the measurement accuracy which will guide us in the determination of the feasibility of various rat studies as well as a determination of the superiority of the segmented attenuation correction method compared to the measured one.

Experiment LS60

The physiological role of copper in marine phytoplankton

(*M.T. Maldonado, UBC*)

The short-lived radionuclides ^{64,67}Cu are used to investigate the physiological role of copper in Fe-limited phytoplankton. Physiological research during the last two years in our laboratory suggests that Fe-limited diatoms have a higher demand for Cu than Fe-sufficient cells, and that Cu limitation impairs their high-affinity Fe transport system. These results are the first to demonstrate Cu limitation of marine phytoplankton growth and a role for Cu in phytoplankton Fe uptake. During 2004, we have investigated the mechanistic role of Cu in high-affinity Fe transport systems in coastal and oceanic diatoms, using the radioisotope ⁶⁴Cu provided by TRIUMF.

Using the methods we have developed in our laboratory, we have measured rates of Fe uptake, Fe oxidation, and Fe reduction. Since the summer, we have measured intracellular levels of Cu in Fe-limited and Fe-sufficient coastal and oceanic phytoplankton using ⁶⁴Cu. In 2005 we hope to focus on determining Cu levels in various cellular compartments, and the kinetics of Cu transport of these microorganisms will be determined using ⁶⁴Cu.

During 2004, we processed a limited number of the samples we have collected to determine preliminary cellular Cu and Fe requirements of our diatom species using graphite furnace atomic absorption spectrometry (GFAAS). The samples were obtained from laboratory diatom cultures grown under various Fe and Cu levels, as well as from offshore, Fe-limited regions in the Antarctic and sub-Arctic Pacific Ocean. These data are limited, given how time consuming it is to process these samples and the high demand for these analytical instruments. However, these GFAAS data have been invaluable to validate the use of ⁶⁴Cu to determine intracellular Cu levels of Fe-limited marine phytoplankton.

An examination of published estimates of Cu:C ratios (based on linear relationships between dissolved Cu and PO₄³⁻ concentrations in oceanic nutriclines and Redfield ratios) in Fe-deficient waters determined that they are twice as high as those from other oceanic regions, suggesting that Cu uptake by the biota is significantly elevated in low Fe waters. This puzzling result is consistent with a physiological role of Cu in Fe acquisition. Yet, at present, no direct comparison has been made between particulate Cu:C ratios in low and high Fe waters. Our measurements of intracellular Cu concentrations, using ⁶⁴Cu, have allowed us to demonstrate that indeed the cellular Cu levels in low Fe cultures are elevated relative to Fe-replete cultures, and that phytoplankton in Fe-limited open ocean waters have high particulate copper values relative to those in non Fe-limited regions. A manuscript summarizing these findings will be submitted during the summer, 2005.

Experiment LS63

Non-invasive monitoring of tumour progression in the Shionogi tumour model for prostate cancer

(*M.J. Adam, TRIUMF; D. Yapp, BCCA*)

In the first 8 months of this project, efforts were focused on optimizing the synthesis of ¹⁸F-EF5 and time for distribution of the radiolabelled tracer to obtain images with the best signal-to-noise ratios. In addition, we have also used ¹⁸F-FDG (fluorodeoxyglucose) to image viable tumour tissue and thus locate the po-

sition of the tumour on the mouse image.

Mice bearing androgen dependent (AD) and androgen independent (AI) tumours have been imaged with ^{18}F -EF5 followed by ^{18}F -FDG. In a typical experiment, the animals were anesthetized (halothane), and placed on the scanning bed. ^{18}F -EF5 was injected intravenously (tail vein) and the animal was scanned, initially for 4 hours; subsequent scans were carried out 3 hours after injection of the labelled EF5 for 30 minutes. Once the EF5 scans were completed, ^{18}F -FDG was injected and the animal was re-scanned.

These experiments indicated that $\sim 60 \mu\text{Ci}$ of ^{18}F -EF5 was appropriate for imaging tumour hypoxia in Shionogi tumours grown in DD/S mice. A similar dose for ^{18}F -FDG was also used in the same animal. The 4 hour scan was done to obtain a time-activity curve (TAC) to determine the kinetics of EF5 uptake in tumour tissue. The ratio of ^{18}F -EF5 activity between tumour and non-tumour areas was found to be as high as 1.9. Areas of uptake in AI tumours were generally more consistent and well distributed compared to AD tumours. FDG uptake was useful for delineating the edges of the tumour, differentiating between viable and necrotic areas in the tumour. No significant differences between FDG uptake in AD and AI tumours were found. Funding has been provided by a one year grant from the Prostate Cancer Research Foundation.

Experiment LS69

In-vivo studies on regulation of dopamine turnover using a Parkinson's disease rat model and a microPET

(V. Sossi, UBC)

In preparation for the initiation of this study two aspects were examined: PET estimate of lesion severity and effect of anesthesia.

A key aspect of the studies described in this proposal is the determination of relative changes in vesicular monoamine transporter (VMAT2) marker ^{11}C -dihydrotetrabenzine (DTBZ) and dopamine transporter (DAT) marker ^{11}C -methylphenidate (MP) binding in rat striata. It was thus essential to determine if lesion severity could be properly assessed by PET and not be confounded by instrumental limitation such as the finite PET resolution. One of the methods to quantify lesion severity in a rat model with PET is to compare tracer binding in the lesioned side to that of the healthy side. In a preliminary study we have scanned 6 unilaterally 6-HODA lesioned rats with DTBZ and MP, and determined the BP for both striata. Subsequently we sacrificed four of the six rats and performed post-mortem ^3H WIN35,428 (for DAT) and ^{11}C DTBZ (for VMAT2) binding. The PET studies were done in identical conditions for two anesthetics:

isoflurane and ketamine/xylazine. This was done to compare the effect of two anesthetics on the PET measures, since anesthesia is known to influence binding potential (BP) measures in a tracer and receptor type dependent manner.

Lesion severity was estimated as $\text{BP}_{\text{lesion}}/\text{BP}_{\text{healthy}}$ for both PET and post-mortem measures. Results are shown in Fig. 139. Excellent correlation was found between PET measures and post-mortem measures indicating that lesion severity can be accurately assessed with PET. For DTBZ the linear correlation coefficient (r^2) between the two PET estimates was 0.98 with $\text{BP}_{\text{iso}} = 1.22 \text{BP}_{\text{ket}} + 0.1662$. r^2 between BP_{iso} (BP_{ket}) and $\text{BP}_{\text{post-mortem}}$ was 0.93 (0.91) with BP_{iso} (BP_{ket}) = 0.0077 (0.0055) $\text{BP}_{\text{post-mortem}} + 0.19$ (0.16). For MP the r^2 between the two PET estimates was 0.92 with $\text{BP}_{\text{iso}} = 1.47 \text{BP}_{\text{ket}} - 0.0939$. r^2 between BP_{iso} (BP_{ket}) and $\text{BP}_{\text{post-mortem}}$ was 0.99 (0.96) with BP_{iso} (BP_{ket}) = 0.16 (0.093) $\text{BP}_{\text{post-mortem}} + 0.036$ (0.141).

We thus found that for both tracers there is an excellent linear relation between the two PET BP estimates and between PET BP and post-mortem measures. We also found that the coefficients of the linear relation are different for each tracer and anesthetic (even accounting for a different scale in the post-mortem BP assessment). Anesthesia effects thus need to be accounted for when comparing relative changes in ligand-receptor BP between different tracers. To this end we are now planning to extend this study to 10 rats.

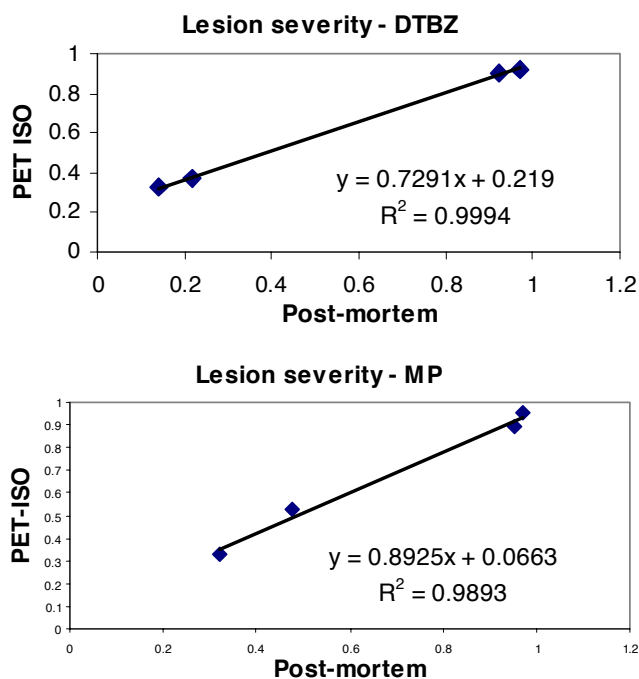


Fig. 139. Relation between lesion severity assessment with PET (under isoflurane anesthesia) and post-mortem measures for DTBZ (above) and MP (below).

These results have been submitted as an abstract to the 2005 AMI meeting [Sossi *et al.*, Proc. AMI meeting (in press)].

Most of the instrumentation and methodological advances described in LS57 will be directly applicable to the studies proposed in this research description. In particular the short scanning protocol will be used for DTBZ scans in conjunction with post-injection transmission scanning (see LS57).

Experiment LS70

Quantification of high resolution brain imaging (*V. Sossi, UBC*)

Implementation of cluster and data archival system

An IBM blade server composed of 8 blades with two xenon 2.8 GHz processors and 1 MB of RAM has been installed and configured to run a parallelized version of OSEM3D (provided by CPS) under Windows. Performance tests have been done and the cluster is now ready for routine reconstructions. Likewise an automated archiving procedure has been developed.

List mode image reconstruction

The development of the list mode reconstruction was published this year [Rahmim *et al.*, Phys. Med. Biol. **49**, 4239 (2004)]. In continuation of that work we have focused on the study of convergent algorithms; i.e. iterative algorithms which (with further iterations) consistently improve such figures of merit as resolution and contrast, relevant to research and clinical tasks [Rahmim *et al.*, Proc. IEEE/MIC, Rome, Italy (2004)]. We have furthermore investigated various interpolation techniques, used in the forward- and back-projection operations in statistical list-mode reconstruction: 1) Siddon interpolation (fastest), 2) bilinear and 3) trilinear (most accurate) interpolation techniques. We have

demonstrated that bilinear interpolation results in an approximately 15% improvement in resolution (2.7 mm as opposed to 3.1 mm in the centre of the field of view), while increasing the reconstruction time only by 20%.

We are currently performing final testing of the quantification accuracy of the list mode reconstruction (both the ordinary and convergent subset versions, using bilinear interpolation and a comparison of image reconstruction algorithms.

Patient motion correction

The paper describing the inclusion of motion correction into image reconstruction has been published [Rahmim *et al.*, IEEE Trans. Nucl. Sci. (in press)]. We have now acquired the PolarisTM tracking system and are currently in the process of setting it up and defining its optimum position with respect to the HRRT field of view. We found that with the current marker plate the sensor was able to see the passive marker tool in the scanner at distances of 155 cm and greater, however, often only three of the four markers were visible. These experimental results agree with the calculated FOV values. We are currently investigating the possibility of building a smaller plate, which would decrease the required distance between the Polaris system and the scanner.

The current Polaris marker geometry has a maximum distance of 164.0 mm between the markers. The restrictions on the marker separation and positions are that each segment is at least 5 mm apart from all others, and that the minimum distance between markers is 50 mm. Using these guidelines, we could have a smaller tool with a maximum distance between markers of 91.2 mm thus making the use of the marker plate more practical.

THEORETICAL PROGRAM

Introduction

The TRIUMF Theory group provides a centre for theoretical research at TRIUMF and a group of active people involved in research in a wide variety of areas. Some of these areas are of direct relevance to the on-site experimental program. Others are more closely related to projects elsewhere involving TRIUMF and other Canadian scientists. Still others are more general, contributing to, and participating in, the efforts of the subatomic physics community both in Canada and elsewhere.

At present the group consists of four permanent staff members, six to seven research associates and a number of students and visitors. Currently the main research interests are nuclear structure and reactions, nuclear astrophysics and cosmology, lattice QCD, effective field theories and chiral perturbation theory, few-body systems, and particle physics beyond the standard model.

The four permanent staff members of the group are: Harold W. Fearing, Byron K. Jennings (group leader), John N. Ng, and Richard M. Woloshyn. Erich W. Vogt (professor emeritus, UBC) is an associate member. Research associates during 2004 were: R. Allahverdi, S. Ando, C. Barbieri, P. Capel (from November), W. Chang (until September), R. Cyburt, W. Liao (from October), J.-M. Sparenberg (until September), and L. Theussl. The graduate students associated with the group during 2004 were: N. Supanam, supervised by H. Fearing, and K. Wong, supervised by R. Woloshyn. B. Barrett (University of Arizona) was on sabbatical with the group for several months.

The short term visitors to the Theory group this year included: J. Al-Khalili, K. Amos, C. Aubin, N. Auerbach, S. Bogner, J. Bowers, M. Buechler, W. Dickhoff, B. Fields, K. Foley, H.W. Hammer, S. Hands, D. Harnett, W. Haxton, I. Horvath, F. Khanna, A. Krassnigg, D. Lin, H. Lipkin, M. Mebel, D. Renner, M. Savage, A. Schwenk, A. Steiner, M. Toharia, E. Tomusiak and D. Wilkinson

As usual members of the group have been quite active, and below we briefly describe some of the many projects undertaken during the year by members of the group and longer term visitors.

Nuclear Structure and Reactions

Time-dependent analysis of the breakup of ^{11}Be on ^{12}C at 67 MeV/nucleon

(P. Capel; G. Goldstein, D. Baye, Brussels Free Univ.)

The breakup of ^{11}Be on ^{12}C at 67 MeV/nucleon has recently been studied experimentally at RIKEN [Fukuda *et al.*, Phys. Rev. **C70**, 054606 (2004)]. We

analyze this dissociation reaction in a semi-classical framework. The resulting time-dependent Schrödinger equation is solved numerically by expanding the projectile wave function upon a three-dimensional spherical mesh. The nuclear interaction between the projectile fragments and the target are modelled by optical potentials. The low-lying $\frac{5}{2}^+$ resonance of ^{11}Be induces a narrow peak in the breakup cross section. The nuclear interactions between the projectile and the target are found to be responsible for the transition towards this resonance. The good agreement with recent experimental data confirms the validity of the model and leads us to suggest that nuclear induced breakup of halo nuclei may be used as a quantitative probe of their internal structure.

Coupling-in-the-continuum effects in Coulomb dissociation of halo nuclei

(P. Capel; D. Baye, Brussels Free Univ.)

Coulomb dissociation is one of the main tools used to study the halo structure. It also provides an indirect method for determining the astrophysical S -factor of radiative capture reactions at stellar energies. In both cases, the experimental data are usually interpreted with a first-order approximation restricted to the E1 multipole with a possible E2 correction. In this perturbative technique, the breakup is assumed to occur in a single-step transition from the initial bound state towards the continuum. However, higher-order effects corresponding to multi-step transitions occurring in the continuum may still be non-negligible, even at high energies. It is therefore of great importance to assess the validity of the first-order approximation so as to avoid biased analyses of experimental results.

We investigated these higher-order effects by comparing the first-order perturbation theory to the numerical resolution of a time-dependent Schrödinger equation. The calculations have been performed for the breakup on a lead target of ^{11}Be and ^8B . The populations of the different partial waves composing the ^{10}Be -neutron or ^7Be -proton continuum reveal that couplings in the continuum remain significant even at high impact parameters and high projectile-target relative velocities. Although the total breakup cross section is fairly well described at a first-order approximation, its partial-wave components reached by the first-order transitions are significantly depleted towards other partial waves after the closest approach. The information extracted by assuming the validity of the first-order approximation is affected by an energy distortion. Another distortion is caused by the presence of a resonance as exemplified by the $\frac{5}{2}^+$ resonance

of ^{11}Be . Such effects may partly explain discrepancies between direct and indirect measurements of the astrophysical S -factor of the $^7\text{Be}(p,\gamma)^8\text{B}$ reaction at stellar energies.

Determination of $S_{17}(0)$ from published data

(*R.H. Cyburt, B. Davids, B.K. Jennings*)

The experimental landscape for the $^7\text{Be}+p$ radiative capture reaction is rapidly changing as new high precision data become available. We present an evaluation of existing data, detailing the treatment of systematic errors and discrepancies, and show how they constrain the astrophysical S factor (S_{17}), independent of any nuclear structure model. With theoretical models robustly determining the behaviour of the sub-threshold pole, the extrapolation error can be reduced and a constraint placed on the slope of S_{17} . Using only radiative capture data, we find $S_{17}(0) = 20.7 \pm 0.6$ (stat) ± 1.0 (syst) eV b if data sets are completely independent, while if data sets are completely correlated we find $S_{17}(0) = 21.4 \pm 0.5$ (stat) ± 1.4 (syst) eV b. The truth likely lies somewhere in between these two limits. Although we employ a formalism capable of treating discrepant data, we note that the central value of the S factor is dominated by the recent high precision data of Junghans *et al.*, which imply a substantially higher value than other radiative capture and indirect measurements. Therefore we conclude that further progress will require new high precision data with a detailed error budget.

Universal energy dependence of radiative capture cross sections

(*R.H. Cyburt, B.K. Jennings*)

We continue the work by Jennings, which determined that the low energy shape of radiative capture cross sections to be dominated by the non-linear nature of the sub-threshold pole. We show that these cross sections, or equivalently the astrophysical S -factor is determined primarily by the sub-threshold pole and the normalization of the regular Coulomb function. With this behaviour established, we provide simple functional forms that can be used to fit cross section data. We also show that this analysis is consistent with other studies of the $E \rightarrow 0$ behaviour of S -factors, though such expansions have a small radius of convergence, making them ill-suited for determining the shape outside the radius of convergence. We present results for $^3\text{He}(\alpha,\gamma)^7\text{Be}$, $^3\text{H}(\alpha,\gamma)^7\text{Li}$, $^7\text{Be}(p,\gamma)^8\text{B}$, and $^7\text{Li}(n,\gamma)^8\text{Li}$.

Three-particle model for halo/deformed nuclide reactions

(*R.H. Cyburt, B. Davids, B.K. Jennings*)

We set out to describe two particle systems, one a composite of two particles, being either a halo nucleus or deformed by its interaction with the third. We find a set of 2-body potentials describing each 2-body channel. Using these potentials, we solve the three-body problem for several benchmark nuclei, including ^6He , ^6Be , ^8Li and ^8B . We show that we can reproduce the structure of these compound nuclei as well as their production cross sections.

Hybrid potential/R-matrix models for the $^{12}\text{C}+\alpha$ system

(*J.-M. Sparenberg*)

Hybrid models which combine the potential model, for the description of the background, with the R-matrix model, for the description of discrete states, have been developed. Physical parameters of discrete states are converted into formal R-matrix parameters, taking into account the potential background. The nuclear part of this potential is constructed by a new variant of an inversion method based on supersymmetric quantum mechanics. The method has been applied to $^{12}\text{C} + \alpha$ S -wave elastic phase shifts.

Construction of a Λ - Λ effective interaction for the calculation of hypernuclei

(*J.-M. Sparenberg; Y. Fujiwara, Kyoto; K. Miyagawa, Okayama Science Univ.; M. Kohno, Kyushu Dental College; Y. Suzuki, Niigata; D. Baye, Brussels Free Univ.*)

The 1S_0 Λ - Λ phase shifts generated by a QCD-inspired spin-flavour SU_6 quark model have been analyzed by a supersymmetric inversion method. This leads to a local potential which has been approximated by the sum of two Gaussian functions. This effective potential, together with Λ - N effective interactions obtained in the same way, has been used in microscopic calculations of the $^6_{\Lambda\Lambda}\text{He}$ and $^9_{\Lambda}\text{Be}$ hypernuclei with a new three-cluster Fadeev formalism based on the two-cluster resonating-group-method kernel.

Rescattering contribution to $(e, e'p)$ cross section at high missing energy and momenta

(*C. Barbieri; L. Lapikás, NIKHEF; D. Rohe, Basel, for the E97-006 collaboration*)

The contribution of rescattering to final state interactions in the $(e, e'p)$ cross section was studied using a semi-classical model. This approach considers a two-step process with the propagation of an intermediate nucleon and uses Glauber theory to account for the reduction of the experimental yield due to $N-N$ scattering. This calculation has relevance for the analysis

of data at high missing energies and in particular at the kinematics of the E97-006 experiment done at Jefferson Lab. It is found that rescattering is strongly reduced in parallel kinematics with respect to perpendicular ones.

The one-hole spectroscopic function has been measured at Jefferson Lab for different nuclei, by the E97-006 collaboration. This experiment focused on the region at high missing energy and missing momenta, where the effects of short-range and tensor correlations can be studied directly. The data obtained show that a sizable contribution to the experimental cross section comes from processes involving the rescattering of the detected proton, against other nucleons in the target. These effects are to be subtracted in order to obtain meaningful results.

Comparison of the experimental data with both theoretical predictions of short-range correlated strength and our rescattering calculations suggests that the results in parallel kinematics are reliable up to the pion emission threshold for ^{12}C . Other effects, such as meson exchange currents, will have to be addressed in order to explain the data in perpendicular kinematics.

Nucleon-nucleus optical potential at low energy and proton capture

(C. Barbieri, B.K. Jennings)

Nucleon capture reactions at low energy like $^7\text{Be}(p, \gamma)^8\text{B}$ play an important role in the understanding of stellar evolution. In this regime, the nuclear optical potential that describes the nucleon-nucleus interaction can present substantial energy dependence and is expected to be sensitive to the surface of the target nucleus. Such low-energy correlations have been considered for ^{16}O in earlier works, based on the self-consistent Green's function theory (SCGF).

We have considered the nuclear self-energy obtained from SCGF calculations in a restricted model space and extended it the full momentum or coordinate spaces. This has been applied to proton scattering and the $^{16}\text{O}(p, \gamma)^{17}\text{F}$ reaction. The results show that this method can lead to a simultaneous description of the bound nucleons (both particle and hole orbitals) and scattering states. However, the phase shifts for the $l=1$ partial waves present difficulties analogous to those encountered in reproducing the corresponding hole spectroscopic factors.

Hadron masses in medium and neutron star properties

(C.Y. Ryu, C.H. Hyun, S.W. Hong, Sungkyunkwan Univ.; B.K. Jennings)

We have investigated the properties of the neutron star with relativistic mean-field models. We incorporate in the quantum hadrodynamics and in the quark-

meson coupling models a possible reduction of meson masses in nuclear matter. The equation of state for neutron star matter is obtained and is employed in the Oppenheimer-Volkov equation to extract the maximum mass of the stable neutron star. We find that the equation of state, the composition and the properties of the neutron stars are sensitive to the values of the meson masses in medium.

The shell model and projection operator formalisms

(B.K. Jennings)

Shell models try to solve the nuclear many-body problem in a restricted space and take into account the restricted space by using effective interactions. In this paper two different approaches to generating the effective interaction are considered, one based on the projection operator formalism and the other on unitary transformations. The two approaches are derived in a parallel manner so that the difference becomes apparent. The effective interaction obtained in the two approaches is very different. For example in one approach it is energy independent while in the other it is energy dependent.

Effective operators within the *ab initio* no-core shell model

(B.R. Barrett, I. Stetcu, Arizona; P. Navratil, Lawrence Livermore National Lab; J.P. Vary, Iowa State)

We implement an effective-operator formalism for general one- and two-body operators, obtaining results consistent with the no-core shell-model (NCSM) wave functions. In the NCSM formalism, we compute electromagnetic properties using the two-body cluster approximation for the effective operators and obtain results which are sensitive to the range of the bare operator. To illuminate the dependence on the range, we employ a Gaussian two-body operator of variable range, finding weak renormalization of long range operators (e.g. quadrupole) in a fixed model space. This is understood in terms of the two-body cluster approximation which accounts mainly for short-range correlations. Consequently, short-range operators, such as the relative kinetic energy, will be well-renormalized in the two-body cluster approximation.

Nuclear Astrophysics, Cosmology

Precision primordial ^4He measurement with CMB experiments

(R.H. Cyburt; G. Huey, B.D. Wandelt, UIUC)

Big bang nucleosynthesis (BBN) and the cosmic microwave background (CMB) are two major pillars of cosmology. Standard BBN accurately predicts the primordial light element abundances (^4He , D, ^3He and

${}^7\text{Li}$), depending on one parameter, the baryon density. Light element observations are used as a baryometer. The CMB anisotropies also contain information about the content of the universe which allows an important consistency check on the big bang model. In addition CMB observations now have sufficient accuracy not only to determine the total baryon density, but also resolve its principal constituents, H and ${}^4\text{He}$. We present a global analysis of all recent CMB data, with special emphasis on the concordance with BBN theory and light element observations. We find $\Omega_B h^2 = 0.025 + 0.0019 - 0.0026$ and $Y_p = 0.250 + 0.010 - 0.014$ (fraction of baryon mass as ${}^4\text{He}$) using CMB data alone, in agreement with ${}^4\text{He}$ abundance observations. With this concordance established we show that the inclusion of BBN theory priors significantly reduces the volume of parameter space. In this case, we find $\Omega_B h^2 = 0.0244 + 0.00137 - 0.00284$ and $Y_p = 0.2493 + 0.0006 - 0.001$. We also find that the inclusion of deuterium abundance observations reduces the Y_p and $\Omega_B h^2$ ranges by a factor of ~ 2 . Further light element observations and CMB anisotropy experiments will refine this concordance and sharpen BBN and the CMB as tools for precision cosmology.

New BBN limits on physics beyond the standard model from ${}^4\text{He}$

(R.H. Cyburt; B.D. Fields, UIUC; K.A. Olive, E. Skillman, Minnesota)

A recent analysis of the ${}^4\text{He}$ abundance determined from observations of extragalactic HII regions indicates a significantly greater uncertainty for the ${}^4\text{He}$ mass fraction. The derived value is now in line with predictions from big bang nucleosynthesis when the baryon density determined by WMAP is assumed. Based on this new analysis of ${}^4\text{He}$, we derive constraints on a host of particle properties which include: limits on the number of relativistic species at the time of BBN (commonly taken to be the limit on neutrino flavours), limits on the variations of fundamental couplings such as α_{em} and G_N , and limits on decaying particles.

Exotic particle decay scenarios in the early universe

(R.H. Cyburt; J. Ellis, CERN; B.D. Fields, UIUC; K.A. Olive, V.C. Spanos, Minnesota)

We generalize our treatment of the radiative decay of an unstable particle in the universe to include decay channels which can produce hadrons as well as electro-magnetic radiation. Just as the EM-decay case, the highly non-thermal injection spectra of injected particles are rapidly “cooled” and brought into a quasi-static or thermal equilibrium with the background plasma. Further interactions with the plasma, either $n - p$ conversion or nuclide dissociation, will

change the predictions of the standard big bang nucleosynthesis (BBN) scenario. Due to the general concordance between standard BBN and observations, this non-standard model of the early universe is highly constrained. We present detailed discussions of the thermalization history of the particle spectra, and the subsequent change to the light element abundances. By adopting these constraints and a particular model for the decaying particle, we can place strong limits on its mass and the temperature of reheating.

What’s next for big bang nucleosynthesis?

(R.H. Cyburt)

Big bang nucleosynthesis (BBN) plays an important role in the standard hot big bang cosmology. BBN theory is used to predict the primordial abundances of the lightest elements, hydrogen, helium and lithium. Comparison between the predicted and observationally determined light element abundances provides a general test of concordance and can be used to fix the baryon content in the universe. Measurements of the cosmic microwave background (CMB) anisotropies now supplant BBN as the premier baryometer, especially with the latest results from the WMAP satellite. With the WMAP baryon density, the test of concordance can be made even more precise.

Any disagreement between theory predictions and observations requires careful discussion. Several possibilities exist to explain discrepancies: (1) observational systematics (either physical or technical) may not be properly treated in determining primordial light element abundances, (2) nuclear inputs that determine the BBN predictions may have unknown systematics or may be incomplete, and (3) physics beyond that included in the standard BBN scenario may need to be included in the theory calculation. Before we can be absolutely sure new physics is warranted, points (1) and (2) must be addressed and ruled out. All of these scenarios rely on experimental or observational data to make definitive statements of their applicability and range of validity, which currently is not at the level necessary to discern between these possibilities with high confidence. Thus, new light element abundance observations and nuclear experiments are needed to probe these further.

Assuming concordance is established, one can use the light element observations to explore the evolution from their primordial values. This can provide useful information on stellar evolution, cosmic rays and other nuclear astrophysics. When combined with detailed models, BBN, the CMB anisotropy and nuclear astrophysics can provide us with information about the populations or environments in which the light elements are observed. Precision cosmology becomes pre-

cision astrophysics.

Primordial nucleosynthesis and the age of cosmological enlightenment

(R.H. Cyburt)

Big bang nucleosynthesis (BBN) theory has long predicted the light element abundance pattern produced during the first minutes after the big bang. These predictions rely on careful analyses of nuclear cross section data to accurately and precisely describe this early epoch. We review the current status of BBN, discussing its concordance with light element abundance observations and the parameter determinations from the anisotropies in the cosmic microwave background. The future of primordial nucleosynthesis hinges on new experimental and observational data. BBN remains a powerful probe of the early universe, which can help illuminate and constrain fundamental questions in nuclear and particle astrophysics.

Lattice QCD

An alternate smearing method for Wilson loops

(F. Okiharu, Nihon; R.M. Woloshyn)

A gauge field link smearing method developed for calculations with staggered fermions, namely the use of unitarized fat7 links, is applied to mesonic and baryonic Wilson loop calculations. This method is found to be very effective for reducing statistical fluctuations for large Wilson loops. Examination of chromo-electric field distributions shows that self-interactions of the static sources are reduced when unitarized fat7 smearing is used but long-distance inter-quark effects are unchanged. This method was applied to the calculation of the static quark-antiquark potential and the three-quark potential in the baryon. The colour field distribution in the baryon was calculated but there was not enough sensitivity to see, unambiguously, the formation of flux tubes in the three quark system.

Staggered fermions and topology in lattice QCD

(K.Y. Wong, SFU; R.M. Woloshyn)

The spectral properties of a variety of improved staggered operators are studied in quenched QCD. The systematic dependence of the infrared eigenvalue spectrum on i) improvement in the staggered operator, ii) improvement in the gauge field action, iii) lattice spacing and iv) lattice volume, is analyzed. It is observed that eigenmodes with small eigenvalues and large chirality appear as the level of improvement increases or as one approaches the continuum limit. These eigenmodes can be identified as the “zero modes” which contribute to the chirality associated, via the index theorem, with the topology of the background gauge field.

This gives evidence that staggered fermions are sensitive to gauge field topology. After successfully identifying these would-be chiral zero modes, the distribution of the remaining non-chiral modes is compared with the predictions of random matrix theory in different topological sectors. Excellent agreement is obtained.

Lattice simulations with twisted mass QCD

(A. Abdel-Rehim, R. Lewis, Regina; R.M. Woloshyn)

Recently a new variation of Wilson-like fermions has been proposed for lattice QCD. It features an axial rotation of the Wilson term relative to the mass term. This removes the possibility of accidental zero modes at non-zero quark mass thus solving the “exceptional configuration” problem. However the new action violates invariance and quark-flavour symmetry at non-zero lattice spacing. A quenched QCD simulation with the twisted mass action is being undertaken to investigate questions such as the effect of using different definitions of the twist angle and the size of flavour symmetry breaking in the hadron mass spectrum. The scaling of hadron masses with lattice spacing is also being investigated.

Effective Field Theories and Chiral Perturbation Theory

Neutron beta-decay in effective field theory

(S. Ando, H.W. Fearing; V. Gudkov, K. Kubodera, F. Myhrer, South Carolina; S. Nakamura, T. Sato, Osaka)

Radiative corrections to the lifetime and angular correlation coefficients of neutron beta-decay are evaluated in effective field theory. We also evaluate the lowest order nucleon recoil corrections, including weak-magnetism. Our results agree with those of the long-range and model-independent part of previous calculations. In an effective theory the model dependent radiative corrections are replaced by a well-defined low energy constant. The effective field theory allows a systematic evaluation of higher order corrections to our results to the extent that the relevant low-energy constants are known.

Radiative corrections and internal degrees of freedom in ChPT

(N. Supanam, Suranaree Univ. of Technology; H.W. Fearing)

In the usual approach photons, leptons, and weak currents are included in ChPT as fixed external fields. For radiative corrections however, and for calculating things like electromagnetic isospin violation, such fields have to be included as explicit degrees of freedom so that they can be included as internal lines in diagrams. To do this one first needs to derive the most general ChPT Lagrangian involving nucleons, pions,

photons, leptons, Ws and Zs all as internal degrees of freedom. As a first application we intend to apply this Lagrangian to radiative corrections to neutron beta decay, which should give as a result expressions for the two constants of the EFT approach in terms of the low energy constants of ChPT. This should resolve a major flaw in the EFT approach, namely the fact that the EFT constants are specific to the given process whereas the ChPT LECs can be obtained from other processes, thus in principle allowing a prediction of the radiative corrections to beta decay.

Ordinary muon capture in RelChPT and relativistic renormalization schemes

(*S. Ando, H.W. Fearing*)

A major effort this past year has been devoted to understanding the various approaches to relativistic chiral perturbation theory (RelChPT) and specifically to a calculation of ordinary muon capture in this formalism. RelChPT has the advantage over the standard heavy baryon ChPT of allowing one to easily obtain a result to one higher order. However there are difficulties with the renormalization and there have been several proposals to resolve these difficulties. One of our primary goals has been to explore in the context of a practical calculation these various proposals and to try to understand what is best for doing real calculations.

We have now completed the main calculation of ordinary muon capture on the proton in the sense that we have results for the weak form factors g_V , g_A , g_M , and g_P and for the isovector and isoscalar nucleon electromagnetic form factors in terms of the low energy constants (LEC's) of the relativistic theory. We are now looking at and comparing the additional finite renormalizations required by the various proposed schemes. The longer term goal is to apply these same techniques to radiative pion capture, RMC, and perhaps other simple processes.

Effective field theory of the deuteron with dibaryon field

(*S. Ando; C.H. Hyun, Seoul/Sungkyunkwan*)

Pionless effective field theory with dibaryon fields is reexamined for observables involving the deuteron. The electromagnetic form factors of the deuteron and the total cross section of radiative neutron capture on the proton, $np \rightarrow d\gamma$, are calculated.

The low energy constants of vector(photon)-dibaryon-dibaryon vertices in the effective Lagrangian are fixed by the one-body vector(photon)-nucleon-nucleon interactions. This scheme for fixing the values of the low energy constants satisfactorily reproduces the results of the effective range theory. We also show that, by including higher order corrections, one can

obtain results that are close to those of the accurate potential model.

The $np \rightarrow d\gamma$ cross sections at the BBN energies

(*S. Ando, R.H. Cyburt; S.-W. Hong, Sungkyunkwan; C.H. Hyun, Seoul/Sungkyunkwan*)

The total cross sections for the radiative neutron capture on a proton, $np \rightarrow d\gamma$, and its inverse reaction $d\gamma \rightarrow np$ are evaluated at the big bang nucleosynthesis energies. We employ the effective field theory with dibaryon field to describe the two-nucleon reactions with external electromagnetic probe. Electromagnetic transition amplitudes are obtained up to next-to leading order and the total cross sections for the inverse reaction are calculated up to 2.3 MeV above the threshold photon energy. We compare our results with relevant experimental data and other theoretical calculations, and discuss the impact on BBN predictions. We show that the error in the cross section at BBN energies is not lower than 1%. Higher order calculations do not improve this accuracy.

Few-Body and Medium Energy Processes

Exact numerical solution of a 3-body Bethe-Salpeter equation

(*L. Theussl*)

We present a benchmark calculation of binding energies and wave functions of a bound state composed of three equal-mass, scalar particles in the Bethe-Salpeter framework. Ground and excited states, including different orbital angular momenta, as well as different masses of the exchanged particle are considered.

Bethe-Salpeter equation with non-planar diagrams

(*L. Theussl*)

We present a formalism that allows the inclusion of an infinite number of crossed diagrams in a Bethe-Salpeter equation. The method is illustrated and numerical benchmark results are presented for a simple two-body system of scalar particles.

Form factors in the “point-form” of relativistic quantum mechanics: single- and two-particle currents

(*B. Desplanques, Grenoble; L. Theussl*)

Electromagnetic and Lorentz-scalar form factors are calculated for a bound system of two spin-less particles exchanging a zero-mass scalar particle. Different approaches are considered including solutions of a Bethe-Salpeter equation, a “point form” approach to relativistic quantum mechanics and a non-relativistic one. The comparison of the Bethe-Salpeter results, which play the role of an “experiment” here, with

the ones obtained in “point form” in single-particle approximation, evidences sizable discrepancies, pointing to large contributions from two-body currents in the latter approach. These two-body currents are constructed using two constraints: ensuring current conservation and reproducing the Born amplitude. The two-body currents so obtained are qualitatively very different from standard ones. Quantitatively, they turn out to be insufficient to remedy all the shortcomings of the “point form” form factors evidenced in impulse approximation.

Particle Physics

Toward precision measurements in solar neutrinos

(*P.C. de Holanda, Campanis State; W. Liao; A.Yu. Smirnov, Moscow/INR*)

Solar neutrino physics enters a stage of precision measurements. In this connection we present a precise analytic description of the neutrino conversion in the context of LMA MSW solution of the solar neutrino problem. Using the adiabatic perturbation theory we derive an analytic formula for the ν_e survival probability which takes into account the non-adiabatic corrections and the regeneration effect inside the Earth. The probability is averaged over the neutrino production region. We find that the non-adiabatic corrections are of the order $10^{-9} - 10^{-7}$. Using the formula for the Earth regeneration effect we discuss features of the zenith angle dependence of the ν_e flux. In particular, we show that effects of small structures at the surface of the Earth can be important.

Lepton flavour violation in extra dimension models

(*W.-F. Chang, J.N. Ng*)

Models involving large extra spatial dimension(s) have interesting predictions on lepton flavour violating processes. We consider some 5D models which are related to neutrino mass generation or address the fermion masses hierarchy problem. We study the signatures in low energy experiments that can discriminate the different models. The focus is on muon-electron conversion in nuclei, $\mu \rightarrow e\gamma$ and $\mu \rightarrow 3e$ processes and their τ counterparts. Their links with the active neutrino mass matrix are investigated. We show that in the models we discussed, the branching ratio of $\mu \rightarrow e\gamma$ -like rare process is much smaller than the ones of $\mu \rightarrow 3e$ -like processes. This is in sharp contrast to most of the traditional wisdom based on four dimensional gauge models. Moreover, some rare tau decays are more promising than the rare muon decays.

Charged lepton electric dipole moments from TeV scale right-handed neutrinos

(*W.-F. Chang, J.N. Ng*)

We study the connection between charged lepton electric dipole moments, d_l ($l = e, \mu, \tau$), and seesaw neutrino mass generation in a simple two Higgs doublet extension of the standard model plus three right-handed neutrinos (RHN) N_a , $a = 1, 2, 3$. For RHN with hierarchical masses and at least one with mass in the 10 TeV range we obtain the upper bounds of $|d_e| < 9 \times 10^{-30}$ e-cm and $|d_\mu| < 2 \times 10^{-26}$ e-cm. Our scenario favors the normal mass hierarchy for the light neutrinos. We also calculated the cross section for $e^-e^- \rightarrow W^-W^-$ in a high luminosity collider with constraints from neutrinoless double beta decay of nuclei included. Among the rare muon decay experiments we find that $\mu \rightarrow e\gamma$ is most sensitive and the upper limit is $< 8 \times 10^{-13}$.

Leptogenesis from a sneutrino condensate re-examined

(*R. Allahverdi; M. Drees, Munich*)

We re-examine leptogenesis from a right-handed sneutrino condensate, paying special attention to the B -term associated with the see-saw Majorana mass. This term generates a lepton asymmetry in the condensate whose time average vanishes. However, a net asymmetry will result if the sneutrino lifetime is not much longer than the period of oscillations. Supersymmetry breaking by thermal effects then yields a lepton asymmetry in the standard model sector after the condensate decays. We explore different possibilities by taking account of both the low-energy and Hubble B -terms. It will be shown that the desired baryon asymmetry of the universe can be obtained for a wide range of Majorana mass.

Scenarios of modulated perturbations

(*R. Allahverdi*)

In an alternative mechanism recently proposed, adiabatic cosmological perturbations are generated at the decay of the inflaton field due to small fluctuations of its coupling to matter. This happens whenever the coupling is governed by the vacuum expectation value of another field, which acquires fluctuations during inflation. We discuss generalization and various possible implementations of this mechanism, and present some specific particle physics examples. In many cases the second field can start oscillating before perturbations are imprinted, or survive long enough so as to dominate over the decay products of the inflaton. The primordial perturbations will then be modified accordingly in each case.

Enhanced reheating via Bose condensates

(*R. Allahverdi; R. Brandenberger, A. Mazumdar, McGill*)

In supersymmetric extensions of the particle physics standard model, gauge invariant combinations of squarks and sleptons (flat directions) can acquire large expectation values during a period of cosmological inflation. If the inflaton sector couples to matter fields via these flat directions, then new channels for efficient reheating, in particular via parametric resonance instabilities, are opened up. These can lead to efficient reheating induced by the flat directions even if the bare coupling constants are small. We discuss various channels which yield this “enhanced reheating” effect, and we address some cosmological consequences.

Leptogenesis as the source of dark matter and density perturbations

(*R. Allahverdi; M. Drees, Bonn*)

We investigate the possibility that the entropy producing decay of a right-handed sneutrino condensate can simultaneously be the source of the baryon asymmetry, of gravitino dark matter, and of cosmological density perturbations. For generic values of soft supersymmetry breaking terms in the visible sector of 1–10 TeV, condensate decay can yield the dark matter abundance for gravitinos in the mass range 1 MeV to 1 TeV, provided that the resulting reheat temperature is below 10^6 GeV. The abundance of thermally produced gravitinos before and after sneutrino decay is then negligible. We consider different leptogenesis mechanisms to generate a sufficient asymmetry, and find that low-scale soft leptogenesis works most naturally at such temperatures. The condensate can easily generate sufficient density perturbations if its initial amplitude is $\sim \mathcal{O}(M_{\text{GUT}})$, for a Hubble expansion rate during inflation $>10^9$ GeV. Right-handed sneutrinos may therefore at the same time provide a source for baryogenesis, dark matter and the seed of structure formation.

Gravitino production from reheating in split supersymmetry

(*R. Allahverdi; A. Jokinen, A. Mazumdar, NORDITA*)

We discuss gravitino production from reheating in models where the splitting between particle and sparticle masses can be larger than TeV, as naturally arising in the context of split supersymmetry. We show that such a production typically dominates over thermal contributions arising from the interactions of gauginos, squarks and sleptons. We constrain the supersymmetry breaking scale of the relevant sector for a given reheat temperature. However, the situation changes when the gravitinos dominate the universe and decay before nucleosynthesis. We briefly describe prospects for a successful baryogenesis and a viable neutralino dark matter in this case.

Miscellaneous

Creating nuclear data representations and error budget accounting

(*R.H. Cyburt*)

Great effort is exerted by experimentalists to beat down and understand the overall error budget in their experiments, in particular nuclear cross section data. In principle, an equally rigorous formalism for combining data should be used when determining data representations and their uncertainties. We present such a formalism here. We detail the treatment of statistical and systematic uncertainties, showing how correlations impact a maximum likelihood analysis. We also clarify the nature of discrepant data and how to quantify the magnitude of the discrepancy. Though the precise definitions presented here are not set in stone, their results are particularly robust, thus other types of analyses should agree quantitatively. Data analysis is limited directly by the data, and can be improved upon in two ways: (1) new, more accurate and precise data are obtained, and (2) old data can be excluded given sufficient reason. We conclude with a discussion of propagating cross section representations into thermal rates and uncertainties, which are then readily available for use in nuclear astrophysics calculations.

EXPERIMENTAL FACILITIES

Proton and Neutron Irradiation Facilities

(E.W. Blackmore, TRIUMF)

This year was the busiest year yet for proton and neutron irradiations. TRIUMF has become recognized as a premier test site for space radiation effects using variable energy protons and now, with the capability of providing a neutron energy spectrum similar to that found at aircraft altitudes and at ground level, neutron beam time is also becoming heavily subscribed. A large fraction of the proton users are Canadian space-related companies, while the neutrons are used primarily by foreign companies for avionics and microelectronics testing.

Proton irradiation facility

During the year there were five scheduled periods for proton testing on the low energy beam line BL2C and during two of these periods the high energy beam line BL1B was also available.

The group from Sandia National Laboratories and CEA in France carried out Expt. 948, Proton Radiation Effects in Silicon-on-Insulator and Bulk-Silicon Devices, in two beam periods, one on BL2C at lower energies in May and then on BL1B at energies up to 500 MeV in December. This experiment had a number of studies, including investigating the effects of total dose on single-event upsets, the effects of proton energy on single-event latchup and simulating the terrestrial neutron environment using protons. The Sandia group also used commercial time for single event testing of various devices.

Groups from MD Robotics visited the facility five times during the year, testing components of a LIDAR system, and various other cards and devices. A special set-up with a 15 cm by 15 cm proton beam spot was used for one test. Other Canadian space companies using beam this year included Routes Astro Engineering and Xiphos. Tests of radiation effects on fibre optic cables were carried out for the space group at the University of Calgary. Foreign users included QinetiQ and BAE Systems from the UK.

Neutron irradiation facility

A schematic of the neutron facility is shown in Fig. 140. Protons are stopped in an aluminum plate beam dump located at the end of BL1A. The proton beam – 500 MeV and typically 120–140 μA – is degraded to about 400 MeV by passing through the T1 and T2 meson production and a series of isotope production targets. The beam dump is immersed in a cylindrical water tank and four horizontal neutron beam channels emerge from the steel shielding surrounding the beam dump. These 20 cm wide by 8 cm

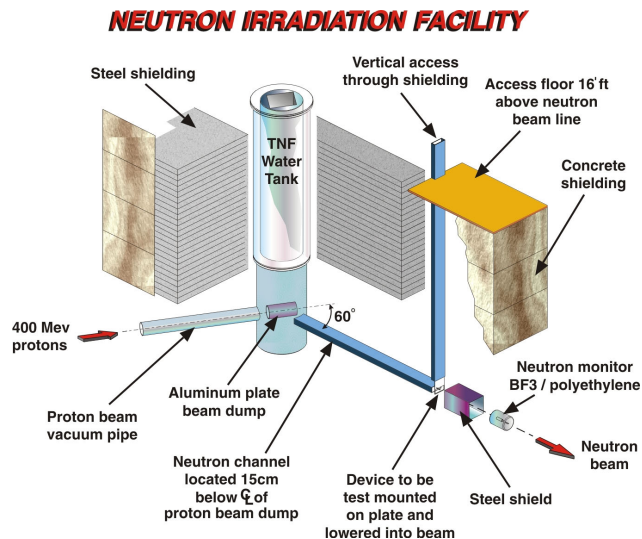


Fig. 140. The TRIUMF neutron irradiation facility.

tall channels are offset vertically from the proton beam line so that they look at the water moderator below the beam dump. Neutrons must scatter in the water moderator at least once in order to enter the beam pipe. Thermalized neutrons are also present in this beam. One of the channels can be accessed through a vertical slot in the shielding and this is where devices are tested.

The neutron spectrum follows the terrestrial spectrum from below 1 MeV to the highest neutron energies around 400 MeV. The rate is about 10^9 times higher than the ground level neutron fluence of about 20 neutrons/cm² s⁻¹ above 10 MeV, so accelerated testing can be carried out very efficiently. The only other similar facility is at LANSCE in Los Alamos but it was shut down through most of 2004.

The users in 2004 included avionics testing by a Swedish/UK collaboration called SPAESRANE and a US company Smiths Aerospace, along with two microelectronics testing companies, HIREX from France and IROC Technologies from US/France.

Proton Therapy Facility

(E.W. Blackmore, TRIUMF)

In 2004 there were 6 patients treated with protons during four scheduled treatment sessions. This brings the total number of patients treated at TRIUMF to 95. This is a lower number than in previous years but seems to be just a statistical variation.

There were no significant changes made to the treatment system or the treatment planning software during 2004.

A radiobiology experiment was carried out using 50 MeV protons to compare the RBE (relative biological effectiveness) of protons to antiprotons to determine the effectiveness of antiprotons for cancer therapy. The antiproton measurements were carried out using the AD (antiproton decelerator) at CERN. The biological samples were Chinese hamster V-79 WNRE immobilized in gelatin, using a technique developed by L. Skarsgard of the BC Cancer Research Centre. To match the antiproton energy spread a one-step modulator was designed for the protons. This work is a collaboration of institutions in Europe, Canada and the United States. A publication of the results is being pursued.

Centre for Molecular and Materials Science (μ SR + β -NMR) User Facility (*S. Kreitzman, TRIUMF*)

Overview

Proposals and funding The primary news regarding Centre for Molecular and Materials Science (CMMS) operations was the coupled results of our 2004 Major Facilities Access Grant (MFAG) submission and the TRIUMF Five-Year Plan, also submitted in 2003. For the second time, our MFAG was renewed only for a single year, due to exactly the reasons that this occurred during our previous MFA application. The MFAG selection committee simply was not aware of the funding status of the Five-Year Plan, as this was to be announced after the MFAG selection committee concluded its decision making process.

As of the end of 2004, the TRIUMF Five-Year Plan is advocating two major μ SR beam line facility upgrades. The M9A beam line is the highest priority and will provide a new high luminosity surface muon beam fitted with an achromatic spin rotator/separator. Further plans include a state-of-the-art turnkey spectrometer at the end of this beam line, suitable for the broad range of general researchers who wish to use μ SR as one of many tools in the investigation of their materials of interest. The second μ SR proposed beam line upgrade is to split M20 into two legs, one of which supports “muons on request”, a configuration which allows one to do μ SR experiments on a longer time scale. With these TRIUMF plans in place, the CMMS will again submit an expanded MFAG application to support the new planned infrastructure.

Funding support for our user groups continues to be strong, and major funding in the 2004 competitions has been received (including equipment and group operations) to support condensed matter high pressure work in exotic materials.

Beam utilization Browsing the beam scheduling Web pages <http://tcmmms.ca/sched/sch105a.html>

and <http://tcmmms.ca/sched/sch106a.html> shows that apart from some lost time on M9B (due to solenoid difficulties) no other significant beam delivery losses impacted the CMMS μ SR schedule in 2004. However, the β -NMR/ β -NQR schedule was reduced from historical levels due to technical difficulties with targets. Summarizing this data, the schedules reflect experiments, taking 882 12 hour shifts or 73.5 beam weeks on four beam lines. The breakdown for the major spectrometers was (in weeks): OMNI/SFUMU – 9; DR – 10; LAMPF – 12; HiTime – 14; Helios – 24.5; β -NMR/ β -NQR – 4.

Developments

Significant facility developments may be categorized into two broad components, the first with evolutions in beam line operation and the second regarding technical progress on specific instruments or inserts.

Operational evolutions

- Spin rotated tunes for high-momentum muons in M9B are being developed utilizing a differentially powered split quad after the solenoid section. This allows for high muon momentum (but lower rate) tunes with predominantly left/right polarization. Such tunes are now routinely being used to do transverse field μ SR in moderate to high fields without suffering the beam steering effects of injecting into a magnetic field perpendicular to the beam momentum.
- Switched and/or simultaneous β -NMR/ β -NQR operation has led to much more efficient use of the precious ISAC unstable beams. Now T_1 spin lattice relaxation measurements can be done on one leg while simultaneous frequency scan (or T_1) techniques are carried out on the other.

Technical progress and developments

- The new high field, high timing front end for our DR is now in fabrication. It utilizes wave shifting technology for the backward and veto counters, and an optimized HiTime-like muon counter (see Fig. 141).
- With the significant field modelling efforts of Bassam Hitti, the problems at very high fields with respect to beam steering and inhomogeneity have been identified and corrected in the HiTime spectrometer. The field steering was due to a 1° misalignment of the magnet within the bore. A reorientation of the magnet now predominantly removes this effect. High field homogeneity (capability to lock an NMR probe from 2–7 T) has been achieved by appropriately placed magnetic shims within the bore.

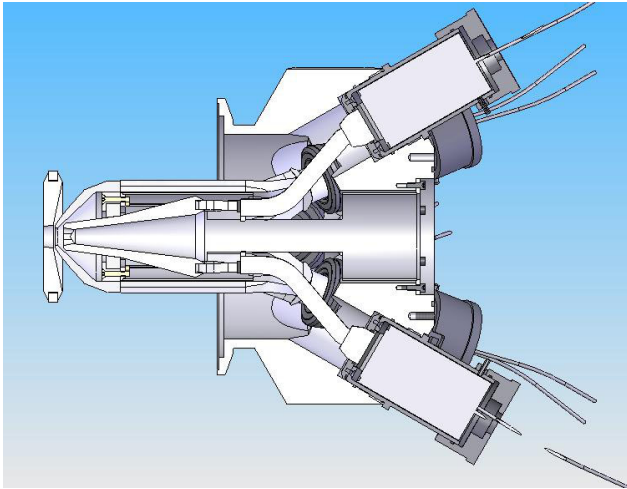


Fig. 141. A cut away view of the new high timing resolution front end for the DR. The back, muon and active collimator scintillators are shown.

- A high pressure cell cryogenic alignment insert for our gas flow cryostats has been designed and built. It contains two in-cryostat scintillators which help define and range the muon beam. Additionally, a dummy cell with a sanitization counter in the sample space of the high pressure cell is available to establish appropriate muon momenta for different cells (see Fig. 142).
- Design of a dual walled high pressure cell (capable of 2.5 GP) continues.
- A third generation temperature stable variable frequency microwave (0.8–2.5 GHz) transmitter/cavity system has been designed, and is now in fabrication.
- The new OMNI' fabrication and assembly is complete and the spectrometer is in operation.
- A second generation β -NMR/ β -NQR frequency synthesizer has now been designed and proof of principle tests successfully conducted. This allows for a single module to be utilized to generate the $1/3/5F$ β -NQR pulses and the $0/90/180/270^\circ$ β -NMR pulses with the change of a switch and appropriate software initialization parameters.
- On a more prosaic level, scheduled maintenance on critical subsystems to minimize start-up or beam time problems is now being more widely implemented.

Future perspectives

The most significant future initiatives are the preparations to operate μ SR at a higher level of user mode, initiated by the building of the new M9A beam line and spectrometer. The beam line will be unique at TRIUMF in so far as having extensive diagnostic and warning elements built into it so that nascent prob-

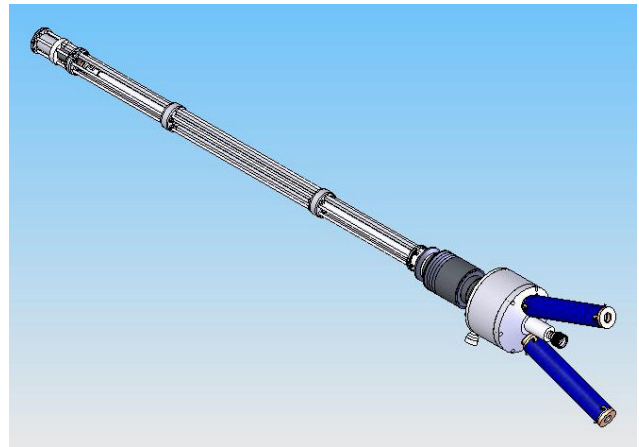


Fig. 142. The pressure cell insert showing muon entry and exit counters, with the centre removable cell rod.

lems can be detected before they become serious. Its achromatic dual spin rotator/separators will yield high luminosity (comparable to M15) in both spin polarizations. The spectrometer will be a turnkey operation and it is anticipated that additional MFAG personnel increases will allow full facility support for novice users, including first pass data analysis.

The model set by this beam line will then filter into the operation of our legacy facilities, leading to increased efficiency and utility in the CMMS operation.

Information and documentation

Please refer to our Web site <http://tcmmms.ca> for full access to a broad range of facility resources and information.

Computing Services

(C. Kost, TRIUMF)

Overview

While 2003 was the year of the massive migration of Computing Services to the new ISAC-II building, 2004 was the year of consolidating and expanding the new network and computing infrastructure.

The UBC-TRIUMF component of WestGrid, the core of which is the 1008 3.06 GHz Xeon CPU cluster called Glacier, came into full operation in 2004 and was heavily used by TWIST – which was often the catalyst for both hardware and software upgrades to enable stable operation of Glacier. Migrating from NFS to IBM's GPFS and requiring raiding of the pair of disks in each node (due to the high failure rate of the Toshiba 40 GB drives) were just two examples.

The decision to have TRIUMF as the CERN ATLAS Tier1 for Canada is expected to have a significant impact on our group (and TRIUMF) as there are many elements that need to be integrated between our small

service group and the expected much larger ATLAS team planned for TRIUMF.

To improve performance and reliability several servers were replaced with more powerful machines – mostly Dell 2650s.

Network

We successfully configured and tested the TRIUMF new secure wireless LAN (WLAN) router from Colubris. This device will be used to automate IP assignments to the TRIUMF users in general and visitors in particular, once the single flat B space IP addresses have been separated into VLANs.

To address the vulnerability of a single point of failure to all non-commodity network traffic to/from TRIUMF via the coarse wave division multiplexer (CWDM) a second, more powerful pair of CWDMs (see Fig. 143) was installed between TRIUMF and BCNET (located in downtown Vancouver). Contrary to plans envisioned last year, commodity traffic continued to be serviced via (now upgraded to a 1 Gbit link) UBC (which is supported by 3 redundant service providers) as the bandwidth manager effectively maintains this at an acceptable low rate.

Additional fibres were laid from the main office building to ISAC-II – providing full redundancy between almost all main nodes at TRIUMF.

Two students spent most of their summer designing and implementing Web based tools to build a network database of most of the equipment connected to the network backbone at TRIUMF.

Computer security

The reliability and regulation of the air-conditioners cooling the main compute server room in ISAC-II continue to be questionable and plans are under way for 2005 to address this with improved

monitoring and supplementary heating to further reduce temperature excursions.

In accordance with TRIUMF policy all Linux machines on the network now require “back-door” access – preferably privileged, but minimally with a normal user account to readily allow examination of any errant machine. It is also required that critical Windows updates be performed in a timely manner. The mandatory move to Windows SP2 has been deferred till sometime in 2005.

Although we avoided being infected by the Mydoom virus attacks of January, August was a busy month for viruses with some 20 PCs, either through lack of appropriate updates or the unauthorized use of KaZaA, infected with the w32.spybot.worm, while some were infected with W32.Mydoom, or W32.Beagle by running e-mail attachments before Symantec released a “cure”.

To further improve security we now require Linux on networked computers to be updated as much as possible to the latest Red Hat version or Scientific Linux (released on May 10, 2004 and generously provided through the joint efforts of Fermilab and CERN). Computing Services provides local users with the required kickstart CDs as well as maintains an on-site mirror of Scientific Linux.

E-mail

Due to both aggressive e-mail filtering (typically rejecting 6000 messages/day) before e-mail is passed to the end user, and increased use of e-mail filtering by the end user, unwanted e-mails have been steadily declining. Early in the year a dual CPU Dell 2650 mail server running Redhat 9 was installed to address poor disk I/O performance. However, due to heavy growth in this area, the long term solution will likely require two or more machines – splitting the load by having one machine handle incoming mail, AntiVirus, and AntiSpam filtering to a second machine for user mail access. A third machine would handle outgoing mail.

Servers

Figure 144 shows the current status of the main components of the Computing Services facilities. Almost all servers have two or more power supplies which are connected to two or more networked power bars so as to provide redundancy, remote current monitoring, and power control to the servers. As the year-end approached it was clear that more circuits would need to be provided than were available in the main server room. Plans are to double the number to this room by mid-2005.

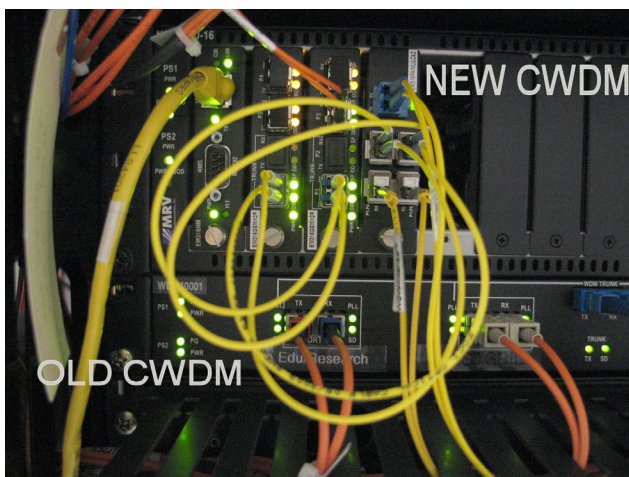


Fig. 143. New and old coarse wave division multiplexer (CWDM) connecting TRIUMF to BCNET.

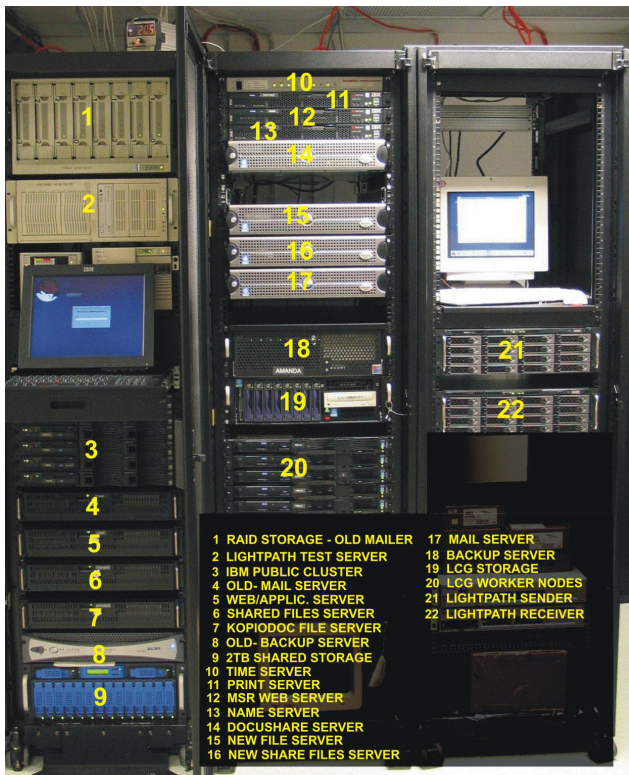


Fig. 144. Status of main components of the Computing Services hardware facilities.

CERN/ATLAS service challenges / IGT and 10 GbE developments

In order to develop an LCG presence at TRIUMF (reported elsewhere in this Annual Report) and in preparation for dealing with the upcoming service challenges relating to the CERN ATLAS experiment scheduled to start production mid-2007, two new staff members were hired. Hardware, based largely on the experiences acquired with the high-speed, long distance data transfers relating to the IGT developments (described below), is being ordered for delivery in early 2005.

A great deal of experience has been acquired as a result of various tests run over a 10 GbE linking TRIUMF and CERN. TRIUMF acquired two powerful servers with dual 3.2 GHz Xeon processors on a SuperMicro X5DPE-G2 motherboard with 4 GB of memory and 16 SATA150 120 GB disk drives connected to four 3Ware-9500S-4LP (later two 9500S-8) controllers as shown in Fig. 145.

Disk to disk I/O for the machines connected back-to-back via 10 GbE S2IO network cards transferred 10 TB in about 17 hours – an average rate of 180 MB/s. To test robustness a pair of 80 GB files were read continuously for 67 hours – some 120 TB, at an average rate of 524 MB/s. A short test was done to a single disk machine at CERN – limiting the rate to



Fig. 145. Servers used for back-to-back and TRIUMF-CERN data transfers over a 10 GbE lightpath.

30 MB/s – over a 10 GbE lightpath that was available for a limited time. Much was learned from back-to-back tests conducted between the two local servers in order to achieve sustainable, reliable, and cost effective high speed transfers across long distance networks.

Software developments

Physica and other data analysis Physica, is an internationally popular, general purpose data analysis/visualization program running on UNIX/Linux. The enhanced version for Windows, called Extrema, has now been largely ported back to Linux and converted to Open Source, making it more accessible to the global community.

Locally, this code was instrumental in merging the various field maps of the cyclotron's extraction region, contributing to the resolution of a long standing error in the transfer matrices used for extracted beam tuning.

User requested enhancements to Physica were added, including a new user interface based on the readline (FSF, Inc.) package and a new fitting technique based on the Marquardt algorithm. The libraries and executables are updated regularly on multiple platforms, and made available via anonymous ftp and download via the Internet.

Work continued on ROODY, a GUI written in C++ based on CERN-ROOT, which displays histograms and other objects (especially useful for monitoring on-line histograms). Significant enhancements were made to ROODY, including an XML save session facility, many on-line histogram display and control features, and context sensitive menu additions.

Beam dynamics

ACCSIM The multiparticle simulation code ACCSIM continues to be used in a wide variety of accelerator applications, principally for high-intensity synchrotrons and storage rings.

Consultation and support activities with new and existing users continued. New ACCSIM applications emerging during the year included:

- J-PARC 50 GeV ring space charge studies;
- Beta beam decay ring for radioactive ions; and
- CERN-PS injection and acceleration of radioactive ions for beta beam.

The latter two applications are being prepared as part of TRIUMF's participation in the EURISOL beta beam study. This study, part of the four year EU-funded EURISOL project, will develop the design for a new type of neutrino factory using radioactive light ions, which are produced in an ISOL front end, accelerated to highly relativistic energies, and then injected into a racetrack-shaped storage ring where copious neutrinos will be produced from the ions via the beta decay process.

Numerical computing

FEMLAB The multi-physics PDE solver FEMLAB has a small but growing community of users at TRIUMF. It offers an interactive 2D and 3D modelling facility to define the geometry of the problem domain and boundary conditions, as well as the ability to import geometries from CAD systems. Via finite-element methods, solutions to a wide variety of physics problems can be efficiently obtained. The built-in graphics includes sophisticated 2D and 3D visualization and plotting capabilities.

For TRIUMF applications, there is a need for a scripting mechanism to control FEMLAB runs, and an efficient access mechanism to FEMLAB's data structures for accurate field interpolation and other post-processing. At present these functionalities are provided only through a third party product, Matlab, which fortunately is already licensed and available at TRIUMF. We have been in ongoing consultation with the maker of FEMLAB regarding performance and compatibility issues arising from this Matlab link. In the course of our discussions and local tests we upgraded FEMLAB to the new release 3.1 and Matlab to its latest release 7.0, which brought some performance improvement. Given effective scripting and application-programming aspects, and continued competitive pricing and support, FEMLAB has potential as an important scientific and engineering tool at TRIUMF.

Parallel computing Using a parallel application BeamX which simulates LHC beam-beam effects (see the CERN Collaboration section of this Annual Report), we conducted a benchmark survey of available parallel computing resources including the WestGrid Lattice CLUMP (CLUster of MultiProcessors) system at the Univ. of Calgary, the WestGrid Glacier facility at UBC, and the new Openlab cluster at CERN. Of these, the Lattice cluster was the clear leader, with performance at least a factor 2 better than the other clusters in a series of timing trials. The CLUMP architecture is designed to support rapid low-latency communication among small groups of processors in shared memory configurations, whereas the WestGrid-UBC and CERN clusters are based on commodity processors in blade or white-box packages, respectively. Additional performance tests on the blade system showed that the interprocessor communication speed for this application was independent of the location of processors. There was no performance advantage in allocating all processors within a single blade unit, utilizing only the blade's internal networking, as opposed to having them distributed among two or more blade units.

Infrastructure software

Agenda The TRIUMF Central Document Server Agenda was installed. It is a multi platform (Linux, Windows and Mac OS) tool used to help plan meetings, workshops and conferences, and associate for a long-term storage all possible attachments such as minutes of meetings, slides and even multi media. Agenda is used both to display schedules of meetings, and create and modify new ones. This tool, originally created at CERN for the CERN environment, required extensive modifications to many scripts and PHP files to make it useful for the TRIUMF users community.

The TRIUMF Central Document Server (TCDS), a product based on CERN's central document server (<http://cdsweb.cern.ch>) which uses a powerful search engine with Google-like syntax, electronic submissions and uploading of various types of documents, was initially proposed as the Central Document Server for hosting various kinds of collections. Creating it required a MySQL database, compiled PHP and Python applications. However, it was decided that Docushare, which can be found at <http://documents.triumf.ca>, would be used on site instead of TCDS until some real needs exceed Docushare's capabilities.

Docushare The document management system from Xerox, Docushare, was chosen largely because it was accessible for all platforms: Linux, Mac OS, as well as Windows. About \$25 k was spent for a 100 user license and the Dell 2650 server running Redhat 8. So far the system has run smoothly for 6 months and it is planned

to expand to a 200 user license early in 2005. There are currently about 3000 documents on the system.

Printing-Scanning-Copying

The new Kyocera colour printer has proven to be a reliable, cost effective alternative to the costly to run HP colour laser printers. In addition, a Xerox Pro40C colour laser printer/scanner/copier, installed in the office building mail room, is providing printing at a reduced overall cost – in the same manner as was done last year for monochrome printing. Due to the problematic and costly nature of printing, there is an ongoing process to review site printing-scanning-copying needs with the goal of reducing overall costs while improving capabilities.

Miscellaneous

After many years of neglect the public TRIUMF Web pages have been completely revamped – setting the stage for all the internal pages to be upgraded to this new style and standard in 2005.

TRIUMF, along with 11 other laboratories, submitted proposals to become the host site for a Central Design Team (CDT) of the next generation machine known as the International Linear Collider (ILC). This potentially enormous future project would have initially a very small management team coordinating resources in major laboratories around the world. If the CDT is awarded to TRIUMF, Computing Services would be involved with setting up infrastructure – mostly desktop computing and network connections to Paprican, a facility adjacent to TRIUMF.

Expanded support for videoconferencing included operating a Web cast server to record and transmit a number of events, including the EMMA review, TUG meetings, and some EEC sessions. In further support of videoconferencing at TRIUMF a second H.323 video appliance and projector were installed in the main office conference room, along with AccessGrid software on the PC used for VRVS video, which was moved from the adjacent small office. We continued to participate in the SLAC pinger and other network measurement efforts.

Data Acquisition Systems

(*R. Poutissou, TRIUMF*)

Overview

In 2004, the DAQ group continued to expand the number of DAQ systems around the site. Most of the new hardware deployed came from LADD purchases (see LADD section, p.128, this Annual Report). It now stands at 35 PCs (Table XXIII), 10 VME PowerPCs 604 and 9 VME VMICs, all managed by members of the group. These machines also provide some off-line analysis resources and disk storage

(http://daq.triumf.ca/triumf_nodeinfo). Performance is monitored via Ganglia (<http://daq.triumf.ca/ganglia>).

Development of an on-line analysis package based on ROOT (<http://root.cern.ch>) continued. The package is now called ROODY.

MIDAS and ROODY

The basic MIDAS data acquisition package is in a stable condition and it is used throughout TRIUMF. Although its operation is stable, constant efforts are dedicated to improve MIDAS in order to keep it up-to-date with current analysis packages such as ROOT. This year this has been achieved with the help of Dr. Stefan Ritt and Matthias Schneebeli from PSI who came to TRIUMF for two weeks in September. The main improvements added are listed here. The MIDAS data logger can now produce ROOT files. On-line DAQ access to external databases such as MySQL (equivalent to the “runlog” option) has been added. The transition scheme has been modified allowing better control of the run transition sequences. The event builder scheme has been improved for simplified and more flexible handling of frontend equipment.

In parallel to these tasks, Matthias Schneebeli, the author of ROME, gave an introduction to this latest ROOT based stand-alone analyzer. ROME (<http://midas.psi.ch/rome>) is an OO generic analyzer framework builder, where the analysis definition is provided in XML format. The experiment specific class templates are then generated automatically, ready to receive the user code. ROME is fully MIDAS compatible for on-line and off-line data retrieval, and contains an interface to a standard database.

The other main project of the DAQ group is the development of a ROOT based GUI for histogram display. This is a continuation of the MIROODAS project started in 2003. This application has been renamed ROODY (ROOT display) to reflect the disconnect from MIDAS (<http://midas.triumf.ca/roody/html>). While ROODY can be used for on-line data display through the MIDAS analyzer, MIDAS is not a prerequisite for running ROODY. ROODY can also be coupled with the user specific ROME analyzer. Development and maintenance of ROODY is managed mainly by Joe Chuma.

DAQ systems

β -NMR and β -NQR at ISAC The operating system on all the DAQ machines for β -NMR and μ SR experiments, and the test systems (dasdevpc, daqlabpc) were updated to Linux Red Hat 9. The DAQ systems had to be upgraded to work correctly under the new OS.

The “Dual Channel Mode” was proposed by the β -NMR group, where the beam will be alternated between the β -NMR and β -NQR beam lines. Required

hardware modifications to the PPG boards for this mode were determined and made. The frontend code

Table XXIII. Computer systems managed by the DAQ group.

Name	Location	Type
daqlabpc	DAQ lab machine	PII/232
dasdevpc	DAQ development Web server	PIV/1700
e614slow	TWIST Slow Control	2xPIII/750
epicsdragon	DRAGON EPICS Display	PII/300
epicsm15	M15 μ SR EPICS	PIII/871
epicsm20	M20 μ SR EPICS	PIII/400
epicsm9b	M9B μ SR EPICS	PIII/550
isdaq01	ISAC-LE β -NMR TRINAT	2xPIII/450
isdaq02	ISAC-LE, GP2, LTNO	Cel/795
isdaq03	ISAC-HE, TUDA	2xPIII/550
isdaq04	ISAC-HE, DRAGON	2xAMD Ath/2000
isdaq05	ISAC-LE, ISAC users	PIII/1000-256
isdaq06	ISAC-HE ISAC users	PIII/1000
isdaq08	ISAC-LE, 8π	2xAMD Opt/2000
ladd00	LADD server	2xAMD Opt/1800
linm15	M15 μ SR users	AMD Ath/1500
linm20	M20 μ SR users	AMD Ath/1500
linm9b	M9B μ SR users	AMD Ath/1500
ltno01	LTNO CR DAQ	2xPIII/600
midm15	M15 μ SR DAQ	2xPIII/1000
midm20	M20 μ SR DAQ	2xPIII/1000
midm9b	M9B μ SR DAQ	2xPIII/1000
midmes01	Detector Facility	PIII/500
midmes03	RMC DAQ	2xPIII/550
midmes04	M11 DAQ	2xPIII/750
midmes05	Detector Facility	Celeron/335
midmes07	Neutrino Development DAQ	PII/400
midtis01	TRINAT DAQ	2xPIII/550
midtis02	Detector Facility	2xPII/450
midtis03	LTNO platform DAQ	PII/350
midtis04	GP2 DAQ	2xPIII/550
midtis05	8π Cryo	PII/300
midtis06	Osaka DAQ	AMD Ath/2000
midtis07	Pol/CFBS Slow Control	Cel/375
midtwist	TWIST DAQ	2xPIII/1000

was modified to incorporate the Dual Channel Mode, and to ensure that the “Single Channel Mode” works in a similar way to the old code. Work began on the “randomized frequency scan” and the requested change in helicity flipping for mode 1g.

Syd Kreitzman designed a new Pol Synth Module (PSM) which was built by the Electronics group. With the help of Syd, a new mode called the “Quadrature Modulation Mode” was implemented to exploit this new module, and the PSM was thoroughly debugged for use in the β -NQR experiment. The frequency scan code in the frontend was rearranged to incorporate the PSM code.

For POL, a new DAC scan was added to control the power supply for Expt. 920, replacing the old CAMP DAC scan. A readback of the DVM and Wavemeter was implemented. Support for a new experiment (P. Levy) to scan the NaCell was added, with a readback of the Faraday cup. A jump in the scan values (i.e. a discontinuous scan) was implemented for POL, also an up/down scan and a variable offset for the NaCell readback.

During 2004, Dave Morris continued to offer some much appreciated support to the DAQ group. In particular, we used his expertise with GPIB drivers on Linux and his knowledge of Agilent DVM instruments

to set up hardware and software slow control for a high voltage unit. This HV provides retardation voltage for the collinear fast beam spectroscopy set-up and was a crucial element in the DAQ system used by Expt. 920 last year.

μ SR systems

With the help of Stefan Ritt, during his September visit, the annoying μ SR fragmented buffer problem for large data buffers was finally solved. The latest version of MIDAS (1.9.5) was installed on all μ SR DAQ machines. The μ SR DAQ systems seemed to be quite stable throughout 2004, with relatively small modifications required.

No progress was made to commission a MULTI type μ SR system due to the lack of a μ SR software expert to write a suitable filter. In MULTI mode, the detector is segmented in 8 sections and the DAQ has to handle the equivalent of 8 parallel experiments.

TWIST DAQ activities

Ongoing modernization of the slow controls software was the main development activity on the TWIST DAQ in 2004. In particular, improvements to the M13 B1 and B2 dipole regulators were implemented. High precision measurements of muon polarization by the TWIST experiment require that the M13 beam line elements be controlled with precision and stability higher than that provided by standard TRIUMF magnet power supplies and power supply controls. We see 0.5–1 G changes in the magnetic field of the B1 and B2 dipoles caused by day-and-night temperature variations. We also see long term drifts in B1 and B2, up to 1–2 G over half a week. To improve the long term stability of B1 and B2, in 2002–2003, high precision fine DACs were added to the B1 and B2 magnet power supply controls and a closed-loop software regulation scheme was implemented. The MIDAS-based slow controls frontend reads the NMR probes installed inside the M13 B1 and B2 dipoles, filters the NMR readings, compares them with the NMR setpoints and minimizes the difference by adjusting the fine DAC controls via the M13 EPICS control system. Special care had to be taken to monitor and filter the NMR readings in order to avoid misregulation in the presence of spurious NMR readings caused by NMR signal degradation from radiation damage of the NMR probes. During the 2003 running of TWIST, B1 and B2 were regulated with a precision of 0.1 G, compared to the precision of 1–2 G without using the regulators. In early 2004 a hardware problem was identified and corrected in the implementation of the fine DAC controls, resulting in the improvement of controls precision from 0.03 G/LSB to 0.003 G/LSB. This resulted in an improvement of regulation precision from 0.1 G during 2003 to 0.02 G

during the 2004 running of TWIST. The achieved regulation precision is better than what is required for TWIST. Further precision improvements are limited by the very-short-term stability of the magnet power supplies and by the quality of NMR measurements. The regulator system is highly robust and reliable and is now routinely used by experiment operators with minimal training and minimal expert intervention.

Another important improvement was the development of a “muon stopping position regulator”. The TWIST experiment stops the beam muons in a stopping target in the middle of the TWIST detector. To minimize the systematic errors in TWIST measurements, it is important to always stop the muons in the same place, to minimize any variation of the muon stopping position. The muon stopping position is controlled by adjusting the mixture of CO₂ and He gases in the gas degrader volume in the muon path: because muon loses more energy in CO₂, compared to He, increased CO₂ content makes the muons stop faster, moving their stopping position upstream. During off-line analysis, the muon stopping position is measured using one of several methods. While analyzing the 2003 data, we observed a correlation between the atmospheric pressure and the muon stopping position: the CO₂/He gas degrader is at atmospheric pressure and higher atmospheric pressure yields increased density of the CO₂ gas, with a bigger muon stopping power, so the muons stop faster and the stopping position moves upstream. This effect was estimated to be big enough to affect the ultimate precision of the experiment and, based on our positive experience with the B1/B2 magnet regulators, we decided to implement a regulator for the muon stopping position. This task turned out to be harder than expected. There is no direct control over the CO₂/He gas mixture: one controls only the gas flow rates into the degrader volume; gas mixture follows changes in flow rates, but the exact relation is unknown. There is no direct measurement of the muon stopping position: to obtain an adequate measurement, one has to analyze about 10–20 minutes worth of data, fill histograms and compute the average stopping position. Meanwhile, the atmospheric pressure changes and the stopping position moves. These difficulties with both controls and measurements reduce the reliability and robustness of normal proportional regulation schemes, like those used to control B1 and B2. Instead, a very simple relay regulator was used. If the muons stop too fast (too far upstream), the CO₂ flow is reduced by 1%, otherwise the CO₂ flow is increased by 1%. The gas flows are adjusted each time a new measurement of the stopping position is available from the on-line data analysis (QOD), with at least 20 minutes between subsequent adjustments, to let the gas mix-

ture settle. The TWIST experimenters are presently assessing the effectiveness of this regulation scheme. Preliminary results indicate improved stability compared to 2002 operation.

Other experimental stations

The DRAGON system was upgraded from a standalone CAMAC system to a mixed VME/CAMAC system for additional functionality and speed increases.

The Canadian T2K Neutrino group which occupies the former ATLAS clean room continued their program of detector development studies. One of the standard CAMAC DAQ test stations deployed last year was replaced by a VME LADD system where software drivers were developed for the new hardware as well as support for on-line analysis and ROODY.

Support for external MIDAS users is still ongoing. Pierre Amaudruz spent one week at Los Alamos as a consultant on MIDAS.

Detector Facility

(*R.S. Henderson, TRIUMF*)

The TWIST experiment at TRIUMF (Expt. 614) is a sophisticated attempt to measure the Michel parameters to ten times the precision they are now known. The various subsystems of this experiment continued to function extremely well, but unfortunately, a human error with the gas system resulted in broken wires in 14 wire-planes from 11 detector modules. The cradle and detector stack were brought back to the facility for several months of module repair and bench testing. This has been completed. The cradle was returned to TWIST, the services connected. All detectors and readout channels are being tested prior to re-installation in the magnet for upcoming data-taking.

A low pressure time expansion chamber (TEC) has also been built for use just upstream of the TWIST spectrometer. It will be used to measure the muon beam properties. The TEC was built and tested in the facility. These tests led Grant Sheffer to make some design changes that greatly improved performance. The TEC has also been thoroughly tested in the muon beam and will be used in the next data-taking run. A spare TEC will be fabricated and tested. This will mark the completion of the facility participation in the TWIST experiment, except for maintenance and repair.

The facility also had two other major repair efforts this year. The large drift chamber built and used for the RMC suffered major damage. The cause isn't certain, but a problem with the HV software is suspected. Many wires were broken and the repair took many months. This chamber has been re-installed and the readout is being checked for an upcoming experiment. Coincidentally, two of the MWPCs we built for the KVI

spectrometer (Netherlands) also suffered damage. This was caused by the quenching gas running out. The two damaged chambers were shipped to TRIUMF, repaired and sent back to KVI.

The scintillator shop continues to function as the heavily used machining centre for the facility. This year has seen a wide variety of scintillators fabricated for μ SR and the $G\theta$ experiment (at TJNAF). The small 4-axis NC mill (refitted) in the shop allowed us to machine the complex curved scintillator pieces for $G\theta$. All seven scintillator sectors have been completed and shipped to TJNAF. Steve Chan also helped design a new yield station for the ISAC beam line and it was fabricated in the shop. More KOPIO prototype detectors were also fabricated in this shop, as were various pieces for the T2K liquid scintillator R&D.

The KOPIO experiment has been down-sized, the inner region (called the detector unit) was previously planned to have an active area of $2.1\text{ m} \times 2.1\text{ m}$. This has now been reduced to $1.5\text{ m} \times 1.5\text{ m}$, cutting the number of readout channels by approximately 25%. The updated design of the KOPIO module and components is complete and design studies for the difficult KOPIO installation issues are under way.

The KOPIO design (see Fig. 146) has four quadrants of preradiator modules, each quadrant eight modules deep, for a total of thirty-two modules (plus two spares). Each of the modules would consist of two parts. The detector unit consists of eight drift chamber layers sandwiched between nine layers of extruded scintillator. The outer region (called the L-unit) will connect to, and support, the preradiator unit at the two orthogonal readout faces. Thirty-six Shashlyk calorimeter blocks will be mounted on these two edges of this L-unit, giving full calorimeter coverage in the experiment. Miniature coax cables will transport the 4608 anode/cathode signals past the Shashlyk blocks to six readout crates also mounted on the L-unit. In addition, both ends of approximately 1370 WLS fibres will pass the Shashlyk blocks to 40 PMTs (or APDs).

With each of the thirty-four preradiator modules $3.3\text{ m} \times 3.3\text{ m} \times 0.17\text{ m}$ in size and weighing approximately 1.8 tonnes, the scale of the project becomes apparent. A great deal of development and testing is required. The detector facility is already contributing much of its manpower to this project in areas of design, prototyping, thermal expansion testing, wire-chamber structural tests and scintillator painting tests. A full size module is scheduled for completion in early 2006.

KOPIO is awaiting approval by the US funding agencies and NSERC. If approved, the KOPIO project will be a very large detector project at TRIUMF, considerably larger and more complex than previous projects such as the ATLAS calorimeter fabrication, the BABAR drift chamber or the HERMES TRDs.

Detector-Unit

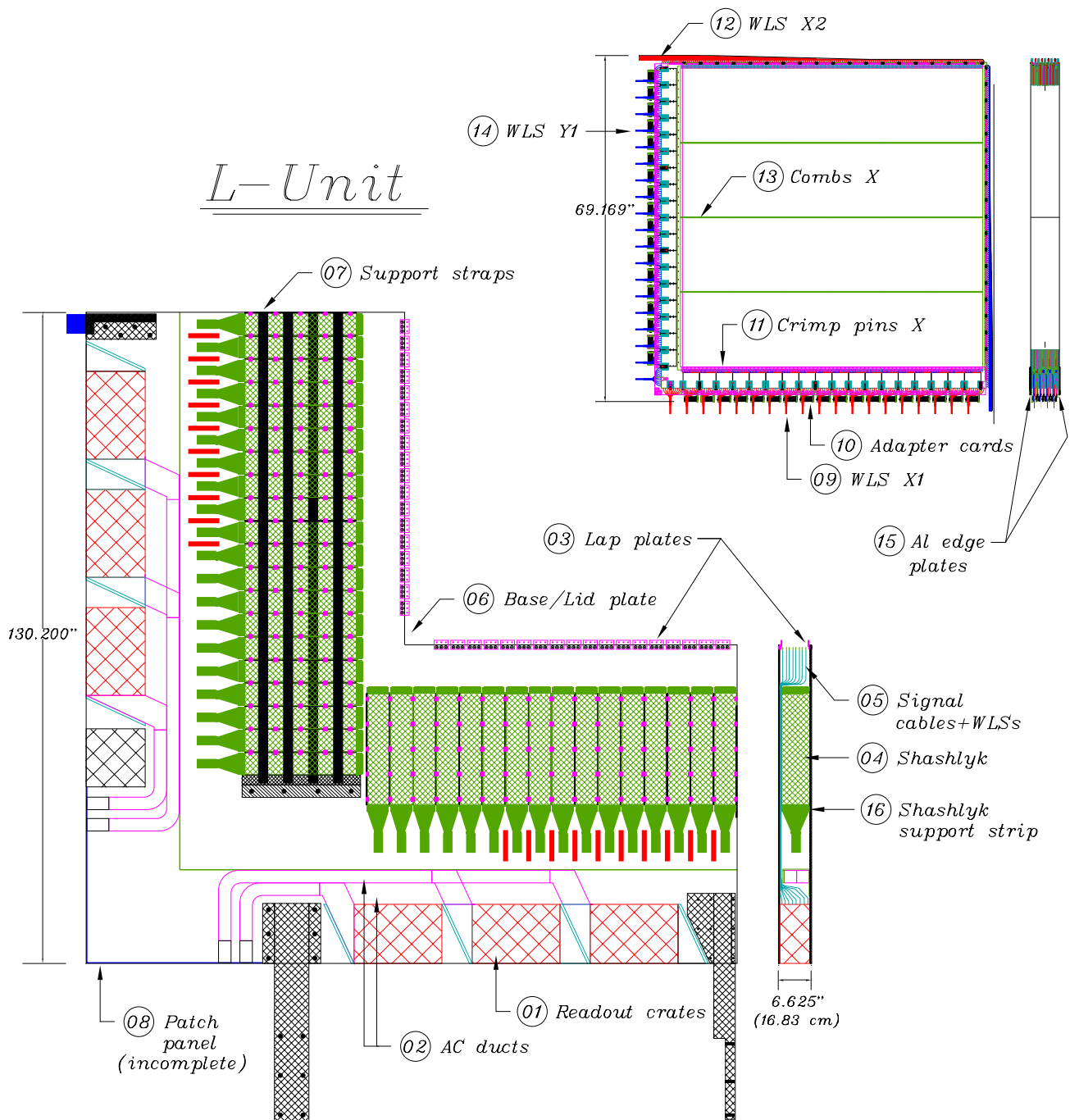


Fig. 146. Present design of KOPIO preradiator module.

A second major project is the T2K experiment planned for J-PARC in Japan. The TRIUMF T2K group and the detector facility are responsible for two of the major detector components. The first is the six large tracking TPCs (2.2 m × 1.25 m × 0.67 m). A

small prototype of this TPC has been designed and is scheduled for fabrication by early 2006 (see Fig. 147).

The second is the two types of fine grain detectors (FGDs) that are between the three double-ended TPC gasboxes. These FGDs are ~2 m × 2 m × 0.3 m. The

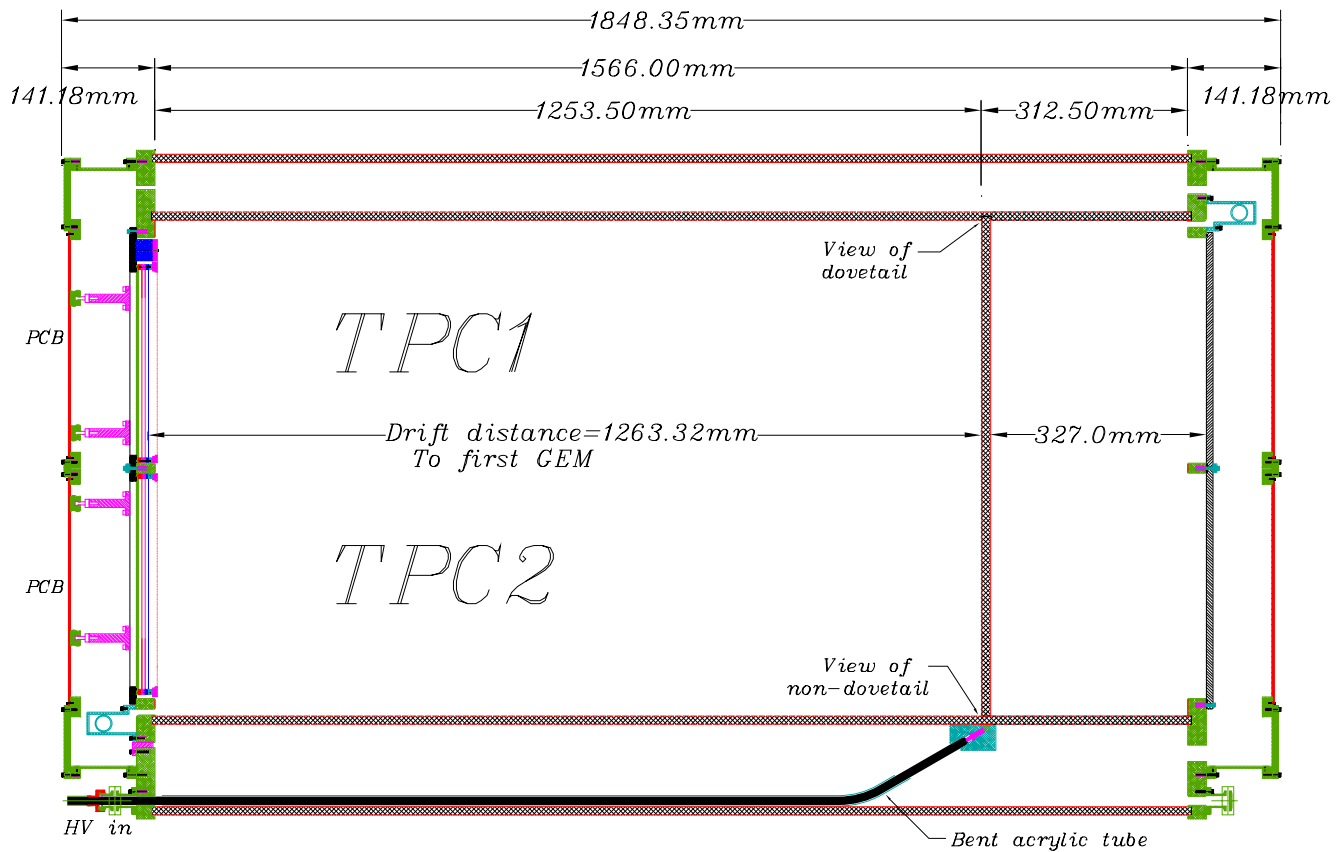


Fig. 147. Side view of T2K prototype TPC.

first type is made from thirty layers (alternating X and Y) made from extruded scintillator. Each layer would consist of two hundred $10\text{ mm} \times 10\text{ mm}$ pieces with central holes). These 6000 scintillator pieces would be read out with WLS fibres and APDs. The second type of FGD would be thirty layers (alternating X and Y), each layer made from two extruded plastic panels ($1\text{ m} \times 2\text{ m}$), each having one hundred $10\text{ mm} \times 10\text{ mm}$ cells. These panels would be filled with liquid scintillator and read out with 1.5 mm diameter WLS fibres. Again, the 6000 fibres will be read out with APDs.

CFI funding for LADD has been approved and spending has started. This money will be used to boost the detector development infrastructure at TRIUMF. LADD will take considerable time and effort to set up, and is planned to give TRIUMF a world class facility for continuing development of detector technologies, not just for physics experiments, but potentially for a wide range of R&D projects including a variety of medical detectors. An important item that LADD will provide is a large ($3\text{ m} \times 3\text{ m}$) router that will be used for both inspection and fabrication of the KOPIO and T2K detectors. Another LADD item already purchased and installed is a precision 5 ton crane in the large clean room.

GEANT4

(P. Gumplinger, TRIUMF)

Modern particle and nuclear physics experiments require large-scale, accurate and comprehensive simulations of the particle detectors used in these experiments. The same is true for other disciplines, such as space science, nuclear medicine, accelerator design and radiation physics. In response to this demand, a new object-oriented toolkit, GEANT4, has been developed for the simulation of particles passing through matter. It provides a comprehensive, diverse, yet cohesive set of software components which can be employed in a variety of settings, from small standalone applications to large scale detector simulations for experiments at the LHC and other facilities. At the heart of this software system is an abundant set of physics models, including electromagnetic, hadronic and optical processes, over a wide energy range starting, in some cases, from 250 eV and extending in others to the TeV energy range.

GEANT4 was designed and is being developed by an international collaboration, formed by individuals from a number of cooperating institutes, HEP experiments, and universities. It builds on the accumulated experience in Monte Carlo simulations of many physi-

cists and software engineers around the world. The major players in the current collaboration are the international organizations CERN and ESA/ESTEC, the national laboratories INFN (Italy), IN2P3 (France), Helsinki Institut of Physics (Finland), Karolinska Institutet (Sweden), KEK (Japan), PPARC (UK), SLAC (USA) and TRIUMF (Canada), with strong support from these HEP experiments: BaBar (SLAC), ATLAS, CMS, HARP, LHCb (CERN). Additional expertise comes from 14 European, 4 Japanese, and 5 North-American universities and 4 Russian institutes, for a total of about 150 collaborators. The TRIUMF group is active in some of the core activities of the collaboration, in areas of user support, documentation, testing and quality assurance. We have representation in the Technical Steering Board and in the Collaboration Board.

GEANT4 is an ideal framework for modelling the optics of scintillation and Čerenkov detectors and their associated light guides. This is founded in the toolkit's unique capability of commencing the simulation with the propagation of a charged particle and completing it with the detection of the ensuing optical photons on photo sensitive areas, all within the same event loop. This functionality of GEANT4 is now employed world-wide in experimental simulations as diverse as ALICE, ANTARES, AMANDA, Borexino, ICARUS, LHCb, HARP, KOPIO, the Pierre Auger Observatory, and the GATE (Imaging in Nuclear Medicine) Collaboration. This functionality is also exploited as part of the investigation to understand the optical properties of extruded plastic scintillator tiles for KOPIO and for the Near Detector of the Long Base-Line Neutrino Experiment at J-PARC/SuperK. We are constantly responding to inquiries posted on the G4 Users Forum regarding the optical photon tracking. Questions and feedback arrive from people working in medical PET research, cosmic shower research, neutrino detectors, HEP experiments and also from cooperate research laboratories. During the last year alone, we responded to inquiries from EXO (Enriched Xenon Observatory for Double Beta Decay), Milagro Gamma-Ray Observatory (a Water-Cherenkov detector in the Jemex mountains near Los Alamos), ICARUS (a LAr TPC proton decay and neutrino interactions detector at the Gran Sasso), from the LHC Physics Center (LPC) at FNAL, from CAST (CERN Axion Solar Telescope), n_TOF collaboration at CERN, the MACFLY project studying air fluorescence, the Panda experiment at GSI, Borexino, the LLNL/SNL Applied Antineutrino Physics Project, LHCb and CMS. We collected links to these experiments at <http://www.triumf.ca/g4triumf/users/users.html>

A computer science coop student from SFU, Trevor

MacPhail, worked in our group for the first six months of 2004. As a result of his efforts, the G4 source distribution now comes with an excellent, extended, optical photon example. This application also helps the design of an advanced next generation LXe PET camera with improved background rejection. A phi-angle correlation exists in polarized Compton scattering between the two scattered annihilation photons because of their definite relative polarization at birth. This information becomes accessible in an active tracking medium where the photon interaction points can be observed individually. We also finalized the capability of spin tracking in GEANT4, spin precession at rest, followed by Michel decay relative to the momentary spin direction. This was a vital development before the TWIST experiment at TRIUMF could adopt GEANT4 as their simulation engine.

The G4 toolkit is now in public release version 7.0 and is available for a variety of operating systems.

GEANT4 collaborators at TRIUMF: P. Gumplinger, F.W. Jones and C.J. Kost, M. Losty.

Laboratory for Advanced Detector Development (LADD)

(J. McKay, TRIUMF; D. Bryman, UBC)

During the past year, LADD funds were used to purchase equipment to support a variety of detector development directions as indicated in the LADD CFI proposal.

The electronics laboratory component of LADD continued development of infrastructure for design and development of electronics readout systems. The KOPIO and Liquid Xenon projects will make particular use of this equipment. Purchases this year have focused mostly on additional test and measurement equipment (such as waveform/pulse generators and power supplies), tools, and parts storage. There have also been some new software items purchased to aid in design tasks.

The LADD electronics equipment has been extensively used for development and evaluation of detector components. KOPIO and T2K have instrumented their prototypes with LADD equipment such as NIM and VME crates, VME data acquisition modules, high voltage systems, etc. as well as auxiliary devices such as oscilloscopes, multimeters, power supplies and computers. The nature of this development requires advanced electronic equipment which is essential to a proper development set-up. The contribution of LADD has significantly facilitated this development by providing state of the art electronic infrastructure.

Equipment has also been purchased for the detector facility. Major purchases include a quadrupole mass spectrometer and a crane for the clean room. This

equipment will be used to facilitate projects with large complex detectors such as KOPIO, Liquid Xenon, and neutrino detector projects.

As mentioned above, equipment purchased for the electronics laboratory and the detector facility are being used to support the KOPIO project. KOPIO chamber development and prototyping has been taking place. Mechanical development and prototype work has been aided by various hand tools, computers, and software. One large development project has been the fibreglass wire chamber frames and sheets. The maximum size of G10 sheets commercially available is too small for our chambers if we want to keep them joint free. Working with a Vancouver Island company (Profile Composites), a method has been developed to make G10 sheets and chamber frames as large as the wire chambers. This will result in chambers with higher mechanical strength and make the assembly easier and more economical.

Another part of KOPIO is scintillator development. KOPIO is developing a technique to produce extruded scintillator at a local company (Celco Plastics). The scintillator planks will be glued using a tongue and groove method to make large sheets of scintillator of the desired size. There is substantial cost savings in using this extrusion technique over buying cast scintillator sheets. These sheets will be machined at TRIUMF using a machine purchased by LADD. Research and testing to determine the best type of machine has been taking place. The machine will also be used to machine wire chamber frames and cathode strips, among other things. Good results have been achieved with a router, which will likely be purchased in 2005, and will double as an inspection table.

The Liquid Xenon facilities development project has also been made possible by LADD. Various materials (such as ceramic feedthroughs, UHV valves, UHC flanges, vacuum fittings, macor, and stainless) and instrumentation were purchased for building a cryostat and gas handling system. A control system has been developed, and assembly of the cryostat and gas handling system are well under way, with testing to start in 2005.

In addition, equipment has been purchased for DAQ systems, including VME scalers, high voltage modules, TDCs, ADCs, and VME crates. Another advanced detector development area that is being enhanced by LADD infrastructure involves neutrino detectors.

During 2004, LADD funds were used to purchase extensive computing, real time data acquisition, high voltage supply equipment, and advanced photodetectors. This equipment was used to evaluate different photosensors for use in the fine-grained neutrino de-

tector (FGD) to be built for the T2K neutrino oscillation experiment at Tokai in Japan. As part of the reference design for this detector, it is planned to use extruded bars of scintillator with either an active or passive water component, and with wavelength shifting (WLS) fibre used to transport the light to some kind of photon detector.

Measurements were carried out with this apparatus to compare the performance of the SiPMs with multi-anode PMTs (MAPMTs). Work using LADD facilities has reached the following conclusions:

1. The SiPMs work best at a bias voltage of around 52 V, where the gain is a few $\times 10^5$. This is about an order of magnitude lower than that of a MAPMT, and will necessitate the use of a preamp with a gain of 20–30 if the SiPM is chosen.
2. The quantum efficiency of the SiPM is about 30% better than the MAPMT, and is about equivalent to that of a good green-extended PMT.
3. The pulse height resolution of the SiPM is much better than the MAPMT, and clear peaks corresponding to 1 pe, 2 pe, 3 pe... can be seen.
4. The timing resolution of the SiPM is adequate, and almost certainly better than the time spread produced by the WLS fibre at low light levels.
5. The single photoelectron noise (or dark current) count rate is substantially higher for the SiPM compared with the MAPMT. It is a function of bias voltage, and was measured to be about 1 MHz at 52 V.

Scientific Services

(*M. Comyn, TRIUMF*)

The Scientific Services group encompasses the Publications Office, Library, Information Office, and Conferences. Its activities during 2004 included: producing the 2003 Annual Report, conference abstract booklet and proceedings, and the TRIUMF preprints; maintaining the Library; coordinating TRIUMF tours and assisting with the production of public relations materials; and supporting eleven past, present and future conferences and workshops. The primary focus of the group throughout the year concerned all aspects of hosting the NIC8 conference in Vancouver in July.

Publications Office

The TRIUMF Annual Report Scientific Activities has been truly electronic since 1998. Electronic files have been used throughout, from initial contributor submission, through editing, transmission to the printer, and subsequent direct printing on a Xerox Docutech system. The same files are used for the WWW versions of the report which are available at

<http://www.triumf.ca/annrep> in both Portable Document Format and PostScript file formats. Unlike the monochrome paper version, the electronic versions allow those figures which were submitted in colour to be both viewed and printed in colour. The WWW version of the 2003 report was available to readers five weeks before the printed version. It contained a record 331 pages and 320 figures. The Annual Report mailing list has been reduced and the trend is expected to continue as people become more accustomed to accessing the information over the WWW. This will result in less copies having to be printed and mailed, with subsequent major cost savings.

TRIUMF preprints are only produced electronically, and immediately posted on the WWW at <http://www.triumf.ca/publications/home.html> to allow rapid dissemination of the publications. This has replaced the traditional distribution of paper copies by mail, resulting in significant savings of both cost and labour.

The year began on two fronts with the kickoff for the TRIUMF Annual Report Scientific Activities 2003 submissions, and the receipt and processing of abstracts for the Eighth International Symposium on Nuclei in the Cosmos (NIC8), which was held in Vancouver, July 19–23. Many aspects of handling the abstracts were based on those developed for the EMIS-14 conference in 2002. However, this time the abstracts were ranked by the International Advisory Committee via a secure Web form to determine which should be presented orally rather than as a poster. Although the abstract submission deadline was April 2, half of the 211 accepted abstracts were submitted later. A draft program was produced in late May by the local organizing committee, and an almost final version was posted on the conference Web site in early June. However, the program remained fluid with late cancellations, additions and changes, resulting in the final 224 page abstract booklet only being sent to the printer a week before the conference began. Publications Office staff manned the Proceedings Office during the conference, accepting manuscripts in both hardcopy and electronic formats. As the proceedings will be published as an edition of Nuclear Physics A in 2005, all contributions had to be refereed. This is a complex, time-consuming procedure which had still not been completed at year end. Unlike EMIS-14, no manuscripts were assigned to referees at the conference. Therefore, to speed up the process, nearly all communications with the referees were via e-mail with scanned manuscripts and referee information sheets being sent as PDF attachments. By avoiding the use of conventional mail (which often added a month in transit time for the EMIS-14 refereeing, even within North America), communica-

tions were much faster. All transactions were logged on a database.

Web site and other support was provided for the TRIUMF Summer Institute, held July 5–16.

Due to the workload this year, activities on the Joint Accelerator Conference Website (JACoW) committee were completely curtailed.

Library

The Library budget was increased in 2004 to compensate for rising journal subscription costs, thereby maintaining the list of journals which have been acquired since the last cutbacks in 1998. However, the journal subscription budget and electronic access alternatives are constantly under review. The Library continues to rely on donations for most of its book acquisitions. The Library operates on a self-serve basis and manages with minimal support for day-to-day operations.

Information Office

The Information Office coordinated 194 tours for 1663 people during 2004. The general public tours were conducted by a summer student during the June to August period when tours were offered twice a day. 153 people attended one of the 46 tours conducted during the three month period. Throughout the remainder of the year for the twice weekly general public tours, and for the many pre-arranged tours given to high school students and others, a small, dedicated group of TRIUMF staff acted as tour guides.

Table XXIV shows the number of people taking tours, the number of tours, and the number of tour guides required to conduct them (groups of more than 15 require multiple tour guides) for each of the years 1999–2004. 2004 saw a decline in all numbers in all categories, except for science, compared to recent years. The 2004 numbers were very similar to those for 1999. This can be ascribed to many factors. For the general public, TRIUMF had not featured so prominently in the local media during 2004. For students, the lack of a professional development day event for the BC physics teachers in October, 2003 undoubtedly had an effect. Finally, there were fewer VIP visitors in 2004 following increased numbers in the previous three years associated with ISAC-II construction and the Five-Year Plan review in 2003. The four categories are defined as follows:

- General public: tours provided for members of the general public twice a week September–May and twice a day June–August, on a drop-in basis.
- Science: pre-arranged tours conducted for university/college physics, chemistry or science students with a specific interest in TRIUMF, scien-

tists at TRIUMF for a conference or workshop, and scientific groups.

- Students: pre-arranged tours conducted for elementary and high school students and university/college non-science students.
- VIP: specific tours, often conducted by senior management personnel, arranged for VIPs, review/advisory committee members, and the media.

The summer student also assisted with the production of presentation materials, with the TRIUMF Summer Institute, and as the coordinator of many student activities throughout the summer.

The TRIUMF Welcome Page, which is accessible directly at <http://www.triumf.ca/welcome>, continues to receive well over 5000 visits each year. No maintenance was performed during the year as the content is being superceded by the new public Web site <http://www.triumf.info> which became operational during the year.

Various TRIUMF images found on the Web pages continue to be in demand for use in text books and on other Web pages.

Substantial support was provided to the TRIUMF Users' Group throughout the year by the TUEC Liaison Officer.

Table XXIV. Breakdown of TRIUMF tour numbers for the period 1999–2004.

Category	1999	2000	2001	2002	2003	2004
General						
Public						
# people	350	368	421	499	482	399
# tours	96	107	110	131	126	109
# guides	96	107	111	134	126	111
Science						
# people	384	294	383	592	651	729
# tours	18	20	30	23	34	36
# guides	33	26	43	57	59	70
Students						
# people	794	612	839	894	626	440
# tours	46	40	30	40	38	23
# guides	70	53	60	70	50	35
VIP						
# people	145	171	258	193	260	95
# tours	37	37	59	53	63	26
# guides	38	40	65	55	71	26
Total						
# people	1673	1445	1901	2178	2019	1663
# tours	197	204	229	247	261	194
# guides	237	226	279	316	306	242

Conferences

Support was provided for four conferences and workshops, along with preparations for seven conferences and workshops in 2005 and beyond. Registration databases were created and managed for all of the conferences and workshops.

TRIUMF hosted or supported the following conferences and workshops in 2004:

- Fixed Field Alternating Gradient Workshop (FFAG 2004), TRIUMF, April 15–21 (23 delegates).
- TRIUMF Summer Institute 2004 (TSI2004), TRIUMF, July 5–16 (38 delegates plus 8 lecturers).
- Eighth International Symposium on Nuclei in the Cosmos (NIC8), Vancouver, July 19–23 (237 delegates).
- Fifth International Symposium on Radiohalogens (5ISR), Whistler, September 11–15 (74 delegates).
- TRIUMF Users' Group Annual General Meeting, TRIUMF, December 8 (58 delegates).

In addition, preparations were made for the following future conferences and workshops.

- ICFA Workshop, February 10–11, 2005.
- Western Regional Nuclear and Particle Physics Conference (WRNPPC'05), Banff, AB, February 18–20, 2005.
- 2005 CAP Congress, UBC, June 5–9, 2005.
- TRIUMF Summer Institute 2005, TRIUMF, July 11–22, 2005.
- Trapped Charged Particles and Fundamental Interactions (TCPFI 2006), Parksville, September, 2006.
- Linear Accelerator Conference (LINAC08), Vancouver, September 29 – October 5, 2008.
- Particle Accelerator Conference (PAC09), Vancouver, May, 2009.

The DRAGON Facility

(*D. Hutcheon, TRIUMF*)

DRAGON is a facility at ISAC for the study of radiative capture reactions by inverse kinematics, in which the beam is the heavy reactant and the target is the lighter one. The focus of study is to measure reaction strengths of relevance in nuclear astrophysics, but the facility has been used for nuclear structure experiments as well.

The principal parts of the facility are a windowless gas target, an array of scintillators around the target to detect capture γ -rays, a mass separator to transmit

heavy recoil products while suppressing beam particles, and a gaseous or solid-state detector of the recoil ions.

DRAGON was used to study radiative capture of protons by unstable beams of ^{21}Na (Expt. 821) or ^{26}Al (Expt. 989), capture of alpha particles by a stable beam of ^{12}C (Expt. 952) and capture of ^{12}C target nuclei by nuclei of a ^{12}C beam. Results from these experiments are presented elsewhere in this Annual Report. Here we describe improvements in the DRAGON facility in 2004 and tests aimed at possible future improvements.

Data acquisition system

Noise problems with elastic-scattering surface-barrier detectors were fixed, with implementation of a second surface-barrier detector at a higher lab angle with respect to the beam axis.

Electronics housed in one crate near the gas target were split between two crates, one still at the gas target and one at the tail of DRAGON. All required signal exchange between the two crates is now performed via ECL. Both crates are housed in racks which have improved cooling to suppress erratic behaviour of the electronics at high temperatures, a problem which can occur with hot weather in the summer months. The number of ADCs and TDCs in the tail crate was doubled to allow a more permanent addition of extra detectors. The existing scaler modules were upgraded, doubling the number of available scaler channels. The DSSSD electronics have been upgraded to allow readout of both front and back strips providing complete detector pixelization. MCP local time of flight has also been implemented and can be used in conjunction with other heavy-ion detectors at the tail of DRAGON to improve ion separation.

Traditional CAMAC readout of the data has been replaced in favour of readout through a vxWorks-based VME interface, decreasing dead-time on each memory module readout. The frontend software has been changed to run on the vxWorks system to enable the new readout scheme. The on-line analysis was rewritten using the ROOT framework in a totally object-oriented manner.

The HV calibration program has been rewritten to allow interaction with the new on-line system and to provide a quick means to change the BGO detector-array voltages rapidly.

Ion chamber gas control system

The ion chamber detector of recoil ions uses isobutane gas at pressures that are typically in the range 5 to 15 torr with gas flow of about 100 cc/min. Ions enter the gas through a window which must be as thin as possible to minimize energy straggling. The pump-down, filling, operation and venting of the ion chamber

must be carried out very carefully to avoid destruction of the thin window. Initially, these operations were carried out by users operating manual valves and following a lengthy written procedure.

In order to make ion chamber operation easier and safer, the manual system was replaced by one controlled through EPICS and having interlock protection provided by a programmable logic controller (PLC). Some interlocks on valves had to change in a state-dependent way, according to whether the chamber was being roughed, filled, operated or vented. A different set of conditions had to be applied when the ion chamber was replaced by the vacuum box for solid-state detectors.

The connection of vacuum and gas handling devices to the PLC was accompanied by installation of a “burst-puck” and shield, as a safety measure for the (unlikely) scenario of formation and ignition of an air-isobutane mixture in the ion chamber. High voltage to the ion chamber grid wires is enabled only when there is an expected isobutane flow rate, indicating the absence of dangerous air leaks into the system.

Monitors of beam contamination

For certain experiments it is necessary to monitor the level of beam contamination. We have installed two additional diagnostics at the mass slit box to accomplish this feat: 1) a germanium detector mounted beside mass slit box at beam height, and 2) a positron-catcher plate coupled to two NaI detectors mounted oppositely in close geometry surrounding the plate on top of the mass slit box. These detectors take advantage of the mass dispersion at the mass slit box which causes the beam to be deposited on the left mass slit plate while passing recoils through the slit opening. These new detectors complement the pre-existing plastic scintillator for counting betas that is sensitive to both electrons and positrons. The positron catcher assembly can be used to identify positron emission only, while the germanium detector can be used to identify characteristic γ -rays emitted from either the beam or a contaminant thereof.

As an example, in the case of Expt. 989 ($^{26}\text{Al}(p, \gamma)$), two beam contaminants were identified in early running, first by our beta counter then later at the yield station and finally using our new set-up. The possible beam contaminants are $^{26}\text{Na}(\beta^-, T_{1/2} = 1.08\text{s}, E_\gamma = 1.809\text{ MeV})$, $^{26\text{m}}\text{Al}(\text{EC}, T_{1/2} = 6.34\text{ s}, \beta^+)$, $^{26}\text{Si}(\text{EC}, T_{1/2} = 2.23\text{ s}, \beta^+, E_\gamma = 0.829\text{ MeV (BR} = 21\%))$, and $^{26}\text{Mg}(\text{stable})$. Due to the nature of the SiC surface ion source, the magnesium and silicon components are absent. Thus, the positron-catcher is used to determine the level of $^{26\text{m}}\text{Al}$ contamination only, while the germanium detector monitors the level of ^{26}Na (via detection of $E_\gamma = 1.809\text{ MeV}$) and $^{26\text{m}}\text{Al}$ (via detection of E_γ

= 0.511 MeV). The ^{26}Al beam with its 720,000 year half-life is effectively stable.

For a more detailed description visit <http://dragon.triumf.ca/nai.html>.

A “switchyard” for end detectors

Two vacuum enclosures have been used to contain recoil ion detectors: a machined box in the form of a 20 cm cube housed silicon strip detectors, and a 25 l cylinder enclosed a low-pressure gas ionization chamber. The two types of detector have been exchanged frequently, sometimes during the course of a single experiment. The ionization chamber was mounted on a trolley which could be rolled forward when that detector was to be used, but the heavy strip detector box had to be lifted into place by hand in a procedure that required two people.

The installation of the strip detector box was simplified by the addition of a linear bearing running at right angles to the trolley track. It allows the box to be moved into the correct position without lifting, so that one person can carry out a change of detectors much more easily and quickly than before.

Improved ion chamber energy resolution

Standard mylar windows with a thickness of $130\ \mu\text{g}/\text{cm}^2$ and thin polypropylene (PP) windows of $55\ \mu\text{g}/\text{cm}^2$ have been used as entrance window for the DRAGON ion chamber (IC) at higher energies with sufficient resolution (e.g. $\Delta E/E = 1.7\%$ FWHM for ^{28}Si at 750 keV/u) [Chen for the DRAGON collaboration, Nucl. Instrum. Methods **B204**, 614 (2003)]. However, for $A > 20$ ions at low energies the energy-loss straggling in the entrance window, about 24% for PP and 45% for mylar, degrades the energy resolution to 5–10%, not enough for a separation of recoils from leaky beam at the end detector. In order to improve the separation power of the IC at low energies (e.g. 188 keV/u ^{26}Al), new foils were tested.

Amorphous silicon nitride (SiN) membranes can be made as thin as a few times 10 nm. For our tests we used 50 nm (=17 $\mu\text{g}/\text{cm}^2$) SiN membranes with a size of $5 \times 5\ \text{cm}^2$ up to pressures of a few 10s of torr. The anode of the IC was modified to have two main segments each of 10 cm length and a third segment of 5 cm length at the end as an optional veto. First spectra of ^{12}C and ^{16}O at 179 keV/u show the improved energy resolution of 3.1% and 2.6% (Fig. 148). Due to the high homogeneity of the SiN membranes, low-energy tails are significantly reduced. This is particularly important for proton capture reactions where the expected recoils have slightly less energy than the leaky beam. With this set-up the resolution is dominated by electronic noise, mainly from the preamplifier, which is in the order of 40 keV. As a next step we plan to

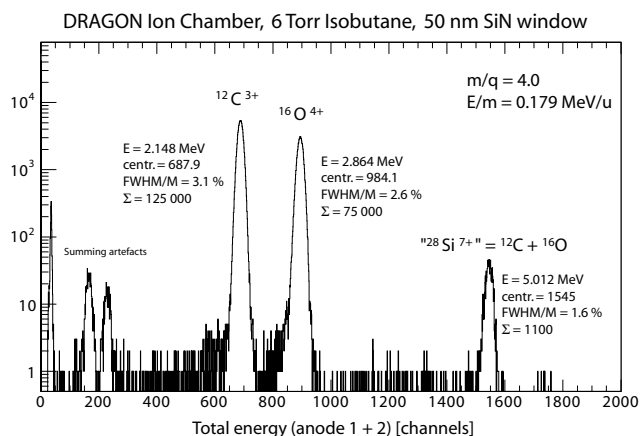


Fig. 148. DRAGON segmented ionization chamber response to C and O ions.

install new low-noise preamplifiers directly onto the anode board, which will greatly reduce input capacitance and noise pick-up. For heavier ions at low energy it has been shown [Doebeli *et al.*, Nucl. Instrum. Methods **B219-220**, 415 (2004)] that an improved ion chamber with thin SiN entrance window can outperform silicon solid-state detectors, which suffer from relatively large intrinsic dead layers (about 600 nm Si equivalent).

Local time of flight (TOF) can provide better separation than energy measurement at low ion energies, since flight time increases at lower energies, while the time resolution is independent of the flight time. Even with a moderate TOF resolution of 1.5 ns FWHM and a 0.5 m flight path, TOF gives better separation than E-detectors with 3% resolution for energies below 500 keV/u [Lamey, M.Sc. thesis, Simon Fraser University (2004)]. However, thin carbon foils ($20\ \mu\text{g}/\text{cm}^2$) used for the start MCP detector can introduce significant energy-loss straggling and angular scattering. To improve the detector performance, we tested ultrathin diamond-like carbon (DLC) foils having a thickness of only $0.6\ \mu\text{g}/\text{cm}^2$, which are supported by a mesh of about 80% transmission [Liechtenstein *et al.*, Nucl. Instrum. Methods **A521**, 197 (2004)]. With ^{21}Ne beam we could demonstrate negligible angular scattering compared to $20\ \mu\text{g}/\text{cm}^2$ carbon foils. However, the thickness of these DLC foils is less than the escape length of secondary electrons (about 5 nm), reducing the number of secondary electrons and thus the pulse height at the MCP anode, which is used for a position signal. For our planned second MCP we will install a large DLC foil with a thickness of about $4\ \mu\text{g}/\text{cm}^2$ and supported by a mesh of 99% transmission, a compromise between secondary electron yield and angular scattering.

Solid target mount

The 9-position solid target system was used successfully by Expt. 947, which required a target of ^{12}C

in the form of a thin foil. Mounted on a plate which could replace the standard side-plate of the windowless gas target box, the chain of targets could be driven under EPICS control of a stepping motor to any one of 9 pre-set positions. Two target positions were dedicated to collimators used in beam tuning. A third target, a microscope glass slide coated by a thin carbon layer, gave a visible spot when struck by beam and was an additional beam-tuning diagnostic.

Beam visualization by CCD camera

A CCD camera viewing the target cell along the zero-degree axis is able to detect light produced when ion beams of nanoampere intensity pass through hydrogen or helium in the gas target. It is displayed using commercial software designed for amateur astronomers. Thanks to a custom modification of the software, it is possible to log beamspot intensities and $x - y$ centroids while data-collection runs are in progress.

8 π Spectrometer

(G.C. Ball, TRIUMF)

During the past year the ancillary detector systems for the 8 π spectrometer were further augmented with the fabrication, installation and commissioning of PACES, a pentagonal array of SiLi detectors for conversion electron spectroscopy measurements. A view of PACES, which replaces the upstream half of SCEPTAR, is shown in Fig 149. The first experiment to use PACES and SCEPTAR was the study of coexisting collective phases in ^{156}Dy from a detailed measurement of the β -decay of ^{156}Ho . The results of this experiment led by D. Kulp are reported separately (see Expt. 973, this Annual Report).

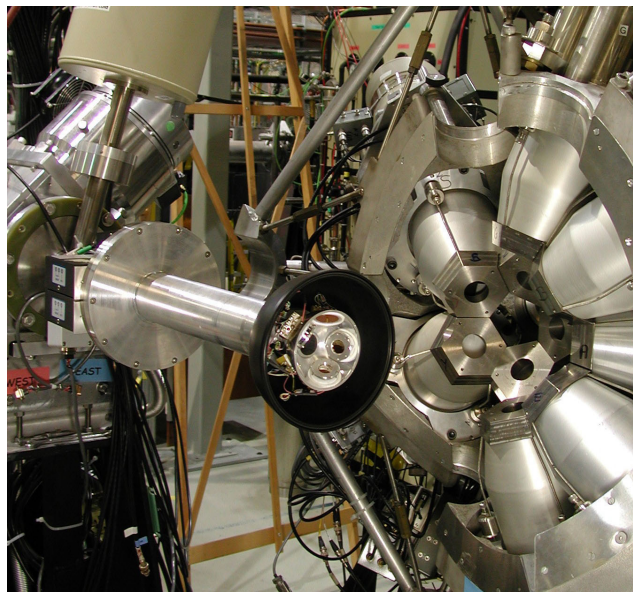


Fig. 149. Photo of PACES installed on the 8 π beam line.

In June a ^{26}Na beam was used to measure the time response of SCEPTAR and characterize the performance of BaF_2 detectors when integrated into the 8 π array. A proposal led by P. Garrett (see Expt. 984, this Annual Report for details) to build an array of 10 BaF_2 detectors for fast (down to 10 ps) lifetime measurements of gamma-decaying excited states populated in the β -decay of exotic nuclei was submitted to NSERC in October.

Once again, the 8 π data acquisition system (see TRIUMF 2002 Annual Report for details) was extended to include separate FERA readout buses and VME triple port memory modules for both the PACES and BaF_2 arrays.

During the initial running of Expt. 921 (see Expt. 921, TRIUMF 2003 Annual Report) it was determined that to prevent contaminating the 8 π vacuum chamber with small quantities of long-lived isobaric contaminants the vacuum in the section of LEBT immediately upstream of the 8 π spectrometer had to be improved to reduce the probability of charge exchange collisions and subsequent loss of beam. As a result, an additional 550 l/s turbo pump was added and the 550 l/s turbo pump on the LEBT box connected to the 8 π vacuum chamber was replaced with a 1000 l/s pump. In addition, the SCEPTAR array was removed and replaced with a simplified chamber with removable liners. In the spring, extensive measurements were carried out searching for new high-K isomers in the mass 170 region. A new 2.3 s isomer was discovered in ^{174}Tm (see Expt. 921, this Annual Report).

The use of the 8 π γ -ray spectrometer for high-precision β -decay lifetime measurements is also being pioneered at ISAC. This lifetime technique has been investigated extensively for the β -decay of ^{26}Na (see Expt. 909, TRIUMF 2002–2003 Annual Reports). The first high-precision lifetime measurement of a superallowed β -emitter was carried out for the $T_z = 1$ nucleus ^{18}Ne for which the Fermi decay to the analogue 0^+ level in ^{18}F at 1042 keV is only a 7.7% branch. A beam of $\sim 4 \times 10^5$ ^{18}Ne ions/s was obtained during the first ECR ion source development run (see Expt. 985, this Annual Report for more details).

Two other 8 π experiments received beam in 2004, namely a study of the beta-delayed neutron decay of ^{11}Li (Expt. 1008) and a high-precision measurement of the branching ratio for the superallowed β -emitter ^{62}Ga (Expt. 823). These experiments demonstrated that SCEPTAR, in combination with the 8 π spectrometer, is a powerful tool for studying the beta decay of exotic nuclei. In particular, since the SCEPTAR array has approximately the same geometry as the HPGe detector array, by vetoing those events where the β particle and the γ -ray are detected in the corresponding

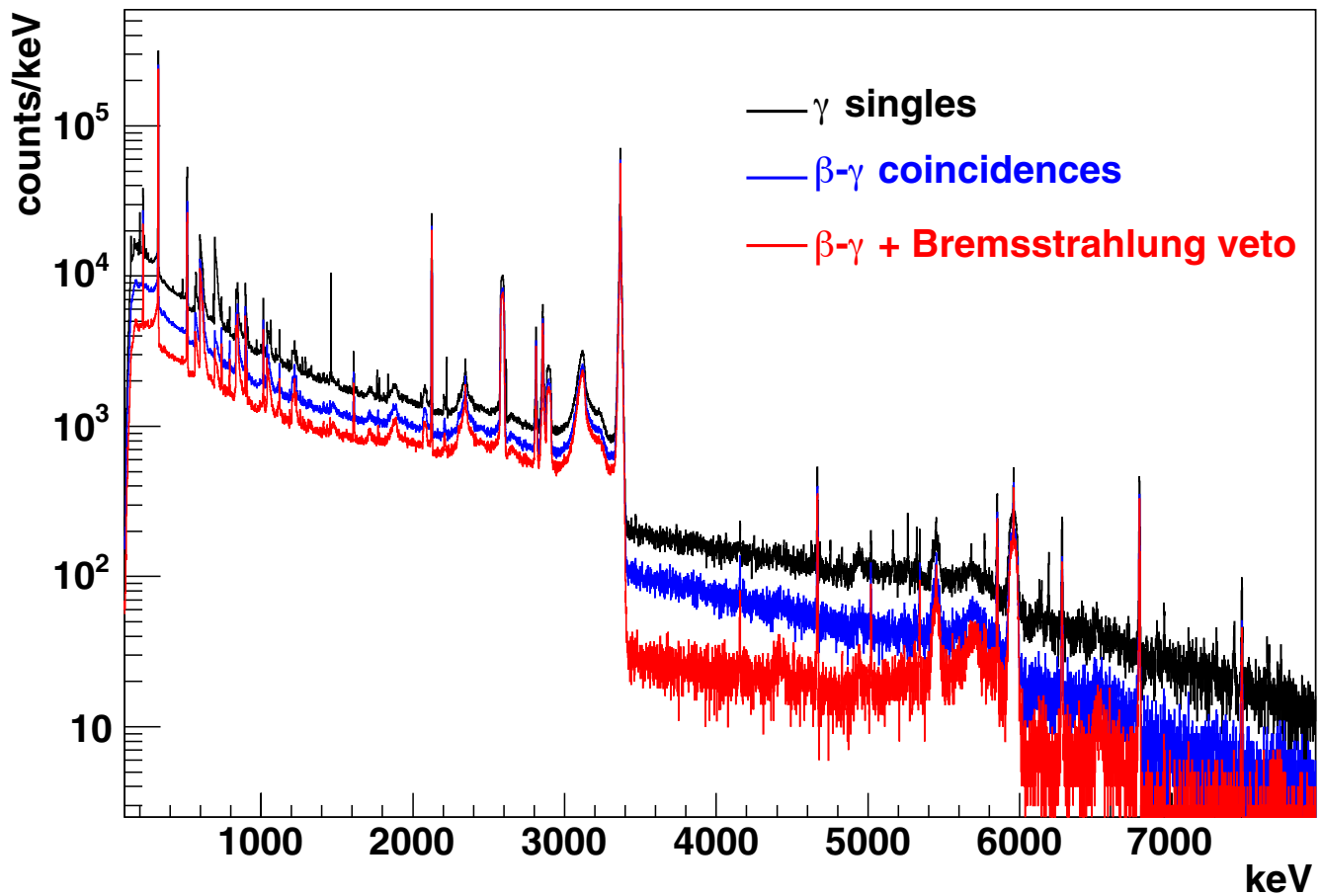


Fig. 150. γ -ray spectra observed in the β -decay of ^{11}Li : 1) the upper (black) histogram is γ singles, 2) the middle (blue) histogram is the γ spectrum obtained in coincidence with β s detected in SCEPTAR, and 3) the lower (red) histogram is the γ spectrum obtained in coincidence with SCEPTAR and with the bremsstrahlung veto condition applied.

plastic and HPGe detectors, the bremsstrahlung background can be reduced substantially. This is illustrated in Fig 150. Both of these experiments are reported in more detail elsewhere in this Annual Report.

There are currently 15 approved ISAC experiments that will use the 8π spectrometer (Expts. 823, 909, 921, 929, 954, 955, 957, 961, 973, 984, 985, 988, 1007, 1008, 1028) including three which were approved by the TRIUMF EEC in 2004. During the past year a total of 40 collaborators from 14 institutions actively participated in the development and/or use of the 8π spectrometer, including: 3 undergraduate students, 7 graduate students and 10 post-doctoral fellows.

TIGRESS

(G. Hackman, TRIUMF)

To take full advantage of the physics opportunities presented by ISAC-II beams, a state-of-the-art γ -ray detector array with high efficiency and high energy resolution is needed. TIGRESS (TRIUMF-ISAC gamma-ray escape suppressed spectrometer) will satisfy this need. Two key features of TIGRESS are: a)

rapidly reconfigurable escape suppression, and b) digital sampling of waveforms from high-purity germanium signals. These have been discussed in previous Annual Reports.

In 2004 the collaboration has built on last year's accomplishments, highlighted by: 1) continued testing of the high-purity germanium (HPGe) clover, and specification and ordering of twelve clover germanium units; 2) assembly of the prototype support structure; 3) suppressor performance testing; 4) signal simulations; 5) production of the first, revision 0 TIG-10 card. Many of the details of these developments may be found in recent publications [Scraggs *et al.*, Nucl. Instrum. Methods **A543**, in press; Svensson *et al.*, Nucl. Instrum. Methods **A540**, in press].

HPGe clovers

The prototype HPGe was returned to France for installation of two retrofits, one for the side- and back-suppressor mounting hardware, and one for electromagnetic shielding between outer-contact FETs. On return, integrated noise spectra and position sensitivities were measured. The full results of all the proto-

type clover tests have now been published [Scraggs *et al.*, *op. cit.*; Svensson *et al.*, *op. cit.*]. Based on these tests, the production HPGe clover units were specified and ordered, to be delivered at a constant rate with the twelfth unit scheduled for arrival in 2009.

Support structure

One of the key features of TIGRESS is its ability to be redeployed from a close-packed, high-efficiency configuration to a fully-suppressed, high peak-to-total configuration (Fig. 151). This presents a mechanical design challenge, and a prototype single-detector stand was fabricated for this purpose. Components for the single-detector stand were fabricated at TRIUMF and the University of Guelph (Fig. 152).

The prototype identified several operational deficiencies, primarily in the motion of detectors in their fully-inserted configurations. For the clovers, this has been addressed by repositioning the stop rods on their carriages. The side shield mechanisms continue to be reviewed. Nevertheless, the overall support system is adequate, and a mechanical engineering analysis will be performed in parallel with detailed design in 2005.

Suppressor tests

The single-unit prototype support structure also facilitated measurements of suppressor performance. Prototype suppressor shields (Fig. 153) were mounted

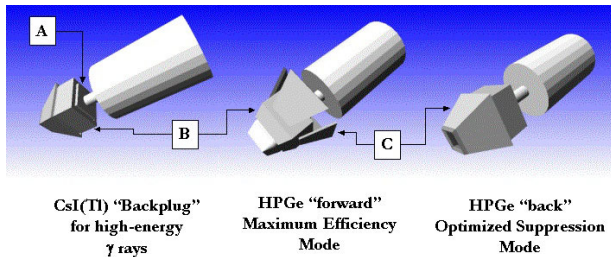


Fig. 151. Suppression scheme comprising three components: A) back-catcher, B) side shields, and C) front shields.

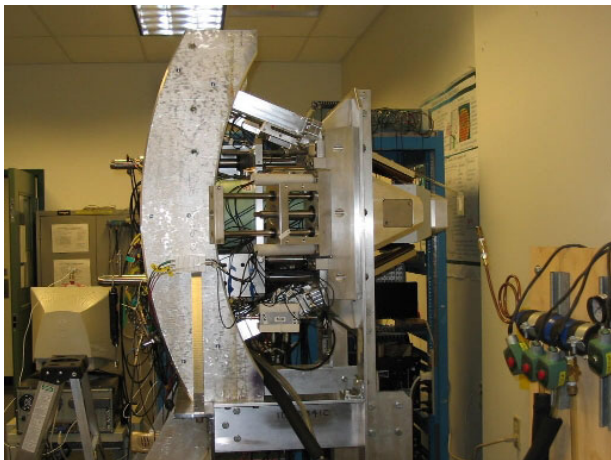


Fig. 152. Single-detector stand for testing mechanical mounting scheme and suppressor performance.



Fig. 153. Prototype suppressor shields.

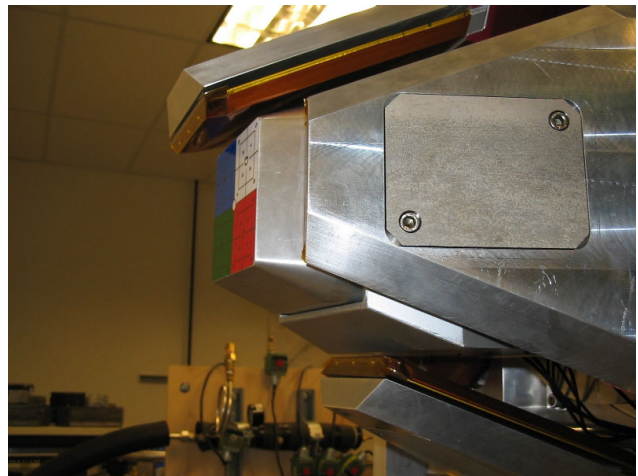


Fig. 154. Close-up view of clover and front plates. The side and bottom plates in the picture are withdrawn to show the clover and top plate in their high peak-to-total configuration.

in the single-unit stand (Fig. 154). Figure 155 compares the spectral shapes for a typical monoenergetic source, while Table XXV gives efficiency and peak-to-total performance for the prototype clover and shields in the fully-suppressed, collimated, configuration. The full details of the analysis with a variety of sources and detector configurations are to be published in the Master's thesis of Mike Schumacker at the University of Guelph.

Revision 0 TIG-10 card

Because ISAC-II beams will approach 10% the speed of light, any nuclear reactions involving these beams will emit γ -rays from sources moving up to that speed as well. The Doppler shift in the resulting γ -rays can be corrected and transformed back to the source frame if the angle of emission relative to the source velocity direction is known. This requires knowledge

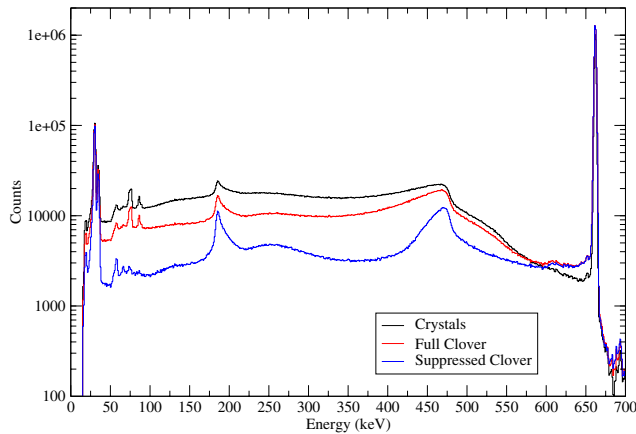


Fig. 155. Spectrum of a ^{137}Cs source with the detectors in the fully suppressed configuration, in single-crystal mode, addback mode, and addback with suppression.

Table XXV. Experimentally determined peak-to-total ratios (P/T) for test sources, measured with the prototype TIGRESS detector in the back (optimized peak-to-total) configuration, with heavymetal collimation.

Source	Parameter	Value
^{137}Cs	P/T crystals	24.9%
	P/T clover	39.7%
	Add-back factor	1.340
	P/T suppressed clover	59.9%
	Photopeak veto probability	0.19%
^{60}Co	P/T crystals	16.5%
	P/T clover	28.8%
	Add-back factor	1.437
	P/T suppressed clover	49.9%
	Photopeak veto probability	1.58%
^{88}Y	P/T crystals	16.0%
	P/T clover	27.7%
	Add-back factor	1.435
	P/T suppressed clover	47.7%
	Photopeak veto probability	1.39%

of the first interaction location of the γ -ray. The electrical waveforms generated by the nuclear event carry information about interaction locations, so that one can measure the emission angle of the γ -ray, in principle, with enough precision that the uncertainty introduces an error in energy comparable to the intrinsic energy resolution of germanium. The two key elements needed to realize this are sufficiently segmented outer contacts [Svensson *et al.*, *op. cit.*] and waveform sampling and analysis.

In the case of TIGRESS, waveforms will be sampled and events compiled using technologies similar to those developed for KOPIO (see the Particle Physics section of this Annual Report). The TIGRESS data acquisition will be built on “TIG-10” modules, ten-

channel 14-bit 100 MHz digitizers in VXI-C packages. The single-channel 14-bit 100 MHz flash-ADC sampler developed and tested last year has been integrated into a Rev 0 prototype TIG-10 module. This was delivered from Université de Montréal in late 2004. The prototype is configured and read out by a VME interface. By the end of the year, the TIG-10 prototype was incorporated into a TRIUMF-standard MIDAS set-up. Waveforms were captured and logged, demonstrating the basic functionality of the module. Further testing to improve pole-zero corrections and to implement a low-voltage differential serial (LVDS) communication to so-called “collector” (TIG-COL) and master trigger cards will continue in 2005.

Signal simulations

To fully exploit the pulse shape analysis potential of TIGRESS, it is necessary to understand the response of the detector at all positions. While these responses can be measured, it is very time consuming, and it is impossible for the inner quadrants of each detector. Instead, the pulse shapes must be simulated. Although the theory for pulse shape generation is well established, the simulations must nevertheless be verified.

Work in 2004 focused on two major efforts. The first was to rewrite the codes to be more maintainable, in particular to perform the electrostatics calculations with FEMLAB and the charge-carrier dynamics and signal generation in C++. The second was to directly compare the simulations to selected data from the coincidence scans [Svensson *et al.*, *op. cit.*].

Figure 156 demonstrates how the simulations compare to measurements of the centre-contact rise times in the outer quadrant of one crystal along the diagonal. Nominally these data points are along the $\langle 100 \rangle$

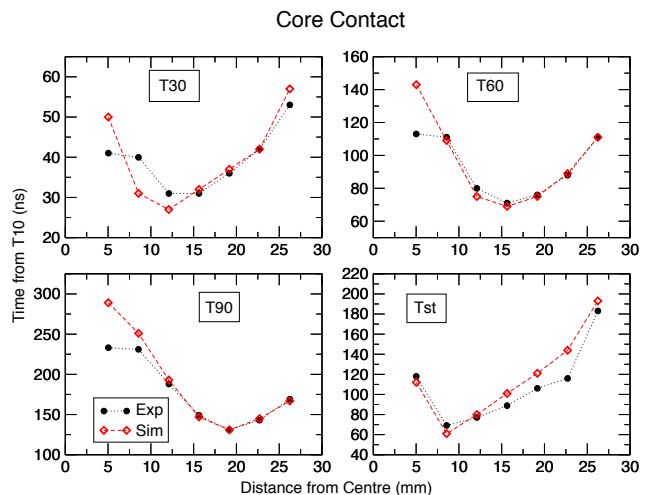


Fig. 156. Simulated vs. measured times to rise from 10% to 30%, 60%, and 90% of maximum, and to the time of steepest slope, for the core contact of one crystal.

crystallographic axis where the drift velocities are best known and are parallel to the electric field axis. The agreement is best near the outer edge of the crystal. Sources of error near the core continue to be investigated. Work in 2005 will include full implementation of the anisotropic drift velocities, including lateral deflection of charge carriers when the electric field is not along a crystallographic axis, improved treatment of edge effects, and improved modelling of the impurity distribution in the crystals.

This work earned undergraduate student Nick Cowan the award for Best Student Talk and an opportunity to present his results at the 2005 Western Regional Nuclear and Particle Physics Conference. Nick is currently a graduate student at the University of Washington.

Collaboration

The TIGRESS family grew with the addition of three NSERC grant-eligible collaborators: Prof. Roby Austin (St. Mary's), Prof. Paul Garrett (Guelph), and Prof. Jo Ressler (SFU). Of the three research associates who were part of the TRIUMF-based TIGRESS team last year, Prof. Fred Sarazin (Colorado School of Mines) remains an active member of the collaboration. Andrei Andreyev, Colin Morton and Chris Pearson have joined TIGRESS as research scientists, working with staff scientists Gordon Ball and Greg Hackman. A workshop is planned for University of Guelph in early 2005 to invite and encourage American and European involvement in TIGRESS auxiliary detectors.

Status of the TITAN System

(J. Dilling, TRIUMF, for the TITAN Collaboration)

TITAN (TRIUMF's ion trap for atomic and nuclear science) is a facility for a variety of high precision experiments. The main goal is accurate atomic mass measurements on short-lived radioactive isotopes. In order to achieve this the nuclei, produced at ISAC, undergo various preparations, before the actual mass measurement in a Penning trap. What sets this facility apart from all other Penning trap mass spectrometers for radionuclides is the fact that we boost the charge state of the ions. The atomic mass of the ions is determined by measuring the cyclotron frequency $\nu_c = q/m \cdot B$ of the ions with q/m being the mass-to-charge ratio and B the magnetic field strength of the Penning trap. The precision of this determination is limited by the observation or preparation time available, and is proportional to $\approx T \cdot q$. To overcome this limitation of observation time for short-lived isotopes, one can make use of charge bred highly charged ions. The charge breeding is done employing a high current EBIT (electron beam ion trap). In order to achieve a high efficient charge breeding process, the beam has to be converted from a

dc beam to a bunched beam, and an additional reduction of the phase space or emittance is desired. These two important steps are carried out by a gas-filled linear Pauli trap or radio frequency quadrupole (RFQ).

After the charge breeding additional cooling is required. A dedicated cooler Penning trap is foreseen for this task. The TITAN system comprises in total 4 main components: the RFQ cooler and buncher, the EBIT charge breeder, a Penning trap for cooling of highly charged ions, and the Penning trap for high precision mass measurements. The sub-systems can be tested independently using the off-line ion source and will be installed on a platform in the low energy area of the ISAC-I experimental hall. Figure 157 shows a rendered drawing outlining the location of the different components with respect to the ground-level ISAC beam line. Figure 158 shows a recent photograph of the TITAN platform.

In the following, the various components will be described in more detail.

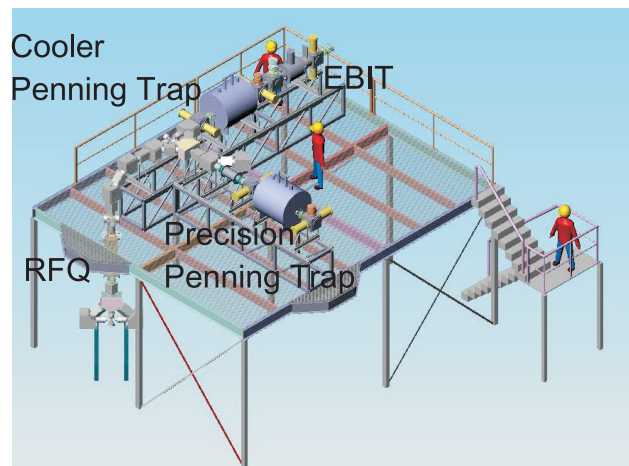


Fig. 157. Rendered drawing of the TITAN system located on, or just below, the platform in the ISAC-I experimental hall. The four main components are identified.



Fig. 158. Photograph of the recently installed TITAN platform in the low-energy ISAC area.

The TITAN RFQ beam cooler and buncher

The motivations for beam handling arise from the need to manipulate the beam properties for a variety of post processes, in our case charge breeding in the TITAN EBIT. Cooling and bunching of beams are of most interest. In this method, the incoming radioactive ion beam is cooled and subsequently delivered in bunches at a prescribed repetition rate, adjusted to the breeding cycle of the EBIT. Cooling the incoming beam reduces the energy spread both in the longitudinal and transverse directions. This improves the quality of the beam which allows us to match the emittance of it to the acceptance of the EBIT, and hence achieve an increased efficiency. The RFQ beam cooler is the first beam processing device in the TITAN experimental set-up as it processes and delivers the ISAC beam to a variety of experimental end stations, both on and off the TITAN beam line. The TITAN RFQ beam cooler is currently undergoing operational tests in the TITAN test stand (see Fig. 159). The initial tests are designed to characterize the system prior to the final coupling of the beam cooler to the ISAC beam line. The TITAN beam cooler is a radio-frequency quadrupole device that is driven by an oscillating square waveform as opposed to traditional sinusoidal driven devices. The RFQ driver developed (in collaboration with the Kicker group) for the TITAN system is capable of generating a rectangular voltage waveform of peak to peak amplitudes up to 600 V with a variable duty cycle and pulse repetition rates up to 3 MHz. This system is frequency agile as it has a flat frequency response over the entire operational range. This allows for frequency scanning without the tedium of changing circuit components as required in traditional tuned circuit systems.



Fig. 159. The RFQ off-line test stand. Composed of an off-line source, the RFQ inside the high voltage cage, and a Faraday cup diagnosis system behind the exit, on ground potential.

Initial injection tests, comparing the beam on a Faraday cup straight up from the ion source, compared to a cup on the high voltage platform, behind the final retardation electrode, have shown that around 70% of the incident beam has been successfully decelerated into the RFQ confines. Of this, 20% has been transmitted through the length of the RFQ with the RFQ operated in continuous (transmission) mode, without buffer gas. For the latter measurements a Faraday cup was mounted on ground potential behind the extraction system of the RFQ. The first test using buffer gas at a pressure of $p_{\text{Ne}} \approx 4 \times 10^{-3}$ mbar showed a rise in transmission efficiency, indicating cooling of the beam. Proper optimization of the parameters, like dc gradient, buffer gas pressure and rf parameters, are under way. Trapping and subsequent ejection of a cooled bunched beam will follow shortly. Transverse and longitudinal emittance measurements will be performed to measure the extent of beam cooling and to assess the quality of the extracted bunched beam. A specially engineered support structure will hold the RFQ beam cooler in the vertical position above the ISAC-I experimental floor in the final set-up. In this position, the beam cooler will couple the TITAN beam line, situated on the recently constructed platform, to the ISAC beam line. In addition to delivering the beam to the TITAN EBIT, the beam bunches can be extracted at the bottom end. This allows the experiments along the ISAC beam line to be provided with cooled bunched beams. Experiments that would benefit from this include the collinear laser spectroscopy and the β -NMR system. Detailed ion transport calculations based on the standard ISAC matrix code were carried out to insure that a proper injection and extraction from and into the ISAC beam line are possible. The same code was used to determine the ion optical needs for the beam transfer to the upper level of the TITAN platform. Further simulations for the complete beam line will follow.

Figure 160 shows details of how the RFQ will be mounted in the vertical position, and how the removal could be done. The concept is based on a rails system, that will allow a careful extraction of the RFQ structure from the vacuum tank, and a precise insertion, reproducing the position on a sub-millimetre level.

The TITAN high-current EBIT progress

The TITAN electron beam ion trap (EBIT) for charge breeding of radionuclides is currently under construction in the EBIT group at the MPI for nuclear physics in Heidelberg. An electron beam is produced with a thermionic cathode and then electrostatically accelerated and injected into a strong magnetic field. Here the electrons are radially confined by the Lorentz

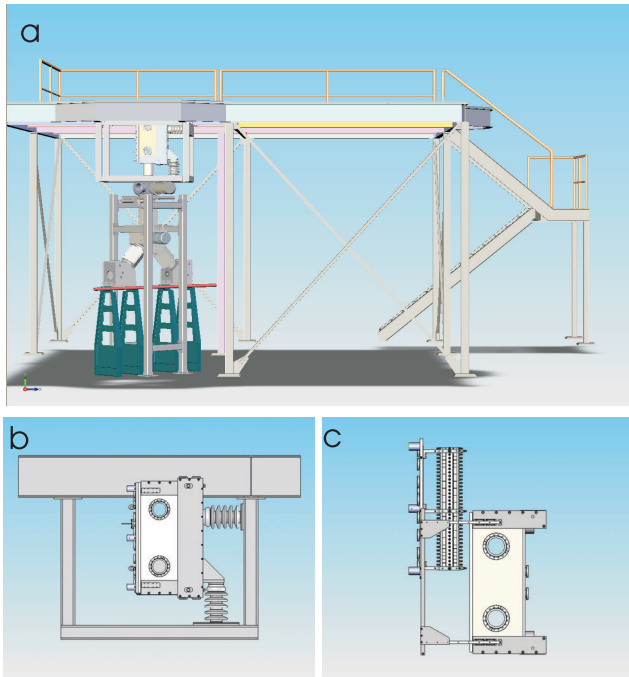


Fig. 160. Rendered drawings of the side view of the TITAN beam line, connecting the upper level (on the TITAN platform) to the ISAC beam line. Picture a) shows the RFQ in the planned location, together with the high-voltage cage frame, and support for the beam line. The lower pictures (b and c) show details of the support system for the RFQ, based on high-voltage insulators and the concept of removing the system from the vacuum tank for servicing purposes.

force, and the beam is compressed as the electrons enter the region of high magnetic field. A field of 6 T is generated by a cryogen-free superconducting magnet operating at a temperature of 3.5 K. The electron beam acceleration voltage will be variable up to 80 kV, and a beam current of 5 A is envisaged. With these parameters a compression of the electron beam down to $150\ \mu\text{m}$ is expected. The confinement of such an amount of negative electric charge provides a space charge potential, which is more than 5 kV deep. This space charge potential traps the ions radially. Axial confinement is accomplished by applying appropriate potentials to cylindrical electrodes, which are lined up coaxially in the bore of the magnet. While trapped in the dense electron beam, the ions undergo further ionization through successive electron impact processes. To obtain highly charged ions in charge states such as Xe^{44+} , typical ionization times are in the order of 10 to 50 ms.

Figure 161 shows a schematic overview of the TITAN EBIT. The radionuclides enter the EBIT as cooled bunches of singly charged ions (in the figure, from the left side through the collector). The extraction after charge breeding takes place along the same path in the opposite direction. The extraction and the

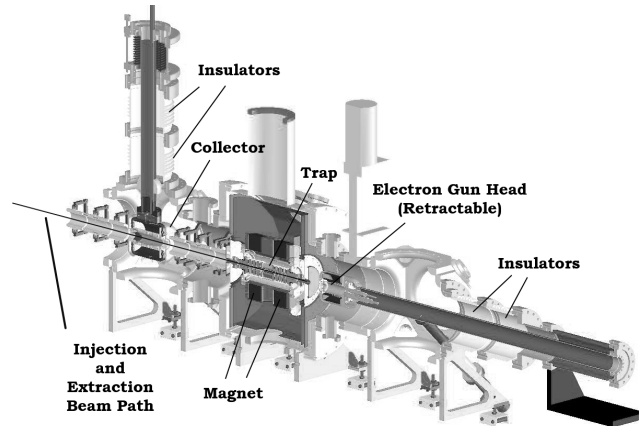


Fig. 161. Schematic overview of the TITAN EBIT. A superconducting 6 T magnet with cold bore houses the actual trap set-up. Both the electron gun head and the electron collector unit are adjustable with respect to the magnetic field and relative to each other to provide an optimal electron beam performance. The electron gun and the collector are floating on negative high voltage whereas the trap is held at ground potential.

transport to the precision Penning trap will be accomplished by means of floatable drift tubes and pulsed cavities.

Recently the TITAN EBIT assembly was completed (see Fig. 162). Some last components are expected shortly, including the final version of the trap electrodes. Using a prototype trap assembly in the first test, an electron beam current of more than 180 mA and a kinetic energy of 14 keV was achieved. Besides trapping and ionizing, the electron beam gives rise to excitation of the trapped ions and recombination. A germanium detector was placed on one of the seven radial ports to observe X-rays from the trap region through a beryllium vacuum-window. A sample X-ray spectrum taken during the first week of operation is shown in Fig. 163. Barium (and tungsten) which is

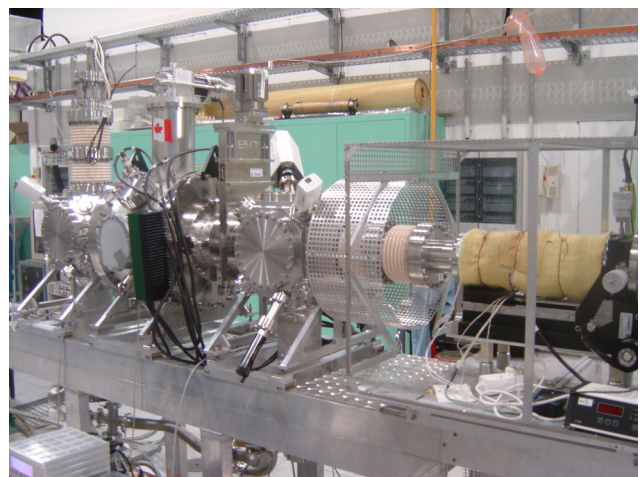


Fig. 162. Photo of the TITAN EBIT set-up.

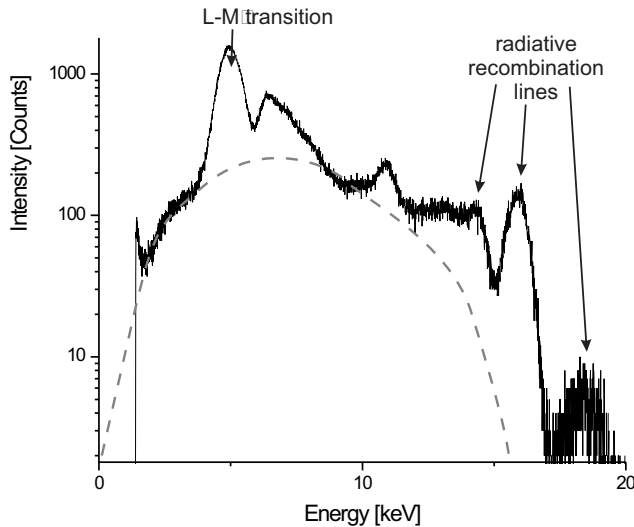


Fig. 163. X-ray spectrum from trapped highly charged Ba ions. On top of the bremsstrahlung-continuum (dashed line) spectral direct transitions, of which the L-M transition is the most prominent one, resonances at energies much higher than the kinetic energy (16.5 keV) of the electrons are observed. They are emitted by electrons which are captured in radiative recombination processes from the continuum into the $n = 4, 3$ and 2 shell of Ba.

evaporated from the cathode surface makes its way as neutral atoms into the trapping region where it gets ionized to high charge states. The spectrum gives clear evidence for trapping and ionizing of Ba. The most prominent excitation and recombination lines were observed.

In the near future the TITAN EBIT will be equipped with a gas injection system to increase the variety of elements to test with and to allow for insertion of cooling gas such as argon or neon. Furthermore a test ion source, a position sensitive particle detector and a charge-to-mass ratio analyzing magnet, all of them being operational already, will be attached to the set-up. Charge breeding and extraction of externally produced ions will be proven in the fall of 2005 and quantitative values for breeding times, temperature and beam emittance of extracted highly charged ions will become available. Shipping of the TITAN EBIT and its incorporation into the TITAN set-up is foreseen to occur in early 2006.

TITAN cooler Penning trap

The energy spread of highly charged ions (HCI) extracted from the EBIT has not been measured yet. In fact, it is rather difficult to estimate since experience with such high electron charge densities doesn't exist. However, it will most likely be too high for direct injection into the mass measurement trap. Typically, energies of <1 eV/ q are required for the cyclotron resonance technique (q is the charge of the ion). Current

experience with EBITs indicates that energy spreads of >10 eV/ q must be expected. In addition, the TITAN EBIT is designed to provide currents up to 5 A, leading to significantly higher electron densities and collisional heating rates compared to current devices. To remedy this, we plan to insert a cooler Penning trap between the charge breeding and the mass measurement. The proven method of buffer gas cooling is ruled out by the unacceptably large charge transfer; resistive cooling requires a cryogenic environment and is highly q/m specific. We are currently exploring two promising routes towards cooled HCI – sympathetic cooling with electrons and light, cold ions such as protons or He^{2+} . Electron cooling is attractive as electrons are easily produced and self-cool to the temperature of the environment via the emission of synchrotron radiation with a time constant of ≈ 100 ms in a 6 T field. A complication is the possibility of electron-ion recombination. For typical parameters such as an electron temperature of 300 K, an electron density of 10^7 cm $^{-3}$, and $q = 50$, the radiative recombination rate amounts to ≈ 0.1 s $^{-1}$. This would be tolerable; however, higher electron densities, effects of dielectronic recombination and three-body recombination could shorten the lifetime significantly. In addition, the opposite charge of electrons and ions requires the use of a nested trap, where electrons are trapped in one or multiple inverted wells inside a larger ion trap. At ion energies corresponding to the height of the inverted well, the two species start to decouple spatially, halting the cooling process. As an alternative, we are looking into light-ion cooling of HCI. In this scheme, sub-eV protons from an ion source are injected into the trap. Preliminary calculations show (see Fig. 164) that this method can cool HCI at time scales much shorter than 1 s.

The Manitoba group has recently received a CFI grant to build the cooler trap. The set-up will be flexible to explore electron-ion and ion-ion cooling. For effective synchrotron radiation cooling, the magnet needs to produce at least a 6 T field. Efficient capture

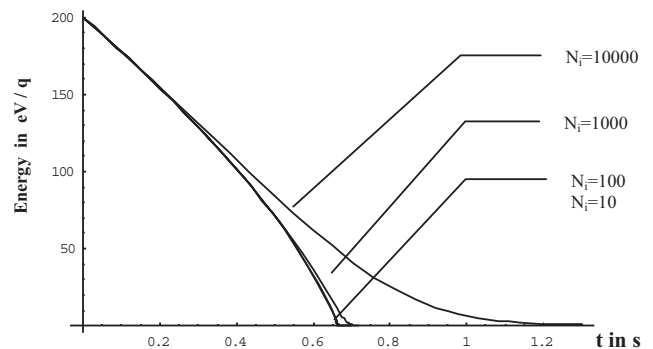


Fig. 164. U^{90+} with an initial energy of 200 eV/ q and different numbers of injected ions. Cooled by 10^7 protons with a density of $n = 10^7$ cm $^{-3}$.

of HCI bunches from the TITAN EBIT requires a long trap (≈ 50 cm). A cylindrical electrode structure with about a dozen separately controllable electrodes can produce various geometries for a nested trap potential. Construction will start in 2005.

TITAN mass measurement Penning trap

Penning trap design Mass measurements in a Penning trap are carried out by determining the cyclotron frequency of the charged particles in the magnetic field of a strong homogeneous magnet. Naturally, special care has to be taken in selecting the magnet, since deviations from the homogeneous field couple directly to the uncertainty in the mass determination. One of the first things for the precision Penning trap project was to establish the specifications of the Penning trap magnet. In the first round of negotiations with magnet manufacturers it was determined that the desired parameters would put the price of the magnet outside the budget goal. Since the highly charged ions used for mass measurements at TITAN would not require as high a field to achieve the desired accuracy, the decision was made to acquire a magnet with magnetic field strength of 4 T. The magnet is scheduled for delivery in December, 2005. Measurements on the highly charged ions require UHV to XHV (10^{-9} – 10^{-12} mbar) vacuum conditions in the vacuum chamber. Additional stringent requirements from the magnetic field homogeneity restrict the choice of materials for the Penning trap vacuum system. The main vacuum chamber that will contain the measurement trap has been designed from pure titanium and is currently being manufactured. To achieve the required vacuum conditions, a vacuum system concept was developed that consists of two pumping stations with the ion getter pumps and NEG pumps. A support structure design for the Penning trap and the ion optics electrodes has been finalized.

Figure 165 shows the rendered overview drawing of the Penning trap, including the magnet, the titanium vacuum chamber, with feedthrough vessel and vacuum

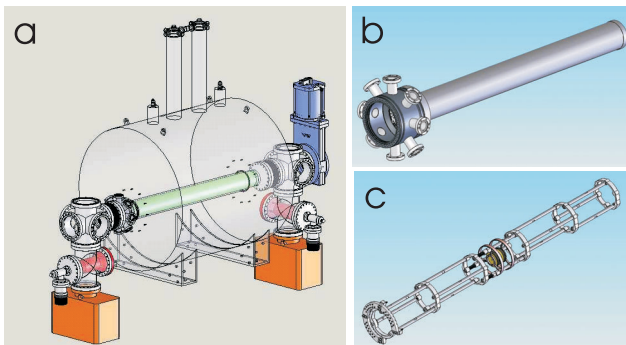


Fig. 165. Mechanical and vacuum design of the Penning trap: a) vacuum system concept; b) main vacuum chamber; c) Penning trap support structure.

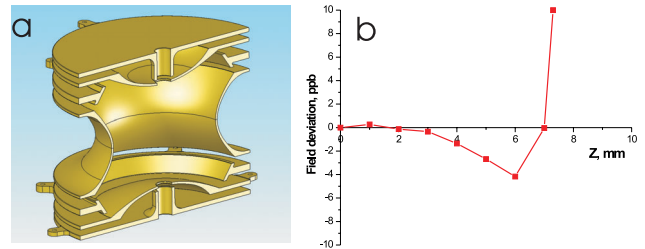


Fig. 166. a) Section view of the electrode design of the precision Penning trap; b) disturbance to the magnetic field homogeneity by the Penning trap electrodes.

pumps (a). Figures 165b and c show details of the vacuum chamber and the Penning trap electrode structure support.

The electric and magnetic field homogeneity in the mass measurement Penning trap is crucial for achieving the target accuracy. Therefore, a series of electrostatic calculations was performed to achieve the best electric field parameters. The material along the trap electrodes was then redistributed by successive optimizations to obtain the best possible magnetic field homogeneity. The magnetic field calculations were incorporated into a CAD design program (SolidWorks). The produced trap geometry and the corresponding magnetic field inhomogeneity are shown in Fig. 166. The calculations indicate that the required field homogeneity of ≈ 10 ppb can be reached or surpassed.

Ion injection and extraction simulations Careful ion transport into the precision Penning trap through the fringe field of the superconducting magnet is very important for the mass measurement. The magnetic field gradient can produce a magnet mirror, reflecting the incoming ions, and leading to substantial losses of the radioactive isotopes. Hence, extensive simulations of the ion injection into the trap to optimize the ion optical parameters and to determine the position of the optical elements were performed. Under the conservative assumption of a beam of charge bred ions with an emittance of 100π mm mrad (beam without cooling), it is impossible to achieve the necessary initial ion distribution in the Penning trap. Similar calculations were carried out with a beam emittance of 10π mm mrad (employing the cooler Penning trap). The results of the simulations for the 100π mm mrad beam are shown in Figs. 167 and 168.

Test ion source and emittance meter For the calibration of the Penning trap during the mass measurements, an off-line ion source is desired. It should supply the reference ions with a mass-to-charge ratio close to that of a highly charged ion, hence probing the same phase space inside the Penning trap. Ions that could be used as reference ions are the hydrogen molecular ions H^{2+} and H^{3+} , and helium ion He^+ with mass to charge

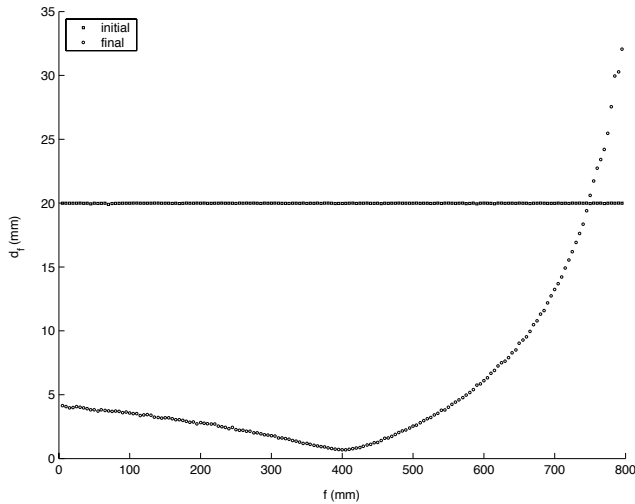


Fig. 167. Ion injection into the precision Penning trap as a function of final focal point before the Penning trap. Graph: size of the injected beam inside the trap (initial size top dots).

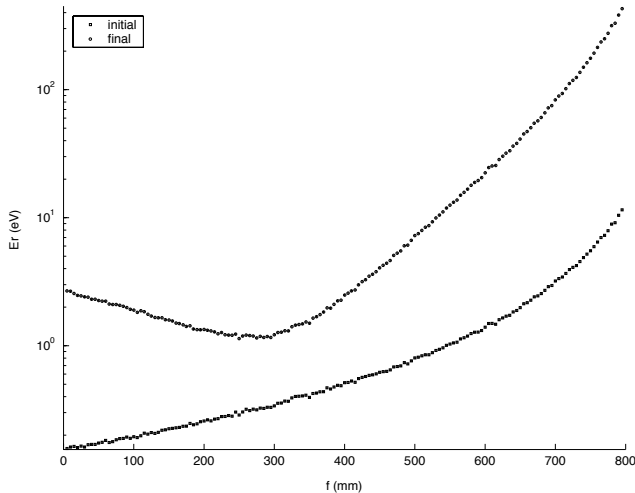


Fig. 168. Cyclotron energy of the ions inside the magnetic field as a function of final focal point (initial energy bottom dots).

ratios of 2, 3, and 4 respectively. A cooler Penning trap based on protons as a coolant would, of course, also require a source of protons. We have pursued a dc plasma discharge ion source based on a commercial design. The initial version of the ion source was quickly put together and successfully tested for Xe ion beam delivery. The design was then modified to conform with UHV requirements of the TITAN transfer beam line and ability to be used as a multi-purpose unit with differential pumping station and built-in Faraday cup diagnostics. The source is now undergoing tests and delivering $3 \mu\text{A}$ of Xe ion beam. It can be used for all four traps at various locations in the TITAN set-up.

A device to measure the emittance of a charged particle beam was designed and built, in order to characterize the ion beam from the test ion source, the



Fig. 169. Photo of the ion source test stand, with Wien-filter and emittance meter.

RFQ cooler and buncher, and the EBIT. It is based on the ISAC emittance meter rig design. The original design was modified in the following way: the materials used in the device are UHV compatible, the design was lightened, and made significantly more compact (it fits into the standard 8 in. conflat 4-way cross). First measurements of the emittance of the Xe beam from the plasma ion source have been carried out. Figure 169 shows a photograph of the test set-up with the ion source (inside the high voltage cage), extraction optics, a Wien-filter and the emittance meter on a linear feedthrough.

Summary and conclusion

The TITAN facility set-up and construction is well under way. Some of the main components, the gas-filled RFQ cooler and buncher, and the charge breeder EBIT are already in the test or operational phase. The progress on the Penning trap project allows a projection to first tests in early 2006, after the mass measurement Penning trap magnet is received in December, 2005. The key infrastructure component, the TITAN platform, is already erected. The move of the RFQ system to the ISAC hall is foreseen for later in 2005. First laser spectroscopy experiments are possible at this stage. The advantage of having an off-line ion source built into the system will become evident during the set-up and commissioning phase of the individual components and the test of the transfer of beam from one subsystem to the next. This is planned for the coming year.

Linear Collider TPC Development

(D. Karlen, Victoria/TRIUMF)

The Victoria time projection chamber (TPC) prototype, designed for use in magnetic fields at TRIUMF and DESY, had a successful data-taking run at

DESY in the summer. The prototype was operated with GEMs and micromegas gas amplification and its performance was investigated with cosmic and laser tracks. This work was performed in order to demonstrate the capabilities of such a device as a large volume gaseous central tracking system for a linear collider experiment. As a result of the success of this program, the long baseline neutrino experiment, T2K, now includes these types of devices in the design of the near detector tracker, and the Victoria/TRIUMF groups are leading the T2K TPC project.

Introduction

Given the precise three dimensional information it provides, a large volume TPC is a leading candidate for the central tracker for an experiment at the International Linear Collider. Starting in 2003, the Victoria prototype TPC has demonstrated the performance of TPCs with micropattern gas detectors operated in magnetic fields. The TPC is of modest scale, with an active drift volume of about $300 \text{ mm} \times 85 \text{ mm} \times 64 \text{ mm}$, read out with 256 channels of modified STAR prototype electronics. From data taken in 2003, it was shown that up to the full drift distance, 30 cm, the prototype had a space point resolution of approximately $100 \mu\text{m}$ for a 7 mm sample in P5 gas at magnetic fields above about 1.5 T.

This year, the TPC was modified to allow UV laser pulses to enter the drift volume, which would produce a straight line of ionization, in a repeatable fashion. A laser delivery system was designed and built at the University of Victoria in order to control the beams sent to the TPC during operation in the DESY magnet. For personnel safety reasons, the system was designed for remote control. Pictures of the laser delivery system are shown in Fig. 170. The YAG laser, provided by DESY, produced a 266 nm wavelength beam.

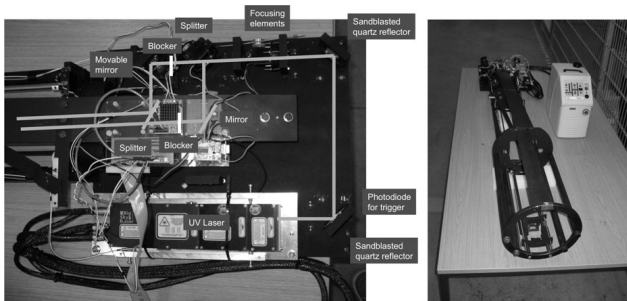


Fig. 170. Photographs of the laser delivery system designed for TPC operation in the DESY magnet. The left image shows the optical components, with movable mirrors and blockers to produce one or two beams of variable separation. The right image shows the TPC holder that includes movable mirrors to direct the laser beams through the TPC at different drift distances.

Results from 2004 DESY run

The prototype was operated with laser and cosmic triggers in P5 (Ar:CH₄ 95:10) and the so-called TDR (Ar:CH₄:CO₂ 93:5:2) gas mixtures. The laser intensity was adjusted to give mean ionization density similar to that of minimum ionizing particles. Primarily it was operated using a double GEM; only a short test using micromegas with a resistive anode was performed.

The laser track position in the TPC was very stable, typically drifting less than $10 \mu\text{m}$ over a period of 24 hours. The laser was found to be very useful to quickly measure the drift velocity, and thereby monitor the equilibrium time after gas changes or after periods of opening the TPC.

Since the laser tracks were stable in location from pulse to pulse, they provide an excellent control sample to demonstrate the techniques used to estimate the tracking resolution for cosmic ray tracks. By using 8 rows of $2 \text{ mm} \times 7 \text{ mm}$ pads, the standard deviation of the horizontal track parameters of the track fits to the laser pulses was typically $28 \mu\text{m}$, corresponding to a single row resolution of $79 \mu\text{m}$. The technique used for cosmic ray tracks (comparing single row fits with all row fits) gives $77 \mu\text{m}$, in good agreement.

By bringing two parallel laser beams close together at the same drift distance, the two track resolution capability of the device was investigated. The two remote control blockers allowed one or the other laser beam to pass through the TPC, or both. Single fits of the individual tracks were compared to a simultaneous fit to the two tracks. For 2 mm wide pads, the resolution of the two track fits was found to only degrade significantly for track separations less than 2 mm, as shown in Fig. 171.

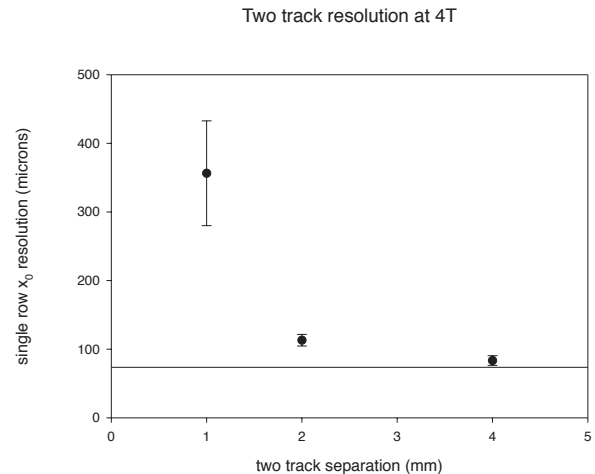


Fig. 171. The two track resolution capability of the TPC is shown for 2 mm wide pads. The horizontal line shows the single pad row resolution for single tracks. The points show the single pad row resolution for two parallel tracks at different separation distances. This represents the first measurement of this property for GEM-TPCs.

To better understand the results from cosmic ray samples, a full GEANT3 simulation of the cosmic events was developed. The energy loss of charged particles as they pass through the gas is simulated by GEANT, and the values are passed to the jtpc TPC simulation package. The simulated events are analyzed with the same program as the real data. The resolution measured in the simulated samples is in good agreement with the real data. The momentum distribution of the muons as estimated by the radius of curvature is in good agreement.

The ionization energy loss, dE/dx , was also examined, and the relativistic rise with momentum is clearly visible. The dE/dx resolution was measured to be 17% for the 85 mm track length, consistent with the expectation from an extrapolation of traditional large gaseous tracking systems.

A set of narrower readout pads, 1.2 mm pitch instead of 2 mm pitch, were also tested. This was done because the defocusing of the GEMs for P5 gas at high fields provides less than optimal charge sharing for the larger pads. For P10, the defocusing is larger, but the use of this gas was not allowed in the DESY set-up.

An initial study showed biases in the data, as if pad rows were offset from their nominal locations by various amounts of order 100 μm . The original gerber file for the PCB layout was reviewed, and it was found that the pads were, in fact, not correctly placed. After correcting for this in the analysis, the biases were found to be less than 5 μm .

The single row resolution for the narrow pad cosmic data is shown in Fig. 172, and compared to the result from the GEANT-jtpc simulation. Single row resolution of approximately 60–80 μm is found. It appears that systematic effects, not included in the simulation, are not influencing the resolution at this level.

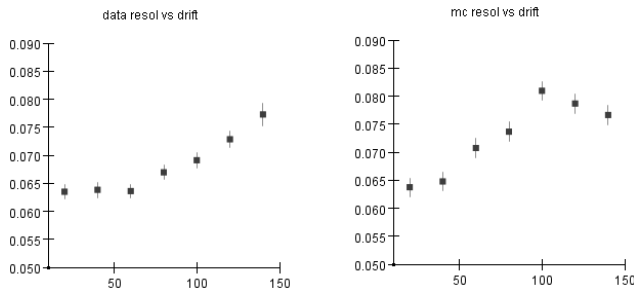


Fig. 172. The single row resolution (mm) of cosmic tracks is shown for 1.2 mm wide pads for 7 mm samples in P5 gas as a function of drift distance (time bins – range from 0 to 300 mm). The figure on the left shows the result from data, and the figure on the right is from the full simulation.

Future work

A full analysis of these data is under way for publication. The results and experience gained with the Victoria prototype will be very helpful in designing a large Linear Collider prototype TPC, in collaboration with physicists from Europe and the US, and in designing the T2K TPC modules over the coming year.

University of Victoria LC TPC group in 2004: Dean Karlen, Mark Lenkowski, Chris Nell, Paul Pofenberger, Gabe Rosenbaum.

TPC R&D for the International Linear Collider (M. Dixit, Carleton/TRIUMF)

Introduction

The time projection chamber (TPC) for the future international linear collider will need to measure about 200 track points with a resolution of better than 100 μm . The resolution goal, close to the fundamental limit from ionization electron statistics and transverse diffusion in gas, is nearly two times better than has been achieved by conventional wire/pad TPCs. A TPC with a micro pattern gas detector (MPGD) readout could, in principle, reach the target resolution. However, it may require sub-millimetre width pads resulting in a large increase in the number of electronics channels and detector cost and complexity over conventional TPCs.

In the recent past, the R&D at Carleton has focused on exploring new ideas to improve TPC resolution (see Fig. 173). We have recently developed a new readout concept based on the phenomenon of charge dispersion in MPGDs with a resistive anode. With charge dispersion, wide pads similar in width to the ones used with wire/pad TPCs can be used without sacrificing resolution.

We have proven the concept of charge dispersion for a collimated X-ray source earlier. We have recently

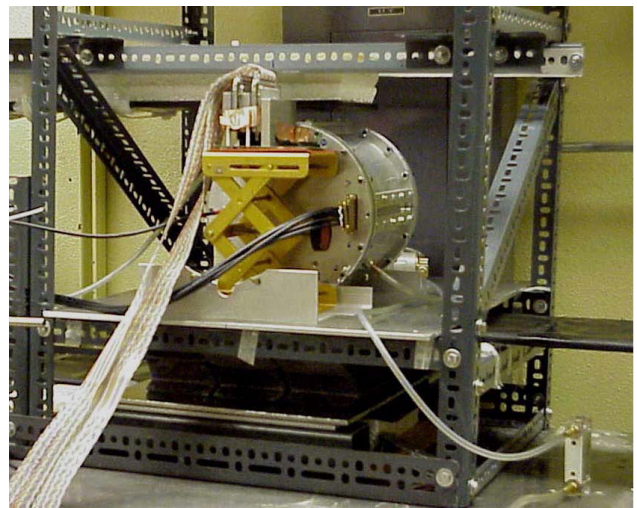


Fig. 173. Cosmic ray GEM-TPC set-up at Carleton.

measured the spatial resolution of a small prototype TPC using the charge dispersion readout as proof of principle. In cosmic ray tests with no magnetic field, we have measured the resolution for a number of gases with different diffusion. The dependence of measured resolution on drift distance was consistent with diffusion in all cases. This is the first time a TPC has achieved a spatial resolution close to the fundamental limit from diffusion. The resistive anode GEM in the TPC endcap was recently replaced with a resistive anode micromegas. Preliminary results from the micromegas TPC with the charge dispersion readout are quite encouraging. These activities are described below.

GEM-TPC resolution from charge dispersion

A small cosmic ray test TPC used earlier with a conventional direct charge GEM readout was modified for charge dispersion studies. The GEM endcap was altered to accommodate a resistive anode. Signals on 60 pads, $2\text{ mm} \times 6\text{ mm}$ each, were read out using Aleph TPC wire preamplifiers and digitized by 200 MHz FADCs.

Figure 174 shows TPC pulses for two pads. Both the pulse rise time and the decay time depend on the position of the charge with respect to the pad. The charge collecting pad has a fast signal. The signal on the adjacent pad has a slower rise and decay time. Figure 175 shows track signals for all the pads for a cosmic ray track.

Since the risetime and the pulse height both depend on the charge position, there are many possible ways to define and use the pad response function (PRF). For the present analysis, we have used only the pulse height information. We used part of the cosmic ray data to determine the PRFs (see Fig. 176). The remaining data were used for resolution studies.

The charge dispersion signals are affected by non-uniformities in the anode resistivity and the capacitance per unit area. Positions measured from PRF need

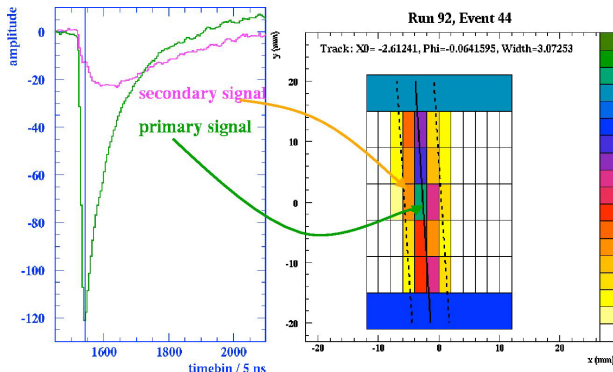


Fig. 174. Charge dispersion signal on a charge collecting pad and its neighbour for a cosmic ray track in the TPC. Ar:CO₂/90:10.

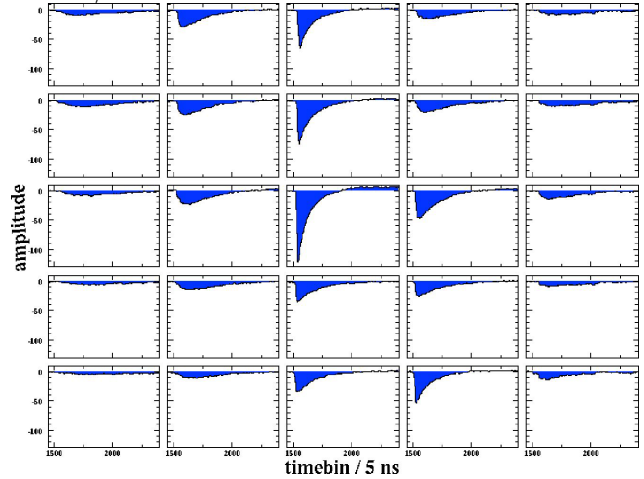


Fig. 175. FADC charge dispersion signals on $2 \times 6\text{ mm}^2$ readout pads for a cosmic ray track. The TPC fill gas was Ar:CO₂/90:10.

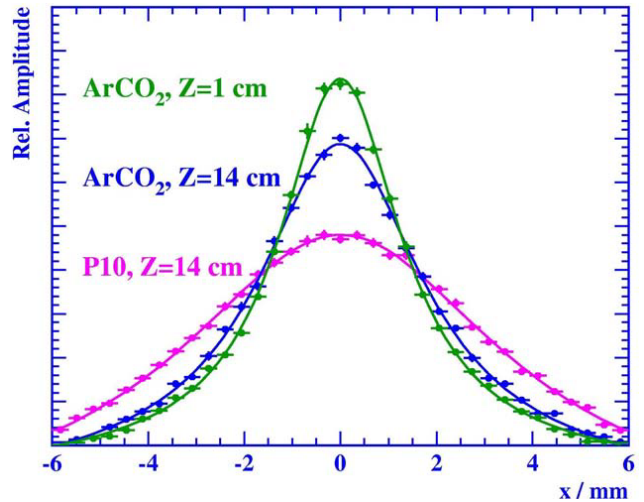


Fig. 176. Example pad response functions (PRF). The PRFs were determined from a subset of the cosmic ray data set.

to be corrected for local RC distortions. The bias corrections were also determined from the calibration data set.

Figure 177 shows the resolution measurements for Ar:CO₂ with and without charge dispersion. P10 results are shown in Fig. 178. The resolution from charge dispersion is significantly better than for the direct charge readout for both gases. Apart from a constant term, the dependence of resolution on drift distance is consistent with diffusion.

A detailed simulation has been done to understand the characteristics of charge dispersion signals. Initial ionization clustering, electron drift, diffusion effects, the MPGD gain, the intrinsic detector pulse-shape and electronics effects have been included. All aspects of

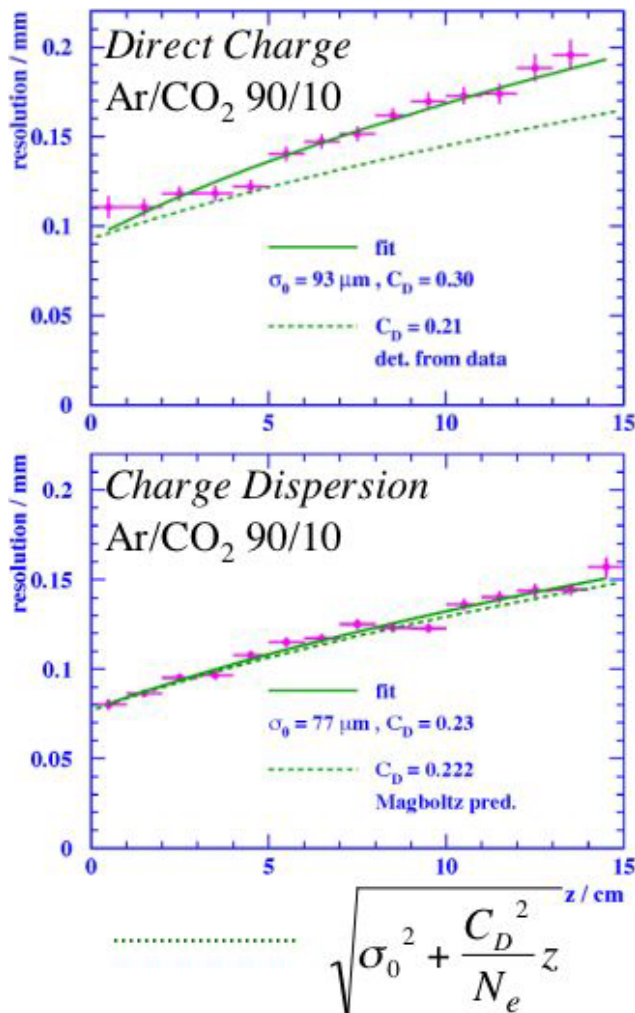


Fig. 177. Charge dispersion improves TPC resolution over that from direct charge for low diffusion gases like Ar:CO₂ with limited charge sharing between pads.

charge dispersion phenomena can be simulated including pulse shapes (see Fig. 179) and the PRF. The simulation is in good agreement with the experiment and can be used to optimize the charge dispersion readout for the TPC.

In summary, the charge dispersion on a resistive anode improves the GEM-TPC resolution significantly over that achievable with conventional direct charge readout. Bias errors due to RC inhomogeneities can be corrected. With no magnetic field, the measured dependence of resolution on drift distance is consistent with diffusion and electron statistics. Charge dispersion resolution studies with a micromegas TPC are in progress. Preliminary results are quite encouraging and are similar to those with the GEM readout.

Future plans

TPC resolution studies for a micromegas TPC with a resistive anode readout will be completed. Beam tests in a magnet are planned for the summer of 2005 in a

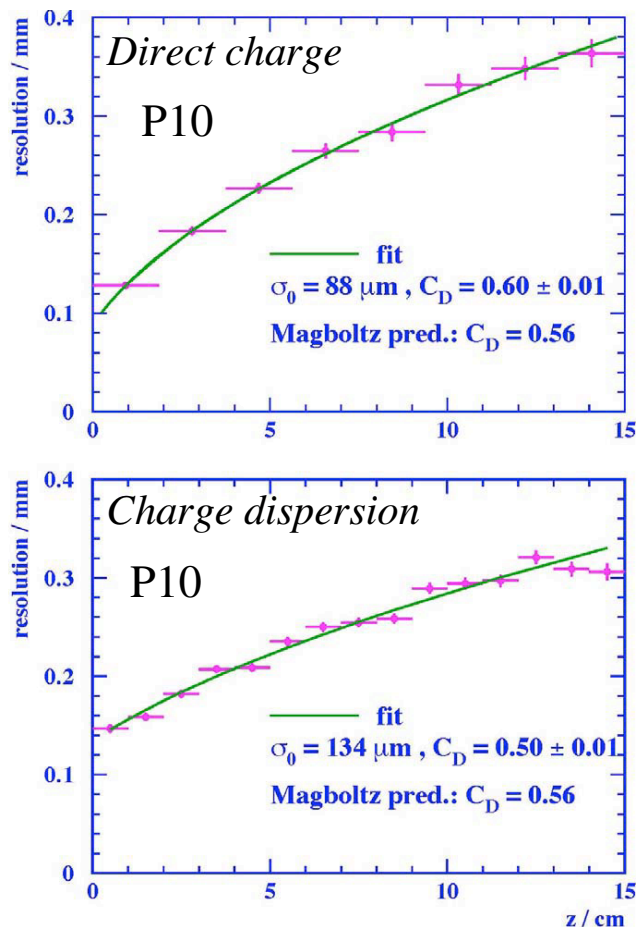


Fig. 178. Charge dispersion improves TPC resolution even if the track charge is spread over several pads due to transverse diffusion, as is the case for P10.

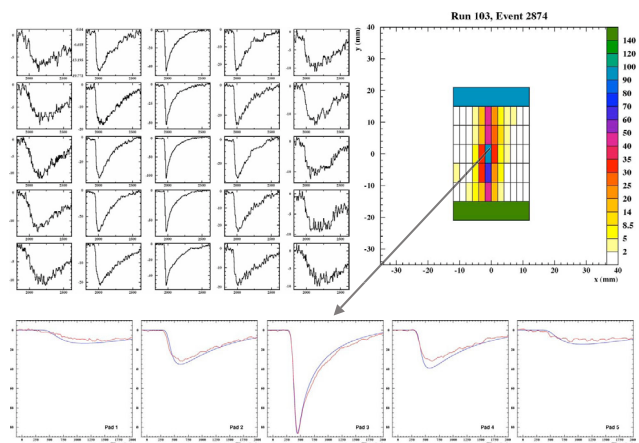


Fig. 179. Simulated and experimental cosmic ray charge dispersion signals on a row of cosmic ray TPC readout pads.

KEK test beam. With the announcement of the choice of superconducting rf structures for the ILC last summer, the TPC R&D effort worldwide is gaining momentum. The time scale is driven by the expectation that the ILC will be operational by 2015. A major ILC-TPC

goal is to choose the readout technology and build and test a large prototype by 2007. If a TPC resolution of less than $100\ \mu\text{m}$ for all drift distances (diffusion limit in a magnet) can be reached, it will have a major impact on the ILC detector design. We expect to

contribute significantly to this effort.

IILC TPC R&D group in Canada: A. Bellerive, K. Boudjemline, R. Carnegie, H. Mes, J. Miyamoto, K. Sachs (Carleton), M. Dixit (Carleton/TRIUMF), J.-P. Martin (Montreal), and D. Karlen (Victoria).

CYCLOTRON OPERATIONS DIVISION

INTRODUCTION

During 2004 the cyclotron was available for 92% of the hours scheduled, which is 4% better than last year. The total number of available hours was 5565, exceeding the 5176 hours available in 2003. The total beam charge delivered was 687 mAh, up 6% from last year, of which 437 mAh were delivered to BL1A for meson production and 108 mAh were delivered to BL2A for RIB production. Beam was delivered for the first time down BL2A3 to the east target station (ITE) of ISAC. Approximately 142 mAh were delivered at 85 MeV to rubidium targets in the solid target facility (STF) in beam line 2C4 for the production of radiopharmaceutical generators.

The cyclotron beam development shifts concentrated on reproducing, understanding and improving the $\sim 300 \mu\text{A}$ tune being developed to satisfy the users' requirements for beam in 2007 when ISAC is scheduled to begin operating at $100 \mu\text{A}$. After several improvements in diagnostics and alignment of the centre region correction plates, the best 2004 high current result achieved was a stable beam with an equivalent current of $320 \mu\text{A}$ at 50% duty cycle with 64% cyclotron transmission and reasonable spills.

The annual downtime of 407 hours was only slightly higher than average, of which the inflector problems cost 138 hours of the total. Most impressive was the lowest ever rf downtime of 77 hours, which is about 1/3 of the long-term average. Site power and power supply problems were the next largest contributors to downtime, followed by beam trips which became a nuisance in 2A operation.

During the winter shutdown, the major beam line activities were the repair of four major vacuum leaks (M20Q1, upstream of Q14, 1AT2-M8 blank-off plate, O-ring at M20B2) in the T2 area of BL1A. Last year's crumbling block replacement program continued this year. However, because of the extent and complexity of the above jobs in mostly high radiation fields, we had to postpone the removal of the M11 septum and the repair of the small M15 vacuum leak. There were many other meson hall activities, which are covered in detail in the Beam Production section. The major vault and tank activities included jack-station maintenance, diagnostic maintenance activities, periscope improvements, installation of new inflector cables and connectors, and chore pad replacements in Q3 and Q4. Removing the STF in BL2C4 to repair limit switches and to correct a skew misalignment, that had caused problems for years, proved to be a very difficult job with mechanical obstacles and persistent water leaks along the way. A new and improved STF is being de-

signed to replace the present one. The new STF will be a water vessel with no water joints to be made up in the vault. The target insertion will be done on rails located in the vessel and the insertion mechanism will be removable to the hot cell for MRO.

In the fall mini shutdown the vault activities included both X1 and X2A foils being replenished, vault BL monitors being gassed, 2C4 protect monitor being repaired, upper correction plate external cabling being repaired, and many other MRO jobs. In BL1A there was the repair of vacuum leaks at 1AVA8 and 1AQ14, a water leak at 1AQ15 and many other MRO jobs, which are covered in more detail in the support group sections. As well as vault and beam line activities, the support groups were also very busy in their own respective areas.

The efforts of the RF group are reflected in the low downtime of 77 hours compared to 234 hours last year. The major activities contributing to this reliability are the upgrade of the HVPS (which includes new thyrite varistor stacks, new water connections to the water-cooled resistors and a newly designed crowbar driver protection board), a new final combiner, major upgrades to the 9 in. and 11 in. transmission line system, and general upgrades in the rf power amplifiers.

In the Probes and Diagnostics group great progress was made on the HE probe refurbishment, including the completion of the probe detailed design and fabrication and testing of the major sub-assemblies. The group was also involved in ISAC work which is covered in that section.

The newly formed Diagnostics Electronics group had a very busy year. The major priority was given to fast signal acquisition from internal probes in the cyclotron. A real step forward in beam measurements in the time domain can be expected with the implementation of broadband signal acquisition and analysis. Improvements were made to the electronics processing the signal from the beam line capacitive probe to make the TOF measurements on the cyclotron more automatic.

The vacuum/cryogenics system operated reliably over the year. Upgrades were made to both B-20 cryogenerators to improve their reliability. Improvements were made to the B-20 cooling water system to improve turn around time during cryogenerator regeneration. Both cyclotron and beam line vacuum systems were efficiently maintained during the year.

In ISIS the CUSP ion source and injection line continued to operate well for the past year. A major effort was unexpectedly required to realign the I1 motor generator set that provides power to the ion source termi-

nal. Variable aperture slits were successfully commissioned and now provide improved beam quality to the cyclotron. Some effort went into restoring the CRM ion source test stand to allow testing of CUSP ion sources by ISIS, Nordion and Dehnel Consulting, and to allow us to study our ion source characteristics.

The Controls group carried out many new developments on the CCS facility, secondary beam lines and other systems, which are too numerous to mention here. The low loss of scheduled beam time attributed to control systems is noteworthy and is a result of the new developments and maintenance efficiently carried out by the Controls group.

Operational Services, which includes Remote Handling, Magnet Power Supplies, Electrical Services and Mechanical Services, continues to play a vital role in the reliable operation of the cyclotron. Their services extend to the whole TRIUMF site and are appreciated site wide.

As part of the ongoing work for safety-critical monitoring for prompt radiation hazards, the reliable termination of beam production in response to beam spill, neutron, access, and emergency safety trip conditions was implemented during the 2004 shutdown. Each secondary channel area safety unit test procedure was written and approved. The operation of nine safety-critical pairs of radiation detectors was checked out on thirty-five maintenance days with no failures reported. The ISAC B1 level electrical room was made an interlock exclusion area and now must be locked up and unoccupied when beam line 2A is on.

BEAM PRODUCTION

Beam delivery for the year was reasonably successful with a total charge production of 687mAh delivered to the high current proton lines (1A, 2A and 2C4), up 6% from last year although still 5% lower than the 2002 record of 723mAh. Performance of the cyclotron was excellent for the most part (barring an emergency inflector repair in August) with a typical operating transmission of 64% and a measured tank beam spill around 1% of the circulating current. These parameters were achieved partly with the help of the rf booster that was sometimes unavailable due to developments in its control system, partly due to a more reproducible ISIS beam (with newly installed slits cutting back a high output source as needed), and partly because of the continuing tuning efforts of the operators. Thirteen weeks of shutdown left 6058 scheduled operational hours (in this 53 week year) of which 5565 were achieved for an availability of 92%, 4% better than last year. These totals, including 316 hours used for development and tuning, are shown in Fig. 180. Note that the 2 week periods preceding shutdowns were dedicated to lower intensity operation, usually involving beam delivery to ISAC with the proton irradiation facility (PIF, using BL1B and BL2C1) running in parallel. BL2C1 was also used at 74 MeV for ocular melanoma treatments for 6 patients during 4 proton therapy (PT) sessions. These PT sessions, with the high intensity source on-line, required the use of the ISIS pepperpot to limit the injected beam current during patient treatment times. Again this year there was no BL4 operation and no polarized source operation.

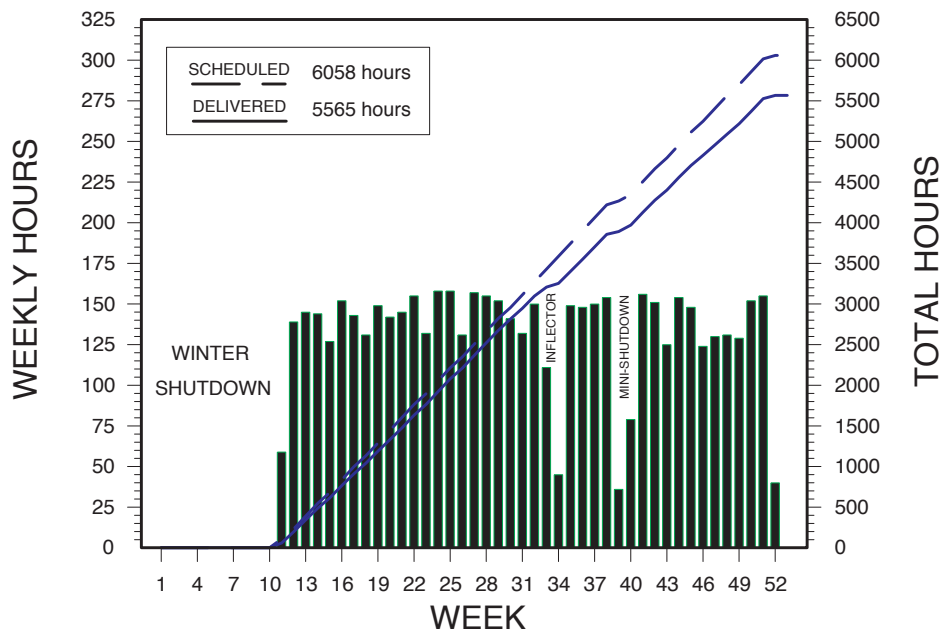


Fig. 180. Operational hours for 2004.

As Fig. 181 shows, the total beam charge delivered to meson hall experiments along BL1A was 437 mAh or 88% of the scheduled amount, down marginally from last year because of vacuum and target considerations described below. In addition to the BL1A charge, there were a significant 142 mAh delivered at 85 MeV to rubidium targets in the solid target facility (STF) in beam line 2C4 for the production of radiopharmaceutical generators and another 108 mAh, 30% more than last year's record, delivered to the two target stations on BL2A for the production of radioactive ion beams (RIB) for experiments in ISAC. A total extracted current exceeding $220 \mu\text{A}$ was sometimes shared by the three proton lines, although $200 \mu\text{A}$ or less was more normal for extended production periods. This was par-

ticularly true for the month when graphite targets were used at 1AT1 for the TWIST experiment, limiting BL1A currents to $100 \mu\text{A}$.

The annual downtime of 407 hours (Fig. 182) was only slightly higher than average even though inflector problems cost 138 hours or 34% of the total. Most impressive was the lowest ever rf downtime, 77 hours or less than 2 hours per operational week, about one-third of the long term average. Site power and power supply problems followed at 9% and 8% respectively while beam trips, particularly a nuisance in 2A operation, came in at a costly 5%. The operational record and beam to experiments for the year are given in Tables XXVI and XXVII.

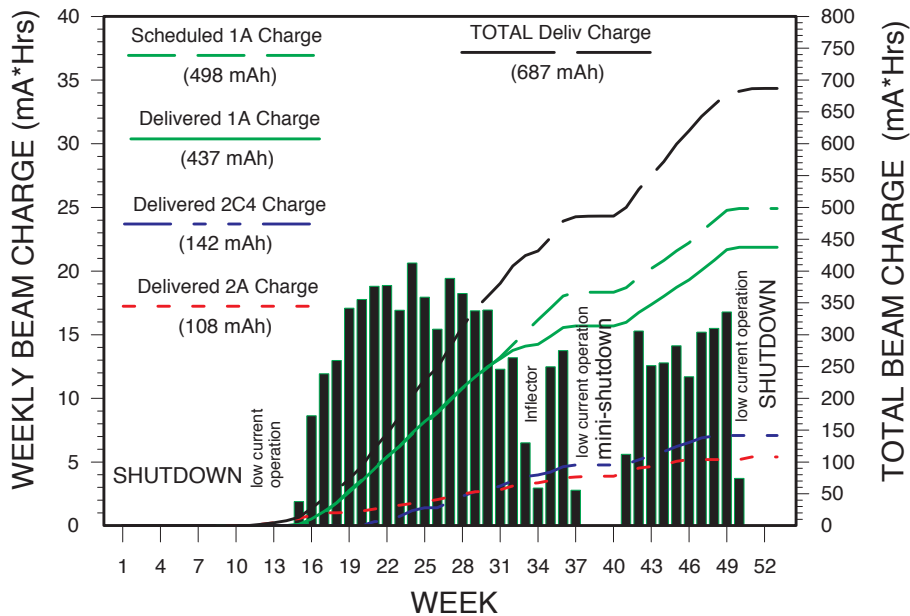


Fig. 181. Beam delivery for 2004.

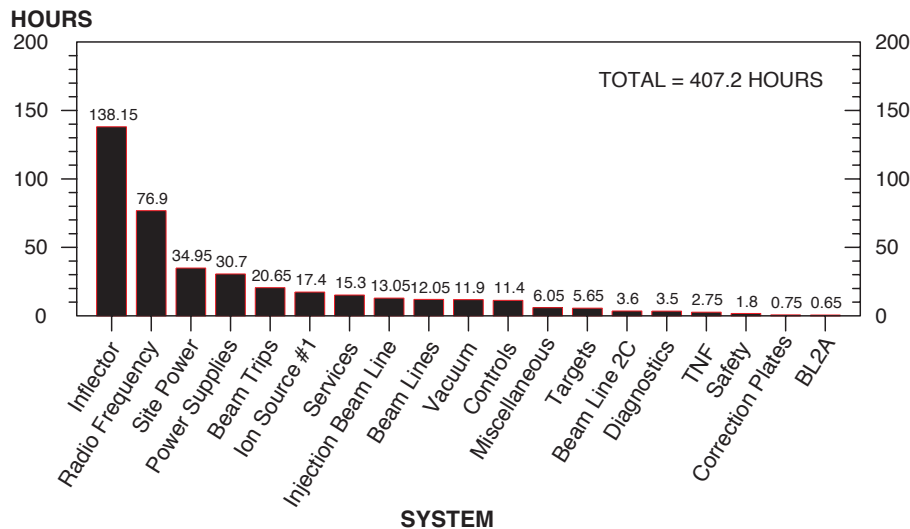


Fig. 182. Cyclotron downtime for 2004.

Table XXVI. Operational record for 2004.*

	Scheduled hours	Actual hours
<u>Cyclotron off:</u>		
Maintenance	528.0	535.25
Startup	178.0	178.30
Shutdown	2,140.0	2,155.50
Other	0.0	0.00
Cyclotron downtime	0.0	407.20
Overhead	0.0	62.75
Totals	2,846.0	3,339.00
<u>Cyclotron on:</u>		
Development	202.5	173.15
Cyclotron tuning	525.0	143.30
Beam to experiments	5,330.5	5,248.55
Totals	6,058.0	5,565.00
Actual / Scheduled = 5,565.0 / 6,058.0 = 91.9% availability		
<u>Beam to experiments:</u>		
1A Production	4,155.0	3,987.65
1A Development/tuning	10.0	35.20
1A Down/open/no user	807.5	854.15
1B Production	335.0	69.45
1B Development/tuning	0.0	3.50
1B Down/open/no user	23.0	298.60
Total 1A+1B production	4,490.0	4,057.10
2A Production	5,029.5	3,577.75
2A Development/tuning	0.0	18.25
2A Down/open/no user	301.0	1,652.55
2C1 Production/tests	1,431.5	192.95
2C1 Development/tuning	0.0	8.90
2C1 Down/open/no user	405.0	1,463.55
2C4 Production/tests	3,378.0	2,523.65
2C4 Development/tuning	0.0	18.00
2C4 Down/open/no user	116.0	1,041.50
1A Beam charge (μ Ah)	498,320.0	437,178.00
2A Beam charge (μ Ah)	148,903.0	107,875.50
2C4 Beam charge (μ Ah)	155,750.0	141,530.00

* There was no BL4 production this year and the polarized source was not used.

Table XXVII. Beam to experiments for 2004.

Experiment*	Channel	Schedule #	Scheduled		Delivered	
			Hours	$\mu\text{A h}$	Hours	$\mu\text{A h}$
614	M13	105	2,542	330,460	2,451.50	275,762
614	M13	106	1,108	124,570	1,048.60	117,473
(614)	M13	105	404	35,220	403.25	33,550
(614)	M13	106	101	7,070	80.30	5,612
782	M15	105	150	19,500	156.75	19,291
842	M9B	105	150	19,500	150.05	19,716
847	M15	105	273	35,490	276.60	35,300
877	M9B	105	123	15,990	139.65	17,113
881	M15	105	81	10,530	81.15	9,637
881	M15	106	79	5,530	58.30	4,080
891	M15	105	127	16,510	124.00	12,565
891	M20B	105	196	25,480	208.25	22,744
912	M15	106	127	16,390	110.60	13,718
917	M20B	105	427	55,510	446.85	51,536
917	M20B	106	273	26,730	239.25	23,729
932	M9B	105	150	19,500	169.90	20,095
938	M15	105	273	35,490	265.85	29,481
938	M15	106	127	16,510	127.45	16,616
939	M20B	105	254	33,020	275.80	34,569
939	M20B	106	277	31,390	238.70	26,373
943	M9B	105	273	35,490	273.45	30,649
944	M20B	106	151	15,100	151.50	14,839
945	M20B	105	150	19,500	147.30	17,971
945	M9B	106	79	5,530	73.45	5,495
945	M20B	106	127	16,510	127.45	16,616
949	M9B	105	300	39,000	278.85	24,210
949	M9B	106	381	49,410	368.55	47,875
950	M15	105	150	19,500	152.65	11,842
951	M20B	105	75	9,750	79.05	7,893
951	M15	106	69	8,970	69.30	8,966
953	M15	105	127	16,510	121.65	15,722
953	M15	106	127	12,700	120.25	11,970
958	M15	105	127	16,510	142.05	18,250
959	M20B	105	150	19,500	150.05	19,716
960	M20B	105	150	19,500	86.30	5,697
960	M15	106	127	12,700	125.25	12,255
962	M20B	105	150	19,500	155.80	20,191
968	M9B	105	438	56,940	371.20	31,995
968	M9B	106	277	27,700	249.35	24,672
969	M15	105	150	19,500	146.90	15,065
974	M15	105	277	36,010	198.50	20,750
975	M15	105	150	19,500	142.30	12,008
976	M15	105	46	5,980	54.95	6,125
976	M15	106	58	7,540	61.20	8,575
977	M20B	105	150	19,500	126.20	12,368
978	M20B	105	63	8,190	63.55	6,397
979	M20B	105	127	16,510	121.65	15,722
981	M20B	106	127	16,510	130.50	17,541
997	M20B	105	150	19,500	152.65	11,842
998	M15	105	127	16,510	143.20	17,180

Table XXVII (cont'd.)

Experiment*	Channel	Schedule #	Scheduled		Delivered	
			Hours	$\mu\text{A h}$	Hours	$\mu\text{A h}$
999	M20B	105	123	15,990	139.65	17,113
1000	M15	105	300	39,000	303.10	38,162
1000	M20B	106	127	12,700	121.25	12,017
1000	M15	106	127	16,510	120.20	14,961
1001	M15	105	138	17,940	142.60	14,290
1002	M15	105	277	36,010	227.65	23,329
1003	M20B	105	127	16,510	142.05	18,250
1004	M20B	105	123	15,990	126.55	15,584
1005	M20B	105	150	19,500	142.30	12,008
1006	M20B	105	150	19,500	64.05	3,813
1011	M15	106	151	15,100	151.50	14,839
1012	M9B	106	127	16,510	120.20	14,961
1013	M15	106	67	4,690	60.75	4,688
1015	M15	106	150	15,000	128.10	12,655
1016	M20B	106	127	12,700	120.25	11,970
M9 test	M9B	105	173	5,190	174.85	10,315
Setup9	M9B	106	151	15,100	151.50	14,839
TBA15	M15	105	173	5,190	174.85	10,315
TBA20	M20B	105	231	12,730	226.70	15,898
TBA9	M9B	105	1,339	174,070	1,296.80	55,219
TBA9	M9B	106	194	17,390	165.85	15,243

* See Appendix D for experiment title and spokesman.

Winter Shutdown

Shutdown activities got under way at the beginning of the year, particularly in BL1A which was scheduled to be off until just before the Easter weekend. Work there was again long and involved, starting with the removal of 60 to 70 large shielding blocks to outside storage. One of the main 1A jobs was the repair of T2 area vacuum leaks, the main one at M20Q1 and another, trickier one discovered just upstream of Q14 that was sensitive to the loading of shielding blocks above it and which proved very challenging to fix because of alignment issues. A third leak was repaired by replacing the 1AT2-M8 blank-off plate and a fourth leak involved replacing a 20-year-old rubber O-ring at M20B2. After these were repaired the best vacuum that area has seen in years was achieved. While the area was accessible, a remote video survey of the front end of M20 was made in preparation for the future installation of new rad-hard components there. At M9Q1 it was discovered that water from a weeping solder joint was getting into hairline cracks on an insulator just below and causing a ground fault. This was fixed by epoxying the joint and insulator, but a residual ground fault was attributed to track marks left on the insulator.

To help reduce dose to the technical experts, volunteers were used to continue last year's crumbling block replacement program, this time starting with the removal of the 1AM10 smokestack monitor to access and replace six blocks in that area. The extent and complexity of the above jobs, most of them in high radiation fields, made it impossible to complete all the scheduled shutdown work so the removal of the M11 septum and the repair of a small M15 vacuum leak were postponed for yet another year. Still, there were numerous other meson hall activities, among them being the replacement of the M20VA5 valve, 1AT1 and 1AT2 water package upgrades and servicing, 1AT2 beam blocker servicing (both M9 and M20), the addition of a gate valve in M13 to remove the vacuum valve functionality of the existing beam blocker there, hose replacements and water leak repairs in M9, M20 and M13, replacement of the TNF resin can, routine filter changes, and so forth.

As in the previous year, the cyclotron was scheduled to start up a month earlier than BL1A in order to deliver beam to PT, PIF and ISAC while shutdown work in the meson hall continued. In the vault some jack-station maintenance took place before the lid was raised for 5 weeks of cyclotron repairs in resid-

ual fields similar to those of the previous year. Diagnostics activities there consisted of the usual probe maintenance as well as probe position measurements. Also some considerable effort was put into improving the periscopes by replacing radiation damaged pentaprisms and wiring. New cables and connectors were installed for the inflector and some maintenance of the inflector was done. RF inspections, chore pad replacement (Q3 and Q4 upper resonators) and thermocouple work went as planned. However resonator adjustments, transmission line improvements and correction plate work (where some subsequent shorts in the tank had to be located and repaired) were more involved than originally considered and pushed the schedule a little.

Remote handling work in the vault consisted of jack-station maintenance before the lid went up and alignment checks after the lid was down. In between were the usual remote installation and removal of shadow shields and copper beam blockers as well as assistance with probes work. Operations group activities consisted mostly of support work for rf resonator and correction plate work as well as overhead for lid cycling and tank inspections.

The main objectives of BL2C4 shutdown work were to remove the STF for limit switch repairs and to correct the misalignment that has caused tuning problems over the last couple of years. The latter proved to be a very difficult exercise with mechanical obstacles each step of the way including a persistent water leak at the seal between the STF target housing and the water column above it. Finally a mock-up in the hot cell and a different style clamp helped get the job done albeit a few weeks into the beam schedule. A new and improved STF is being designed to replace the present one in a couple of years. BL2C4 work ultimately contributed 50 mSv to the total shutdown dose of approximately 190 mSv distributed among 105 workers.

Beam Schedule 105

Startup was relatively straightforward although there was a problem with some upper correction plates that turned out to be environmentally damaged cabling. Quick repairs were made by cutting off the last metre and installing new connectors while planning for a more thorough job for the next shutdown. Beam was first injected and extracted in the middle of March with a notable change in the safety system logic that has reduced the number of beam-tripped devices to three (the ISIS vertical bends, beamstop 165 and the fast target) with the rf now notably removed from the list.

Availability of the cyclotron for this operating period was quite good at 91% of the 4267 scheduled hours and would have been even better had there not been an emergency lid up in mid-August to repair the inflector.

An insulator had become dirty enough to prevent stable high voltage operation in a failure similar to that of the previous spring. Downtime totalled 299 hours, nearly half of which (137 hours) was for the inflector while rf was a distant second at less than 2 hours per week. The cyclotron tune was quite good with a typical transmission of 64% and measured spills around $2 \mu\text{A}$ for total extracted currents of up to $220 \mu\text{A}$ to the three active proton lines. Apart from these beam lines, which are discussed below, there was also beam delivery to 2C1 for both PT (three sessions, five patients) and PIF for two weeks at the end of the beam production schedule as part of lower current operation (placed to provide some cooldown prior to the fall shutdown). BL2C1 currents were less than 7 nA. BL1B scheduled at the same time had user problems and therefore had little use (at currents of less than 1 nA).

There was an unresolved problem in trying to tune 2C1 energies above 105 MeV that appears to have coincided with the emergency inflector repair in August. But, as there were no other pressing reasons for raising the lid and incurring the associated dose during the fall shutdown, it was decided, after confirming that lower energy tunes would suffice for this year, to wait until the spring, 2005 shutdown to resolve this issue.

BL1A ran for 2855 hours or 97% of its scheduled time, receiving 314 mAh or 86% of its scheduled charge. The high hourly availability was helped along by running unscheduled beam overnight during training shifts as well as keeping shorter than usual maintenance days. The impetus for this came from a new vacuum leak around 1AQ14 which would open up after about 6 hours of beam-off and slowly worsen until beam was restored at which time the vacuum would fully recover to its base pressure. However, that base pressure was slowly rising by 10 or 15 mtorr per week due to another vacuum leak around valve 1AVA8 (due to a tall vertical beam in the absence of 1AQ9). Preparations were made for emergency intervention if required earlier than fall shutdown and BL1A currents were for the most part kept to a conservative $130 \mu\text{A}$ as an extra precaution. As it turned out, the steady rise in pressure was kept in check enough by adding extra pumping to last out the schedule.

Later on the BL1A current was further lowered because of cooling problems with the BL1A triplet. This fault ended up in a horse race with the above vacuum problem to see which would curtail BL1A operation before the end of the beam schedule. The coolant flow through two circuits in the 1AQ15 magnet was restricted causing heating problems that could only be alleviated by reducing the current through this quadrupole. This, in turn, compromised the BL1A tune thus forcing lower proton currents in order to main-

tain normal beam spills in the 1AT2-TNF area. Even though some respite was obtained during the emergency inflector repair which offered the opportunity to check out and optimize the 1AQ15 flow, the subsequent deterioration of this cooling had the BL1A currents reduced to $50\ \mu\text{A}$ as the fall shutdown approached. This was a large contributor to the above reduced percentage for current delivery. BL1A production was followed by BL1B operation which finished much sooner than scheduled allowing a welcome early start to the ambitious list of BL1A shutdown activities briefly described below.

BL2A ran for 2792 hours or 75% of its scheduled time, receiving a charge of 77 mAh at currents up to $65\ \mu\text{A}$ but usually around 30 to $40\ \mu\text{A}$. Beam was generally available on demand and the lower availability reflects those times when RIB was not needed due to ISAC target problems or changeovers, stable-beam tuning or other procedures. The chief problem during 2A operation was beam stability. Far too many trips occurred while running as close to the target current limit as possible (to capitalize on exponentially increasing RIB production with current) only to be upset by an approximate $2\ \mu\text{A}$ current variation. This instability may be inherent in the shadowing technique (with extraction 1) that itself was instigated to avoid BSM trips caused by high energy beam tails intercepted when the 2A foil is dipped in at slightly lower (non-shadowed) energies. Beam physicists are investigating the problem while the Controls group is developing stability programs that may help reduce the downtime – largely associated with the longish (2 to 4 minute) beam recovery ramp-up times following each trip).

BL2C4 ran for 1660 hours or 69% of its scheduled time, receiving 95 mAh or 83% of its scheduled charge. Shutdown repair problems, particularly in achieving leak-tight water seals as described above, delayed 2C4 startup by about 5 weeks resulting in the poor statistics as well as some of the higher individual shutdown doses. However, there was little 2C4 downtime once it got going at nominal currents of $60\ \mu\text{A}$. The shutdown goal of a realigned beam line and STF was achieved and some of the best operation in recent years has resulted (wider tuning windows, low collimator temperatures). Nevertheless, a redesign of the STF target is in progress in collaboration with ATG/Nordion.

Fall Shutdown

The scheduled fall shutdown saw a tremendous amount of meson hall work done over a three week period while the week of work in the vault was fairly limited. In BL1A there was the repair of vacuum leaks at 1AVA8 and 1AQ14, the repair of a water leak at 1AQ15 as well as flow improvements to that quadrupole mag-

net, the installation of new target ladders and water package servicing for 1AT1 and 1AT2, the replacement of monitor 1AM9 and servicing of others, the repair of BSM 56, and various routine maintenance jobs such as the replacement of active system filters.

In the vault both X1 and X2A foils were replenished (X2C foils were reloaded when the lid was raised in August), vault BL monitors were gassed, the 2C4 protect monitor wiring was repaired and the 2C4 scanning wire monitor alignment inspected, tank cryopump 2 was installed, the upper correction plate external cabling was refurbished, a vacuum leak at 2AVB1 was repaired, rf transmission line repairs were made at capacitor station 2, the water-cooled probe flow meter was replaced, and a 2C roughing pump was repaired.

Elsewhere a water leak in the main magnet power supply was fixed, AIALCW system control valves were serviced, site air and water filters were replaced, site power supplies were serviced (including a water leak repair at 1VB1), the 2A toroid was calibrated, diesel generator maintenance was done, and several water-pump motor couplers were upgraded. The total dose for all shutdown activities was about 26 mSv distributed among 50 workers. This was in addition to the 9 mSv accrued during the mid-August inflector repair.

Beam Schedule 106

The cyclotron availability for this period was 93% of the 1791 scheduled hours, a reasonably smooth finish to the year. The total downtime was 108 hours, the bulk of which was fairly evenly distributed among the RF, ISIS and Services groups as well as site power disturbances. It should be noted that the rf behaved extremely well with an average weekly downtime of only 1.5 hours. The cyclotron tune was reasonably good with a typical transmission of 64% and measured tank spills around 1% of the total current extracted to the three active proton lines as follows.

BL1A ran for 1133 hours or 94% of the scheduled time and received 123 mAh or 93% of the scheduled charge. The statistics were very good as a result of work done in the fall shutdown although there were still a few problem areas such as slightly rising (but not threatening) triplet temperatures and, more worrisome, a worsening beam line vacuum due to a leak associated with monitor 1AM9. There was also the continuing inability to tune π^+ mode which fortunately was not required. The BL1A current was limited to $100\ \mu\text{A}$ for a month due to the use of graphite targets at 1AT1 but was usually $130\ \mu\text{A}$ when beryllium targets were used. Nine weeks of BL1A production were followed by BL1B operation for PIF.

BL2A ran for 786 hours or 60% of the scheduled time at currents ranging from 20 to $65\ \mu\text{A}$. Beam was

generally available on demand and the low availability reflects those times when RIB was not needed due to ISAC target problems or changeovers, stable beam tuning and other procedures. Beam stability was again an issue when running in a radial split configuration with BL1A but not so much a problem toward the end of the beam schedule when running as sole outside high-current user in parallel with PIF in BL1B and BL2C1. Some time was spent in trying to understand beam density issues with respect to target longevity and the line tune and its diagnostics. A more satisfactory beam spot was obtained by defocusing the last two quadrupoles.

BL2C4 ran for 858 hours or 89% of the scheduled time receiving 46 mAh or 111% of the scheduled charge at currents between 50 and 60 μA . It enjoyed continuing success although some problems with the water package conductivity toward the end of the last run will have to be attended to in the 2005 winter shutdown.

BL2C1 saw a single patient PT session and also ran for 65 hours (of 382 scheduled) primarily for PIF experimenters booked for the last 2 weeks. It was limited to energies less than 105 MeV as reported previously, another problem to be sorted out in the following shutdown. PIF users also ran in BL1B at three energies (225, 355 and 495 MeV) taking beam for 67 of a scheduled 231 hours – fairly heavy use as it goes. Following PIF was a two-day development shift after which most cyclotron systems were turned off just before the Christmas holidays.

Apart from the many tasks associated with beam delivery, various operators were again very involved with fire alarm and card access system improvements, AUTOCAD drawings, training, equipment repair, computer and console upgrades and maintenance, beam transport modelling, coordination software improvements and more as well as actively helping out with many shutdown jobs.

BEAM DEVELOPMENT

Cyclotron Beam Development

Cyclotron beam development concentrated on reproducing, understanding and improving the $\approx 300 \mu\text{A}$ tune being developed to satisfy the users' requirements for beam in 2007 when ISAC is scheduled to begin operating at 100 μA . The installation of emittance limiting slits in ISIS, improved diagnostics, better alignment of the centre region correction plates, and the discovery of improved ISIS tunes all contributed to the development effort.

Beam dependent heating of the beam scrapers attached to the leading edges of the trays holding the

centre region correction plates was a problem. The upper scraper in quadrant 2 and the lower scraper in quadrant 4 both heated. In 2004, the lower trays were re-aligned, and for good tunes this has eliminated the lower quadrant 4 heating problem. The upper trays will be re-aligned in 2005, and that will hopefully eliminate the upper quadrant 2 heating.

Some work was done on low energy probes LE1 and LE2. First, a high resolution probe head with five vertical fingers, identical to the one installed on LE1 in 2003, was installed on LE2. Second, the vertical sag of the cantilevered probes was measured as a function of radius. After the sag in LE1 was partially corrected, the measured displacements were incorporated into the data analysis programs as correction factors so that the position of the beam centroids could be estimated more accurately.

After the above improvements, the position of the centroid of the beam was measured on opposite sides of the tank with LE1 and LE2. As shown in Fig. 183, the beam is higher on LE1 in quadrant 1 than it is on LE2 in quadrant 3. The reason for this median plane tilt is not entirely understood, however, a theoretical analysis done during TRIUMF's early construction suggests that it could be caused by dee mis-alignments. A median plane tilt could also be a contributing factor to the overheating of diagonally opposite upper and lower correction plate scrapers described above.

Decreasing beam losses in the centre region is advantageous when running high currents since it minimizes heating and the risk of component damage. This becomes increasingly important as the beam moves outward and becomes more energetic, so it was encouraging to find improved tunes with significantly better centre region transmissions beyond the first turn.

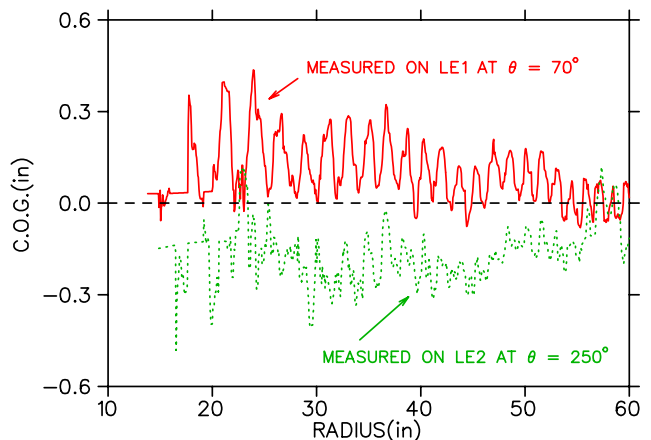


Fig. 183. Vertical positions of beam centroids measured on opposite sides of the tank with LE1 and LE2.

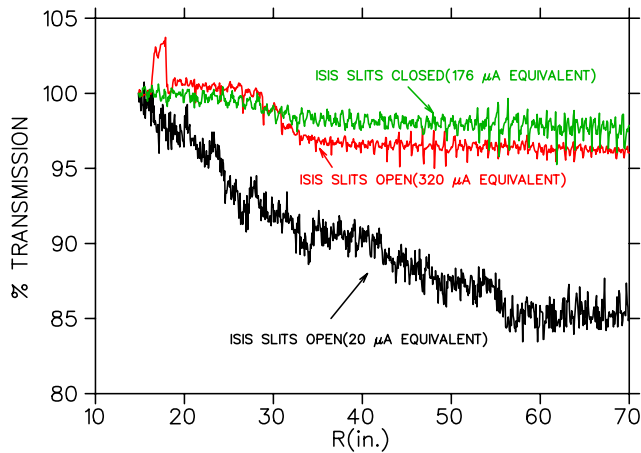


Fig. 184. Centre region transmission measured on low energy probe LE2.

This is illustrated in Fig. 184. On March 30 with $20\ \mu\text{A}$ equivalent current the transmission measured on LE2 between the first turn and $R = 70$ in. was $\approx 85\%$, which was considered typical at the time. By June 15, after some judicious tuning, this increased to $\approx 96\%$ even though the equivalent current was raised to $320\ \mu\text{A}$. Closing the newly installed ISIS emittance limiting slits to decrease the equivalent current to $176\ \mu\text{A}$ increased the transmission to over 97% . This mode of operation is now being used for production runs. The ion source runs continuously at high current and the injected current is controlled with the ISIS slits.

The best 2004 high current result was achieved on June 15 when a stable beam with an equivalent current of $320\ \mu\text{A}$ was obtained at 50% duty cycle with 64% cyclotron transmission and reasonable spills. In previous years we achieved similar results with duty cycles as high as $\approx 85\%$. This was difficult to do in 2004 because during development shifts the current handling capacity of the external beam lines was often limited by hardware problems and BL1, BL2A and BL2C were never all available simultaneously for high current extraction. Although many of the properties of high current beams can be studied at low duty cycle, it is impossible to develop a high current tune with good spills without working at high duty cycles. We hope we will be able to do this in 2005.

Because smoothly operating probes are essential for beam development, beam dynamics studies were done to assist the Diagnostics group in determining if the low energy probe heads could be made lighter for smoother motion and less vertical sagging. Thermal calculations based on calculated and measured beam spot sizes on the probe heads indicated that the weight of the heads could be reduced from 450 g to 190 g by making the radially outward part of the head thinner without decreasing the head's current handling capacity.

ISIS Beam Dynamics Development

During the winter shutdown, two sets of adjustable slits were installed in the horizontal section of ISIS. These proved useful for limiting the emittance of the injected beam and for controlling the current injected into the cyclotron without having to adjust anything upstream of the slits.

Considerable effort went into finding improved tunes for the vertical section of ISIS. The polarity of quadrupole Q340 in the lower section of ISIS was found to be reversed and was corrected. This enabled us to lower the voltage of quadrupole Q336 from 8.9 kV to 4.4 kV, thus reducing the risk of sparking. In addition, the 3 kV supplies attached to the last two periodic sections in ISIS were replaced with 5 kV supplies to provide more tuning room for high current beams. After retuning, the nominal settings for these sections was found to be ≈ 3.6 kV.

The transfer matrix elements in the vertical ISIS line, where the axial magnetic field of the cyclotron couples the transverse movements of beam, were measured and found to agree well with theoretical predictions. This will help us model the beam optics of the vertical section.

BL2A Beam Dynamics Development

ISAC requires a highly stable beam with a relatively large spot size on their target at the end of BL2A. To help achieve this, a development program aimed at obtaining a better understanding and improving the performance of BL2A was begun.

The beam envelopes along BL2A were measured with profile monitors and compared to theoretical predictions. During the course of this work, it was discovered that STRIPUBC, the program used to calculate the transfer matrices between the stripping foil and the BL2A combination magnet, was doing the vertical calculations incorrectly. This error has existed from the start, and so has implications not only for BL2A, but for all the primary beam lines. As shown in Fig. 185, good agreement between the measured and calculated envelopes was obtained after correcting STRIPUBC.

A feedback loop, which will sample the BL2A current and adjust the duty cycle of the ISIS pulser to keep the sampled current constant, is being developed. The software has been debugged and a number of successful simulations have been completed. A test with BL2A will be performed early in 2005.

In 2005 it is anticipated that a substantial portion of the beam development program will be devoted to improving the quality of the beam being delivered to the ISAC target.

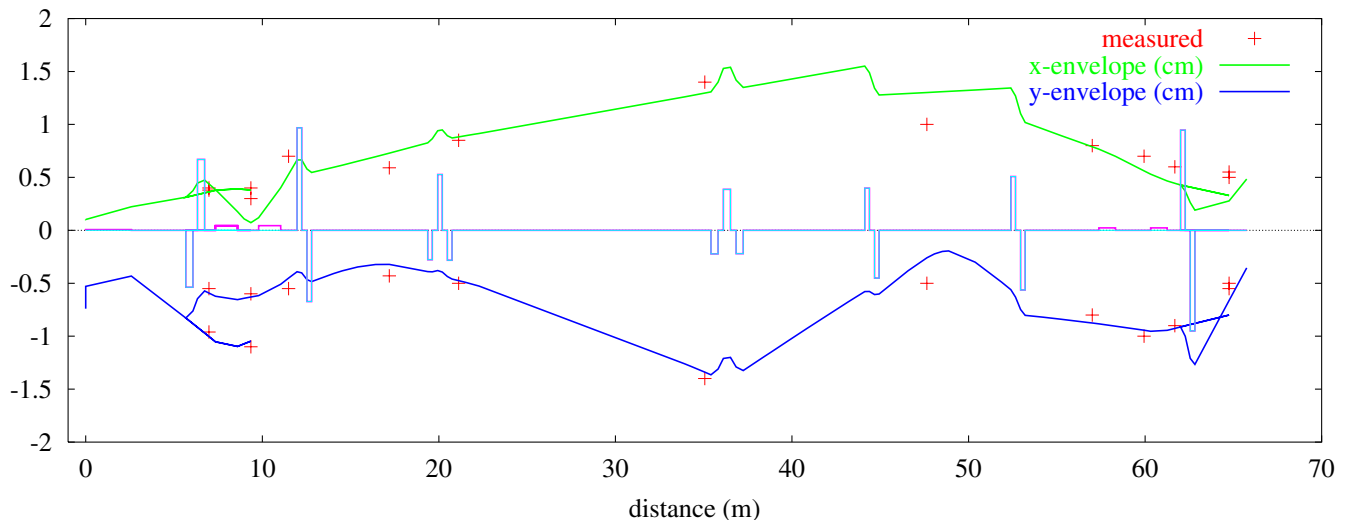


Fig. 185. Measured and calculated BL2A envelopes.

PROBES AND DIAGNOSTICS MECHANICAL MRO

In addition to normal MRO activities and ISAC work, more progress was made on the HE probe refurbishment. This included completion of the probe detailed design and fabrication and testing of the major subassemblies. The group activities are documented in the Diagnostics group meeting notes, which are available electronically via the Operations CYCINFO information service on the site computer cluster (accessible also through the TRIUMF home page on the WWW).

Cyclotron Diagnostics MRO

Prior to the lid-up, the low energy probes (LE1, LE2) were surveyed (via periscopes) for vertical alignment. The LE1 head was found to be low and so the track was adjusted to raise the probe 0.125 in. to bring it into better alignment. Both LE probes were inspected *in situ*. A new five-finger head was installed on LE2, replacing the crossed-wire head that had been installed in the mid-1990s for the alternative extraction studies. LE1 was removed from the tank for service; the re-circulating ball bearings were overhauled and modified slightly to reduce wear. Also, a problem was found with the mounting of the head, which is susceptible to cantilever forces. A new LE head design was developed to lighten the mass and improve the attachment. LE2 is scheduled for similar treatment in 2005.

The extraction probe for beam line 2C was removed for routine service in the winter shutdown. The grease on the vertical drive screw of PIP3 was found to have dried out resulting in stalling. The screw was cleaned and re-lubricated.

In a major effort, the vault wiring for the SE periscope was replaced during the winter shutdown.

The NW periscope cables will be replaced in 2005. The NW periscope prism was replaced.

Beam Line Monitor MRO

All vault and standard beam line monitors were serviced during the shutdowns. The external wiring harness of 1BM5 was tied away from obstructions and the radiation damaged HT cable of 1VM3 was replaced. In addition, assistance was provided to beam line 2C4 service in which several alignment issues have been identified.

ISAC Diagnostics

The external wiring harness of the IMS:DB0 slits was re-routed to solve an interference problem. Conceptual designs were made for a scanning wire monitor to be an alternative to the harps in the target station exit modules because at the high ion-beam intensities possible with some ISAC ion sources, the harp monitors are saturated. As usual, a significant number of foils were prepared and loaded on the MEBT stripper.

HE Probe Refurbishment

The original HE and LE probe designs have ball-screw drives moving travelling intermediate members to perform cable-driven doubling of radial motion along a track that is raised and lowered to retract and insert the probe head into the cyclotron median plane. When not in use, the probes have to be raised at specific radial park positions. The replacement HE probe design utilizes a rack and pinion drive to move a travelling intermediate member moving along a vertically stationary track. The probe head alone is raised or lowered into the beam plane along a wide radial range of probe motion. Extensive tests of the lift mechanism

were done in the lab to ensure reliability of the concept. The probe was assembled in the laboratory before the end of the year, but fabrication of the vertical mounts and laboratory commissioning will delay the installation in the cyclotron until the next opportunity available after March, 2005.

RADIO FREQUENCY SYSTEMS

RF Operation

The total rf downtime for the year was 77 hours. This is a great achievement compared to 234 hours in the previous year.

The main contribution to downtime was sparking with 44 hours. Crowbars caused 12 hours and the remaining hours were caused by various small failures like blown HVPS water cooled resistor and worn filament power supply breakers.

A great deal of activity was devoted to enhance the overall reliability of the rf system. A number of improvements were made in various areas starting from amplifiers all way through to the cyclotron resonators.

RF Power Amplifiers

Acquisition of data concerning the voltages and currents of the power amplifiers (PA) is via CAMAC. A new interface box with the capability to handle up to 112 inputs was installed to provide the good rf filtration and over-voltage protection required for the controls input modules and the ADCs. Also installed were new wiring within the rf room and new shunts for PA screen current measurement. All this was accomplished in the framework of our co-op student project.

Modifications were made to the spare soft-start SCR boxes. Diodes, SCRs, and snubber networks that have higher break-down voltage ratings and new heatsinks were installed. A spare filament power supply was refurbished to provide a tube conditioning voltage of 12.0 V. Because the filament connectors of the original PA tube were very weak and were prone to water leaks, new connectors were designed. A total of sixteen connectors are being installed.

A new, more robust, hairpin inductor less susceptible to water leaks was designed and will be tested in 2005. Meanwhile, a new hairpin cooling concept was tested in the PA1 amplifier. Broken input capacitors' gearboxes were refurbished in PA3 and PA4.

The original elapsed-time counters for the filaments were located at the back of each PA and were non-resettable mechanical meters. Two (of eight) have stopped and there were no spares due to their obsolescence. The new electronics-type counters are compact, easy to read, and have a maximum range of 999999.9 hours. They can be reset to zero, which is very useful when a new or rebuilt tube is put into service. All eight

counters were mounted on a 19 in. rack panel above the main console (see Fig. 186) and commissioned in May.

Anode HVPS

New thyrite varistor stacks with additional air cooling were installed in the main HVPS to improve protection of the chokes (see Fig. 187). Horn spark gaps on the chokes were readjusted to the specified rating. New flexible couplings for the water-cooled resistors were installed because the old ones often cracked and gave a lot of trouble with water leaks. Both the old and the new type of connections are shown in Fig. 188.



Fig. 186. New PA filament elapsed time counters.



Fig. 187. New thyrite varistors in anode HVPS.

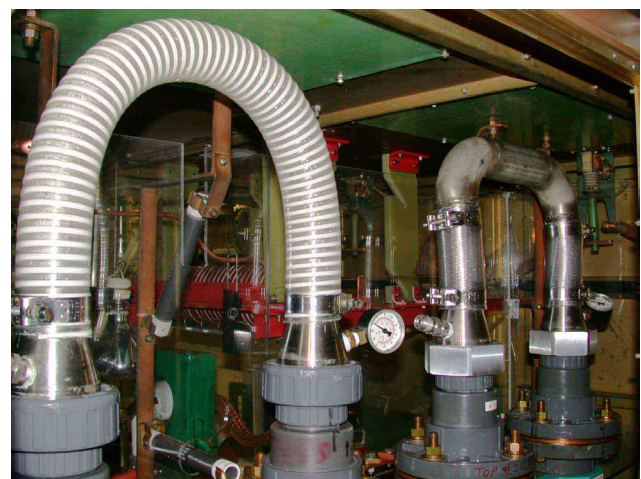


Fig. 188. Old and new (left to right) flexible couplings in the HVPS resistor cooling circuit.

A water filter, purging valves, and pressure release valves were incorporated into the return cooling line. Broken check valves were replaced. New controls were installed for the automatic water supply valve.

The original HVPS diodes in the 24 stacks of 12 series connected high power diodes, with their accompanying RC networks, became obsolete. Two new spare rectifier diode stacks with new diode types were assembled and successfully tested.

The crowbar-driver protection board accepts crowbar firing signals from eight PA tube cathode shunts and is supposed to suppress transients and potentially high voltage spikes, not allowing them to get to the crowbar driver logic board. It also provides signal sources for monitoring continuity of the cathode shunts and interconnecting cables. The old board contained signal diodes that were low-rated in both forward current and reverse breakdown voltage capabilities. These shorted almost every time when the crowbar was fired from a cathode shunt because of the excessive energy of the transient. A shorted diode means a completely shorted input and the PA tube is no longer crowbar-protected! A new crowbar protection board was designed and built. It performs much better transient clamping by means of 2×20 A Schottky diodes for both positive- and negative-going transients. The existing coaxial cables to the old board were removed and replaced with new cables fitted with SMA and BNC connectors and, for ease of maintenance, bulkhead adapters instead of direct soldering. The board was installed (Fig. 189) and commissioned in the September shutdown.

RF Combiners and Coaxial Switch

The final rf combiner (#3) was replaced with a new unit (see Fig. 190) that was tested into a dummy load up to 700kW, limited only by the load cooling capability. All 3 combiner waster loads were relocated

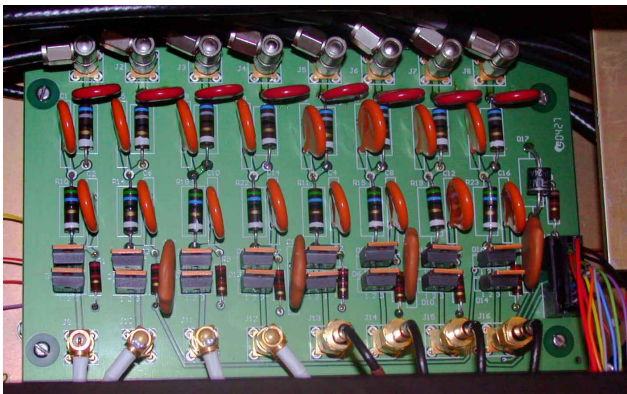


Fig. 189. New HVPS crowbar driver protection board.

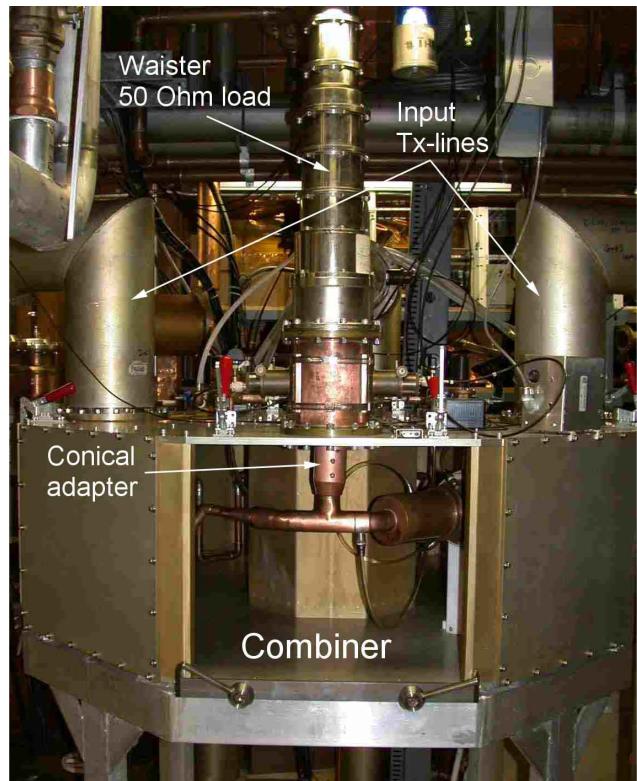


Fig. 190. New final combiner with dummy load on top.

on top of their corresponding combiners and new water cooling circuits were installed. All sharp edges of the 12 conical adapters to transmission lines were chamfered, and an installation procedure for the cones was established to prevent fingerstocks damage.

The rf amplifier system provides up to 1 MW of rf power at the output of combiner #3, which is connected to the cyclotron through a 9 in. transmission line. To simplify troubleshooting the system a 4-port 9 in. coaxial rf switch was purchased in 1995. The idea was to install it at the final combiner output in order to switch rf power either to the cyclotron or to the dummy load. Unfortunately, the manufacturer's power rating did not suit our requirements covering only the range up to 700 kW.

Over the last year the switch was modified by incorporating a water-cooling circuit inside the switch port of the inner conductors and the rotor-blade contacts were air-cooled by 3 blowers attached to the switch. Teflon insulators were replaced with polypropylene ones to prevent substantial deflection due to cooling-water pressure. An inside view of the switch while it was being modified is presented in Fig. 191.

In April the rf switch was tested on a soda-solution dummy load (see Fig. 192). Maximum power at that time was limited to 700kW by the capability of the heat exchanger of the dummy load.

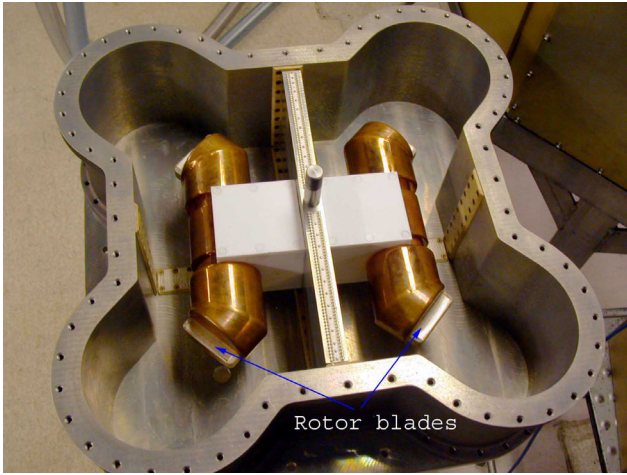


Fig. 191. Inner structure of the rf switch.

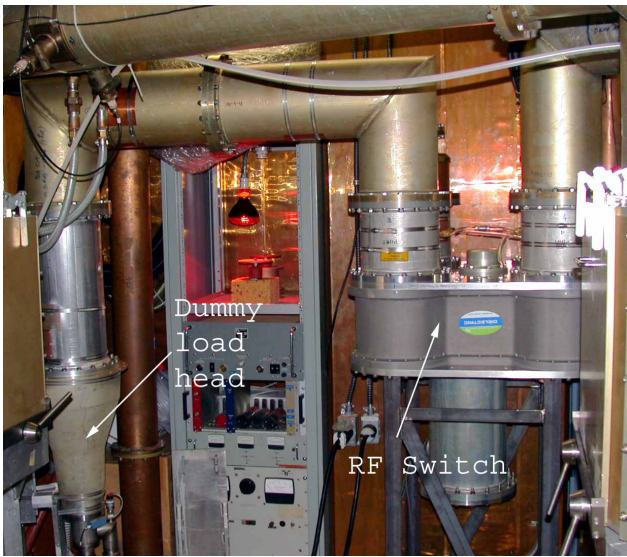


Fig. 192. RF switch with dummy load test set-up.

In June the switch was successfully tested at full power in the cyclotron. This time we extended the length of the transmission line (including the switch) by about 5 m in order to move a transmission line resonance away from the operating frequency. The measured temperatures at the rotor (knife) contact and the water-cooled stator contact group are presented in Fig. 193, and show a minor temperature rise which will not affect the reliability of the operation of the system. The rf switch and soda solution load are being upgraded now with commissioning planned for 2005 winter shutdown.

Transmission Line

The entire section of 9 in. transmission line from the final combiner to the 11 in. matching section was overhauled during winter shutdown. All junction bullets and elbows were serviced and new O-ring water

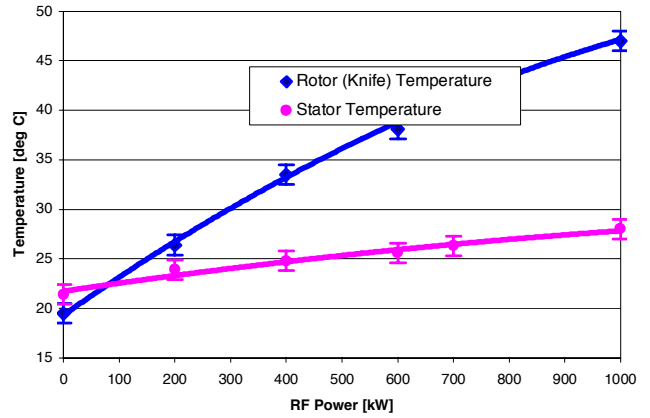


Fig. 193. RF switch temperatures vs. rf power.

seals were installed. Old rubber gaskets, installed some 20 years ago, were found hardened (carbonized), especially in the vault area where they are exposed to radiation. The transmission line water cooling circuit was redesigned. The original design was based on a plastic return pipe buried inside a centre conductor of the transmission line. This pipe was found to be completely disintegrated due to radiation damage. The new design uses an external copper return pipe and requires new combiner adapter cones and centre-conductor water plugs with plastic pipes going out of the transmission line (see Figs. 194 and 195). The new design separates the cooling circuit for active branch from that of the non-active branch.

To reinforce structural stiffness of the transmission line at the water breakouts where water pressure creates a high axial force, new dielectric spacers were fabricated initially of delrin and later of polypropylene. These new spacers were installed at the output of the final combiner, at active/non-active water junction, at 9 in. to 11 in. transmission line junction, and on the



Fig. 194. Parts for new transmission line cooling design.

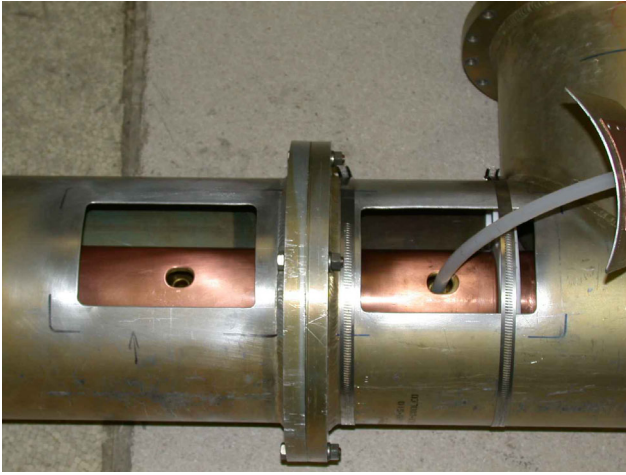


Fig. 195. Water outlets at transmission line junction.

coaxial switch. The new cooling circuit incorporates pressure and flow regulation valves and an interlocked flow switch. Matching section capacitor stations #1 and #3 were replaced with fast-detachable plug-in modules in the winter shutdown. This new approach uses external, quick-detachable cooling lines.

Thus we have eliminated the troublesome cooling lines buried inside the 11 in. transmission line centre conductor. At present we have all of the capacitor stations upgraded; they are independently cooled and interlocked with individual flow switches. The new water distribution set-up is shown in Fig. 196.

During the September shutdown some critical transmission line junctions were inspected. Severe finger-contact damage was detected on the transmission line centre conductor at the matching section capacitor #2 (see Fig. 197). Broken parts were repaired and new stainless steel clamps were built to replace weak copper clamps, ensuring reliable rf contact for copper sleeves at the transmission line centre-conductor junctions.

Cyclotron

We continued the program of the replacement of copper chore pads with fibreglass ones. The aim of this program is to protect the delicate resonator cooling circuit bellows. This year another 20 resonators in the upper octants #3 and #4 were serviced and leak tested.

Ground arm tip (GAT) positions of #10 resonators are not adjustable like the other resonators. From the measurements last year we recognized that some of them are offset with respect to the adjacent resonators. To reduce an impact on the electric field distribution it was decided to compensate this misalignment with hot arm repositioning, aiming for a constant rf gap along the dees.

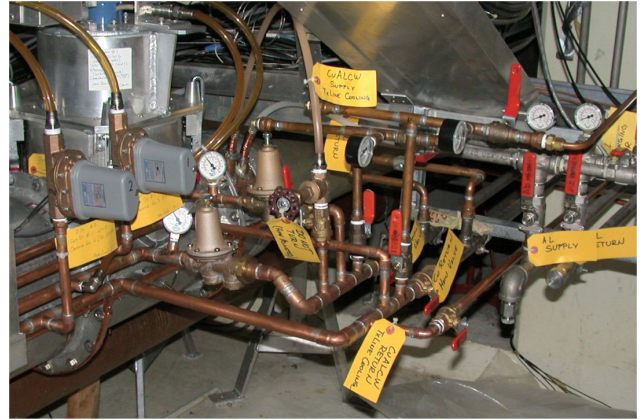


Fig. 196. Capacitor stations water distribution.

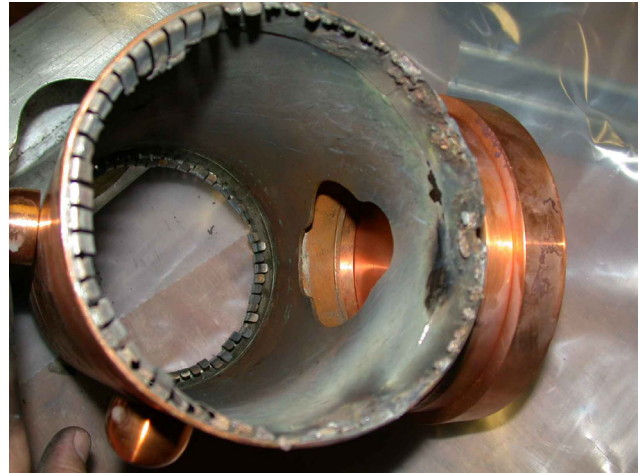


Fig. 197. Burnt transmission line finger contacts at capacitor station #2.

An attempt to measure some of the GAT positions inside the tank was made. However, the planned survey was not completed due to an issue of high dose. The measurements that were completed confirm last year's numbers. These data are the essential part of the dee-voltage monitoring program: the rf gap distances will be included in the calibration factor for the voltage distribution along the dee gap. At present this information is used in the GAT tuning process for minimization of rf leakage patterns. All of the troublesome thermocouples (TC) in the tank were assessed. A few problems were traced down to poor contacts in the connectors and were fixed. Three thermocouples, one on the rf booster, rf deflector, and high-energy spill monitor, were found damaged. A decision was made not to touch them because of the high radiation level in the area. All the above-mentioned devices have other thermocouples in their proximity, which can cover temperature monitoring. The correction plate (CP) trays from quadrant #3 were pulled out of the tank and serviced. All insulators were replaced, burnt marks cleaned, and deformations straightened out. CP trays in Q2 and Q4

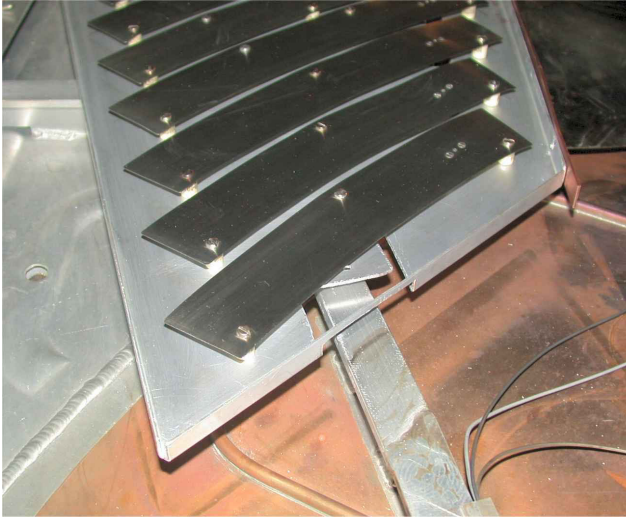


Fig. 198. Modified Q4 correction plates tray.

are known for significant temperature response because of the accelerated beam hitting the CP trays. This time both lower trays were realigned by means of modified supporting spacers. CP Q4 required tray modification to meet the desired elevation (see Fig. 198). Four thermocouples attached to the CP copper beam-scrapers were rearranged to protect them against direct beam exposure.

At the end of the winter shutdown we had found a number of shorts in the correction plates HV feeding cables. The problem was traced to radiation damage in the last part of the cable length near the cyclotron (see Fig. 199). A few broken cable ends were trimmed and new connectors installed, while many other cables remained marginal. During the September shutdown a number of upper vault cables were trimmed back ~ 10 m, where a breakout panel was installed with new sections of cabling to the cyclotron feedthroughs. A replacement program is being planned for the next winter shutdown for the lower CP feeding cables.

RF Booster

The RF Controls group replaced an old rf booster control system with a newly developed hardware and Windows PC-based software. The system interface now looks much the same as for the ISAC rf systems. The motor attachment of the rf booster tuner was modified to ensure reliable operation at the extremes of the tuning range. The coupling-loop window was checked for moisture conditions that had been observed in the past. This inspection showed dry transmission line and ceramics surfaces, as a result of forced air ventilation provided for this area in 2003.

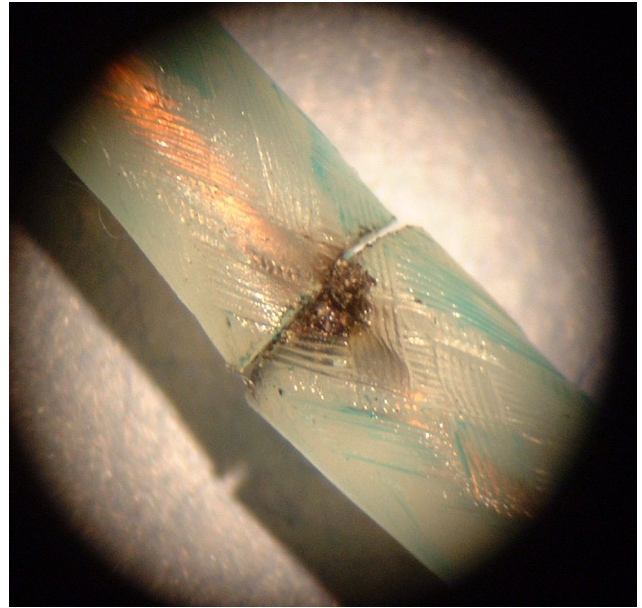


Fig. 199. Broken CP HV cable fragment.

Cyclotron Simulations

A cyclotron electrostatics study was carried out using the 3-D structure simulator software, HFSS (high frequency structure simulator, Ansoft Corporation). This work is aimed at better understanding the rf modes excitation and eventually to suppress cyclotron sparking. The centre post, the flux guides, the quasi-circular vacuum chamber, and the rf structure have been incorporated into the simulation. Fundamental accelerating mode and rf leakage into the beam gap have been studied in details. The rf parameters have been computed and are in close agreement with the parameters measured on the cyclotron (see Table XXVIII). Vertical asymmetry at the dee gap, caused mainly by resonator misalignment, leads to rf leakage fields into the beam-gap tank volume outside the resonators. A number of parasitic modes were identified in the frequency range of 10–40 MHz. Field distribution of one of the nearest parasitic modes is shown in Fig. 200.

Table XXVIII. Calculated and measured rf parameters of the cyclotron.

Parameter	HFSS	Measured
Resonant frequency (MHz)	23.106	23.060
Quality factor	5814	5500
R_{shunt} (k Ω)	38.6	36.0
Power (kW) for dee-gap voltage of 180 kV	840	900
Sensitivity to all ground arm tip displacement (kHz/mm)	83	---

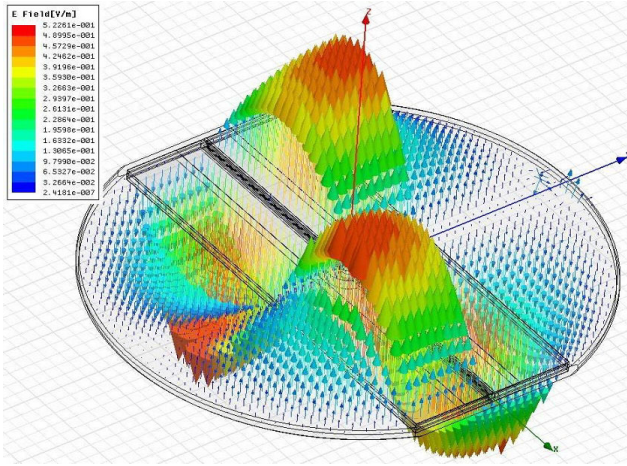


Fig. 200. Medium plane E-vector plot for one of the parasitic modes.

RF Support

The RF group was also dedicated to the following major ISAC projects, which are reported in the ISAC section.

- Operation and maintenance of the ISAC linac.
- ISAC-I rf amplifier remote controls development.
- SCRF cavities and accessories design, test, and characterization.
- Cryomodule alignment (WPM) system commissioning.
- Cryomodule #3 assembly and tests.
- ISAC-II transfer line rebuncher system development.

RADIO FREQUENCY CONTROLS

The RF Control group, in cooperation with the RF group, has continued fine-tuning the main cyclotron rf control system with the goal of reducing rf downtime in the cyclotron. By adjustment of the levels of the smaller sparks, which are ignored, and using a more aggressive recovery of rf voltage on the larger ones, the rf downtime was reduced significantly while reducing stress to the rf power components.

The booster rf control system was commissioned. Internal tuning controllers were added to facilitate the automatic power up sequence.

The rf control system for the ISAC-II superconducting rf module was tested successfully. Each module consists of 4 superconducting rf cavities, each of which are individually amplitude and phase regulated with tuner feedback control. Phase instability that was traced to fan noise in the power amplifier was fixed. Cross-talk within the phase feedback loop was eliminated and the phase loop is now, like the amplitude loop, unconditionally stable. Additional control was

added to the tuner controller with the result that powering up a superconducting cavity can now be fully automatic. Remote interface to EPICS was completed and tested.

CYCLOTRON DIAGNOSTICS

Tank Broadband Diagnostics

The major priority was given to fast signal acquisition from internal probes of the cyclotron. The fastest beam signal currently available for operation is the time-of-flight (TOF) signal with a frequency spectrum extending to a few MHz. With such a limited band this signal represents only the envelope of the multi-bunch beam structure; the rf structure is not retained. The TOF signal is routinely used by Operations to optimize the transit time of the beam through the cyclotron. However, the signal appears not to be sufficiently stable when applied to more delicate measurements of the beam isochronism and the beam energy gain per turn as a function of the orbit radius.

An investigation was undertaken to identify the nature of the noise in the TOF signal derived from the HE2 probe. We observed that the stability $\Delta t/t$ of the TOF remains nearly constant with the radius to a level of 10^{-4} . This implies that the absolute accuracy worsens with the radius as a power of ~ 3 . We conclude that fluctuations in the TOF signal are not related to the signal acquisition instrumentation but rather are generated by the beam itself. While studies of beam instability may be considered as a long term program, interpretation of data may still be unambiguous if adequate statistical analysis, such as data smoothing by cubic splines, is applied. This procedure was implemented in Matlab as a test.

An attempt was made to improve the accuracy of the TOF measurements by increasing the dwell time at each radius and averaging over multiple samples. Though a benefit was noted, the slowness of the procedure makes it impractical unless the data acquisition instrumentation and/or algorithms are improved.

A real step forward in beam measurements in the time domain can be expected with the implementation of broadband signal acquisition and analysis. Applications for these diagnostics include measurement of the TOF, direct bunch phase measurement with respect to the rf, and the shape of the longitudinal bunch. Significant efforts were made in this direction concentrating simultaneously on two devices: the phase capacitive pickups and a new broadband head for the HE3 probe. Only the two outermost pairs (upper and lower) of the capacitive pickups remain of some seven pairs initially installed in the tank. The others were decommissioned because the strong signal induced by the cyclotron rf system, rendered extraction of accurate beam informa-

tion impossible. There is a hope, however, that modern methods of signal analysis can improve the accuracy of measurement to the required level even in the presence of the strong rf background.

The four pickups were inspected visually during the September shutdown and their signals observed in the time and frequency domains. All four are still usable and beam induced spectra were observed up to ~ 2 GHz. Signal-to-noise ratio (SNR) was ~ 0.1 at the fundamental, more than 5 at the second harmonic and drastically increasing above the 7th harmonic. Inspection revealed that some of the coaxial signal cables were partially damaged. A decision was taken to replace the four cables with foam dielectric, low loss, phase stable cables. The cables were installed in the winter shutdown along with two similar cables for the HE3 probe equipped with a new broadband stripline head (see Fig. 201).

The new head is essentially a $50\ \Omega$, parallel-plate transmission line made of a tantalum foil 0.3 mm thick supported by a frame made of BN ceramic. The entire structure was designed with the high-frequency structure simulator program (HFSS) from Ansoft and was optimized to provide a broadband $50\ \Omega$ match (VSWR < 1.2) over a frequency interval from dc to over 2 GHz. The 3 mm inter-plate spacing of the transmission line was chosen as a compromise between two objectives: minimizing transverse geometrical dimensions and reducing the current leakage due to knock-on electrons that was estimated to be $\sim 2\%$. In contrast to capacitive pickups, this broadband monitor intercepts the beam and therefore can be used only for cyclotron tuning at low beam currents. A 3D thermal simulation

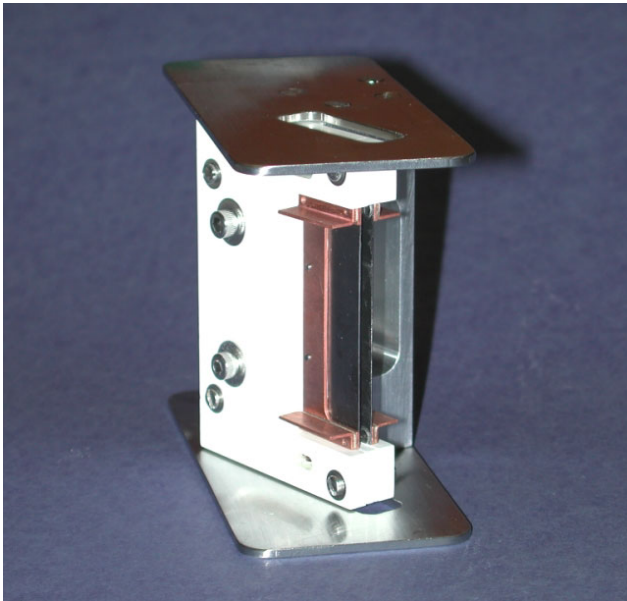


Fig. 201. The new stripline head for the HE3 cyclotron probe.

with ANSYS Workbench has shown that the probe can be operated up to at least $1\ \mu\text{A}$ average. A high peak current at low duty cycle is essential for a good SNR. Minor modifications made to improve the mechanical rigidity of the frame during the mechanical design had a negative impact on the rf performance between 1 and 2 GHz (VSWR increased to almost 2).

The head was built and installed in collaboration with the Probes group on the existing drive mechanism of the former HE4 probe which replaced HE3 in the tank at the end of the winter shutdown. Diplexers permit acquisition of the dc, low frequency TOF (< 3 MHz), and broadband signals.

Beam Line Diagnostics

The signal from the capacitive probe in beam line 1A is used to optimize the overall TOF of the beam through the cyclotron. The raw signal from the probe is a train of pulses at 23.055 MHz modulated by the 1 kHz pulse structure. A CAMAC module was in place to count the number of rf cycles from the start of the ISIS pulser signal to the trailing edge of the capacitive probe signal but the system was never fully commissioned. A prototype module was built which unambiguously detects the leading and trailing edges of the beam pulse from the capacitive probe signal. Applying these new signals to the counter module now allows the machine TOF and the apparent lengthening of the extracted beam pulse to be determined. Since the measurement is automatic, it eliminates the need for the operators to set up the oscilloscope and allows the new parameters to become a part of the shift log. The design was tested with beam and a printed circuit card version will be made.

Diagnostics MRO

In addition to numerous routine checkups and calibrations of diagnostic electronics, several time consuming and dose related jobs were performed over the year. The water cooled pop-in-probe (WCP) cooling flow meter was replaced in the vault. The radiation damaged wiring harness of the SE periscope was replaced completely. An oil-free vacuum test station, consisting of a turbo pump, a scroll pump, gauges, and a test box, is being constructed in the Probes laboratory. Our rf design software was updated and printed circuit card layout software purchased. A USB to GPIB interface was purchased for connecting our notebook computer to various test instruments using LabVIEW.

CYCLOTRON VACUUM AND CRYOGENICS

The cyclotron vacuum/cryogenic system continued to operate well for the year. Minor problems with vacuum equipment caused almost no downtime during

beam production. Cryogenerator #1 is still not very reliable, and it is used for a one to two week interval to make time for overhauling cryogenerator #2.

The lubrication delay device was modified on cryogenerator #1; the lubrication can be turned on manually in the case of a device failure. Major repairs were made to the crank case assembly of cryogenerator #2 to fix a loose displacer rod on the first cylinder. The temperature sensors wiring and some of the sensors were replaced on both cryogenerators. New cables were made and installed connecting the sensors to the new Lakeshore temperature monitor. The monitor readouts are available through the main control system. The helium gas copper lines were replaced with stainless steel lines on both cryogenerators as well as on the gas manifold system.

Cyclotron cryopumps were maintained and serviced regularly throughout the year. Cryopumps 2, 4, 5 and 6 were refurbished. The limit switches were repaired on the gate valves of cryopumps 5 and 6.

In December the main seals of the cyclotron were tested OK by venting the seal space. The Varian ion gauges that were installed in 2003 are operational and readouts are available through the main control system. One of the two inflector ion gauges failed. Both gauges have been replaced with dual filament models for redundancy. The ion gauge power supply was checked and repaired as well as the cable for the inflector ion gauge.

An air leak was registered by the residual gas analyzer (RGA) in December as soon as the rf system was shut off. Helium leak detection with the RGA confirmed the leak in an O-ring seal of the coupling loop.

The cyclotron tank vent valve system failed during the summer emergency shutdown. The tank was vented with nitrogen through a manual valve on the RGA line. Failure of the vent valve was caused by low pressure in the air line due to leaks in other devices using the same air supply. The air leaks have been repaired.

Improvements to the B20 cooling water system were made by removing an inefficient heat exchanger and switching to the city water system.

Beam Line Vacuum

On BL1A the vacuum of the beam line was compromised due to the leaks in the 1AT2 area at 1AQ14 and 1AVA8. The roughing system was modified to accommodate the increased load. The leaks at 1AVA8 were repaired during the summer shutdown by replacing O-rings and refurbishing the valve.

A few leaks developed in the vault section of BL2A because of radiation damage to O-ring material. The O-rings were replaced. All key brass block valves were replaced with refurbished ones. The ion gauge head

2AVIG1 was replaced.

The vacuum system of BL2C worked well. The BL2C radiation hard valve and its N₂ supply were repaired.

The front-end vacuum of BL4 was maintained and kept under nominal vacuum to protect the cyclotron vacuum in case of gate valves failure.

Vacuum and Cryogenic Support

The Vacuum group has been involved in ISAC projects assisting with vacuum designs, vacuum equipment installation, mechanical assemblies, leak checking, cryogenic designs, etc. The details are presented in the ISAC Vacuum section of this Annual Report. The supply of liquid nitrogen and liquid helium was also looked after by the Vacuum group.

ISIS

The CUSP ion source and injection line continued to operate well during the past year with only minor downtime due to a failed turbopump, light-link power supply module, and some vacuum leaks. Although many ISIS personnel were involved in other TRIUMF projects, some extraordinary maintenance as well as a few significant projects were undertaken during the past year.

A major effort was unexpectedly required to realign the I1 motor generator set that provides power to the ion source terminal. The ion source optics were cleaned, realigned and reinstalled. The second of two new CUSP ion source bodies was installed and commissioned in March. This source ran well albeit with shorter than expected filament lifetime during a brief test run. The beam production schedule dictated that, for reliability, the other source be reinstalled. The source was tested off-line later in the year in the CRM and will be installed in the I1 terminal in early 2005.

Last year we reported the design and manufacture of four new sets of motor-driven variable aperture slits. One set of slits (*y*-direction only) residing between the two 45° vertical bend elements were installed in the September, 2003 shutdown to limit the dispersive energy tails of the beam from reaching the cyclotron. Of the other three sets, two sets of slits were installed into the first common periodic section of the ISIS beam line to define the emittance of the beam injected into the cyclotron. This entailed moving some diagnostic and beam trip elements with appropriate interlocks revisions as well as some minor refurbishing of the optics. The final assembly replaced the existing 5:1 slits and provides enhanced beam current control. The slits were successfully commissioned and provide improved beam quality to the cyclotron.

The inflector/deflector system experienced a major failure in August and accounted for 138 hours of down-

time. The failure was due to sputtering from a sharp metallic edge on an insulator in the “cross” providing high voltage to the inflector/deflector. This area had previously been serviced in May, 2003 when all insulators were replaced. The insulators in this region will be inspected and replaced in January, 2005. The inflector/deflector proper was serviced during the winter shutdown and ran well for the entire schedule.

A new equipment rack was installed next to the existing inflector/deflector power supply equipment rack to allow for present and future refurbishing. The oil filled ballast resistors were replaced with new air insulated resistors. New high voltage cables and positive lock connectors at the feedthrough end were installed. New power supplies will be installed in the latter half of 2005.

The prompt radiation safety trip system has been revised to include redundant safety-critical gamma and neutron monitors. Each of these safety-critical trip functions requires three independent ISIS beam control devices. To provide these additional beam control devices we have designed a system of four high-voltage relays to service the four vertical bend electrodes and two beamstops. Each trip function will use two high-voltage relays to switch two electrodes to ground potential and to insert a beamstop. The design is complete and procurement, assembly and off-line testing is under way. Installation will take place in January and February, 2005 with commissioning scheduled for March.

Some effort has gone into restoring the CRM ion source test stands. The first chamber of the 1 MeV cyclotron was restored to operating condition. This has allowed the testing of CUSP ion sources by ISIS, Nordion and Dehnel Consulting. In addition, Dr. Yong-Seok Hwang joined us in August on sabbatical from Seoul National University in South Korea, to study our ion source characteristics.

ISIS has provided assistance to numerous ISAC projects during the course of the year. These include assembly of electronics racks for the TITAN RFQ and high-voltage power supply commissioning. For Expt. 991 an extension of the LEBT was required and ISIS procured, assembled and installed the major mechanical and electrical components including power supplies. A great deal of mechanical effort was directed for the assembling of the ISAC-II cryomodules. Work also continued on the transfer line vacuum and diagnostics systems.

Last year we reported the successful development effort to achieve $412\ \mu\text{A}$ equivalent extracted current at 25% duty cycle. This year our development focused on producing $300\text{--}350\ \mu\text{A}$ equivalent tunes at higher duty cycles and with improved cyclotron beam losses.

This work, as well as centre region work, is described in greater detail in the Cyclotron Beam Development section of this Annual Report.

PRIMARY BEAM LINES

The winter shutdown began on January 5 following the Christmas holidays with replacement of the 1AT2-M20Q1 indium ring. Vacuum leak checking also showed leaks at the collimator B-1AQ14 and 1AS1-1AM10 vacuum joints. The 1AT2-M20Q1 indium ring was removed, remnant indium removed, and new ring installed. A video survey of the front end of the M20 channel was made to aid planning for its refurbishment during next year’s shutdown. A loose nut on the power connection to M20Q2 was carefully tightened to avoid cracking the connector. The location of the ground fault on the M20Q1 magnet was determined. After a successful power test the shielding over the channel was replaced.

M9Q1 was uncovered to investigate its interlock and electrical problems. The former was caused by a broken wire in the Klixon sensor chain, which was repaired, and the latter by a water leak from a Pyrotenax end cap. After its repair no further water leakage was detected at the insulator.

An unexplained vacuum excursion occurred causing another round of leak checking. Three leaks were detected. Load tests determined there was a correlation with tightening/loosening the remote-handling bolts on the buss links of the 1AQ14/15/16 triplet downstream of 1AT2. Indium remnants were found on the impression on the collimator B side on the ring indicating that indium had not been totally removed during 2003 triplet installation. The indium was removed and a blanking plate with a rubber O-ring was installed to allow further leak checking. Tests showed that the 1AQ14 flange did not close parallel to the collimator B flange. A new procedure was employed to close this joint and a new indium ring was installed. Another leak test with block loading resulted in no change in the vacuum. The leaks at 1AT2-M8 blank-off plate and 1AS1-1AM10 joint were, however, still present.

A new beam-spill monitor was installed on the upstream side of the triplet; the bridge and service-chase blocks were installed. The 1AT2-M8 blank-off plate was removed and inspected. The threads of a spring eye were found to be stripped and the knife impression was found to be deep. The leak was repaired by reducing the tension on the springs.

The entire layer of blocks surrounding monitor 1AM10 and the monitor itself were removed to replace crumbling blocks in that region. A broken, lower spring pin explained the vacuum leak at this location. However, because the leak was small and its repair would

increase the total shutdown dose, no repair was made.

More shielding was removed to gain access to the crumbling blocks south of 1AM10. Those that were structurally sound were left in position. Others, however, could not be safely lifted; it was necessary to jackhammer them until they could be removed. All high density blocks were replaced with low density ones except for the high-density suitcase blocks along the south wall of the trench, which were replaced with steel suitcase ones. Because the area was uncovered, the opportunity was taken to replace the cabling to the beam-spill monitor upstream of 1AS3.

Replacement of crumbling blocks north of the 1AM10 area was difficult because many had services attached to them. Removal of the blocks surrounding the crumbling ones had an added bonus of allowing inspection of the services running through the 1AS2/M20 service chase, partially exposing the M20Q5/Q6 and sextupole region of the M20 beam line to allow inspection of the rubber cooling lines. Some were radiation damaged and all hoses of the M20Q5/Q6 and sextupole were replaced; replacement of the M20VA5 valve was also done.

With the work completed at M20 and the crumbling blocks replaced, reinstallation of the beam line shielding began. The smokestack was chain-falled into position, the 1AM10 vacuum can–smokestack joint established, and the 1AT2 vacuum was pumped down. Leak checking found the joint leak tight. The 1AT2 vacuum was vented to install the 1AM10 monitor. A full-power test of the triplet magnets showed no problems and the triplet was covered with its remaining shielding blocks. A new beam line pipe was fitted to the M20Q9-10 doublet to allow a new window and gate valve assembly to be installed.

The Beam Lines group replaced the supply and return hoses of the M9AQ3/4/5 and M20Q5/6/7/8/9/10 magnets as well as those of M20B1. A vacuum leak discovered at the joint between M20Q8-M20B2 was cured by replacing an O-ring. Finally, the remainder of the M20B2 channel was covered with shielding and the shielding blocks that had been stored outside were replaced over beam line 1A.

Following the shutdown, operation continued normally until mid-July when it was noted that the vacuum in beam line 1A was deteriorating. At the same time over-temperature warnings began from quadrupole 1AQ15, the centre quadrupole of the triplet downstream of the 1AT2 target. By the end of July it was necessary to reduce the current to the quadrupole to maintain its operation and reduce the beam line 1A current from 130 μA to 100 μA to prevent excessive beam spill in the beam line. By the middle of August the beam line current was reduced to 60 μA to maintain

operation of the beam line. Then the inflector began sparking and it was removed for cleaning. The opportunity was taken to open the triplet area for assessment of the 1AQ15 problem.

Thermal scans of the quadrupole revealed that two of its cooling circuits were running hotter than the others. One of these was significantly hotter and it was decided to backflush the magnet. A thermocouple was attached to each of the hotter circuits and to one of the circuits that was operating normally, which served as a control measurement. Signals from these thermocouples were fed to the control room where their temperatures were monitored continuously. This was completed as the repaired inflector was being installed in the cyclotron.

Normal operation continued with a beam line 1A current of 100 μA until the end of August, although the beam line vacuum continued to worsen. In early September quadrupole 1AQ15 began tripping again on over temperature with the result that the beam line current had to be reduced to 80 μA and then to 50 μA just before the September shutdown.

Due to the vacuum and overheating problems the September shutdown was extended to allow all the necessary repairs to be made. A vacuum leak in the 1AVA8 area was tackled first. Leak checking indicated problems with the gate valve and both of the body-valve O-rings. Examination of the damaged O-rings showed that the beam was tall vertically in this region and it was speculated that this could be related to the present mode of operation of the beam line. After the replacement of these O-rings back-flushing of the two problem circuits of the 1AQ15 magnet began. Flow rates through the two hottest and control circuits were measured; that of the hottest circuit was found to be one-third that of the control circuit. After backflushing with boosted water pressure, the flow rate through the hottest circuit was doubled and found to be close to that through the next hottest circuit.

The coil interior bore of these hot circuits was examined to see if any obstructions could be removed. A black residue of unknown composition was found on a rod after its removal from the bore. Because back-flushing with water had improved the flow rate, air pressure was used in an attempt to flush out the residue and further improve the flow rates. More black sediment was released and water flow in the circuit was increased. When the triplet was powered it was found that the temperature of the hottest circuit had decreased 30°C to approximately the same temperature as the other hot circuit. That circuit too was air back-flushed and sediment was removed as well. Another full-power test found that the operating temperature for this second-hottest circuit had also been reduced.

Having completed the repair of the triplet the final job was the replacement of the collimator B-1AQ14 indium joint with a new tapered indium ring to which a thermocouple had been attached to monitor its temperature. The new ring is thicker at the top than the bottom to compensate for the vertical misalignment between the 1AQ14 and the collimator B flanges. When the vacuum was re-established a leak check found this joint leak tight.

With the conclusion of the September shutdown normal beam line operation was resumed. Temperatures of the water circuits of 1AQ15 remained normal although toward the end of the running period a slight increase in the temperature of the hottest circuit was noted. Another backflushing of this quadrupole will be scheduled during the spring, 2005 shutdown.

Beam Line 2C

The solid target facility (STF) on BL2C4 was removed during the spring shutdown to repair the target position limit switches and to correct the skew misalignment that had been introduced in 2001 when the STF was previously removed. The alignment was corrected but the limit switches could not be fixed so other indicators were used to determine target position. Reinstalling the STF was very difficult because the flanges between the STF and the vertical water column did not come together when the clamp was tightened. The original clamps and alignment mechanisms were removed and a modified chain clamp was installed on both sides of the latching mechanism between the STF and the vertical water column. This work continued after the shutdown on maintenance days so BL2C startup was delayed by a month and beam production started on May 19. The dose for the STF repairs and the clamping difficulties was 51 mSv to the repair crew and the volunteers with 5 people exceeding the shutdown and sliding quarterly limits.

Strontium-82 production in the STF was very good in 2004 despite the delayed startup. 48.48 Ci were produced from 134.3 mAh in 137 days compared with 41.66 Ci produced from 116.1 mAh in 170 days in 2003. The yields in 2004 with 40 days less operation were similar to 2003 because the 2C beam current was increased to 55–60 μ A. Increased currents were allowed because aligning the STF increased the beam acceptance and extra extraction foils were added in the summer when the cyclotron was raised for inflector repairs. Nine natural rubidium targets were irradiated in 2004 compared with eight targets in 2003. A dose of 180 mAh for 2005 is projected as demand for strontium-82 continues to increase. There were 30 days scheduled for proton therapy on BL2C1 and 42 days scheduled in the proton irradiation facility (PIF) on

BL2C1. PIF operation was compromised because energies above 108 MeV could not be extracted. The BL2C extraction probe and beam line are designed to work from 65 to 120 MeV. It is assumed that the BL2C exit horn beam stop is in the way; this will be corrected in the 2005 shutdown.

A number of meetings were held to discuss the shutdown difficulties and a redesign of the STF. The new STF will be a water vessel with no water joints to be made up in the vault. The target insertion will be done on rails located in the vessel and the insertion mechanism will be removable to the hot cell for MRO. A new vacuum box to facilitate changing the target protect monitor will be attached to the BL2C4 beam line. The beam pipe including the new vacuum vessel will not be attached to the STF water vessel so that the vacuum box can be removed to the vault for servicing. A budget of \$360 K based on the preliminary design has been approved and will be funded by MDS-Nordion.

PROMPT RADIATION HAZARDS

During the 2004 shutdown the electrical room on the B1 level of ISAC was made an interlocked exclusion area. It now must be locked and unoccupied whenever beam line 2A is on. This was necessary because a combination of measurements and calculations had shown that dose rates in that location could exceed the 1 Sv/h policy limit of TRIUMF given a point loss of the total beam for which beam line 2A is licensed. Dose rates at ground level over beam line 2A are within the 1 Sv/h policy limit.

An interim proposal to reliably terminate beam production in response to beamspill, neutron, access, and emergency safety trip conditions was implemented during the 2004 shutdown. Three existing ISIS devices, beamstop 165, the fast target, and components in bend 3/4 were all interlocked to stop beam delivery in response to any of the four trips. The rf system was removed from all safety trips.

A template set of annual area safety unit test procedures was drafted. Specific annual test procedures for each secondary channel area safety unit were written and approved.

There were four safety-critical radiation monitor trips in 2004, but all were associated with power bumps and not with beam delivery.

The operation of the nine safety-critical pairs of radiation detectors was checked on thirty-five maintenance days. No failures were reported.

CONTROLS

Introduction and Summary

The Central Control System (CCS) ran smoothly during 2004. New developments and maintenance were

done as needed. Reliability and performance remained good. The CCS continues to evolve with enhanced functionality and the replacement of aging components, supported in part by the refurbishing program.

The loss of scheduled beam time due to CCS faults during 2004, as recorded by the Operations group, was 11.4 hours. Of this time, 85% was the result of three events: two hardware failures and one software bug. The remaining 1.7 hours were the result of 12 other lesser events. Problems with the site network and the UPS were of concern but did not lead to significant controls downtime.

The goals established in 2003 were mostly attained and numerous unforeseen requirements that arose during 2004 were also met. In the area of planned goals, a number of tasks are worth noting. The hardware and software to support the new ISIS slits, including console support, were completed. Control system support for the rf spark detector was completed for the present state of the detector system. A system to control and display rf power signals was developed and commissioned. In the area of X Window displays, LCD monitors replaced the old CRT displays in the main console and a new X Window terminal configuration capable of replacing the VXT X Window displays is now running smoothly. The old safety touch screen has also been upgraded to this new X Window configuration and it now uses a touch sensitive LCD monitor. An upgrade to OpenVMS version 7.3-2 was done as anticipated. Changing the cyclotron device numbering from octal to decimal is almost completed.

Not all projects were completed as anticipated. The task of decommissioning the old DSSI disk system in the Production Cluster was mostly done but not completed and should be finished during the 2005 shutdown. Work on replacing the old terminal servers also did not progress as well as expected. Work on establishing a reliable terminal server replacement is continuing.

CCS Facilities

Numerous changes were made to the Central Control System hardware. Changes resulted from adding new and removing old equipment, doing regular maintenance, and as a result of trouble shooting problems. An example of a new addition is the crate that was added at the vacuum test stand to support developments. Other areas include items such as cooling tower motor control, inflector power supply control, rf thermocouple readback, M13 gate and window valve control, and correction plate control. One major change, physically removing the development cluster DSSI disks, is now complete. Other disk changes were made including restricting access on the fibre channel

systems and installing new disk drives. An HP Integrity Server using the Intel 64 bit Itanium chip was acquired and set up. To allow this Itanium system to connect to the CCS, a PCI-X to PCI expansion chassis was purchased and configured with the Itanium box.

There were many software developments in the CCS. A few examples are cited here. The safety displays and scans were modified as requested by the Safety group. Further support for the new ISIS slits was provided. The main magnet run up procedure was modified to incorporate new requests from Operations. Important changes were made to the message handling software to allow a better reaction to the message storms that occur when crucial hardware components fail. Changes were also made to most of the major applications in the CCS such as XTpages, Xstrip, the scans, the logged devices, PSU, and Xasset. The standalone rf booster application was normalized by including its functionality in XTpages and some developments were done on dual speed ramping of the ISIS pulser. A significant effort was put into examining improved beam stability by providing feedback with the pulser duty cycle. The goal is to increase stability to beam line 2A and to reduce the number of overcurrent trips. If testing in the new year indicates that improvements to 2A stability can be attained then the software and a standardized user interface will be made operational.

Many CCS users are familiar with the existing system and thumbwheel scheme of specifying a device. A significant effort was put on modifying this cyclotron device numbering system to move from octal numbering to decimal numbering. The related hardware and software components have now been largely changed. A system for simultaneously supporting both numbering systems was established and the phase has been occurring transparently and without interruption.

When problems arose with the quadrupole magnet 1AQ15, a variety of activities took place to support continued running while providing new machine protection.

The computers in the CCS were upgraded to Multi-net version 4.4. To support the new Itanium computer, a field test version of OpenVMS was acquired and a number of applications were ported to this hardware platform. The low level software that does the data acquisition is being ported and modified to support symmetric multi-processing. We expect to have Itaniums in both the development and production clusters and connected to the fibre channel disk systems by the end of next year.

Secondary Beam Lines

There were a number of developments on the secondary beam line controls. A new valve controller for the M20 window and gate valve was built and installed. The backup procedure for the Sun server computers was enhanced. Improvements were made to the control system functionality including such things as a multiplet tuning feature, M11 bender ramping controls, beam line save/restore, new EPICS tools, new display pages, and new scripts. The version of EPICS was upgraded and in the new year the latest build of EPICS will likely be installed.

Other Systems

There are several other areas that also received support during the year. Both the neutron irradiation facility and the proton irradiation facility had changes. The CRM (centre region model) also had activity as the emittance facility was re-activated to support ion source developments. In the new year a variety of other developments are anticipated in the CRM. There were some activities for proton therapy and the environment that supports the dose program for the Safety group was changed to allow more instances.

OPERATIONAL SERVICES

Remote Handling

Cyclotron servicing

Annual remote handling winter shutdown activities for cyclotron maintenance included removal and storage of the interim Cu-blockers, installation of the tank peripheral personnel shadow shields, remote vacuum cleaning, as well as video and tank seal inspection. In the 2004 shutdown the 2C extraction probe and one low energy diagnostics probe were removed for servicing and reinstalled.

Routine maintenance of the elevating system of the cyclotron was performed at the beginning and end of the shutdown. The screw jacks and gear reducers at station #8 were removed for service rebuilding during the year.

During the summer months routine maintenance was performed on the major-use trolleys of the cyclotron servicing system and the remote handling service bridge. High voltage sparking of the ISIS inflector in August required an emergency cyclotron tank lid-up for repair. Two beam stop Cu-blockers in the tank were remotely removed and four others repositioned to reduce personnel exposure during tank access for the inflector removal and repair. The remote handling building access shield door was opened again in September to facilitate vault access for servicing of probes by the Diagnostics group.

The cyclotron elevating system station #8 jacks and gear reducers, which were removed during the winter shutdown, were rebuilt and overhauled. A new, TRIUMF original specification, spare reducer, compatible for either left or right hand operation was acquired from the manufacturer in England. Canadian distribution of this critical TRIUMF component has been discontinued and future supply might be problematic. Replacement reducers from a North American supplier have proven problematic in routine exchange maintenance due to dimensional differences in construction.

Hot cells/targets

In the winter shutdown, the M9 beam blocker was removed for replacement of the vacuum seal gland of the actuator rod. The 1AT1/1AT2 water packages were serviced and the BL2C solid target was brought to the hot cell for repair work and clean-up of the damaged sealing-flange faces.

During the year significant remote handling assistance was provided to the BL2C beam line solid target facility with its hot cell operations. A target mechanism required repair due to bent guide pins on the assembly, Rb targets were loaded into a transport flask, and a 1AT1/1AT2 style resin can was modified for use at the BL2C cooling package. In routine servicing, the BL2C cooling package filters were changed, conductivity cells cleaned, and the resin can to the reservoir lines flushed.

The 1AT2-Mk1 target was serviced in the second quarter. The travel positions of the target cassette were measured and noted, the cassette and profile monitor elevations were changed 3 mm from 1834.5 to 1837.5 mm. The 1AT1-Mk2 target was also serviced with a 4 mm wide by 5 mm high aperture protect monitor replacing the original 5 mm by 5 mm aperture monitor. Target cassette and monitor elevations were changed 2 mm from 1828.0 mm to 1830.0 mm. A "new" (1980 vintage body, 1984 vintage graphite) 2 mm by 45° uncooled pyrolytic graphite target was installed at position #2.

In the spring, work began on three new graphite target assemblies. After production of one target the brazing oven failed and required repair. Of the three targets produced, only one appeared to be satisfactory, the other two evidenced brazing voids in the pyrolytic-to-saddle bond. Redesign of this challenging target production began with Engineering group involvement.

Another rubidium target was swapped in the BL2C hot cell in October with the currently used target-holder float experiencing a weld failure. Again in November a rubidium target was exchanged in the BL2C hot cell. The soda-lime trap on the BL2C cooling package became blocked due to excessive moisture in the trap and required removal for cleaning.

A new graphite target was installed at position #5 on the 1AT1-Mk1 target. Fittings on this ladder are exhibiting signs of wear, causing difficulties in achieving leak-tight joints during target replacements. This target was installed in the beam line in November when the 1AT1-Mk2 target was moved to storage. Subsequent inspection of the Mk2 target in the hot cell noted that the 2 mm 45° graphite target had eroded approximately 0.2 mm back from the top of its 10 mm height.

The BL2C resin can was exchanged due to deteriorating cooling water electrical resistance. Some difficulty was experienced with conductivity and flow in the cooling package and additional adjustment was required before operation could continue. This package will require some rework in the winter shutdown.

A radiation damaged, rubber pneumatic air hose on the M20 beam blocker at 1AT2 ruptured during beam operation in November. These will be replumbed with metal tubing in the winter shutdown.

Another iteration of graphite target brazing was completed in December. Seven graphite targets were produced and look promising before machining. At this same time, as a trial, Diagnostics group requested that we experimentally braze a Ta/Cu/TICUSIL assembly in the oven. This was achieved at 943° C for a 35 minute period. The Ta/Cu bonding was adequate for this use, and could improve with better preparation.

Miscellaneous hot cell facility work included: rebuilding of one air pressure amplifier for the meson hall target areas, dilution and release of 280 l of the 1AT1/1AT2 cooling package water, TNF resin can transfer, thermal cycling tests for the ceramic insulator development program, and barrel scans performed by the Radiation Protection group for active waste disposal. A new target cassette alignment jig (determining beam direction) was also manufactured.

Beam lines servicing

Beam line activities for the winter shutdown centred around the 1AT2 target area. Leak checking with periodic shield block repositioning identified three separate leaks: the 1AT2 target monolith to the former M8 beam line blank-off plate, the collimator B to 1AQ14 joint, and the 1AS1 to 1AM10 vacuum joint. The indium seal at the 1AT2/M20Q1 joint was successfully replaced, and the M20 front-end inspected and documented in preparation for the future M20 refurbishment. The actual location of the M20Q1 ground fault was also determined. Survey of the area revealed a loose connection at an M20Q2 SuperCon electrical connector. This event could have contributed to another catastrophic failure similar to last year's M9Q1 failure. The connector was carefully re-tightened, giving allowance for the radiation damaged materials.

The M9 front-end was uncovered to investigate an

electrical problem at M9Q1. It was eventually determined to be a leaking solder joint at a Pyrotenax end-seal that leaked water into hairline cracks on the insulator beneath. This joint was cleaned and epoxied with a fibreglass reinforcement sleeve.

A vacuum excursion concentrated work on the collimator B to 1AQ14 magnet vacuum leak and its correlation with the electrical buss links solidly mounted to the trench shielding. Heavily loaded shielding causes the magnet to be disturbed by movement of the solid buss links on 1AQ15. The indium joint seal was removed and inspected. A vacuum leak at the M8 blank-off was found to be due to a stripped thread spring eye on one side. This was replaced and a good vacuum achieved.

The work of crumbling block replacement occupied a full five weeks of shutdown. Many crumbling blocks needed to be jack hammered down in size to relieve crumbling expansion pressure against adjacent blocks. Badly crumbled blocks required packaging into metal containers. All suspect "high density" blocks found to be still structurally sound were relocated up from ground level to prevent future standing water damage. Many hand-stack blocks at the south wall opening to the former Bio-Med treatment room were removed and replaced at this time.

Additional shutdown work included new cabling to BSM #61, refastening of the triplet Pyrotenax brackets in the trench, repair of rusted M9/M20 beam blocker control power conduit, re-hosing of the M20 sextupole magnet, installation of new O-rings at Marmion joints in the 1AS2 service chase, repair of a water leak at M9AQ5, replacement of an O-ring at M20Q8, and replacement of the M20VA5 valve. The 1AM10 monitor and monitor smokestack were also replaced after shielding was installed at the area.

Following the major winter shutdown work, activities in the second and third quarter were much quieter, with the majority of effort going into design and planning for the M20 front-end replacement work. New magnet stands, vacuum boxes and remote handling of services were organized for the replacement of the M20Q1/Q2 magnets.

During the mini-shutdown in September a vacuum leak in the 1AVA8 vacuum gate valve between the 1AT1 and 1AT2 volumes required replacement of the all three O-rings.

In the same shutdown a major effort was directed to the 1AQ15 cooling flow problem that was first identified in August. Individual "control" and two problematic circuits were isolated from the magnet cooling header. Tests were performed to determine flow characteristics and found to be significantly lower on the two problematic circuits. As yet unexplained foreign mate-

rial was flushed from both problematic circuits. After both forward and reverse back-flushing of these circuits, flow was greatly improved. Further investigation of the magnet coils revealed an obstruction at the end of circuit #11 coil. This was mechanically opened-up in diameter. Again a foreign substance was removed from the interior of these coils. Further examination of these materials will be performed in the fall. After work was completed on these circuits the magnet was normally replumbed and power tested successfully to run at 917 A as required for the normal beam line 1A 140 μ A beam tune.

Late in the year a decision was made to concentrate the winter 2005 activities on repair of the 1AQ9 magnet thermal switch problem. This decision was taken because the inability to operate this magnet results in higher beam spills downstream, thus further exacerbating radiation damage to 1AVA8 and other organic vacuum seals, as well as some loss of beam tuning beyond this location. This decision will also address the concern of the failed M11 septum magnet, and allow additional time to work on crumbling shielding blocks upstream of 1AT2. Work progressed toward preparation for the new work, with as little impact as possible on the continued effort to complete refurbishment of the M20 front end.

Magnets and Power Supplies

Most of the work in 2004 related to MRO activities in support of the cyclotron, primary and secondary beam lines, and the ISAC facility. Copper chill plates for heat sinks in the series regulated power supplies are being installed to replace leaking pass banks as in previous years. As last year, we prepared trim and harmonic supplies which had to be modified for trim and harmonic bay 1 which will be brought up to code during the spring, 2005 shutdown.

Power supplies for ISAC were purchased for the S-bend dipole supplies as well as some quadrupole supplies for ISAC-II straight section. Further units are to be purchased once the budget is finalized.

Experimental support was provided in the repair of a laser power supply in the ISAC-I laser shack. This was necessary to allow the developmental work to proceed.

A new power supply engineer has joined the group to replace a retiree and is providing good support as he becomes familiar with the existing system. Documentation upgrades are under way which will facilitate trouble shooting and data management.

As part of his workload the group leader also provides coordination of meson hall activities during the winter and fall shutdowns.

Mechanical Services

Efforts to improve the reliability of breathable compressed air met with success with the modifications made to the hand-me-down Sullair compressor (ex-MRS compressor) that fixed a few problems. With the addition of the new breathable-air-monitor air dryer (thanks to ISAC-II) the compressor has passed the breathable air certification and is now acting as a backup site machine. Its large capacity was obtained for a fraction of the cost of a new machine. Until the Sullair was proven to be reliable, the existing Nash compressor was directly connected to the chemistry annex and shown to be capable of running that building by itself. At present the Nash now acts as a backup for the Chemistry Annex. Another new development of note is the new services umbilical installed into a trench between the proton hall extension and the main office building (MOB). When connected it will provide CuLCW to the MOB, along with electrical and control functions. Lastly in compressed air, the MOB air dryer was repaired.

Piping MRO work included replacement of corroded heating water lines in the MOB and Chemistry Annex and city water lines in the service annex. Repairs were undertaken for the sprinkler system, the CuALCW de-ionizing resin, the rf room piping hangers, the rf vault transmission line pressure regulating valve, and the M15 vacuum pump exhaust line.

HVAC MRO work included air conditioning repairs to the MOB board room, AHUs 1 and 5, trailers Gg and Hh, Me140 and 141 pneumatic controls, and the MESA clean room buffalos. An air conditioning duct was attached to the rf floor UPS for direct cooling. The MOB kitchen fan exhaust stack was raised to 15 feet to help reduce cooking smells in the building.

Several meson hall lifting beams were sent out for testing and recertification.

Electrical Services

The centrepiece of the design and engineering effort continued to be the ISAC project and is covered under a separate heading. On the rest of the site, priority was placed on the implementation of the re-design of the power distribution for the Trim Coil Bay 4, the completion of the VFD addition (phase 2) to the cyclotron cooling towers, the supply of emergency power for M15 cryogenic loads, and the phase out of the old CP42 UPS unit. All radioisotope production facilities UPS loads were integrated under the TR30-2 UPS machine installed in 2003. In all about 48 entries of various importance were logged in the engineering log-book of which about 30 belonged to ISAC. Other completed jobs include rationalization of services in the MHESA detector laboratory, services for a new crane in the me-

son hall extension clean room and TR13 nearby, services for a new elevator in TR30-2, and conduit services for the TSG in the vault area. Continuing engineering support was provided to TRIUMF users on electrical matters, and to Nordion and the ATG group for maintaining electrical services for the isotope production facilities. The upgrade of the rf system distribution system was postponed as spare breakers were finally located in the United States.

Typical maintenance activities included servicing lighting systems, motors and associated controls, air conditioning controls, panel boards and transformers, HV switchgear, breakers and capacitor banks, and the fire alarm system. A dedicated electrical crew looks after the electrical installation and maintenance needs of Nordion and the radiochemistry isotope production facilities. Approximately 130 calls were answered from the rest of the site (about 35 from ISAC-I) for other than lighting maintenance. Motors for about 120 HP total were replaced. The fire alarm system annual inspection, carried out during the summer, revealed a few deficiencies that needed attention. Early last March the main emergency power centre, MCC-B suffered the first short circuit of its life when minuscule water infiltration from a conduit run above found its way into the unit. The short circuit occurred on the line side of the breakers. As a result the whole MCC-B tripped leaving the UPS without its natural power back-up. The short circuit destroyed the two breakers feeding the substation main protection breaker relays and caused significant damage to nearby cubicles. The repair was carried out expeditiously, but the source of the water could not be located. The fault also revealed a weakness in the distribution wiring to the UPS for such rare events like this fault that shuts down the emergency power bus while the normal power bus remains functional. To protect against these rare events we plan to add a second feeder line from the normal power bus at the next opportunity.

As equipment ages it becomes crucial to keep up with technology changes. This year brought to light the question of maintainability and reliability of the UPS and spare parts for the power distribution centres. Both are strategically important to the continuing operation of the experimental program. A strategy was developed to cope with this problem and start phasing out obsolete power distribution centres this fiscal year. In addition to increased trouble calls, the main UPS suffered a couple of serious faults, one of which was associated with early battery wear. Plans are under way to replace this unit in the near future.

Power delivery

Power delivery continued to be very reliable without major unscheduled outages. In early fall the site

was shut down to allow for the replacement of a damaged power pole and cracked HV insulators.

Scheduling coordination with Power Tech High Voltage laboratory continued regularly to ensure that the impact on our operation from their short circuit tests is minimized.

The monthly averaged peak power demand increase was more contained this year. It was a mere 2.7% from 7358 to 7560 kVA (Fig. 202). The annual maximum peak demand (8914 kVA) was reached in July and was 2.4% higher than the maximum last year. The electricity consumption jumped about 3.5% from 56.4 GWh to 58.4 GWh (Fig. 203). The largest monthly

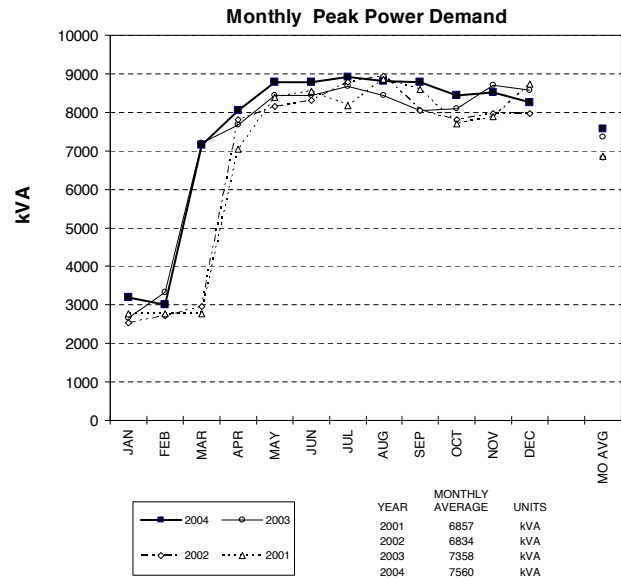


Fig. 202. Monthly peak power demand – four year comparison.

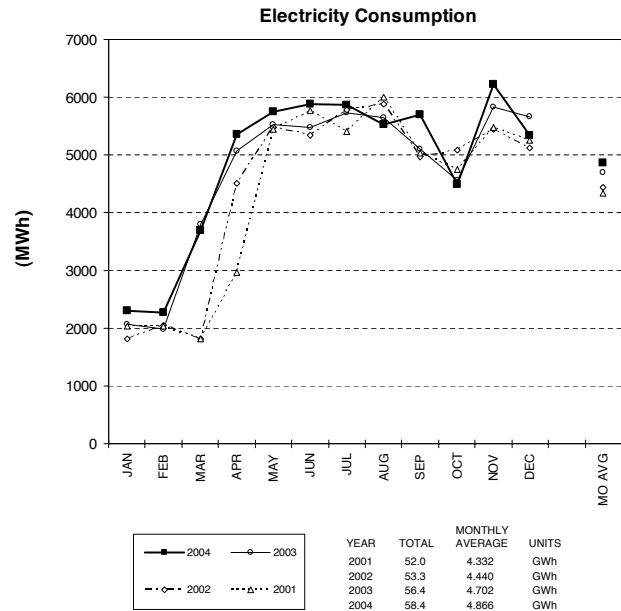


Fig. 203. Electricity consumption – four year comparison.

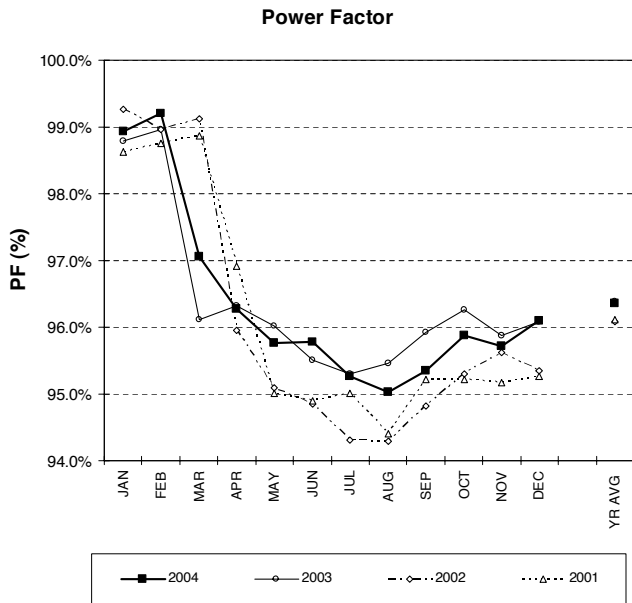


Fig. 204. Electrical system power factor – four year comparison.

consumption was recorded in November (6.22 GWh) and was approximately 6.6% larger than last year's maximum. These increases are in line with the increased activities in both ISAC (primarily ISAC-II) and Nordion.

The power factor (PF), averaged over the calendar year, remained flat at 96.4% (Fig. 204) despite increased activities. This effect can be attributed to the work of the additional capacitor banks in ISAC. The average load duration – the indicator of how well we use our power demand – has increased just slightly by 1.6% to 88.1% (Fig. 205).

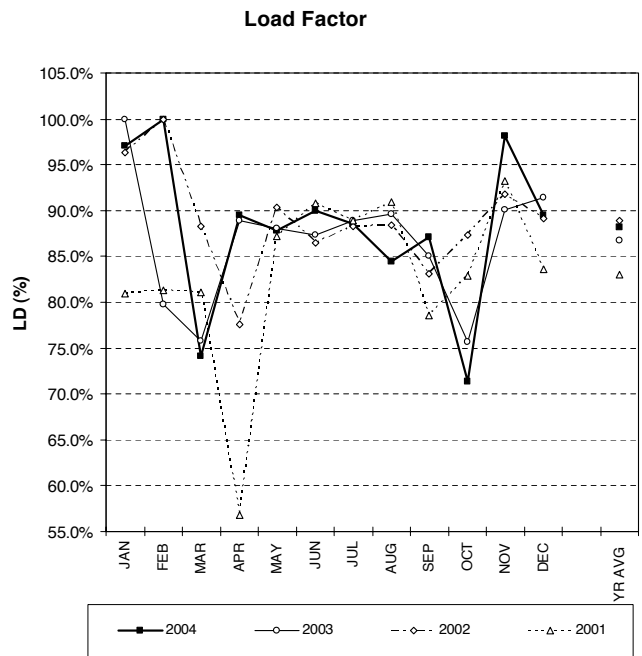


Fig. 205. Electrical system load duration – four year comparison.

ISAC DIVISION

INTRODUCTION

The following ISAC sections describe the various activities in ISAC-I operation, ISAC-I developments and the progress in ISAC-II during 2004. Although there have been many highlights during the year, only a few are outlined here. The availability of the first target station to be commissioned (ITW) was remarkably near 90%, whereas the newer target station (ITE) was only 50%, reflecting the fact that ITE was used extensively for developing high power targets and an ECR ion source. Nine different targets were installed during the year (four Ta, three SiC, one CaZrO₃ and one ZrC). Several were compromised as a result of damage caused by the proton beam. The on-line testing of the ECR ion source has shown that the design must be modified to provide better ionization efficiencies in the high gas environment from the target. The charge state booster was used to examine the charge distribution of various species. A resonant laser ion source was used to provide a beam of ⁶²Ga from a SiC target. Development work during the year focused on developing schemes to provide laser-ionized beams of Al and Ga. In ISAC-II, all of the medium beta superconducting rf cavities have been fabricated, chemically treated and are now at TRIUMF. Two cryomodule tanks have been delivered to TRIUMF. Most of the liquid helium plant has been delivered to ISAC, is being installed, and commissioning will begin early in 2005. Good progress is being made on achieving adequate cavity tuning and rf coupling. Components required for the S-bend HEBT connecting the ISAC-I DTL to the ISAC-II medium beta accelerator are ready for installation during the 2005 winter shutdown. The ISAC-II installation schedule predicts that the medium beta section should be completed in time to accelerate a beam from the DTL through five cryomodules by the end of 2005.

ISAC OPERATIONS

This year, routine RIB operation provided beams to DRAGON and TUDA in the high energy area and to low energy experiments at LTNO, 8 π , GPS1-3, BNMR and Osaka. As in previous years, the first quarter was devoted to shutdown activities. Beam schedule 105 began in the second quarter and carried on through the summer. Beam schedule 106 followed a short shutdown in September. An overview of RIB operation is shown in Fig. 206 in terms of the weekly proton beam exposure of the production targets. The total proton exposure is given for each target. The hours of RIB and stable beam operation for schedules 105 and 106 are shown in Figs. 207–210.

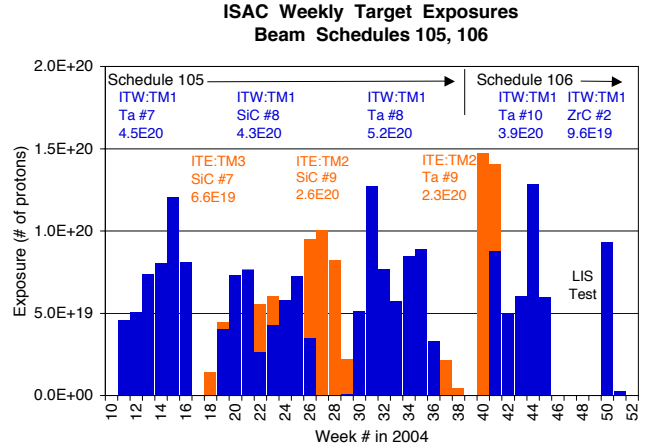


Fig. 206. Integral target exposures by week for RIB delivery in 2004.

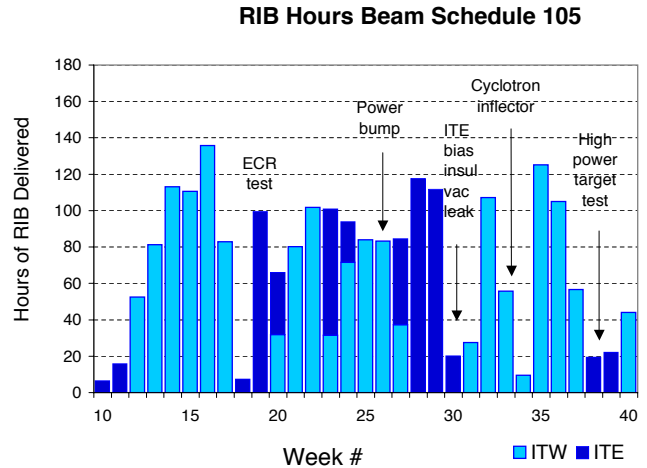


Fig. 207. Weekly hours of RIB beam available to experiments during schedule 105.

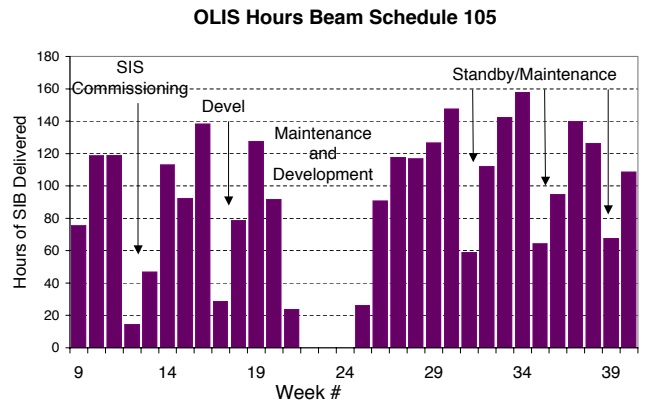


Fig. 208. Weekly hours of stable beam available to experiments during schedule 105.

RIB Hours Beam Schedule 106

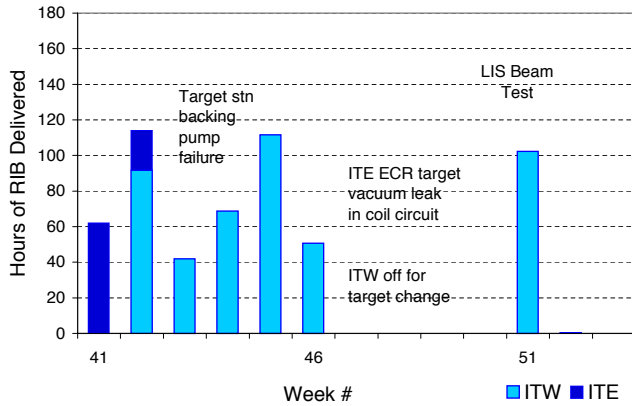


Fig. 209. Weekly hours of RIB beam available to experiments during schedule 106.

OLIS Hours Beam Schedule 106

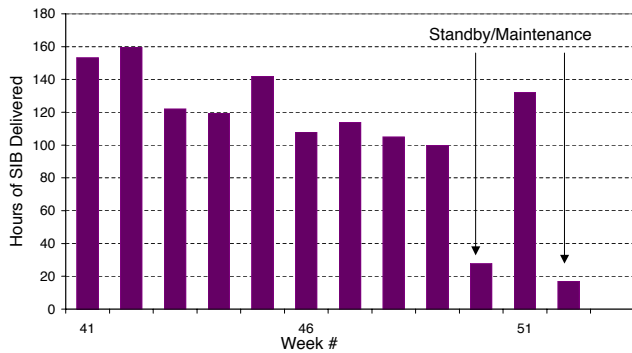


Fig. 210. Weekly hours of stable beam available to experiments during schedule 106.

Operational performance statistics are provided for the ISAC beam production of RIB from ITW and ITE and stable beam from OLIS. These are summarized separately for each beam schedule in Tables XXIX–XL. The summary performance statistics are given in Table XLI. Here it can be seen that 89.2% availability for ITW reflects its nature as a fully commissioned target station, whereas the 50.6% availability for ITE operation reflects the reality of the challenges of commissioning the ECR and high power targets. This summary information includes the effects of experiment operational performance, ISAC system performance and the availability of proton beam from the cyclotron and also includes overhead as well as downtime components. Some interpretation is required to extract the relevance of beam time in the context of operational constraints not accounted for during beam scheduling. This year, several targets were damaged during operation resulting in lower yields and consequently RIB rates to users much less than expected when the beam time was scheduled. There is no easy way to represent this in the performance statistics, other than to acknowledge the fact that yields were low and there

was evidence of target damage. The target damage likely occurred due to a mismatch between the delivered power density of the proton beam compared to that estimated for setting the target operating parameters, the most critical being the central temperature. Efforts are under way to understand and remedy these problems. On the other hand, the ISAC systems were for the most part very reliable. There were only a few notable exceptions. Power outages in week #26 that affected cyclotron availability, a vacuum leak in a HV insulator damaged by sparking that was caused by a water leak in the HV enclosure on top of the east target station in week #30, and finally, a vacuum leak from a coil cooling circuit on TM3 caused the cancellation of ECR operation in November.

A major milestone was achieved in the last weeks of beam schedule 106 when the first RIB operation with a laser ion source was demonstrated.

The summary of beam to experiments for the year is given in Table XLII, and the summary of the isotopic beam delivery is given in Table XLIII.

Two new operators, who had been recruited in October, 2003, completed their training and assumed shift responsibilities in May, 2004, bringing the complement of shift operators to six which is still inadequate to properly serve the needs of a challenging science program at a multiple source RIB facility. The sixth operator provided support for afternoon activities Monday to Friday and filled in for operator absences.

Several new Web based applications were introduced, including a new e-log, NCR (non-conformance report) and revised electronic work permit system. A number of operator environment tools were developed including: improved tuning and save routines, segregated strategic alarm handling, electrostatic steering optimization program, IBRMS bridge display, and fire-wall protection of the ISAC Operations network. Applications and assistance were also provided for the TRILIS and SCRF projects. The ISAC-II control room was equipped with one off-line work station which was used for development purposes.

Documentation and training responsibilities continue to command the full-time attention of the ISAC Operations Documentation and Training Coordinator. After the training of the new operators was completed in April, work resumed on the design phase of the SAT program, which was completed and approved. The development phase will carry over into 2005. Learning objectives were established for all of the previously recorded training videos; an important aspect of the evaluation phase of SAT.

The members of the ISAC Operations group take great pride in their contributions to the successes of the experiments and major ISAC milestones that have

been highlighted elsewhere in this Annual Report. In the coming year, in addition to providing beam for the scheduled experiments and performing systems maintenance, the major effort will be to complete the SAT training program for ISAC operators, migrate many

of the control functions to the ISAC-II Control Room, and continue to improve the ability of ISAC Operations to provide the beams of interest to the ISAC science program.

Table XXIX. ITW beam schedule 105 (surface ion source targets used: Ta #7/8/10 and SiC #8): February 23 – October 4 (weeks 9–40). ITW beam to ISAC experiments (hours).

Expt	Line	Sched	Actual	Tune	Off	Total
Yield	ILY	426	64.4	2.8	0.0	67.2
ICS	ICS	0	1.7	0.0	0.0	1.7
E816	β -NMR	156	0.0	0.0	0.0	0.0
E817	β -NMR	348	270.6	15.4	16.2	302.2
E824	DRAGON	78	22.4	2.9	2.6	27.9
E871	Osaka	192	191.8	0.9	9.8	202.5
E903	Osaka	264	119.6	10.4	0.0	130.0
E909	8π	95	76.3	1.9	6.3	84.5
E920	Polarizer	120	41.7	0.0	0.3	42.0
E921	8π	156	138.7	0.4	19.8	158.9
E973	8π	276	170.0	1.0	6.5	177.5
E984	8π	96	67.9	7.2	3.4	78.5
E989	DRAGON	288	173.0	5.4	1.9	180.3
E991	GPS3	156	81.2	2.3	3.5	87.0
LIS	IMS	180	44.1	0.0	0.0	44.1
Subtotals		2831	1463.4	50.6	70.3	1584.3
Available					44.0	44.0
Totals		2831	1463.4	50.6	114.3	1628.3

Total RIB experiment time = 1628.3 hours
 Combined facility efficiency = 92.9%

Table XXX. ITW beam schedule 105: ITW systems downtime and overhead.

ISAC systems	Hours
<u>Downtime – unscheduled</u>	
Beam lines	1.3
Controls	30.2
Elec P/S	5.1
Mag P/S	0.5
RF controls	2.0
Ion source	45.8
Polarizer	21.9
Safety	0.2
Site power	17.4
Subtotal	124.4
<u>Downtime – scheduled (overhead)</u>	
Cyclotron maintenance	255.8
Cyclotron development	83.4
Beam line 2A off	389.0
ISAC shutdown	168.0
ISAC idle	347.8
Procedures	510.3
Target conditioning	435.5
Target change	1375.9
ITW startup	24.9
ITW cooldown	31.5
Q-exch stripper	0.2
Subtotal	3622.3
Total	3746.7

Table XXXI. ITE beam schedule 105: ITE beam to ISAC experiments (hours).

Expt	Sched	Actual	Tune	Off	Total
Yield	444	57.9	1.3	0.3	59.5
ICS	0	6.5	0.0	0.0	6.5
E816	144	178.7	6.8	2.0	187.5
E824	120	57.6	5.7	0.0	63.3
E984	0	0.0	0.0	0.0	0.0
E985	168	189.4	2.6	13.8	205.8
E989	96	7.8	2.7	0.8	11.3
E991	36	0.0	0.0	0.0	0.0
E995	0	15.4	0.0	0.5	15.9
Totals	1008	513.3	19.1	17.4	549.8

Total RIB experiment time = 593.2 hours
 Combined facility efficiency = 74.1%

Table XXXII. ITE beam schedule 105: ITE systems downtime and overhead.

ISAC systems	Hours
<u>Downtime – unscheduled</u>	
Beam lines	4.0
Controls	10.2
Elec P/S	65.6
Ion source	108.3
Pre-buncher	3.6
DTL rf	0.3
Services	4.5
Site power	0.5
Vacuum	9.9
Subtotal	206.9
<u>Downtime – scheduled (overhead)</u>	
Cyclotron maintenance	86.9
Cyclotron development	36.0
Beam line 2A off	49.5
ISAC development	175.4
ISAC idle	1133.5
ISAC maintenance	20.3
Procedures	273.9
Shutdown	114.3
ITE startup	37.5
ITW cooldown	48.5
Target change	1890.5
Conditioning	708.4
Q-exch stripper	0.2
Subtotal	4574.9
Total	4781.8

Table XXXIII. OLIS beam schedule 105: OLIS beam to ISAC experiments (hours).

Expt	Sched	Actual	Tune	Off	Total
E824	48	6.1	1.0	0.0	7.1
E893	0	0.0	2.3	0.0	2.3
E903	12	1.3	0.5	0.0	1.8
E920	36	9.5	2.8	0.1	12.4
E927	168	43.2	6.5	6.9	56.6
E947	360	238.0	8.7	0.2	246.9
E952	575	385.3	29.8	4.2	419.3
E989	72	84.1	10.5	6.8	101.4
E991	144	78.2	4.7	0.9	83.8
Polarizer	48	95.9	0.0	0.5	96.4
DRAGON	144	96.4	4.8	1.8	103.0
Totals	1607	1038.0	71.6	21.4	1131.0

Total IB experiment time = 2768.1 hours

Combined facility efficiency = 93.1%

Table XXXIV. OLIS beam schedule 105: OLIS systems downtime and overhead.

ISAC systems	Hours
<u>Downtime – unscheduled</u>	
Controls	11.8
Beam lines	5.4
Elec PS	5.0
Magnet PS	26.7
RF controls	3.4
RFQ	0.5
DTL rf	23.7
MEBT rf	18.7
Site power	9.1
Vacuum	19.0
Ion source	81.5
Subtotal	204.8
<u>Downtime – scheduled (overhead)</u>	
ISAC maintenance	175.2
ISAC idle	419.9
ISAC shutdown	540.5
ISAC startup	111.0
ISAC development	702.7
Procedures	419.4
Q-exch stripper	33.4
Subtotal	2402.1
Total	2606.9

Table XXXV. ITW beam schedule 106 (surface ion source targets used: Ta #10 and ZrC #2): September 29 – December 29 (weeks 41–53). ITW beam to ISAC experiments (hours).

Expt	Line	Sched	Actual	Tune	Off	Total
Yield	ILY	168	21.4	0.3	0.0	21.7
E823	8 π	132	86.2	0.0	0.0	86.2
E893	LTNO	97	53.3	0.6	0.0	53.9
E956	LTNO	156	93.3	0.2	0.2	93.7
E991	GPS3	0	89.8	0.5	0.8	91.1
E1008	8 π	216	78.8	2.5	0.0	81.3
Subtotals		769	422.8	4.1	1.0	427.9
Available					39.4	39.4
Totals		769	422.8	4.1	40.4	467.3

Total RIB experiment time = 467.3 hours
 Combined facility efficiency = 78.5%

Table XXXVI. ITW beam schedule 106: ITW systems downtime and overhead.

ISAC systems	Hours
<u>Downtime – unscheduled</u>	
Controls	3.8
Ion source	20.5
Services	21.3
Site power	2.5
Vacuum	80.0
Subtotal	128.1
<u>Downtime – scheduled (overhead)</u>	
Cyclotron maintenance	115.0
Cyclotron development	50.4
Beam line 2A off	81.4
ISAC maintenance	8.0
ISAC development	112.0
ISAC shutdown	288.0
ISAC idle	417.8
Procedures	149.9
Target conditioning	109.9
Target change	247.3
ITW startup	6.2
ITW cooldown	3.7
Subtotal	1589.6
Total	1717.7

Table XXXVII. ITE TM3 beam schedule 106 (Ta #4 target with ECR source and gases; commissioning and development of new facility): ITE beam to ISAC experiments (hours).

Expt	Line	Sched	Actual	Tune	Off	Total
Yield	ILY	24	11.7	0.0	0.0	11.7
E991	GPS3	288	53.9	10.3	1.4	65.6
GPS	GPS1	24	0.0	0.0	0.0	0.0
Subtotals		336	65.6	10.3	1.4	77.3
Available					7.1	7.1
Totals		336	65.6	10.3	8.5	84.4

Total RIB experiment time = 84.4 hours

Combined facility efficiency = 15.6%

Table XXXVIII. ITE TM3 beam schedule 106: ITE systems downtime and overhead.

ISAC systems	Hours
<u>Downtime – unscheduled</u>	
Controls	0.8
Ion source	428.0
Safety	0.5
Vacuum	26.0
Subtotal	455.3
<u>Downtime – scheduled (overhead)</u>	
Cyclotron maintenance	28.0
Cyclotron development	24.0
Beam line 2A off	43.0
ISAC maintenance	60.5
ISAC idle	465.3
Procedures	43.0
Shutdown	288.0
Target change	693.5
Subtotal	1645.3
Total	2100.6

Table XXXIX. OLIS beam schedule 106: OLIS beam to ISAC experiments (hours).

Expt	Line	Sched	Actual	Tune	Off	Total
E893	LTNO	12	0.7	0.0	0.0	0.7
E909	8 π	0	3.5	0.0	0.0	3.5
E920	Polarizer	120	48.5	0.0	0.0	48.5
E952	DRAGON	108	42.1	3.9	2.3	48.3
E972	Polarizer	84	46.6	0.9	0.0	47.5
E989	DRAGON	30	6.9	0.0	0.0	6.9
E991	GPS3	276	60.4	2.3	0.0	62.7
E1029	TUDA	36	4.2	0.6	0.5	5.3
DRAGON	DRAGON	121	78.5	4.3	2.6	85.4
8 π	8 π	0	4.0	0.0	0.0	4.0
Laval	HEBT	228	172.7	0.3	8.0	181.0
Yen	HEBT	12	5.7	0.0	0.0	5.7
Subtotals		1027	473.8	12.3	13.4	499.5
Available					800.2	800.2
Totals		1027	473.8	12.3	813.6	1299.7

Total OLIS experiment time = 1299.7 hours
 Combined facility efficiency = 96.4%

Table XL. OLIS beam schedule 106: OLIS systems downtime and overhead.

ISAC systems	Hours
<u>Downtime – unscheduled</u>	
Controls	7.3
Elec PS	4.2
RF controls	6.9
Pre-buncher	0.3
RFQ	2.8
DTL rf	18.4
Services	6.3
Vacuum	0.3
Ion source	2.2
Subtotal	48.7
<u>Downtime – scheduled (overhead)</u>	
ISAC maintenance	50.5
ISAC idle	94.7
ISAC shutdown	288.0
ISAC development	130.8
Procedures	271.1
Q-exch stripper	1.5
Subtotal	836.6
Total	885.3

Table XLI. Summary of overall performance for 2004.

	Schedule 105	Schedule 106	2004
ITW	92.9%	78.5%	89.2%
ITE	74.1%	15.6%	50.6%
OLIS	93.1%	96.4%	94.1%

Table XLII. Summary of beam to experiments for 2004.

Expt	Line	Sched	Beam	Tune	Off	Perf	Type
E816	β -NMR	300	178.7	6.8	2.0	63%	RIB
E817	β -NMR	348	270.6	15.4	16.2	87%	RIB
E823	8π	132	86.2	0.0	0.0	65%	RIB
E824	DRAGON	198	80.0	8.6	2.6	46%	RIB
E871	Osaka	192	191.8	0.9	9.8	100%	RIB
E893	LTNO	97	53.3	0.6	0.0	56%	RIB
E903	Osaka	264	119.6	10.4	0.0	49%	RIB
E909	8π	95	76.3	1.9	6.3	89%	RIB
E920	Polarizer	120	41.7	0.0	0.3	35%	RIB
E921	8π	156	138.7	0.4	19.8	100%	RIB
E956	LTNO	156	93.3	0.2	0.2	60%	RIB
E973	8π	276	170.0	1.0	6.5	64%	RIB
E984	8π	96	67.9	7.2	3.4	82%	RIB
E985	8π	168	189.4	2.6	13.8	100%	RIB
E989	DRAGON	384	180.8	8.1	2.7	50%	RIB
E991	GPS3	480	224.9	13.1	5.7	51%	RIB
E995	ICS	0	15.4	0.0	0.5	100%	RIB
E1008	8π	216	78.8	2.5	0.0	38%	RIB
GPS	GPS1	24	0.0	0.0	0.0	0%	RIB
ICS	ICS	0	8.2	0.0	0.0	100%	RIB
Yield	ILY	1062	155.4	4.4	0.3	15%	RIB
8π	8π	0	4.0	0.0	0.0	100%	SIB
DRAGON	DRAGON	265	174.9	9.1	4.4	71%	SIB
E824	DRAGON	48	6.1	1.0	0.0	15%	SIB
E893	LTNO	12	0.7	2.3	0.0	25%	SIB
E903	Osaka	12	1.3	0.5	0.0	15%	SIB
E909	8π	0	3.5	0.0	0.0	100%	SIB
E920	Polarizer	156	58.0	2.8	0.1	39%	SIB
E921	8π	0	0.0	0.0	0.0	0%	SIB
E927	TUDA	168	43.2	6.5	6.9	34%	SIB
E947	DRAGON	360	238.0	8.7	0.2	69%	SIB
E952	DRAGON	683	427.4	33.7	6.5	68%	SIB
E972	Polarizer	84	46.6	0.9	0.0	57%	SIB
E989	DRAGON	102	91.0	10.5	6.8	100%	SIB
E991	GPS3	420	138.6	7.0	0.9	35%	SIB
E1029	TUDA	36	4.2	0.6	0.5	15%	SIB
Laval	HEBT	228	172.7	0.3	8.0	79%	SIB
LIS	IMS	180	44.1	0.0	0.0	25%	SIB
Polarizer	ILE2	48	95.9	0.0	0.5	100%	SIB
Yen	HEBT	12	5.7	0.0	0.0	48%	SIB

Table XLIII. Isotopic beam delivery for 2004.

TIS nuclide	Hours	OLIS nuclide	Hours
${}^6\text{Li}$	79.0	${}^6\text{Li}$	97.1
${}^8\text{Li}$	516.4	${}^7\text{Li}$	59.9
${}^9\text{Li}$	58.2	${}^{12}\text{C}$	626.8
${}^{11}\text{C}$	20.4	${}^{12}\text{C}^{3+}$	41.8
${}^{11}\text{Li}$	219.2	${}^{14}\text{N}$	17.8
${}^{12}\text{C}$	1.5	${}^{16}\text{O}^{4+}$	4.5
${}^{18}\text{Ne}$	177.5	${}^{19}\text{F}$	124.1
${}^{19}\text{Ne}$	5.7	${}^{20}\text{Ne}$	43.2
${}^{20}\text{Na}$	145.7	${}^{21}\text{Ne}$	151.9
${}^{21}\text{Al}$	7.8	${}^{21}\text{Ne}^{5+}$	172.7
${}^{21}\text{Na}$	81.8	${}^{23}\text{Na}^{6+}$	66.4
${}^{22}\text{Na}$	1.7	${}^{26}\text{Mg}$	40.7
${}^{23}\text{Ne}$	2.8	${}^{28}\text{Si}^{7+}$	6.9
${}^{24}\text{Ne}$	3.4	${}^{139}\text{La}$	42.1
${}^{26g}\text{Al}$	176.0	${}^{141}\text{Pr}$	15.9
${}^{26}\text{Na}$	145.4		
${}^{27}\text{Na}$	42.3		
${}^{62}\text{Ga}$	84.4		
${}^{63}\text{Ga}$	0.5		
${}^{64}\text{Ga}$	0.3		
${}^{65}\text{Ga}$	0.2		
${}^{66}\text{Ga}$	0.8		
${}^{69}\text{Ga}$	44.1		
${}^{79}\text{Rb}$	53.3		
${}^{80}\text{Rb}$	93.3		
${}^{130}\text{La}$	2.2		
${}^{134}\text{La}$	39.5		
${}^{156}\text{Ho}$	170.0		
${}^{170}\text{Tm}$	20.0		
${}^{172}\text{Lu}$	37.5		
${}^{174}\text{Tm}$	67.4		
${}^{178}\text{Lu}$	13.1		
${}^{174}\text{LuO}$	0.7		
${}^x\text{Ga}$	11.4		
${}^x\text{Li}$	21.7		

The target hall and hot cell operations have become quite well organized. The services in the west MAA were redone to the standard that was set in the east MAA. Careful planning is required to be able to manage the service requirements of the off-line target station during brief maintenance periods in the beam schedule. There were eight target changes done this year, involving all three of the commissioned target modules. Each target change was completed as planned

and without incident. In post-operation inspections, three targets were found to have evidence of beam damage: Ta #7 had a hole in the side of the cassette at the central support; Ta #8 had material damage without breach along the side of the cassette; and Ta #9, a high power cassette, had three holes in the front and rear faces. The history of operation of ISAC production targets for 2004 is given in Table XLIV.

Table XLIV. ISAC target history for 2004.

Target ID	In Date	Out Date	Exposure # of protons	Power $\mu\text{A h g/cm}^2$	Comments
ITW:TM1:Ta #7	09-Mar-04	28-Apr-04	4.53×10^{20}	568,915	28.22 g/cm ² Ta in the form of 680×0.025 mm foils. Yield low, <i>p</i> -beam had not been centred; hole at cassette support.
ITE:TM3:SiC #7	20-Apr-04	17-Jun-04	6.56×10^{19}	60,373	20.69 g/cm ² SiC in the form of 460 × 0.26 mm SiC on 0.13 mm C disks.
ITW:TM1:SiC #8	05-May-04	08-Jul-04	4.25×10^{20}	338,864	17.9 g/cm ² SiC in the form of 375 × 0.26 mm SiC on 0.13 mm C disks.
ITE:TM2:SiC #9	17-Jun-04	11-Aug-04	2.64×10^{20}	205,257	17.5 g/cm ² SiC in the form of 680 × 0.025 mm foils. Excessive sparking – small external water leak at TGTHTTR connection.
ITW:TM1:Ta #8	13-Jul-04	15-Sep-04	5.20×10^{20}	504,438	21.79 g/cm ² Ta in the form of 525 × 0.025 mm foils. Evidence of beam hitting along side of cassette. No holes.
ITE:TM2:Ta #9	18-Aug-04	27-Oct-04	2.26×10^{20}	219,359	21.79 g/cm ² Ta in the form of 525 × 0.025 mm foils. High power cassette, yields dropped significantly during operation. Beam too dense – 3 holes in front and rear faces of target.
ITW:TM1:Ta #10	21-Sep-04	18-Nov-04	3.87×10^{20}	374,984	21.79 g/cm ² Ta in the form of 525 × 0.025 mm foils.
ITE:TM3:CaZrO ₃ #2	01-Nov-04	26-Nov-04	0	0	1.21 g/cm ² Ca + 2.76 g/cm ² Zr + 0.48 g/cm ² O 6 cm length of CaZrO pellets. No beam due to vacuum leak in ECR coil cooling.
ITW:TM1:ZrC #2	02-Dec-04	02-Feb-05	9.60×10^{19}	90,801	21.25 g/cm ² Zr + 5.79 g/cm ² C in the form of 200 ZrC + C composite foils.

ISAC ION SOURCES

Operation of the 2.45 GHz ECRIS at ISAC

A 2.45 GHz ECRIS was built at TRIUMF for on-line applications at the ISAC facility. The source cavity is a single mode TE₁₁₁ that operates at 2.45 GHz. In order to avoid large containment time the plasma volume is limited using a 12 mm diameter quartz tube located at the centre of the cavity [Jayamanna *et al.*, Rev. Sci. Instrum. **73**(2), 792 (2002)]. Figure 211 shows a drawing of the ECR ion source and target assembly. The quartz tube lies in the centre of the plasma chamber. The electron cyclotron resonance (ECR) ion source has the following characteristics:

- 2.45 GHz operating frequency,
- Single mode cavity,
- Radial injection of the radio frequency (rf) power,
- No radial magnetic field confinement,
- The axial magnetic field confinement is very shallow. (The magnetic field longitudinal distribution is superimposed onto the mechanical drawing in Fig. 211.)

In May on-line tests with a SiC target were undertaken. The goal was to produce ¹⁸Ne for a high precision half-life determination. The ECRIS was operated with the same tune developed during the off-line tests, where a 2% neon ionization efficiency was obtained. A

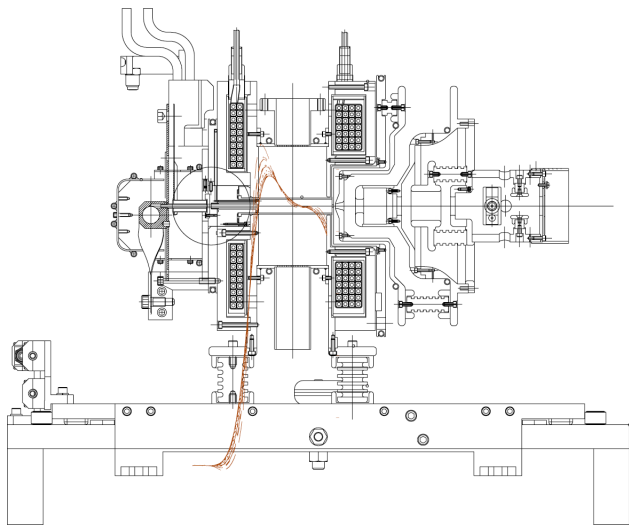


Fig. 211. Drawing of the ECR and target assembly as installed on the tray at the bottom of the target module.

flow of 1 SCCM helium was used as the support gas. The ^{18}Ne yield was measured with $1\ \mu\text{A}$ to $5\ \mu\text{A}$ and followed the proton beam. Above $7\ \mu\text{A}$ the yield did not increase and at $10\ \mu\text{A}$ it was lower than at $5\ \mu\text{A}$. The on-line neon ionization efficiency was measured and it decreased from 1% at $5\ \mu\text{A}$ to 0.05% at $10\ \mu\text{A}$.

Furthermore, due to carbon coating of the quartz liner in the plasma chamber, the ECRIS had to run with an Ar-He mixture. The Ar provides a way to reduce the carbon coating on the quartz tube. Unfortunately, the addition of Ar also reduces the ionization efficiency by a factor 3. Figure 212 shows the trend of the ^{18}Ne yield as a function of the proton beam current on target. The dots and squares represent the measured ^{18}Ne yield when the ECRIS was operating with He. The sudden drop at $6\ \mu\text{A}$ corresponds to the addition of the Ar with He as support gas. We then reduced the amount of injected gas into the ECR. We then changed the support gas from He to Ar. In those conditions we were able to operate the ECRIS with a proton beam up to $30\ \mu\text{A}$ on the SiC target and the ^{18}Ne yield just scaled with the proton beam. The open dots and squares in Fig. 212 show the ^{18}Ne yield when we were operating the ECRIS with only 0.003 SCCM Ar.

During the on-line run we observed that the ionization efficiency was dropping significantly when the proton beam was increased to $10\ \mu\text{A}$. We changed the support gas from 1 SCCM of He to 0.003 SCCM of Ar only and we were able to maintain the ionization efficiency relatively constant up to $30\ \mu\text{A}$, which is the nominal beam current we can run on the SiC target.

An on-line run was scheduled in November but unfortunately a water leak in one of the coil cooling circuits was found. The leak rate was such that it was impossible to operate the ion source. An extensive search

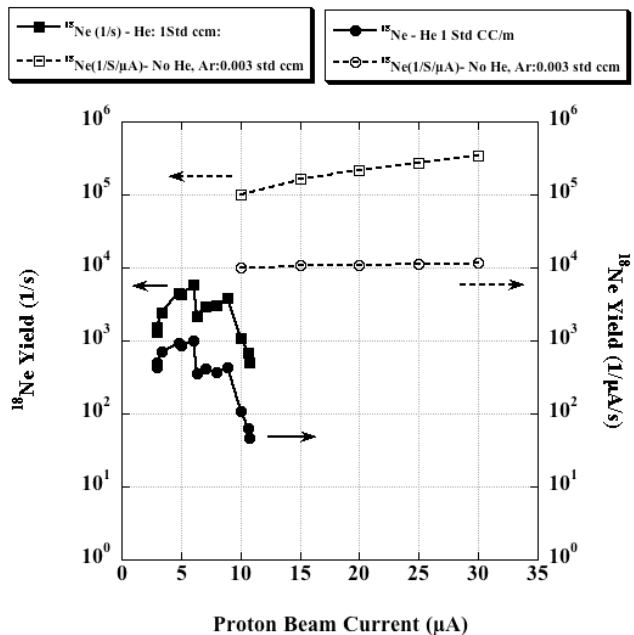


Fig. 212. ^{18}Ne yield as a function of the proton beam current. Solid lines show the ^{18}Ne yield operating the ECRIS with the nominal parameters. The dashed lines show the yield operating the ECRIS without He and only 0.003 SCCM of Ar as support gas.

for the leak was performed during the winter shutdown but did not produce any results. The ECRIS was then put back into the target station vacuum box and once again the leak was confirmed. This time we were able to determine that the water leak was present only if one end of the cooling circuit was hooked to the input. When hooked to the return we did not see the water leak. This was explained in the following way: on the return, the pressure is much smaller than at the supply side (20 psi instead of 120 psi). The ECRIS was then brought back to the hot-cell and the efforts were concentrated on the identified end. The leak was located on one of the water-blocks at a solder joint.

Taking apart the support tray to correct the leak would take too much time so we decided to clog the tiny leak using a vacuum anaerobic sealer that penetrates into the occlusion. A layer of epoxy glue was applied to cover the region. The ECRIS was again brought back into the target station vacuum box and tested. To be on the safe side the two ends of the water-cooling circuit were identified so that we always placed the repaired ends on the return side. Now the ECRIS is ready for a run schedule in May, 2005.

OLIS

Originally OLIS was assembled from parts of I3, only the filaments were removed and a 2400 MHz wave guide installed. When the Y box was installed in 2002 that could accommodate the surface source it was soon

realized that it made servicing of the optics in the original DB2 difficult. Thus in early 2004 DB2 was replaced with a standard LEPT chamber; this allowed the optics of this chamber to be mounted on the chamber lids and thus be quickly removable for cleaning.

Read backs were installed on upstream OLIS skimmers, and on a few downstream of the magnetic bend. They are single gain range and at time of writing will read back a maximum of 30 μA . The reason for this is that the rf source can produce currents greater than 1 mA and it is possible with such large currents to cause damage to optics if there is too much heating or sputtering. These read backs can aid in tuning OLIS and will eventually be used for interlocks or warning should there be changes in the OLIS operating point

during experimental runs. Note after mass separation at the magnetic bend the currents are normally greatly reduced.

There was a request for emittance selection slits for OLIS. In December two flanges with 5 mm apertures were installed 1 m apart to reduce the emittance for experiment at the polarizer. This also was to test the idea of improved emittance as an aid to tuning. As it turned out the variation of energy of the OLIS beam was then found to be too large. The original OLIS specifications did not include a precise bias supply, hence the energy variation is greater than that of the target stations.

Table XLV lists the OLIS beams delivered in 2004.

Table XLV. OLIS beams delivered in 2004 (MW means microwave source and SS means surface source).

OLIS	Beam	Facility	Experiment	Start date	End date
MW	^{12}C	DRAGON	Detector	26-Feb	27-Feb
MW	^{12}C	DRAGON	947	01-Mar	15-Mar
SS	^{23}Na	TUDA	927	16-Mar	17-Mar
MW/SS	Various	OPS	Training	22-Mar	26-Mar
MW	^{12}C	DRAGON	952	26-Mar	19-Apr
MW/SS	Various	OPS	Training	26-Apr	27-Apr
MW	Ne	TUDA	927	28-Apr	02-May
SS	Li	TUDA	927	03-May	04-May
MW	^{21}Ne	DRAGON	989	06-May	07-May
MW	^{21}Ne	DRAGON	824	13-May	14-May
MW/SS	La		Dev/920		
MW	^{26}Mg	DRAGON	824	14-Jun	15-Jun
MW	Mg	DRAGON	989	15-Jun	
MW/SS	Mg/Li	DRA/GP3	989/991	24-Jun	25-Jun
MW/SS	Mg/La	DRA/POL	989/920	28-Jun	29-Jun
MW	^{21}Ne	DRAGON	Dev/824	08-Jul	12-Jul
MW	Ne	Osaka	903	13-Jul	
SS	La	Pol	920	15-Jul	
SS	Li		991	01-Sep	07-Sep
MW	F	Pol		16-Sep	21-Sep
MW	Ne	DRAGON		01-Oct	04-Oct
MW	N	LTNO		05-Oct	
SS	Li			06-Oct	18-Oct
MW	$^{21}\text{Ne}/^{14}\text{N}$	Laval		21-Oct	25-Oct
SS	Na	DRAGON		28-Oct	31-Oct
MW/SS	La/Pr	Pol	920	05-Nov	09-Nov
MW	^{21}Ne	Laval		12-Nov	15-Nov
MW	$^{12}\text{C}/^{16}\text{O}$	DRAGON		18-Nov	22-Nov
MW	F	Pol		01-Dec	06-Dec
SS	Li	Pol		07-Dec	08-Dec
MW	TUDA	TUDA		13-Dec	16-Dec

Charge State Booster (CSB)

The final installation of the charge state booster (CSB) at the ion source test stand has been completed and commissioning of the system started in April. This includes the 1+ line, consisting of an 2.45 GHz ECR ion source, the 14.5 GHz PHOENIX booster and the analyzing system.

In a first series of measurements the CSB has been operated as ECR source only, without injection of 1+ ions, but with a calibrated gas leak of Ar or Ne. The goal was to condition the plasma chamber and the injection and extraction electrode system and to find the operating parameters for the beam optical elements. As an example the charge state distribution obtained for Ar is shown in Fig. 213. For this measurement the source was operated at 100 W microwave power and with a flow of about 10^{-3} SCCM He as a support gas. The maximum in the distribution is at 7+ with an efficiency of 2.7%. Summing up the efficiencies for all charge states leads to a total efficiency of 12%. This includes the transmission of the extraction and analyzing system. Especially in front of the magnet, the high total beam current causes losses due to space charge effects. Additionally, due to the poor vacuum in the analyzer (1×10^{-6} torr), charge exchange for the higher charge states will occur, resulting in an estimated loss of up to 20%.

The emittances for the different charge states of Ar have been determined at the end of the analyzer. Values of up to 20π mm mrad at 15 kV source potential have been found for 86% of the beam enclosed and no significant dependence on the charge state.

For first charge breeding tests beams of Ne, Ar and Xe have been injected from the 1+ ECR source. Figure 214 shows the efficiencies for the different charge states of Xe. The distribution can be altered by changing the source operating parameters, in this case the microwave power. Most measurements have been done with a very small He gas flow or no support gas. Summing up the efficiencies for the different charge states of Xe results in a total efficiency of 22.5%. In the case of Ar and Ne the maximum in the distribution was at 8+ and 4+ respectively, with a smaller total efficiency, but at this time a microwave power of only 100 W could be used.

The measurements were interrupted in October due to mechanical breakdown of a high voltage insulator. This insulator also supports the inner structure of the source and failed due to mechanical stress, caused by the forces from high magnetic fields. A reinforced replacement has been designed and constructed at TRIUMF. It has been installed and the measurements resumed. First results are that due to improvements in the vacuum inside the plasma chamber the density of

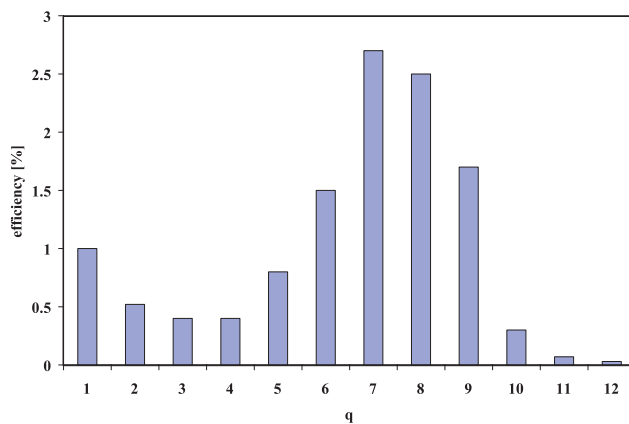


Fig. 213. Charge state distribution of highly charged Ar ions from the CSB. The Ar has been led into the source via a calibrated gas leak.

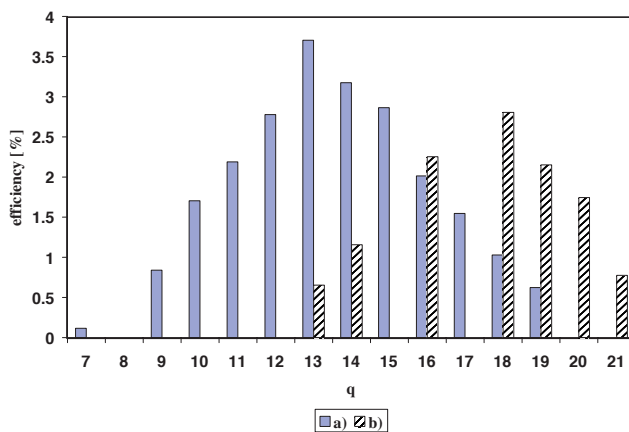


Fig. 214. Charge state distribution of highly charged Xe ions from the CSB. a) $^{129}\text{Xe}^{1+}$ injected with 250 W microwave power, b) $^{136}\text{Xe}^{1+}$ injected with 320 W.

high energy electrons could be increased resulting in a higher X-ray emission of the source. This makes additional shielding necessary.

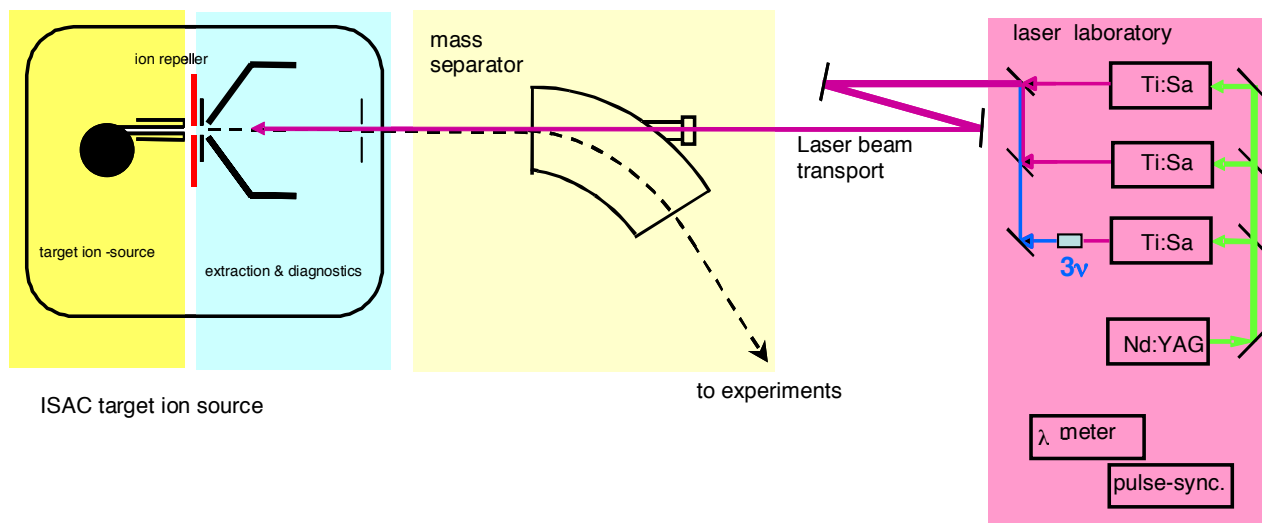
Parallel to the measurements a preliminary design study has been made for the installation of the CSB in the ISAC mass separator room. Based on the first results, ion optical simulations have been performed in order to find ways to minimize the losses at the extraction and increase the efficiency. Improvements will be implemented first at the test stand. The design of the final installation will be finished to prepare for the installation in the beginning of 2006.

RIB Development: Resonant Ionization Laser Ion Source

Within the radioactive ion beam (RIB) development at ISAC the TRIUMF resonant ionization laser ion source (TRILIS) continued with on-line installations and off-line beam development for Ga and Al beam production. In summary, TRILIS on-line installations were completed and a development run pro-

vided a beam of radioactive Ga from a SiC target. ^{62}Ga was delivered to 8π (Expt. 823) with a beam intensity enhancement $2\times$ and an augmentation of $20\times$ in the suppression of ^{62}Cu over surface ionization for branching ratio determination. A radioactive beam was successfully produced and delivered for an experiment one year ahead of the initial schedule.

In principle, TRILIS uses multi-step resonant laser excitation and ionization. This technique capitalizes on the potential for element-selective, efficient photo-excitation and ionization, with the major components of the LIS located 20 m away from the radiation area of the target ion source. The basic set-up of TRILIS is shown in Fig. 215 and is identical for off-line development and on-line beam production. In general, RILIS can supply beams of metals and transition elements that are otherwise difficult to obtain. Tunable, high-power, high repetition rate, narrow bandwidth, pulsed lasers are required which can be synchronized with respect to each other. The TiSa laser systems provide above 2 W output power at 10 kHz rep. rate, with typical pulse widths of 40 ns and a spectral line width around 5 GHz. Measured frequency doubling efficiencies are above 20%. Typical excitation schemes employ two and, more commonly, three laser excitation steps for resonant excitation and ionization, with the laser wavelength for the first excitation step usually being in the blue to ultraviolet region of the spectrum. In a typical laser excitation ladder each additional step requires higher spectral energy density. Therefore either Rydberg- or autoionizing-states are best suited for efficient ionization. These states have to be determined experimentally for each element, as only limited spectroscopic information on these high-lying atomic states exists.



Beam development in 2003/04 focused on Ga and preparation of Al beams. Figure 216 details the choice of laser excitation scheme for Ga. In the development work for Ga beams, performed at Mainz University, it became evident that for efficient ionization of Ga, frequency tripling of the TiSa lasers was necessary. Thus, the laser ion source test stand implementation was put on hold, and TiSa laser frequency tripling (planned for 2005) was developed and implemented. Based on the

Ga I - RILIS excitation scheme

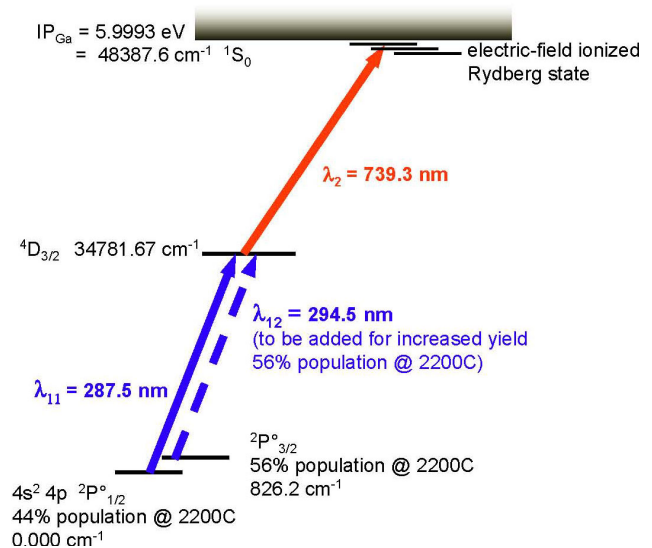


Fig. 216. Two-step resonant laser excitation scheme into a long lived Rydberg state that is subsequently field-ionized. This scheme was the result of detailed development work at TRIUMF and Mainz, and was successfully used for on-line production of ^{62}Ga . For future runs on Ga this scheme will be augmented with a second frequency tripled TiSa laser, to improve yields.

Fig. 215. Schematic of the TRILIS off-line development station with the principal functional groups: target ion source, mass separator and laser system with frequency tripling unit.

ISAC POLARIZER

All experimental groups that use the polarizer beam line were accommodated this year. The β -NMR/QR group was allotted a total of 5 weeks of polarized ^8Li beam time, the Osaka (Minamisono) group was allotted 2 weeks of polarized ^{20}Na and ^{27}Na , and the Osaka (Shimoda) group was allotted 2 weeks of polarized ^{11}Li . The McGill group (Expt. 920) was allotted 1 week of radioactive lanthanum and praseodymium isotopes in the summer and 1 week from OLIS in November. The polarizer beam line and laser systems worked reliably throughout, aside from two brief interruptions due to sodium cell malfunctions. However, other, unrelated problems in the summer shortened the radioactive McGill and Osaka (Shimoda) runs by half. The polarizer dye laser was also run for 4 weeks in September and October, in support of the GSI experiment Expt. 991 that successfully measured the charge radius of ^{11}Li .

We began development of a polarized ^{20}F beam to be used in Expt. 972, which is an extension of the Osaka (Minamisono) group's work on ^{20}Na . All the polarized beams produced to date at ISAC have been alkali metals. In alkali metals the ground state atom has one loosely bound valence electron that can be optically pumped by commonly available lasers. It is not practical to directly pump the ground state of the fluorine atom (or of the ion for that matter), due to the short wavelength light that would be required. A workable fluorine scheme was envisaged based on polarizing the metastable atomic state $3s\ ^4P_{5/2}$ via optical pumping on the closed transition $3s\ ^4P_{5/2} - 3p\ ^4D_{7/2}$ at 686 nm. The metastable state is produced as some fraction of the total atomic beam during neutralization of F^+ in sodium vapour. Its lifetime of $3.7\ \mu\text{s}$ is long enough for an appreciable fraction to survive during the optical pumping process. Collinear laser spectroscopy of ^{19}F was used to investigate the feasibility of the scheme in two OLIS runs in September and December. The aims were 1) to measure the hyperfine splitting of the $^4P_{5/2}$ and $^4D_{7/2}$ energy levels, and 2) to estimate the metastable fraction of the beam. The former is important in devising a practical laser scheme, while the latter determines the maximum beam polarization possible.

The hyperfine structure was determined by observing laser induced fluorescence from the $^4P_{5/2} - ^4D_{7/2}$ transition while scanning the Doppler-shifted laser excitation frequency (see Fig. 219). The hyperfine magnetic dipole coupling constants of ^{19}F (nuclear spin $I = \frac{1}{2}$) were thus determined for both energy levels. The nuclear magnetic moments of ^{19}F and ^{20}F are known, so the hyperfine structure in ^{20}F ($I = 2$) could be calculated, neglecting shifts caused by the electric

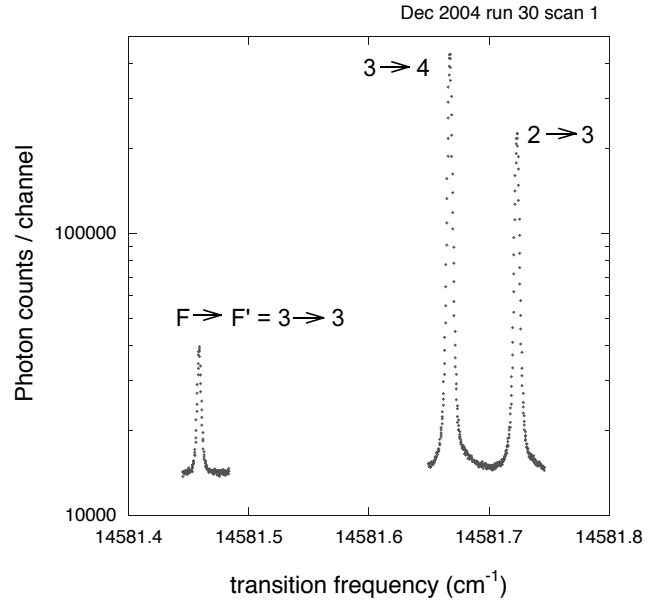


Fig. 219. Laser induced fluorescence showing the hyperfine structure of the $^4P_{5/2} - ^4D_{7/2}$ transition in ^{19}F . The labels F and F' refer to the total angular momentum in the lower and upper state, respectively.

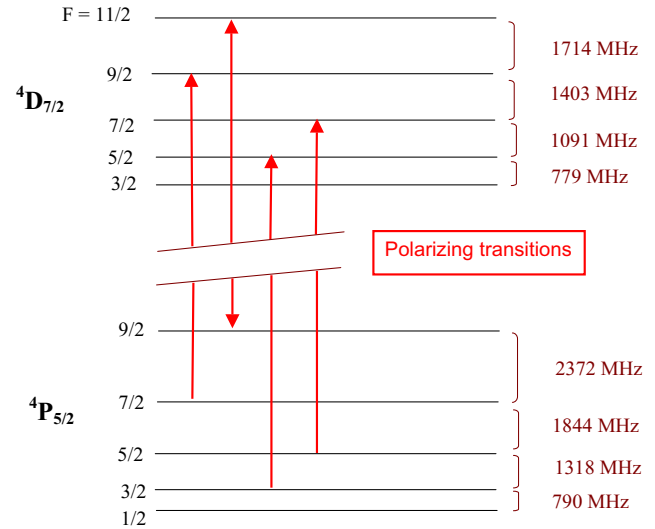


Fig. 220. Calculated hyperfine splitting of $^4P_{5/2}$ and $^4D_{7/2}$ energy levels in ^{20}F .

quadrupole moment (see Fig. 220). It is likely that one laser in combination with a single electro-optic modulator could optically pump most of the metastable population on the strong transitions shown in Fig. 220. This needs to be confirmed with direct measurement of the hyperfine structure of ^{20}F .

The metastable yield was estimated by optically pumping metastable atoms into the ground state via the $3s\ ^4P_{5/2} - 3p\ ^4D_{5/2}$ transition at 677 nm. The optically pumped beam was ionized in a helium gas cell (as in the operational polarizer) and steered to a Faraday cup. Depletion of the metastable population de-

creased the current observed at the Faraday cup, due to preferential ionization of metastable atoms compared to ground state atoms. The hyperfine structure of the transition was determined by scanning the excitation frequency while chopping the laser beam and using lock-in detection of the Faraday cup current. Then, while sitting on the biggest hyperfine peak, the dc ion currents at the Faraday cup were recorded with the laser “on” and “off”. The conclusion was that up to 23% of the ionized beam would be derived from metastables in the limit of zero helium density. One could expect $\sim 10\%$ ^{20}F polarization in an operational system. Although lower than the typical 50–70% achieved with alkali metal beams, this is still a very useful number. (It could be greatly improved by removing the He cell and substituting UV laser ionization of the $^4D_{7/2}$ state.) We plan at least one more ^{19}F test to investigate the effect of varying the He gas density.

The β -NMR group has requested polarized ^{15}O as a spin- $\frac{1}{2}$ probe that could occupy oxygen sites in high temperature superconductors. Like fluorine, optical pumping must begin from a metastable level, in this case on the closed transition $3s\ ^5S_2 - 3p\ ^5P_3$ at 777 nm. The fluorine results are encouraging in this regard, since for several reasons the metastable yield should be higher in oxygen:

- The charge exchange reaction that neutralizes oxygen ions in potassium vapour, creating metastable oxygen, has closer to zero energy defect than the analogous reaction between fluorine and sodium vapour.
- The 5S_2 metastable level in oxygen has no nearby energy levels to reduce its yield during the charge exchange reaction, unlike metastable fluorine, which has two very short-lived levels $^4P_{3/2, 1/2}$ nearby.
- Metastable oxygen is so long-lived that decay losses during transit in the polarizer are negligible.

The only disadvantage of oxygen is that preferential ionization of the metastable atom in helium is expected to be slightly less efficient than with fluorine, and therefore less efficient at removing unpolarized background from the ion beam going to experimenters.

ISAC REMOTE HANDLING

The Remote Handling group continued to support ISAC activities throughout the year, servicing the target stations, remote handling of modules and ISAC hot cell operations, along with engineering support in the construction of the latest target module.

The ITW module access area services were fully rebuilt during the winter shutdown with the installation

of new cable trays. All new electrical power and controls cabling, as well as new cooling water lines and revised vacuum plumbing were installed. This updating of the west target station will greatly improve service access, reduce risk to services and facilitate contamination control in the area.

Engineering support on ISAC continued with group technicians rebuilding the TM4 target module towards a more conventional arrangement after the unique set-up required for the 100 μA target tests completed in 1998. This is now being rebuilt to a standard surface-source configuration for use with high power targets, laser ion source operation or actinide target testing as scheduled in 2005.

The module transport carrier, previously used only for shuttle transport of new modules to the target hall, has been modified both for improved personnel access safety and to provide a vacuum pumping chamber for new module construction leak checking.

ISAC CONTROLS

This year was a “maintenance” year at the ISAC-I control system with no major new system installations. A lot of effort went into peripheral systems, such as TITAN, the charge state booster, etc. During the impending installation of ISAC-II, the group will have to support maintenance of the existing ISAC-I installations without additional manpower. Improvement of tools, which enhance the group’s productivity, was therefore given high priority.

As in the years before, the Electronics Development group supplied the hardware support for the ISAC control system, both for design and maintenance.

New Systems

ISAC-II

In preparation for the installation of the ISAC-II systems, which will happen during 2005, the hardware and software structure of the control system was reviewed.

Tests of a new generation of VME CPUs (Pentium based) were concluded successfully. These will be used instead of the 68040 based SBCs used in ISAC-I.

A new system of PLC I/O (Modicon Advantys) was evaluated. This system allows the distribution of I/O modules in small clusters along the beam lines, leading to a substantial reduction in cabling costs and effort. The S-bend transfer beam line between the DTL and the superconducting SCB accelerator will be instrumented with this system. Beam lines in the ISAC-II experimental hall are further candidates.

Advantys I/O was also used for a small PLC system, which was implemented to support the commissioning and the acceptance tests of the Linde helium

liquefier system. Associated EPICS support was provided to allow strip-charting and archiving of selected data.

In order to integrate the Linde system into the ISAC operations, a software driver was written for reading the Siemens PLC, which controls the Linde helium liquefier.

Two group members visited the Canadian Light Source in Saskatoon in order to discuss control system issues, in particular with respect to the Linde helium liquefier plant.

RF amplifier monitoring

Following last year's conceptual design, the system for monitoring all relevant parameters of the 14 ISAC rf amplifiers was produced. PLC drops for all amplifiers, using the distributed Advantys I/O system, were built for 10 amplifiers. The system is ready for installation, but is waiting for parts delivery for signal conditioning boards.

Integration of ISAC building controls

The ISAC building control system is a commercial system, using the BACNET network protocol for communication between devices and supervising PC workstations. This system stands alone, does not provide satisfactory data archiving facilities, and suffers from a host of operational insufficiencies.

A major project was begun to integrate this facility into the ISAC control system. The starting point was open-source BACNET drivers for Linux, which were essentially alpha state. These drivers were debugged and made functional. A BACNET application was developed, which allows fast startup of the monitoring system from a locally stored database. This local database is acquired by lengthy on-line exploration of the installed system. The BACNET application was interfaced to an EPICS soft IOC running on the same Linux machine. This will allow monitoring of all building control parameters through the ISAC control system.

The BACNET/soft IOC combination is undergoing final testing at the moment.

Functionality Enhancements

ISAC-I diagnostics

Software drivers for the VQSX beam current amplifiers were upgraded to provide auto-ranging and logarithmic output capability.

In the IOS section, software support for a new set of beam skimmers was implemented.

CAN-bus based beam current integrators were installed at some Faraday cups in the IMS, 8π , and TUDA beam lines in order to increase readout sensitivity.

Charge state booster

At the ion source test stand, the control system for the charge state booster was completed. Support for all beam diagnostics elements was implemented. Beam current amplifiers with higher current capability were installed. A new water flow controller box with analogue flow read-out was added to the system. Control of the CSB power supplies was moved from CAN-bus to the PLC, in order to support a changed interlock specification. The PLC interlock system was enhanced in software and hardware to allow the CSB HV to be run independently from the ion source or from a common HV supply. MATLAB applications for better visualization of emittance scans and correlation plots were developed.

TITAN RF cooler

The components of the TITAN control system were implemented and commissioned. This included the new rf cooler optics, which uses TRIUMF developed VME-based voltage supplies. An EPICS operator interface was supplied. EPICS driver and device support for the TITAN-specific VME modules was enhanced and commissioned.

ISAC-II cryomodule

Ongoing support was given to the SCRF facility. The EPICS interface to the rf control system was changed. The unstable portable channel access server was replaced with a "soft IOC", a new software tool, which became available with EPICS release 3.14. The soft IOC was interfaced to the rf controls with a software "glue" layer based on a shared memory protocol. This upgrade improved the stability of the system dramatically. It will be used for ISAC-II and should also be retro-fitted to the ISAC-I rf controls if time and resources permit.

A similar soft IOC was integrated with the commercial Windows-based system for cavity alignment. This gives the alignment system access to EPICS facilities like archiving and strip-charting of data.

Target conditioning box

At the target conditioning box, many small modifications were made to support changing requirements for testing of the laser ion source, high current targets, and the development of a FEBIAD source.

Miscellaneous

Changes were made to the PLC software to implement "soft" roughing of several diagnostics boxes in the HEBT sections.

In order to make IOC development easier, separate small PC104-based IOCs were deployed for the supervision of the evaporator, TIGRESS detector fill, and M9/M15 vacuum system PLCs.

At the laser ion source, a Windows-based PC runs a commercial software package to read and process wave-meter data. A soft IOC was provided to allow data visualization and logging by EPICS.

Experiment Support

PLC and EPICS support was implemented for Expt. 991 at the end of the ILE2 beam line.

Temporary modifications were made in the ILE2 polarizer section to accommodate Expt. 990.

For DRAGON, the PLC program was enhanced to support new devices and configuration change between different detector systems at the end chamber.

System Support

System maintenance on the development and production nodes occupies an ever increasing amount of time. In addition to the console machines, there are now 9 Solaris servers, 4 Linux servers, and 4 Linux firewalls.

The protection of all EPICS based control systems with firewalls was finished. The production machine(s), IOC(s), and PLC(s) are grouped behind separate firewalls for

- ISAC
- Ion source test stand and TITAN
- SCRF, target conditioning station, evaporator.

In addition, a firewall protects the development systems in Trailer GgExt.

The EPICS CA gateway program was installed on a Linux machine with the intent to concentrate all user connections to IOCs, thereby reducing the network and memory load on the IOCs. This led to the discovery of serious bugs in the gateway software, which was reported back to the EPICS collaboration. Until a fix is available, the system was reverted to the previous configuration.

EPICS auto-save/restore routines were modified to use the IOC's NVRAM, and installed on some IOCs to allow bumpless reboots.

The logging configuration of the EPICS IOCs was reconfigured. A separate IOC log server for each IOC accepts console output logging and writes to a set of rotating logs. CA output logging, the operator activity log, is handled by a dedicated IOC log server.

Two new SUN servers were acquired to replace two mission-critical servers, which had been in faultless operation since 1997. One of the new servers failed catastrophically in December. This exposed a weakness in our server redundancy configuration. Bringing the backup server on-line required more intervention of a system expert than expected. As a consequence, a new server hot-sparing concept is being implemented.

All production servers were relocated to the ISAC-II controls development room.

All IOCs were upgraded to EPICS release 3.13.10. The new EPICS release 3.14 was compiled and used for support of soft IOCs and the CA gateway. All ISAC device drivers were modified to support 3.14. No decision has been made yet to upgrade to 3.14.

Development and QA Support

Device database

The ISAC control system relational database and associated Web-application was further enhanced to include more checking tools. IOC configuration and roll-back was refined, CAN-device configuration was included, Capfast symbol import was improved, and a better device name aliasing system was implemented.

Perl tools were written to support PLC interlock checking and device control panel building for the Concept PLC programming software, which is used with the new Advantys I/O systems.

NCR system

A new version of the Web-based ISAC fault report system was designed and implemented following specifications by the ISAC Operations group. The new "non-conformance reporting" (NCR) system uses the PostgreSQL relational database system as back-end. The system complies with the TRIUMF QA program and supports the full life-cycle of an NCR.

Bypass and force tracking

New tools were developed in order to improve tracking of interlock bypasses and device forces. Issuing of bypass and force commands to the control system is now limited to operators. The reasons for bypasses and forces are tracked in a relational database, so that status and history can be easily queried.

Operation

In general, operation of the control system during 2004 was not too eventful. There are still too many IOC reboots required to revive "hung" IOCs. These reboots usually do not cause loss of beam, but are a nuisance nevertheless. Reasons for the hang-ups are task crashes on the IOC or starvation of resources. Due to the intermittent nature of these problems, progress in addressing them has been slow.

VACUUM

ISAC-I

The Vacuum group maintained and repaired the vacuum equipment on accelerators and the beam transfer lines. Assistance was provided with setting up vacuum systems for different experiments by GSI, Laval University, etc. on GPS2, GPS3 and on the end of the HEBT. The last vacuum section of 8π has been

upgraded with a Varian dry Scroll 300 mechanical pump. The vacuum diagram was produced for the TITAN/RFQ cooler, and two V-1000 turbo pumps were repaired also for TITAN. The Vacuum group assisted the CS-booster development with vacuum services.

Targets

Both target stations performed well during the year, at an average vacuum of about 8.0×10^{-7} torr. Diaphragm gauges were installed on decay and operating storage tanks for better vacuum monitoring. The diaphragm gauge is not a gas-dependent type as is the convectron. The failure of a hermetically-sealed mechanical pump required the installation of the spare. The second hermetically-sealed pump was also replaced as a preventive maintenance precaution. Replacement pumps have been ordered. Two Varian V-1000 turbomolecular pumps failed during the year and both have been replaced with new pumps. The faulty pumps had bearings replaced and rebalancing done. The Penning gauges had stability problems related to controllers, grounding and due to work in excessive outgassing during target initial bake out. The Vacuum group looked after retrieving samples from the decay storage tank for survey before each gas removal. The group has also been involved in intensive leak checking of heat shield cooling lines for target module #1 and the ECR target module.

Mass separator area

A few tests have been done with the goal to find a way of improving vacuum in between the mass separator and RFQ for the beams with a high charge transfer. The cryopump and electrical tape heaters have been installed for the test. The data obtained is compatible with ISIS experience with cryopumps. The baking with heaters to reasonable (about 50–60°C) temperatures did not change the vacuum. Two convectron gauges were replaced on the mass separator platform. The baking mechanical pump on the platform had a complete overhaul several times during the year. The quick oil quality degradation has been noted.

LEBT

The Varian turbo pump V-551 on the polarimeter has been replaced as well as turbo pumps ILE2:TP21 and ILE1:TP10. One turbo pump controller has been repaired. Two mechanical pumps have been replaced.

RFQ

The water cooling has been added to all RFQ Leybold turbo pumps.

DTL

The DTL roughing pump has been repaired.

HEBT

Installation of the S-bend take off dipole magnet with vacuum chamber is scheduled for the winter shutdown. The HEBT vacuum system modification is planned for the same time. The modification will involve the splitting of the vacuum system into separate sub-systems with separate roughing/backing pumps in each sub-section. This will shorten the pump downtime and will simplify control system interlocks.

The cold finger cryopump has been maintained and the new high pressure helium lines were installed. Two ion gauges, one mechanical pump, and one turbo pump controller have also been replaced.

ISAC-II

Vacuum and cryogenics

The Vacuum group assisted the ISAC-II project with vacuum and cryogenic services in the SC Linac development and the S-bend. A lot of leak checking was done on cryomodule components during manufacturing, and cold tests were performed on the first cryomodule. A 1000 l helium dewar, manufactured by CRYOFAB in 1983, has been restored and installed as a part of the helium refrigeration system. The current leads for the SC-solenoid have been designed and assembled.

Liquid helium and liquid nitrogen

The Vacuum group is looking after liquid helium and liquid nitrogen deliveries and distribution on site.

The new 9000 US gallon nitrogen tank replaced the smaller tank located by the east wall of the ISAC-I building. It is serving users connected through the ISAC-II nitrogen distribution system and portable dewar fill station inside ISAC-I.

The old helium refrigerator, which occupied space in the helium building, has been sold.

The Linde TCF-50 helium refrigerator system is under construction with commissioning scheduled for February–March, 2005.

ISAC-I RF SYSTEMS

ISAC rf systems performed very well over 2004 with availability of about 97% and total downtime of 81 hours.

LEBT Pre-buncher

The LEBT pre-buncher was routinely operated to bunch the dc beam in the LEBT into a desired bunch structure for injection into RFQ. The rf amplifier misbehaved twice. The first time it was a solder joint failure of one of the resistors in the amplifier module. The second time was a loose rf connector failure. Both troubles caused beam instabilities.

RFQ

The RFQ operated well in 2004, and system downtime was mainly associated with the computer control system. Major developments done on the RFQ system were:

- RF control computer and VXI control system were powered from a UPS;
- Cooling circuits of tuners, coupler and tank structure were refurbished to incorporate water flow controls and interlock;
- All 6 RFQ vacuum turbo pumps were equipped with water cooling;
- An updated version of the anode power supply soft start circuit board has been manufactured and commissioned into the system;
- RF controls hardware was modified to perform the frequency tuner initial position alignment. Corresponding software upgrade is under way.

Bunch Rotator

The MEBT 105 MHz bunch rotator was routinely used in operation to achieve the desired beam quality.

During the winter shutdown the bunch rotator cavity was taken off-line and dismantled to investigate the problem of multipactor discharge, which made the startup procedure rather difficult. A visual inspection revealed a few areas with multipactor marks around the stem and rings. A surface coating with Ti to reduce secondary electron emission was considered and rejected due to unacceptable impact on the beam schedule. Instead we painted the troublesome areas with Aquadag (see Fig. 221). In the past this kind of treatment had been proven to reduce the multipactoring in the main cyclotron rf structure. After Aquadag treatment the rotator cavity was tested at a test bench at signal and high power levels. An improvement in conditioning time has been achieved, though we were not able to completely suppress multipactor discharge.

A new, smaller coupling loop was installed for the cavity, which significantly reduced the capacitive coupling and improved system stability. To compensate the frequency shift introduced by smaller coupling loops, a 5 cm diameter tuner plate was used to replace the existing 3.8 cm one.

An amplifier tetrode tube degraded in performance with an indication of aging, though it has operated only about 4000 hours. A spare 3CX 3000 tube was installed and easily gave 5 kW output power (required power is 2.6 kW). To increase tube lifetime, the filament voltage was reduced from 7.7 V to 6.8 V after the tube was conditioned for 200 hours.

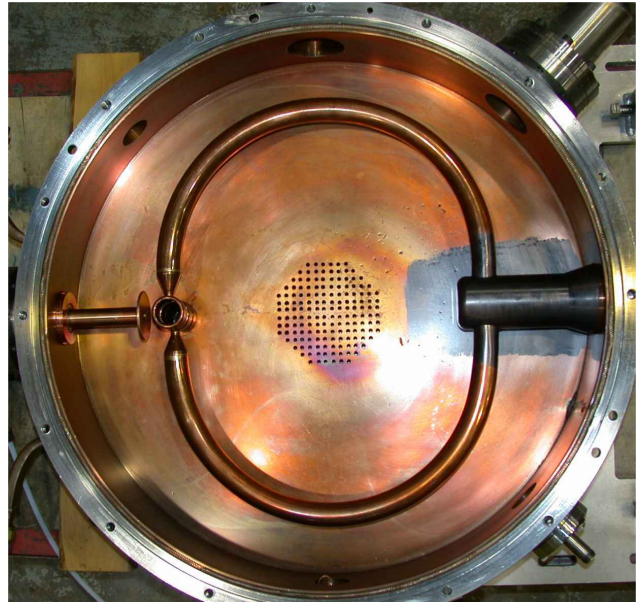


Fig. 221. MEBT bunch rotator painted with Aquadag.

MEBT Rebuncher

The MEBT rebuncher operated very reliably this year. The rebuncher cavity was tested to operate without endplate cooling and the frequency tuner taken out of regulation loop. Despite these changes the system has shown stable operation without any trouble during the year.

DTL

Due to cooling water pollution coming from rusting steel endplates, the DTL tank #1 had also gone through a similar test in 2003. We had run it at nominal rf power (4 kW) without endplate cooling. Structure temperature rapidly rose and the fine tuner could not compensate frequency change due to the tuning range limit. Subsequently an external water-cooling of the endplates had to be implemented instead of original internal cooling. In June, 2004 we installed 4 detachable heat sinks to both endplates. The system has operated well ever since. Recent investigation on the deionized water quality has not revealed any contaminants in the return circuits.

In January there was an incident, when DTL tank #4 was tested at high rf power while the DTL cage was open and accessible to personnel. An investigating committee has identified some deficiencies in the procedures which caused a failure in the hardware (interlock relay). Following committee recommendations, the DTL cage safety interlock has been upgraded during last year. The trip signals of X-ray or high rf levels should now turn off all DTL rf driver and screen power supplies. The trip status is latched in the safety system and in the rf amplifier controls. The rf amplifiers can

be powered again only after clearing and resetting the interlock status. The interlock status is now displayed at the DTL rf control consoles, advising the operator about DTL cage safety status.

DTL amplifiers

After extensive maintenance in 2002 the DTL amplifiers did not require any specific service over the past two years and worked very reliably. The only failure was in the DTL tank #1 PA. A homemade anode blocking capacitor experienced a destructive spark, which produced a 2 mm diameter hole in the kapton insulator. A broken capacitor was replaced with a spare one.

The amplifier remote control system was developed. New data processing and interface boards are housed in the shielded metal boxes in each of the 8 DTL amplifiers. Adequate HV protection and rf filtering are incorporated into the design. All PA voltages, currents and status signals are provided to the ISAC main control system via a PLC. An EPICS control page is being developed. The amplifier hardware upgrade included installation of new 3 ft Tx-line directional couplers, rf driver 1 kW directional couplers, rectifiers, voltage dividers, current sensors, and associated wiring. Final commissioning of the remote control systems for all 8 DTL PAs is planned for spring, 2005. Control systems for the rest of the PAs will be upgraded afterwards.

HEBT High Beta Buncher

Following the test results of 2003, the upgrade of the frequency tuner for the 35 MHz buncher has been completed during the winter shutdown. A modified tuner does not comprise rf fingerstocks, which rapidly deteriorated due to friction in the past. Removal of finger contacts caused resonant frequency shift, which was adjusted by means of the coarse tuner. The fine tuner new operational range covers cavity detuning due to heating by rf power in the full working range from 0.5 to 13 kW. Maximum heat dissipation on the tuner itself leads to an insignificant temperature increase of 15°C. The new tuner is interchangeable with DTL tank 2, 3, 4 and 5 tuners. This reduces the required number of spare parts for the rf system.

RF Controls

Over the year the RF Controls group regularly provided routine tune up of the rf control system. A number of spare rf control boards for different frequencies of the ISAC rf systems have been tested during shutdown time.

ISAC DIAGNOSTICS

Cryomodule Alignment Hardware

The ISAC-II superconducting cavities must remain aligned at liquid He temperatures: cavities to $\pm 400 \mu\text{m}$ and solenoids $\pm 200 \mu\text{m}$ after a vertical contraction of $\sim 4 \text{ mm}$. A wire position monitor (WPM) system based on a TESLA design has been developed, built, and tested with the prototype cryomodule. The system is based on the measurement of signals induced in pickups by a 215 MHz signal carried by a wire through the WPMs. The 0.5 mm diameter copper-bronze wire is stretched between the warm tank walls parallel to the beam axis providing a position reference. The sensors, one per cavity and two per solenoid, were attached to the cold elements to monitor their motion during pre-alignment, pumping and cool down. A WPM consists of four 50Ω striplines spaced 90° apart. A GaAs multiplexer scanned the WPMs and a Bergoz card converted the rf signals to dc X and Y voltages. National Instruments I/O cards read the dc signals. The data acquisition is based on a PC running LabVIEW. System accuracy is $\sim 7 \mu\text{m}$.

Alpha Acceleration Hardware

For the experiment on acceleration of alpha particles from a radioactive source in superconducting cavities, a ^{244}Cm source with an intensity of 10^7 Bq was attached to the upstream diagnostics box on the front of the cryomodule. In order to prevent possible contamination, the source was separated from the cryomodule vacuum by an $8 \mu\text{m}$ kapton window of 2 mm diameter and a copper mesh screen. The detector consisted of a silicon surface barrier detector in a vacuum box connected to the downstream end of the cryomodule. The source and detector could be valved off and a magnet could be turned on to sweep away electrons from the cryomodule before reaching the detector. The absolute measurement of the energy of the accelerated alphas was crucial. To calibrate the detector, a low level alpha source could be moved in front of it. It produced a spectrum of three lines between 5 and 6 MeV and consisted of a mixture of isotopes: ^{239}Pu , ^{241}Am and ^{244}Cm . It was found that the cavity tuner motors induced significant switching noise despite the use of double shielded signal cables. To alleviate the noise, the detector ground was floated and the pre-amp moved close to the detector. The electronics was standard: an +80 V bias supply for the detector, a charge-sensitive preamplifier, a pulse amplifier. The alpha particle spectra were collected by a multichannel analyzer and read by a laptop running acquisition software under LabVIEW.

Stripline FFC

A fast Faraday cup (FFC) in the diagnostics box of the cryomodule will be used to tune the buncher in the new transfer line to ISAC-II. The existing FFCs are too long in the beam direction, ~ 6 cm, for this location. A thinner, ~ 2 cm, FFC was designed based on a water cooled ceramic printed circuit board (pcb). A biased screen in front of the pickup electrode shields it from the EM wave which precedes the ion bunch, yielding a fast time response. A fine copper mesh screen was supported by a 0.5 mm spacer in front of the electrode and this assembly was soldered to a separate track on the pcb. The device was tested

Other Activities

Certain attention was given to the diagnostics capable of monitoring beams with intensities from a few to 10^6 – 10^7 ions per second. Current emphasis is placed on two types of devices: secondary electron emission monitors (SEM) and CVD diamond detectors. Both detector types are considered radiation hard and, therefore, suitable for beam diagnostics purposes. They will be used complementarily depending on requests and experimental conditions and, hopefully, will satisfy current demands on “low-intensity” diagnostics. It should be noted that in contrast to the SEMs, diamond detectors will require additional R&D but are potentially very attractive since they are very robust and simple in operation. Two detector grade CVD diamond wafers from Element Six Ltd. have been acquired for prototyping. Several devices of both types will be developed and built in the upcoming year.

The vacuum stand for testing detectors and other equipment is complete. The multipurpose diagnostics box arrived from the shop at the end of the year and successfully underwent vacuum leak tests. The final assembly was delayed in connection with a decision to replace the existing roughing pump with an oil-free scroll pump to prevent contamination and eventual damage of sensible detectors, e.g. microchannel plates. The pump is currently being commissioned.

ISAC-I CONVENTIONAL FACILITIES AND INFRASTRUCTURE

Two significant failures tarnished what would have otherwise been a relatively quiet year. A required upgrade in chiller #2 was postponed due to financial constraints. Regular engineering support continued to be provided to users on electrical and mechanical services matters. This included participation in engineering design reviews for accelerator as well as experimental facilities, cost estimating, services design and specification, procurement and installation supervision as well as attending to operational problems and maintenance.

Preliminary work started on TITAN and β -NQR services design. A review of the CSB services requirements indicated that they could be housed in the mechanical room next to the mass separator vault. Safety interlocks for the 8π experimental facility obtained final approval of the engineering review panel. They will be installed next spring.

A number of improvements were brought about. The overload of the LEBT 208 V power distribution was resolved and the local capacity expanded to accommodate an increased demand in the area. A safety concern with one of the main LEBT cable trays was attended to. A water leak in the electrical room was fixed and the feeder to DTL tank 5 was increased. UPS power was supplied to the RFQ controls that were experiencing too frequent nuisance trips.

The most important maintenance activity was the replacement of both variable frequency drives (VFD) and motors for both cooling tower units in late October. This equipment has been in service for about 8 years. The cooling tower system is critical to the continuing operation of ISAC and is required to be highly reliable. We have experienced serious problems in finding replacement parts when the first unit failed, but the problem became critical when the second unit failed. We were left with little support from the manufacturer’s local service representative. Our vulnerability to the outside service support was evident. After a careful review of the technical problems and the required reliability, the decision was made to change manufacturer of the VFD. We also improved on the previous design to better protect the motors from the damaging effects of impulses created internally to the VFD. Chokes were added to both line and load side. The first unit was commissioned early in November. The reliability of the VFD from the same manufacturer installed in the radiation exhaust system came into closer scrutiny as more frequent troubles were reported. In the process, we decided to replace in time that VFD as well. This task is planned for next year. Another major failure occurred in one of the uninterruptible power supply units, when one of its inverter’s card burned. UPS reliability and availability are also critical to continuing ISAC operation. The repair of these units is expensive and we are looking at replacing the whole UPS system with a more reliable one.

About 22 installation orders were processed for ISAC-I, amongst them services to Expt. 991, TITAN test stand, TRINAT lasers and DTL-8 amplifier.

Mechanical Services

Several large projects dominated activity. The NALCW system for ISAC-II was started up and provided water to its first consumer, the rf test stand. Be-

cause of the contamination of the mains in ISAC-II for this system during construction, cleaning and repeated flushing was required before water could be allowed to return to ISAC-I. After water was allowed to flow, the return water to ISAC-I was filtered for several weeks to ensure all loose materials were captured. One casualty was the de-ionizing resin which faithfully polished the new piping system before expiring. After having to polish the ISAC-I piping and five more years of service it was near the end anyway.

ISAC-I room 06 (actinide lab) fume hoods had HEPA filters installed which required new ductwork squeezed into the tight space available, exhaust fan speed up, installation of a new fume hood, and re-piping of services including changing the cup sink drains from the active to the sanitary system.

The cryogenics project called for action on several fronts. Room 164 required rotation of the existing ventilation fan, relocation of a sprinkler main, and installation of water and air piping. In the helium compressor building the existing fans were removed and a new roof top system installed to meet the high demand for compressor ventilation. A new flow switch was installed in the incoming sprinkler line to alert controls in the event of a fire.

A compromise design exhaust fan was installed in each of the glass enclosed stairwells. Compressed air service was provided to room 03. MRO work included TRINAT heating coils and piping modifications, and a new radio operation system for the ISAC-I experimental hall crane.

ISAC PLANNING

This year the Planning group was involved in planning, scheduling, coordinating and expediting several sub-projects for ISAC-II (medium beta cavities, wire position monitor, cryogenics system, high beta cavities, charge state booster, HEBT transfer, H-HEBT, ECR); planning and coordinating activities for two shutdowns (December 22 – mid April and September 13 – October 6); ISAC experimental facilities (TIGRESS, TITAN); and M20Q1, Q2 refurbishing.

Technical details and progress on PERTed activities are described elsewhere in this Annual Report under the respective principal group. However, following is a summary of the main projects along with the major milestones achieved.

ISAC-I

Various plans and PERTs were prepared and updated regularly with manpower estimates and analysis to identify critical areas and resolve any problems. ISAC priorities were evaluated and higher priority was assigned where necessary to optimize the scientific output and meet overall milestones.

ISAC-II

Medium beta cavities

The remaining cavities, #8–20, were fabricated, inspected, chemically treated and received at TRIUMF. Cavities for the first two cryomodules (SCB3 and SCB1) were cold tested, with the remaining cavities to be tested by May, 2005. The cold test results indicated that three flat type cavities (#7,9,12) did not meet our quality specifications. The plan is to electro polish cavity #7 at Argonne for now in order to resolve this quality issue and establish an agreement with Jefferson Lab to chemically treat our cavities as needed. Tuners and coupling loops for the first 2 cryomodules have been received and are prepared for installation. The remaining components are expected to arrive early in 2005. Cryomodule tanks 2 and 3 were received and the LN₂ shielding fabricated and installed in the tanks. Cold tests and rf tests on cryomodule SCB3 were completed in November, and the assembly of cryomodule SCB1 started in December with an aim to move it to the clean room in February, 2005. Considerable effort was put in by the machine shop to fabricate the components for cryomodules SCB1 and 2. Cold tests and rf tests on cryomodules SCB1 and 2 will still require extensive expediting of components and appropriate manpower allocations to meet the scheduled completion dates. As an intermediate milestone, the plan is to test SCB1 with final cabling, rf controls and configuration by June, 2005. The plan is to install the last cryomodule #5 and be ready for beam in December, 2005. The fabrication of components for SCB4 and 5 was delayed to the 2005/06 fiscal year due to budget constraints.

Cryogenics system

Process and instrumentation drawings (PID) were completed which specified all the components required. The contract for the cold box, compressor/ORS and He ambient vapourizer was awarded in November, 2003 to Linde. These components began arriving at TRIUMF on schedule in July and September, 2004. After an extensive search the buffer tank was procured, cleaned, leak checked and installed on its pad in October. The plan is to install refrigeration systems and distribution systems in early 2005 with the overall system commissioning by Linde in March, 2005.

High beta cavities

Preliminary physics specs for the high beta systems were completed by December with an aim to review the initial conceptual design to finalize the decision regarding the cavity frequency by March, 2005. The aim is to finalize the design followed by an evaluation of a local company for manufacturing cavities, and then

fabrication, testing and evaluation of a prototype cavity by March, 2006. The specifications of all cavities can then be finalized and the fabrication order will be placed. The plan is to complete the high beta system by summer, 2008.

Charge state booster (CSB)

ECR mode and breeding mode commissioning continued in 2004. Several tests had to be done to specify the shielding required for X-rays. Tests with the rf cooler will take place in spring, 2005, and optimization will continue until the end of the year when the CSB will be ready to move to its final location. After the rf cooler tests are complete, optics design will begin for the CSB implementation in the mass separator room due to required shielding constraints. The aim is to have all the components fabricated and assembled and prepare for installation in the January, 2006 shutdown.

HEBT transfer line

Many components for the HEBT transfer line were fabricated and procured during 2004. Two of the four dipoles were received in June. The other two needed repairs, were sent back to Alpha, and were received in August. The main support frame, service trays and racks were installed by August. The rebuncher was received at TRIUMF, and assembly of the components onto the rebuncher continued with an aim to be ready to install in the DSC line after the January, 2005 shutdown. Installation of all the components continued up to December, 2004. The plan is to install MB0 with its associated vacuum system, services and controls and connect with ISAC-I HEBT during the January, 2005 shutdown.

H-HEBT

Physics specifications of the H-HEBT have begun with the aim to have the layout finalized by February, 2005, after which the design and fabrication of the components will begin. The plan is to have the vault section of the H-HEBT ready for beam by December, 2005, and finish the installation into the first experimental station by April, 2006.

TIGRESS

The stand and substructure for one detector were fabricated and all the related electronics, readout systems and electronics for the prototype substructure were ordered and procured. The prototype substructure was tested in June, and as a result a new front suppressor block was designed in December. The new block will be installed in January, 2005 and new test results will be analyzed and evaluated with an aim to then be able to start on the design of the components for the remaining 4 detectors in May, 2005.

The optics design of the beam line has been completed and the overall engineering design will commence after May, 2005. The aim is to have all the beam line components assembled and installed and ready for beam in August, 2006.

TITAN

The TITAN platform was designed and ordered in December. It will be fabricated and then will be installed in location during the January, 2005 shutdown. Tests on the rf cooler in the proton hall started in the summer and will continue up to spring, 2005. The plan is to move it for tests with CSB in the test stand in May, 2005. The EBIT is being fabricated, assembled and tested in Heidelberg, Germany with the plan to be ready to ship to TRIUMF in the spring, 2005. The Wien filter has been received from McGill and is being prepared for installation on the platform. The transfer beam line system has been designed and fabrication began in the fall. The aim is to be able to install the transfer beam line in June, 2005. The Penning trap has been designed, and the superconducting magnet ordered. Design work will continue on the Penning trap components up to spring, 2005. The overall plan is to be able to install all the components on the platform and be ready for experiments by the end of 2005.

Actinide Target Test

A task force was formed to define the overall project scope with an aim to do preliminary tests and prepare a safety report for CNSC to get a license to do tests with RIB. A work breakdown structure was developed and the major subprojects included: alpha monitoring system, hot lab and target preparations and hot cell modifications. The project progress was slow in 2004 due to the longer time required to answer many outstanding questions in order to start proper engineering conceptual design.

Shutdown Activities

There were two shutdowns during the year: the winter shutdown (December 22, 2003 – March 17 for ISAC beam production), and a fall mini shutdown (September 13 – October 6).

The major jobs completed for ISAC included: rf system maintenance (coated surfaces of bunch rotator with Aquadag, commissioned spare control boards, design modifications for DTL #1 cooling system, commissioned remote controls for DTL #5 amp), implementation of access control system for electrical services room and DRAGON, OLIS work (MRO, source commissioning, controls MRO).

Completed target hall work included: ITW module access area MRO (rerouted cabling, cooling and vacuum services to tidy up the original installation), ITE

(EX1 harp MRO), TM1 work (replace target at ITW, replace faulty connector with new wiring harness for steering magnet), laser ion source alignment at ITW, installed modified ECR on TM3 and ECR tests (without target) at ITE.

CONTRACT ADMINISTRATION

In the past year three contracts were awarded: Linde Kryotechnik Agisac of Switzerland supplied and commissioned the refrigerator system for Phase I of the ISAC-II linac. The ISAC-II cryogenic refrigeration system warm piping was supplied and installed by Lockerbie and Hole Contracting Limited of New Westminster, BC. The ISAC-II Phase I helium gas storage tank was purchased from Gary L. Nadon Enterprises of Vancouver, BC.

Personnel Resources

ISAC-I

In 2004 the average monthly personnel effort for ISAC-I decreased by approximately 1 person per month to an average of 42.20 FTE people per month

(see Fig. 222). In 2003 the FTE effort per month was 43.28 people. The total work effort expended on ISAC-I from the start of the project January 1, 1996 to December 31, 2004 has been 559.01 years, based on a FTE work-month of 150 hours per person.

ISAC-II

The recording of work effort for ISAC-II started October 1, 2000 (see Fig. 223). The work effort was recorded as “Project Management and Administration” up until March 31, 2002. Commencing April 1, 2002 the work effort was monitored by section. In 2004 the average monthly personnel effort for ISAC-II increased by approximately 1.5 people per month to an average of 21.11 FTE people per month (see Fig. 223). In 2003 the FTE effort per month was 19.53 people. The total work effort expended on ISAC-II from the start of the project October 1, 2000 to December 31, 2004 has been 56.91 years, based on a FTE work-month of 150 hours per person. Figure 224 shows the FTE years of work effort for each section of ISAC-II since the project began.

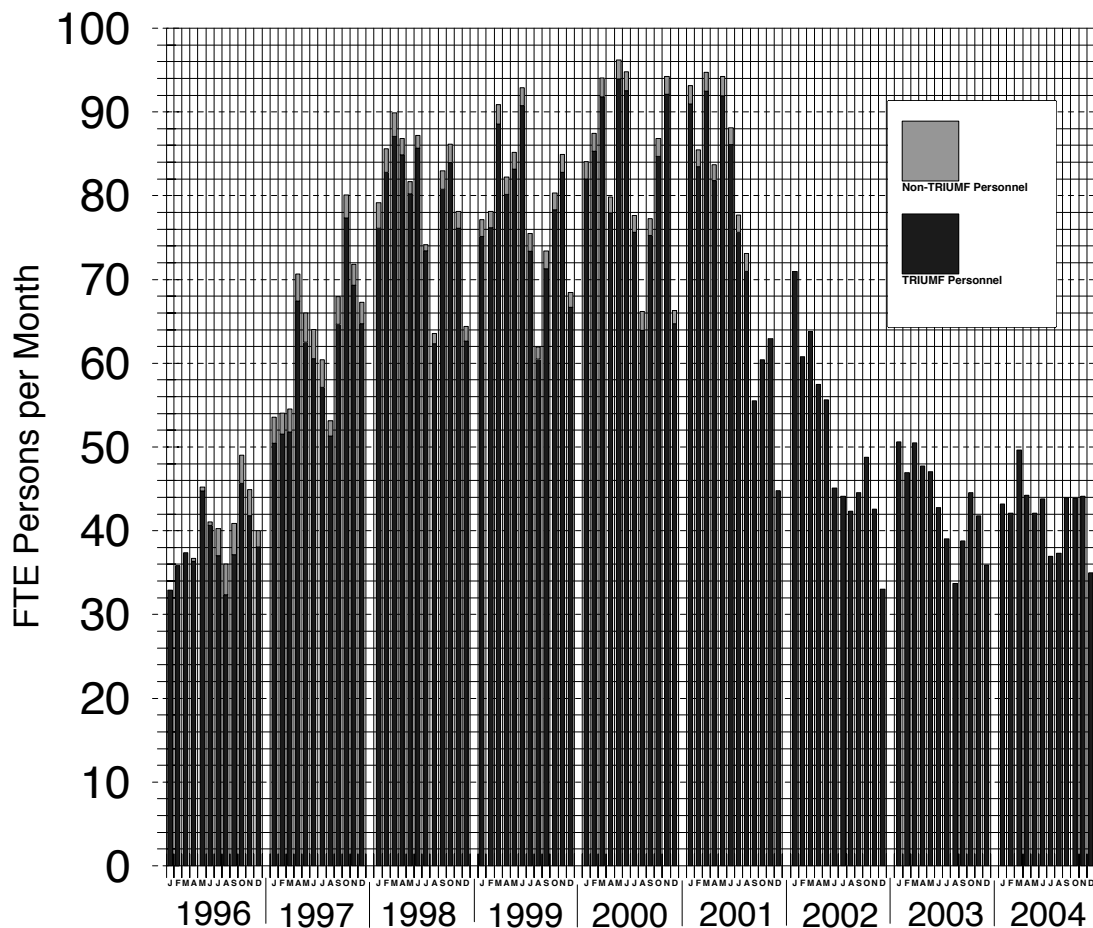


Fig. 222. ISAC-I monthly personnel effort, January 1, 1996 to December 31, 2004.

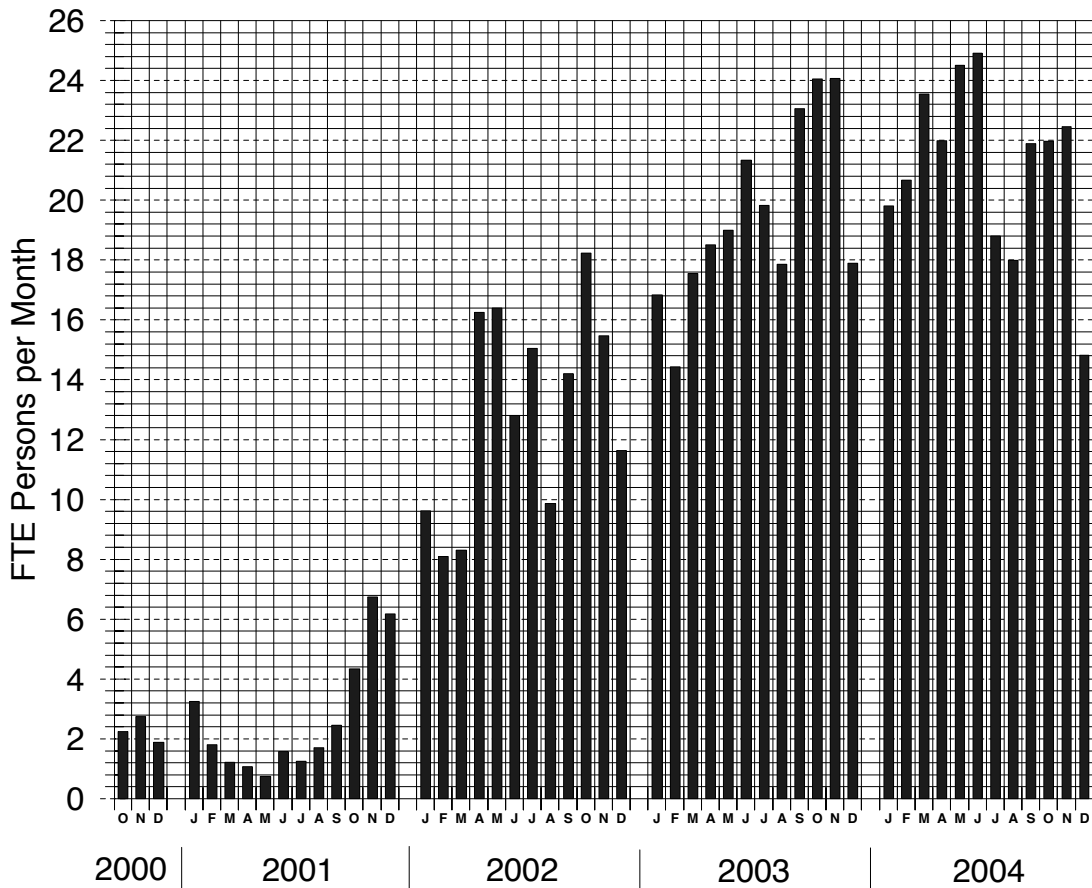


Fig. 223. ISAC-II monthly personnel effort, October 1, 2000 to December 31, 2004.

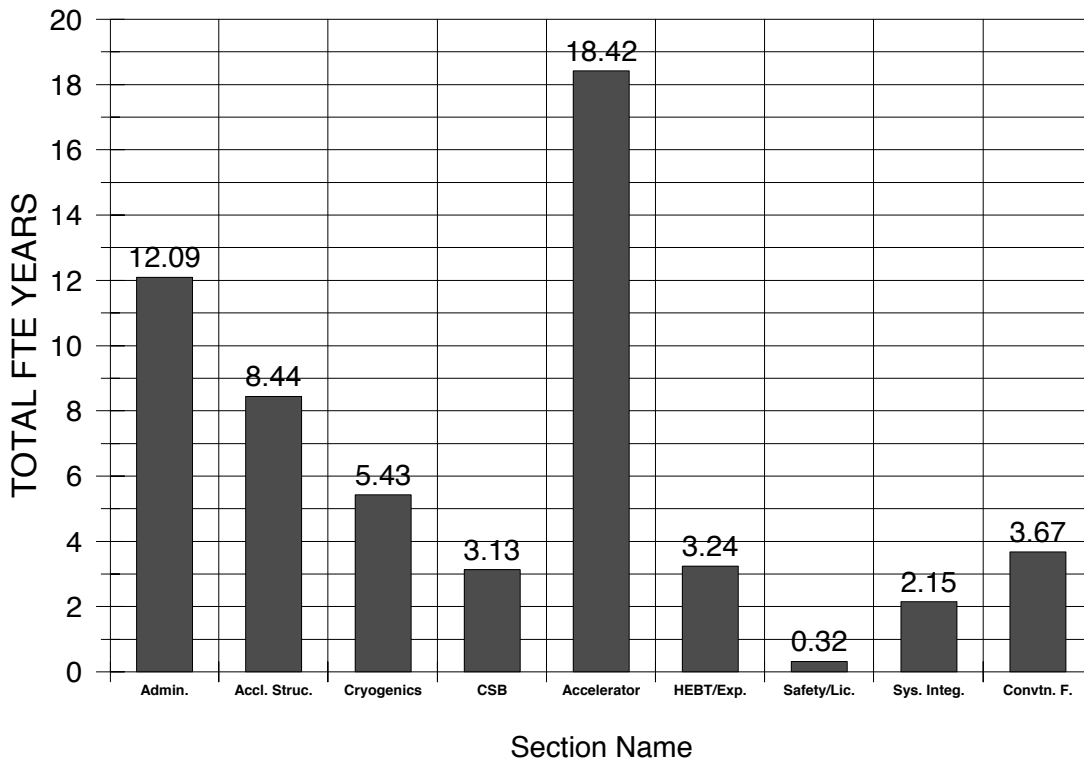


Fig. 224. ISAC-II total personnel effort, October 1, 2000 to December 31, 2004 shown by section.

ISAC-II CONVENTIONAL FACILITIES AND INFRASTRUCTURE

Activities in ISAC-II were mostly design and construction projects. In addition, we continued to provide engineering support to other groups and users and were involved in the preparation of specifications documents, and sat on several engineering review panels. Concurrently, civil construction deficiencies and warranty repairs continued, with the exception of the vault door deficiency. TRIUMF has taken this project into its own hands since the contractor was unwilling to properly fix the problem. We are currently reviewing the design concept, which includes using Thompson rollers instead of Hillman rollers.

On the mechanical services front, the depleted oxygen sensor system went through the entire process of design, review, tendering and construction. It was started up successfully just before Christmas, however, a few minor deficiencies remained and will be addressed during the winter shutdown. Air conditioning to the network computing centre continues to be scrutinized as it appears the thermal cycling provided by these units may not be sufficient for the sensitive electronics, in particular disk drives. There is some indication that temperature fluctuations greater than $1^{\circ}\text{C}/3$ min affect the performance and increase the failure rate of these devices. A solution is being studied. Several large mechanical projects came to an end. The NALCW system was started up and provided water to its first consumer, the rf test stand. Because of the contamination of the mains during construction of ISAC-II, cleaning and repeated flushing was required before water could be allowed to return to ISAC-I. After water was allowed to flow, the return water to ISAC-I was filtered for several weeks to ensure all loose materials were captured. One casualty was the de-ionizing resin which faithfully polished the new piping system before expiring. After having to polish the ISAC-I piping and five more years of service it was near the end anyway. A major upgrade of the air exhaust in the helium compressor room was also completed. The existing system was not able to meet the 40,000 CFM required.

On the electrical services front, we record the successful completion of the services for the helium refrigeration system, which was commissioned during the winter shutdown and the installation of the S-bend beam transport services. Activities in the latter will continue well into next spring, with commissioning expected in early June, 2005. Other activities to report include: the installation of a crane for the rf test area on the NW side of the experimental hall; a study to determine whether the services for the CSB would fit into the service room next to the mass separator vault in ISAC-I; the design of the upgrade of the UPS power

distribution for the network computer system and the expansion of the UPS distribution to supply the liquefier room and the S-bend. The review of the electrical power needs of the ISAC facility was also completed. It pointed to a few significant upgrades and re-alignments of the main power distribution centres to accommodate future load growth. The first of these upgrades, the MCC-S, will start during this coming winter shutdown with the remainder to follow over the next couple of years. Redundant fibre links were installed between ISAC-II and the administration building. These included 6 strands of single-mode fibres, and 48 strands of multi-fibres (24 of which are spares). DATA cabling was completed for room 163, the rf services and S-bend, room 164, the liquefier room, room 166, the helium compressor room, the vault and the experimental hall. The power supply room DATA cabling is planned for next year.

ISAC-II ACCELERATORS

Introduction

The ISAC-II linac is being installed in stages. The superconducting linac is composed of two-gap, bulk niobium, quarter wave rf cavities, for acceleration, and superconducting solenoids, for periodic transverse focusing, housed in several cryomodules. The initial stage to be completed in 2005 includes the installation of a transfer line from the ISAC DTL ($E = 1.5$ MeV/u) and twenty medium beta cavities in five cryomodules to produce 20 MV of accelerating voltage for initial experiments.

Cavity Testing

To date, fifteen cavities have been characterized via cold tests. Typical treatment involves a 30–40 minute high pressure water rinse and 24 hour air dry in a clean room, followed by vacuum pumping and bakeout at 95°C for 48 hours, then an LN_2 pre-cool to 160 K over 48 hours followed by helium transfer and test. A distribution of the cavity performance is shown in Fig. 225 for both the characteristic fields at 7 W cavity power and at maximum power. Four cavities out of the fifteen have not met specification with one cavity limited to 3 MV/m. Developments are under way to determine the cause of the reduced performance. A further chemical polishing may be required.

Medium Beta Cryomodule

The vacuum tank consists of a stainless steel rectangular box and lid. All services and feedthroughs are located on the lid. The entire cold mass is surrounded by a forced flow, liquid nitrogen cooled, copper thermal shield. A μ -metal magnetic shield, consisting of 1 mm Conetic panels is attached to the inside of the vacuum tank outside the LN_2 shield. A single LN_2 panel and

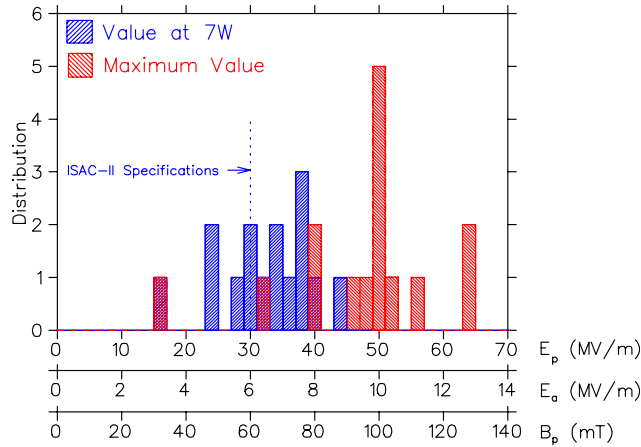


Fig. 225. Histogram summarizing cavity performance for fifteen tested cavities. Shown are the numbers of cavities achieving a certain gradient at 7 W helium load (blue) and the numbers of cavities achieving a certain maximum field (red).

μ -metal shield suspended from the lid make up the top thermal and magnetic enclosure respectively. The μ metal is designed to suppress the ambient field by a factor of twenty. Cavities and solenoids are suspended from a common support frame itself suspended from the tank lid (Fig. 226). Each cryomodule has a single vacuum system for thermo-isolation and beam acceleration. The cavities must be aligned to within 0.4 mm and the solenoid to 0.2 mm. A wire position monitor system has been developed to monitor the position of the cold mass during thermal cycling.

The ISAC-II medium beta cavity design goal is to operate up to 6 MV/m across an 18 cm effective length with $P_{\text{cav}} \leq 7$ W. The gradient corresponds to an acceleration voltage of 1.1 MV, a challenging

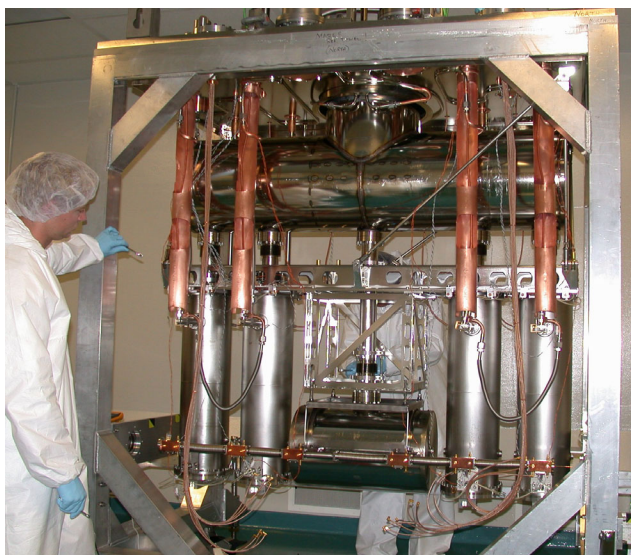


Fig. 226. Cryomodule top assembly in the assembly frame prior to the cold test.

peak surface field of $E_p = 30$ MV/m and a stored energy of $U_o = 3.2$ J and is a significant increase over other operating heavy ion facilities. To achieve stable phase and amplitude control, the cavity natural bandwidth of ± 0.1 Hz is broadened by overcoupling to accommodate detuning by microphonic noise and helium pressure fluctuation. The chosen tuning bandwidth of ± 20 Hz demands a cw forward power of ~ 200 W ($\beta \simeq 200$) and peak power capability of ~ 400 W to be delivered to the coupling loop. A new coupler has been developed that reduces the helium load to less than 0.5 W at $P_f = 200$ W. The tuning plate on the bottom of the cavity is actuated by a vertically mounted permanent magnet linear servo motor at the top of the cryostat using a “zero backlash” lever and push rod configuration through a bellows feed-through. The system resolution at the tuner plate centre is ~ 0.055 μm (0.3 Hz). The solenoids are equipped with bucking coils to reduce the fringe field in the adjacent cavities to < 50 mT.

Cryomodule Testing

The cryomodule assembly and commissioning tests are conducted in the clean laboratory area in the new ISAC-II building. Three cold tests have been completed. An EPICS based control interface is used to interact remotely with the cryomodule systems during the test.

An initial cold test I in April, without rf ancillaries installed, characterized cryogenic performance and determined the warm off-set required to achieve cold alignment. In cold test II the integrity of the rf and solenoid systems was checked as well as the repeatability of the initial cold alignment. In cold test III the cavities were prepared for final installation with a final high pressure water rinse before reassembly with machined alignment shims. During this third test the cryomodule was outfitted with an alpha source and acceleration was demonstrated for the first time.

Alignment

The position of the cold mass as monitored by the WPM at three cold LN₂ temperatures is repeatable to within ± 50 μm vertically and ± 100 μm horizontally. Due to the different materials involved, the solenoid experiences more vertical contraction, with 4.4 mm at LN₂ and 5 mm at LHe temperatures while the cavities contract 3.3 mm at LN₂ and 3.8 mm at LHe temperatures. For beam dynamics reasons we require the cavity beamport centre line to be 0.75 mm below the beam centre line as defined by the solenoid. Cold tests I and II results show that final alignment is achieved by aligning the cavities while warm to (0,0,0) horizontally and (+0.28,+0.38,+0.38,+0.28) vertically with the solenoid at $(x, y) = (0, 0)$. Optical targets are then

placed in the upstream and downstream solenoid bore for cold test III. The beam axis is defined by optical targets on the beam aperture of the tank. Adjusters located on the lid are used to align the solenoid targets to the beam axis targets after cooling the cold mass.

Cryogenics

The helium transfer line fits to a manifold in the helium space that delivers helium in parallel to a series of 3 mm tubes that are routed to the bottom of each of the cold mass elements. This system works well to efficiently cool the cryomodule. At a total flow of 75 l/hr the cavities cool together at a rate of 100 K/hr while the solenoid cools at a rate of 20 K/hr due to its larger mass. The static load on the helium in the three tests is measured to be 11 W, 16 W and 13 W respectively. The differences are due to the variations in the internal cabling and equipment used in each test. The final value of 13 W is representative of the load for the on-line system and compares well to estimates during the design phase. The LN₂ flow required to keep the side shield less than 100 K is ~ 5 l/hr, matching design estimates.

Cavities and solenoid

The cavities are first baked at $\sim 90^\circ\text{C}$ for 24 hours. The cold mass is pre-cooled with LN₂ to about 200 K before helium transfer. The quality factor of each cavity is determined by measuring the time constant of the field decay in pulsed mode at critical coupling. The Q_0 values for test II, presented in Table XLVI, are similar to those measured in the single cavity cryostat indicating that the μ -metal reduces the remnant magnetic field to a sufficient level. In the first rf test (cold test II) the solenoid is ramped up to 9 T with cavities 2 and 3 ON. The cavities remain ON and the measured Q_0 values do not change. The solenoid and cavities are then warmed above transition. After a subsequent cooldown the cavity Q_0 values are again measured. There is no change in the values showing that fields induced by the solenoid in the region of the cavities are tolerably small.

After test I the cold mass is removed from the cryomodule and the top plate is replaced by sheets of μ metal. The remnant field inside measured longitudinally at the beam axis and vertically in the cryomodule (-1 is at the top) are shown in Fig. 227. Also plotted are values from new cryomodule SCB1 after assembly and before powering the solenoid. Note that the fields in SCB3 are significantly higher especially in the middle of the cryomodule in close proximity to the solenoid. It appears that the solenoid is magnetizing the μ metal enclosure or the nickel in the LN₂ shield. In subsequent tests a hysteresis cycling of the cryomodule will be employed to reduce the remnant field. A field higher than $5 \mu\text{T}$ will start affecting the performance.

Table XLVI. Cavity performance during cold tests II and III.

Test	Cavity 1 $Q/10^9$	Cavity 2 $Q/10^9$	Cavity 3 $Q/10^9$	Cavity 4 $Q/10^9$
II	1.5	1.4	1.5	1.3
III-1	1.25	1.03	1.42	1.13
III-2	0.745	0.89	1.17	0.76
III-3	0.41	0.20	0.19	0.28
III-4	1.12	0.76	1.18	0.75

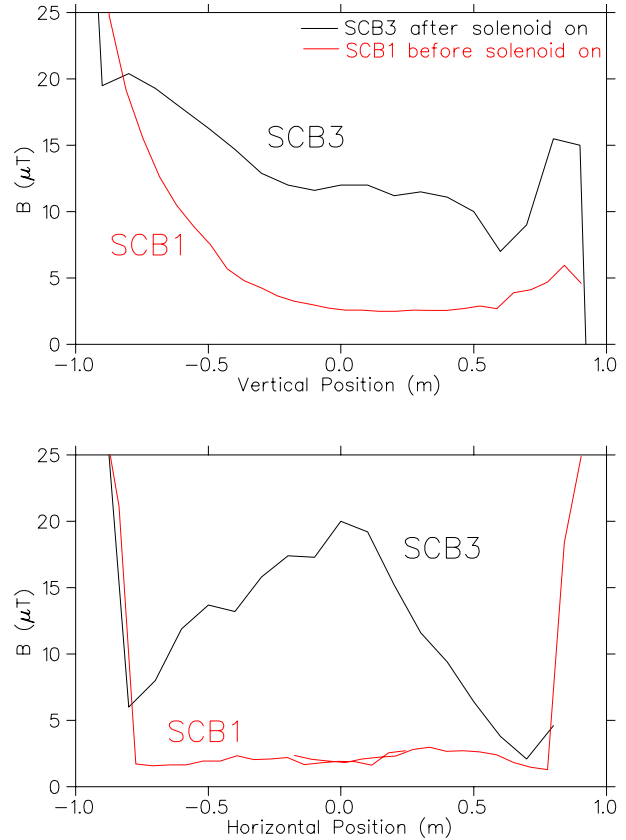


Fig. 227. Longitudinal and vertical magnetic field maps inside cryomodule SCB3 (warm) after test II compared to a mapping on new cryomodule SCB1.

nally at the beam axis and vertically in the cryomodule (-1 is at the top) are shown in Fig. 227. Also plotted are values from new cryomodule SCB1 after assembly and before powering the solenoid. Note that the fields in SCB3 are significantly higher especially in the middle of the cryomodule in close proximity to the solenoid. It appears that the solenoid is magnetizing the μ metal enclosure or the nickel in the LN₂ shield. In subsequent tests a hysteresis cycling of the cryomodule will be employed to reduce the remnant field. A field higher than $5 \mu\text{T}$ will start affecting the performance.

In test II Q_0 values are taken periodically and the results are reported in Table XLVI. We attribute the large range in values to trapped flux in the solenoid. Since the modules are filled from dewars the cryomodules are allowed to warm overnight. Fig. 228 gives the temperature of the solenoid and cavities during the test. Labels Q1–Q4 indicate the time of Q measurements corresponding to III-1 to III-4 in Table XLVI. Labels S1–S5 indicate powering of the solenoid. The cavity temperatures rise above transition during the night but portions of the solenoid remain below transition. In addition for cases S1, S4 and S5 a hysteresis cycling of the solenoid occurs. For cases S2 and S3 no

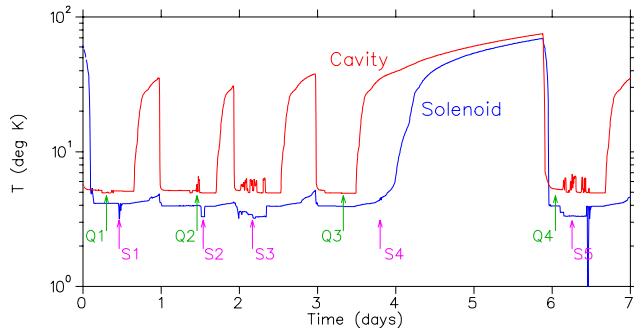


Fig. 228. Temperature history of cavities and solenoid during test III. Q1–Q4 indicate the time of the Q_0 measurements reported in Table XLVI and S1–S5 indicate solenoid on periods.

cycling is done. Taking the Q_0 values for case III-1 as a base and assuming the subsequent reduction in Q_0 is due to an increase in R_{mag} gives an estimate of the magnetic field increase. The resulting estimations are summarized in Fig. 229. Note that the field increase is largest near the solenoid.

RF control and tuning

A new EPICS GUI interface provided remote tuning control for the four cavities during test III. All four cavities were locked at ISAC-II specifications, $f = 106.08$ MHz, $E_a = 6$ MV/m with a coupling $\beta \simeq 200$ for tuning bandwidth. Stable operation was maintained for several hours. Tuner operation is tested by forcing pressure variations in the helium space. The tuner plate position of the four cavities during one perturbation cycle is shown in Fig. 230.

Alpha Acceleration

The cold tests establish the integrity of the cryomodule and rf ancillaries but do not qualify the unit as an accelerator. An off-line acceleration test with alpha particles from a radioactive source has several key motivations: to establish the integrity of the cryomodule as an accelerator months before an on-line beam

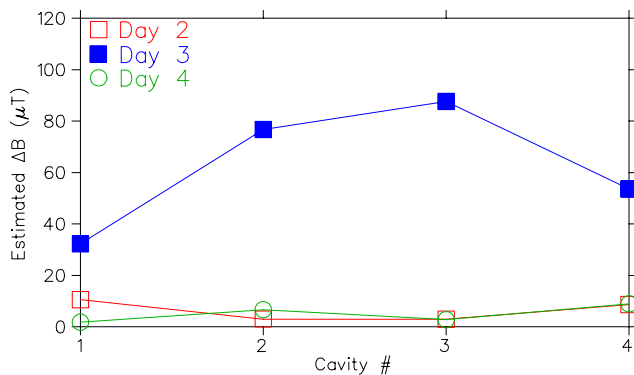


Fig. 229. Estimated change in background magnetic field at times corresponding to Q2–Q4 compared to field at Q1.

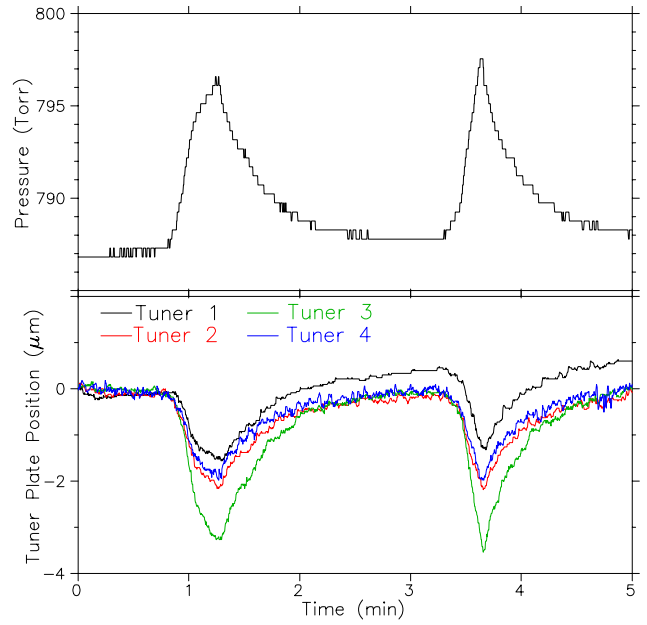


Fig. 230. Tuner position response for forced pressure fluctuations in the helium space. The cavity gradient is 6 MV/m with a bandwidth of ± 20 Hz.

test is possible, to measure directly the total voltage of the cryomodule, and to gain first experience with the proposed ISAC-II accelerator control system and GUI interface.

Test set-up

The cryomodule tests are done in the test pit of the ISAC-II clean room. The source is installed in the beam aperture of the upstream diagnostic box and the silicon detector is mounted in a diagnostic box positioned at the exit of the cryomodule downstream of the isolation valve as shown in Fig. 231.

A ^{244}Cm alpha source, borrowed for the experiment, emits alpha particles with energies 5.76 MeV (24%) and 5.81 MeV (76%) with a half life of 18 years and an activity of 10^7 Bq. It is covered by a $5 \mu\text{m}$ foil of Ti to contain the radioactive material. Due to safety concerns over foil rupture and possible migration of

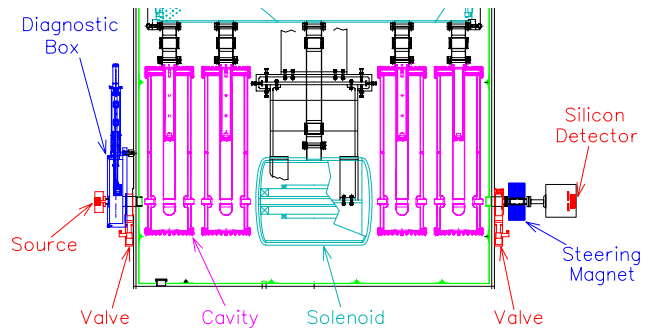


Fig. 231. The test set-up for the alpha particle acceleration. The particles are accelerated from left to right.

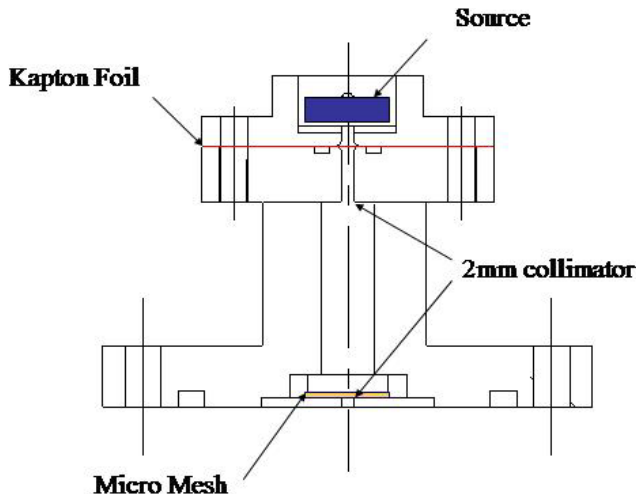


Fig. 232. The source and holder.

the alpha emitters the source remains at atmosphere. A source holder (Fig. 232) is equipped with an $8\ \mu\text{m}$ kapton window over a 2mm aperture that serves as a vacuum window. Another 2mm aperture lies downstream to further collimate the alpha beam and limit the molecular conductance in case of window failure. A foil micro-mesh (60% transmission) is installed in the downstream 2mm aperture to catch foil fragments in the case of window rupture. The source holder has a vacuum flange on the downstream end that mates with the upstream diagnostic box of the cryomodule. The Ti and kapton foils degrade the energy spectrum of the alphas to 2.85 MeV with a standard deviation of 200 keV.

A diagnostic box is placed 40 cm downstream of the cryomodule and is connected to the vacuum space by a 5 cm diameter vacuum pipe that can be isolated by a VAT valve connected to the module. A steering magnet is placed between the cryomodule and the diagnostic box to clear any electrons accelerated by the cavities. A silicon surface barrier detector is mounted on the back of the box with a moveable collimator wheel assembly in front to intercept the deflected electrons.

An accelerating gradient of 6 MV/m corresponds to a peak voltage gain of 1.08 MV for an effective length of 18 cm. The alpha particle average initial energy of 2.85 MeV/u ($\beta = 3.9\%$) is low with respect to the design geometry of the cavity. The expected transit time factors, energy gain/cavity and expected final energy are given in Table XLVII.

Multi-particle simulations are done with the linac code LANA. The source collimator geometry is modelled to generate a realistic initial transverse phase space. The transverse beam parameters after collimation are $\alpha_{x,y} = -1.0$, $\beta_{x,y} = 0.0055$ mm-mrad and $\beta\epsilon_{x,y} = 0.45\ \pi$ mm-mrad. Realistic three-dimensional fields generated by HFSS are used to represent the

Table XLVII. Expected energy gain for 2.85 MeV alpha particles accelerated through four ISAC-II cavities at 6 MV/m.

Cavity	E_{in}	T/T_0	ΔE (MeV)	E_{out}
1	2.85	0.46	0.99	3.84
2	3.84	0.75	1.62	5.46
3	5.46	0.92	1.99	7.45
4	7.45	0.99	2.14	9.59

cavities and the solenoid is modelled with the standard linear matrix. Previous modelling studies have shown that the solenoid matrix represents a ray traced solution to close approximation.

Test results

The collimation reduces the intensity to ~ 40 pps while the accelerator acceptance reduces this further to ~ 4 pps. Since the beam is unbunched, the actual count distribution for the higher energy particles of interest is very weak. The cavities are turned on sequentially starting at the upstream end. Each cavity is first set to the correct voltage. The solenoid is set to the optimal value found from the simulations. With the exception of cavity 1, the cavity phase is scanned in 30° phase increments to find the optimum phase. Each phase set point takes 5–10 minutes before a reasonable spectra is obtained. Once the correct phase is determined, the spectra for the optimized settings are taken for twenty minutes.

The spectrum for the cavities off as well as the four spectra as the cavities are turned on sequentially are plotted in Fig. 233. Maximum particle energies for the four cases are 4.2, 5.8, 7.4 and 9.4 MeV. The results for the first two cavities are higher than the calculated single particle values in Table XLVII due to the large energy spread in the initial beam. The maximum final energy depends on the phasing of the cavities and the relationship of the cavity phases to the initial energy of the beam. During the test, cavity phases are chosen to optimize the energy of a statistically significant number of particles. These particles would come from some energy band located between the mean initial energy and the highest initial energy.

A true analysis of the cavity voltage can only be done with a simulation. Due to the poor quality of the injected beam, most of the ions are only partially accelerated. The spectra for the unbunched, uncollimated beam provide, however, a spectral fingerprint. As the voltage and phase of the cavities in simulation are varied the distribution of the most energetic ions, as well as that of the lower energy peaks, shifts and an unambiguous fit of cavity voltage is possible. The best fit simulations are superimposed on the test data in Fig. 233. The corresponding

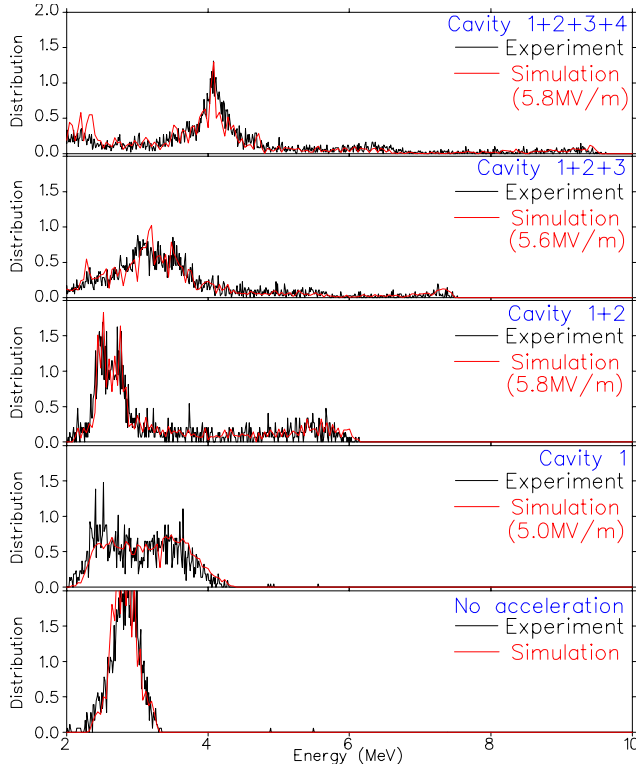


Fig. 233. Experimental spectra (black) and simulation result (red) for no acceleration, and for each case with cavities from 1 to 4 on sequentially at the nominal voltage of 6 MV/m.

cavity voltages for these cases are 5, 5.8, 5.6, and 5.8 MV/m for cavities 1 through 4 respectively for an average gradient of 5.6.

High Beta Cavities

The linac for ISAC-II comprises twenty cavities of medium β quarter wave cavities now in the installation phase. A second stage will see the installation of ~ 20 MV of high β quarter wave cavities. The cavity structure choice depends on the efficiency of operation, cost, stability, beam dynamics and schedule. Three cavity variants are considered and shown in Fig. 234. The benchmark cavity, (a) *round141*, has identical transverse dimensions to the medium beta cavity but is designed as a 141 MHz cavity by shortening the overall length and adjusting the gap. In a second variant,

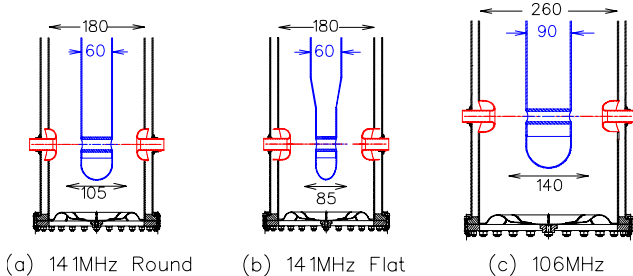


Fig. 234. Three cavity variants considered in the study.

(c) *round106*, the cavity frequency is kept at 106 MHz but the cavity transverse dimensions are scaled to increase the beta from 7.1% to 10.4%. The quadrupole asymmetry in the accelerating fields is somewhat larger in the high frequency case by virtue of the smaller inner conductor. A third variant, (b) *flat141*, is also considered where the 141 MHz cavity inner conductor is flattened near the beam ports to produce a smaller quadrupole asymmetry. This variant has a lower optimum beta, 9%, suitable for use in the beginning of the high beta section.

Previous beam dynamics studies have shown that the reduced quadrupole asymmetry in the *round106* cavity results in less asymmetry in the transverse envelope compared to the other two 141 MHz variants. However, the transverse and longitudinal emittance growth for the three cases are virtually identical. The beam centroid shifts are tolerably small in all cases.

RF characteristics

The rf parameters of the three cavity variants are given in Table XLVIII. The cavity rf properties are simulated in HFSS. We compare all cavities at a gradient of 6 MV/m calculated over the cavity length defined as the inside diameter of the outer rf surface. There is little difference between the two 141 MHz variants except for the higher peak surface field in the *flat141* variant. Instead we concentrate here on the comparison of the *round141* and the *round106* variants. Due to the increased voltage the main practical difference is that fewer sub-systems (14 as compared to 20) would be required for the lower frequency. However, due to the higher stored energy and somewhat higher Q_0 (see

Table XLVIII. Parameters of cavity variants.

Parameter	<i>round141</i>	<i>flat141</i>	<i>round106</i>
f (MHz)	141.4	141.4	106.1
β_0	0.104	0.09	0.103
TTF ₀	0.089	0.086	0.093
Bore (mm)	20	20	20
Gap (mm)	45	45	50
Drift tube (mm)	60	40	90
L_{eff} (mm)	180	180	260
Height (mm)	577	577	737
Δy (mm)	1.3	1.0	2.0
f_{mech} (Hz)	150	150	134
E_a (MV/m)	6	6	6
V (MV) @ 6 MV/m	1.08	1.08	1.56
E_p/E_a	4.7	5.6	4.6
B_p/E_a (mT/MV/m)	10.3	10.5	9.9
U/E_a^2 (J/(MV/m) ²)	0.073	0.078	0.194
$R_s Q_0$ (Ω)	24.8	24.9	26.8
R_{sh}/Q (Ω)	499	470	521

below) more power is required to provide a sufficient tuning bandwidth.

Let us examine the role of rf frequency in cavity scaling. The surface resistance is given by

$$R_s = R_{BCS} + R_{\text{mag}} + R_0$$

where

$$R_{BCS} = 2 \times 10^{-4} \frac{1}{T} \left(\frac{f}{1.5} \right)^2 e^{-17.7/T}$$

and

$$R_{\text{mag}} = 0.3n\Omega \cdot H_{\text{ext}}(mOe) \sqrt{f(GHz)}.$$

Results of these expressions are shown in Table XLIX assuming a magnetic field attenuation factor of five from the earth's field. The TRIUMF medium beta cavity has a typical Q of 1.5×10^9 at low field that droops to 5×10^8 at a gradient of 6 MV/m. Since $R_s Q = 19 \Omega$ for this cavity, this corresponds to surface resistance values of 12.7 and 38.2 n Ω . Assuming R_0 is independent of frequency we can estimate that the high-field surface resistance for the 141 MHz cavity is enhanced due to the increased values of R_{BCS} and R_{mag} to be 42.5 n Ω , an increase of 11%. Using these values of R_s and the tabulated values of $R_s Q_o$ gives expected Q_o values of 5.8×10^8 and 7×10^8 respectively for the *round141* and *round106* cavity respectively. The cavity power dissipation, $P_{\text{cav}} = \omega_o U / Q_o$, is listed in Table XLIX.

The increased quality factor of the 106 MHz cavity increases the amount of overcoupling required to achieve a specified rf bandwidth (in our case $\Delta f / f = 4 \times 10^{-7}$). The forward power can be calculated from the coupling factor, β , and the cavity power using $P_f = P_{\text{cav}} * (\beta + 1)^2 / (4\beta)$. To provide for the bandwidth the peak amplifier power must be sufficient to deliver twice the required forward power after considering the line losses. These deliberations lead us to estimate that the required amplifier would be almost a factor of two larger in the 106 MHz case.

Table XLIX. Frequency dependence of surface resistance and cavity power.

Parameter	106 MHz	141 MHz
R_{BCS} (n Ω)	3.5	6.3
R_{mag} (n Ω)	9.8	11.3
R_0 (n Ω)	25	25
R_s (n Ω)	38.2	42.5
Q_o @ 6 MV/m	7×10^8	5.8×10^8
P_{cav} (W) @ 6 MV/m	6.7	4.2
β	280	230
P_{amp} (W) @ 6 MV/m	1200	620

Cavity choice

There is no strong beam dynamics argument to choose one variant over another. The total dissipated cavity power is 17% less in the high frequency cavity and the total amplifier power is 29% less. The high frequency cavity is also somewhat more mechanically stable. These advantages are not sufficient to force a cavity choice. The most compelling argument is that the design time for the 141 MHz cavity, the ancillaries and the cryomodule will be significantly less. This is balanced somewhat by the attractiveness of reducing the number of sub-systems by adopting the lower frequency. However, the 141 MHz option has been chosen as the high beta cavity for ISAC-II.

Cryogenics

The ISAC-II Phase I cryogenic system was specified for tender in early 2003. Initially a complete turnkey system including refrigerator, warm and cold piping, buffer tank, helium dewar, compressors, gas management and oil removal system was requested. All returning bids were overbudget. TRIUMF decided to take on a larger role in the project in order to reduce the capital costs. The scope of the initial contract was restricted to the major refrigerator components: refrigerator, main and recovery compressor and ORS/gas management. TRIUMF assumed the responsibility for installation of the Linde refrigerator components as well as the management of the contract for the installation of the warm piping by a local installer. In addition TRIUMF acquired and installed the buffer tank and helium dewar. The cold distribution is now specified by TRIUMF and the contract for manufacture and installation will be awarded in 2005.

In the first phase, to be completed by December, 2005, five medium beta cryomodules will be installed. The linac cryomodules will be cooled by 4.5 K LHe at 1.4 bar. The measured static heat load for a single cryomodule is 13 W with a LN₂ feed of 61/hr. Together with estimated thermal losses from the cold distribution of 72 W this gives a total static load of 137 W. The budget for active load component is 8 W per cavity giving 160 W for the twenty medium beta cavities for a total estimated heat load of 297 W. A TC50 cold box complete with oil removal and gas management system, main and recovery compressors was purchased from Linde and installed by TRIUMF with commissioning slated for early 2005.

Cold distribution

The refrigerator supplies liquid helium to a dewar via a Linde supplied transfer line. The main trunk supply line is fed LHe from the dewar. The cryomodules are fed in parallel from a helium supply trunk line through variable supply valves and field joints. The

cold return from the cryomodules comes back to the trunk cold return line through open/close valves and field joints. During cooldown, when warmer than 20 K, the returning gas is sent back to the suction side of the compressor through the warm return piping. Keep cold sections with proportional valves are required at the end of the trunk lines to join the trunk supply and the trunk cold return. Future expansion will involve demounting the keep cold sections, extending the trunk and cryomodule feed lines and remounting the keep cold sections. A second refrigerator will be added in two years. Pipe sizes and expected mass flows for the cold distribution are given in Table L. Valves specified for the middle of the two trunk lines are for future installations to divide flows between two refrigerators. They can be installed as just valve seats with the stems left out, and run continuously open for Phase I. In addition to the branch lines supplying the five cryomodules, a secondary line off the main trunk supply is required to deliver LHe to the ISAC-II test/assembly area. All supply and cold return piping is vacuum jacketed and, except for the short cryomodule feed lines, is cooled with LN₂.

A cross section of vault and refrigerator room is shown in Fig. 235.

Table L. Cold distribution specifications.

Pipe	Supply ID (mm)	Return ID (mm)	Mass flow (gm/s)
Dewar to trunk	18	45	25
Trunk	18	45	25
Cryomodule	13.8	32	5
Clean room	13.8	32	5
Keep cold	–	13.8	2

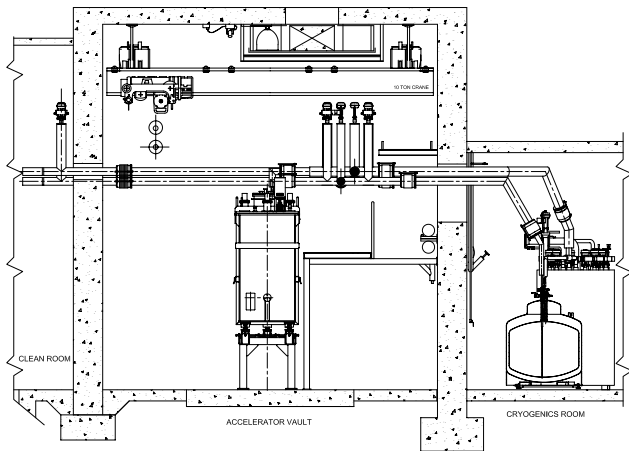


Fig. 235. Vault and refrigerator room cross section showing cryomodule, cold piping, service platform, helium dewar and cold box.

Beam Lines

The S-bend transport line from the ISAC-I hall to the superconducting linac is almost complete. The line consists of two achromatic bend sections of $\sim 120^\circ$ with two 4Q straight segments between. A 35 MHz buncher between straight segments matches the beam from the ISAC-I DTL to injection into the SC linac.

The high energy beam line is designed with a removable section to be compatible with the installation of the high beta cryomodules. This represents a full length of 8.84 m so two 4.42 m long 4Q sections are used. This periodicity is maintained to the end of the vault within all five 4Q sections. The sections can be tuned to unit cells with double focus points at the end of each section or to periodic doublet sections with a phase advance of $\sim 90^\circ$ for multicharge transport. Previous studies have shown that the accelerator can accommodate multicharge beams up to $\Delta Q/Q = \pm 10\%$. The present beam line design will accommodate such beams with some emittance growth due to the mismatch at the first cell after the linac.

At present the plan is to use existing dipoles from Chalk River to deliver beam up to three experimental stations. The installation of these beam lines will be staged over the next several years.

ISAC-II HEBT AND EXPERIMENTAL HALL

The ISAC-II accelerator will take the beam from the DTL-1. To increase the mass range from 30 u to 150 u, we will rely on a charge state booster. Consequently, the expected beam emittance is larger than the one used for the DTL-1. Figure 236 shows the beam emittance as a function of the output beam energy. The solid curve is the nominal beam emittance, the dotted line represents the expected beam emittance if the charge state booster is in use. We have to assume the largest expected emittance in order to make sure that the transport calculations are realistic.

The design of the beam lines is based on the available magnets and quadrupoles from the Chalk River Laboratory. We have two Y-magnets and 18 magnetic quadrupoles that can be used for the ISAC-II beam lines.

Figure 237 shows the layout of the ISAC-II experimental area. The beam lines will be built in stages. For the moment, four facilities that we know about are to be installed in the ISAC-II experimental hall:

1. TIGRESS, a gamma ray spectrometer;
2. HERACLES, a heavy ion detector array for the study of reaction mechanisms;
3. A large acceptance light ion detector array for (p, p) , (α, p) , ... reactions; and
4. EMMA, a recoil spectrometer.

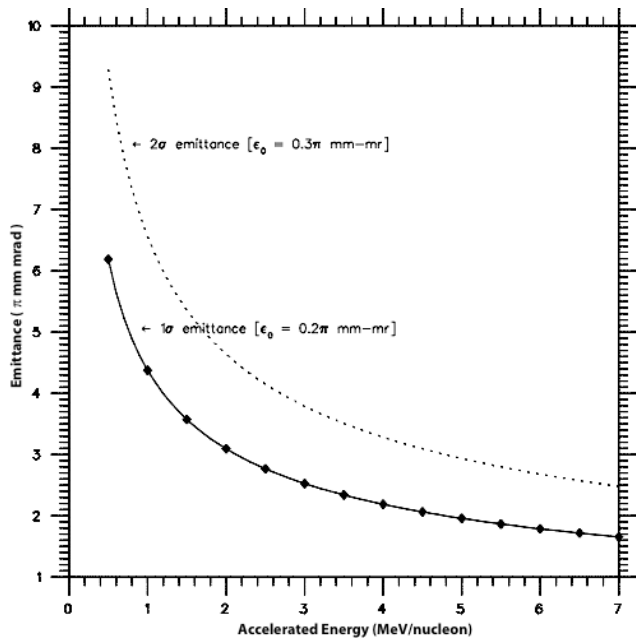


Fig. 236. Plot of the expected emittance as a function of the output energy.

Phase 0 in April, 2006 will accommodate a short beam line to perform the first beam experiment. It will most likely be a ^{21}Na Coulomb excitation experiment, which requires very little infrastructure.

Phase I (represented in light blue) will accommodate the TIGRESS facility with the beam dump. It will be completed during the fall, 2006.

Phase II is represented in red. Once the second leg is installed, we will be able to accommodate the HERACLES detector (light green), the TUDA-II detector facility, and the EMMA recoil spectrometer. The next step will be an expansion with a linear rail system which will allow TIGRESS to move from its stand-alone station to EMMA.

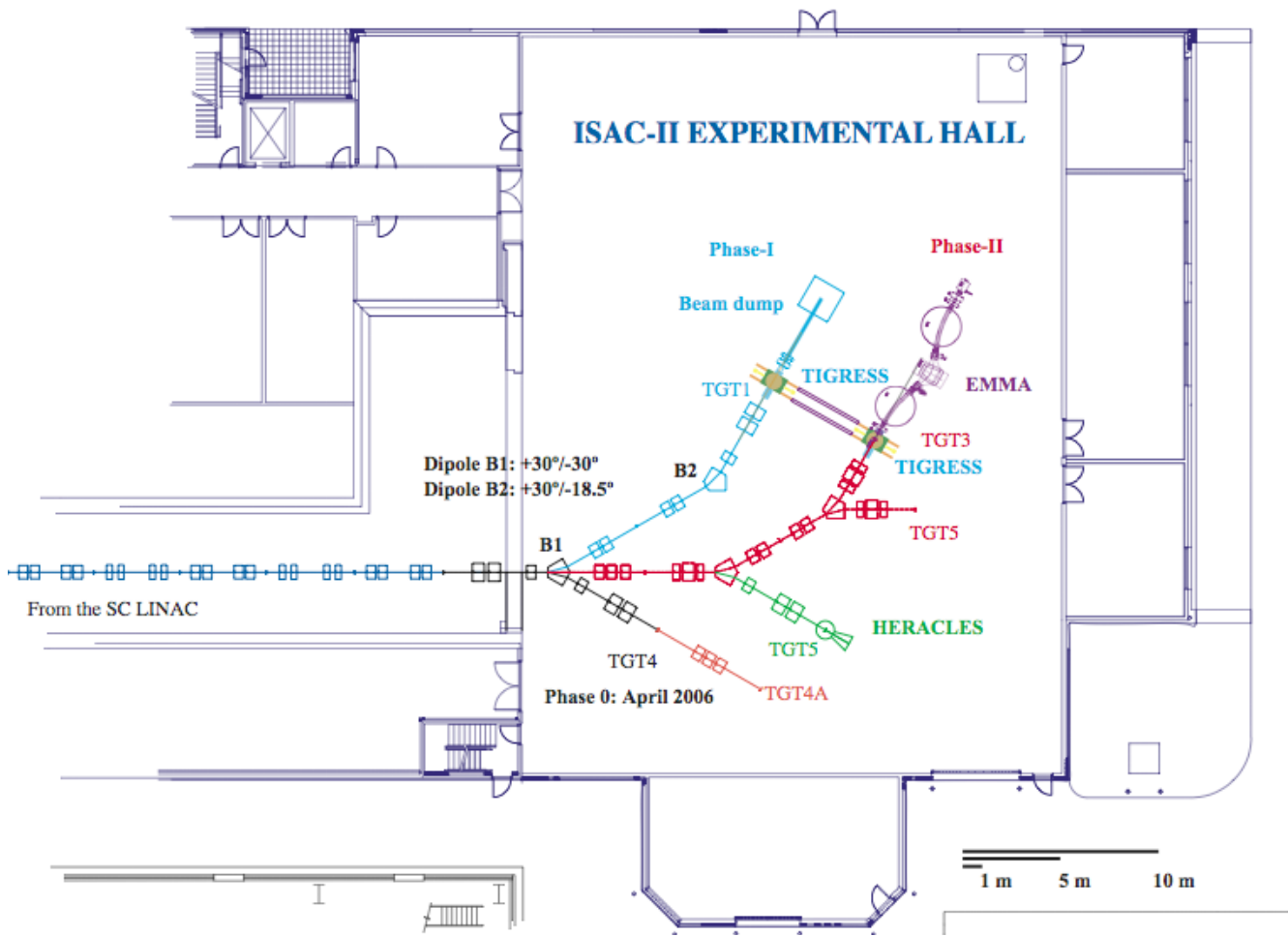


Fig. 237. Layout of the proposed beam lines for the ISAC-II experimental hall.

ACCELERATOR TECHNOLOGY DIVISION

INTRODUCTION

The Accelerator Technology Division is responsible for most of the engineering, design and fabrication at TRIUMF. Other responsibilities include planning for projects and shutdowns, electronics development and services, the Building department, the Design Office and Machine Shop. The site beam dynamics effort is also now coordinated through the division. This year, as for the past number of years, much of the available effort went into supporting the ISAC-II project. In the Requests for Engineering Assistance (REA) that were submitted during the year, there were 40 ISAC related jobs and 34 non-ISAC in mechanical engineering and design. In electronics development there were 29 REAs and in electronics services there were 16 REAs.

On external projects, the Beam Dynamics group continued their work on the design of FFAG accelerators with special effort on the specification of an electron model.

Magnet work included the supervision of contracts for the superconducting solenoids being fabricated by Accel Instruments, the S-bend dipoles for the ISAC-II transfer line, and the large coils for the Q_{weak} experiment at Jefferson Lab. The Kicker group started on the design of a kicker for the Brookhaven AGS upgrade project and also made improvements and repairs to the MuLan kicker developed for an experiment at PSI.

Among the achievements in the engineering and design groups, and for many other groups at TRIUMF, was the first ISAC-II cryomodule assembly and tests and the successful commissioning of the 500 W refrigeration system by Linde Kryotechnik. Support was also given to TITAN, TIGRESS and external projects, KOPIO at Brookhaven and K2K, T2K at J-PARC in Japan. The Design Office has decided to adopt SolidWorks 3D modelling software as the site standard.

The Planning group looked after the scheduling and coordinating of the many ISAC projects, the planning of the cyclotron shutdowns and the priority scheduling in the Machine Shop. The Machine Shop purchased a second CNC vertical machining centre to increase the efficiency and capability in meeting the demanding requirements for fabrication.

The Building department was involved in several structural projects for ISAC, including the installation of the large helium tank for the ISAC-II refrigeration system and the TITAN platform. The usual building and site maintenance and repair jobs were supervised, and some architectural designs for a new lobby and cafeteria were proposed.

In the Electronics Services group, hardware support was given to a large number of experimental groups,

the MuLan kicker repairs and vault cabling replacement. The computer network for TRIUMF House was commissioned and requests for PC support at TRIUMF continue to increase. An interesting motor control project was the LaserBall manipulator system developed for the K2K collaboration.

The Electronics Development group continued to provide all of the hardware installation, maintenance and upgrades for the ISAC control system. The controls interface for the helium refrigeration system was commissioned and there were new developments in the control systems for vacuum and in other areas. Several new types of modules were designed and built for experiments and for ongoing developments on ISAC. Assistance was given to the PET group in upgrading the pneumatic delivery system between TRIUMF and the UBC Hospital.

Once again it was a busy year for the division which resulted in several notable achievements.

BEAM DYNAMICS

Muon and Electron Acceleration in FFAGs

The collaboration with BNL and FNAL on the design of FFAG accelerators for a future neutrino factory has widened in scope, to include an electron demonstration model, and in composition, with the participation of Daresbury, UK as a probable host for the model. Two types of investigations have been completed: parameter optimizations of general applicability, and design work specific to the electron model.

For the US Neutrino Factory, FFAGs are the preferred acceleration model to high energy due to their significantly reduced cost and larger acceptance, implying a factor of 4 reduction in transverse cooling and total elimination of longitudinal cooling relative to recirculating linear accelerators. These are not MURA-style scaling FFAGs, but a new breed of accelerator, using strictly linear elements, with characteristics well matched to the rapid acceleration of beams with large 6D emittances. Physically, they will bear a strong resemblance to electron storage rings, but will be operable over a tremendous momentum range.

Magnet Lattices

The thin element models of F0D0, doublet and triplet based lattices were developed further to cover unequal integrated quadrupole strengths. These models indicate that when the horizontal focusing strength is greater than the vertical, as occurs when the tunes are split, the path-length variation is reduced by $\simeq 20\%$ with a corresponding increase in the number of turns. The scope of the thick element models was widened to include cells with two sector bends, one of them

reverse bending to reduce the aperture requirements, and by the addition of doublet cells to the stable of FODO and triplet types. These analytic models, which are more accurate for large momentum offset than the optics program MAD, neglect terms of second order in displacement divided by bending radius ($\Delta x/\rho$). Computations with the differential algebra program COSY show the errors to be 5% or more for rings with fewer than 30 cells, but negligible for the $\simeq 100$ cell muon rings. The models form the basis for scripts that automatically optimize lattice parameters to minimize time-of-flight variation, subject to constraints on betatron tunes and peak pole-tip fields, etc.

Acceleration

The longitudinal dynamics has two key parameters: voltage and radio frequency (V, f). The serpentine channel responsible for acceleration may pinch closed for small variations in V or f , and the muon machine will operate close to these conditions. The parameter choice depends upon a compromise between acceleration range, dwell time and decay losses, acceleration efficiency, emittance growth and matching conditions for the phase-space ellipse. Based on analytic expressions for all these quantities, a lower-emittance working point has been found which reduces the ellipse distortion due to stalling at the fixed-points.

Electron Model

The linear-field FFAG lattices demonstrate compaction of a very large range of momenta into remarkably narrow apertures. The FFAG operates at fixed magnetic field, and with a range of momenta many times larger than a synchrotron. This has two consequences: (i) *asynchronous acceleration* within a rotation manifold outside the rf bucket; and (ii) *multi-resonance crossing*: the combination of a $\pm 50\%$ $\delta p/p$ momentum span and uncorrected, natural chromaticity leads to the beam crossing many betatron resonances including integer and $\frac{1}{2}$ -integer. Both features rely on untested beam dynamics and it is proposed to investigate in detail the complex parameter dependencies, of the non-scaling FFAG, in a few MeV electron model at a tiny fraction of the cost of the multi-GeV muon machines. Initial plans, led by BNL, focused on a near-table-top device with 25 cells, or less, and 3 GHz rf cavities. TRIUMF expertise has successfully reshaped this model into one that better emulates the resonance-crossing behaviour of the full-sized rings. The present model has lower frequency, 1.3 GHz rf, more cells, 42, and operates over a greater number of turns – proportional to the square of cells. At fixed length, the magnets become a smaller number of rf wavelengths long, leading to a smaller phase slip, and yet more turns. The 42 cell design entails a three-fold symme-

try to cancel 1/3-integer structure resonances. Since the summer, the Daresbury Laboratory has identified itself as a probable host and, along with UK and EU collaborators, has begun overtures to potential funding agencies for construction of the electron model downstream of their ERLP, a ring-like energy recovery linac prototype.

EURISOL Beta Beam

The Beta Beam Study is part of the EU-funded EURISOL initiative which will develop a proposal for a new European ISOL-based radioactive ion beams facility. Beta Beam is a novel concept for a neutrino factory which utilizes radioactive light ions produced by the ISOL front end. These ions are collected, accelerated to highly relativistic energies in order to extend their lifetime, and then injected into a racetrack-shaped storage ring (the “decay ring”) where copious neutrinos will be produced from the ions via the radioactive beta decay process. The EURISOL Beta Beam Study will formally commence in January, 2005 and will run for four years.

TRIUMF was invited to participate in Beta Beam in the area of multiparticle simulations of the operation of the decay ring, using our tracking and simulation code ACCSIM and other available tools such as GEANT4 and/or MARS. ACCSIM’s space charge capabilities will also be of use in studying beam-intensity limitations in the ion acceleration stages of the Beta Beam facility.

Some preparatory work was done in order to assess the needs and objectives of the simulation program and to specify some needed extensions to ACCSIM for handling radioactive ions, decay products, and ion interactions in matter.

A survey was also conducted of other computational tools which would complement ACCSIM. It was noted that there is current interest from several fields in extending the physics reach of particle simulation codes to include ions, and that advanced models of ion physics processes are being pursued by groups involved with GEANT4, MARS, and Tech-X corporation. Of particular note is the Quark Gluon String Model (QGSM) being developed for GEANT4, which extends into the comparatively high energy regime of the decay ring.

A comprehensive simulation of the decay ring, capable of supporting the needs of the ring design and operational phases, represents a considerable challenge and will require advancements in both the particle tracking and physics aspects of existing codes. For the near future, we expect that ACCSIM, which will provide the large-scale particle tracking and particle loss information for the beta beam rings, will be used in concert with codes such as GEANT4 and MARS which

will act as post-processors to give a detailed account of the ion interactions in matter and resulting secondary particles.

MAGNETS

The ISAC-II superconducting linac uses superconducting solenoid magnets to focus the ion beam. Accel Instruments (Germany) tested and delivered 5 solenoids for the medium-beta section (see Fig. 238). The specification calls for these magnets to operate at 9 T. All of these magnets operated at over 10 T before quenching. Since the solenoids operate next to the superconducting rf cavities, the specification limits the fringe and residual fields in the cavity area. When operating at 9 T, the field at the cavity is less than 0.1 T. After operating at 9 T and degaussing, the residual field is less than 1 mT. The linac designers had hoped that the residual field would be less than 0.1 mT. This can be achieved, but only by warming the magnet above the transition temperature to release the flux trapped in the coil winding. Based on the success of the medium-beta solenoids, three solenoids for the high-beta linac were ordered.

A concept design of a new septum magnet for the M11 beam line was written [TRI-DN-04-12]. This



Fig. 238. ISAC-II SC solenoid in test at Accel Instruments (photo courtesy of Accel).

design lowers the magnet's resistance and power by about 6%.

The high field ISAC HEBT (S-bend) transfer line dipoles that were designed last year, were manufactured by Alpha Magnetics (California) and Sunrise Engineering (Delta, BC). These magnets were field mapped and met the design specifications. At year-end, one magnet was installed and the others were ready to be installed.

To assist the Canadian contingent to the Q_{weak} experiment at the Jefferson Lab, TRIUMF ordered nine coils for the QTOR spectrometer magnet from Sigmaphi (France). The copper conductor was delivered to France by Jefferson Lab. At year-end, Sigmaphi was developing a technique to splice the large cross section conductor. These coils are expected to be delivered in July, 2005.

Magnet Measurements

Magnets surveyed this year include twenty-three ISAC-II L2 experimental hall quadrupoles, a UCLA dipole (Clyde), five ISAC-II L5 experimental hall quadrupoles, four S-bend double steering magnets, four S-bend dipole magnets, a HiTime superconducting solenoid for M15 (measured from 2 T to 7 T with test shimming), a Belle superconducting solenoid at 6.2 T field, and finally a repeat mapping of the HiTime superconducting solenoid twisted on physical axis at 7 T field.

Experiment 614 – TWIST

TOSCA 3D simulations have previously been carried out for the TWIST magnet. These simulations provide important information because the measurements provide only one component (B_z) of the field at a limited number of space points. By contrast a good TOSCA computer model can provide the three-field components at any point. A detailed comparison was made between field maps taken for the TWIST solenoid, at a field of approximately 2 T, and the TOSCA predictions. The maximum discrepancy between the predicted and measured B_z field is 8 mT; this reduced to 3 mT when a simplified representation of the iron of two upstream quadrupoles and a dipole was included. The TOSCA model also confirms that the solenoid results in an offset-field being added to the pole tip field of the Q7 quadrupole; means of shielding the Q7 quadrupole, from the solenoid generated field, are currently being investigated.

KICKERS

AGS collaboration

The present AGS injection kickers at the A5 location were designed for 1.5 GeV proton injection (see Fig. 239). Recent high intensity runs have pushed the

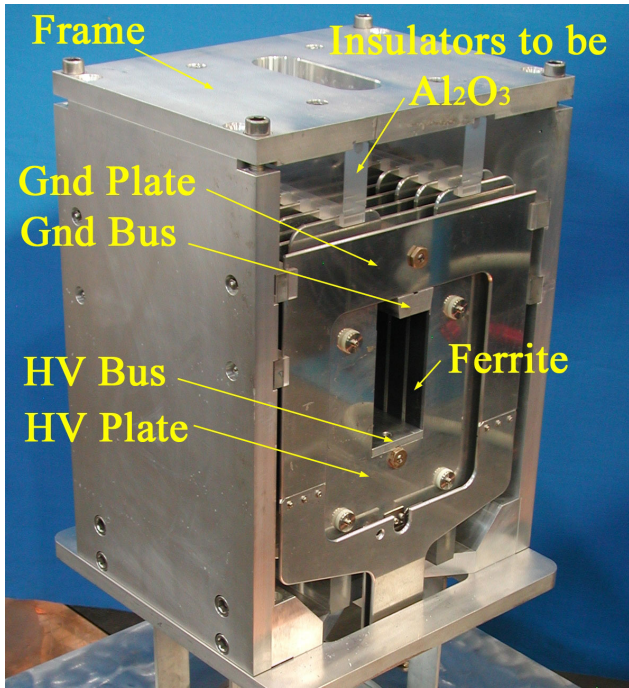


Fig. 239. Photo of KAON kicker assembly that is similar to proposed AGS kicker.

transfer kinetic energy to 1.94 GeV, but with an imperfect matching in transverse phase space. Space charge forces result in both fast and slow beam size growth and beam loss as the size exceeds the AGS aperture. A proposed increase in the AGS injection energy to 2 GeV with adequate kick strength would greatly reduce the beam losses making it possible to increase the intensity from 70 TP (70×10^{12} protons/s) to 100 TP. However, the integral of flux density over the length of the present AGS A5 injection kickers is insufficient for injection at 2 GeV. R&D studies are being undertaken by TRIUMF, in collaboration with BNL, to design two new kicker magnets for the AGS A10 location to provide an additional kick of 1.5 mrad to 2 GeV protons. The kick strength rise and fall time specifications are 100 ns, 3% to 97%; the design goal is to achieve a field uniformity of $\pm 1\%$ over 85% of the cross sectional area of the aperture. TRIUMF has proposed a design for a 12.5 W transmission line kicker magnet powered by a matched 12.5 W pulse forming line.

To achieve low ripple and minimize field rise/fall time the impedance of the kicker magnet must be close to 12.5 W. Hence detailed electromagnetic simulations of the proposed A10 kicker magnets have been used during the design stage:

- 3D modelling to accurately predict capacitance of capacitance plates (including edge effects);
- 2D modelling of electric and magnetic field in the aperture to optimize the aperture geometry to achieve a kick uniformity of $\pm 1\%$ over 85%

of the aperture without unduly increasing cell inductance. Ferrite and ground conductor have been shaped to achieve this;

- A modified equivalent circuit of the kicker magnet has been developed. The revised model has been shown to give almost identical predictions to the previous model but negative mutual coupling between cells is represented in a more intuitive manner, simplifying the derivation of values for the model;
- Incorporation of a model of beam bunches into PSpice equivalent circuit, for the 3 different operating modes, to allow a better optimization of the kicker system.

Two co-op students worked on this project at TRIUMF during 2004.

NLC collaboration

The collaboration with SLAC, to analyze the failure mechanism of the IGBTs under fault conditions in the prototype NLC modulator, was successful. A paper was co-authored with SLAC and presented at the 2004 Power Modulator Conference. A more complete version of the paper has been accepted for publication in a special issue of the IEEE Transactions on Plasma Science.

PSI MuLan collaboration

An international collaboration plans to measure the lifetime of the muon to a precision of 1 ppm. The MuLan experiment will take place at PSI in northern Switzerland. The central idea employed in MuLan invokes an artificial time structure on an otherwise dc beam. The MuLan method requires a fast beam line kicker, which can turn the beam on and off at a repetition rate of up to 40 kHz: the TRIUMF Kicker group designed and built the kicker. The kicker runs with a standard “on-off time cycle”, or in a “muon on request” mode. The MuLan kicker consists of 2 pairs of deflector plates mechanically in series, driven by 4 FET modulators. Each pair of plates is 0.75 m long. One plate of each pair is driven by a +12.5 kV FET based modulator and the other plate is driven by a -12.5 kV modulator. The potential difference between a pair of deflector plates is variable up to 25 kV. Each modulator consists of two stacks of FETs operating in push pull mode.

The kicker was successfully commissioned at PSI in July, 2003. However, as a result of the very fast switching times of the MOSFETs (< 2 ns compared with approximately 30 ns in the previous generation of the FET cards), and the external interconnections required for the 4 kicker racks, significant rf noise was generated. In addition the specifications for the flatness of the voltage pulse were modified, now calling

for a pulse flatness of 1 V in 12500 V, compared to the achieved 22.5 V in 12500 V. The kicker was returned to TRIUMF in January, 2004, and extensive changes were made which were based on detailed PSpice modelling of the system. The rf was reduced by a factor of approximately 5000. The flat top droop, for a 20 ms pulse duration, was reduced from 0.18% (22.5 V) to less than 0.001% (100 mV). In addition the pulse overshoot, at the front and back edges of the pulse, which occurs for ~ 70 ns duration, was reduced from 10% to 2%. The kicker was successfully recommissioned at PSI during October. However, some of the MOSFETs were destroyed during physics runs in December. The cause of the failures is not completely understood but is believed to be due to several reasons including a short circuit on the output of a kicker and damaged fibre optic cables. The MOSFET cards have been returned to TRIUMF: a gate-resistor is being incorporated on the PCB to make the MOSFETs less susceptible to failure resulting from timing mismatch (e.g. due to minor damage to the fibre optic cables). In addition the timing of all the cards is being measured and adjusted, where necessary.

One co-op student worked on this project at TRIUMF during 2004.

A very similar kicker is required at TRIUMF as part of the Five-Year Plan. The co-op student also investigated using magnetic coupling to trigger the MOSFETS, rather than using fibre optics.

Research into a thyatron replacement

Starting in September, with the return of a previous co-op student, now a graduate student at UBC, the Kicker group commenced a research project into replacing high-power thyatrons with IGBT modules for kicker systems. The collaboration with SLAC, into the cause of IGBT failures in the SLAC klystron modulator, resulted in a good understanding of some of the problems associated with using IGBTs in pulsed power applications.

After an initial period researching manufacturers and devices, attention has been turned towards Westcode branded IGBT modules from the UK. These modules differ from the previously analyzed (EUPEC) modules, in that they are encapsulated in a disc-like “hockey puck” package with the top and bottom of the package being the emitter and collector respectively (Fig. 240 – right). The EUPEC modules are encased in a more conventional “brick-type” package with the collector and emitter contacts being bolt-on terminals on the top of the device (Fig. 240 – left).

If the hockey puck device fails it does so to a short circuit, allowing a series stack with redundancy to continue to operate, whereas because of internal bond wires in the brick package, a brick package can fail

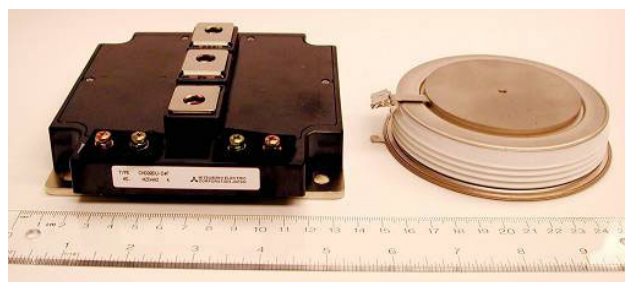


Fig. 240. Comparison of IGBT module packaging (EUPEC module on left, Westcode module on right).

to open circuit. The fact that the hockey puck package does not fail to an open circuit is a significant advantage over the brick package as it provides improved reliability in a series stack.

In the Westcode IGBT module, each current “path” through the individual IGBT die is the same length and has the same fundamental geometry. In addition the gate-trace is almost completely orthogonal to the main current flow, making it less susceptible to magnetic coupling to the main current paths than was evidenced in the EUPEC IGBT module.

However, while the physical geometry of each path in the Westcode IGBT is identical, mutual coupling to return path(s) is not. During a high rate of change of current, as a result of differences in mutual coupling to the return paths, current crowds to the outermost IGBT die. The current imbalance could potentially be of sufficient magnitude to destroy the IGBT, or at least raise its switching impedance to a degree that would make it unusable for the intended application. Additionally, unlike the EUPEC modules, the placement of the return current paths is very important in this case because of the effect of the return path on the current distribution within the IGBT module.

Using techniques developed while analyzing the EUPEC module, an investigation has commenced into the current sharing between the IGBT die during fast switching. This analysis is being undertaken using several electromagnetic analysis codes, including: Fast-Henry, Vector Field’s Opera2D and Opera3D, and Integrated Engineering Software’s Oersted. The results from these simulations are cross-checked with each other, and then fed into the PSpice circuit simulator as linear resistor and coupled-inductor parameters.

The initial results from these simulations show that current sharing might, in fact, be a significant issue with the Westcode IGBT module, and the determining factor appears to be the conductivity of the actual silicon IGBT die. As this parameter varies considerably during the switching process, and is dependent upon the gate-emitter voltage, it is planned to include a non-linear model of IGBT die in the PSpice simulation. In

addition it is planned to carry out measurements, during fast switching, on a representative IGBT module. These experiments are set to commence shortly with the assistance of an IGBT expert, Dr. Patrick Palmer, of the Department of Electrical Engineering at UBC.

TITAN

The TITAN radio frequency quadrupole (RFQ) beam cooler is a device that is employed to cool and collect ions with short half-lives created by ISAC. An rf square wave driver performs 2 dimensional focusing of the ion beam within the RFQ, along a plane normal to the beam's intended trajectory, in an effort to confine ion motion along a stable path; hence the ions can be trapped and collected for extraction. The rf square wave driver, which is based on the MuLan kicker design, employs two stacks of MOSFETs, operating in push-pull, to generate high voltage rectangular waveforms at a prescribed frequency and duty cycle. Currently a 500 V, 2 MHz drive system is in operation, however, the system configuration allows for operation with higher voltage and a repetition rate from 300 kHz up to 3 MHz, continuous.

The Kicker group has provided significant design support for the TITAN RFQ driver, providing advice and carrying out simulations. Simulations include analyses of the capacitance of the RFQ using Coulomb, 3D modelling software from Integrated Engineering Software (Canada), and modelling of the equivalent circuit using PSpice.

MECHANICAL ENGINEERING

Mechanical engineering and design work is initiated by the submission of a Request for Engineering Assistance (REA) form. These are assessed weekly and assigned according to the size, complexity and schedule of the work. Larger tasks requiring engineering input often require a team approach guided by a project engineer. The KOPIO project and the ISAC-II linac project fall into this category.

During 2004 there were 40 ISAC REAs and 34 non-ISAC REAs submitted (this differentiation has been dropped for 2005). There are also lengthy projects that are carried forward from the previous year. As well there is participation of engineering personnel in engineering analyses, FEA, on-site safety issues, design reviews, etc.

ISAC-I

Target module 4, which was scheduled for completion in 2004 to be used for target and ion source development, was rescheduled to coincide with the Febiad ion source development program which will occur in 2005. Work on the module was interrupted as a result

of this schedule change and also due to the redeployment of manpower to support the cyclotron shutdown. Work will recommence in the spring of 2005.

ISAC-II

TRIUMF is currently constructing a 43 MV superconducting heavy ion linear accelerator (linac) to accelerate radioactive ion beams from the current ISAC-I level of 1.5 MeV/u to 6.5 MeV/u. The initial stage, phase 1, currently under way, involves the manufacture, assembly and installation of 5 medium-beta cryomodules and phase 1 of the liquid helium refrigeration system necessary to support their operation (500 W at 4.5 K). This phase is scheduled for completion by the end of 2005 and will add 18 MV of accelerating voltage for initial experiments. Phase 2 will add 3 high-beta cryomodules, an extension to the helium distribution system, and doubling of the refrigeration capacity.

Cryomodules

A medium-beta cryomodule consists of 4 two-gap, bulk niobium, quarter wave rf cavities and one superconducting solenoid magnet housed in a vacuum tank and supported from the tank lids. A helium reservoir provides a total inventory of 190 l of liquid helium at 4.5 K under constant replenishment from the refrigeration system during normal operation. The vacuum tank is lined with μ -metal to protect the cryo elements from the earth's magnetic field. There is also a separate box and lid inside, cooled with liquid nitrogen which acts as a thermal shield surrounding the cryo elements. The engineering challenge in the design of a cryogenic accelerator module such as this is the internal support and alignment of the cryo elements. The cryo elements must be as thermally isolated as possible and supported in such a way as to allow for thermal contraction without inducing stored energy in the support structure such that alignment repeatability of $\pm 200 \mu\text{m}$ can be achieved over repeated cooldown cycles.

The first cryomodule constructed (designated SCB3) was completed in April, 2004. Thermal testing commenced shortly thereafter in the test area of the SCRf clean room. Thermal migrations of the cryo elements were measured by means of a wire position monitor (WPM) installed in the cryomodule on each of the cryo elements at the beam port level. This allows thermal migrations to be continuously monitored during cooldown and warm-up. This information is backed up by optical targets installed in the beam ports of the end rf cavities. The cooldown cycles were conducted down to liquid nitrogen levels where 85% of the contraction occurs. Three cooldown/warm-up cycles were performed and the repeatability was $80 \mu\text{m}$ vertically and $120 \mu\text{m}$ horizontally which is well within the specified

limit. Subsequent to these tests there were 2 cooldowns to liquid helium temperature in order to establish the “cold offset” (contraction compensation). The cryo elements were adjusted by use of the adjustable support posts such that the beam ports were concentric to the tank beam ports.

The cold-offset was measured as 3.8 mm for the rf cavities and 5 mm for the solenoid. Subsequent to these tests the cryomodule was prepared for rf testing by removal of the WPM and installation of rf ancillaries and the rf tuner. A more detailed report on all of the tests performed on SCB3 appear in the ISAC section of this Annual Report.

SCB3 served as the prototype for the remaining medium-beta cryomodules. There were a number of problems that were dealt with such as the cryo element mounting beam suspension system which was simplified over the original design; the nitrogen thermal shield had a number of fit problems and the μ -metal panels were difficult to install. These and more were changed for the manufacture and assembly of the next two units SCB1 and SCB2. A second new and improved assembly frame was also manufactured such that one was available for both the initial experimental hall assembly stage and for the class 3 clean room final assembly. The initial assembly of SCB1 began in December, 2004 with cold tests scheduled for April, 2005.

Refrigeration system

Due to budget constraints the phase 1 refrigeration system was broken down into subsystems which were all managed by TRIUMF personnel. The subsystems were as follows:

1. Refrigeration system major components, i.e. compressors, cold box, gas management system, oil removal system, and control system.
2. Warm piping subsystem – all the stainless steel pipe work necessary to connect all the refrigeration components.
3. Buffer storage tank – for the storage of gaseous helium.
4. LHe dewar – for the storage of liquid helium produced by the cold box and to be distributed by the CPS/s.
5. Cold piping subsystem (CPS/s) – to transport LHe from the dewar to the cryomodules and clean room test area.

Item 1 – a contract was signed in November, 2003 with Linde Kryotechnik AG of Switzerland to provide a 500 W class helium refrigerator. The components were delivered to TRIUMF starting in early 2004 with the final component, the model TCF50 cold box, being delivered in July (see Fig. 241). Included in this contract



Fig. 241. Cold box arriving at TRIUMF from Linde Kryotechnik.

were process and instrumentation diagrams specifying line sizes and valves. The contract included commissioning the system in April, 2005.

Item 2 – Linde Kryotechnik provided process and instrumentation diagrams as part of the contract. TRIUMF used these to create 2 and 3 dimensional drawings of the warm piping subsystem and the installation within the building in order to create a specification and tender package and engage a contractor. Lockerbie and Hole was the contractor selected and they began work in September.

Item 3 – A custom made, single, vertical storage tank of 90000 USG proved to be far too expensive and it was suggested that 3 smaller 30000 USG horizontal tanks of the propane storage type would work well. These could be stacked on a special frame. Phase 1 would only require one tank initially. Gary L. Nadon Enterprises was engaged to locate one, and a new tank was found at a price within budget. A pad was poured east of the experimental hall and the tank was installed in the fall.

Item 4 – This was supplied from the Chalk River inventory of equipment that TRIUMF acquired. It is an older 1000l dewar by Cryofab. It was inspected and

found to be adequate for the job. It will be installed in early 2005.

Item 5 – This is the most complex task for TRIUMF to manage. It is a specialized technology with only a few manufacturers in the world to deal with. The TRIUMF distribution team visited several laboratories and met with many groups in order to learn as much as possible about the technology. This resulted in a set of drawings depicting what was deemed to be the best solution from the point of view of distribution and thermal losses as well as cost. A specification was drawn up and submitted for tender in December.

SCRF cavity tuner system

Considerable progress was made this year on the development and integration of the SCRF cavity tuner system for the prototype cryomodule SCB3 of the ISAC-II superconducting linac. We successfully completed the assembly and debugging of the electronic wiring/cabling, inside and out, of the prototype servo amp cabinet in the ISAC-II clean room. Stable, low noise, closed loop motor control was achieved for all tuners installed onto the completed 4 cavity cryomodule.

As well, extensive servo control and communication systems integration was performed successfully. Extensive safety interlock software and control subroutines were written for integrating functional control of the tuner motors from the rf supervisory control system. All interlocks and control functions were tested and found to perform as required. This performance was maintained throughout the alpha beam acceleration tests where the tuner position control specifications well exceeded the required specifications.

Engineering – Other

FEA analysis

The TRIUMF 54ton spreader beam is used for moving the long shielding blocks by crane. Extensive theoretical and FEA calculations were done to determine the safety factors involved after non-destructive testing revealed cracks in the welds in sensitive areas of the spreader beam. An approach was developed for the maintenance of similar spreader beams at TRIUMF, and a company found to independently proof test and certify the beam. All lifting beams at TRIUMF are now being maintained and certified in this manner.

The design of a very high pressure, cryogenic temperature, high performance compound hydrostatic pressure cell was studied for producing very high pressures in target materials. This job is for the μ SR group and the final products will be used in local experiments and for export to other laboratories.

The usual salvo of analysis was performed on freshly designed mechanical structures for determina-

tion of design integrity, safety factors and approval for fabrication.

KOPIO

Scintillator extrusion Work continued to improve the external profile and shape of the holes in the KOPIO scintillator extrusion. It was nearly perfected to achieve the desired tolerances on size, flatness and straightness for the $1\text{ cm} \times 7.2\text{ cm}$ cross section. The process was refined and made fully automatic to run the extruder without operator intervention to fill the die and produce consistent profile. This profile was acceptable enough to go into production.

Then the KOPIO collaboration decided to make the scintillator thinner to 8 mm. A new die was designed and manufactured for this new thickness. Modifications were made on this die and the profile produced is fairly close to the final size. The next run is planned after die and spider plates are polished and electroless nickel plated. We expect to have a mini production run to produce enough scintillator for one module in the spring of 2005.

These 7.2 cm wide extruded scintillator planks will be machined to have tongue on one side and groove on the other side. A gluing jig has been designed to glue 35 of these planks to make $8\text{ ft} \times 8\text{ ft}$ sheets for the KOPIO preradiator. This jig is designed to give flat sheets with equi-spaced holes from plank to plank with no glue protruding out of the surface of the sheet. This jig is out for manufacture and has a tolerance of $200\ \mu\text{m}$ over the entire front surface area of $236\text{ cm} \times 236\text{ cm}$.

Preradiator fibreglass panels Preradiator wire chambers required fibreglass sheets varying in thickness from 0.011 in. to 0.25 in. $8\text{ ft} \times 8\text{ ft}$ size with 1 oz copper on one or both sides of some of these panels. These sheets are required to have quasi-isotropic mechanical properties. The commercially available standard size is $4\text{ ft} \times 8\text{ ft}$. After a worldwide search, a company (Profile Composites) has been located in Sydney, BC that is willing to try to make these sheets. They have successfully produced $4\text{ ft} \times 4\text{ ft}$ sheets meeting our tolerances, with their existing tooling with minimal cost to us. We have obtained quotes from this company to produce sheets for prototype. A visit is planned to look at the facilities and products of this company. So far it looks promising.

Structural The above-mentioned preradiator wire chambers are pressurized with chamber gases. It was desired to optimize the thickness of the lid and the base made of the above-mentioned fibreglass sheets, and also to optimize the location and number of fasteners holding the lid and the base together, to minimize bulging of these thin sheets. A finite element program

ANSYS was used to analyze and optimize these parameters. Based on this study, a thickness of 0.055 in. was chosen for both the base and the lid.

Figure 242 shows a plot of displacements in the lid of the KOPIO preradiator wire chamber under chamber gas pressure.

Cathode strips KOPIO needs a flexible circuit of polyamide base Nova clad material as cathode plane for the wire chambers of the KOPIO preradiator. A company (Sheldahl) has been selected which could make rolls of as much as 12 in. wide kapton based material with 1/2 oz glueless copper deposit. This company has promised an accuracy of 0.001 in. between the traces of copper strips. A minimum quantity for testing has been ordered.

Q_{weak}

Contract management services are being provided to supply coil carrier and coil carrier stiffener plates for the QTOR spectrometer for the Q_{weak} experiment at Jefferson Lab. Four 5 in. × 81 in. × 206 in. plates and sixteen 1.25 in. × 36 in. × 152 in. aluminum plates are needed. Aluminum supply has been very tight in 2004 and mills were not accepting orders until late into the fall at which time they would assess their positions and may or may not take orders. Suppliers have been found who, because of their quota allocations with the aluminum producing mills, were able to place orders of aluminum plates in these circumstances for timely delivery to the project.

Budgetary quotes have been obtained from several machining centres to machine these plates to final shapes.

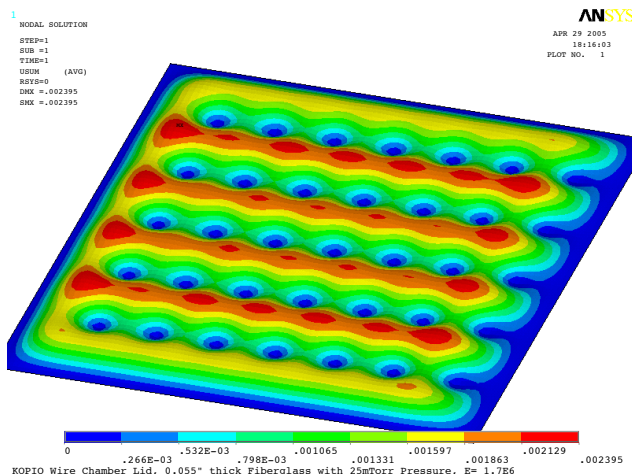


Fig. 242. Plot of displacements in the lid of the KOPIO preradiator wire chamber.

Engineering – Victoria

ISAC target development

High temperature vacuum chamber The design and construction of a high temperature vacuum chamber is complete, which includes a double-walled tubular graphite filament and an effusion cell capable of reaching 2300°C. The crucible, made from tantalum, was used for a series of tests with samples such as lithium, sodium, potassium, rubidium, cesium, boron, aluminum, gallium, tin, lead, arsenic, antimony, bismuth, and indium, to determine the out-gassing properties of materials at high temperatures for future consideration in target development.

From the data that were collected and analysed at the University of Victoria through the summer, modifications are under way to include a 45° filament ribbon. This will increase the opportunity to observe diffusion characteristics as the atomic beam from the crucible interacts with the 45° filament and is directed into the RGA through a cross beam ionizer. The design of this vacuum chamber has also been used for other experiments at TRIUMF, and a patent application is under way for its design.

ISAC Febiad ion source An improved filament design for the ISAC Febiad ion source was required to replace the traditional wound wire filament, which began sagging and causing electrical shorts. With the success of the tubular filament in the high temperature vacuum system, a similar concept was considered to replace the existing filament.

A single-walled tubular design was created by replacing the graphite from the high temperature vacuum system with welded tantalum foil, as the higher vapour pressure of graphite prevented its use for this application. Initial testing at TRIUMF has shown that this design is more stable, demonstrating a resistance to sagging while being subjected to high temperature, around 2200°C, from power supply heating.

A double-walled tubular filament has also been created, and testing for this design will begin in 2005. Using a double-walled system increases the length of the filament, allowing twice the thickness of tantalum foil to be used without an increase in current, which doubles the expected lifespan of the filament. Further analysis and design for both the single-walled and double-walled concepts will continue in 2005, which should provide a more reliable filament for the ISAC Febiad ion source.

Time projection chamber (TPC)

A TPC is the leading candidate for the central tracking system of an experiment at the international linear collider. The physics goals for the project require an exceptionally precise tracker, and the University of

Victoria Engineering group has been involved in the proof of principle demonstrations with a prototype detector. The prototype was modified to accept UV laser beams and a complex laser delivery system (LDS) was constructed for the TPC test to be performed in a 5 T SC magnet at the DESY Laboratory. The system was capable of delivering one or two beams at various locations within the TPC chamber under remote control. The mechanical design for the LDS was completed in the summer, and was operated with the TPC prototype at DESY in early fall. The tests were very successful and results are explained in the Science Division section of this Annual Report. The experience gained from the TPC studies for the linear collider has opened the door for the Engineering group to be involved in leading the construction of the TPC modules for the T2K experiment in 2005.

K2K calibration manipulator arm

A device was needed to extend the calibration capabilities for the K2K neutrino detector at KEK, Japan, to provide off axis calibration beyond the current system, which consists of hanging a wire dropped through a tube into the water filled detector. The Engineering group prepared an initial concept for a multi degree of freedom manipulator arm, which could be positioned with locking segments into the detector and used remotely for precise calibration of the photomultiplier tubes (PMT).

After successful presentation of the PMT calibration proposal while visiting the facilities at KEK, the conceptual design was approved and final dimensions were confirmed. Drag force analyses were performed to determine safe working speeds, applied torques on the joints and motor specifications for the manipulator, as it will be submerged in water during use. The formal design of the K2K calibration manipulator arm was designed and is being manufactured with plans for assembly and testing at TRIUMF prior to operation at KEK in 2005.

ISAC charge state booster (CSB) insulator

A strength analysis for the ISAC CSB insulator that failed in operation was required so recommendations could be made for an improved design with appropriate materials. Forces acting on the insulator were determined from the magnetic field acting on the steel pole of the CSB; however, it appears that improper sizing and possible material flaws of the supplied insulator were to blame for the failure. The improved design has successfully replaced the original insulator after minor modifications were made.

Safety

Technical support was provided to better understand the certification requirements for radioactive ma-

terial packaging as part of TRIUMF's waste removal system in conjunction with TRIUMF's quality assurance program. After determining the annual leak testing and servicing procedures required for continued use of the packaging, along with the appropriate codes for the transportation of radioactive materials, this information was given to Safety personnel to develop appropriate flow charts.

Remote handling

An engineering load review was needed for the cyclotron elevating system hoist frame used by Remote Handling. This hoist is used during shutdown periods for removal of the cyclotron elevation system bearings and their components. While initial calculations suggested that continued use of the system was safe, the use of the system could be simplified if several modifications were considered. The re-design of this system will continue in 2005.

Engineering – Carleton

Enriched Xenon Observatory (EXO)

Engineering at Carleton University assumed the lead engineering role in the development and design of the EXO 200 kg prototype. With the copper cryostat already designed, the next major components to be designed were the lead shielding and an overhead crane, that resides in the clean room with the experiment, used to assemble the shielding (see Fig. 243). As the experiment is to be set up and tested first at Stanford University, then moved to an underground location at

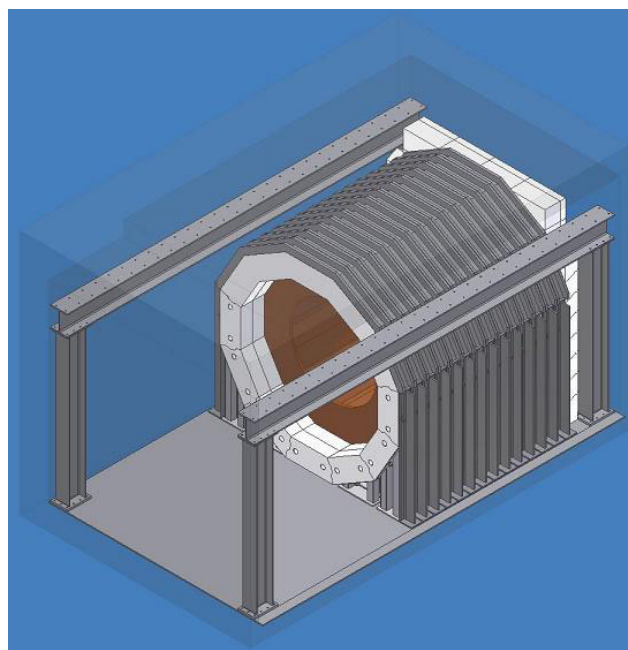


Fig. 243. Model of clean room with cryostat and lead shielding in place.

the Waste Isolation Pilot Plant (WIPP) in New Mexico, the lead shielding is designed in blocks that can easily be assembled, disassembled and reassembled in the two locations. It is necessary to disassemble the lead for moving because the total mass of lead is approximately 54 tonnes and the handling equipment at WIPP has a maximum load rating of 30 tonnes.

The experiment occupies 6 portable clean room modules that need to be lowered into the mine and transported approximately 640 m underground to the experiment location. Engineering is under way to be able to move these modules, the heaviest being 27 tonnes, in the confined tunnels of the mine.

PLANNING

This year the Planning group was involved in planning, scheduling, coordinating and expediting several sub-projects for ISAC-II (medium-beta cavities, wire position monitor, cryogenics system, high-beta cavities, charge state booster (CSB), HEBT transfer, H-HEBT, ECR); planning and coordinating activities for two shutdowns (December 22, 2003–April 15, 2004 and September 13–October 6); ISAC experimental facilities (TIGRESS, TITAN); and M20Q1,2 refurbishing. The Planning group was also extensively involved in preparing manpower and cash flow estimates for the Five-Year Plan (2005–2010), as well as setting up a new job recording system for the Machine Shop, and setting priorities in the Machine Shop to meet various milestones for ISAC, Cyclotron and Science division projects.

Technical details and progress on PERTed activities for ISAC are described elsewhere in this report.

Shutdown Activities

There were two shutdowns during the year: the winter shutdown (December 22, 2003–March 17, 2004 for ISAC beam production, and beam to proton therapy and PIF, and to April 14, for BL1A), and a fall mini shutdown (September 13–October 6).

Winter shutdown

BL1A activities started early with the removal of 60–70 shielding blocks from the meson hall on December 29–30, to get a headstart for shutdown work.

Major jobs completed by the Remote Handling, Beam Lines, Vacuum and Diagnostics groups in the meson hall included: repairing several BL1A vacuum leaks in the T2 area, 1AQ14, M8 blank-off flange, M20Q1 and M20B2 O-ring, removal and replacement of several crumbling blocks near 1AM10 and T2 water package, and installation of new custom designed shielding blocks (as needed), repairs of M20Q1 water leaks, M20 separator window valve, M13 beam blocker work, T1 and T2 target, and water packages MRO.

Very good vacuum was achieved in the T2 area after repairing these vacuum leaks. While the area was accessible, a remote video survey was taken of the M20 front-end area to prepare for a future installation of radiation hard components. To help reduce the dose to technical experts, several volunteers were used to help with the replacement of up to 6 crumbling blocks. Due to several additional MRO jobs and high dose levels, the removal of the M11 septum and the repairs of a small vacuum leak in M15 were postponed to the January, 2005, shutdown.

In the vault, the cyclotron lid was not raised until January 19 in order to do the elevating jacks maintenance (station #8 and some calibrations). After that the lid was up until February 23 to complete the maintenance jobs for probes (2C extraction foils, LE inspection, replace NW periscope prism), engineering physics (MRO on Q3 correction plate, replacement of radiation damaged cabling for some upper correction plates as a quick repair with a plan to do a more thorough job in the next shutdown). The RF group completed several jobs that included: periscope survey, GAT position measurement, HAT adjustment for resonator #10, thermocouple replacement, chore pads replacement in UQ3 and UQ4, and resonator water leak test. The removal and reinstallation of the STF target was also completed to correct the misalignment and repair the limit switch. This job became more complex and took longer than scheduled due to a persistent leak (at the seal between the STF target housing and the water column above it) that was finally repaired by using a different style clamp and mocking up the repairs in the hot cell.

Vault work on the jacks (station #11, check all jack counters) continued with the lid down while the cyclotron was baking, pumping and leak checking. The main magnet was energized on March 4, followed by injection and cyclotron tuning and a beam in 2A with TM1 at ITW on March 17. BL1A beam production started on April 14, due to the heavy workload planned in the meson hall.

Beam line 2C contributed up to 50 mSV to the total dose of 190 mSV for the whole shutdown distributed over 105 workers.

Fall mini shutdown

1A shutdown was from September 13 to October 6; 2A shutdown was from September 22 to October 4.

It was decided to shut beam off to 1A a week early in order to repair 1AV8 and to allow the triplet to cool down for 2 weeks before doing repairs to it. The major jobs completed in the meson hall included: repair 1AVA8 leak, 1AQ15 water flush and flow test, 1AQ14 vacuum leak, T1 and T2 water package MRO, replace

HV cables to beam spill monitor #56, as well as many MRO jobs.

In the vault, the beam was off September 22, and turned back on September 28. During that time the major jobs completed were: 2C4 monitor wiring and check wire scanner alignment, replace WCP flow meter, check phase probe wiring, C/P cabling, as well as MRO jobs by RF, Vacuum and Plant groups.

DESIGN OFFICE

ISAC received the majority of billable hours again this year (55% or approximately 8540 hours). ISAC-II used 5160 hours for the design of the S-bend to ISAC-II, the SCB3 prototype and SCB2 production medium-beta cryomodule, and LN2 shield; GHe (from storage to compressor and refrigerator), LHe (from refrigerator to cryomodule) and LN2 distribution subsystems; TIGRESS prototype, EMMA proposal, charge state booster (CSB) development and ISAC-II experimental beam lines.

ISAC development and MRO used the rest, with target and target module improvements, laser spectroscopy (source and port shielding), OLIS upgrades, LEBT extension to GP3, CSB development, TITAN (RFQ off-line test and platform for installation in experimental hall), LTNO Faraday cup and beam transport upgrades, conceptual design for β -NQR and on HEBT, improvements to rf tuners, DRAGON and TUDA.

TRIUMF's main program, MRO and upgrades, continued with beam line upgrades on 1A, M9, M11, M13, and M20. Cyclotron upgrades were made to: rf power switching devices, PA tube filament and hairpin inductor, development of new HE and LE probes. Proposals were made for future upgrades to the 2C solid target facility. (Total main program = 26% or approximately 4110 hours.)

External projects continued with CERN 66 kV power supplies as-built documentation, xenon detector for LADD, KOPIO detector prototype, and AGS Brookhaven upgrade and kicker design (external projects = 17% or approximately 2670 hours).

Photographic and visual art services provide support for seminars, conferences, and publications, such as the Annual Financial and Administrative Report, the Five-Year Plan brochure and material for TRIUMF's corporate presentation and Outreach Program. A large part of our miscellaneous hours go to visual art services and, this year, included training hours for our SolidWorks users and a new junior/intermediate designer.

Following the policy statement of December, 2003, "CAD Strategy at TRIUMF", SolidWorks 3D modelling software has been adopted as the platform of

choice for all TRIUMF users. We will extend this to support a network of designers through the next Five-Year Plan. The close relationship between software for engineering analysis (COSMOS) and CNC machining (MasterCam) is proving to be both powerful and efficient. Network 2D CAD is available through PC Support and currently provides access for 75 part-time users on a 9-seat network. This represents a considerable savings on the maintenance required by the (previously) 55 single seat users.

MACHINE SHOP

Over the past year the Machine Shop has gone through a restructuring process that entailed implementing the following procedures:

1. Initiating a system of setting priorities by collaborating with TRIUMF's project coordinator.
2. Restructuring the shifts in order to maximize efficiency.
3. Purchase of a second CNC vertical machining centre. Both machines have already had a major impact on the quality, quantity and versatility of work produced in the shop.
4. Recruitment of four highly skilled technicians, three of whom are experienced programmer/machinists using software such as MasterCam and SolidWorks.
5. Linking up to the Design Office database to expedite the transfer of solid/Autocad files to the HAAS machining centres and to facilitate the speedy procurement of quotes by e-mailing drawings to companies we consider awarding contracts to.

Major projects worked on included the TIGRESS prototype, TITAN RFQ, and cryomodules 1 and 2. The Machine Shop kept pace despite a heavy workload and the continual shortage of manpower due to retirements and lag time, as a result of the recruitment process.

The Machine Shop continues to support local industries by sub-contracting out work that is beyond the capacity of the shop or large volume components that are extremely time sensitive in nature. Speciality companies which provide anodizing, electro-polishing and copper plating among others are also supported.

Table LI demonstrates utilization of the Machine Shop by TRIUMF divisions and other user groups.

The goal for the coming Five-Year Plan is to continually upgrade and modernize the Machine Shop by replacing old and obsolete machinery that is not cost effective to maintain. As designs are becoming more complex it is becoming increasingly difficult to machine these components on manual machines, consequently CNC machining is the only option (see Fig. 244).

Table LI. Machine Shop utilization.

ISAC development	4.48%
Science	22.14%
ISAC operations	7.27%
Nordion	5.78%
ISAC-II	41.94%
Cyclotron operations	7.59%
Cyclotron refurbishing	5.48%
CERN	0.16%
Affiliated institutions	2.42%
NSERC	1.80%
Miscellaneous (CFI)	0.16%
Site infrastructure	0.38%
Accelerator Technology and Administration	0.19%
AGSUPER and Royalty	0.18%

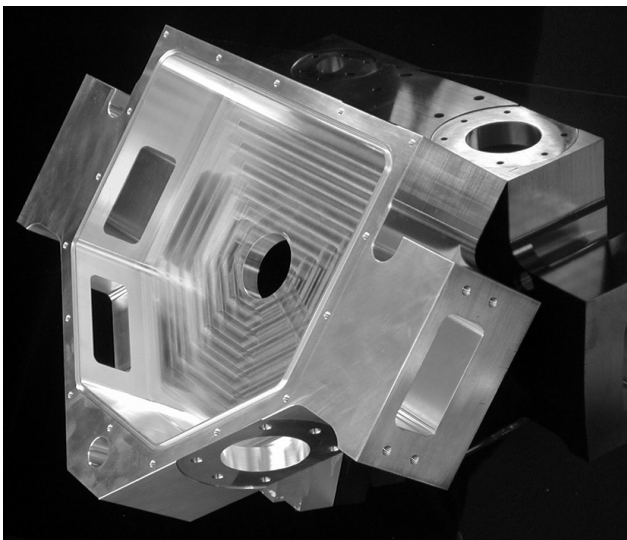


Fig. 244. Part made from a solid block of aluminum using the CNC machine.

BUILDING PROGRAM

Design and management of minor construction projects

The department was involved in a number of small construction projects around the site such as the He compressor room roof reinforcement, CRM water pipes trench, and the He tank slab (see Fig. 245).

Structural design and engineering review

Structural design was done for a variety of structures including the TITAN installation platform and the He tank slab. Engineering review was performed for various small structures like cranes, trench bridges, etc.

Construction review

Besides the reviews of minor construction projects managed by the department, construction reviews of



Fig. 245. He tank for the ISAC-II refrigeration system.

the free standing crane in the ISAC-II building and the clean room bridge crane were also done.

Architectural design

The Building department worked on the architectural re-design of the lobby and cafeteria areas in the main office building. Architectural re-design was also done for the mailroom in the main office building.

Management of maintenance and repair work

During the course of the year, approximately \$100 K was spent on maintenance and repair work at various TRIUMF buildings and around the site. This included the annual maintenance and repair contract, interior and exterior painting, upgrading the parking lot and repairing some of the access roads.

Management of landscaping work

The Building department continued with the management of the landscaped areas on the site. Most of this work is done through an annual landscape maintenance contract.

Drawing library maintenance and services

The department continued with organizing and updating the site and buildings drawing library, and provided services of creating new and issuing existing drawings to many “in-house” clients.

ELECTRONICS SERVICES

Overview

In 2004, the Electronics Services group continued the tradition of offering services to a large percentage of the site. This year was no exception from commissioning a computer network at the new TRIUMF House, down to repairing cables in the bowels of the cyclotron vault. Twelve members of this group handled a great variety of services including: consulting, design,

assembly, repair, manufacturing, testing, programming and debugging. This department also handled approximately 12 tons of electronics goods for recycling.

Electronics Repair Shop

Significant effort was put into implementing the directives of the new recycling program (necessitated by the large volume of dated equipment deemed to be obsolete) wherein otherwise unavailable parts are salvaged for re-use, before the equipment is sent out for environmentally sound disposal. Also, numerous repairs were performed on the readout displays, motor controllers, and servo controllers for the Machine Shop lathe and milling machines. Otherwise, most of the maintenance activity involved the repair and calibration of a total of 193 various electronic devices, including: 26 monitors and terminals (comprising 15 colour units and 11 monochrome units), 50 power supplies (of which 8 were NIM types, 13 were CAMAC types, 11 were high-voltage types, and the remaining 18 were miscellaneous types), 74 nucleonics modules (including 62 NIM devices and 12 CAMAC devices), 11 test and measurement instruments, and 32 miscellaneous devices of an electronic nature (vacuum pump controllers, etc.).

PC Support/Desktop Services

The Desktop Services department continues to provide a strong support service for the TRIUMF community. Typical responsibilities include support for Windows operating systems and common Windows applications as well as recommending and maintaining PC, notebook, and server hardware. Other provided services include file serving, scheduled backup services, virus control, stocking spare parts, as well as assisting with network, e-mail, and printer connection issues.

The PC backup service has been upgraded from a tape based system to disk based utilizing a new server with RAID protection and new backup software. This has improved the capacity, speed, and reliability of the backup service. Several Dell servers and Windows 2003 server licenses were purchased to create a Windows server environment that will replace our Novell services and allow the Windows services provided by TRIUMF computing services to be amalgamated with our services.

The increasing threat of spyware and malware has caused us to review many products to help protect our Windows systems. This is a quickly evolving problem requiring immediate attention yet no single product is available to adequately protect us. Solutions will be available soon but in the meantime we are spending many hours cleaning up infected systems.

PC hardware specifications remained relatively static this year as there was not much new product be-

ing introduced. This has led to many nearly identical PCs being ordered this year. The Intel motherboards being used in most configurations are very stable hence leading to fewer service calls for our department. We continue to see higher than expected hard disk failures, however, the problem is not confined to a single manufacturer. We are now recommending disks with a five-year warranty in the hope that reliability is improved. It appears that the LCD monitor has achieved a price point where it has replaced the CRT monitor. Over 90% of new monitor orders are for LCDs.

Help desk activities have increased in comparison to 2003. PC hardware related tasks have grown by 20% to 369 tasks. Software related jobs increased by 57% to 514 tasks, and network related activities decreased by 23% to 107 tasks. The number of people accessing this department's servers has increased by 32% to 162. The PC backup service is utilized by 60 PCs which is up from 51 PCs last year. The backup size is now at 194 Gbytes for the PCs and 99 Gbytes for the servers. The networked AutoCAD 2000 pool consisting of nine licenses has 76 registered users.

Experimental and Target Technical Support

Much of the year was spent on rework and repair of the MuLan Kicker project. Another major project involved work on the ISAC cryomodule tuner system and packaging a prototype system. For the 8π group, an equipment protection and fire alarm system was proposed, designed and installed. Ongoing background tasks included items such as target maintenance and repairs.

High Level Software Support

The past year included several projects for a variety of groups at TRIUMF.

The principal project was the control system for the LaserBall manipulator system for the K2K collaboration. This system used four motors, solid state inclinometers, MIDAS and MatLab to operate the arm. Preliminary design of an automated wire plane measurement system was started for the detector facility. This is a motorized camera system that will measure wire positions on drift chamber frames. A solid state bridging firewall was implemented to protect the BL2A and BL2C extraction probe computers from uncontrolled access over the network. This also resolved problems with an excessively noisy network affecting the computer's operation. A rewrite of the magnet survey system was started to replace the software running on a DECStation 5000 and the ULTRIX operating system. The Java acquisition system (JACQ) was used for this. Support for the Data Acquisition group included work on TIGRESS, Expt. 920 and LTNO. This

included data acquisition equipment, software development, and hardware repair. The ISAC-II superconducting cavity washer was completed, allowing automated washing of the cavities before installation into the accelerator.

Technical Support

Major work for Technical Support included the design and installation of a prototype servo system and supporting electronics for the ISAC-II cryomodule tuners. Another main project involved the design, construction and installation of a PLC-based control system for the TWIST experiment TEC chamber. Support was provided for the re-cabling of the cyclotron main tank periscope systems. Printed circuit boards were designed to support LTNO as well as some mechanical design, and assembly and wiring for a gas control system for TIGRESS. There were approximately 30 small jobs, which included items such as helping the RF group debugging software and improving documentation for an rf multiplexer switch.

Site Communications

Site Communications worked closely with the Central Computing department to plan and prepare for installation of redundant fibre optics cable links on the site. A related job was the transfer of existing copper cabling to the new rack in the MOB. Communications was also involved in planning, coordinating, and preparation, with a pressing deadline, to reach an agreement to dig a trench from the MOB to the proton hall extension and install various conduits and pipes. A direct savings of \$10,000 was realized by TRIUMF. With only a few hours notice, the group coordinated with fibre installers to determine the routing requirements at TRIUMF House, as well as patching the copper network in time for the opening day. In order to preserve data and save space, help was given in archiving some 270 floppy disks and transferring them to CD media.

Electronics Shop

Work for CERN was a major component for our group. The Electronics Shop spent a lot of hours every month in 2004 producing and modifying boards and making up fibre optic cables for CERN. Controls required modifications to 20 units of our power and diagnostic 0918 modules. We replaced two large sets of correction plate cables that had suffered radiation damage over the last 30 years. For the KOPIO project we assembled delay boxes. Other best sellers during the year were visual scalers and flowswitches. Making cables for all projects on site is a priority of the Electronics Shop. Groups like DRAGON, TUDA, TITAN, LADD, TIGRESS and all others require lemo cables,

ribbon cables, high voltage, delay cables and other one-off specials on a regular basis.

ELECTRONICS DEVELOPMENT

The majority of the group's work this year was again in support of the ISAC control system. Several specialized hardware modules were constructed for ISAC and further development continued on the data acquisition board (DAB) for CERN. Two members of the group visited the Canadian Light Source (CLS) to discuss controls for the helium refrigeration system for ISAC-II. Two members attended a one-week course on new PLC programming tools. The group received 29 requests for engineering assistance (REA) and 23 engineering change requests (ECR).

ISAC Support

The group continued to provide all the hardware installation, maintenance and upgrade support for the ISAC control system.

For TITAN, an existing 6-channel 500 V VME module design was modified to provide 6 channels at 2 kV. The group also assisted in the manufacture of FET modules used for the TITAN RFQ. A module was designed and installed to handle the gas and vacuum on the HV platform.

Assistance was provided for the installation of the Linde Kryotechnik helium refrigeration control system.

With the experience gained from the rf amplifier monitoring system, it was decided to move towards a more distributed vacuum control system with the installation of the S-bend beam line. Higher density convectron gauge readout modules were redesigned as single channel versions to allow for installation at the device, which eliminates the need for extra cabling.

Modifications were undertaken in the ICB target conditioning station to accommodate the testing and development of a Febiad ion source.

The CAN-bus controllers' installation and cabling for the 85-magnetic element HEBT, MEBT, and DTL power supplies were reconfigured to allow for better maintenance and individual controller reset.

Three beam current integrator modules were installed for 8π .

A hall probe readout module was modified to allow faster magnet scanning and installed in the CSB test stand.

CERN

The DAB-64x design in VME-64 form-factor was finalized and manufactured. Five prototypes were assembled, two of which were sent to CERN for beam loss monitor mezzanine development. Firmware development is ongoing.

The group assisted in the production of 30 DAB-III modules for CERN.

Engineering Support

The group provided engineering support as members of technical committees, design review panels and the QA task force. The group also provides electronics engineering assistance to other groups at TRIUMF. These included the Central Controls group, the Safety group, and the RF Controls group.

This year a new version of the PET rabbit pneumatic transmission controller was implemented. Eleven new transmitters were designed, built and installed in the manholes along Wesbrook Mall between TRIUMF and the UBC Hospital. The new transmitters provide both the hospital and PET staff with information about the location of the rabbit during the trip from TRIUMF to the hospital. The controller for the send station was replaced with a PLC based system.

Layout, assembly, and wiring of a methyl iodide chemistry control box were also started for the PET group.

A photo detector and amplifier/shaping module has been designed for evaluation as a gamma detector for PET. A frequency to voltage stage will be added if the detector is suitable for the application.

Experimental Support

The DRAGON 300 kV power supply stack was rebuilt with a redesigned capacitor board after the stack failed in operation.

More functionality was added to the VME based Gate Logic board as requested by the μ SR group.

Work continued on the design of pre-amplifier electronics for a silicon E-deltaE detector for the DRAGON beam line.

PSpice simulations were performed to evaluate and improve the pick-up circuit and rf transmission system of the LTNO detector.

A 200/400/800 MHz summation amplifier capable of the faster rise times achievable with the new detectors was constructed.

Secondary Channel Support

A plug-in ADC module was designed and retrofitted into the M13 secondary channel motor controller. This module provided a more accurate position readback and hence a more accurate positioning of the M13 slits and jaws.

New Hardware Designs

Several new modules were designed and built:

- The VME high voltage module was redesigned to accommodate ELCO HV plug-in modules, as the Spellman modules have been discontinued.
- The VME QSX module was reworked to include a DAC and an upgraded FPGA.
- A CAN-bus to GPIB and serial converter module was developed to provide greater flexibility in interfacing to more exotic devices, such as laser controllers.
- In order to generate the necessary frequencies required for the TITAN RFQ, a version of the previously built VME POL SYNTH module was built with modified firmware.
- Optical isolation was added to the remote integrator module.
- The pulse controller module, originally developed for the PSI kicker, was modified for use with the TITAN RFQ.
- An Altera Cyclone board was designed and built for KOPIO development. Additional support was provided for developing applications with the NIOS-II embedded processor.
- A pre-amplifier and VME digitizing/signal processing module was built for use in the Q_{weak} experiment at Jefferson Lab.
- A 4-channel modulated frequency synthesizer has been designed as a VME module for β -NMR.

Infrastructure

The group's Web-based REA tracking system was expanded. Search and browse capabilities were increased. NCR tracking was included and automatic communication with the ISAC NCR system was implemented.

The group's computer network was expanded to include the controls working area next to the ISAC control room and the controls development room in the ISAC-II building.

The use of the Mentor Graphics Expedition software package for schematic design and PCB layout was abandoned after a time-consuming trial period because the package proved to be non-stable. The newest versions of the Protel tools have addressed most of the group's concerns, which had earlier prompted the switch to Mentor Graphics.

CERN COLLABORATION

INTRODUCTION

TRIUMF's collaboration with CERN on producing accelerator components for the Large Hadron Collider (LHC) is now essentially complete with only a few small tasks continuing up to first collisions. For the period 1995–2005 the amount of this contribution that TRIUMF is coordinating on behalf of Canada is \$41.5 million. The largest contribution has been the manufacture of 52 twin aperture quadrupoles, completed and shipped to CERN last year. These magnets are being field mapped at CERN and this work is expected to be completed by May, 2005.

The LHC injection kicker components designed and built at TRIUMF underwent some final long term high voltage testing using the CERN provided control system. High voltage measurements were carried out to demonstrate that the rise time, fall time, and pulse uniformity were within the required specifications. The PFNs are being shipped to CERN in a special shock-absorbing container and all components should arrive by June, 2005.

The remaining hardware project is the design and prototyping of the digital acquisition boards for the LHC beam pick-up monitors. This design has become a CERN standard and is now planned for use in the transfer lines and for the beam loss monitors. TRIUMF has manufactured prototypes of the latest version for testing at CERN. The series production will be carried out at CERN.

The two beam dynamics efforts continue to be supported. The first is a continuation of the beam tracking efforts taking into account field errors in the magnets, beam-beam interactions and misalignments to determine methods of correcting these non-linearities. The second study looks at beam-beam effects in the collision region and the potential instabilities that might be caused by the electric forces between the bunches. This task requires extensive computing power and makes use of the parallel processing available from WestGrid.

The LHC schedule presently calls for an injection test into an octant of magnets to take place in late 2006, with first collisions scheduled for July, 2008. More details of the TRIUMF LHC work can be found in the following sections.

BEAM DYNAMICS

Beam Optics and Collimation

After completion, in late 2003, of the tasks related to collimation set-up and optics, a request was made by the CERN beam-dynamics group for assistance in studies of LHC at collision. This is a part of an intensive tracking campaign planned by CERN for 2004–

2005 aiming to optimize the machine parameters at collision and evaluate the realistically achievable luminosity.

During 2004, in collaboration with CERN, a tracking model was developed, which includes weak-strong beam-beam interactions, simulated alignment and field errors in both rings, and procedures for their correction. The resultant programming tools mostly consist of already existing modules. They were thoroughly tested at TRIUMF and, on several occasions, improvements were made.

The tracking job is built in several stages: preparation of optics for an imperfect machine, correction, short-term (1000 turns) tracking performed with the code MADX, and a million-turns tracking with Six-track to obtain the domain of stable trajectories (dynamic aperture). The short-term tracking allows us to observe the effect of non-linearities on the beam-beam tune footprint. The long-term jobs are built locally, but executed on dedicated clusters at CERN and worldwide. Being intended to assist the actual machine operation, the correction algorithm takes into account only measurable observables, i.e. such that can be accessed from the LHC control room.

The non-linear particle motion in an accelerator can be described by a symplectic 6-D map acting on initial coordinates. Using the well established theory of such maps, several programming tools were created allowing us to build the Lie-algebraic map of a beam line or a ring in either factorized, or Taylor form. Such maps were applied for the LHC triplet correction, where an analytical treatment was made, and on beam dynamics problems arising at TRIUMF – to reproduce the 7th order Taylor map (COSY) of an FFAG cell. In perspective, such tools may serve to analyze the Linear Collider interaction region.

Beam Optics and Stability

Coherent beam-beam effects in the LHC

Our study of beam-beam interactions in the LHC seeks to identify potentially unstable coherent modes excited by the electric forces between counter-rotating bunches of protons as the two beams meet and cross in the collision regions. Large-scale multiparticle simulations are a principal tool in this type of investigation and our parallel beam-beam simulation code BeamX is one of the first to include a fully 3-dimensional model of the collision process.

In 2004 BeamX was migrated to three new computing platforms in order to evaluate their parallel performance and to establish resource criteria for supporting large-scale simulations that would allow the explo-

ration of the beam-beam parameter space and help to predict and optimize LHC collision scenarios.

The systems used were: the WestGrid Lattice CLUMP (CLUster of MultiProcessors) system at the University of Calgary, the WestGrid Glacier facility at UBC, and the new Openlab cluster at CERN. This provided a diverse set of testbeds. The WestGrid-UBC and CERN clusters are based on dual 32- or 64-bit commodity processors in blade or rackmount configurations, respectively. In contrast, the CLUMP architecture uses specialized hardware and is designed to support rapid low-latency communication among small groups of processors in shared memory configurations.

To benchmark these systems, a series of full-scale BeamX runs (131078 simulated collisions), employing from 1 to 9 processors, were performed on each cluster. Consistently, the lattice CLUMP system was the clear leader, with performance at least a factor of 2 better than the commodity clusters, making it the preferred platform for BeamX in its current form. However, further developments in parallel beam-beam simulation for LHC will likely involve increasing numbers of processors, to handle multiple interaction regions and bunch trains, and this may swing the preference back to the larger commodity clusters.

We would like to acknowledge the support of WestGrid (funded by the Canadian Foundation for Innovation and other agencies) whose facilities were essential to the timely validation, scaling up, and benchmarking of our parallel code in collaboration with CERN.

CONTROLS AND INSTRUMENTATION

LHC Orbit System Components

The digital acquisition board (DAB64x) was redesigned to meet the latest LHC specification (LHC-BP-ES-0002 Rev 2.0). Five prototype boards were manufactured and assembled for preliminary hardware testing. Two modules were sent to CERN for beam loss monitor mezzanine development. Firmware development and hardware testing is ongoing. Software for DAB control and monitoring was rewritten to support the new power PC processor and the latest Lynx OS operating system.

Assistance was also provided in the production of 30 DABIII modules which were used for beam tests at CERN.

KICKER MAGNETS

Each of two LHC injection kicker magnet systems must produce a kick of 1.3 T m with a flattop duration variable up to 7.86 ms, and rise and fall times of less than 900 ns and 3 μ s, respectively. A kicker magnet system consists of four 5 Ω transmission line magnets

with matching terminating resistors, four 5 Ω pulse forming networks (PFN) and two resonant charging power supplies (RCPS). Six RCPS and nine PFNs, together with associated switch tanks, and dump switch terminating resistors have been built at TRIUMF and all have been tested at high voltage (60 kV) to ensure that the performance is within specification.

Each 5 Ω PFN is composed of two parallel 10 Ω lumped element delay lines; each line consists of a 28 cell, 4.36 m long precision wound coil, high voltage and high current capacitors and damping resistors in parallel with the coil. There is a thyatron switch tank at each end of the 5 Ω PFN.

Each PFN and associated thyatron switch tank was operated at 54 kV and 0.1 Hz for more than 24 hours. Detailed measurements were carried out with 54 kV on the PFNs: 54 kV was chosen as it is the expected operating voltage at CERN. Pulses of magnitude 27 kV are produced when a PFN is charged to 54 kV and discharged into a matched terminating resistor. CERN provided a terminating resistor and 10 RG220 cables to connect the main switch (MS) CX2003 thyatron to the main switch terminator (Fig. 246). The kicker pulse length is controlled by a dump switch (DS) CX2503 hollow anode thyatron that connects to a water-cooled DS terminating resistor. A total of 10 precision terminating resistors was built and tested at TRIUMF with a measured resistance of $4.74 \Omega \pm 0.01 \Omega$ at 25°C at low voltage. The MS terminating resistance was measured at low voltage to be 4.96 Ω . The voltage dependence of the MS and DS terminating resistors is, according to HVR, $-1.33\%/(\text{kV}/\text{cm})$. Each resistor consists of a stack of 10 resistor disks each 1 in. thick, thus the MS terminator resistor at 27 kV is 4.89 Ω , and the DS terminator resistance at 27 kV is 4.68 Ω .



Fig. 246. PFN test set-up at TRIUMF with RCPS, and 4 CERN controls racks.

Each PFN system was set up and controlled by a CERN computer control system consisting of 4 racks of electronics, that was set up at TRIUMF. Thus testing of the PFNs and thyatron switches and RCPS was controlled in a representative manner. The operational status of the kicker system located at TRIUMF could be monitored from CERN via an Internet connection. Several modifications to the controls and interlocks were made remotely from CERN during the initial setup phase.

The high voltage pulse measurements are in excellent agreement with the low voltage measurements and with PSpice predictions. The pulse waveforms, measured at the MS terminating resistor, were used to calculate the field in a PSpice simulation that includes the kicker magnet (Fig. 247). The 0.5% to 99.5% rise time for PFN2 is 800 ns (cf 900 ns) and the 99.5% to 0.5% fall time 2.4 ms (cf 3.0 ms). The fall time is 2.0 ms if the 0.6% undershoot at the tail of the pulse is neglected. The standard deviation of the magnetic field variation for PFN2 during the flat top is $\pm 0.09\%$. The largest flat top standard deviation is $\pm 0.16\%$ for PFN9.

An important design consideration was the absolute precision of the PFN construction so that the PFNs are interchangeable with a minimum change in the relative calibration. All 9 PFNs were operated at a voltage of 54 kV: the high voltage was set by the CERN control system. The measurements were made in 2-month intervals over an 18-month period. The

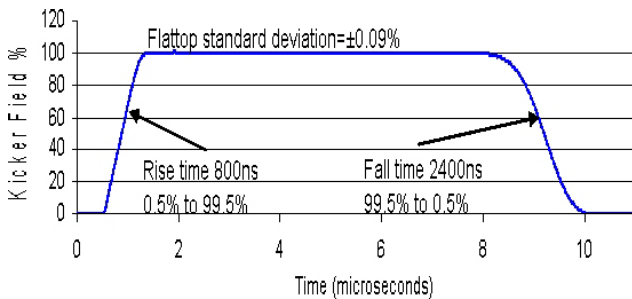


Fig. 247. Kicker magnet field calculated from PFN2 measured voltage pulse.

standard deviation in the relative calibration of the fields (Fig. 248) for the 9 PFNs is $\pm 0.11\%$: this is a good indication of the long-term stability of the system as well as the precision of the PFN fabrication. Thus the overall system is well within the required specifications of $\pm 0.5\%$. The maximum relative field calibration is 0.33%.

The TRIUMF shipping container, with special new shock absorbing frame, was used to ship 4 RCPS in 2003. One RCPS remains at TRIUMF and was used for all of the HV tests on the PFNs, switch tanks and terminating resistors. Special mounting brackets for clamping the PFNs to the shock absorbing frame were designed and installed in the spring, and there were 3 shipments of 2 PFNs each in 2004. There are 2 more shipments of the container scheduled for 2005, one shipment containing 2 PFNs to leave TRIUMF in February, and one shipment containing the final RCPS and PFN to leave TRIUMF in May. The CERN controls racks will be crated and sent separately in April. Thus all of these systems will be at CERN by June, 2005 for final testing and preparation for installation into the LHC tunnel.

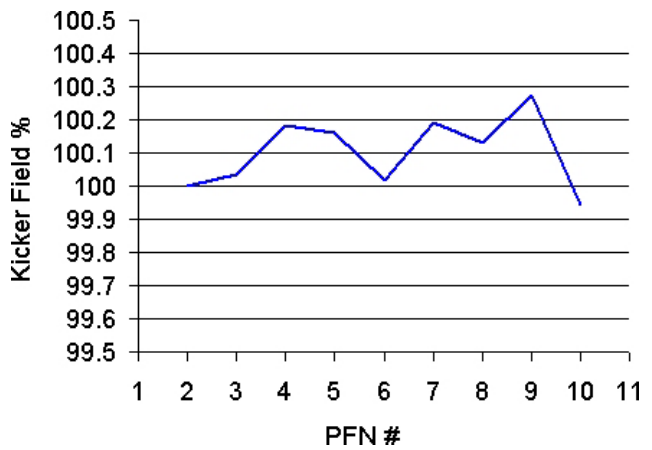


Fig. 248. PFNs (2 to 9) kicker fields normalized to PFN2.

TECHNOLOGY TRANSFER DIVISION

INTRODUCTION

The Technology Transfer Division at TRIUMF is responsible for the laboratory's commercial interactions. It is composed of a small group dedicated to optimizing the commercialization of technologies emanating from TRIUMF research, plus the Applied Technology group that is responsible for the operation of the on-site commercial cyclotrons on behalf of MDS Nordion.

TECHNOLOGY TRANSFER

The mandate of the division is the pursuit of all financially and technically viable opportunities for commercializing technologies emanating from the research at TRIUMF. This mandate must recognize the preeminence of the scientific research at the laboratory, and proceed in a manner that optimizes the impact on TRIUMF and the Canadian economy while minimizing the impact on scientific activities at the facility.

The current Contribution Agreement between the National Research Council (NRC) and TRIUMF includes the requirement for TRIUMF to enhance its impact on the Canadian economy. This impact is measured through the benefits provided to Canadian industry, both through the transfer of TRIUMF's technical knowledge and through its purchasing practices.

APPLIED TECHNOLOGY GROUP

500 MeV Isotope Production Facility

During this year, the 500 MeV irradiation facility received 327.6 mAh. Thirteen targets were irradiated, nine targets delivered to produce $^{82}\text{Sr}/^{82}\text{Rb}$ for MDS Nordion.

CP42 Facility

The total beam delivery for 2004 was 670 mAh. The weekly beam delivery graph is shown in Fig. 249, the quarterly time evolution of the beam delivery is shown in Fig. 250. The downtime and maintenance statistics are analyzed in Fig. 251 and compared with the TR30-1 and TR30-2.

The upgrade of the CP42 control system is nearing completion.

TR30-1 Facility

The total beam delivery for 2004 was 1982 mAh. The weekly beam delivery graph is shown in Fig. 252, the quarterly time evolution of the beam delivery is displayed in Fig. 250. The downtime and maintenance statistics are analyzed in Fig. 251 and compared with the CP42 and TR30-2.

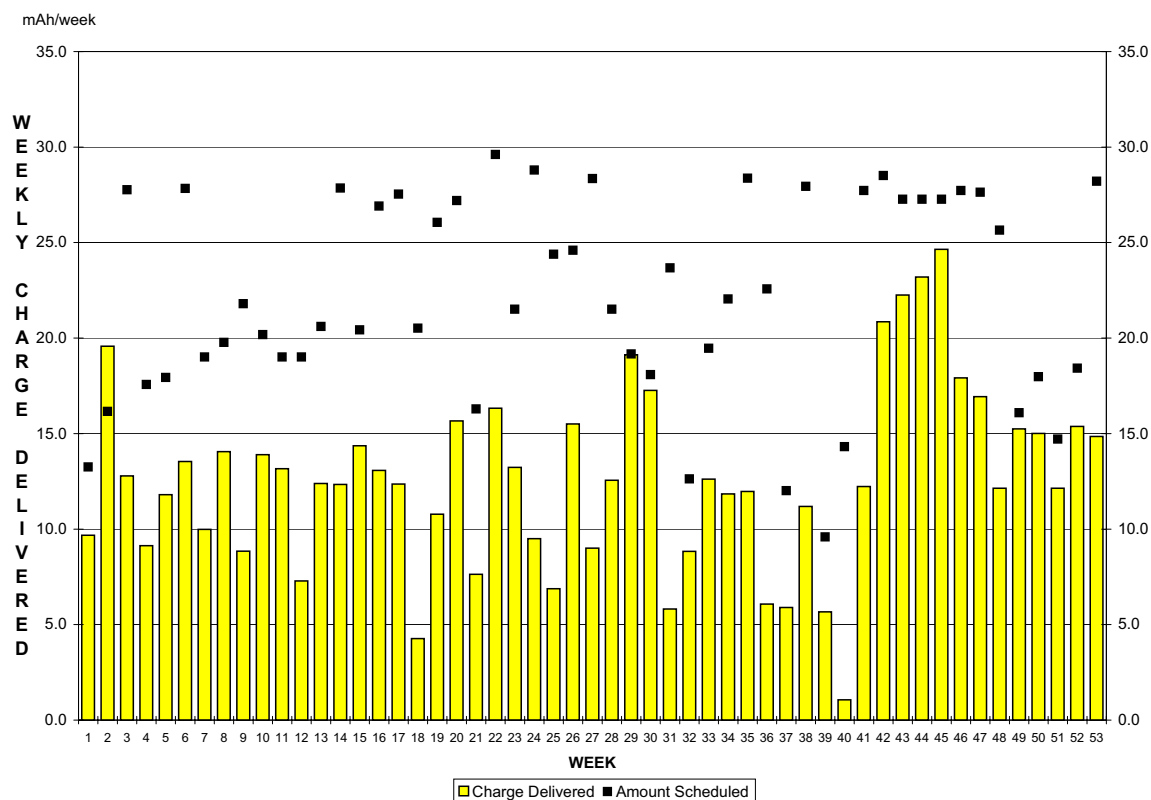


Fig. 249. Weekly beam delivery for the CP42.

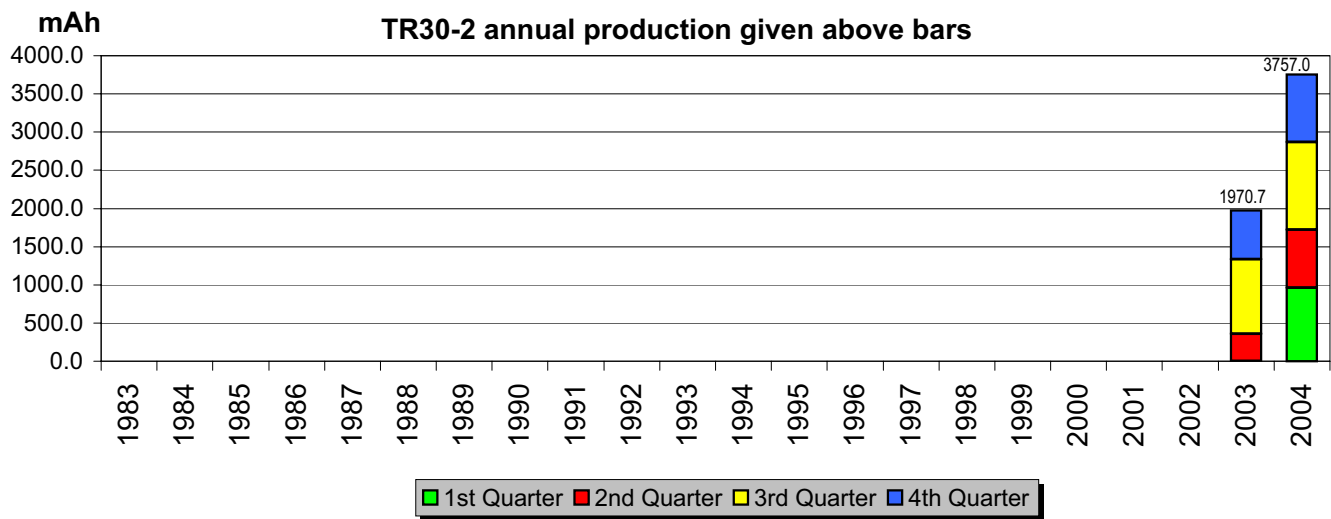
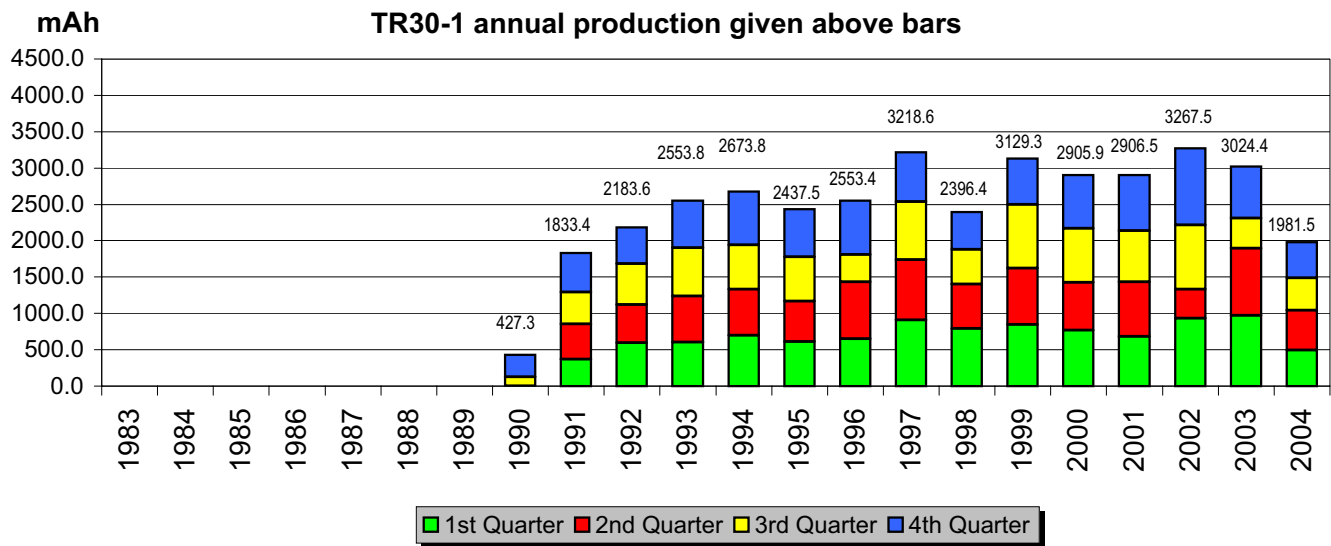
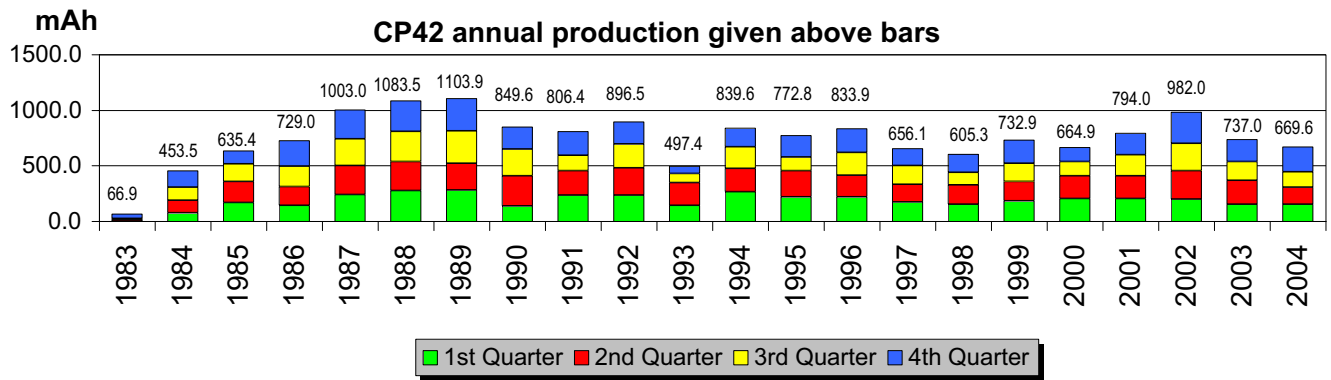
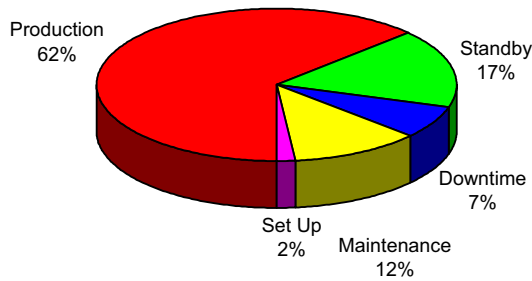
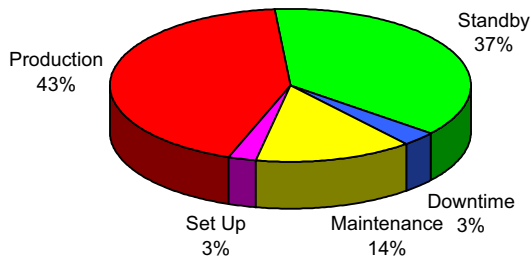


Fig. 250. Quarterly time evolution of the beam delivery for the CP42 (top), TR30-1 (middle) and TR30-2 (bottom).

CP42 2004



TR30-1 2004



TR30-2 2004

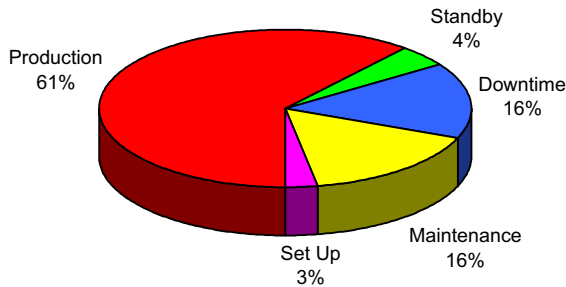


Fig. 251. Breakdown of downtime and maintenance for the CP42 (top), TR30-1 (middle) and the TR30-2 (bottom) during operational hours.

TR30-2 Facility

In 2004, the TR30-2 had the highest ever beam production of all ATG cyclotrons. The total beam delivery was 3757 mAh. The weekly beam delivery graph is shown in Fig. 253, the quarterly time evolution of the beam delivery is displayed in Fig. 250. The downtime and maintenance statistics are analyzed in Fig. 251 and compared with the CP42 and TR30-1.

ATG Development Projects

ATG is working towards a consolidation of the cyclotron control rooms. The CP42 and TR30-1 controls are scheduled to be moved into the TR30-2 control room by the end of 2005.

The upgrade of the CP42/TR30 Radiation Monitoring System has been completed. Work is in progress to replace the obsolete CP42 Access Control System.

Improvements to the existing solid target station collimators are in progress. The new design uses collimator heads manufactured from a specific high strength tantalum-tungsten alloy.

Collaborations are ongoing with the Université de Sherbrooke, Quebec, and the University of Washington Medical Center in Seattle.

RADIOISOTOPE PROCESSING (MDS NORDION)

During the year 2004, MDS Nordion shipped large quantities of short-lived medical radioisotopes produced using the two TR30 cyclotrons and the CP42 cyclotron. The main radioisotopes produced and shipped were iodine-123 used for thyroid imaging and research, palladium-103 used in prostate brachytherapy, and indium-111 used for monoclonal antibody imaging.

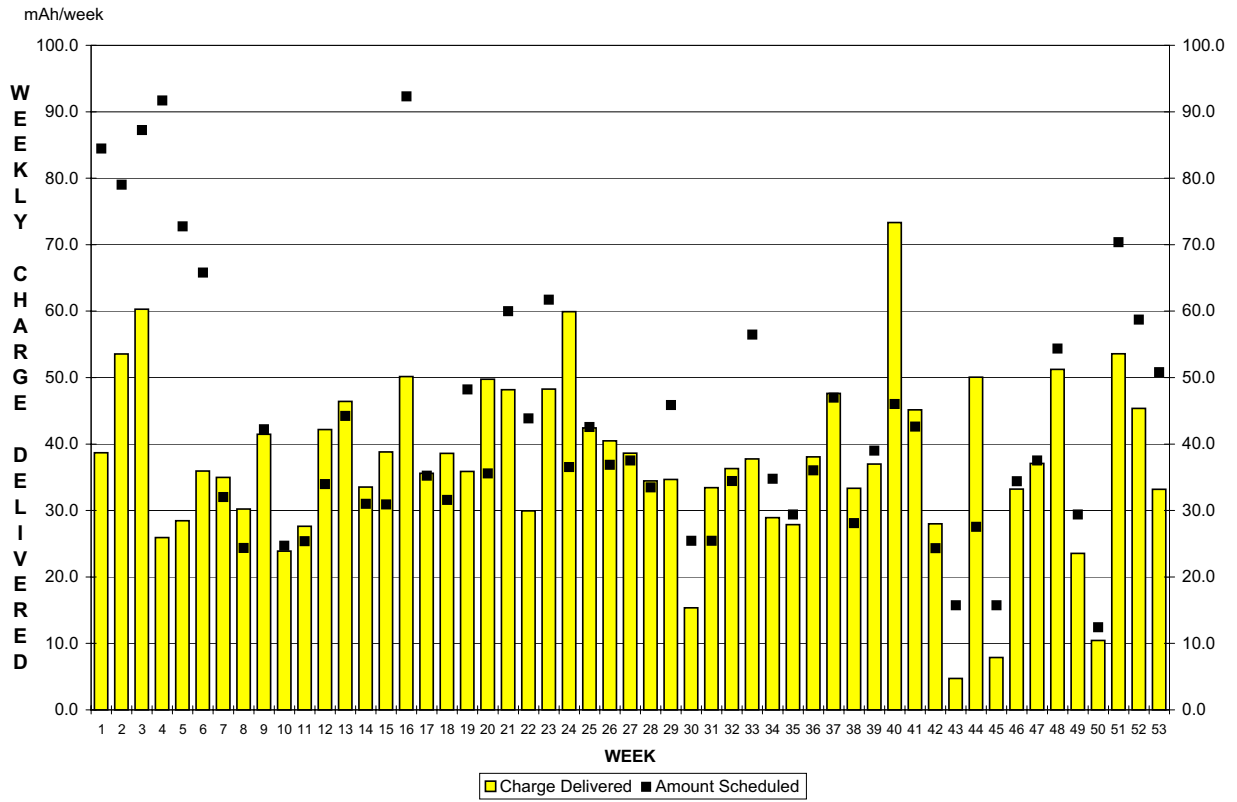


Fig. 252. Weekly beam delivery for the TR30-1.

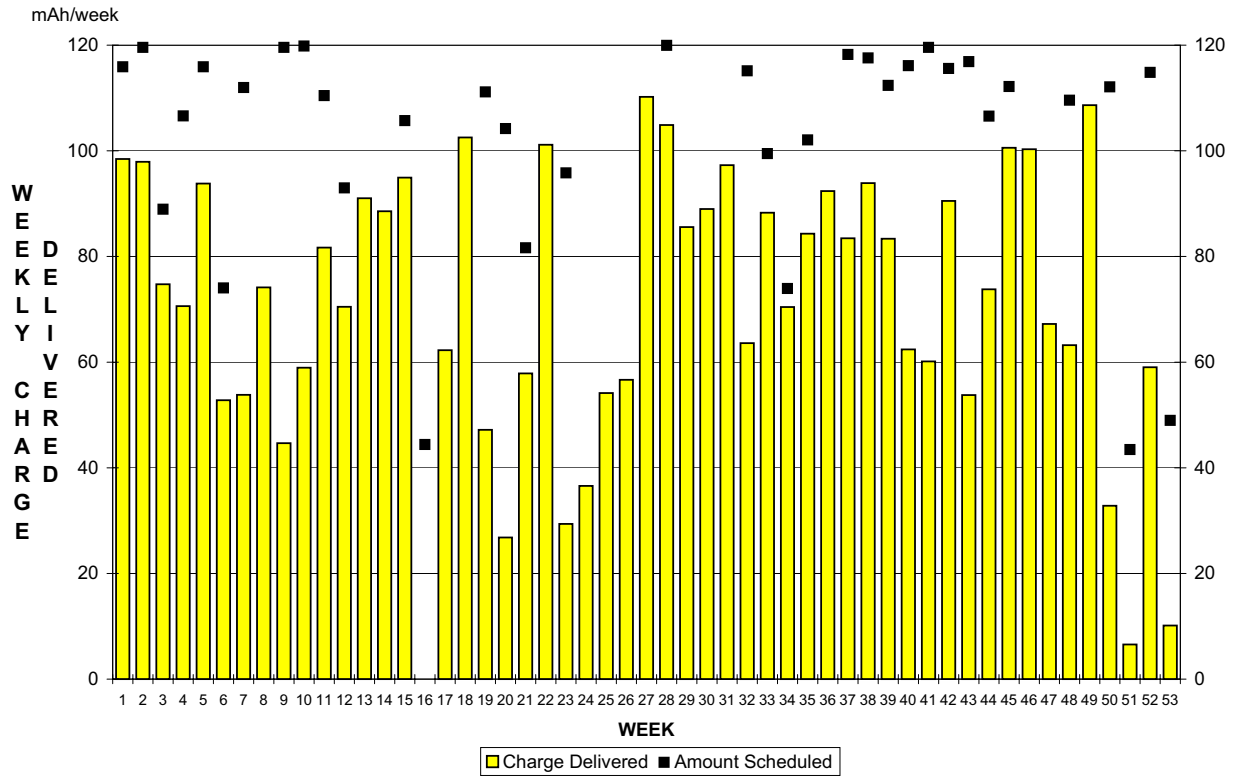


Fig. 253. Weekly beam delivery for the TR30-2.

ADMINISTRATION DIVISION

INTRODUCTION

The Administration Division is made up of Human Resources and Administration, Accounting and Materials Control, Administrative Computing, and Safety. The manager of each group reports to the Director. A summary of Division activities is included in this report.

HUMAN RESOURCES AND ADMINISTRATION

All employees are reviewed for performance on an annual basis. The period covered for Performance Planning and Review coincides with the calendar year.

TRIUMF has a very strong student program and hires on average some 35 summer students per year in addition to approximately 10 university co-op students who are hired each term.

In 2004 TRIUMF awarded researcher emeritus status to two retired scientists. The researcher emeritus position is intended to mark the past accomplishments of retired researchers and to express TRIUMF's appreciation for their willingness to continue active research in TRIUMF related activities. Initial planning was completed for the establishment of a TRIUMF alumni group. All retired TRIUMF employees and regular visitors to TRIUMF will be eligible to become members of this alumni group. A Web site with relevant alumni information is currently being constructed.

The Administration Division maintains all long-term visitor information such as home institution, length of stay, contact person at TRIUMF, radiation badge, and keys issued.

The TRIUMF security card access system is working well with approximately 1100 active security cards. All employees and long-term visitors are required to wear a photo ID card. All short-term visitors, those visiting less than three weeks, are required to wear a Visitor badge. Security guard coverage continues between 6:00 pm and 6:00 am on working days with twenty-four hour coverage on weekends and statutory holidays. All vehicles accessing the site behind the security fence are required to have a permit.

The insurance program was renewed with an approximate 13% increase in premiums over the previous year as a result of market conditions. Third party liability coverage remains at \$50 M. All buildings operated by TRIUMF are owned by the University of British Columbia and insurance coverage for these buildings and contents is provided by the Canadian Universities Reciprocal Insurance Exchange (CURIE).

There are currently six full member and seven associate member universities in the Joint Venture. Ef-

fective April 1, 2004, the University of Toronto became a full member and on December 1, 2004, Saint Mary's University became an associate member.

TRIUMF complies with Federal Treasury Board requirements under a results-based Management and Accountability Framework. The purpose of this framework is to establish a mechanism to help the National Research Council (NRC) and TRIUMF: i) collect performance information related to this initiative; ii) track delivery of commitments and reporting; iii) describe how the success of TRIUMF will be evaluated over time; and iv) provide direction for on-going and future planning. No Management and Accountability Framework report was required to be submitted in 2004 due to the review of the reports submitted by TRIUMF to the NRC in support of TRIUMF's 5 year funding request for the period 2005–2010.

In 2004 TRIUMF completed construction of its new housing facility, TRIUMF House. This facility offers modern amenities in a soundproof environment that ensures visitors to TRIUMF enjoy their home away from home. Official occupancy began on December 13. Construction of this facility was completed earlier than scheduled and under budget.

ENVIRONMENT HEALTH AND SAFETY

Licensing

The latest version of the TRIUMF Preliminary Decommissioning Plan was accepted by the Canadian Nuclear Safety Commission (CNSC). Such a plan is a regulatory requirement under the new CNSC regulations for all nuclear facilities and must be accompanied by financial guarantees to cover the cost of eventual decommissioning. At year's end, TRIUMF was still negotiating the form of these guarantees with the federal government.

The TRIUMF Quality Management System as defined in the Quality Manual and ten TRIUMF Standard Operating Procedures (TSOPs) was accepted by the CNSC. These documents are available at <http://www.triumf.ca/EHS/> by clicking on "Quality Assurance". As part of the Quality Assurance program, the TRIUMF QA Assessment Team performed 13 internal assessments of compliance with the TSOPs of a number of TRIUMF groups. The assessments have been published as Internal Assessment Reports and are available to those TRIUMF users with an account on the TRIUMF Document Server <http://documents.triumf.ca/docushare/dsweb/HomePage>. A new list of assessments planned for 2005 was published at the end of the year.

Table LII. Collective dose for TRIUMF personnel by group.

Group	Dose (mSv)	Fraction of total (%)	Median (mSv)
Applied Technology	129.8	31.5	3.4
Remote Handling	33.7	8.2	3.2
500 MeV Operations	28.3	6.9	1.5
Safety Group	29.9	7.3	1.1
RF Group	16.8	4.1	0.7
Vacuum Group	30.8	7.5	4.4
Plant Group	31.6	7.7	0.6
Beam Lines/Probes	29.0	7.0	4.0
Tech Support	32.5	7.9	4.7
Life Sciences	28.3	6.9	0.7
ISAC Operations	8.4	2.0	0.2
Science Division	10.5	2.5	0.3
Outside Contractors	2.5	0.6	0.2
Others	24.7	5.6	—
Total	436.9	100.0	0.6

In September TRIUMF was visited by a team of IAEA inspectors to verify TRIUMF's compliance with international safeguards on nuclear materials. The inspectors examined all hot cells at TRIUMF and obtained swipes of the exterior for analysis.

Personnel Dosimetry

The collective dose for TRIUMF personnel for the year 2004 was 436.9 mSv as measured by the direct reading dosimeter service. Table LII shows the breakdown of the collective dose by various work groups. The collective dose was somewhat lower than for 2003. ISAC continues to make a relatively minor direct contribution to the collective dose.

Interlocks and Monitoring

ISAC B1 electrical room was interlocked to the 500 MeV Central Safety System and the ISAC DRAGON experimental area was interlocked to the Ion Beam Safety System. Both were commissioned early in the year.

Designs were completed for the ISAC-II Access Control System and the extension of the ISAC Radiation Monitoring System to ISAC-II. No funds were available to start installation within this fiscal year.

A design for a new prototype secondary channel area safety unit was started. This is in anticipation of a program to refurbish the meson channel interlock systems.

Occupational Health and Safety

All TRIUMF's Occupational Health and Safety Programs continued to run smoothly. The fire alarm system, sprinkler systems and fire extinguishers were all inspected and verified for 2005.

A workshop on ladder safety was presented in June after a rash of ladder related accidents. In order to address the possibility of falls in other areas such as, for example, working on the 500 MeV cyclotron jacking system, fall arrest equipment was purchased for use in these areas and training provided for its use.

ADMINISTRATION COMPUTING AND COMMUNICATIONS

Management Information Systems

No major changes were made to the MIS systems and database in 2004.

Public Web Services

Testing of the new TRIUMF Web server, <http://www.triumf.info/>, was completed, and it became the default public Web site in the last half of 2004. The site was set up with two home pages, one addressed to the general public, the other to TRIUMF users and employees. The former presents headline stories that may be of interest to outsiders, and has menu items that lead to areas of general interest. The Users and Employees home page, on the other hand, presents current site announcements and status information, and has menu items that lead to areas more specific to the TRIUMF community itself. In both cases, some menu items lead to pages that remain on the old Web server; it will be a continuing project to migrate and reorganize these Web pages onto the new Web server.

In 2004, additional Web based utilities were implemented to support on-line beam requests. Unlike previous forms, these new forms are interactive, in that the form structure varies depending on what type of beam request is being made. The forms themselves are fully database-driven, so that they can be adjusted as new experimental facilities are brought on-line. These forms were first used for beam schedule 106, and formed the second component of the Web beam scheduling tools (the first component, publishing the schedules, was completed in 2003).

Development continued on the third component of the beam scheduling tools, which will allow a schedule to be built directly from the request database, without having to print the requests and prepare the schedule off-line. This component is expected to have two interfaces – a graphic interface that uses timelines, and a spreadsheet-like interface. It is expected that this tool will be available for use in 2005.

The administration Web server, admin.triumf.ca, was used to support the registration and payment of three conferences in 2004: NIC-VIII, 5ISR, and WRNPPC. The NIC-VIII conference was the first to use the reusable conference forms, which will continue to be used for other conferences hosted by TRIUMF.

Telephones

No major changes were made to the site telephone infrastructure during 2004. Towards the end of the year, planning was started on how to provide telephone service to the new TRIUMF House. The decision was made to add TRIUMF House to the existing TRIUMF telephone system rather than install an independent system. The TRIUMF House portion would be connected to the main site using IP telephony, which would also allow sharing of infrastructure with the TRIUMF House data network. This would be the first use of IP telephony for TRIUMF, and in future, the same technology may be used within the main site as well.

TRIUMF OUTREACH PROGRAM

The TRIUMF Outreach Program (TOP) continues to evolve and grow in its second year, after being officially launched in 2003 with generous grants from the Vancouver Foundation and the TRIUMF Technology Transfer office. TOP has been focusing its outreach efforts on high school students and teachers, as well as the general public, and good progress has been made in all of these areas.

The high school teacher internship program has continued to attract keen interest from teachers across BC, with 7 teachers having participated in TRIUMF experiments so far and over a dozen more on the waiting list. We expect this program to attract 3–6 teachers a year to TRIUMF for years to come.

TRIUMF/ISCBC High School Fellowship

In 2004, TRIUMF instituted a new High School Fellowship program for an outstanding graduating high school student from BC. This fellowship is being run in conjunction with the Innovation and Science Council of BC (ISCBC). In 2004 about 100 of the top students from across BC were nominated by their schools for the award, from which the ISCBC selected a short list of seven students. TRIUMF selected Reka Moldovan from Kelowna as the inaugural winner of the \$3000 fellowship. She spent a six week summer research ex-

perience at TRIUMF working with Prof. Jess Brewer of UBC. This fellowship was considered to be very successful, so the plan is to make it an annual award with hopefully more student winners in the future.

Future Directions

TOP has committed to joining the Alberta Large-Area Time coincidence Array (ALTA) cosmic-ray detector in the schools project by funding research and development of the next generation data acquisition system. Two such systems are under development at the University of Alberta under the direction of Jim Pinfold, and TRIUMF can expect to see the completed units late in 2005. TOP is also gearing up for the United Nations World Year of Physics 2005, with many events being planned throughout the year. Plans are also under way to create a new Outreach Web site for use by teachers and students seeking information and updates about TOP programs.



Fig. 254. Kelowna high school student Reka Moldovan receiving her TRIUMF High School Fellowship award from TRIUMF Director Alan Shotter. Ms. Moldovan is presently a science student at UBC.

CONFERENCES, WORKSHOPS AND MEETINGS

FFAG 2004 WORKSHOP

Fixed-field alternating-gradient (FFAG) accelerators, which were intensively studied in the 1950s and '60s but never progressed beyond the model stage, have in recent years been the focus of renewed attention. Two proton machines have now been built, three more (plus an electron FFAG and a muon phase rotator) are under construction, and a variety of designs are under study for the acceleration of protons, heavy ions, electrons and muons, with applications as diverse as cancer therapy, industrial irradiation, driving sub-critical reactors, boosting high-energy proton intensity, and producing neutrinos. These advances have been underpinned by a series of international workshops held at CERN, KEK, LBNL, BNL and now TRIUMF (April 14–21). A valuable feature of these workshops has been their small and informal nature, with as much time as possible allocated to work and discussion. At TRIUMF, the 23 participants were certainly hard-working, giving no less than 36 talks between them. Their presentations can be found at the workshop Web site: <http://www.triumf.ca/ffag2004>. The workshop was very capably organized by Shane Koscielniak and Elly Driessen.

With their fixed magnetic fields, modulated rf, and pulsed beams, FFAGs operate just like synchrotrons – with the central region removed and the magnet broken into radial or spiral sectors to provide edge and strong focusing. The fixed magnetic field leads to a spiral orbit, so the vacuum chamber and magnets tend to be larger than for synchrotrons, but the repetition rate (and hence beam intensity) can be much higher, as it is set purely by rf considerations. High rep rate and large momentum acceptance are the two features where FFAGs offer advantages over synchrotrons, and it is applications needing one or both of these features that have driven the current surge of interest.

In order to avoid the slow crossing of betatron resonances associated with conventional low energy-gain per turn, all FFAGs so far constructed have been based on the “scaling” principle, which means keeping the orbit shape, optics, and betatron tunes fixed, independent of energy, just as in synchrotrons. This requires magnets with constant field index (log gradient) over a wide radial aperture, and either constant spiral angle or, for radial-sector designs, focusing (F) and defocusing (D) gradient magnets with equal and opposite fields.

Y. Mori described the two proton FFAGs recently built at KEK using DFD radial-sector triplets. The 1 MeV 6-sector POP (proof of principle) FFAG came

into full operation in 2000, while the 12-sector, 5 m radius, 150 MeV ring, a prototype for proton therapy and neutron production, recently reached full energy.

Another 150 MeV FFAG of the same design is being installed at the Kyoto University reactor (KURRI), in collaboration with Mitsubishi, to test accelerator-driven sub-critical reactor operation. Two further FFAGs act as injector (a 2.5 MeV betatron with 8 spiral sectors) and booster (20 MeV with 8 radial sectors). Initially the rep rate will be 120 Hz, yielding a 1 μ A beam, later 1 kHz, providing 100 μ A.

FFAGs are also of interest for muons at both low and high energies. Y. Kuno described PRISM (phase-rotated intense slow muon source), a 10-cell DFD radial-sector FFAG of 6.5 m radius, now under construction at RCNP Osaka for eventual installation at J-PARC. It will collect 5-ns-wide bunches of 68 MeV/c \pm 30% muons and use a sawtooth rf field to rotate them in phase space, reducing the momentum spread to \pm 3%. With a rep rate of 100–1000 Hz the muon intensity will be $10^{11} - 10^{12}$ /s, making possible ultra-sensitive rare-muon-decay studies. PRISM will also be used for ionization cooling of muons. Another scheme for ionization cooling came from Garren (UCLA) and Kirk and Kahn (BNL), who proposed a small 12-sector gas-filled FFAG (1 m radius) for cooling 250 MeV/c \pm 30% muons, using superconducting magnets.

Mori also described the ambitious plan to build a neutrino factory at J-PARC based on a sequence of four muon FFAGs with top energies of 1, 3, 10, and 20 GeV. The largest would have a radius of 200 m (total orbit spread 50 cm) and consist of 120 cells, each containing a superconducting DFD triplet. Most cells would also contain rf cavities to provide an overall energy gain of \approx 1 GeV/turn, restricting the muon decay loss to 50% overall. The use of low-frequency rf (24 MHz) keeps the buckets wide enough to contain the phase drift occurring as the orbit expands. A major advantage of FFAGs over linacs – either single or recirculating – is that their large acceptance obviates the need for muon cooling or phase rotation. There are also significant cost savings.

The rapid acceleration essential for muons allows betatron resonances no time to damage beam quality. Scaling can therefore be abandoned, the betatron tunes allowed to vary, and lattices explored for properties favourable to muons. In particular, in 1999 C. Johnstone (FNAL) showed that it would be very advantageous to use constant-gradient magnets, with positively bending Ds stronger and longer than the Fs. The circumference could be shortened, the radial orbit



Fig. 255. Attendees at the FFAG2004 Workshop at TRIUMF, including AG pioneer Ernest Courant and FFAG pioneer Andy Sessler (4th and 5th from left).

spread reduced (allowing the use of smaller vacuum chambers and magnets), and the orbit length made to pass through a minimum at mid-energy (instead of rising monotonically), thus reducing the variation in orbit time with energy – a vital consideration since there is no time for rf frequency modulation. Moreover, constant field gradients could be used (rather than constant field index), simplifying the magnet design and rendering non-linear resonances harmless.

Lattices along these lines were described by Johnstone, by Berg, Courant, Trbojevic and Palmer (BNL), by Keil (CERN) and Sessler (LBNL), and by Koscielniak (TRIUMF). The latest results from an ongoing cost-optimization study by Berg *et al.* favoured the use of linacs up to 2.5 GeV followed by 2.5–5, 5–10 and 10–20 GeV FFAGs; the main ring, composed of ≈ 100 doublet or FDF triplet cells, would have a circumference of ≈ 700 m, with orbit lengths varying by only 20 cm.

With the orbit time first falling and then rising, Koscielniak and Berg have shown that, by exceeding a critical rf voltage, an acceleration path can be created which stays close to the voltage peak (crossing it three times), snaking between neighbouring buckets (rather than circulating inside them). Their latest results showed that by using high-field superconducting 200 MHz cavities it should be possible to accelerate from 10 to 20 GeV in 16 turns, with decay loss 10% (25% in the three rings).

Several presentations were dedicated to particular technical features, including resonance crossing, injection and extraction, and magnet and rf hardware design. Some novel features of non-scaling designs – particularly acceleration outside buckets and the crossing of many integer and half-integer resonances – were felt to deserve demonstration in an electron model (prob-

ably 10–20 MeV/ c) and some preliminary studies of lattices and hardware were presented.

A different non-scaling approach has been taken by Ruggiero (BNL), who described a design for a 1.5 GeV proton FFAG to replace the AGS booster, or for high-power applications up to 4 MW. Here acceleration is relatively slow (>1000 turns) so that resonances must be avoided. The tune is therefore kept essentially constant by using a non-linear field profile for which the changes in gradient balance those in flutter, while the non-scaling virtue of low dispersion is retained by using FDF cells with stronger D than F magnets. The 136-cell FFAG, located in the AGS tunnel, would accelerate 10^{14} ppp at 2.5 Hz, providing a 40 μ A beam.

With this wide variety of new ideas and new projects, FFAGs seem at last to have come into their own. These matters were to be followed up at the next workshop, held at KEK in October, 2004.

TRIUMF SUMMER INSTITUTE

The TRIUMF Summer Institute (TSI) has a long standing tradition, and has over the years attracted many students from Canada and around the world to lectures on a wide variety of topics, all in direct relation to forefront physics pursuit at TRIUMF. The 2004 TSI was the 16th in the series, and took place at TRIUMF from the July 5–16. It was entitled Lectures in Nuclear Astrophysics: Experiment, Theory, and Observations. The Institute is tailored towards graduate students and young researchers in the field. This year's Institute was organized to go hand-in-hand with a major international conference, also organized by TRIUMF: the 8th International Symposium on Nuclei in the Cosmos (NIC 8), which started the following week. This combination of the summer school together with the conference allowed for an excellent introduction

to the field and attracted 38 students from 4 continents. The Institute is structured with formal lectures in the morning and a tutorial session in the afternoon, where open discussions were encouraged. The presence of various lecturers during these open sessions made for interesting discussions and allowed the students to tackle a broad variety of questions from different viewpoints, both experimental and theoretical. In addition to the formal part, 3 excursions were organized, including an ocean kayak trip, which allowed for excellent interaction between the lecturers and students, leading to many interesting and enlightening conversations (and unwanted swimming actions). Nevertheless, the Institute is recognized by many universities as a formal course and students used this opportunity to arrange for credit, which is given based on homework. The lecturers and topics this year were:

- T. Beers (Michigan State University, USA) Astrophysical Observations
- F. Bosch (GSI Darmstadt, Germany) Mass Measurements of Astrophysical Interest
- A. Cummings (McGill University) Explosive Nucleosynthesis
- B. Davids (TRIUMF) Indirect Reaction Studies Relevant for Nucleosynthesis
- C. Illiadis (University of North Carolina, USA) Direct Reaction Studies
- T. Kajino (National Astronomical Observatory of Japan) Big Bang Nucleosynthesis
- B. Mayer (Clemson University, USA) Stellar Evolution
- A. Mezzacappa (Oak Ridge National Lab, USA) Supernovae and Gamma-Ray Bursts

The organizing committee was chaired by Jens Dilling and included Lothar Buchmann, Barry Davids and Byron Jennings.

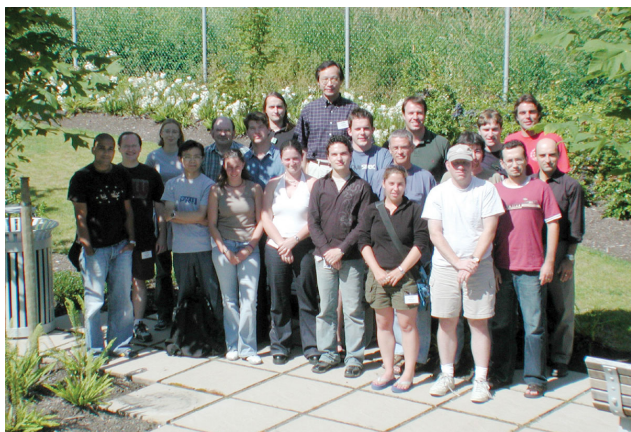


Fig. 256. Group photo of the TRIUMF Summer Institute participants and lecturers in the TRIUMF backyard.

NUCLEI IN THE COSMOS

The 8th International Symposium on Nuclei in the Cosmos was held from July 19–23 at the Coast Plaza Hotel, located in the West End of Vancouver. There, two hundred and thirty-seven participants were treated to the latest news from the world of nuclear astrophysics and related fields as well as a multitude of other means to keep the body and soul refreshed. This series of conferences was established under its present name in 1990, with the inaugural meeting being held in Baden, Austria. The initial emphasis on experimental nuclear astrophysics has now been extended to include a wide range of topics from observational astronomy to stellar modelling of extreme conditions, all bound together by the common subject of interest which is how elements are produced and distributed in the cosmos.

After an introductory address by Sam Sullivan, the deputy mayor of Vancouver, the conference was opened for talks with Tom Lehrer's rendition of "The Elements", as the focus of these meetings is the origin of the elements in the universe. Opening talks on core collapse supernovae reported significant advances in understanding these mechanisms which have led to (nearly) working models of such SN explosions; impressive colour movies of such explosion simulations were shown. Additional data on many processes, e.g. electron capture rates for medium mass nuclei in the iron region are, however, needed. The observation by satellites of the γ emitting isotope ^{26}Al ($t_{1/2} = 7.4 \times 10^5$ yr), most likely resulting largely from core collapse supernovae (and maybe other explosive events), has stimulated the drive to measure reaction rates for its production and destruction in such events. Such reactions involve both stable and radioactive heavy ion beams. As not all reactions can be measured directly, there is a strong need for nuclear theory input, a topic that was discussed extensively.

The focus of the conference then shifted to observation of specific isotopes by non-optical means. An exciting development is the observation of ^{60}Fe ($t_{1/2} = 1.5 \times 10^6$ yr) in ferromanganese crust in the Pacific. This isotope can only have been produced in a SN explosion which occurred in the solar vicinity about three million years ago. The Cosmic Ray Isotope Spectrometer (CRIS) on the ACE spacecraft, which is measuring the isotopic composition of cosmic rays, observes a source similar to the elements in the solar system except for a few, not well understood isotopes. Since 2002 the European Space Agency's INTEGRAL satellite has been observing γ -rays emitted from specific isotopes in our galaxy, including those from positron annihilation radiation and from the decay of ^{26}Al . Since in many core collapse supernovae models ^{60}Fe is produced at

about the same rate as ^{26}Al , the fact that its decay has not been observed by satellites has become critical.

A large fraction of the conference was dedicated to the observation of early nucleosynthesis in the atmospheres of old, small halo stars and the modelling of the galactic chemical evolution. There is remarkable evidence that early r-process nucleosynthesis and the distribution of iron peak elements is often close to solar, closer than models would predict. Early s-process nucleosynthesis leads to a relative enhancement of lead, while some isotopes show not well understood irregularities.

The measurement of nuclear reactions with stable isotopes is still at the forefront of research. In particular, the reaction considered to be the most important for understanding the production of medium mass elements in stellar environments is $^{12}\text{C}(\alpha, \gamma)^{16}\text{O}$. It was the subject of many experimental studies reported at the symposium which attempt to determine its rate at stellar temperatures with greater precision. While significant progress has been achieved by various groups, more work is needed. The LUNA (Laboratory Underground for Nuclear Astrophysics) facility, located in the Gran Sasso tunnel in Italy, allows measurements of important reactions such as radiative proton capture on ^{14}N at very low energies where the stellar reaction rate has lately been lowered considerably. With the reduction of cosmic ray background, studies down to the Gamow energy window can be achieved.

A highlight of the conference was the series of talks on SN and γ -ray bursts (GRBs), exhibiting total energy outputs of $\approx 10^{52}$ ergs and more. Overwhelming evidence over the last 6 years indicates that a large fraction of GRBs are accompanied by SNIc events, although the inverse is not necessarily true. Models of such violent explosions, known as collapsars, were presented as a work in progress; the role of rotation and the formation of jets are important aspects of such scenarios. Of equal importance is a good understanding of SNIa, which are excellent cosmological distance indicators (standard candles). The maximum light output versus decay width calibration seems to be understood now theoretically; however, second order variations in models and the exact deflagration mechanism need more attention.

Considerable progress has been made in understanding the s-process but more work is needed, especially with initiation reactions and for reactions of low cross section and at very low energies as the paradigm for s-process nucleosynthesis has moved to low mass stars. A new facility, the n_TOF system at CERN, is now operational and providing valuable (n, γ) cross sections over a wide mass range.

A number of talks were centred on the r-process, which is believed to be the mechanism responsible for the production of half of the elements heavier than those in the iron peak. Identification of the astrophysical site and the specific conditions under which the r-process takes place remains a major mystery, along with predictions of properties of very neutron-rich exotic nuclei involved in this process. Studies on presolar grains are also providing a wealth of new information and setting constraints on models of nucleosynthesis and stellar evolution for a multitude of stellar scenarios.

Originally, this conference series sought to bring together experimentalists to discuss programs in nuclear astrophysics. This is still a main focus of attention and there were a number of overview talks on studies with both stable and radioactive heavy ion beams. Areas of focus for radioactive isotope studies are measurements related to the r-process, the rp-process and the p-process. The combination of these data coupled with improved stellar models leads to a better understanding of nucleosynthesis in stellar environments prior to and during explosive scenarios. Therefore mechanisms for cataclysmic stellar events, including novae and X-ray bursts, were the subject of various talks at the conference. New techniques involving radioactive beams and recoil separators are providing new avenues to obtain necessary information previously considered inaccessible. Additional reaction rates involving exotic nuclei are still required for a clearer understanding of the mechanism leading to the production of particular isotopes.

In addition, there were talks on reactions occurring in the sun, measurements of the solar neutrino flux using the Sudbury Neutrino Observatory (SNO) which have led to a clear confirmation of neutrino flavour mixing, and the status of information on reactions in big bang nucleosynthesis.

At the banquet held at the University of British Columbia's Museum of Anthropology, all were treated to an introspective view of the early days of studies at the first centre for experimental nuclear astrophysics at Caltech by D.D. Clayton. His talk was entitled "Phive Years of Physics Phun with Phowler", presenting stories of working with Willie Fowler (Nobel Laureate in 1983). The talk can be found in the conference proceedings, including the Kellogg Laboratory's battle song.

A closing talk was given by Claus Rolfs with a particular emphasis on experimental measurements in Bochum. The next symposium, Nuclei in the Cosmos IX, will be hosted by CERN in Geneva, Switzerland in 2006.

The conference proceedings will be published as an edition of Nuclear Physics A early in 2005. The edi-

tors are Lothar Buchmann, Martin Comyn and Jana Thomson.

The following people are acknowledged for ensuring the successful staging of the conference. With her impressive organizational skills, Elly Driessen made the conference possible in the first place. Lorraine King's dedicated work on the proceedings helped ensure their timely publication. Thanks are extended to the staff of the Coast Plaza Hotel and to Mindy Hapke for taking the conference photographs. UBC Catering Services and the Romanza String Quartet, both involved with the banquet, are also gratefully acknowledged. The work of the Local Organizing Committee, in particular J. D'Auria, P. Gardner, K.P. Jackson, G. Jones, H. Leslie, J. Rogers and A. Shotter, deserves high praise as does the TRIUMF accounting office for help and personnel during registration, and the many tour guides who assisted at the TRIUMF tour on the Saturday morning following the conference. Finally, hosting the conference would not have been possible without the generous sponsorship provided by MDS Nordion, NSERC and TRIUMF.

VICTORIA LINEAR COLLIDER WORKSHOP

The Victoria Linear Collider Workshop was held July 28–31 at the Hotel Grand Pacific in downtown Victoria. This was a meeting in the series of North American workshops on the physics, detector, and accelerator issues of the future International Linear Collider.

The workshop was attended by 150 physicists, the large majority from the United States, but with many participants from Canada, Europe, and Asia.

Alan Shotter, TRIUMF director, opened the meeting by welcoming the participants to Victoria and giving a brief introduction to TRIUMF and its role in Canadian particle physics. The rest of the first day consisted of plenary talks on the status of linear collider plans around the world, the status of accelerator research and development, and on a number of theoretical developments. The closing talk of the first day, *The Linear Collider and the Rest of the Universe*, by Jonathan Feng, was very well received.

The second and third days had parallel sessions, typically five at any time, of the 21 working groups covering all aspects of physics, detector, and accelerator issues. In the late afternoon of the second day, a review of detector research and development was presented in plenary session.

In the afternoon of day three, the plenary session included a presentation by Barry Barish on the status of the International Technology Recommendation Panel (ITRP). That panel was charged to select be-

tween the two competing accelerator technologies, so that the world community could focus on a single design. At ICHEP in Beijing in August, the ITRP announced its recommendation to use superconducting accelerating structures. Subsequently, Barry has been asked to lead the organization to develop the single design of the International Linear Collider.

Other plenary presentations on the third day included talks from representatives of the US funding agencies, and from the leaders of the world wide physics and detector studies.

The final day of the program had a set of summary presentations covering some of the parallel sessions, and concluded with a fine talk by Michael Peskin from SLAC.

More information about the workshop, including all of the presentations given at the meeting, can be found on the Web at www.linearcollider.ca/victoria04.

The workshop was a great success. The participants and organizers were very pleased with the hotel services and staff. The chair of the organizing committee (D. Karlen) would like to acknowledge the financial support for this meeting from TRIUMF, University of Victoria, IPP Canada, and NSERC.

FIFTH INTERNATIONAL SYMPOSIUM ON RADIOHALOGENS

The Fifth International Symposium on Radiohalogens (5ISR) was held September 11–15 in Whistler. 5ISR was the most successful Radiohalogen symposium in the series with more than 70 attendees from Canada, Europe, Japan, China, and the USA. While most attendees were from academic research facilities, several participants came from companies such as Bristol-Myer Squibb, MDS Nordion, Merck, Nihon Medi-Physics, Schering AG, Theragenics, and Molecular Insight Pharmaceuticals. Topics discussed at the meeting included: production of radiohalogens, fluorine chemistry, iodine chemistry, bromine chemistry, radiohalogens in radiotherapy, drug development, and industrial issues. Sponsorship for the meeting came from the US Department of Energy (DOE), MDS Nordion, the University of Washington, TRIUMF, and the Society of Radiopharmaceutical Sciences (SRS). With the DOE and SRS contributions we were able to provide travel awards for 11 graduate students and postdoctoral fellows to attend the meeting. The 5ISR Web site (<http://www.triumf.ca/5ISR>) contains a PDF version of most of the scientific presentations, an attendees list, and various photos from the meeting.

TRIUMF USERS' GROUP ANNUAL GENERAL MEETING

The 2004 TRIUMF Users' Group Annual General Meeting was held in the TRIUMF auditorium on

Wednesday, December 8, prior to the Subatomic and Materials Science two-day EEC meetings. The meeting had 48 registrants and several users who were unable to travel to TRIUMF watched the live video stream on the Web. The video files are archived on <http://video.triumf.ca/cgi-bin/archive/tug04>.

The meeting began with the traditional set of talks by the Director and Division Heads reporting on the state of the laboratory, the science highlights and future beam schedule, the cyclotron status and plans for future refurbishing and upgrades, and the status of ISAC-I and ISAC-II. All of the presentations contemplated future developments outlined in the 2005–2010 Five Year Plan which was awaiting government approval.

In anticipation of the new funding, the TRIUMF Users' Executive Committee (TUEC) had conducted a long range planning survey as an initial step in developing a vision beyond 2010. Jeff Sonier, the TUEC Chair, presented a summary of the 43 responses received. Many were provocative and prompted a lively discussion from the floor, which extended into the lunch break. It was generally agreed that it had been a worthwhile exercise, and the collated responses were later given to the Director and Division Heads for their consideration.

After lunch, there were talks by Isao Tanihata of ANL and two TRIUMF graduate students, Julie Lefebvre and Dan Melconian.

In the TUEC Business Meeting, Jeff Sonier outlined what TUEC had achieved during 2004 and then announced the results of the election for the vacant 2005 TUEC positions. By acclamation, P. Garrett (U. Guelph) was elected as chair elect for 2005. For the first time in the history of the TRIUMF Users' Group (TUG), there was a second place tie in the vote for the two representatives. As the TUG by-laws did not specify what to do in such a situation, it was agreed by a majority of the members present that in this instance there would be three representatives for 2005/2006. They are G. Gwinner (U. Manitoba), M. Nozar (TRIUMF) and F. Sarazin (Colorado School of Mines). To avoid a recurrence in the future and, more importantly, to specify what to do in the case of a tied vote for chair elect, TUEC will propose an amendment to the by-laws

early in 2005 and conduct a ballot which will require a two-thirds majority of the members voting in order to be adopted.

TUEC also nominates two members to represent the Users on the TRIUMF Operating Committee. In 2004 S. Yen (TRIUMF) and L. Lee (U. Manitoba) remained as the on-site member and alternate, respectively, while G.M. Luke (McMaster U.) and J.E. Sonier (SFU) remained as the off-site member and alternate, respectively.

This ended the formal part of the TUG AGM, but instead of finishing with a buffet dinner at TRIUMF, everyone moved to TRIUMF House for a reception and a final chance to reminisce and say farewell to the old building before the move to the new facility the following week.

Welcome	Jeff Sonier
State of the Laboratory	Alan Shotter
Science Division Report	Jean-Michel Poutissou
Cyclotron Status	Roger Poirier
ISAC Report	Paul Schmor
TUG LRP Survey Results	Jeff Sonier
Radii and Density	
Distributions of Nuclei	Isao Tanihata, ANL
Chemistry and Physics of Gold-Cyanide Coordination	
Polymers	Julie Lefebvre
Searching for Right-Handed Currents in the β -Decay of Laser-Cooled Polarized ^{37}K	Dan Melconian
TUEC Business Meeting	Jeff Sonier
Reception - Farewell to the Old TRIUMF House	

TUEC Membership for 2004

J.E. Sonier	SFU	<i>Chair</i>
J. Dilling	TRIUMF	<i>Chair Elect</i>
W.D. Ramsay	U. Manitoba	<i>Past Chair</i>
A.A. Chen	McMaster U.	2003/2004
T.A. Porcelli	U. Northern BC	2003/2004
P. Bricault	TRIUMF	2004/2005
A. Laird	U. York, UK	2004/2005
M. Comyn	TRIUMF	<i>Liaison Officer</i>

ORGANIZATION

Board of Management (BOM)

The Board of Management of TRIUMF manages the business of the facility and has equal representation from each of the five member universities. The Board met 3 times during the year. At the end of 2004 the Board comprised:

University of Alberta	Dr. W.J. McDonald Dr. A. Noujaim	Chairman
University of British Columbia	Dr. D. Brooks Dr. J. Young	
Carleton University	Dr. R. Carnegie Dr. F. Hamdullahpur	
Simon Fraser University	Dr. M. Plischke Dr. C.H.W. Jones	
University of Toronto	Dr. P. Sinervo Dr. R. Orr	
University of Victoria	Dr. R. Keeler Dr. M. Taylor	
Private Sector	Ms. G. Gabel Dr. H. Ing	Environmental Sensors Inc. Bubble Technologies Inc.

Towards the end of 1987, Board membership was expanded in anticipation of a broadening of the TRIUMF joint venture to include a more national representation of Canadian universities long associated with the TRIUMF experimental program. The University of Manitoba and Université de Montréal became associate members, and the University of Toronto joined as an observer. At the end of 1988, University of Toronto's status changed from that of observer to associate member. In March, 1989 the University of Regina became an associate member. In December, 1998 Carleton University and Queen's University became associate members. In March, 2000 Carleton University's status changed from that of associate member to full member. In 2001 two private sector positions were added. In October, 2001 McMaster University became an associate member and effective April 1, 2003 the University of Guelph became an associate member. In April, 2004, the University of Toronto became a full member. Associate membership at year-end:

Non-voting Associate members:	Dr. P. Tremaine Dr. W.T.H. van Oers Dr. A.J. Berlinsky Dr. C. Leroy Dr. A. Hallin Dr. K. Bergman TBA Dr. R. Orr	University of Guelph University of Manitoba McMaster University Université de Montréal Queen's University University of Regina Saint Mary's University University of Toronto
<i>ex officio</i> members:	Dr. W. Davidson Dr. R.G.H. Robertson Dr. A. Shotter Dr. J.-M. Poutissou Mr. J. Hanlon	National Research Council ACOT Director, TRIUMF Associate Director, TRIUMF TRIUMF, Recording Secretary

Administration

Under the directorship of Dr. A. Shotter, TRIUMF personnel were grouped into Divisions, with Division Heads as follows:

Division Head, Science Division	J.-M. Poutissou
Division Head, Accelerator Technology Division	E.W. Blackmore
Division Head, Cyclotron Operations Division	R. Poirier
Division Head, Technology Transfer Division	P.L. Gardner
Division Head, ISAC Division	P.W. Schmor
Division Head, Administration Division	A. Shotter

Operating Committee

The TRIUMF Operating Committee advises the Director and the TRIUMF Board of Management (through the Director) on matters relating to the scientific productivity and direction of the TRIUMF laboratory. The Operating Committee consists of one voting member from each of the five full-member universities, two voting members representing the interests of the Users, and one representing TRIUMF staff. The Associate Director is a non-voting member. The Operating Committee met 5 times in 2004. Members of the committee (alternate members in parentheses) at the end of 2004 were:

Dr. A. Shotter	Chairman	Director	
Dr. J.-M. Poutissou	<i>(ex officio)</i>	Associate Director	
Dr. J. Pinfeld		University of Alberta	(Dr. D. Gingrich)
Dr. G. Oakham		Carleton University	(Dr. S. Godfrey)
Dr. J.M. D'Auria		Simon Fraser University	(Dr. P. Percival)
Dr. P. Savard		University of Toronto	(Dr. R. Orr)
Dr. D. Karlen		University of Victoria	(Dr. R. Sobie)
Dr. T. Mattison		University of British Columbia	(Dr. S. Oser)
Dr. G.M. Luke		Users	(Dr. J. Sonier)
Dr. S. Yen		Users	(Dr. L. Lee)
Mr. R. Baartman		TRIUMF Employee Group	(Mr. R. Ruegg)
Mr. J. Hanlon	Recording Secretary	TRIUMF	
Dr. W. Davidson	<i>(ex officio)</i>	National Research Council	

Agency Committee on TRIUMF (ACT)

The role of the Agency Committee on TRIUMF is to oversee the Government of Canada's investment in TRIUMF and the economic benefits derived from that investment, with a particular focus on financial and commercialization matters. The Committee provides advice to the Minister of Industry, in conjunction with the reports of the NRC Advisory Committee on TRIUMF on scientific matters. The Agency Committee on TRIUMF usually meets twice a year.

Dr. M. Raymont	Chairman	Acting President, National Research Council
Dr. T. Brzustowski		President, Natural Sciences and Engineering Research Council
Ms. S. Hurtubise		Deputy Minister, Industry Canada
Dr. W. Davidson	Secretary	National Research Council

NRC Advisory Committee on TRIUMF (ACOT)

The Advisory Committee on TRIUMF advises the National Research Council on all aspects of the TRIUMF program insofar as they relate to the determination and administration of the federal contribution to TRIUMF. The Committee provides scientific program advice to the Director of TRIUMF. The Committee reports to the National Research Council each year on its findings and recommendations, with particular reference to the arrangement entered into by the National Research Council and TRIUMF under which contribution payments are made, thereby ensuring that TRIUMF utilizes its program in support of its defined role as a national facility and works with all constituencies of the Canadian subatomic physics community to sustain a national program in the field of research, within the context of the funds available.

Dr. R.G.H. Robertson	Chairman	University of Washington
Dr. W. Davidson	Secretary	National Research Council
Dr. J. Äystö		University of Jyväskylä
Dr. W.J.L. Buyers		National Research Council
Dr. J. Guigné		Guigné International Ltd.
Dr. S. Houle		University of Toronto
Dr. G. Kalmus		Rutherford Appleton Laboratory
Dr. W. Nazarewicz		University of Tennessee
Dr. C. Rolfs		Ruhr-Universität Bochum
Dr. J. Siegrist		University of California, Berkeley
Dr. H. Tennant		National Research Council
Dr. P. Vincett		FairCopy Services Inc.
Dr. E. Brash	<i>(ex officio)</i>	University of Regina
Dr. W.J. McDonald	<i>(ex officio)</i>	University of Alberta
Dr. W. Trischuk	<i>(ex officio)</i>	University of Toronto
Ms. K. Wilson	<i>(ex officio)</i>	Natural Sciences and Engineering Research Council

TRIUMF Safety Management Committee

Dr. A. Shotter	Director, TRIUMF
Dr. J.-M. Poutissou	Associate Director/Head, Science Division
Dr. E.W. Blackmore	Head, Accelerator Technology Division
Dr. R. Poirier	Head, Cyclotron Operations Division
Mr. P.L. Gardner	Head, Technology Transfer Division
Dr. P.W. Schmor	Head, ISAC Division
Mr. M. Stenning	Head, Operations Group
Mr. D. Preddy	TAPC Chairman
Mr. G. Wood	Industrial Safety Officer/TAPC
Mr. L. Moritz	Head, Environmental Health & Safety
Mr. J. Hanlon	Manager, Human Resources & Administration
Dr. S. Zeisler	Head, Applied Technology Group
Dr. B. Abeysekera	MDS-Nordion
Mrs. K. Gildert	Recording Secretary

Experiments Evaluation Committees (EEC)

In July, 1994 the Experiments Evaluation Committee was formally split into two committees representing subatomic physics and μ SR physics. In 2000 the μ SR Committee changed its name to the Materials Science Committee and in 2003 the name was changed to Molecular and Materials Science Experiments Evaluation Committee. In 2004 these committees comprised:

Subatomic Committee:

Dr. B.M. Sherrill	Chairman	NSCL/Michigan State University
Dr. J.-M. Poutissou	Associate Director/ <i>(ex officio)</i>	TRIUMF
Dr. B. Jennings	Secretary	TRIUMF
Dr. W. Ramsay	<i>(ex officio)</i>	TUEC Past Chairman/TRIUMF
Dr. S.J. Freedman		Lawrence Berkeley Laboratory
Dr. I. Tanihata		Argonne National Laboratory
Dr. F.K. Thielemann		Universität Basel
Dr. R.E. Tribble		Texas A&M University

Molecular and Materials Science Committee:

Dr. B. Gaulin	Chairman	McMaster University
Dr. J.-M. Poutissou	Associate Director/ <i>(ex officio)</i>	TRIUMF
Dr. P.W. Percival	Secretary/ <i>(ex officio)</i>	SFU/TRIUMF
Dr. J. Sonier	<i>(ex officio)</i>	TUEC Chairman/Simon Fraser University
Dr. M. Gingras		University of Waterloo
Dr. F. Marsiglio		University of Alberta
Dr. S. Roorda		Université de Montréal
Dr. G.A. Sawatzky		University of British Columbia

Life Sciences Project Evaluation Committee (LSPEC)

Dr. J. Link	Chairman	University of Washington
Dr. J.-M. Poutissou	Associate Director/ <i>(ex officio)</i>	TRIUMF
Dr. L.P. Robertson	Secretary	University of Victoria
Dr. J. DaSilva		University of Ottawa
Dr. S. Houle		PET Centre – CAMH/University of Toronto
Dr. W. Jagust		Lawrence Berkeley Laboratory
Dr. R. Lecomte		Université de Sherbrooke
Dr. A.J.B. McEwan		Cross Cancer Clinic

PUBLICATIONS

This appendix lists publications describing work performed at TRIUMF and also work conducted elsewhere by TRIUMF personnel and TRIUMF users.

Journal Publications

Particle, Nuclear and Atomic Physics

P. Dubé and M. Trinczek, *Hyperfine structure splittings and absorption strengths of molecular iodine transitions near the trapping frequencies of francium*, J. Optical Society of America **B21**, 1113 (2004).

Z. Salman, E.P. Reynard, R.F. Kiefl, W.A. MacFarlane, J. Chakhalian, K.H. Chow, S. Daviel, S. Kreitzman, C.D.P. Levy and R. Poutissou, *Beta-detected nuclear quadrupole resonance with a low energy beam of $^8\text{Li}^+$* , Phys. Rev. **B70**, 104404 (2004).

U. Greife, S. Bishop, L. Buchmann, M.L. Chatterjee, A.A. Chen, J.M. D'Auria, S. Engel, D. Gigliotti, D. Hunter, D.A. Hutcheon, A. Hussein, C.C. Jewett, A.M. Laird, M. Lamey, W. Liu, A. Olin, D. Ottewell, J. Rogers and C. Wrede, *Energy loss around the stopping power maximum of Ne, Mg and Na ions in hydrogen gas*, Nucl. Instrum. Methods **B217**, 1 (2004).

M. Hunyadi, C. Bäumer, A.M. van den Berg, N. Blasi, M. Csatlós, L. Csige, B. Davids, U. Garg, J. Gulyás, M.N. Harakeh, M. de Huu, B.C. Junk, A. Krasznahorkay, S. Rakers, D. Sohler and H.J. Wörtche, *Particle decay of the isoscalar giant dipole resonance in ^{208}Pb* , Nucl. Phys. **A731**, 49 (2004).

J. Guillot, D. Beaumel, A.M. van den Berg, S. Brandenburg, B. Davids, S. Fortier, M. Fujiwara, S. Galés, M.N. Harakeh, M. Hunyadi, M. de Huu and H.J. Wörtche, *Investigation of IVGRs via the $^{58}\text{Ni}(t, ^3\text{He})^{58}\text{Co}$ reaction*, Nucl. Phys. **A731**, 106 (2004).

E.W. Grewe, C. Bäumer, A.M. van den Berg, N. Blasi, B. Davids, D. De Frenne, D. Frekers, P. Haefner, M.N. Harakeh, M. Huynyadi, E. Jacobs, B. Junk, A. Korff, A. Negret, P. von Neumann-Cosel, L. Popescu, S. Rakers and H.J. Wörtche, *Gamow-Teller transitions to ^{32}P studied through the $^{32}\text{S}(d, ^2\text{He})$ reaction at $E_d = 170$ MeV*, Phys. Rev. **C69**, 064325 (2004).

S. Rakers, C. Bäumer, A.M. van den Berg, B. Davids, D. Frekers, D. De Frenne, Y. Fujita, E.-W. Grewe, P. Haefner, M.N. Harakeh, M. Hunyadi, E. Jacobs, H. Johansson, B.C. Junk, A. Korff, A. Negret, L. Popescu, H. Simon and H.J. Wörtche, *Nuclear matrix elements for the ^{48}Ca two-neutrino double- β decay from high-resolution charge-exchange reactions*, Phys. Rev. **C70**, 054302 (2004).

A. Korff, P. Haefner, C. Bäumer, A.M. van den Berg, N. Blasi, B. Davids, D. De Frenne, R. de Leo, D. Frekers, E.-W. Grewe, M.N. Harakeh, F. Hofmann, M. Hun-

yadi, E. Jacobs, B.C. Junk, A. Negret, P. von Neumann-Cosel, L. Popescu, S. Rakers, A. Richter and H.J. Wörtche, *Deuteron elastic and inelastic scattering at intermediate energies from nuclei in the mass range $6 \leq A \leq 116$* , Phys. Rev. **C70**, 067601 (2004).

G.S. Mitchell, C.S. Blessinger, J.D. Bowman, T.E. Chupp, K.P. Coulter, M. Gericke, G.L. Jones, M.B. Leuschner, H. Nann, S.A. Page, S.I. Penttila, T.B. Smith, W.M. Snow and W.S. Wilburn, *A measurement of parity-violating gamma-ray asymmetries in polarized cold neutron capture on ^{35}Cl , ^{113}Cd , and ^{139}La* , Nucl. Instrum. Methods **A521**, 468 (2004) [nucl-ex/0401009].

A. Bacchetta, U. D'Alesio, M. Diehl and C.A. Miller, *Single-spin asymmetries: the Trento conventions*, Phys. Rev. **D70**, 117504 (2004) [DESY-04-193, hep-ph/0410050].

F. Sarazin, J.S. Al-Khalili, G.C. Ball, G. Hackman, P.M. Walker, R.A.E. Austin, B. Eshpeter, P. Finlay, P.E. Garrett, G.F. Grinyer, K.A. Koopmans, W.D. Kulp, J.R. Leslie, D. Melconian, C.J. Osborne, M.A. Schumaker, H.C. Scraggs, J. Schwarzenberg, M.B. Smith, C.E. Svensson, J.C. Waddington and J.L. Wood, *Halo neutrons and the β decay of ^{11}Li* , Phys. Rev. **C70**, 031302 (2004) [TRI-PP-04-13].

S. Shimizu, K. Horie, M. Aliev, Y. Asano, T. Baker, P. Depommier, M. Hasinoff, Y. Igarashi, J. Imazato, A.P. Ivashkin, M.M. Khabibullin, A.N. Khotjantsev, Y.G. Kudenko, A. Levchenko, G.Y. Lim, J.A. Macdonald, O.V. Mineev, C. Rangacharyulu and S. Sawada, *Measurement of $K^+ \rightarrow \pi^0 \pi^0 e^+ \nu$ (K_{e4}^{00}) decay using stopped positive kaons*, Phys. Rev. **D70**, 037101 (2004) [hep-ex/0408098].

J.T.M. Goon, D.J. Hartley, L.L. Riedinger, M.P. Carpenter, F.G. Kondev, R.V.F. Janssens, K.H. Abu Saleem, I. Ahmad, H. Amro, J.A. Cizewski, C.N. Davids, M. Danchev, T.L. Khoo, A. Heinz, T. Lauritsen, W.C. Ma, G.L. Poli, J. Ressler, W. Reviol, D. Seweryniak, M.B. Smith, I. Wiedenhöver and J.-Y. Zhang, *Shape coexistence and band crossings in ^{174}Pt* , Phys. Rev. **C70**, 014309 (2004).

J.M. D'Auria, R.E. Azuma, S. Bishop, L. Buchmann, M.L. Chatterjee, A.A. Chen, S. Engel, D. Gigliotti, U. Greife, D. Hunter, A. Hussein, D. Hutcheon, C.C. Jewett, J. José, J.D. King, A.M. Laird, M. Lamey, R. Lewis, W. Liu, A. Olin, D. Ottewell, P. Parker, J. Rogers, C. Ruiz, M. Trinczek and C. Wrede, *The $^{21}\text{Na}(p, \gamma)^{22}\text{Mg}$ reaction from $E_{c.m.} = 200$ to 1103 keV in novae and x-ray bursts*, Phys. Rev. **C69**, 065803 (2004).

R.J. Peterson, C.E. Allgower, V. Bekrenev, W.J. Briscoe, J.R. Comfort, K. Craig, D. Grosnick, D. Isenhower, N.

- Knecht, D. Koetke, A.A. Kulbardiš, G. Lolos, V. Lopatin, D.M. Manley, R. Manweiler, A. Marušić, S. McDonald, B.M.K. Nefkens, J. Olmsted, Z. Papandreou, D.C. Peaslee, N. Phaisangittiskaul, J. Price, D.E. Prull, A.F. Ramirez, M. Sadler, A. Shafi, H. Spinka, T.D.S. Stanislaus, A. Starostin, H.M. Staudenmaier, I. Strakovsky and I. Supek, *y scaling in quasifree pion-single-charge exchange*, Phys. Rev. **C69**, 064612 (2004).
- E. Friedman, M. Bauer, J. Breitschopf, H. Clement, H. Denz, E. Doroshkevich, A. Erhardt, G.J. Hofman, R. Meier, G.J. Wagner and G. Yaari, *The in-medium isovector πN amplitude from low energy pion scattering*, Phys. Rev. Lett. **93**, 122302 (2004) [nucl-ex/0404031].
- P.A. Zolnierczuk, D.S. Armstrong, E. Christy, J.H.D. Clark, T.P. Goringe, M.D. Hasinoff, M.A. Kovash, S. Tripathi and D.H. Wright, *Search for exotic baryons in double radiative capture on pionic hydrogen*, Phys. Lett. **B597**, 131 (2004) [nucl-ex/0403046].
- C.D. O'Leary, R. Wadsworth, P. Fallon, C.E. Svensson, K. Ragnarsson, D.E. Appelbe, R.A.E. Austin, G.C. Ball, J.A. Cameron, M.P. Carpenter, R.M. Clark, M. Cromaz, M.A. Deleplanque, R.M. Diamond, D.F. Hodgson, R.V.F. Janssens, D.G. Jenkins, N.S. Kelsall, G.J. Lane, C.J. Lister, A.O. Macchiavelli, D. Saranites, F.S. Stephens, D. Seweryniak, K. Vetter, J.C. Waddington and D. Ward, *High spin study of rotational structures in ^{72}Br* , Phys. Rev. **C69**, 034316 (2004).
- N.S. Kelsall, C.E. Svensson, S.M. Fisher, D.E. Appelbe, R.A.E. Austin, D.P. Balamuth, G.C. Ball, J.A. Cameron, M.P. Carpenter, R.M. Clark, M. Cromaz, M.A. Deleplanque, R.M. Diamond, P. Fallon, D.F. Hodgson, R.V.F. Janssens, D.G. Jenkins, G.J. Lane, C.J. Lister, A.O. Macchiavelli, C.D. O'Leary, D.G. Saranites, F.S. Stephens, D.C. Schmidt, D. Seweryniak, K. Vetter, J.C. Waddington, R. Wadsworth, D. Ward, A.N. Wilson, A.V. Afanasjev, S. Frauendorf and I. Ragnarsson, *High spin structure of $N-Z$ nuclei around the $A=72$ region*, Eur. Phys. J. **A20**, 131 (2004).
- R. Meier, M. Cröni, R. Bilger, B. van den Brandt, J. Breitschopf, H. Clement, J.R. Comfort, H. Denz, A. Erhardt, K. Föhl, E. Friedman, J. Gräter, P. Hautle, G.J. Hofman, J.A. Konter, S. Mango, J. Pätzold, M.M. Pavan, G.J. Wagner, G. von Wrochem, *Low energy analyzing powers in pion-proton elastic scattering*, Phys. Lett. **B588**, 155 (2004) [nucl-ex/0402018].
- G.D. Morris, W.A. MacFarlane, K.H. Chow, Z. Salman, D.J. Arseneau, S. Daviel, A. Hatakeyama, S.R. Kreitzman, C.D.P. Levy, R. Poutissou, R.H. Heffner, J.E. Elenewski, L.H. Greene and R.F. Kiefl, *β -detected NMR of ^8Li implanted in a thin silver film*, Phys. Rev. Lett. **93**, 157601 (2004).
- P. Camerini, E. Fragiaco, N. Grion, S. Piano, R. Rui, J. Clark, L. Felawka, E.F. Gibson, G. Hofman, E.L. Mathie, R. Meier, G. Moloney, D. Ottewell, K. Raywood, M.E. Sevior, G.R. Smith and R. Tacik, *General properties of the pion production reaction in nuclear matter*, Nucl. Phys. **A735**, 89 (2004) [nucl-ex/0401018].
- P.-N. Seo, J.D. Bowman, M. Gericke, J. Long, G.S. Mitchell, S.I. Penttila and W.S. Wilburn, *A measurement of the Flight Path 12 cold moderator brightness at LAN-SCE*, Nucl. Instrum. Methods **A517**, 285 (2004).
- S. Adler *et al.* (BNL E787 collaboration), *Further search for the decay $K^+ \rightarrow \pi^+ \nu \bar{\nu}$ in the momentum region $P < 195 \text{ MeV}/c$* , Phys. Rev. **D70**, 037102 (2004) [BNL-72163-2004-JA, hep-ex/0403034].
- V.V. Anisimovsky *et al.* (BNL E949 collaboration), *Improved measurement of the $K^+ \rightarrow \nu \bar{\nu}$ branching ratio*, Phys. Rev. Lett. **93**, 031801 (2004) [TRI-PP-04-07, BNL-72164-2004-JA, KEK-PREPRINT-2004-2, FERMILAB-PUB-04-173-E, hep-ex/0403036].
- K.A. Aniol *et al.* (HAPPEX collaboration), *Parity violating electroweak asymmetry in polarized $\bar{e}p$ scattering*, Phys. Rev. **C69**, 065501 (2004) [JLAB-PHY-04-4, nucl-ex/0402004].
- A. Airapetian *et al.* (HERMES collaboration), *Flavor decomposition of the sea quark helicity distributions in the nucleon from semi-inclusive deep-inelastic scattering*, Phys. Rev. Lett. **92**, 012005 (2004) [DESY-03-067, hep-ex/0307064].
- A. Airapetian *et al.* (HERMES collaboration), *Nuclear polarization of molecular hydrogen recombined on a non-metallic surface*, Eur. Phys. J. **D29**, 21 (2004) [DESY-03-168, physics/0408138].
- A. Airapetian *et al.* (HERMES collaboration), *Evidence for a narrow $|S| = 1$ baryon state at a mass of 1528 MeV in quasi-real photoproduction*, Phys. Lett. **B585**, 213 (2004) [DESY-03-213, HERMES-DC-56, hep-ex/0312044].
- A. Airapetian *et al.* (HERMES collaboration), *Hard exclusive electroproduction of $\pi^+ \pi^-$ pairs*, Phys. Lett. **B599**, 212 (2004) [DESY-04-097, hep-ex/0406052].
- M. Abe *et al.* (KEK-E246 collaboration), *A new limit of T -violating transverse muon polarization in the $K^+ \rightarrow \pi^0 \mu^+ \nu$ decay*, Phys. Rev. Lett. **93**, 131601 (2004) [hep-ex/0408042].
- G. Abbiendi *et al.* (OPAL collaboration), *Tests of models of color reconnection and a search for glueballs using gluon jets with a rapidity gap*, Eur. Phys. J. **C35**, 293 (2004) [CERN-EP-2003-031, hep-ex/0306021].
- G. Abbiendi *et al.* (OPAL collaboration), *Search for R -parity violating decays of scalar fermions at LEP*, Eur. Phys. J. **C33**, 149 (2004) [CERN-EP-2003-036, hep-ex/0310054].
- G. Abbiendi *et al.* (OPAL collaboration), *Search for anomalous production of dilepton events with missing transverse momentum in $e^+ e^-$ collisions at $\sqrt{s} = 183\text{--}209 \text{ GeV}$* , Eur. Phys. J. **C32**, 453 (2004) [CERN-EP-2003-040, hep-ex/0309014].

- G. Abbiendi *et al.* (OPAL collaboration), *Measurement of charged current triple gauge boson couplings using W pairs at LEP*, Eur. Phys. J. **C33**, 463 (2004) [CERN-EP-2003-042, hep-ex/0308067].
- G. Abbiendi *et al.* (OPAL collaboration), *A study of $W^+W^- \gamma$ events at LEP*, Phys. Lett. **B580**, 17 (2004) [CERN-EP-2003-043, hep-ex/0309013].
- G. Abbiendi *et al.* (OPAL collaboration), *A study of charm production in beauty decays with the OPAL detector at LEP*, Eur. Phys. J. **C35**, 149 (2004) [CERN-EP-2003-050, hep-ex/0308050].
- G. Abbiendi *et al.* (OPAL collaboration), *Tests of the standard model and constraints on new physics from measurements of fermion pair production at 189–209 GeV at LEP*, Eur. Phys. J. **C33**, 173 (2004) [CERN-EP-2003-053, hep-ex/0309053].
- G. Abbiendi *et al.* (OPAL collaboration), *Experimental studies of unbiased gluon jets from e^+e^- annihilations using the jet boost algorithm*, Phys. Rev. **C69**, 032002 (2004) [CERN-EP-2003-067, hep-ex/0310048].
- G. Abbiendi *et al.* (OPAL collaboration), *Flavor independent search for Higgs bosons decaying into hadronic final states in e^+e^- collisions at LEP*, Phys. Lett. **B597**, 11 (2004) [CERN-EP-2003-081, hep-ex/0312042].
- G. Abbiendi *et al.* (OPAL collaboration), *Measurement of the partial widths of the Z into up and down type quarks*, Phys. Lett. **B586**, 167 (2004) [CERN-EP-2003-082, hep-ex/0312043].
- G. Abbiendi *et al.* (OPAL collaboration), *W boson polarization at LEP2*, Phys. Lett. **B585**, 223 (2004) [CERN-EP-2003-088, hep-ex/0312047].
- G. Abbiendi *et al.* (OPAL collaboration), *Search for chargino and neutralino production at $\sqrt{1/2} = 192\text{--}209$ GeV at LEP*, Eur. Phys. J. **C35**, 1 (2004) [CERN-EP-2003-090, hep-ex/0401026].
- G. Abbiendi *et al.* (OPAL collaboration), *Constraints on anomalous quartic gauge boson couplings from $\nu\bar{\nu}\gamma\gamma$ and $q\bar{q}\gamma\gamma$ events at LEP2*, Phys. Rev. **D70**, 032005 (2004) [CERN-PH-EP-2004-003, hep-ex/0402021].
- G. Abbiendi *et al.* (OPAL collaboration), *Study of Bose-Einstein correlations in $e^+e^- \rightarrow W^+W^-$ events at LEP*, Eur. Phys. J. **C36**, 297 (2004) [CERN-PH-EP-2004-008, hep-ex/0403055].
- G. Abbiendi *et al.* (OPAL collaboration), *Measurement of the strange spectral function in hadronic τ decays*, Eur. Phys. J. **C35**, 437 (2004) [CERN-PH-EP-2004-010, hep-ex/0406007].
- G. Abbiendi *et al.* (OPAL collaboration), *Scaling violations of quark and gluon jet fragmentation functions in e^+e^- annihilations at $\sqrt{s} = 91.2$ GeV and 183–209 GeV*, Eur. Phys. J. **C37**, 25 (2004) [CERN-PH-EP-2004-011, hep-ex/0404026].
- G. Abbiendi *et al.* (OPAL collaboration), *Search for neutral Higgs boson in CP-conserving and CP-violating MSSM scenarios*, Eur. Phys. J. **C37**, 49 (2004) [CERN-PH-EP-2004-020, hep-ex/0406057].
- G. Abbiendi *et al.* (OPAL collaboration), *Determination of the LEP beam energy using radiative fermion-pair events*, Phys. Lett. **B604**, 31 (2004) [CERN-PH-EP-2004-042, hep-ex/0408130].
- B. Aharmim *et al.* (SNO collaboration), *Electron antineutrino search at the Sudbury Neutrino Observatory*, Phys. Rev. **D70**, 093014 (2004) [hep-ex/0407029].
- S.N. Ahmed *et al.* (SNO collaboration), *Measurement of the total active 8B solar neutrino flux at the Sudbury Neutrino Observatory with enhanced neutral current sensitivity*, Phys. Rev. Lett. **92**, 181301 (2004) [nucl-ex/0309004].
- S.N. Ahmed *et al.* (SNO collaboration), *Constraints on nucleon decay via ‘invisible’ modes from the Sudbury Neutrino Observatory*, Phys. Rev. Lett. **92**, 102004 (2004) [hep-ex/0310030].
- R.A. Scalzo *et al.* (STACEE collaboration), *High-energy gamma-ray observations of W Comae with STACEE*, Astrophys. J. **607**, 778 (2004) [astro-ph/0403114].

Instrumentation/Accelerator Physics/Computing Sciences

M. Craddock, *The rebirth of the FFAG*, CERN Courier **44**(6), 23 (2004).

S. Koscielniak and C. Johnstone, *Mechanisms for non-linear acceleration in FFAGs with fixed rf*, Nucl. Instrum. Methods **A523**, 25 (2004).

M.S. Dixit, J. Dubeau, J.-P. Martin and K. Sachs, *Position sensing from charge dispersion in micro-pattern gas detectors with a resistive anode*, Nucl. Instrum. Methods **A518**, 721 (2004) [physics/0307152].

Ch. Rauth, Ch. Geppert, R. Horn, J. Lassen, P.G. Bricault and K. Wendt, *First laser ions at an off-line mass separator of the ISAC facility at TRIUMF*, Nucl. Instrum. Methods **B215**, 268 (2004).

Ch. Geppert, P. Bricault, R. Horn, J. Lassen, Ch. Rauth and K. Wendt, *Resonance ionization laser ion source – off-line tests at TRIUMF*, Nucl. Phys. **A746**, 631c (2004).

J. Baggio, V. Ferlet-Cavrois and O. Flament, *Comparison of SER test methods for commercial SRAMs*, IEEE Trans. Nucl. Sci. **51** (2004).

J.R. Schwank, P.E. Dodd, M.R. Shaneyfelt, G.L. Hash, V. Ferlet-Cavrois, P. Paillet and J. Baggio, *Issues for single-event proton testing of ICs*, IEEE Trans. Nucl. Sci. **51** (2004).

C. Cojocaru *et al.* (ATLAS Liquid Argon EMEC/HEC collaboration), *Hadronic calibration of the ATLAS liquid argon end-cap calorimeter in the pseudorapidity region 1.6*

$\langle |\eta| \rangle < 1.8$ in beam tests, Nucl. Instrum. Methods **A531**, 481 (2004) [MPP-2004-81, physics/0407009].

D. Binosi and L. Theussl, *JaxoDraw: A graphical user interface for drawing Feynman diagrams*, Comput. Phys. Commun. **161**, 76 (2004) [FTUV-03-0902, hep-ph/0309015].

Molecular and Materials Science

K.M. Kojima, J. Yamanobe, H. Eisaki, S. Uchida, Y. Fudamoto, I.M. Gat, M.I. Larkin, A. Savici, Y.J. Uemura, P.P. Kyriakou, M.T. Rovers and G.M. Luke, *Site-dilution in quasi one-dimensional antiferromagnet $Sr_2(Cu_{1-x}Pd_x)O_3$: reduction of Néel temperature and spatial distribution of ordered moment sizes*, Phys. Rev. **B70**, 094402 (2004).

R.L. Lichti, W.A. Nussbaum and K.H. Chow, *Hyperfine spectroscopy of muonium in 4H and 6H silicon carbide*, Phys. Rev. **B70**, 165204-1 (2004).

V.G. Storchak, D.G. Eshchenko and J.H. Brewer, *Formation and dynamics of muonium centres in semiconductors – a new approach*, J. Phys. Condens. Matter **16**, 4761 (2004).

J.E. Sonier, K.F. Poon, G.M. Luke, P. Kyriakou, R.I. Miller, R. Liang, C.R. Wiebe, P. Fournier and R.L. Greene, *Field-induced antiferromagnetic order in $Pr_{2-x}Ce_xCuO_4$* , Physica **C408-10**, 783 (2004).

W. Higemoto, K. Ohishi, A. Koda, S.R. Saha, R. Kadono, K. Ishida, K. Takada, H. Sakurai, E. Takayama-Muromachi and T. Sasaki, *Possible unconventional superconductivity in $Na_xCoO_2 \cdot yH_2O$ probed by muon spin rotation and relaxation*, Phys. Rev. **B70**, 134508 (2004).

R. Kadono, W. Higemoto, A. Koda, M.I. Larkin, G.M. Luke, A.T. Savici, Y.J. Uemura, K.M. Kojima, T. Okamoto, T. Kakeshita, S. Uchida, T. Ito, K. Oka, M. Takigawa, M. Ichioka and K. Machida, *Expansion of vortex cores by strong electronic correlation in $La_{2-x}Sr_xCuO_4$ at low magnetic induction*, Phys. Rev. **B69**, 104523 (2004).

R. Kadono, K. Ohishi, A. Koda, W. Higemoto, K.M. Kojima, S. Kuroshima, M. Fujita and K. Yamada, *Strong correlation between field-induced magnetism and superconductivity in $Pr_{0.89}LaCe_{0.11}CuO_4$* , J. Phys. Soc. Jpn. **73**, 2944 (2004).

S. Kuroiwa, H. Takagiwa, M. Yamazawa, J. Akimitsu, K. Ohishi, A. Koda, W. Higemoto and R. Kadono, *Unconventional behavior of field-induced quasiparticle excitation in $Ca(Al_{0.5}Si_{0.5})_2$* , J. Phys. Soc. Jpn. **73**, 2631 (2004).

A. Koda, R. Kadono, W. Higemoto, K. Ohishi, H. Ueda, C. Urano, S. Kondo, M. Nohara and H. Takagi, *Spin fluctuation in LiV_2O_4 studied by muon spin relaxation*, Phys. Rev. **B69**, 012402 (2004).

S. Hirano, J. Sugiyama, T. Noritake and T. Tani, *Chemical pressure effect on magnetic properties in electron-doped Perovskite manganites $(Gd_{0.08}Ca_ySr_{0.92-y})MnO_3$*

$(0 \leq y < 1)$: percolation transition of ferromagnetic clusters, Phys. Rev. **B70**, 094419 (2004).

J. Sugiyama, J.H. Brewer, E.J. Ansaldo, B. Hitti, M. Mikami, Y. Mori and T. Sasaki, *Electron correlation in the two-dimensional triangle lattice of Na_xCoO_2* , Phys. Rev. **B69**, 214423 (2004).

D.E. MacLaughlin, R.H. Heffner, O.O. Bernal, K. Ishida, J.E. Sonier, G.J. Nieuwenhuys, M.B. Maple and G.R. Stewart, *Disorder, inhomogeneity and spin dynamics in f-electron non-Fermi liquid systems*, J. Phys. Condens. Matter **16**, S4479 (2004).

J.E. Sonier, *Investigations of the core structure of magnetic vortices in type-II superconductors using muon spin rotation*, J. Phys. Condens. Matter **16**, S4499 (2004).

J.E. Sonier, F.D. Callaghan, R.I. Miller, E. Boaknin, L. Taillefer, R.F. Kiefl, J.H. Brewer, K.F. Poon and J.D. Brewer, *Shrinking magnetic vortices in V_3Si due to delocalized quasiparticle core states: confirmation of the microscopic theory for interacting vortices*, Phys. Rev. Lett. **93**, 017002 (2004).

D.R. Harshman, W.J. Kossler, X. Wan, A.T. Fiory, A.J. Greer, D.R. Noakes, C.E. Stronach, E. Koster and J.D. Dow, *Nodeless pairing state in single-crystal $YBa_2Cu_3O_7$* , Phys. Rev. **B69**, 174505 (2004).

J. Sugiyama, J.H. Brewer, E.J. Ansaldo, H. Itahara, T. Tani, M. Mikami, Y. Mori, T. Sasaki, S. Hébert and A. Maignan, *Dome-shaped magnetic phase diagram of thermoelectric layered cobaltites*, Phys. Rev. Lett. **92**, 017602 (2004).

Life Sciences

S.R. Bayly, C.L. Fisher, T. Storr, M.J. Adam and C. Orvig, *Carbohydrate conjugates for molecular imaging and radiotherapy: $^{99m}Tc(I)$ and $^{186}Re(I)$ tricarbonyl complexes of $N-(2'-hydroxybenzyl)-2-amino-2-deoxy-D-glucose$* , Bioconjugate Chemistry **15**, 923 (2004).

K.R. Buckley, S. Jivan and T.J. Ruth, *Improved yields for the in situ production of $[^{11}C]CH_4$ using a niobium target chamber*, Nucl. Med. Biology **31**, 825 (2004).

A.R. Studenov, S. Jivan, M.J. Adam, T.J. Ruth and K.R. Buckley, *Studies of the mechanism of the in-loop synthesis of pharmaceuticals*, Appl. Radiat. Isot. **61**, 1195 (2004).

A. Rahmim, M. Lenox, A.J. Reader, C. Michel, Z. Burbar, T.J. Ruth and V. Sossi, *Statistical list-mode image reconstruction for the high resolution research tomograph*, Phys. Med. Biol. **49**, 4239 (2004).

A. Rahmim, P. Bloomfield, S. Houle, M. Lenox, C. Michel, K.R. Buckley, T.J. Ruth and V. Sossi, *Motion correction in histogram-mode and list-mode EM reconstruction: beyond the event-driven approach*, IEEE Trans. Nucl. Sci. **51**, 2588 (2004).

H. Zaidi and V. Sossi, *Point-counterpoint: correction for image degrading factors is essential for accurate quantification of brain function using PET*, Med. Phys. **31**, 423 (2004).

R. de la Fuente-Fernández, V. Sossi, Z. Huang, S. Furtado, J.-Q. Lu, D.B. Calne, T.J. Ruth and A.J. Stoessl, *Levodopa-induced changes in synaptic dopamine levels increase with progression of Parkinson's disease: implications for Dyskinesias*, Brain **127**, 2747 (2004).

C.S. Lee, M. Schulzer, R. de la Fuente-Fernández, E. Mak, L. Kurtamoto, V. Sossi, T.J. Ruth, D.B. Calne and A.J. Stoessl, *Lack of regional selectivity during the progression in Parkinson's disease: implications for pathogenesis*, Ann. Neurol. **61**, 1920 (2004).

V. Sossi, R. de la Fuente-Fernández, J.E. Holden, M. Schulzer, T.J. Ruth and A.J. Stoessl, *Changes of dopamine turnover in the progression of Parkinson's disease as measured by positron emission tomography: their relation to disease-compensatory mechanisms*, J. Cereb. Blood Flow & Metab. **24**, 869 (2004).

D.J. Doudet and J.E. Holden, *[¹¹C]raclopride PET studies of dopamine release by amphetamine: dependence on presynaptic integrity*, Biol. Psychiat. **54**, 1193 (2004).

D.T. Britto, T.J. Ruth, S. Lapi and H.J. Kronzucker, *Cellular and whole-plant chloride dynamics in barley: insights into chloride-nitrogen interactions and salinity responses*, Planta **218**, 615 (2004).

S.E. Unkles, R. Wang, Y. Wang, A.D.M. Glass, N. Crawford and J.R. Kinghorn, *Nitrate reductase is required for nitrate uptake into fungal but not plant cells*, J. Biol. Chem. **279**, 28182 (2004).

Theoretical Program

D. Baye and J.-M. Sparenberg, *Inverse scattering with supersymmetric quantum mechanics (Topical Review)*, J. Phys. **A37**, 10223 (2004).

P.C. de Holanda, W. Liao and A.Yu. Smirnov, *Toward precision measurements in solar neutrinos*, Nucl. Phys. **B702**, 307 (2004) [hep-ph/0404042].

P. Capel, G. Goldstein and D. Baye, *Time-dependent analysis of the breakup of ¹¹Be on ¹²C at 67 MeV/nucleon*, Phys. Rev. **C70**, 064605 (2004).

K. Tsushima and F.C. Khanna, *Λ_c^+ , Σ_c , Ξ_c and Λ_b hypernuclei in the meson-quark coupling model*, J. Phys. **G30**, 1765 (2004) [Alberta THy 07-03].

J. Ho, F.C. Khanna and B.C. Choi, *Dynamical invariant method and radiation-spin interaction to calculate magnetisation damping*, Phys. Rev. **B70**, 172402 (2004).

E.S. Santos, M. Montigny, F.C. Khanna and A.E. Santana, *Gauge covariant Lagrangian models*, J. Phys. **A37**, 9771 (2004).

G. Gour, F.C. Khanna, A. Mann and M. Revzen, *Optimisation of Bell's inequality violation for continuous variable systems*, Phys. Lett. **A324**, 415 (2004).

J. Ho, F.C. Khanna and B.C. Choi, *Radiation-spin interaction, Gilbert damping and spin torque*, Phys. Rev. Lett. **92**, 097601 (2004).

M.D. Oliviera, M.C.B. Fernandes, F.C. Khanna, A. Santana and J.D.M. Vianna, *Symplectic quantum mechanics*, Ann. Phys. **312**, 492 (2004).

G. Gour, F.C. Khanna and M. Revzen, *Self adjoint extensions of phase and time operators*, Phys. Rev. **A69**, 014101 (2004).

M. Kobayashi, F.C. Khanna, M. Revzen, A. Mann and A. Santana, *Maximal Bell's inequality violation for non-maximal entanglement*, Phys. Lett. **A323**, 190 (2004).

W.-F. Chang and J.N. Ng, *Phenomenology of a 5-D orbifold SU(3)(W) unification model*, Phys. Rev. **D69**, 056005 (2004) [hep-ph/0312199].

T. Gorringer and H.W. Fearing, *Induced pseudoscalar coupling of the proton weak interaction*, Rev. Mod. Phys. **76**, 31 (2004) [TRI-PP-02-08, nucl-th/0206039].

B. Desplanques and L. Theussl, *Form factors in the 'point form' of relativistic quantum mechanics: single and two-particle currents*, Eur. Phys. J. **A21**, 93 (2004) [LPSC-03-15, hep-ph/0307028].

L. Theussl, S. Noguera and V. Vento, *Generalized parton distributions of the pion in a Bethe-Salpeter approach*, Eur. Phys. J. **A20**, 483 (2004) [nucl-th/0211036].

G. Huey, R.H. Cyburt and B.D. Wandelt, *Precision primordial ⁴He measurement from the CMB*, Phys. Rev. **D69**, 103503 (2004) [astro-ph/0307080].

R.H. Cyburt, B.D. Fields and K.A. Olive, *Solar neutrino constraints on the BBN production of Li*, Phys. Rev. **D69**, 123519 (2004) [astro-ph/0312629].

C.Q. Geng, I.-L. Ho and T.H. Wu, *Axial-vector form factors for $K_{l2\gamma}$ and $\pi_{l2\gamma}$ at $\mathcal{O}(p^6)$ in chiral perturbation theory*, Nucl. Phys. **B684**, 281 (2004) [hep-ph/0306165].

B. Davids and S. Typel, *Reply to comment on electromagnetic dissociation of ⁸B and the astrophysical S factor for ⁷Be(p, γ)⁸B*, Phys. Rev. **C70**, 039802 (2004).

C. Barbieri and L. Lapikas, *Effects of rescattering in (ee'p) reactions within a semiclassical model*, Phys. Rev. **C70**, 054612 (2004) [TRI-PP-04-15, nucl-th/0409032].

R. Allahverdi, R. Brandenberger and A. Mazumdar, *Enhanced reheating via Bose condensates*, Phys. Rev. **D70**, 083535 (2004) [TRI-PP-04-12, hep-ph/0407230].

P.H. Beauchemin, G. Azuelos and C.P. Burgess, *Dimensionless coupling of bulk scalars at the LHC*, J. Phys. **G30**, N17 (2004) [MCGILL-04-12, ATL-COM-PHYS-2004-031, hep-ph/0407196].

- B.K. Jennings and K. Maltman, *Z* resonances: phenomenology and models*, Phys. Rev. **D69**, 094020 (2004) [YU-PP-I-E-03-KM-3, hep-ph/0308286].
- C.B. Das, S. Das Gupta and B.K. Jennings, *Grand canonical model predictions for nuclear fragmentation*, Phys. Rev. **C70**, 044611 (2004) [nucl-th/0406073].
- R.H. Cyburt, B. Davids and B.K. Jennings, *Determination of $S_{17}(0)$ from published data*, Phys. Rev. **C70**, 045801 (2004) [nucl-th/0406011].
- Y. Fujiwara, K. Miyagawa, M. Kohno, Y. Suzuki, D. Baye and J.-M. Sparenberg, *Faddeev calculations of 3α and $\alpha\alpha A$ systems using $\alpha\alpha$ resonating-group method kernel*, Phys. Rev. **C70**, 024002 (2004) [nucl-th/0404071].
- Y. Fujiwara, M. Kohno, K. Miyagawa, Y. Suzuki and J.-M. Sparenberg, *Faddeev calculation of ${}^6_{\Lambda\Lambda}\text{He}$ using SU_6 quark-model baryon-baryon interactions*, Phys. Rev. **C70**, 037001 (2004) [nucl-th/0405056].
- R. Allahverdi, *Scenarios of modulated perturbations*, Phys. Rev. **D70**, 043507 (2004) [TRI-PP-04-06, astro-ph/0403351].
- J.-M. Sparenberg, *Clarification of the relationship between bound and scattering states in quantum mechanics: application to ${}^{12}\text{C} + \alpha$* , Phys. Rev. **C69**, 034601 (2004).
- C.P. Liu, C.H. Hyun and B. Desplanques, *Parity nonconservation in the photodisintegration of the deuteron at low energy*, Phys. Rev. **C69**, 065502 (2004) [nucl-th/0403009].
- S. Ando, H.W. Fearing, V. Gudkov, K. Kubodera, F. Myhrer, S. Nakamura and T. Sato, *Neutron beta decay in effective field theory*, Phys. Lett. **B595**, 250 (2004) [TRI-PP-04-05, USC-NT-04-04, nucl-th/0402100].
- C. Barbieri, C. Giusti, G.D. Pacati and W.H. Dickhoff, *Effects of nuclear correlations on the ${}^{16}\text{O}(e, e'pN)$ reactions to discrete final states*, Phys. Rev. **C70**, 014606 (2004) [TRI-PP-04-04, nucl-th/0402081].
- W.H. Dickhoff and C. Barbieri, *Self-consistent Green's function method for nuclei and nuclear matter*, Prog. Part. Nucl. Phys. **52**, 377 (2004) [TRI-PP-03-40, nucl-th/0402034].
- F. Okiharu and R.M. Woloshyn, *An alternate smearing method for Wilson loops in lattice QCD*, Eur. Phys. J. **C35**, 537 (2004) [hep-lat/0402009].
- R. Allahverdi and M. Drees, *Leptogenesis from a sneutrino condensate revisited*, Phys. Rev. **D69**, 103522 (2004) [TRI-PP-04-01, hep-ph/0401054].
- R. Allahverdi and M. Drees, *Leptogenesis as the source of gravitino dark matter and density perturbations*, Phys. Rev. **D70**, 123522 (2004) [TRI-PP-04-14, hep-ph/0408289].
- R.H. Cyburt, *Primordial nucleosynthesis for the new cosmology: determining uncertainties and examining concordance*, Phys. Rev. **D70**, 023505 (2004) [astro-ph/0401091].
- D.H. Wilkinson, *Super-allowed Fermi beta-decay: a further visit*, Nucl. Instrum. Methods **A526**, 386 (2004) [TRI-PP-03-41].
- R. Allahverdi, C. Bird, S.G. Nibbelink and M. Pospelov, *Cosmological bounds on large extra dimensions from non-thermal production of Kaluza-Klein modes*, Phys. Rev. **D69**, 045004 (2004) [TRI-PP-03-07, UVIC-TH-05-03, hep-ph/0305010].
- N. Knecht, Z. Papandreou, G.J. Lolos, K. Benslama, G.M. Huber, S. Li, V. Bekrenev, W.J. Briscoe, D. Grosnick, D. Isenhower, D.D. Koetke, N.G. Kozlenko, S. Kruglov, D.M. Manley, R. Manweiler, S. McDonald, J. Olmsted, A. Shafi and T.D.S. Stanislaus, *Relative branching ratio of the $\eta \rightarrow \pi^0 \gamma \gamma$ decay channel*, Phys. Lett. **B589**, 14 (2004).

Journal Publications In Press or Submitted

Particle, Nuclear and Atomic Physics

- M. Agnello, G. Beer, L. Benussi, M. Bertani, S. Bianco, E. Botta, T. Bressani, L. Busso, D. Calvo, P. Camerini, P. Cerello, B. Dalena, F. De Mori, A. D'Erasmus, D. Di Santo, F.L. Fabbri, D. Faso, A. Feliciello, A. Filippi, V. Filippini, R. Fini, E.M. Fiore, H. Fujioka, P. Gianotti, N. Grión, V. Lucherini, S. Marcellò, T. Maruta, N. Mirfakhrai, O. Morra, T. Nagae, A. Olin, H. Outa, E. Pace, M. Pallotta, M. Palomba, A. Pantaleo, A. Panzarasa, V. Paticchio, S. Piano, F. Pompili, R. Rui, G. Simonetti, H. So, S. Tomassini, A. Toyoda, R. Wheadon and A. Zenoni, *Evidence for a kaon-bound state $K^- pp$ produced in K^- absorption reactions at rest* (Phys. Rev. Lett., in press).
- M. Agnello, G. Beer, L. Benussi, M. Bertani, H.C. Bhang, S. Bianco, E. Botta, T. Bressani, M. Bregant, L. Busso, D. Calvo, P. Camerini, P. Cerello, B. Dalena, F. De Mori, A. D'Erasmus, D. Di Santo, R. Dona, D. Elia, F.L. Fabbri, D. Faso, A. Feliciello, A. Filippi, V. Filippini, E.M. Fiore, H. Fujioka, P. Gianotti, N. Grión, V. Lucherini, S. Marcellò, T. Maruta, N. Mirfakhrai, O. Morra, T. Nagae, A. Olin, H. Outa, E. Pace, M. Pallotta, M. Palomba, A. Pantaleo, A. Panzarasa, V. Paticchio, S. Piano, F. Pompili, R. Rui, G. Simonetti, H. So, S. Tomassini, A. Toyoda, R. Wheadon and A. Zenoni, *First results on ${}^{\Lambda^2}\text{C}$ production at DAΦNE* (Phys. Lett. B, in press).
- T. Warner, G. Ball, J.A. Behr, T.E. Chupp, P. Finlay, G. Hackman, M.E. Hayden, B. Hyland, K. Koopmans, S.R. Nuss-Warren, M.R. Pearson, A.A. Phillips, M.A. Schumaker, M.B. Smith, C.E. Svensson and E.R. Tardiff, *Diffusion of Xe in Zr, Ta, and Pt* (submitted to Nucl. Instrum. Methods A).
- Y. Hirayama, T. Shimoda, H. Izumi, A. Hatakeyama, K.P. Jackson, C.D.P. Levy, H. Miyatake, M. Yagi and H. Yano, *Structure of ${}^{11}\text{Be}$ studied in β -delayed decays from polarized ${}^{11}\text{Li}$* (Phys. Lett. B, in press).
- W.S. Wilburn, J.D. Bowman, S.I. Penttila, M.T. Gericke, *A low-noise current-mode preamplifier for gamma asymmetry measurements* (Nucl. Instrum. Methods A, in press).

- B. Davids and C.N. Davids, *EMMA: a recoil mass spectrometer for ISAC-II at TRIUMF* (Nucl. Instrum. Methods A, in press).
- A. Mills, J.A. Behr, L.A. Courneyea and M.R. Pearson, *Lifetime of the potassium $5P_{1/2}$ state* (submitted to Phys. Rev. A).
- H.C. Scraggs, C.J. Pearson, G. Hackman, M.B. Smith, R.A.E. Austin, G.C. Ball, A.J. Boston, P. Bricault, R.S. Chakravarthy, R. Churchman, N. Cowan, G. Cronkhite, E.S. Cunningham, T.E. Drake, P. Finlay, P.E. Garrett, G.F. Grinyer, B. Hyland, B. Jones, J.R. Leslie, J.-P. Martin, D. Morris, A.C. Morton, A.A. Phillips, F. Sarazin, M.A. Schumaker, C.E. Svensson, J.J. Valiente-Dobón, J.C. Waddington, L.M. Watters and L. Zimmerman, *TIGRESS highly-segmented high-purity germanium clover detector* (Nucl. Instrum. Methods A, in press) [TRI-PP-04-23].
- C.E. Svensson, G. Hackman, C.J. Pearson, M.A. Schumaker, H. Scraggs, M.B. Smith, C. Andreoiu, A. Andreyev, R.A. Austin, G.C. Ball, A.J. Boston, R.S. Chakravarthy, R. Churchman, N. Cowan, T.E. Drake, P. Finlay, P.E. Garrett, G.F. Grinyer, B. Hyland, B. Jones, J.P. Martin, A.C. Morton, A.A. Phillips, R. Roy, F. Sarazin, N. Starinsky, J.J. Valiente-Dobon, J.C. Waddington and L.M. Watters, *Position sensitivity of the TIGRESS 32-fold segmented HPGE clover detector* (Nucl. Instrum. Methods A, in press).
- J.R. Musser, R. Bayes, Yu.I. Davydov, P. Depommier, J. Doornbos, W. Faszer, C.A. Gagliardi, A. Gaponenko, D.R. Gill, P. Green, P. Gumplinger, M.D. Hasinoff, R.S. Henderson, J. Hu, B. Jamieson, P. Kitching, D.D. Koetke, A.A. Krushinsky, Yu.Yu. Lachin, J.A. Macdonald, R.P. MacDonal, G.M. Marshall, E.L. Mathie, L.V. Miasoedov, R.E. Mischke, P.M. Nord, K. Olchanski, A. Olin, R. Openshaw, T.A. Porcelli, J.-M. Poutissou, R. Poutissou, M.A. Quraan, N.L. Rodning, V. Selivanov, G. Sheffer, B. Shin, F. Sobratee, T.D.S. Stanislaus, R. Tacik, V.D. Torokhov, R.E. Tribble, M.A. Vasiliev and D.H. Wright (TWIST collaboration), *Measurement of the Michel parameter ρ in muon decay* (Phys. Rev. Lett., in press) [TRI-PP-04-21, hep-ex/0409063].
- D. Bryman, *Further study of the decay $K^+ \rightarrow \pi\nu$* (in press) [TRI-PP-04-08].
- A. Gorelov, D. Melconian, W.P. Alford, D. Ashery, G. Ball, J.A. Behr, P.G. Bricault, J.M. D'Auria, J. Deutsch, J. Dilling, M. Dombisky, P. Dubé, J. Fingler, U. Giesen, F. Glück, S. Gu, O. Häusser, K.P. Jackson, B.K. Jennings, M.R. Pearson, T.J. Stocki, T.B. Swanson and M. Trinczek, *Scalar interaction limits from the $\beta - \nu$ correlation of trapped radioactive atoms* (Phys. Rev. Lett., in press) [TRI-PP-04-27, nucl-ex/0412032].
- M.T. Gericke, C. Blessinger, J.D. Bowman, R.C. Gillis, J. Hartfield, T. Ino, M. Leuschner, Y. Masuda, G.S. Mitchell, S. Muto, H. Nann, S.A. Page, S.I. Penttilä, W.D. Ramsay, P.-N. Seo, W.M. Snow, J. Tasson and W.S. Wilburn, *A current mode detector array for gamma-ray asymmetry measurements* (Nucl. Instrum. Methods, in press) [LA-UR-1055, nucl-ex/0411022].
- A. Gaponenko, R. Bayes, Yu.I. Davydov, P. Depommier, J. Doornbos, W. Faszer, M.C. Fujiwara, C.A. Gagliardi, D.R. Gill, P. Green, P. Gumplinger, M.D. Hasinoff, R.S. Henderson, J. Hu, B. Jamieson, P. Kitching, D.D. Koetke, A.A. Krushinsky, Yu.Yu. Lachin, J.A. Macdonald, R.P. MacDonal, G.M. Marshall, E.L. Mathie, L.V. Miasoedov, R.E. Mischke, J.R. Musser, P.M. Nord, M. Nozar, K. Olchanski, A. Olin, R. Openshaw, T.A. Porcelli, J.-M. Poutissou, R. Poutissou, M.A. Quraan, N.L. Rodning, V. Selivanov, G. Sheffer, B. Shin, F. Sobratee, T.D.S. Stanislaus, R. Tacik, V.D. Torokhov, R.E. Tribble, M.A. Vasiliev and D.H. Wright, *Measurement of the muon decay parameter δ* (Phys. Rev. D, in press) [TRI-PP-04-22, hep-ex/0410045].
- G. Azuelos, P.H. Beauchemin and C.P. Burgess, *Phenomenological constraints on extra dimensional scalars* (J. Phys. G, in press) [MCGILL-03-17].
- A. Airapetian *et al.* (HERMES collaboration), *Quark helicity distributions in the nucleon for up, down, and strange quarks from semi-inclusive deep-inelastic scattering* (Phys. Rev. D, in press) [DESY-04-107, hep-ex/0407032].
- A. Airapetian *et al.* (HERMES collaboration), *The HERMES polarized hydrogen and deuterium gas target in the HERA electron storage ring* (Nucl. Instrum. Methods A, in press) [DESY-04-128, physics/0408137].
- A. Airapetian *et al.* (HERMES collaboration), *Single-spin asymmetries in semi-inclusive deep-inelastic scattering on a transversely polarized hydrogen target* (Phys. Rev. Lett., in press) [DESY-04-141, hep-ex/0408013].
- A. Airapetian *et al.* (HERMES collaboration), *Search for an exotic $S = -2$, $Q = -2$ baryon resonance at a mass near 1862 MeV in quasi-real photoproduction* (Phys. Rev. D, in press) [DESY-04-239, hep-ex/0412027].
- E. Aliu *et al.* (K2K collaboration), *Evidence for muon neutrino oscillation in an accelerator-based experiment* (Phys. Rev. Lett., in press) [hep-ex/0411038].
- G. Abbiendi *et al.* (OPAL collaboration), *Flavor independent h^0A^0 search and two Higgs doublet model interpretation of neutral Higgs boson searches at LEP* (Eur. Phys. J. C, in press) [CERN-PH-EP-2004-039, hep-ex/0408097].
- G. Abbiendi *et al.* (OPAL collaboration), *Search for radions at LEP2* (Phys. Lett. B, in press) [CERN-PH-EP-2004-041, hep-ex/0410035].
- G. Abbiendi *et al.* (OPAL collaboration), *Measurement of event shape distributions and moments in $e^+e^- \rightarrow$ hadrons at 91-209 GeV and a determination of α_s* (Eur. Phys. J. C, in press) [CERN-PH-EP-2004-044, hep-ex/0503051].
- G. Abbiendi *et al.* (OPAL collaboration), *Measurement of R_b in e^+e^- collisions at 182-209 GeV* (Phys. Lett. B, in press) [CERN-PH-EP-2004-051, hep-ex/0410034].

Instrumentation/Accelerator Physics/Computing Sciences

J. Lassen, P. Bricault, M. Dombisky, J.P. Lavoie, Ch. Gépert, K. Wendt, *TRIUMF resonant ionization laser ion source project* (submitted to Hyp. Int.).

Yu.I. Davydov, R. Openshaw, V. Selivanov and G. Sheffer, *Gas gain on single wire chambers filled with pure isobutane at low pressure* (submitted to Elsevier) [physics/0410004].

Yu.I. Davydov, *On the first Townsend coefficient at high electric field* (submitted to Elsevier) [TRI-PP-04-09, physics/0409156].

R.S. Henderson, Yu.I. Davydov, W. Faszer, D.D. Koetke, L.V. Miasoedov, R. Openshaw, M.A. Quraan, J. Schaapman, V. Selivanov, G. Sheffer, T.D.S. Stanislaus and V. Torokhov, *Precision planar drift chambers and cradle for the TWIST muon decay spectrometer* (Nucl. Instrum. Methods, in press) [TRI-PP-04-20, hep-ex/0409066].

R. Sturrock *et al.* (ATLAS DC1 Task Force collaboration), *A step towards a computing grid for the LHC experiments: ATLAS data challenge 1* (submitted to Nucl. Instrum. Methods) [CERN-PH-EP-2004-028].

R.K. Carnegie, M.S. Dixit, J. Dubeau, D. Karlen, J.P. Martin, H. Mes and K. Sachs, *Resolution studies of cosmic ray tracks in a TPC with GEM readout* (Nucl. Instrum. Methods A, in press) [physics/0402054].

Molecular and Materials Science

J.H. Brewer, A.M. Froese, B.A. Fryer and K. Ghandi, *Relativistic shifts of bound negative muon precession frequencies* (submitted to Phys. Rev.).

A. Koda, W. Higemoto, K. Ohishi, S.R. Saha, R. Kadono, S. Yonezawa, Y. Muraoka and Z. Hiroi, *Possible anisotropic order parameter in the pyrochlore superconductor KOs_2O_6 probed by muon spin rotation* (J. Phys. Soc. Jpn., in press).

J. Sugiyama, J.H. Brewer, E.J. Ansaldo, J.A. Chakhalian, H. Nozaki, H. Hazama, Y. Ono and T. Kajitani, *Spin state transition in Ca-doped $Na_{0.7}CoO_2$ with the nominal Co valence below 3.16* (submitted to Solid State Commun.).

J. Sugiyama, D. Andreica, H. Itahara and T. Tani, *The effect of pressure on the spin density wave transition in the layered cobaltites $[Ca_2CoO_3]_{0.62}[CoO_2]$ and $[Ca_2Co_{4/3}Cu_{2/3}O_4]_{0.62}[CoO_2]$* (submitted to Solid State Commun.).

J. Sugiyama, H. Nozaki, J.H. Brewer, E.J. Ansaldo, T. Takami, H. Ikuta and U. Mizutani, *Two dimensionality in quasi one-dimensional cobalt oxides* (submitted to Phys. Rev. B).

C. Xia, J. Sugiyama, H. Itahara and T. Tani, *Platelet crystals of thermoelectric layered cobaltites; pure and Sr-doped $[Ca_2CoO_3]_{0.62}[CoO_2]$* (J. Crystal Growth, in press).

J.H. Brewer, K. Ghandi, A.M. Froese and B.A. Fryer, *Negative muon spin precession measurement of the hyperfine*

states of muonic sodium (Phys. Rev. C, in press).

D.R. Noakes, R. Wäppling, G.M. Kalvius, M.F. White Jr. and C.E. Stronach, *Singlet ground-state fluctuations in praseodymium observed by muon spin relaxation in PrP and PrP_{0.9}* (J. Phys. Condens. Matter, in press).

R.F. Kiefl, K.H. Chow, W.A. MacFarlane, C.D.P. Levy and Z. Salman, *Application of low energy spin polarized radioactive ion beams in condensed matter research* (Nucl. Phys. News, in press).

V.G. Storchak, D.G. Eshchenko, J.H. Brewer, B. Hitti, R.L. Lichti and B.A. Aronzon, *Magnetic freezeout of electrons into muonium atoms in GaAs* (Phys. Rev. B, in press).

V.G. Storchak, D.G. Eshchenko, J.H. Brewer, R.L. Lichti, B.A. Aronzon and S.P. Cottrell, *Deep muonium state in InSb: recombination center vs. trapping center* (submitted to Phys. Rev. Lett.).

Life Sciences

R. Mungur, A.D.M. Glass, D.B. Goodenow and D.A. Lightfoot, *Metabolite fingerprinting in transgenic Nicotiana tabacum altered by the Escherichia coli glutamate dehydrogenase* (J. Biomed. Biotech., in press).

V. Sossi, K.R. Buckley, P. Piccioni, A. Rahmim, M-L. Camborde, S. Lapi, E. Strome and T.J. Ruth, *Printed sources for positron emission tomography (PET)* (IEEE Trans. Nucl. Sci., in press).

E.M. Strome, S. Jivan and D.J. Doudet, *Quantitative in-vitro phosphor imaging using $[^3H]$ and $[^{18F}]$ radioligands: the effects of chronic desipramine treatment on serotonin 5-HT₂ receptors* (J. Neurosci. Methods, in press).

V. Sossi, M-L. Camborde, G. Tropini, D. Newport, A. Rahmim, D.J. Doudet and T.J. Ruth, *The influence of measurement uncertainties on the evaluation of the distribution volume ratio and binding potential in rat studies on a microPET[®] R4: a phantom study* (submitted to Phys. Med. Biol.).

Theoretical Program

E. Vogt, *Pervasive and extreme neutron halos* (resubmitted to Phys. Rev. C) [TRI-PP-01-23].

P. Capel and D. Baye, *Coupling-in-the-continuum effects in Coulomb dissociation of halo nuclei* (Phys. Rev. C, in press).

C. Barbieri and B.K. Jennings, *Nucleon-nucleus optical potential in the particle-hole approach* (submitted to Phys. Rev. C) [TRI-PP-04-26, nucl-th-0501072].

D. Wilkinson, *Super-allowed Fermi beta-decay: Vale!* (submitted to Nucl. Instrum. Methods) [TRI-PP-04-17].

K.Y. Wong and R.M. Woloshyn, *Systematics of staggered fermion spectral properties and topology* (Phys. Rev. D, in press) [hep-lat/0412001].

H. Queiroz, J.C. da Silva, F.C. Khanna, J.M.C. Malbouisson, M. Revzen and A.E. Santana, *Thermofield dynamics and Casimir effect for fermions* (Annals Phys., in press) [hep-th/0411228].

C. Barbieri, D. Rohe, I. Sick and L. Lapikas, *Effect of kinematics on final state interactions in (e, e', p) reactions* (Phys. Lett. B, in press) [TRI-PP-04-19, nucl-th/0411066].

W.-F. Chang and J.N. Ng, *Charged lepton electric dipole moments from TeV scale right-handed neutrinos* (New J. Phys., in press) [hep-ph/0411201].

J.L. Fisker, J. Gorres, M. Wiescher and B. Davids, *The importance of $^{15}O(\alpha, \gamma)^{19}Ne$ to X-ray bursts and superbursts* (submitted to Astrophys. J.) [astro-ph/0410561].

R. Allahverdi, A. Jokinen and A. Mazumdar, *Gravitino production from reheating in split supersymmetry* (Phys. Rev. D, in press) [TRI-PP-04-25, NORDITA-2004-80, hep-ph/0410169].

R.H. Cyburt, B.D. Fields, K.A. Olive and E. Skillmann, *New BBN limits on physics beyond the standard model from 4He* (Astropart. Phys., in press) [UMN-TH-2316-04, FTPI-MINN-04-28, astro-ph/0408033].

S. Ando and C.H. Hyun, *Effective field theory on the deuteron with dibaryon field* (submitted to Phys. Rev. C) [TRI-PP-04-10, nucl-th/0407103].

D.U. Matrasulov, F.C. Khanna, U.R. Salomov and A.E. Santana, *Quantum chaos in the Yang-Mills-Higgs system at finite temperature* (Eur. Phys. J., in press) [hep-ph/0306162].

Conference Publications

Particle, Nuclear and Atomic Physics

C. Maggiore, N. Agazaryan, N. Bassler, E. Blackmore, G. Beyer, J.J. DeMarco, M. Doser, C.R. Gruhn, M.H. Holzschneider, T. Ichioka, K.S. Iwamoto, H.V. Knudsen, R. Landua, W.H. McBride, S.P. Meller, J. Petersen, J.B. Smathers, L.D. Skarsgard, T.D. Solberg, U.I. Uggerhoj, H.R. Withers and B.G. Wouters, *Biological effectiveness of antiproton annihilation*, Proc. **7th Int. Conf. on Low-Energy Antiproton Physics (LEAP 03)**, Yokohama, Japan, March 3–7, 2003 (Nucl. Instrum. Methods **B214**, 2004). p.181.

D.S. Armstrong, T.D. Averett, J. Birchall, J.D. Bowman, R.D. Carlini, S. Chattopadhyay, C.A. Davis, J. Doornbos, J.A. Dunne, R. Ent, J. Erler, W.R. Falk, J.M. Finn, T.A. Forest, D.J. Gaskell, K.H. Grimm, C. Hagner, F.W. Hersman, M. Holtrop, K. Johnston, R.T. Jones, K. Joo, C. Keppel, E. Korkmaz, S. Kowalski, L. Lee, A. Lung, D. Mack, S. Majewski, G.S. Mitchell, H. Mkrtchyan, N. Morgan, A.K. Oppen, S.A. Page, S.I. Penttila, M. Pitt, M. Poelker, T. Porcelli, W.D. Ramsay, M.J. Ramsey-Musolf, J. Roche, N. Simicevic, G.R. Smith, R. Suleiman, S. Taylor, W.T.H. van Oers, S.B. Wells, W.S. Wilburn, S.A. Wood and C. Zorn

(Qweak collaboration), *Qweak: a precision measurement of the proton's weak charge*, Proc. **8th Conf. on the Intersections of Particle and Nuclear Physics (CIPANP 2003)**, New York, NY, May 19–24, 2003, ed. Z. Parsa (AIP Conf. Proc. **698**, New York, 2004) p.172 [LA-UR-03-6031, hep-ex/0308049].

C.A. Gagliardi, *TWIST: measuring the space-time structure of muon decay*, *ibid.* 234.

P. Kitching *et al.* (TWIST collaboration), *A precision measurement of μ^+ decay*, Proc. **5th Int. Workshop on Neutrino Factories and Superbeams (NuFact03)**, New York, NY, June 5–11, 2003 (AIP **721**, 2004) p.301.

W.D. Ramsay, *Selected parity violation experiments*, Proc. **Advanced Study Inst. on Symmetries and Spin (SPIN-PRAHA-2003)**, Prague, Czech Republic, July 12–19, 2003 (Czech. J. Phys. **54**, 2004), p.B207 [TRI-PP-04-02, nucl-ex/0401028].

M. Dombisky, P. Bricault and V. Hanemaayer, *Increasing beam currents at the TRIUMF-ISAC facility; techniques and experiences*, Proc. **6th Int. Conf. on Radioactive Nuclear Beams (RNB6)**, Argonne, IL, September 22–26, 2003 (Nucl. Phys. **A746**, 2004) p.32 [TRI-PP-03-35].

Y. Hirayama, T. Shimoda, H. Izumi, H. Yano, M. Yagi, A. Hatakeyama, C.D.P. Levy, K.P. Jackson and H. Miyatake, *Structure of ^{11}Be studied in β -delayed neutron and γ -decay from polarized ^{11}Li* , *ibid.* 71.

C.D.P. Levy, R. Baartman, J.A. Behr, R.F. Kiefl, M. Pearson, R. Poutissou, A. Hatakeyama and Y. Hirayama, *The collinear laser beam line at ISAC*, *ibid.* 206 [TRI-PP-03-36].

D. Hutcheon *et al.* (DRAGON collaboration), *Study of $^{21}Na(p, \gamma)^{22}Mg$ using the DRAGON separator*, *ibid.* 359 [TRI-PP-03-37].

K. Minamisono, K. Matsuta, T. Minamisono, C.D.P. Levy, T. Nagatomo, M. Ogura, T. Sumikama, J.A. Behr and K.P. Jackson, *Quadrupole moments of $^{20, 21}Na$* , *ibid.* 501.

M.B. Smith, P.M. Walker, R.S. Chakravarthy, R.A.E. Austin, G.C. Ball, J.J. Carroll, E. Cunningham, P. Finlay, P.E. Garrett, G.F. Grinyer, G. Hackman, B. Hyland, K. Koopmans, W.D. Kulp, J.R. Leslie, A.A. Phillips, R. Propri, P.H. Regan, F. Sarazin, M.A. Schumaker, H.C. Scraggs, T. Shizuma, C.E. Svensson, J. von Schwarzenberg, J.C. Waddington, D. Ward, J.L. Wood, B. Washbrook and E.F. Zganjar, *Studies of high-K isomers at TRIUMF-ISAC*, *ibid.* 617.

K. Minamisono, K. Matsuta, T. Minamisono, C.D.P. Levy, T. Nagatomo, M. Ogura, T. Sumikama, J.A. Behr, K.P. Jackson, H. Fujiwara, M. Mihara and M. Fukuda, *Alignment correlation term in the β -ray angular distribution from spin aligned ^{20}Na* , *ibid.* 673.

J. Lu *et al.* (HERMES collaboration), *Exclusive deeply inelastic electroproduction at HERMES*, Proc. **3rd Int. Symp.**

on the Gerasimov-Drell-Hearn Sum Rule and its Extensions (GDH 2004), Norfolk, VA, June 2–5, 2004 (Norfolk, 2004) p.216.

M. Agnello *et al.* (FINUDA collaboration), *First results of FINUDA on hypernuclear spectroscopy*, Proc. **Workshop on Physics at Meson Factories (DAΦNE 2004), Frascati, Italy, June 7–11, 2004** (Frascati 2004, DAPHNE 2004) p.189.

M. Agnello *et al.* (FINUDA collaboration), *First observations of hypernuclear non mesonic weak decays with FINUDA*, *ibid.* 195.

M. Agnello *et al.* (FINUDA collaboration), *Search for neutron rich hypernuclei in FINUDA: preliminary results*, *ibid.* 201.

M. Agnello *et al.* (FINUDA collaboration), *Examining sigma-bound states with FINUDA*, *ibid.* 209.

M. Agnello *et al.* (FINUDA collaboration), *Search for deeply-bound kaonic nuclei at FINUDA*, *ibid.* 225.

D.R. Gill (TWIST collaboration) *TWIST: TRIUMF weak interaction symmetry test*, *ibid.* 427.

G. Abbiendi *et al.* (OPAL collaboration), *Multi-photon events with large missing energy in e^+e^- collisions at $\sqrt{s} = 192\text{--}209$ GeV*, Proc. **2nd High-Energy Physics Conf. in Madagascar, Antananarivo, Madagascar, September 27–October 3, 2004** (eConf C0409272:012; Phys. Lett. **B602**, 2004), p.167 [CERN-PH-EP-2004-035, hep-ex/0412011].

Instrumentation/Accelerator Physics/Computing Sciences

T. Yoshioka, M. Nomachi, A. Artamanov, B. Bhuyan, J.S. Frank, T. Fujiwara, K. Higa, S.H. Kettell, T.K. Komatsubara, A. Konaka, A. Kozjevnikov, A. Kushnirenko, N. Muramatsu, T. Nakano, T. Nomura, S. Petrenko, R. Poutissou, G. Redlinger, T. Sekiguchi, T. Shinkawa, S. Sugimoto and T. Tsunemi, *Upgrade of the level-0 trigger system for BNL-E949*, Proc. **13th IEEE – NPSS Real Time Conf. (RT 2003), Montreal, PQ, May 18–23, 2003** (IEEE Trans. Nucl. Sci. **51**, 2004) p.334 [KEK-PREPRINT-2003-109, OULNS-03-02, BNL-71879-2003-JA].

D.M. Gingrich, N.J. Buchanan, S. Liu, S. Boettcher, J.A. Parsons and B.W. Sippach, *Radiation tolerant ASIC for controlling switched-capacitor arrays*, *ibid.* 1324.

R. Poutissou, P.-A. Amaudruz, A. Gaponenko, P. Green, K. Olchanski and A. Olin, *The TWIST data acquisition system at TRIUMF*, *ibid.* [TRI-PP-04-16].

J.B. Jeanneret *et al.*, *Beam loss and collimation in the LHC*, Proc. **29th ICFA Advanced Beam Dynamics Workshop (HALO'03), Montauk, NY, May 19–23, 2003** (AIP **693**, 2004) p.180.

S. Koscielniak and C.J. Johnstone, *Nonlinear acceleration modes in FFAGs with fixed rf*, Proc. **5th Int. Workshop on**

Neutrino Factories and Superbeams (NuFact03), New York, NY, June 5–11, 2003 (AIP **721**, 2004) p.467.

M.J. Barnes and G.D. Wait, *A 25 kV, 75 kHz kicker for measurement of muon lifetime*, Proc. **IEEE Int. Pulsed Power Conf., Dallas, TX, June 15–18, 2003** (IEEE Trans. Plasma Sci. **32**, 2004) p.1932 [TRI-PP-03-28].

M.J. Barnes, G.D. Wait, J. Dilling, J.V. Vaz, L. Blomeley, O. Hadary and M.J. Smith, *A high frequency MOSFET driver for the TITAN facility at TRIUMF*, *ibid.*

K. Jayamanna, D. Yuan, M. Olivo, R. Baartman, G. Dutto, M. McDonald, A. Mitra, P. Schmor and G. Stanford, *Commissioning the TRIUMF/ISAC ECR source for radioactive ion beams*, Proc. **10th Int. Conf. on Ion Sources (ICIS 2003), Dubna, Russia, September 8–13, 2003** (Rev. Sci. Instrum. **75**, 2004) p.1621 [TRI-PP-03-42].

G. Stanford, R.E. Laxdal, C. Marshall, T. Ries and I. Sekatchev, *Design of the medium-beta cryomodule for the ISAC-II superconducting heavy ion accelerator*, Proc. **2003 Cryogenic Engineering Conf. (CEC) and Int. Cryogenic Materials Conf. (ICMC), Anchorage, AL, September 22–26, 2003** (AIP, New York, Advances in Cryo. Eng. **49**, 2004) p.552 [TRI-PP-03-30].

K.S. Lee, E.M. Tikhomolov, J.E. Richards, E. Klassen and T. Tateyama, *TRIUMF secondary beam line control system upgrade using EPICS*, Proc. **IX Int. Conf. on Accelerator and Large Experimental Physics Control Systems (ICALEPCS 2003), Gyeongju, South Korea, October 13–17, 2003** (Pohang Accelerator Laboratory, 2004, ISBN:89-954175-2-8 98420 (CD-ROM)) p.199.

R. Keitel, J. Richards and E. Tikhomolov, *Upgrade of the ISAC device database from Paradox to PostgreSQL*, *ibid.* 202.

J.J. Pon, E. Klassen, K.S. Lee, M.M. Mouat and P.J. Yogendran, *Preliminary use of PDAs in TRIUMF's central control system*, *ibid.* 380.

J.J. Pon, E. Klassen, K.S. Lee, M.M. Mouat and P.J. Yogendran, *Early control system applications using PDAs at TRIUMF*, *ibid.* 383.

G. Waters and R. Nussbaumer, *TRIUMF/ISAC EPICS IOCs using a PC104 platform*, *ibid.* 466.

R. Nussbaumer and G. Waters, *Inexpensive IOCs for GPIB support in the TRIUMF/ISAC control system*, *ibid.* 515.

E. Tikhomolov, G. Waters and R. Keitel, *EPICS portable channel access server for multiple Windows applications*, *ibid.* 518.

M.J. Barnes, G.D. Wait, Y. Shirakabe and Y. Mori, *Conceptual design of a bipolar kicker magnet for the J-PARC-Kamioka neutrino project*, Proc. **18th Int. Conf. on Magnet Technology (MT18), Morioka, Japan, October 20–24, 2003** (IEEE Trans. Applied Superconductivity, 2004) p.465.

M.J. Barnes, E.W. Blackmore, G.D. Wait, J. Lemire-Elmore, B. Rablah, G. Leyh, M. Nguyen and C. Pappas, *Analysis of high power IGBT short circuit failures*, Proc. **26th Int. Power Modulator Symp. and High-Voltage Workshop, San Francisco, CA, May 23–26, 2004** (IEEE conference record, 2004) p.424.

R.W. Assmann, O. Aberle, A. Bertarelli, H.-H. Braun, M. Brugger, L. Bruno, O.S. Brüning, S. Calatroni, E. Chiaveri, B. Dehning, A. Ferrari, B. Goddard, E.B. Holzer, J.-B. Jeanneret, J.M. Jimenez, V. Kain, M. Lamont, M. Mayer, E. Mètral, R. Perret, S. Redaelli, T. Risselada, G. Robert-Demolaize, S. Roesler, F. Ruggiero, R. Schmidt, D. Schulte, P. Sievers, V. Vlachoudis, L. Vos, G. Vossenber, J. Wenninger, I.L. Ajguirei, I. Baishev, I.L. Kurochkin, D. Kaltchev and H. Tsutsui, *An improved collimation system for the LHC*, Proc. **9th European Particle Accelerator Conf. (EPAC 2004), Lucerne, Switzerland, July 5–9, 2004** (EPS Accel. Group, Geneva, 2004) p.536 [EPAC-2004-MOPLT005, CERN-LHC-PROJECT-REPORT-773].

R.W. Assmann, O. Aberle, O.S. Brüning, S. Chemli, D. Gasser, J.-B. Jeanneret, J.M. Jimenez, V. Kain, E. Mètral, G. Peon, S. Ramberger, C. Rathjen, T. Risselada, F. Ruggiero, L. Vos and D. Kaltchev, *The new layout of the LHC cleaning insertions*, *ibid.* 539 [EPAC-2004-MOPLT006, CERN-LHC-PROJECT-REPORT-774].

C. Johnstone and S.R. Koscielniak, *Optimizing non-scaling FFAG lattices for rapid acceleration*, *ibid.* 800 [EPAC-2004-MOPLT112].

M.P. Laverty, S.F. Fang and K. Fong, *TRIUMF ISAC-II rf control system design and testing*, *ibid.* 953 [EPAC-2004-TUPKF002].

A. Facco, W. Lu, F. Scarpa, E. Chiaveri, R. Losito and V. Zviagintsev, *Construction and testing of the beta=0.31, 352 MHz superconducting half-wave resonator for the SPES Project*, *ibid.* 1012 [EPAC-2004-TUPKF022].

A. Facco, W. Lu, F. Scarpa, E. Chiaveri, R. Losito, T.L. Grimm, W. Hartung, F. Marti, R.C. York and V. Zviagintsev, *Construction of a 161 MHz, beta = 0.16 superconducting QWR with steering correction for RIA*, *ibid.* 1015 [EPAC-2004-TUPKF023].

S.R. Koscielniak and M.K. Craddock, *Simple analytic formulae for the properties of non-scaling FFAG lattices*, *ibid.* 1138 [EPAC-2004-TUPLT006].

L. Ahrens, J.M. Brennan, K.A. Brown, J. Glenn, M. Sivertz, N. Tsoupas and S.R. Koscielniak, *Mini-bunched and micro-bunched slow extracted beams from the AGS*, *ibid.* 1544 [EPAC-2004-TUPLT179].

D. Kaltchev, *Building truncated Taylor maps with Mathematica and applications to FFAG*, *ibid.* 1822 [EPAC-2004-WEPLT005].

S.R. Koscielniak, *A comparison of COSY DA maps with analytic formulae for orbit functions of a non-scaling FFAG accelerator*, *ibid.* 2469 [EPAC-2004-THPLT006].

Molecular and Materials Science

J. Sugiyama, J.H. Brewer, E.J. Ansaldo, H. Itahara, K. Dohmae, Y. Seno, C. Xia and T. Tani, *Successive magnetic transitions in thermoelectric layered cobaltite, [Ca₂CoO₃]_{0.62}[CoO₂]*, Proc. **8th IUMRS Int. Conf. on Advanced Materials, Yokohama, Japan, October 8–13, 2003** (Trans. MRS-Japan **29**, 2004) p.2737.

J. Sugiyama, H. Itahara, J.H. Brewer, E.J. Ansaldo, T. Motohashi, M. Karppinen and H. Yamauchi, *Magnetism in Na_{0.75}CoO₂ detected by μ SR*, *ibid.* 2745.

J. Sugiyama, J.H. Brewer, E.J. Ansaldo, B. Hitti, M. Mikami, Y. Mori and T. Sasaki, *μ SR studies on thermoelectric cobalt oxides V: Na_xCoO₂ crystals*, Proc. **Physical Society Japan March Meeting, Fukuoka, Japan, 2004** (Meeting Abstracts Phys. Soc. Jpn. **59**(1), 2004) p.549 (in Japanese).

Life Sciences

M.J. Adam, C.L. Fisher, S.R. Bayly, C.B. Ewart, C. Orvig and S. Lapi, *Synthesis of radiometal complexes of glucose*, Proc. **51st Annual Meeting of the Society of Nuclear Medicine, Philadelphia, PA, June 19–23, 2004** (J. Nucl. Med. **45**, 2004) p.467P.

S. Lu, M.J. Adam, V. Kennedy, J. Lu and T.J. Ruth, *Preparation of iodo-TZDM for PET/SPECT imaging*, *ibid.* 467P.

A.R. Studenov, M.J. Adam, T.J. Ruth and J.S. Wilson, *Exploring new radiolabelling chemistry: synthesis of the compounds with phosphorus-fluorine-18 bonds*, *ibid.* 469P.

Theoretical Program

C. Barbieri, L. Lapikas and D. Rohe, *Rescattering contributions to final state interactions in (e, e'p) reactions*, Proc. **2nd Conf. on Nuclear and Particle Physics with CEBAF at JLab (NAPP 2003), Dubrovnik, Croatia, May 26–31, 2003** (Croatian Phys. Soc. Fizika **B13**, 2004) p.185 [TRI-PP-03-29, nucl-th/0309024].

B. Desplanques, A. Amghar and L. Theussl, *'Point-form' estimate of the pion form factor revisited*, Proc. **17th Int. IUPAP Conf. on Few-Body Problems in Physics (FB 17), Durham, NC, June 5–10, 2003**, eds. W. Gloeckle and W. Tomow (Nucl. Phys. **A737**, 2004) p.3 [hep-ph/0308219].

W.T.H. van Oers, *Symmetries and symmetry breaking*, *ibid.* 267 [TRI-PP-03-27, hep-ph/0307285].

M. de Montigny, F.C. Khanna and A. Santana, *Some Lorentz-like formulation of Galilean invariance*, Proc. **Int. Conf. on Symmetry in Non-Linear Mathematical Physics (SNMP'03), Kyiv, Ukraine, June 23–29, 2003**, eds. A.G. Nikitin *et al.* (Inst. of Mathematics of Ukraine **50**, 2004) p.677.

F. Okiharu and R.M. Woloshyn, *A study of color field distributions in the baryon*, Proc. **21st Int. Symp. on Lattice Field Theory (LATTICE 2003)**, Tsukuba, Ibaraki, Japan, July 15–19, 2003 (Elsevier, Nucl. Phys. Proc. Suppl. **129**, 2004) p.745 [hep-lat/0310007].

C. Barbieri and L. Lapikas, *Rescattering contributions to final state interactions in $(e, e'p)$ reactions at high (p_m, E_m)* , Proc. **6th Workshop on Electromagnetically Induced Two Hadron Emission**, Pavia, Italy, September 24–27, 2003, eds. A. Braghieri, C. Giusti and P. Grabmayr (CD, ISBN:88-85159-20-6, 2004) p.68 [TRI-PP-03-39, nucl-th/0401010].

J.N. Ng, *Neutrino mass models in extra dimensions*, Proc. **2nd Int. Conf. on Flavor Physics (ICFP 2003)**, Seoul, Korea, October 6–11, 2003 (J. Korean Phys. Soc. **45**, 2004) p.S341 [hep-ph/0311352].

J.-M. Sparenberg and B. Jennings, *On the practical interest of one-body overlap functions*, Proc. **Int. Symp.: A New Era of Nuclear Structure Physics**, Niigata, Japan, November 19–22, 2003, eds. Y. Suzuki *et al.* (World Scientific, Singapore, 2004) [nucl-th/0401049].

Y. Fujiwara, K. Miyagawa, M. Kohno, Y. Suzuki, D. Baye and J.-M. Sparenberg, *A realistic baryon-baryon interaction in the SU_6 quark model and its applications to few-body systems*, *ibid.*

J.-M. Sparenberg, *Deducing the asymptotic normalization constant of the 2^+ subthreshold state in ^{16}O from $^{12}C + \alpha$ elastic scattering*, Proc. **8th Int. Conf. on Clustering Aspects of Nuclear Structure and Dynamics (CLUSTER 03)**, Nara, Japan, November 24–29, 2003, eds. K. Ikeda, I. Tanihata and H. Horiuchi (Nucl. Phys. **A738**, 2004) p.416.

Y. Hirayama T. Shimoda, H. Izumi, H. Yano, M. Yagi, A. Hatakeyama, C.D.P. Levy, K.P. Jackson and H. Miyatake, *Spectroscopic study of ^{11}Be through β -delayed neutron- and γ -decays of spin-polarized ^{11}Li* , *ibid.*

Y. Fujiwara, K. Miyagawa, M. Kohno, Y. Suzuki, D. Baye and J.-M. Sparenberg, *A consistent 3α and $2\alpha A$ Faddeev calculation using the 2α RGM kernel*, *ibid.* 495.

Y. Fujiwara, K. Miyagawa, M. Kohno, Y. Suzuki, D. Baye and J.-M. Sparenberg, *$2\alpha A$ Faddeev calculation using the quark-model $S = -2$ hyperon hyperon interaction*, *ibid.*

Conference Presentations

Particle, Nuclear and Atomic Physics

A. Konaka, *The JHFNU experiment and the systematic uncertainties*, Proc. **8th Int. Workshop on Topics in Astroparticle and Underground Physics (TAUP 2003)**, Seattle, WA, September 5–9, 2003 (Nucl. Phys. B138, in press).

M. Agnello, G. Beer, L. Benussi, M. Bertani, S. Bianco, E. Botta, T. Bressani, L. Busso, D. Calvo, P. Camerini,

P. Cerello, B. Dalena, F. De Mori, A. D'Erasmus, D. Di Santo, F.L. Fabbri, D. Faso, A. Feliciello, A. Filippi, V. Filippini, E.M. Fiore, H. Fujioka, P. Gianotti, N. Grion, A. Krasnoperov, V. Lucherini, S. Marcello, T. Maruta, N. Mirfakhrai, O. Morra, A. Olin, E. Pace, M. Pallotta, M. Palomba, A. Pantaleo, A. Panzarasa, V. Patricchio, S. Piano, F. Pompili, R. Rui, G. Simonetti, H. So, S. Tomassini, R. Wheadon and A. Zenoni, *First results from the FINUDA experiment at DAΦNE*, Proc. **VIII Int. Conf. on Hypernuclear and Strange Particle Physics**, Newport News, VA, October 14–18, 2003 (Nucl. Phys. A Proc. Suppl., in press) [LNF-03/23].

S. Piano, M. Agnello, G. Beer, L. Benussi, M. Bertani, S. Bianco, E. Botta, T. Bressani, L. Busso, D. Calvo, P. Camerini, P. Cerello, B. Dalena, F. De Mori, A. D'Erasmus, D. Di Santo, F.L. Fabbri, D. Faso, A. Feliciello, A. Filippi, V. Filippini, E.M. Fiore, H. Fujioka, P. Gianotti, N. Grion, A. Krasnoperov, V. Lucherini, S. Marcello, T. Maruta, N. Mirfakhrai, O. Morra, A. Olin, E. Pace, M. Pallotta, M. Palomba, A. Pantaleo, A. Panzarasa, V. Patricchio, F. Pompili, R. Rui, G. Simonetti, H. So, S. Tomassini, R. Wheadon and A. Zenoni, *Preliminary results from the FINUDA experiment*, Proc. **XLII Int. Winter Meeting on Nuclear Physics**, Bormio, Italy, January 25–February 1, 2004.

R. MacDonald, *Validating the simulation and response function in TWIST*, Proc. **41st Western Regional Nuclear and Particle Physics Conf. (WRNPPC04)**, Lake Louise, AB, February 13–15, 2004.

A. Olin, *Precision measurement of muon decay*, *ibid.*

B. Jamieson, *Status of the TWIST measurement of $P_\mu\xi$ and systematics*, *ibid.*

R. MacDonald, *Precision measurement of the muon decay spectrum*, Proc. **Lake Louise Winter Institute (LLWI04)**, Lake Louise, AB, February 15–21, 2004 (World Scientific, Singapore, in press).

B. Jamieson, *Estimating P_μ for the TWIST measurement of $P_\mu\xi$* , *ibid.*

S.A. Page, J.D. Bowman, R.D. Carlini, T. Case, T.E. Chupp, K.P. Coulter, M. Dabaghyan, D. Desai, S.J. Freedman, T.R. Gentile, M.T. Gericke, R.C. Gillis, G.L. Greene, F.W. Hersman, T. Ino, S. Ishimoto, G.L. Jones, B. Lauss, M.B. Leuschner, B. Losowski, R. Mahurin, Y. Masuda, G.S. Mitchell, H. Nann, S.I. Penttila, W.D. Ramsay, S. Santra, P.-N. Seo, I.I. Sharapov, T.B. Smith, W.M. Snow, W.S. Wilburn, V. Yuan and H. Zhu, *Measurement of parity violation in np : the NPDGamma experiment*, Proc. **Int. Conf. on Precision Measurements with Slow Neutrons**, Gaithersburg, MD, April 5–7 2004 (NIST J. Research, in press).

M.T. Gericke, J.D. Bowman, R.D. Carlini, T.E. Chupp, K.P. Coulter, M. Dabaghyan, D. Desai, S.J. Freedman, T.R. Gentile, R.C. Gillis, G.L. Greene, F.W. Hersman, T. Ino, S. Ishimoto, G.L. Jones, B. Lauss, M.B. Leuschner, B. Losowski, R. Mahurin, Y. Masuda, G.S. Mitchell, S.

- Muto, H. Nann, S.A. Page, S.I. Penttila, W.D. Ramsay, S. Santra, P.-N. Seo, E.I. Sharapov, T.B. Smith, W.M. Snow, W.S. Wilburn, V. Yuan and H. Zhu, *Commissioning of the NPDGamma detector array: counting statistics in current mode operation and parity violation in the capture of cold neutrons on B_4C and ^{27}Al* , *ibid*.
- S.R. Nuss-Warren, E.R. Tardiff, T. Warner, G. Ball, J.A. Behr, T.E. Chupp, K.P. Coulter, G. Hackman, M.E. Hayden, M.R. Pearson, A.A. Phillips, M.B. Smith and C.E. Svensson, *On-line collection and transfer of radioactive noble gas isotopes for radon EDM measurements*, Proc. **APS April Meeting, Denver, CO, May 1–4, 2004** (Nucl. Instrum. Methods A, in press) [TRI-PP-04-03].
- S.A. Page, *The Q_{weak}^p experiment: a precision search for new physics beyond the standard model via parity violating $e-p$ scattering at low Q^2* , Proc. **From Zero to Z^0 – A Workshop on Precision Electroweak Physics, Fermilab, Batavia, IL, May 12–14, 2004**.
- D. Koetke, *The TRIUMF weak interaction symmetry test*, *ibid*.
- S. Su, *Probing new physics with neutral current measurements*, *ibid*.
- M. Bertani, M. Agnello, G. Beer, L. Benussi, S. Bianco, E. Botta, T. Bressani, L. Busso, D. Calvo, P. Camerini, P. Cerello, B. Dalena, F. De Mori, A. D’Erasmus, D. Di Santo, F.L. Fabbri, D. Faso, A. Feliciello, A. Filippi, V. Filippini, E.M. Fiore, H. Fujioka, P. Gianotti, N. Grion, A. Krasnoperov, V. Lucherini, S. Marcello, T. Maruta, N. Mirfakhrai, O. Morra, A. Olin, E. Pace, M. Pallotta, M. Palomba, A. Pantaleo, A. Panzarasa, V. Patichio, S. Pivano, F. Pompili, R. Rui, G. Simonetti, H. So, S. Tomassini, R. Wheadon and A. Zenoni, *First results on hypernuclear spectroscopy from the FINUDA experiment at DAΦNE*, Proc. **8th Int. Workshop on Meson Production, Properties and Interaction (MESON04), Kraków, Poland, June 4–8, 2004** (Int. J. Mod. Phys. A, in press).
- K.H. Grimm, *The Q_{weak}^p tracking system. Measurement of the average Q^2 and the dilution by background events*, Proc. **Int. Workshop on Parity Violation and Hadronic Structure (PAVI 2004), Grenoble, France, June 8–11, 2004**.
- G.R. Smith, *Q_{weak}^p , a precision measurement of the proton’s weak charge*, *ibid*.
- M.A. Quraan, *A high precision measurement of muon decay parameters*, Proc. **CAP Congress, Winnipeg, MB, June 13–16, 2004**.
- K. Olchanski, *Data analysis techniques for high precision measurement of muon decay parameters*, *ibid*.
- G.A. Beer *et al.* (FINUDA collaboration), *Hypernuclear physics with FINUDA*, *ibid*.
- A.K. Opper, *The Q_{weak}^p experiment: a search for new physics at the TeV scale via a measurement of the proton’s weak charge*, Proc. **Jefferson Users Group Workshop and Annual Meeting, JLab, Newport News, VA, June 16–18, 2004**.
- K. Minamisono, *Alignment correlation term of ^{20}Na and quadrupole moments of $^{20,21}Na$* , Proc. **Int. Nuclear Physics Conf. (INPC 2004), Göteborg, Sweden, June 27–July 2, 2004** (Nucl. Phys. A, in press).
- M. Agnello, G. Beer, L. Benussi, M. Bertani, S. Bianco, E. Botta, T. Bressani, L. Busso, D. Calvo, P. Camerini, P. Cerello, B. Dalena, F. De Mori, A. D’Erasmus, D. Di Santo, F.L. Fabbri, D. Faso, A. Feliciello, A. Filippi, V. Filippini, E.M. Fiore, H. Fujioka, P. Gianotti, N. Grion, A. Krasnoperov, V. Lucherini, S. Marcello, T. Maruta, N. Mirfakhrai, O. Morra, A. Olin, E. Pace, M. Pallotta, M. Palomba, A. Pantaleo, A. Panzarasa, V. Patichio, S. Pivano, F. Pompili, R. Rui, G. Simonetti, H. So, S. Tomassini, R. Wheadon and A. Zenoni, *First results from the FINUDA experiment*, *ibid*.
- J. Mildemberger *et al.* (E949 collaboration), *Latest results from the search for $K^+ \rightarrow \pi^+ \nu \bar{\nu}$* , Proc. **6th Int. Conf. on Hyperons, Charm and Beauty Hadrons (BEACH 2004), Chicago, IL, June 27–July 3, 2004** (Nucl. Phys. B, in press).
- L. Buchmann, *Comments on the $^{12}C(\alpha, \gamma)^{16}O$ reaction rate*, Proc. **8th Symp. on Nuclei in the Cosmos (NICVIII), Vancouver, BC, July 19–23, 2004** (Nucl. Phys. A, in press) [TRI-PP-04-35].
- C. Ruiz, M. Aliotta, R.E. Azuma, R.N. Boyd, L. Buchmann, A. Chen, N.M. Clarke, J.M. D’Auria, T. Davinson, B.R. Fulton, D. Groombridge, D. Hutcheon, A.M. Laird, A.S. Murphy, J. Pearson, I. Roberts, A. Robinson, F. Sarazin, A.C. Shotter, P. Walden and P.J. Woods, *Multichannel R-matrix analysis of elastic and inelastic resonances in the $^{20,21}Na+p$ compound systems*, *ibid*. [TRI-PP-04-39].
- G. Ruprecht, K. Czerski, D. Bemmerer, M. Hoefft and P. Heide, *Excitation of giant resonances in deuteron stripping reactions on ^{10}B far below the Coulomb barrier*, *ibid*. [TRI-PP-04-40].
- M. Trinczek, C.C. Jewett, J.M. D’Auria, S. Bishop, L. Buchmann, A.A. Chen, S. Engel, D. Gigliotti, U. Greife, D. Hunter, A. Hussein, D. Hutcheon, J. José, A.M. Laird, M. Lamey, R. Lewis, A. Olin, D. Ottewell, P. Parker, M.M. Pavan, J.E. Pearson, J. Rogers, C. Ruiz and C. Wrede, *Direct measurement of the $^{21}Na(p, \gamma)^{22}Mg$ reaction: resonance strengths and gamma-gamma analysis*, *ibid*. [TRI-PP-04-43].
- S.-M. Chen *et al.* (BNL E949 collaboration), *Rare kaon decay from E949 at BNL: $K^+ \rightarrow \pi^+ \nu \bar{\nu}$* , Proc. **32nd Int. Conf. on High-Energy Physics (ICHEP 04), Beijing, China, August 16–22, 2004** (World Scientific, Hackensack, NJ, in press) [hep-ex/0409064].
- W.T.H. van Oers, *The Qweak experiment*, Proc. **Hall-C Summer Physics Workshop, JLab, Newport News, VA, August 19–20, 2004**.

- A. Sher *et al.* (E865 collaboration), *E865 result: an improved upper limit on the decay $K^+ \rightarrow \pi^+\mu^+e^-$* , Proc. **Annual Meeting of the Division of Particles and Fields (DPF 04)**, Riverside, CA, August 26–31, 2004 (Int. J. Mod. Phys. A, in press).
- R. Tacik *et al.* (CHAOS collaboration), *Low energy pion-nucleon scattering*, Proc. **10th Int. Symp. on Meson-Nucleon Physics and the Structure of the Nucleon (MENU 2004)**, Beijing, China, August 29–September 4, 2004 (Int. J. Mod. Phys., in press).
- H. Fujioka *et al.* (FINUDA collaboration), *Evidence for a kaon-bound state K^-pp produced in K^- absorption reactions at rest*, Proc. **Japan Physical Society Meeting, September, 2004**.
- R.S. Chakrawarthy, P.M. Walker, M.B. Smith, A.N. Andreyev, S.F. Ashley, G.C. Ball, J.A. Becker, J.J. Daoud, P.E. Garrett, G. Hackman, G.A. Jones, Y. Litvinov, A.C. Morton, C.J. Pearson, C.E. Svensson, S.J. Williams and E.F. Zganjar, *Discovery of a new 2.3s isomer in neutron-rich ^{174}Tm* , Proc. **4th Int. Conf. on Exotic Nuclei and Atomic Masses (ENAM04)**, Pine Mountain, GA, September 12–16, 2004 (Eur. Phys. J. A, in press).
- J.A. Behr, A. Gorelov, D. Melconian, M. Trinczek, W.P. Alford, D. Ashery, P.G. Bricault, L. Courneyea, J.M. D’Auria, J. Deutsch, J. Dilling, M. Dombisky, P. Dubé, F. Glück, S. Gryb, S. Gu, O. Häusser, K.P. Jackson, B. Lee, A. Mills, E. Paradis, M.R. Pearson, R. Pitcairn, E. Prime, D. Roberge and T.B. Swanson, *Weak interaction symmetries with atom traps*, *ibid.*
- G. Sikler, J.R. Crespo López-Urrutia, J. Dilling, S. Epp, C.J. Osborne and J. Ullrich, *A high-current EBIT for charge-breeding of radionuclides for the TITAN spectrometer*, *ibid.*
- V.L. Ryjkov, L. Blomeley, M. Brodeur, P. Grothkopp, M. Smith, P. Bricault, F. Buchinger, J. Crawford, G. Gwinner, J. Lee, J. Vaz, G. Werth, J. Dilling and the TITAN collaboration, *TITAN project status report and a proposal for a new cooling method of highly charged ions*, *ibid.*
- M.T. Gericke *et al.*, *A low noise CsI detector array for the precision measurement of parity nonconservation in $\bar{n} + p \rightarrow d + \gamma$* , Proc. **Int. Conf. on Nuclear Data for Science and Technology 2004 (ND2004)**, Santa Fe, NM, September 26–October 1, 2004 (AIP, in press).
- P.N. Seo *et al.*, *The 2004 NPDGamma commissioning run – measurement of parity-violating gamma-ray asymmetries in neutron capture on Al, Cu, Cl, In, and B*, *ibid.*
- P.N. Seo *et al.*, *A new pulsed cold neutron beam for fundamental nuclear physics at LANSCE*, *ibid.*
- R.D. Carlini, *The Q_{weak}^p experiment: a search for new physics beyond the standard model and the TeV scale*, Proc. **16th Int. Spin Symp. (SPIN 2004)**, Trieste, Italy, October 10–16, 2004.
- B. Davids, *EMMA, the proposed recoil separator for ISAC-II*, Proc. **American Physical Society Fall Meeting, Chicago, IL, October 27–30, 2004**.
- Instrumentation/Accelerator Physics/Computing Sciences
- R. Poutissou (TWIST collaboration), *Using the WestGrid Glacier cluster to untangle TWIST*, Proc. **5th Annual BC-NET Advanced Networks Conf., Vancouver, BC, 2004**.
- G.C. Ball, *High resolution gamma-ray spectroscopy at TRIUMF-ISAC: the new frontier of radioactive ion beam research*, Proc. **Workshop on Production and Utilization of Radioactive Ion Beams from ISOL Type Facilities, Puri, India, February 16–19, 2004**.
- G.C. Ball, *High resolution gamma-ray spectroscopy at TRIUMF-ISAC: the new frontier of radioactive ion beam research*, Proc. **Seaborg Symp. in Honour of Don Fleming, National ACS Meeting, Anaheim, CA, March 30, 2004**.
- M.K. Craddock, *An analytic approach to FFAG optics*, Proc. **FFAG Workshop, TRIUMF, Vancouver, BC, April 15–21, 2004**.
- R.K. Carnegie, M.S. Dixit, H. Mes, E. Neuheimer, A. Rankin, K. Sachs and J.-P. Martin, *First tracking experience for MPGD TPC readout with charge dispersion on a resistive anode*, Proc. **Int. Linear Collider Workshop (LCWS 2004)**, Paris, France, April 19–23, 2004.
- D. Karlen, P. Poffenberger and G. Rosenbaum, *GEM-TPC performance in a magnetic field*, *ibid.*
- W.R. Rawnsley, Y. Bylinski, K. Fong, R.E. Laxdal, G. Dutto and D. Giove, *Alignment of the ISAC-II medium beta cryomodule with a wire monitoring system*, Proc. **20th Int. Cryogenic Engineering Conf., Beijing, China, May 11–14, 2004**.
- M.S. Dixit *et al.*, *Resolution of a MPGD readout TPC using the charge dispersion signal*, Proc. **Victoria Linear Collider Workshop (ALCPG2004)**, Victoria, BC, July 28–31, 2004.
- R.E. Laxdal, Y. Bylinskii, G.S. Clark, K. Fong, A.K. Mitra, R.L. Poirier, B. Rawnsley, T. Ries, I. Sekatchev, G. Stanford and V. Zvyagintsev, *Cold test results of the ISAC-II medium beta high gradient cryomodule*, Proc. **XXII Int. Linear Accelerator Conf. (LINAC 2004)**, Lübeck, Germany, August 16–24, 2004 (GSI, Germany, in press).
- R.L. Poirier, K. Fong, P. Harmer, R.E. Laxdal, A.K. Mitra, I. Sekatchev, B. Waraich and V. Zvyagintsev, *RF coupler design for the TRIUMF ISAC-II superconducting quarter wave resonator*, *ibid.*
- W. Rawnsley, Y. Bylinski, G. Dutto, K. Fong, R. Laxdal, T. Ries and D. Giove, *A wire position monitor system for the ISAC-II cryomodule components alignment*, *ibid.*
- P. Schmor, *Developments and future plans at ISAC/TRIUMF*, *ibid.*

K. Fong, S. Fang and M.P. Laverly, *Status of rf control system for ISAC-II superconducting cavities*, *ibid.*

R.E. Laxdal and Z.H. Peng, *High beta cavity optimization for ISAC-II*, *ibid.*

G. Stanford, Y. Bylinskii, R.E. Laxdal, B. Rawnsley, T. Ries and I. Sekatchev, *Engineering and cryogenic testing of the ISAC-II medium beta cryomodule*, *ibid.*

M. Dixit, *A review of tracking sessions*, Proc. **2nd Workshop of the ECFA Physics and Detectors for a Linear Collider**, Durham, UK, September 1–4, 2004.

M.S. Dixit *et al.*, *GEM-TPC resolution from charge dispersion*, *ibid.*

F. Ames, K. Jayamanna, D.H.L. Yuan, M. Olivo, R. Baartman, P. Bricault, M. McDonald, P. Schmor and T. Lamy, *Charge state breeding with an ECRIS for ISAC at TRIUMF*, Proc. **16th Int. Workshop on Electron Cyclotron Resonance Ion Sources (ECRIS'04)**, Berkeley, CA, September 26–30, 2004 (AIP, in press).

G.C. Ball, *High resolution gamma-ray spectroscopy at TRIUMF-ISAC: the new frontier of radioactive ion beam research*, Proc. **18th Int. Conf. on the Application of Accelerators in Research and Industry**, Fort Worth, TX, October 10–15, 2004.

M.S. Dixit *et al.*, *MPGD-TPC resolution from charge dispersion on a resistive anode*, Proc. **IEEE Nuclear Science Symp.**, Rome, October 16–24, 2004.

D.M. Gingrich *et al.* (STACEE collaboration), *The STACEE ground-based gamma-ray detector*, *ibid.* [astro-ph/0506613].

R. Baartman and S. Martin, *Summary of session H: FFAGS and cyclotrons*, Proc. **33rd ICFA Advanced Beam Dynamics Workshop: High Intensity High Brightness Hadron Beams (ICFA HB2004)**, Bensheim, Darmstadt, Germany, October 18–22, 2004 (AIP Conf. Proc., in press).

G. Dutto, *TRIUMF high intensity cyclotron development for ISAC*, Proc. **17th Int. Conf. on Cyclotrons and Their Applications**, Tokyo, Japan, October 18–22, 2004 (in press) [TRI-PP-04-28].

S. Koscielniak, *Novel constant-frequency acceleration technique for non-scaling muon FFAGs*, *ibid.* [TRI-PP-04-29].

I. Bylinski, *TRIUMF cyclotron rf system refurbishing*, *ibid.* [TRI-PP-04-30].

A. Mitra *et al.*, *Simulation of rf structure of TRIUMF cyclotron with HFSS*, *ibid.* [TRI-PP-04-31].

P. Schmor, *TRIUMF ISAC-II and beyond*, *ibid.* [TRI-PP-04-32].

M.K. Craddock, *Cyclotrons and FFAGs in 2004*, *ibid.* [TRI-PP-04-33].

Molecular and Materials Science

J.E. Sonier, *Interplay of magnetism and superconductivity in electron-doped cuprates*, Proc. **American Physical Society March Meeting**, March 20–26, 2004, Montreal, PQ.

I. McKenzie, P.W. Percival and J.A.C. Clyburne, *A computational study of the reactions of a beta-diketiminatoaluminium(I) complex with the hydrogen atom and the electron*, Proc. **American Chemical Society National Meeting**, Anaheim, CA, March 28–30, 2004 (Chem. Comm., in press).

I. McKenzie, *Organic free radicals probed by muonium*, *ibid.*

P.W. Percival, *Pressure-cooker chemistry: probing chemical reactions in high temperature water with muons*, Proc. **Canada-US Joint Workshop on Innovative Chemistry in Clean Media**, Montreal, PQ, May 20–21, 2004.

J. Sugiyama, J.H. Brewer, E.J. Ansaldo, J.A. Chakhalian, H. Nozaki, H. Hazama, R. Asahi, T. Tani, Y. Ono and T. Kajitani, *Spin state transition in Ca-doped $\text{Na}_{0.7}\text{CoO}_2$: muon spin rotation and relaxation in the layered cobaltites with the nominal Co valence below 3.16*, Proc. **Int. Conf. on Thermoelectrics**, Adelaide, Australia, July 25–29, 2004 (IEEE, Piscataway, in press).

J. Sugiyama, J.H. Brewer, E.J. Ansaldo, B. Hitti, M. Mikami, Y. Mori and T. Sasaki, *Electron correlation in the two-dimensional triangular lattice of Na_xCoO_2 with $x \geq 0.6$* , Proc. **Int. Conf. on Strongly Correlated Electron Systems**, Karlsruhe, Germany, July 26–30, 2004 (Physica B, in press).

R.F. Kiefl, K.H. Chow, S. Daviel, W. Dong, M. Hossain, T. Keeler, S.R. Kreitzman, C.D.P. Levy, W.A. MacFarlane, G.D. Morris, T. Parolin, R. Poutissou and Z. Salman, *Beta-detected NMR and NQR using low energy beams of polarized radioactive nuclei: a novel probe of thin films and interfaces*, Proc. **12th Int. Conf. on Hyperfine Interactions**, Bonn, Germany, August 23–27, 2004 (Hyp. Int., in press).

J. Sugiyama, H. Nozaki, H. Itahara, T. Tani, J.H. Brewer, E.J. Ansaldo, J.A. Chakhalian and H. Hazama, *μSR studies on thermoelectric cobalt oxides VI: muonic Knight shift*, Proc. **Physical Society Japan Autumn Meeting**, Aomori, Japan, 2004 (Meeting Abstracts Phys. Soc. Jpn., in press).

H. Nozaki, J. Sugiyama, J.H. Brewer, E.J. Ansaldo, T. Takami, H. Ikuta and H. Hazama, *μSR studies on thermoelectric cobalt oxides VII: one-dimensional system*, *ibid.*

P.W. Percival, *Hydrogen atom chemistry studied via its isotope muonium*, Proc. **5th Int. Conf. on Low Temperature Chemistry**, Berlin, September 7–10, 2004.

J. Sugiyama, D. Andreica, H. Itahara and T. Tani, *Magnetism of layered cobaltites under hydrostatic pressure as probed by $\mu^+\text{SR}$; $[\text{Ca}_2\text{CoO}_3]_{0.62}[\text{CoO}_2]$ and $[\text{Ca}_2\text{Co}_{4/3}\text{Cu}_{2/3}\text{O}_4]_{0.62}[\text{CoO}_2]$* , Proc. **1st Workshop on Anisotropic Science and Technology of Materials and**

Devices, Osaka, October 31–November 1, 2004 (TIC, Kyoto, in press).

Life Sciences

D.T. Yapp, T.J. Ruth, M.J. Adam, C.J. Koch, M.E. Gleeve and K.A. Skov, *Non-invasive evaluation of tumour hypoxia with ^{18}F -EF5 and microPET in androgen dependent murine model for prostate cancer*, Proc. **95th American Association for Cancer Research, Orlando, FL, March 26–31, 2004**.

C.L. Fisher, B.O. Patrick, M.J. Adam and C. Orvig, *Cyclopentadienyltricarbonyl rhenium (I) and technetium (I) complexes containing pendant glucose derivatives: potential radiopharmaceuticals for imaging and therapy*, Proc. **Int. Conf. Organometallic Chemistry, Vancouver, BC, July 2004**.

C. Ewart, S.R. Bayly, M.J. Adam and C. Orvig, *PADA-glucosamide-complexation of a new tridentate ligand based on glucosamine to the $[M(\text{CO})_3]^+$ core ($M = \text{Tc}, \text{Re}$)*, *ibid.*

V. Sossi, J.E. Holden, T.J. Ruth, A.J. Stoessl and D. Doudet, *Strategies to reduce scanning time in receptor imaging with positron emission tomography*, Proc. **5th Int. Conf. on Neuroreceptor Mapping, Vancouver, BC, July 15–18, 2004**.

C.L. Fisher, D.E. Green, T. Storr, S.R. Bayly, S. Lapi, M.J. Adam and C. Orvig, *Radiometal complexes with pendant glucose derivatives for molecular imaging and radiotherapy*, Proc. **228th American Chemical Society Meeting, Philadelphia, PA, August 22–26, 2004**.

M.N. Fedoruk, H. Dougan, C.M. Ludgate and C.C. Nelson, *Auger therapy for prostate cancer*, Proc. **5th Int. Symp. on Radiohalogens, Whistler, BC, September 15, 2004**.

A. Rahmim, T.J. Ruth, and V. Sossi, *Study of a convergent subsetized list-mode EM reconstruction algorithm*, Proc. **IEEE/MIC, Rome, Italy, October 16–24, 2004**.

M-L. Camborde, A. Rahmim, D.F. Newport, S. Siegel, K.R. Buckley, E. Vandervoort, T.J. Ruth and V. Sossi, *Effect of normalization method on image uniformity and distribution volume ratio estimates on microPET[®] R4*, *ibid.*

V. Sossi, M-L. Camborde, D. Newport, A. Rahmim, G. Tropini, D. Doudet and T.J. Ruth, *The influence of measurement uncertainties on the evaluation of the distribution volume ratio in rat studies on a microPET[®] R4: a phantom study*, *ibid.*

Theoretical Program

A. Czarnecki, *Theoretical summary of Moriond 2004: QCD and hadronic interactions*, Proc. **39th Rencontres de Moriond on QCD and High-Energy Hadronic Interactions, La Thuile, Italy, March 28–April 4, 2004** [TRI-PP-04-11, Alberta-thy-1604, hep-ph/0407251].

C. Barbieri and L. Lapikás, *Two-step rescattering in $(e, e'p)$ reactions*, Proc. **VIII Conf. on Electron-Nucleus Scattering, Isola d'Elba, Italy, June 21–25, 2004** (Eur. Phys. J., in press) [TRI-PP-04-18].

K.Y. Wong and R.M. Woloshyn, *Topology and staggered fermion action improvement*, Proc. **22nd Int. Symp. on Lattice Field Theory (Lattice 2004), Batavia, IL, June 21–26, 2004** (Elsevier, in press) [hep-lat/0407003].

C. Barbieri and B.K. Jennings, *Study of the $^{16}\text{O}(p, \gamma)$ reaction at astrophysical energies*, Proc. **8th Symp. on Nuclei in the Cosmos (NICVIII), Vancouver, BC, July 19–23, 2004** (Nucl. Phys. A, in press) [TRI-PP-04-34, nucl-th/0408017].

R.H. Cyburt, *What's next for big bang nucleosynthesis?*, *ibid.* [TRI-PP-04-36].

R.H. Cyburt, *Creating nuclear data representations and error budget accounting*, *ibid.* [TRI-PP-04-37].

R.H. Cyburt, *The $^7\text{Be}(p, \gamma)^8\text{B}$ reaction and its future*, *ibid.* [TRI-PP-04-38].

J.-M. Sparenberg, *Hybrid potential/R-matrix models for the $^{12}\text{C} + \alpha$ system*, *ibid.* [TRI-PP-04-41].

E. Tikhomolov, *Large-scale vortical flows and penetrative convection in the sun*, *ibid.* [TRI-PP-04-42].

Y. Fujiwara, K. Miyagawa, M. Kohno, Y. Suzuki, D. Baye and J.-M. Sparenberg, *Faddeev calculations of light Λ hypernuclei based on the SU_6 quark model baryon-baryon interactions*, Proc. **Int. Workshop on Strangeness Nuclear Physics, Osaka University, Japan, July 29–31, 2004** (World Scientific, in press).

W. Liao, *Toward precision measurements in solar neutrinos*, Proc. **32nd Int. Conf. on High-Energy Physics (ICHEP 04), Beijing, China, August 16–22, 2004** (World Scientific, Hackensack, NJ, in press).

M.C.B. Fernanades, A.E. Santana, J.D.M. Vianna and F.C. Khanna, *Unitary representations of the Poicare group in a symplectic manifold*, Proc. **XXV Brazilian National Meeting on Particles and Fields, Sao Paulo, Brazil, September, 2004**.

A.P.C. Malbouisson, H. Queiroz, J.C. de Silva, J.M.C. Malbouisson, F.C. Khanna and A.E. Santana, *Spontaneous symmetry breaking in the 3-dimensional Gross-Neveu model at finite temperature*, *ibid.*

B.R. Barrett, P. Navratil, A. Nogga, W.E. Ormand, I. Stetcu, J.P. Vary and H. Zhan, *Ab initio large-basis no-core shell model*, Proc. **Int. Conf. on Nuclear Data for Science and Technology 2004 (ND2004), Santa Fe, NM, September 26–October 1, 2004** (AIP, in press).

H.G. Miller, A.R. Plastino, A. Plastino, A.R. Ritchie and F.C. Khanna, *Pairing phase transitions in nuclear physics*, Proc. **28th Int. Workshop on Condensed Matter Theo-**

ries, Washington Univ., St. Louis, MO, September 27–October 2, 2004.

C. Barbieri and W.H. Dickhoff, *Self-consistent Green's function calculation of ^{16}O at small missing energies*, Proc. **Workshop on Nuclear Forces and Many-Body Problems, Seattle, WA, October 4–8, 2004** (J. Phys. G, in press) [TRI-PP-04-24, nucl-th/0410082].

F.C. Khanna, J.M.C. Malbouisson and A.E. Santana, *Thermofield dynamics: generalised Bogoliubov transformations and Casimir effect*, Proc. **NATO-ARW, Tashkent, Uzbekistan, October 10–16, 2004**.

A.E. Santana, A.P.C. Malbouisson, J.M.C. Malbouisson and F.C. Khanna, *Thermofield dynamics and confined systems: applications to physical systems*, *ibid.*

L. Theussl, S. Noguera and V. Vento, *Generalized parton distributions of the pion in a Bethe-Salpeter approach*, Proc. **Int. Conf. on the Structure of Baryons, Palaiseau, France, October 25–29, 2004** (Nucl. Phys. A, in press).

Technology Transfer

P.L. Gardner, A.Y. Fong and L. Graham, *From innovation to enterprise – the role of technology commercialization in sustaining economic development and growth*, Proc. **Int. Engineering Management Conf. 2004 (IEMC 2004), Singapore, October 18–21, 2004**.

A.Y. Fong and P.L. Gardner, *The role of basic research in economic development*, Proc. **4th Int. Symp. on Management of Technology (ISMOT'04), Hangzhou, China, October 24–26, 2004**.

P.L. Gardner and A.Y. Fong, *An analysis of international achievements in technology commercialization*, *ibid.*

Books

J.E. Holden and D.J. Doudet, *PET receptor assay with multiple ligand concentrations: an equilibrium approach* in Methods in Enzymology: Imaging, ed. M. Conn (Academic Press, in press).

Theses

L.A. Courneyea, *Photoionization of the $5P_{1/2}$ state of cooled and trapped potassium atoms* (B.Sc., Physics, University of British Columbia).

A. Bebington, *Investigating the $^{13}\text{C}(p, \gamma)^{14}\text{N}$ reaction and using GEANT to test the DRAGON's acceptance* (M.Sc., Physics, University of Surrey, UK).

E.S. Cunningham, *The development of SCEPTAR, the new scintillator array for the 8π spectrometer and its use in the study of the ^{32}Na decay* (M.Sc., Physics, University of Surrey, UK).

D. Gigliotti, *Efficiency calibration measurement and GEANT simulation of the DRAGON BGO gamma array at TRIUMF* (M.Sc., Physics, University of Northern British Columbia).

G.F. Grinyer, *High precision measurements of ^{26}Na β^- decay* (M.Sc., Physics, University of Guelph).

S. Kecman, *Muonium kinetics and free radical formations in solutions of fullerenes* (M.Sc., Chemistry, Simon Fraser University).

M. Lamey, *A microchannel detection system for DRAGON* (M.Sc., Physics, Simon Fraser University).

J.G. Publicover, *Energy mapping of scattered protons within a gas target* (M.Sc., Physics and Astronomy, University of Victoria).

M. Gericke, *The NPDGamma experiment – the weak interaction between nucleons and parity violation in cold neutron capture* (Ph.D., Physics, Indiana University).

H. Itahara, *Processing design, synthesis and thermoelectric properties of textured cobaltite ceramics* (Ph.D., Engineering, Nagoya University).

I. McKenzie, *Investigations of the structure and dynamics of novel muoniated radicals* (Ph.D., Chemistry, Simon Fraser University).

SEMINARS*

The following seminars were presented at TRIUMF this year.

- 08/01 *Transverse Structure of Nucleon Parton Distributions*, Dru Renner, MIT.
- 12/01 *Self Organization Phenomena in Particle Beams: How to Use Them to Build an X-Ray Laser, and How to Avoid Them to Build a Linear Collider*, Claudio Pellegrini, UCLA.
- 15/01 *Using Staggered Chiral Perturbation Theory to Calculate Pion and Kaon Properties*, Christopher Aubin, U. Washington.
- 16/01 *From Cosmology to Cosmic Rays: Nucleosynthesis Beyond the Stars*, Brian Fields, U. Illinois.
- 22/01 *Measuring Beta Decay Correlations in Laser Trapped ^{21}Na* , Nick Scielzo, ANL.
- 29/01 *Charge Symmetry Breaking in the Reaction $np \rightarrow d\pi^0$* , Dave Hutcheon, TRIUMF.
- 05/02 *Measuring the Charge Radii of $^6, ^8\text{He}$ in an Atom Trap*, Peter Mueller, ANL.
- 06/02 *Effective Interactions and Pairing in Neutron Stars*, Achim Schwenk, Ohio State U.
- 09/02 *Initial Experience with a New Scintillator; LFS*, Tom Lewellen, U. Washington.
- 11/02 *Fine Structure of Giant Resonances – A Quest for Experiments at Highest Resolution*, Achim Richter, Institut für Kernphysik, Darmstadt.
- 12/02 *Nuclear Astrophysics in Two Acts: r-Process Nucleosynthesis in Neutrino-Driven Winds and the Nuclear Symmetry Energy*, Andrew Steiner, U. Minnesota.
- 19/02 *Playing Billiards with Microwaves: Quantum Manifestations of Classical Chaos*, Achim Richter, Institut für Kernphysik, Darmstadt.
- 24/02 *Fermion Localization in Compact Extra-Dimensions*, Manuel Toharia, UC Davis.
- 11/03 *Insights into Nuclear Molecules from Studies of the Heavy Ion Radiative Capture Reaction*, David Jenkins, U. York.
- 18/03 *Adventures of a Proton Named Bob*, Richard Cyburt, TRIUMF.
- 23/03 *New Results from E949*, Joe Mildenberger, TRIUMF.
- 25/03 *Violation of Parity and Time-Reversal in Atoms: Precision Tests of the Standard Model of Elementary Particles*, Jacinda Ginges, U. Alberta.
- 26/03 *Production of High-Spin Isomers in Proton-Induced Reactions at 100–500 MeV*, Boris Zhuikov and Mikhail Mebel, INR, Moscow.
- 01/04 *The Physiological Role of Copper in Fe-Limited Marine Phytoplankton*, Maite Maldonado, UBC.
- 02/04 *Intermediate Energy Particle Nuclear Reactions: A Dynamical Statistical Approach*, Mikhail Mebel, INR, Moscow.
- 08/04 *Physics at the Energy Frontier: Results from the D0 Experiment*, Dugan O’Neil, SFU.
- 13/04 *The Status of ISOLDE*, Mats Lindroos, ISOLDE, CERN.
- 14/04 *1/2 Day Symposium on FFAGs*, Shinji Machida, KEK; Yoshitaka Kuno, U. Osaka; Carol Johnstone, Fermilab; and Shane Koscielniak, TRIUMF.
- 15/04 *Flemfest: In Celebration of Don Fleming’s Glen Seaborg Award*, Khashayer Ghandi and Andrew MacFarlane, UBC.
- 20/04 *R&D Activities on ADS and Proposal of China Spallation Neutron Source*, ShouXian Fang, IHEP, Beijing.
- 22/04 *New Potential Models for Nuclear Astrophysics Illustrated with $^7\text{Be}+p$ and $^{12}\text{C}+\alpha$* , Jean-Marc Sparenberg, TRIUMF.
- 30/04 *Furious Fuss about Five Quarks*, Andy Miller, TRIUMF.
- 06/05 *Neutron Decay and the Standard Model – The Question of the Unitarity of the Cabbibo-Kobayashi-Maskawa Matrix*, Stefan Baeßler, U. Mainz.
- 07/05 *New Lattice Calculations for V_{ub} Determination from $B \rightarrow \pi$ Semileptonic Decays*, Kerryann Foley, Cornell U.
- 13/05 *Lamb Shift in Muonic Hydrogen: Toward the Proton Charge Radius*, Françoise Mulhauser, U. Illinois at Urbana-Champaign/PSI.
- 18/05 *High Performance Computing at SLAC*, Alf Wachsmann, SLAC.
- 20/05 *Correlations in Finite Nuclei (What Does a Proton Do Inside the Nucleus?)*, Carlo Barbieri, TRIUMF.
- 26/05 *Rn and Other Radio-Chemical Backgrounds in the SNO Detector*, Richard Lange, SNO/BNL.
- 03/06 *Nuclear Structure from Cold, Trapped Atoms*, Matt Pearson, TRIUMF.
- 07/06 *Silicon Photomultiplier: Investigation and Comparison*, Vitaly Kovaltchouk, U. Regina.
- 11/06 *Heavy Flavor at RHIC and the STAR MicroVertex Detector Upgrade*, Fabrice Retiere, LBL.
- 22/06 *Multi-Channel Digital Delay/Trigger System*, Shengli Liu, U. Alberta.
- 23/06 *The ATLAS Muon Spectrometer*, Isabel Trigger, CERN.
- 24/06 *Deep Underground Science and the Possibility of a Cascades Site for DUSEL*, Wick Haxton, U. Washington.
- 25/06 *Dilepton Events at Hadron Colliders*, Reda Tafirout, U. Toronto.
- 30/06 *Electronic Eavesdropping on Nuclei – Whispers About the Charge Radii of $^8, ^9, ^{11}\text{Li}$* , Wilfried Noertershaeuser, GSI Darmstadt/U. Tübingen.

- 08/07 *Flashes in the Ashes: A New Probe of the rp -Process on Accreting Neutron Stars*, Andrew Cumming, UC Santa Cruz.
- 16/07 *New Results of K2K Experiment*, Issei Kato, Kyoto U.
- 19/07 *Measurement of the Top Quark Mass at CDF*, Igor Volobouev, LBNL.
- 20/07 *Heavy Flavor Production at HERA and Elsewhere*, Leonid Gladilin, DESY.
- 22/07 *The Optical Data Link for ATLAS Liquid Argon Calorimeter Front End Electronics Readout*, Jingbo Ye, Southern Methodist U.
- 26/07 *The CIAE Facility in Beijing and the BRIF RIB Facility*, Tianjue Zhang, CIAE.
- 26/07 *The Evolution of Elementary Particle Physics at NSF*, Marvin Goldberg, National Science Foundation.
- 27/07 *Innovative Techniques for PET Imaging – Progress and Perspectives*, Patrick Le Du, Saclay.
- 27/07 *Electromagnetic Moments with Radioactive Nuclear Beams*, Michael Hass, Weizmann Inst.
- 29/07 *“Super-Radiance” and the Width of the Θ^+ , $S=1$ Baryon*, Naftali Auerbach, Tel Aviv U.
- 03/08 *Breakup of Halo Nuclei by a Time-Dependent Method*, Pierre Capel, U. Libre Bruxelles.
- 12/08 *The ab initio Large-Basis No-Core Shell Model*, Bruce Barrett, U. Arizona.
- 16/08 *Grid Security and Data Access*, John White, Helsinki Inst. Physics @ CERN.
- 18/08 *Towards Preparing Physics Analysis at LHC*, Hans-Peter Wellisch, CERN.
- 19/08 *The University of Washington Penning Trap Mass Spectrometer; New Apparatus for Precision Measurements*, David Pinegar, U. Washington.
- 31/08 *g-Factor Measurements on Highly Charged Ions in a Penning Trap*, Guenter Werth, U. Mainz.
- 07/09 *Probing the Structure of Radioactive Ion Beams (RIBS)*, Ken Amos, U. Melbourne.
- 09/09 *High-Precision Lattice QCD Confronts Experiment*, Howard Trotter, SFU.
- 23/09 *Commissioning and Initial Operation of the Canadian Light Source*, Mark de Jong, CLS, Saskatoon.
- 30/09 *Isomers and Seniority in the Trans-Pb Nuclei*, Jo Ressler, SFU.
- 04/10 *Emergent Physics: A Condensed-Matter Primer*, Gregory Volovik, Landau Inst. Theoretical Physics, Russia.
- 07/10 *Measurement of the Michel Parameter ρ in Muon Decay*, Jim Musser, Texas A&M U.
- 14/10 *New Shell Structure in Neutron-Rich Nuclei Above Doubly-Magic ^{48}Ca* , Robert Janssens, ANL.
- 21/10 *New Measurement of Michel Parameter δ* , Andrei Gaponenko, U. Alberta.
- 26/10 *Windows on the Dark Side of the Universe*, Bernard Sadoulet, UC Berkeley.
- 01/11 *Analogue Electronics and Signal Processing for ATLAS LAr Calorimetry*, Leonid Kurchaninov, CERN.
- 04/11 *Towards Precision Mass Measurements of Radioactive Ions with a Penning Trap at IGISOL*, Juha Äystö, U. Jyväskylä.
- 08/11 *Report from Cyclotrons 2004 (Tokyo) and FFAG’04 (KEK)*, Michael Craddock, UBC/TRIUMF.
- 10/11 *Nucleosynthesis in the Beginning*, Jennifer Johnson, Herzberg Inst. Astrophysics, Victoria.
- 12/11 *Why Pentaquarks Are Seen in Some Experiments and Not in Others*, Harry Lipkin, Weizmann Inst./ANL.
- 19/11 *Experimental Study of the Pentaquark*, Takashi Nakano, RCNP, Osaka U.
- 24/11 *Beta-Detected NMR and Its Applications in Condensed Matter Physics*, Zaher Salman, TRIUMF.
- 25/11 *An Overview of the Founding and Current Activities of Bubble Technology Industries*, Harry Ing, Bubble Technology Industries.
- 02/12 *Polarized Parton Distributions Measured at the HERMES Experiment*, Jeurgen Wendland, UBC/SFU.
- 16/12 *Nucleosynthesis in Asymptotic Giant Branch Stars*, Amanda Karakas, St. Mary’s U.

The following ISAC seminars were presented at TRIUMF this year.

- 21/04 *The UK Gamma-Ray Tracking Project*, Chris Pearson, TRIUMF.
- 05/05 *Beta Decay Studies with Fast Fragment Beams*, Colin Morton, TRIUMF.
- 19/05 *Design of a Double Time-of-Flight Spectrometer for Fission Fragment Spectroscopy at FZR*, Hariprakash Sharma, U. Manitoba.
- 02/06 *Production of Radioisotopes for Diagnosis and Therapy*, Suzy Lapi, SFU.
- 11/08 *An Introduction to the TITAN Electron Beam Ion Trap (EBIT) – A Status Report*, Chris Osborne, MPI Heidelberg/TRIUMF.
- 25/08 *Superallowed Fermi Beta Decay Studies Using the 8π Spectrometer*, Martin Smith, TRIUMF.
- 08/09 *Measurement of Radiative Lifetimes, Branching Ratios, Hyperfine Structure, and Isotope Shifts in Lanthanide Ions*, David Rosner, U. Western Ontario.
- 24/09 *Solid-State Laser Ion Source Developments for High Purity Ion Beams*, Christopher Geppert, Johannes-Gutenberg U., Mainz.
- 20/10 *Accelerator Mass Spectrometry – ^{14}C Dating and Beyond*, Christof Vockenhuber, TRIUMF.
- 01/12 *Laser Cooling and Sympathetic Cooling of Ions*, Vladimir Ryjkov, TRIUMF.

The following UBC/TRIUMF joint colloquium was presented this year.

- 16/09 *Relativistic Heavy Ion Collider and Ultra-Dense Matter*, Larry McLerran, BNL.

The following technical seminars were presented this year.

- 14/01 *The Charge Breeding System at REX-ISOLDE*, Friedhelm Ames, CERN.
- 31/03 *Isotope Investigation and Production at INR*, Boris Zhuikov, INR, Moscow.
- 13/08 *WIENER VME Crates and Power Supplies for Physics*, Andreas Ruben, WIENER, Plein & Baus Electronics.
- 16/09 *ROME: A New Framework for Object-Oriented Data Analysis with ROOT and MIDAS*, Matthias Schneebeli, PSI.
- 01/10 *Participate/Collaborate: Reciprocity, Design, and Social Networks*, Access Grid Collab., Banff New Media Centre.
- 25/10 *HEPNET Canada Presentation*, Randy Sobie, U. Victoria.
- 27/10 *WestGrid Collaboration and Visualization Presentation*, Brian Corrie, SFU.

The following lunchtime seminars were presented at TRIUMF this year.

- 22/03 *RIA Workshop Summary*, Paul Schmor, John D'Auria, Lutz Moritz and Bob Laxdal, TRIUMF.
- 29/03 *Report on the SLAC ROOT Workshop and ROOT Activities at TRIUMF*, Konstantin Olchanski, TRIUMF.
- 19/04 *Design Status for a 2-Step Target at ISAC, and Predicted Yields*, Will Talbert, TechSource, Inc.
- 14/06 *Report on the CanSecWest Computer Security Conference*, Andrew Daviel, TRIUMF.
- 25/10 *CHEP04 and HEPIX, Learn All the New Buzzwords in Computing*, Renée Poutissou and Corrie Kost, TRIUMF.

* All matters concerning TRIUMF seminars should be referred via e-mail to seminar@triumf.ca

The latest listing of TRIUMF seminars can be seen at <http://admin.triumf.ca/netdata/seminars/list>

USERS GROUPS

TRIUMF USERS' GROUP

From the TRIUMF Users' Group Charter:

The TRIUMF Users' Group is an organization of scientists and engineers with special interest in the use of the TRIUMF facility. Its purpose is:

- (a) to provide a formal means for exchange of information relating to the development and use of the facility;
- (b) to advise members of the entire TRIUMF organization of projects and facilities available;
- (c) to provide an entity responsive to the representations of its members for offering advice and counsel to the TRIUMF management on operating policy and facilities.

Membership of the TRIUMF Users' Group (TUG) is open to all scientists and engineers interested in the TRIUMF program. At the end of 2004 the TUG had 316 members from 12 countries.

TRIUMF Users' Executive Committee (TUEC)

The TRIUMF Users' Executive Committee (TUEC) is a committee of elected members whose role is to represent the interests of the TUG to the TRIUMF administration.

Among other things, TUEC maintains the TUG Web site at <http://www.triumf.ca/tug/> where detailed information is available about its membership, that of related committees, and various TUG activities.

TUEC Membership for 2004

J.E. Sonier	SFU	<i>Chair</i>
J. Dilling	TRIUMF	<i>Chair Elect</i>
W.D. Ramsay	U. Manitoba	<i>Past Chair</i>
A.A. Chen	McMaster U.	2003/2004
T.A. Porcelli	U. Northern BC	2003/2004
P. Bricault	TRIUMF	2004/2005
A. Laird	U. York, UK	2004/2005
M. Comyn	TRIUMF	<i>Liaison Officer</i>

By acclamation, P. Garrett (U. Guelph) was elected as chair elect for 2005.

G. Gwinner (U. Manitoba), M. Nozar (TRIUMF) and F. Sarazin (Colorado School of Mines) were elected as members for 2005/2006.

TUEC nominates two members to represent the Users on the TRIUMF Operating Committee. In 2004 S. Yen (TRIUMF) and L. Lee (U. Manitoba) remained as the on-site member and alternate, respectively, while G.M. Luke (McMaster U.) and J.E. Sonier (SFU) remained as the off-site member and alternate, respectively.

μ SR USERS GROUP

Full details regarding the μ SR Users Group and μ SR facilities can be obtained via the WWW at <http://cmms.triumf.ca/>.

EXPERIMENT PROPOSALS

The following lists experiment proposals received up to the end of 2004 (missing numbers cover proposals that have been withdrawn or replaced by later versions, rejected, or combined with another proposal). Experiments 1–699 are omitted from this listing (except for those reporting results in this Annual Report). Please refer to the 1999 Annual Report or see <http://www.triumf.ca/annrep/experiments.html> for a full listing of these earlier experiments. Page numbers are given for those experiments which are included in this Annual Report.

Page

614. TWIST - precise measurement of the ρ , δ and $(\mathcal{P}_\mu\xi)$ parameters in muon decay [active], R. Bayes, Y. Davydov, J. Doornbos, W. Faszler, M.C. Fujiwara, D.R. Gill, P. Gumplinger, R. Henderson, J. Hu, J.A. Macdonald*, G. Marshall, R. Mischke, M. Nozar, K. Olchanski, A. Olin, R. Openshaw, T.A. Porcelli, J.-M. Poutissou, R. Poutissou, G. Sheffer, W. Shin (*TRIUMF*), A. Gaponenko, P. Kitching, R.P. MacDonald, M. Quraan, N. Rodning*, J. Schaapman, G.M. Stinson (*U. Alberta*), M. Hasinoff, B. Jamieson (*UBC*), P. Depommier (*U. Montréal*), E.L. Mathie, R. Tacik (*U. Regina*), V. Selivanov, V. Torokhov (*Kurchatov Inst.*) C.A. Gagliardi, J.R. Musser, R.E. Tribble, M.A. Vasiliev (*Texas A&M U.*), D.D. Koetke, P. Nord, T.D.S. Stanislaus (*Valparaiso U.*)
700. Measuring cross sections of long-lived radionuclides produced by 200-500 MeV protons in elements found in meteorites and lunar rocks [completed], J. Vincent (*TRIUMF*), J.M. Sisterson (*Harvard U.*), K. Kim (*San Jose State U.*), A.J.T. Jull (*U. Arizona*), M.W. Caffee (*Lawrence Livermore Nat. Lab*), R.C. Reedy (*Los Alamos Nat. Lab*)
702. Measurement of kaon-nucleon elastic scattering at 16 MeV [active], G.A. Beer, P. Knowles, G.R. Mason, A. Olin, L.P. Robertson (*U. Victoria*), P. Amaudruz, D.R. Gill, G. Smith, S. Yen (*TRIUMF*), L. Lee (*U. Manitoba*), G. Tagliente (*UBC*)
703. Study of the decay $\pi^+ \rightarrow e^+\nu$ phase I – lifetime measurement of the pion [completed], D.A. Bryman, T. Numao, A. Olin (*TRIUMF*)
704. Charge symmetry breaking in $np \rightarrow d\pi^0$ close to threshold [completed], R. Abegg*, P.W. Green, D.A. Hutcheon (*TRIUMF-U. Alberta*), L.G. Greeniaus (*U. Alberta-TRIUMF*), R.W. Finlay, A.K. Opper, S.D. Reitzner (*Ohio U.*), E. Korkmaz, T.A. Porcelli (*UNBC*), J.A. Niskanen (*U. Helsinki*), P. Walden (*TRIUMF-UBC*), S. Yen (*TRIUMF*), C.A. Davis (*TRIUMF-U. Manitoba*), D.V. Jordan (*Ohio U.-U. Alberta*), E. Auld (*UBC*)
705. Development of modular gas microstrip chambers as in-target tracking devices for an experiment to detect $\Lambda\Lambda$ hypernuclei at the BNL AGS (BNL885) [completed data-taking], C.A. Davis (*TRIUMF-U. Manitoba*), B. Bassalleck, R. Stotzer (*U. New Mexico*), A.R. Berdoz, A. Biglan, D.S. Carman, G.B. Franklin, P. Khaustov, P. Koran, R. Magahiz, R. McCrady, C.A. Meyer, K. Paschke, B. Quinn, R.A. Schumacher, (*Carnegie-Mellon U.*), J. Birchall, L. Gan, M.R. Landry, L. Lee, S.A. Page, W.D. Ramsay, W.T.H. van Oers (*U. Manitoba*), T. Bürger, H. Fischer, J. Franz, H. Schmitt (*U. Freiburg*), D.E. Alburger, R.E. Chrien, M. May, P.H. Pile, A. Rusek, R. Sawafta, R. Sutter (*Brookhaven Nat. Lab*), A. Ichikawa, K. Imai, Y. Kondo, K. Yamamoto, M. Yosoi (*Kyoto U.*), F. Takeuchi (*Kyoto Sangyo U.*), V.J. Zeps (*U. Kentucky*), P.D. Barnes, F. Merrill (*Los Alamos Nat. Lab*), V.J. Zeps (*U. Kentucky*), T. Iijima (*KEK*), J. Lowe (*U. Birmingham*)
706. μ SR studies of spin fluctuations in CePt₂Sn₂ and other Kondo spin systems [completed], A. Keren, K. Kojima, G.M. Luke, Y.J. Uemura, W.D. Wu (*Columbia U.*), K. Andres, G.M. Kalvius (*Tech. U. Munich*), H. Fujii, G. Nakamoto, T. Takabatake, H. Tanaka (*Hiroshima U.*), M. Ishikawa (*ISSP U. Tokyo*), B. Andraka (*U. Florida*), D.L. Cox (*Ohio State U.*)
707. μ SR measurements on two-dimensional site-diluted antiferromagnets [active], K. Kojima (*Columbia U.-U. Tokyo*), A. Keren, G.M. Luke, Y.J. Uemura, W.D. Wu (*Columbia U.*), H. Ikeda (*KEK-KENS*), R.J. Birgeneau (*MIT*), K. Nagamine (*U. Tokyo*)
708. The spin relaxation and chemical reactivity of muonium-substituted organic radicals in the gas phase [completed], D.G. Fleming, J.J. Pan, M. Shelley (*UBC*), D.J. Arseneau (*TRIUMF-UBC*), M. Senba (*TRIUMF*), J.C. Brodovitch, P.W. Percival (*SFU*), H. Dilger, E. Roduner (*U. Zürich*), S.F.J. Cox (*Rutherford Appleton Lab*)
709. $^{90,92,94,96}\text{Zr}(n,p)^{90,92,94,96}\text{Y}$ reaction at 200 MeV [completed data-taking], A.G. Ling, P.L. Walden (*TRIUMF*), J. Rapaport (*Ohio U.*), D.A. Cooper, D.L. Prout, E.R. Sugarbaker (*Ohio State U.*), M. Halbert (*Oak Ridge Nat. Lab*), D. Mercer (*U. Colorado*), J. Campbell (*U. Manitoba-TRIUMF*), M. Hartig (*U. Muenster*)
710. Dynamics of muonium in Ge and GaAs [completed], R.L. Lichti (*Texas Tech. U.*), S.F.J. Cox (*Rutherford Appleton Lab*), R.F. Kiefl (*UBC*), K.H. Chow (*Lehigh U.*), T.L. Estle (*Rice U.*), B. Hitti (*TRIUMF*), E.A. Davis (*Leicester U.*), C.R. Schwab (*CNRS, Strasbourg*)

5

712. μ SR study of superconducting spin glasses [completed], V. McMullen, D.R. Noakes, C.E. Stronach (*Virginia State U.*), E.J. Ansaldò (*U. Saskatchewan*), J.H. Brewer (*UBC*), G. Cao, J.E. Crow (*NHMFL*), S. McCall (*Florida State U.–NHMFL*)
713. Muonium chemistry in supercritical water [completed], B. Addison-Jones, J.-C. Brodovitch, K. Ghandi, I. McKenzie, P. Percival (*SFU*), J. Schüth (*U. Bonn*)
714. Atomic PNC in francium: preparations [inactive], J.A. Behr, L. Buchmann, M. Domsbky, P. Jackson, C.D.P. Levy (*TRIUMF*), J.M. D’Auria, P. Dubé, A. Gorelov, D. Melconian, T. Swanson, M. Trinczek (*SFU*), O. Häusser* (*SFU–TRIUMF*), U. Giesen (*U. Alberta*), I. Kelson, A.I. Yavin (*Tel Aviv U.*), J. Deutsch (*U. Catholique de Louvain*), J. Dilling (*SFU–Heidelberg*)
715. Weak interaction symmetries in β^+ decay of optically trapped $^{37,38\text{m}}\text{K}$ [active], J.M. D’Auria, A. Gorelov, D. Melconian, M. Trinczek (*SFU*), J.A. Behr, P. Bricault, M. Domsbky, K.P. Jackson, B.K. Jennings (*TRIUMF*), S. Gu, M. Pearson (*UBC*), U. Giesen (*U. Notre Dame*), W.P. Alford (*U. Western Ontario*), J. Deutsch (*U. Catholique de Louvain*), D.A. Ashery, O. Aviv (*Tel Aviv U.*), F. Glück (*U. Mainz*)
716. Complete beta-delayed particle emission study of ^{31}Ar [deferred], J. Cerny, D.M. Moltz, T. Ognibene, M.W. Rowe, R.J. Tighe (*Lawrence Berkeley Lab*), L. Buchmann (*TRIUMF*), J. D’Auria (*SFU*), M. Domsbky (*SFU–U. Alberta*), G. Roy (*U. Alberta*)
717. Muon hyperfine transition rates in light nuclei [completed], J.H. Brewer, E. Gete, M.C. Fujiwara, J. Lange, D.F. Measday, B.A. Moftah, M.A. Saliba, T. Stocki (*UBC*), T.P. Gorringer (*U. Kentucky*)
718. Superconductivity and magnetism in quaternary boron carbides [completed], A. Keren, G.M. Luke, Y.J. Uemura, W.D. Wu (*Columbia U.*), K. Kojima (*Columbia U.–U. Tokyo*), S. Uchida (*U. Tokyo*)
719. $^4\text{He}(\pi^+, \pi^- pp)$ invariant mass measurement with CHAOS [completed data-taking], P. Amaudruz, L. Felawka, D. Ottewell, G. Smith (*TRIUMF*), E.T. Mathie, R. Tacik, D.M. Yeomans (*U. Regina*), H. Clement, J. Gräter, R. Meier, G.J. Wagner (*U. Tübingen*), J. Clark, M. Seviar (*U. Melbourne*), A. Ambardar, G.J. Hofman, M. Kermani, G. Tagliente (*UBC*), F. Bonutti, P. Camerini, N. Grion, R. Rui (*U. di Trieste*), J. Brack, R. Ristinen (*U. Colorado*), E. Gibson (*California State U., Sacramento*), M. Schepkin (*ITEP Moscow*)
720. Muonium’s nucleophilicity [active], G.B. Porter, D.C. Walker (*UBC*), J.M. Stadlbauer* (*Hood Coll.*), K. Venkateswaran (*Hindustan Lever Ltd.*), M.V. Barnabas (*Proctor & Gamble Ltd.*)
721. The delta nucleon reaction in CHAOS [completed data-taking], F. Farzanpay, P. Hong, E.L. Mathie, N. Mobed (*U. Regina*), R. Tacik (*TRIUMF–U. Regina*), P.A. Amaudruz, L. Felawka, R. Meier, D. Ottewell, G.R. Smith (*TRIUMF*), N. Grion (*INFN, Trieste*), P. Camerini, R. Rui (*U. di Trieste*), E. Gibson (*California State U., Sacramento*), G. Hofman, G. Jones, M. Kermani (*UBC*), M.E. Seviar (*U. Melbourne*), J.T. Brack, R.A. Ristinen (*U. Colorado*)
722. Pion initial state interactions in the $^{12}\text{C}(\pi^+, ppp)$ reaction [completed data-taking], T. Mathie, R. Tacik (*U. Regina*), P.A. Amaudruz, L. Felawka, D. Ottewell, K. Raywood, G.R. Smith (*TRIUMF*) M. Kermani, S. McFarland (*UBC*), F. Bonutti, P. Camerini, R. Rui (*U. di Trieste*), N. Grion (*INFN, Trieste*), E.F. Gibson (*California State U., Sacramento*), M. Seviar (*U. Melbourne*), J. Brack, G. Hofman (*U. Colorado*), R. Meier (*U. Tübingen*)
723. Study of pion-nucleus double-scattering reactions [completed data-taking], R. Tacik (*TRIUMF–U. Regina*), T. Mathie (*U. Regina*), P. Amaudruz, L. Felawka, D. Ottewell, K. Raywood, G. Smith (*TRIUMF*), M. Kermani, S. McFarland (*UBC*), F. Bonutti, P. Camerini, R. Rui (*U. di Trieste*), N. Grion (*INFN, Trieste*), J. Brack, G. Hofman (*U. Colorado*), R. Meier (*U. Tübingen*), M. Seviar (*U. Melbourne*), E. Gibson (*California State U. Sacramento*)
724. μ SR measurements on spin ladder systems [completed], A. Keren, G.M. Luke, Y.J. Uemura, W.D. Wu (*Columbia U.*), K. Kojima (*Columbia U.–U. Tokyo*), M. Takano (*Kyoto U.*), K. Nagamine (*U. Tokyo*)
725. Pion double charge exchange reactions on $^{3,4}\text{He}$ in the energy range 50–100 MeV [completed], P. Amaudruz, L. Felawka, R. Meier, D. Ottewell, G. Smith (*TRIUMF*), T. Mathie, R. Tacik, M. Yeomans (*U. Regina*), J. Graeter, G. Wagner (*U. Tübingen*), J. Clark, M. Seviar (*U. Melbourne*), G. Hofman, M. Kermani, P. Tagliente (*UBC*), F. Bonutti, P. Camerini, N. Grion, R. Rui (*U. di Trieste*), J. Brack, R. Ristinen (*U. Colorado*), E. Gibson (*California State U., Sacramento*), O. Patarakin (*Kurchatov Inst.*), E. Friedman (*Hebrew U. Jerusalem*)
726. Beta-delayed proton and γ -decay of ^{65}Se , ^{69}Kr and ^{73}Sr [active], D. Anthony, J. D’Auria, M. Trinczek (*SFU*), R.E. Azuma, J.D. King (*U. Toronto*), L. Buchmann, K.P. Jackson, J. Vincent (*TRIUMF*), M. Domsbky (*SFU–U. Alberta*), U. Giesen (*TRIUMF–U. Alberta*), J. Görres, H. Schatz, M. Wiescher (*U. Notre Dame*), C. Iliadis (*TRIUMF–U. Toronto*), G. Roy (*U. Alberta*)

728. Search for population and de-excitation of low-spin superdeformed states in Po-Hg region via β^+ and α decays [completed data-taking], Y.A. Akovali, M. Brinkman (*Oak Ridge Nat. Lab*), J.M. D’Auria (*TRIUMF-SFU*), J.A. Becker, E.A. Henry (*Lawrence Livermore Nat. Lab*), M. Dombisky (*SFU*), P.F. Mantica (*UNISOR*), W. Nazarewicz (*Joint Inst. for Heavy Ion*), J. Rikovska, N.J. Stone (*Oxford U.*), M.A. Stoyer (*Lawrence Berkeley Nat. Lab*), R.A. Wyss (*MSI, Sweden*)
729. Gamow-Teller and spin-dipole strengths from $^{17,18}\text{O}(n, p)$ [completed data-taking], D.P. Beatty, H.T. Fortune, P.P. Hui, R.B. Ivie, Z.Q. Mao, M.G. McKinzie, D.A. Smith (*U. Pennsylvania*), W.P. Alford (*U. Western Ontario*), K.P. Jackson, A.G. Ling, C.A. Miller, P. Walden, S. Yen (*TRIUMF*)
730. The solar neutrino problem and a new measurement of $^7\text{Be}(p, \gamma)^8\text{B}$ [deferred], R.E. Azuma, J.D. King (*U. Toronto*), P. Bricault, L. Buchmann, T. Ruth, H. Schneider, J. Vincent, S. Zeisler (*TRIUMF*), J. D’Auria, R. Korteling (*SFU*), M. Dombisky (*SFU-U. Alberta*), U. Giesen (*TRIUMF-U. Alberta*), C. Iliadis (*TRIUMF-U. Toronto*), G. Roy (*U. Alberta*), M. Wiescher (*U. Notre Dame*)
731. Investigation of spin-polarized muonium in metallic semiconductors [completed], K.H. Chow, S. Dunsiger, R.F. Kiefl, W.A. MacFarlane, J. Sonier (*UBC*), S.F.J. Cox (*Rutherford Appleton Lab*), E.A. Davis, A. Singh (*Leicester U.*), T.L. Estle, B. Hitti (*Rice U.*), R.L. Lichti (*Texas Tech. U.*), P. Mendels (*Orsay U.*), C. Schwab (*CRN, Strasbourg*)
732. Quantum impurities in one dimensional spin 1/2 chains [completed], I. Affleck, J.H. Brewer, K. Chow, S. Dunsiger, S. Eggert, R.F. Kiefl, A. MacFarlane, J. Sonier (*UBC*), A. Keren, Y.J. Uemura (*Columbia U.*)
733. Probing high T_c superconductor with “paramagnetic” ($\mu^- \text{O}$) system [active], H. Kojima, I. Tanaka, E. Torikai (*Yamanashi U.*), K. Nishiyama (*U. Tokyo*), K. Nagamine (*U. Tokyo-RIKEN*), I. Watanabe (*RIKEN*), T.P. Das (*State U. New York*), S. Maekawa (*Nagoya U.*)
734. Radiative muon capture on nickel isotopes [completed], D.S. Armstrong, P. McKenzie (*Coll. of William & Mary*), G. Azuelos, P. Depommier (*U. de Montréal*), P. Bergbusch, P. Gumplinger, M. Hasinoff, E. Saettler (*UBC*), B. Doyle, T.P. Gorringer, R. Sedlar (*U. Kentucky*), M. Blecher, C. Sigler (*Virginia Polytechnic Inst.*), J.A. MacDonald, J.-M. Poutissou, R. Poutissou, D. Wright (*TRIUMF*)
735. Studies of single layer cuprate superconductors [completed], G.M. Luke, B. Nachumi, Y.J. Uemura (*Columbia U.*), K. Kojima (*Columbia U.-U. Tokyo*), S. Uchida (*U. Tokyo*), R.H. Heffner, L.P. Le (*Los Alamos Nat. Lab*), R. MacLaughlin (*U. California, Riverside*), M.B. Maple (*U. California, San Diego*)
736. Tests of electro-weak theory using ^{14}O beam [deferred], M. Bahtacharya, A. Garcia, R. Rutchi, M. Wayne (*U. Notre Dame*), L. Buchmann (*TRIUMF*), C. Iliadis (*TRIUMF-U. Toronto*), B. Fujikawa (*Lawrence Berkeley Lab*), S.J. Freedman, J. Mortara (*U. California, Berkeley*)
737. Magnetic and superconducting behaviour in selected oxide materials [completed], R.H. Heffner, L.P. Le (*Los Alamos Nat. Lab*), D.E. Maclaughlin (*U. California, Riverside*), G. Luke, B. Nachuma, Y.J. Uemura (*Columbia U.*), K. Kojima (*Columbia U.-U. Tokyo*)
740. Irradiation of silicon tracker components [completed], R. Lipton, L. Spiegel (*Fermilab*), K.F. O’Shaughnessy (*U. California, Santa Cruz*), B. Barnett, J. Cameratta, J. Skarha (*Johns Hopkins U.*), N. Brunner, M. Frautschi, M. Gold, Y. Ling, J. Matthews, S. Seidel (*U. New Mexico*), D. Bortoletto, A. Garfinkel, A. Hardman, K. Hoffman, T. Keaffaber, N.M. Shaw (*Purdue U.*)
741. Beta-delayed proton decay of ^{17}Ne to α -emitting states in ^{16}O [completed], R.E. Azuma, J. Chow, J.D. King, A.C. Morton (*U. Toronto*), L. Buchmann, M. Dombisky (*TRIUMF*), U. Giesen (*U. Notre Dame*), T. Davinson, A.C. Shotton (*U. Edinburgh*), R.N. Boyd (*Ohio State U.*), C. Iliadis (*U. North Carolina*), J. Powell (*U. California, Berkeley*),
742. Scattering of muonic hydrogen isotopes [completed], V.M. Bystritsky, V.A. Stolupin (*JINR*), R. Jacot-Guillarmod, P.E. Knowles, F. Mulhauser (*U. Fribourg*), G.M. Marshall (*TRIUMF*), M. Filipowicz, J. Wozniak (*Fac. Phys., Nucl. Tech., Krakow*), A. Adamczak (*Inst. Nucl. Physics, Krakow*), A.R. Kunselman (*U. Wyoming*), V.E. Markushin, C. Petitjean (*PSI*), T.M. Huber (*Gustavus Adolphus Coll.*), G.A. Beer, M. Maier, A. Olin, T.A. Porcelli (*U. Victoria*), P. Kammel (*U. California, Berkeley*), M.C. Fujiwara (*UBC*), J. Zmeskal (*IMEP Vienna*), S.K. Kim (*Jeonbuk Nat. U.*)
743. Gamow-Teller strength in $^{64,66,68}\text{Zn}$ and $^{63,65}\text{Cu}(n, p)$ [completed data-taking], W.P. Alford (*U. Western Ontario*), D. Beatty, H.T. Fortune, P.P. Hui, R.B. Ivie, Z. Mao, M.G. McKinzie, D.A. Smith (*U. Pennsylvania*), S. Yen (*TRIUMF*)
744. Hadronic weak and electromagnetic form factors via $\pi^- p \rightarrow e^+ e^- n$ [active], P. Gumplinger, M.D. Hasinoff (*UBC*), T.P. Gorringer, M.A. Kovash (*U. Kentucky*), D.H. Wright (*SLAC*), E. Christy (*Hampton U.*), P. Zolnierczuk (*IUCF*)

745. μ^- SR measurements on one-dimensional spin systems [active], K. Kojima (*Columbia U.-U. Tokyo*), K. Nagamine, K. Nishiyama, S. Uchida (*U. Tokyo*), G.M. Luke, B. Nachumi, Y.J. Uemura (*Columbia U.*), I. Affleck, S. Dunsiger, S. Eggert, R.F. Kiefl (*UBC*)
746. Muonium dynamics in Si, Ge and GaAs studied by RF- μ SR and μ W- μ SR [active], S.R. Kreitzman (*TRIUMF*), T.L. Estle, B. Hitti (*Rice U.*), R. Lichti (*Texas Tech. U.*), K. Chow (*UBC*), S.F.J. Cox (*Rutherford Appleton Lab*), E.A. Davis (*Leicester U.*), C. Schwab (*CRN Strasbourg*)
747. μ SR study of re-entrant spin glasses a-FeMn, AuFe, and Fe₇₀Al₃₀ [completed], I.A. Campbell (*U. Paris Sud Orsay*), S. Dunsiger, R.F. Kiefl (*UBC*), M.J.P. Gingras (*TRIUMF*), M. Hennion, I. Mirebeau (*Saclay, LLB*), K. Kojima, G.M. Luke, B. Nachumi, Y.J. Uemura, W.D. Wu (*Columbia U.*)
749. Muonium-substituted free radicals [completed data-taking], B. Addison-Jones, J.C. Brodovitch, K. Ghandi, I. McKenzie, P.W. Percival (*SFU*), J. Schüth (*U. Bonn*)
750. Liquid chemistry μ SR [completed], G.B. Porter, D.C. Walker (*UBC*), J.M. Stadlbauer* (*Hood Coll.*), K. Venkateswaran (*Lever Hindustan Ltd.*), M.V. Barnabas *Procter & Gamble Ltd.*)
751. Tests in preparation for μ SR measurements of off-axis internal magnetic fields in anisotropic superconductors [active], E. Csomortani, W.J. Kossler, X. Wan (*Coll. of William & Mary*), D.R. Harshman (*Physikon Research Inc.*), A. Greer (*Gonzaga U.*), E. Koster, D.L. Williams (*UBC*), C.E. Stronach (*Virginia State U.*)
752. Muonium centres in Si and GaAs [completed], K.H. Chow (*Oxford U.*), S.F.J. Cox (*Rutherford Appleton Lab*), E.A. Davis (*Leicester U.*), S. Dunsiger, R.F. Kiefl, W.A. MacFarlane (*UBC*), T.L. Estle (*Rice U.*), B. Hitti (*TRIUMF*), R.L. Lichti (*Texas Tech. U.*), C. Schwab (*CRN Strasbourg*)
753. Studies of magnetic correlations in planar oxides [completed], K. Kojima (*Columbia U.-U. Tokyo*), M. Larkin, G.M. Luke, J. Merrin, B. Nachumi, Y.J. Uemura (*Columbia U.*), B.J. Sternlieb (*Brookhaven Nat. Lab*), S. Uchida (*U. Tokyo*)
754. A search for the muonium substituted hydroxyl radical [deferred], T.A. Claxton, G. Marston (*Leicester U.*), S.F.J. Cox (*Rutherford Appleton Lab*), D. Arseneau, D. Fleming, M. Senba, P. Wassell (*UBC*), J.-C. Brodovitch, P.W. Percival (*SFU*)
755. Muonium formation in Zn-spinels [deferred], G.M. Kalvius, A. Kratzer, W. Potzel (*Tech. U. Munich*), R. Wäppling (*U. Uppsala*), D.R. Noakes (*Virginia State U.*), S.R. Kreitzman (*TRIUMF*), A. Martin (*U. Jena*), M.K. Krause (*U. Leipzig*)
756. Mu+NO spin relaxation: electron exchange or paramagnetism? [deferred], D.G. Fleming, J.J. Pan, M. Senba, M. Shelley (*UBC*), D.J. Arseneau (*TRIUMF*), E. Roduner (*U. Zürich*)
757. Study of muon dynamics in ferroelectric materials and proton ionic conductors – comparison with proton dynamics [completed], W.K. Dawson, K. Nishiyama, S. Ohira, K. Shimomura (*U. Tokyo*), K. Nagamine (*U. Tokyo-RIKEN*), S. Ikeda (*KEK*), S. Shin (*ISSP U. Tokyo*), N. Sata (*Tohoku U.*)
758. Electronic structure of muonium and muonium-lithium complexes in graphite and related compounds [completed], J. Brewer, J. Chakhalian, S. Dunsiger, R.F. Kiefl, W.A. MacFarlane, R. Miller, J. Sonier (*UBC*), J. Dahn (*Dalhousie U.*), J. Fischer (*U. Pennsylvania*), B. Hitti, S.R. Kreitzman (*TRIUMF*)
759. Study of the isotropic hyperfine coupling constant of muonium at high temperature and under uniaxial pressure [completed], W.K. Dawson, K. Nishiyama, S. Ohira, K. Shimomura (*U. Tokyo*), K. Nagamine (*U. Tokyo-RIKEN*), T.P. Das (*U. New York, Albany*)
761. Parity violation in $p-p$ scattering at 450 MeV [deferred], J. Birchall, C.A. Davis, L. Lee, S.A. Page, W.D. Ramsay, A.W. Rauf, G. Rutledge, W.T.H. van Oers (*U. Manitoba*), R. Helmer, R. Laxdal, C.D.P. Levy (*TRIUMF*), P.W. Green, G. Roy, G.M. Stinson (*U. Alberta*), N.A. Titov, S. Zadorozhny, A.N. Zelenski (*INR, Moscow*), J.D. Bowman, R.E. Mischke, S. Penttila, W.S. Wilburn (*Los Alamos Nat. Lab*), E. Korkmaz, (*UNBC*), M. Simonius (*ETH Zürich*), J. Bisplinghoff, P.D. Eversheim, F. Hinterberger (*U. Bonn*), W. Kretschmer, G. Morgenroth (*U. Erlangen*), H. Schieck (*U. Cologne*), P. von Rossen (*KFA Jülich*)
762. Gamow-Teller and spin-flip dipole strengths near $A=90$ [completed data-taking], W.P. Alford (*U. Western Ontario*), D.P. Beaty, H.T. Fortune, P.P. Hui, R.B. Ivie, D. Koltenuk, J. Yu (*U. Pennsylvania*), A. Ling, S. Yen (*TRIUMF*), S. El-Kateb (*King Fahd U.*)
763. Muon cooling and acceleration in an undulating crystal channel [deferred], S.A. Bogacz, D.B. Cline, D.A. Sanders (*UCLA*), L.M. Cremaldi, B. Denardo, Q. Jie, D.J. Summers (*U. Mississippi-Oxford*), G.M. Marshall (*TRIUMF*)
764. Calibration of a segmented neutron detector [completed], E. Korkmaz, G. O’Rielly (*UNBC*), D.A. Hutcheon (*TRIUMF*), A.K. Opper (*U. Alberta*), G. Feldman, N.R. Kolb (*U. Saskatchewan*)

766. The ortho-para transition rate in muonic molecular hydrogen [completed], D.S. Armstrong, J.H.D. Clark, P. King (*Coll. of William & Mary*), T.P. Gorringe, S. Tripathi, P.A. Żolnierczuk (*U. Kentucky*), M.D. Hasinoff, T. Stocki (*UBC*), D.H. Wright (*TRIUMF*)
767. Direct measurement of sticking in muon catalyzed $d - t$ fusion [inactive], J.M. Bailey (*Chester Technology, UK*), G.A. Beer, M. Maier, G.R. Mason, T.A. Porcelli (*U. Victoria*), K.M. Crowe, P. Kammel (*U. California, Berkeley-LBL*), M.C. Fujiwara, E. Gete, T.J. Stocki (*UBC*), T.M. Huber (*Gustavus Adolphus Coll.*), S.K. Kim (*Jeonbuk Nat. U.*), A.R. Kunselman (*U. Wyoming*), G.M. Marshall, A. Olin (*TRIUMF*), C.J. Martoff (*Temple U.*), V.S. Melezhik (*JINR, Dubna*), F. Mulhauser (*U. Fribourg*), C. Petitjean (*PSI*), J. Zmeskal (*IMEP Vienna*)
768. Generalized Fulde-Ferrell-Larkin-Ovchinnikov state in heavy fermion and intermediate valence systems [completed], J. Akimitsu, K. Oishi, T. Muranaka (*Aoyama Gakuin U.*), W. Higemoto, R. Kadono, A. Koda (*KEK-IMSS*), M. Nohara, H. Suzuki, H. Takagi (*U. Tokyo*), R.F. Kiefl, R.I. Miller, A.N. Price (*UBC-TRIUMF*), J.E. Sonier (*SFU*)
769. Effects of uniaxial stress on muonium in semiconductors [completed], K.H. Chow (*Oxford*), B. Hitti (*TRIUMF*), R.F. Kiefl (*UBC*), T.L. Estle (*Rice U.*), R. Lichti (*Texas Tech. U.*)
770. μ SR studies of organic conductors: $(\text{BEDT-TTF})_2\text{-X}$ and $(\text{TMTTF})_2\text{Br}$ [completed], K. Kojima, M. Larkin, G.M. Luke, J. Merrin, B. Nachumi, Y.J. Uemura (*Columbia U.*), P.M. Chaikin (*Princeton U.*), G. Saito (*Kyoto U.*)
771. μ SR studies of geometrically frustrated $S = 1/2$ spin systems [completed], K. Kojima, M. Larkin, G.M. Luke, J. Merrin, B. Nachumi, Y.J. Uemura (*Columbia U.*), M.J.P. Gingras (*TRIUMF*), S. Dunsiger, R.F. Kiefl (*UBC*), D.C. Johnston, S. Kondo (*Iowa State U.*), S. Uchida (*U. Tokyo*), R.J. Cava (*AT&T Bell Labs*)
772. Search for the $\Delta - \Delta$ dibaryon [inactive], R. Abegg*, C.A. Miller, P. Walden, S. Yen (*TRIUMF*), R. Bent (*Indiana U.*), T.Y. Chen, F. Wang, C.H. Ye (*Nanjing U.*), W. Falk (*U. Manitoba*), D. Frekers, M. Hartig (*U. Muenster*), T. Goldman (*Los Alamos Nat. Lab*), M. Heyrat, C.W. Wong (*UCLA*), G. Jones (*UBC*), E. Korkmaz, G. O'Rielly (*UNBC*), C. Rangacharyulu (*U. Saskatchewan*), I. Strakovsky (*Virginia Tech. Inst.*), Z.X. Sun, J.C. Xu (*Inst. Atomic Energy, China*), T. Walton (*Cariboo U. Coll.*)
773. Muon-electron interaction in n -type silicon [completed], D. Arseneau, B. Hitti, S.R. Kreitzman (*TRIUMF*), J.H. Brewer, R.F. Kiefl, G. Morris (*UBC*), K. Chow (*Oxford U.*), S.F.J. Cox (*Rutherford Appleton Lab*), D.G. Eshchenko (*INR, Moscow*), T.L. Estle (*Rice U.*), R. Lichti (*Texas Tech. U.*), V.G. Storchak, (*Kurchatov Inst.*)
774. Muonium dynamics in GaAs studied by rf and μ -wave μ SR [active], B. Hitti, S.R. Kreitzman (*TRIUMF*), T.L. Estle (*Rice U.*), R. Lichti (*Texas Tech. U.*)
775. Electron transport in insulators, semiconductors and magnetic materials [completed], J.H. Brewer, A. Izadi, D.M.C. Liu, K.M. Nichol, S. Sivanandam, A.T. Warkentin (*UBC*), G.D. Morris (*TRIUMF*), V.G. Storchak (*Kurchatov Inst.*), D.G. Eshchenko (*INR, Moscow*), J.D. Brewer (*SFU*)
776. Rare earth materials with disordered spin structures [completed], J.H. Brewer (*UBC*), K. Fukamichi (*Tohoku U.*), G.M. Kalvius (*Tech. U. Munich*), D.R. Noakes, C.E. Stronach (*Virginia State U.*), R. Wäppling (*Uppsala U.*)
777. Vortex state of s -wave superconductors investigated by muon spin rotation [completed], J.C. Chakhalian, K. Chow, R. Miller, A.N. Price (*UBC*), J.H. Brewer, R.F. Kiefl (*UBC-TRIUMF*), G.M. Luke (*McMaster U.*), J.E. Sonier (*SFU*)
778. $\pi^\pm p$ differential cross sections in the Coulomb-nuclear interference region [completed data-taking], P. Amaudruz, D. Ottewell, (*TRIUMF*), P. Camerini, E. Fragiaco, N. Grion, S. Piano, R. Rui (*INFI Trieste-U. Trieste*), K. Babcock, E. Mathie, H. Xu, D.M. Yeomans (*U. Regina*), G. Hofman, M.M. Pavan, K.J. Raywood, R. Tacik (*Regina-TRIUMF*), J. Breitschopf, H. Denz, R. Meier, F. von Wrochem, G. Wagner (*U. Tübingen*), G. Moloney, M. Sevir (*U. Melbourne*), J. Brack, J. Patterson, R. Ristinen (*U. Colorado*), E. Gibson (*California State U., Sacramento*), O. Patarakin (*Kurchatov Inst.*), G. Smith (*Jefferson Lab*)
779. Accelerator mass spectrometry experiments at ISAC [inactive], S. Calvert, A. Glass, R.R. Johnson, T. Petersen (*UBC*), Z. Gelbart, D. Ottewell (*TRIUMF*), R. Schubank (*unaffiliated*), C.S. Wong (*Inst. of Ocean Sciences*), J. Clague (*Geological Survey Canada*), M. Paul (*Hebrew U. Jerusalem*)
780. Deeply bound pionic states through $^{208}\text{Pb}(p, ^3\text{He})^{206}\text{Pb} \otimes \pi^-$ [completed], D. Frekers, W. Garske, K. Grewer, M. Hartig, H. Wörtche (*U. Muenster*), H. Machner (*KFA, Jülich*), D. Hutcheon, P. Walden, S. Yen (*TRIUMF*), A. Opper (*U. Ohio*)
781. Investigations of the $\pi\pi$ invariant mass distributions of nuclear ($\pi^+, \pi^-\pi^+$) reactions with the CHAOS detector [completed data-taking], J. Clark, G. Moloney, M.E. Sevir (*U. Melbourne*), L. Felawka, G. Hofman, D.F. Ottewell, K. Raywood, G.R. Smith (*TRIUMF*), R. Meier (*U. Tübingen*), P. Camerini, E. Fragiaco, R. Rui (*INFN Trieste-U. Trieste*), N. Grion, S. Piano (*INFN, Trieste*), E.L. Mathie, R. Tacik, (*U. Regina*), E.F. Gibson (*Cal. State U., Sacramento*)

782. Non-fermi-liquid behaviour and other novel phenomena in heavy-fermion alloys [completed], J.E. Anderson, D.E. MacLaughlin, L. Shu (*U. California, Riverside*), R.H. Heffner, G.D. Morris (*Los Alamos Nat. Lab*), N.A. Frederick, M.B. Maple, W.M. Yuhasz (*U. California, San Diego*), O.O. Bernal (*Cal. State U., Los Angeles*), F. Callaghan, J.E. Sonier (*SFU*), B. Andraka, G.R. Stewart (*U. Florida*)
783. Paramagnetic frequency shifts in unconventional superconductors [active], R.H. Heffner, G.D. Morris (*Los Alamos Nat. Lab*), D.E. MacLaughlin (*U. California, Riverside*), G.J. Nieuwenhuys (*U. Leiden*), O.O. Bernal (*Cal. State U., Los Angeles*), J.E. Sonier (*SFU*)
784. μ SR studies of spin singlet states in oxides [active], A. Fukaya, I. Gat, M. Larkin, A. Savici, Y.J. Uemura (*Columbia U.*), T. Ito (*Columbia U.-ETL*), H. Kageyama, K. Ueda, Y. Ueda (*U. Tokyo*), P.P. Kyriakou, G.M. Luke, M.T. Rovers (*McMaster U.*)
785. Pion double charge exchange on ^3He with CHAOS [completed data-taking], R. Tacik (*TRIUMF-U. Regina*), E.L. Mathie, M. Yeomans (*U. Regina*), H. Clement, J. Graeter, R. Meier, J. Petzold, G.J. Wagner (*U. Tübingen*), E. Friedman (*Hebrew U. Jerusalem*), N. Grion (*INFN Trieste*), P. Camerini, E. Fragiaco, R. Rui (*U. Trieste*), L. Felawka, D. Ottewell, K. Raywood, G.R. Smith (*TRIUMF*), G. Hofman, B. Jamieson, G. Tagliente (*UBC*), J. Clark, G. Molony, M.E. Sevier (*U. Melbourne*), E. Gibson (*California State U. Sacramento*), H. Staudenmeyer (*U. Karlsruhe*), S. Filippov, Y. Gavrilov, T. Karavicheva (*Moscow Meson Factory*)
786. Low energy structures in the β -delayed particle decays of ^9C , ^{12}N and ^{17}Ne [completed], N. Bateman (*TRIUMF-SFU-U. Toronto*), L. Buchmann, K.P. Jackson, T. Shoppa (*TRIUMF*), J. Chow, J.D. King, C. Mortin (*U. Toronto*), T. Davison, A. Ostrowski, A. Shotter (*U. Edinburgh*), J. D'Auria (*SFU*), E. Gete, D. Measday (*UBC*), U. Giesen (*U. Alberta*)
788. Nuclear and atomic physics with the CPT spectrometer [inactive], B. Barber, K.S. Sharma (*U. Manitoba*), X. Feng (*U. Manitoba-McGill U.*), F. Buchinger, J. Crawford, S. Gulick, J. Lee, B. Moore (*McGill U.*), E. Hagberg, J. Hardy, V. Koslowsky, G. Savard (*Chalk River Nuclear Lab*)
789. μ SR studies of magnetic fluctuations in hydronium jarosites, model Kagomé antiferromagnets [completed], A. Harrison, A.S. Wills (*U. Edinburgh*), Y. Fudamoto, K. Kojima, M. Larkin, G.M. Luke, J. Merrin, B. Nachumi, Y.J. Uemura (*Columbia U.*), T. Mason (*U. Toronto*)
790. μ SR studies of stripe order in $\text{La}_{1.6-x}\text{Sr}_x\text{Nd}_{0.4}\text{CuO}_4$ modified cuprate superconductors [completed], Y. Fudamoto, K. Kojima, M. Larkin, G.M. Luke, J. Merrin, B. Nachumi, Y.J. Uemura (*Columbia U.*), M. Crawford (*Du Pont*), A. Moodenbaugh (*Brookhaven Nat. Lab*), S. Uchida (*U. Tokyo*)
791. Electronic structure and dynamics of charged muonium and muonium-dopant centers in semiconductors [active], K.H. Chow (*Oxford U.*), R.F. Kiefl (*UBC*), B. Hitti (*TRIUMF*), T.L. Estle (*Rice U.*), R. Lichti (*Texas Tech. U.*), S.F.J. Cox (*Rutherford Appleton Lab*), C. Schwab (*CRN, Strasbourg*)
792. Muonium in III-V semiconductors: identification of states and transitions [completed], K.H. Chow (*Oxford U.*), S.F.J. Cox (*Rutherford Appleton Lab*), B. Hitti (*TRIUMF*), T.L. Estle (*Rice U.*), R.L. Lichti (*Texas Tech. U.*), C. Schwab (*CRN, Strasbourg*)
793. Production of an intense ^{15}O beam for ISAC [completed], J. D'Auria, R. Lange (*SFU*), M. Dombisky, T. Ruth, J. Vincent (*TRIUMF*), K. Carter (*Oak Ridge Nat. Lab*), B. Zhuikov (*INR, Moscow*)
794. μ^+ SR study on the magnetic properties of LaCoO_3 and $\text{La}_{1-x}\text{Sr}_x\text{CoO}_3$ [completed], V.V. Krishnamurthy, I. Watanabe (*RIKEN*), K. Asai, N. Yamada (*U. Electro-communications*), K. Nagamine (*U. Tokyo-RIKEN*)
795. μ SR study on non fermi liquid behaviour [completed], Y. Miyako, Y. Yamamoto (*Osaka U.*), S. Murayama (*Muroran Inst. Tech.*), K. Nagamine (*U. Tokyo*), K. Nishiyama (*U. Tokyo-RIKEN*)
796. μ SR studies in ionic crystals doped with either colour centres or impurity [deferred], Y. Miyake, K. Nagamine, K. Nishiyama, K. Shimomura (*U. Tokyo*), A. Matsusita (*RIKEN*)
797. Magnetic correlations in the ternary equiatomic Ce compounds CeT_2Sn [completed], G. Grosse, G.M. Kalvius A. Kratzer (*Tech. U. Munich*), R. Wäppling (*U. Uppsala*), T. Takabatake (*Hiroshima U.*), D.R. Noakes, C.R. Stronach (*Virginia State U.*), Y. Echizen (*Hiroshima U.*), H. Nakotte (*New Mexico State U.*), H.v. Löhneysen (*U. Karlsruhe*)
798. μ SR studies on the competition of RKKY exchange and Kondo effect in CeT_2X_2 compounds (T=transition metal, X=Si,Ge) [completed], H.-H. Klauss, W. Kopmann, F.J. Litterst, W. Wagener, H. Walf (*Tech. U. Braunschweig*), E. Baggio Saitovitch, M.B. Fontes (*CBPF Rio de Janeiro*), A. Krimmel, A. Loidl (*U. Augsburg*)
799. Hyperfine structure and site determination of $(\mu^- \text{O})$ system in LaSuCuO high T_c superconductors [completed], H. Kojima, I. Tanaka, E. Torikai (*Yamanashi U.*), K. Nishiyama (*U. Tokyo-RIKEN*), K. Nagamine, K. Shimomura (*U. Tokyo*), I. Watanabe (*RIKEN*), T.P. Das (*State U. New York*)

801. Studies of multi-phonon states via β -decay [completed], C.J. Barton, M.A. Caprio, R.F. Casten, N.V. Zamfir (*Yale U.*), D.S. Brenner (*Clark U.*), G.C. Ball, K.P. Jackson (*TRIUMF*)
802. Superdeformation and smooth band termination on and near the $N = Z$ line: Part 1 ^{60}Zn [active], J.A. Cameron, S. Flibotte, D.S. Haslip, J. Nieminen, C. Svensson, J.C. Waddington, J.N. Wilson (*McMaster U.*), G. Ball (*TRIUMF*), A. Galindo-Uribarri, D.C. Radford (*Oak Ridge Nat. Lab*), D. Ward (*Lawrence Berkeley Nat. Lab*)
803. Experimental studies of interaction and properties of neutron-rich nuclei at ISAC [inactive], A.S. Iljinov, A.V. Klyachko, E.S. Konobeevsky, M.V. Morodovskoy, M.A. Prohvatilov, A.I. Reshetin, Yu.V. Ryabov, K.A. Shileev, V.A. Simonov, V.M. Skorkin, S.V. Zuyev (*INR, Moscow*)
804. Muonium in gallium nitride [completed], B.A. Bailey, R.L. Lichti (*Texas Tech. U.*), K.H. Chow (*U. Alberta*), B. Hitti (*TRIUMF*), S.F.J. Cox (*Rutherford Appleton Lab*), E.A. Davis (*Leicester U.*)
805. A study of the $^{13}\text{N}(p, \gamma)^{14}\text{O}$ reaction with a ^{13}N beam [active], R.E. Azuma, J. Chow, J.D. King, A.C. Morton (*U. Toronto*), N. Bateman (*TRIUMF-Toronto*), L. Buchmann, K.P. Jackson, T. Shoppa (*TRIUMF*), J.M. D'Auria (*SFU*), U. Giesen (*SFU-TRIUMF*), G. Roy (*U. Alberta*), W. Galster (*U. Catholique de Louvain*), A.C. Shotter (*U. Edinburgh*), R.N. Boyd (*Ohio State U.*), U. Greife, C. Rolfs, F. Strieder, H.-P. Trautvetter (*Ruhr U. Bochum*)
806. Excitation of high-spin isomeric states and compound nucleus formation by intermediate energy protons and stopped pions [completed data-taking], A.S. Iljinov, V.M. Kokhanyuk, B.L. Zhuikov (*INR, Moscow*), I. Liu, J. Vincent, A.Z. Zyuzin (*TRIUMF*)
808. Spin glass order in magnets frustrated by competing ferro- and antiferromagnetic exchange [completed], G.M. Kalvius, A. Kratzer, E. Schreier (*Techn. U. Munich*), R. Wäppling (*U. Uppsala*), D.R. Noakes (*Virginia State U.*), J. Gal (*Beer Sheva U.*), W. Schäfer (*Bonn U.*)
809. Quantum diffusion of muonium in crystals with orientational degrees of freedom [completed], D. Arseneau, B. Hitti, S.R. Kreitzman (*TRIUMF*), J.H. Brewer, A. Izadi, G.D. Morris (*UBC*), D.G. Eshchenko (*INR, Moscow*), V.G. Storchak (*Kurchatov Inst.*), J.D. Brewer (*SFU*)
810. First direct study of the $^{23}\text{Mg}(p, \gamma)^{24}\text{Al}$ reaction with a recoil mass separator (DRAGON) [active], N.P.T. Bateman, J.M. D'Auria, D. Hunter, R. Korteling (*SFU*), R.N. Boyd (*Ohio State U.*), L. Buchmann, R. Helmer, D. Hutcheon, K.P. Jackson, A. Olin, J. Rogers (*TRIUMF*), U. Giesen, G. Roy (*U. Alberta*), L. Gialanella, U. Greife, C. Rolfs, F. Strieder, H.-P. Trautvetter (*Ruhr U. Bochum*), A. Hussein (*UNBC*), M. Junker (*INFN Gran Sasso*), J.D. King (*U. Toronto*), P.D. Parker (*Yale U.*), A. Shotter (*U. Edinburgh*), M. Wiescher (*U. Notre Dame*)
811. A direct study of the $^{19}\text{Ne}(p, \gamma)^{20}\text{Na}$ reaction with a recoil mass separator (DRAGON) [active], N.P.T. Bateman, J.M. D'Auria, D. Hunter, R. Korteling (*SFU*), R.N. Boyd (*Ohio State U.*), L. Buchmann, R. Helmer, D. Hutcheon, K.P. Jackson, A. Olin, J. Rogers (*TRIUMF*), U. Giesen, G. Roy (*U. Alberta*), L. Gialanella, U. Greife, C. Rolfs, F. Strieder, H.-P. Trautvetter (*Ruhr U. Bochum*), A. Hussein (*UNBC*), M. Junker (*INFN Gran Sasso*), J.D. King (*U. Toronto*), P.D. Parker (*Yale U.*), A. Shotter (*U. Edinburgh*), M. Wiescher (*U. Notre Dame*)
812. Proposed study of the $^8\text{Li}(\alpha, n)^{11}\text{B}$ reaction [active], R.N. Boyd, A. Murphy, L. Sahin, E. Smith, M. Zahar (*Ohio State U.*), L. Buchmann, P. Walden (*TRIUMF*), J.M. D'Auria (*SFU*), J.D. King (*U. Toronto*), M. Nishimura, S. Nishimura, I. Tanihata (*RIKEN*)
813. A study of the $^{15}\text{O}(\alpha, \gamma)^{19}\text{Ne}$ reaction at the astrophysically important energy [active], N.P.T. Bateman, J.M. D'Auria, D. Hunter, R. Korteling (*SFU*), R.N. Boyd (*Ohio State U.*), L. Buchmann, R. Helmer, D. Hutcheon, K.P. Jackson, A. Olin, J. Rogers (*TRIUMF*), U. Giesen, G. Roy (*U. Alberta*), U. Greife, C. Rolfs, F. Strieder, H.-P. Trautvetter (*Ruhr U. Bochum*), A. Hussein (*UNBC*), J.D. King (*U. Toronto*), P.D. Parker (*Yale U.*), A. Shotter (*U. Edinburgh*), M. Wiescher (*U. Notre Dame*)
814. μSR studies of unconventional superconductivity in Sr_2RuO_4 [active], Y. Fudamoto, K.M. Kojima, M. Larkin, G.M. Luke, J. Merrin, B. Nachumi, Y.J. Uemura (*Columbia U.*), Y. Maeno (*Kyoto U.*), R.J. Cava (*Princeton U.*)
815. β -NMR investigation of magnetic multilayers and giant magnetoresistance [active], J. Chakhalian, W.A. MacFarlane, R. Miller, (*UBC*), J.H. Brewer, R.F. Kiefl (*UBC-TRIUMF*), P. Amaudruz, R. Baartman, T.R. Beals, J. Behr, S. Daviel, S.R. Kreitzmann, T. Kuo, C.D.P. Levy, M. Olivo, R. Poutissou, Z. Salman, G.D. Wight (*TRIUMF*) S.R. Dunsiger, R. Heffner, G.D. Morris (*Los Alamos Nat. Lab*), C. Bommas (*U. Bonn*), A. Hatakeyama, Y. Hirayama, T. Shimoda (*Osaka U.*), K.H. Chow (*U. Alberta*), J.E. Elenewski, L.H. Greene (*U. Illinois-Urbana-Champagne*)
816. Semiconductor quantum wells investigated by β -NMR [active], J.H. Brewer, J.C. Chakhalian, S. Dunsiger, R. Miller, T. Tiedje (*UBC*), M. Gingras (*U. Waterloo*), B. Ittermann (*U. Marburg*), B. Hitti, P. Levy, S.R. Kreitzman, A. Zelenski (*TRIUMF*), R.F. Kiefl (*TRIUMF-UBC*)

65

65

817. β -NMR investigation of type II superconductors [active], D. Bonn, J.H. Brewer, J.C. Chakhalian, S. Dunsiger, W. Hardy, R. Liang, R.F. Kiefl, W.A. MacFarlane, R. Miller, J. Sonier (*UBC*), M. Gingras (*U. Waterloo*), R. Heffner (*Los Alamos Nat. Lab*), B. Itterman (*U. Marburg*), B. Hitti, P. Levy, S.R. Kreitzman, A. Zelenski (*TRIUMF*), G.M. Luke (*Columbia U.*), J.W. Brill (*U. Kentucky*)
818. μ^+ SR study of magnetic ordering in the one-dimensional spin-1/2 antiferromagnet copper benzoate [completed], J.C. Chakhalian, S. Dunsiger, R.F. Kiefl, W.A. MacFarlane, R. Miller, J. Sonier (*UBC*), C. Broholm, D.C. Dender, P. Hammar, D. Reich (*Johns-Hopkins U.*), G. Luke, T. Uemura (*Columbia U.*)
819. μ^+ SR studies of the antiferromagnetic instability and metastable state in colossal magnetoresistance system $(\text{Nd}_{1-y}\text{Sm}_y)_{1/2}\text{Sr}_{1/2}\text{MnO}_3$ ($y = 0.875$) [completed], W. Higemoto, I. Watanabe (*RIKEN*), K. Nishiyama (*KEK*), K. Nagamine (*RIKEN-KEK*), A. Asamitsu, H. Kuwahara, Y. Tokura (*JRCAT, U. Tokyo*)
821. Shape coexistence and shape mixing in neutron-deficient platinum isotopes: on-line nuclear orientation studies of the decays of ^{182}Au and ^{186}Au [active], K.S. Krane (*Oregon State U.*), J.L. Wood (*Georgia Inst. Tech.*), J. D'Auria (*SFU*)
822. Effect of disorder on quantum spin liquid state [completed data-taking], W. Higemoto, R. Kadono, A. Koda, K. Ohishi, (*KEK-IMSS*), M. Nohara, H. Takagi, H. Ueda, C. Urano (*U. Tokyo*)
823. Pure fermi decay in medium mass nuclei [active], G.C. Ball, R. Beaton, P. Bricault, G. Hackman, P. Klages, J.A. Macdonald*, E. Vandervoort (*TRIUMF*), D.F. Hodgson (*U. Surrey-TRIUMF*), J. Cerny, D.M. Moltz, J. Powell (*Lawrence Berkeley Lab*), G. Savard (*Argonne Nat. Lab*), J.C. Hardy, V. Iacob (*Texas A&M U.*), S. Bishop, J. D'Auria (*SFU*), J.R. Leslie, H.-B. Mak, I.S. Towner (*Queen's U.*), D. Kulp, J.L. Wood (*Georgia Inst. Tech.*), E.F. Zganjar, A. Piechaczek (*Louisiana State U.*)
824. Measurement of the astrophysical rate of the $^{21}\text{Na}(p,\gamma)^{22}\text{Mg}$ reaction [active], S. Bishop, J.M. D'Auria, D. Hunter, M. Lamey, W. Liu, C. Wrede, (*SFU*), L. Buchmann, D. Hutcheon, A.M. Laird, A. Olin, D. Ottewell, J.G. Rogers (*TRIUMF*), S. Engel, F. Strieder (*Ruhr U.*), D. Gigliotti, A. Hussein (*UNBC*), R. Azuma, J.D. King (*U. Toronto*), R. Lewis, P.D. Parker (*Yale U.*), S. Kubono, S. Michimasa (*U. Tokyo*), M. Chatterjee (*Saha Inst., Calcutta*), U. Greife, C. Jewett (*Colorado School of Mines*), A.A. Chen (*McMaster U.*), M. Hernanz, J. José (*Inst. d'Estudis Espacials de Catalunya, Barcelona*)
826. Studies of ultrathin magnetic films with implanted isotopes [active], R. Kiefl, J. Pond, B.G. Turrell (*UBC*), C.A. Davis, P.P.J. Delheij (*TRIUMF*), K.S. Krane, J. Loats, P. Schmelzenbach, C. Stapels (*Oregon State U.*), D. Groh, W. Kumarasiri, P. Mantica (*Michigan State U.*), D. Kulp, J.L. Wood, (*Georgia Inst. Tech.*)
827. Parity violation in ^{182}W [active], J. D'Auria (*TRIUMF-SFU*), C.A. Davis, P.P.J. Delheij (*TRIUMF*), R. Kiefl, A. Kotlicki, J. Pond, B. Turrell (*UBC*), K.S. Krane (*Oregon State U.*)
828. Nuclear moments in the mass-100 region [active], K.S. Krane, J. Loats, P. Schmelzenbach, C. Stapels (*Oregon State U.*), D. Kulp, J.L. Wood (*Georgia Inst. Tech.*), C.A. Davis, P.P.J. Delheij (*TRIUMF*), D. Groh, W. Kumarasiri, P. Mantica (*Michigan State U.*), R. Kiefl, J. Pond, B.G. Turrell (*UBC*)
829. Muonium as a hydrogen isotope: reactions in solution [completed], D.P. Chong, G.B. Porter, D.C. Walker (*UBC*), K. Venkateswaran (*Hindustan Lever Ltd.*), H.A. Gillis (*St. Francis Xavier U.*)
830. The hot entropy bubble and the decay of ^9Li [active], N. Bateman (*TRIUMF-SFU-Toronto*), L. Buchmann, K.P. Jackson, S. Karataglidis, T. Shoppa, E. Vogt (*TRIUMF*), J. Chow, J.D. King, C. Mortin (*U. Toronto*), T. Davison, A. Ostrowski, A. Shotter (*U. Edinburgh*), J. D'Auria, U. Giesen (*SFU*), E. Gete, D. Measday (*UBC*)
831. Magnetic properties of $\text{REBa}_2\text{Cu}_3\text{O}_x$ [completed data-taking], D. Andreica, F.N. Gygax, M. Pinkpank, A. Schenck (*ETH Zürich*), B. Hitti (*TRIUMF*), A. Amato (*PSI*), J.H. Brewer (*UBC-TRIUMF*)
832. Study of the non-magnetic-magnetic transition in the $\text{Yb}(\text{Cu}_{1-x}\text{Ni}_x)_2\text{Si}_2$ system [completed data-taking], D. Andreica, F. Gygax, M. Pinkpank, A. Schenck (*ETH Zürich-PSI*), A. Amato (*PSI*), B. Hitti (*TRIUMF*)
833. μ SR studies of doped MnSi and V_{2-y}O_3 : non-fermi-liquid behaviour, spin fluctuations and itinerant magnetism [active], A. Fukaya, I.M. Gat, M. Larkin, A.J. Millis, P.L. Russo, A.T. Savici, Y.J. Uemura (*Columbia U.*), P.P. Kyriakou, G.M. Luke, C.R. Wiebe (*McMaster U.*), Y.V. Sushko (*U. Kentucky*), R.H. Heffner (*Los Alamos Nat. Lab*), D.E. MacLaughlin (*U. California, Riverside*), D. Andreica (*PSI*), M. Kalvius (*Tech. U. Munich*)
834. μ SR study of transverse spin freezing in bond-frustrated magnets [active], A.D. Beath, D.H. Ryan, (*McGill U.*), J.M. Cadogan (*U. New South Wales*), J. van Lierop (*U. Michigan*)
835. μ SR studies of intercalated HfN and Bi2212 superconductors [active], M. Greven, N. Kaneko, (*Stanford U.*), I.M. Gat, M.I. Larkin, P.L. Russo, A. Savici, Y.J. Uemura, emph(*Columbia U.*), G.M. Luke, G.J. MacDougall, C.R. Wiebe (*McMaster U.*), Y. Ando (*U. Tokyo*)
836. Elasticks [active], R.E. Azuma, J.D. King (*U. Toronto*), G. Ball, L. Buchmann, K.P. Jackson, B. Jennings, S. Karataglidis, E. Vogt (*TRIUMF*), N. Bateman (*TRIUMF-SFU-U. Toronto*), T. Davison, A. Ostrowski, A. Shotter (*U. Edinburgh*), J. D'Auria (*SFU*), W. Galster (*U. Catholique de Louvain*), G. Roy (*U. Alberta*)

837. Pion-induced errors in memory chips [completed], J.T. Brack, G. Hofman, J. Patterson R.J. Peterson, R.A. Ristinen (*U. Colorado*), J.F. Ziegler (*IBM*), M.E. Nelson (*US Naval Academy*), G. Smith (*TRIUMF*)
838. Measurement of the $\pi^-p \rightarrow \gamma\gamma n$ capture mode of pionic hydrogen [completed data-taking], T. Gorringe, M. Kovash, S. Tripathi, P. Żolnierczuk (*U. Kentucky*), D. Armstrong, J. Clark (*Coll. of William & Mary*), M. Hasinoff (*UBC*), D. Healey, D. Wright (*TRIUMF*)
839. Thermal test of prototype high power ISAC target [completed], D. Drake, D. Liska, W.L. Talbert, M. Wilson (*Amparo Corp.*), P. Bricault, M. Dombisky, P. Schmor (*TRIUMF*), E. Dalder, C. Landram, K. Sale, D. Slaughter (*Lawrence Livermore Nat. Lab.*), J. Nolen, G. Savard (*Argonne Nat. Lab.*), G. Alton (*Oak Ridge Nat. Lab.*)
840. Muon transfer from excited states of muonic hydrogen with x-ray measurement [active], S. Sakamoto, K. Shimomura (*KEK*), K. Nagamine (*KEK-RIKEN*), K. Ishida, N. Kawamura, Y. Matsuda, T. Matsuzaki, S.N. Nakamura, P. Strasser (*RIKEN*)
841. ISAC beam and target development [active], P. Bricault, M. Dombisky (*TRIUMF*)
842. Muonium-substituted free radicals in sub- and supercritical water [completed], J.-C. Brodovitch, S. Kecman, B. McCollum, I. McKenzie, P.W. Percival (*SFU*), B. Addison-Jones (*Douglas College*)
843. Quadrupole ordering in dense Kondo system studied by μ LCR [completed data-taking], J. Akimitsu, K. Kakuta, K. Ohishi (*Aoyama Gakuin U.*), W. Higemoto, R. Kadono (*KEK-IMSS*), T. Yokoo (*CREST*)
844. Quantum impurities in one dimensional spin 1/2 chains [completed], I. Affleck, J. Brewer, J. Chakhalian, S. Dunsiger, R.F. Kiefl, R. Miller, A. Price (*UBC*), S. Eggert (*Chalmers U.*), B. Hitti (*TRIUMF*), A.A. Keren (*Israel Inst. Tech.*), W.A. MacFarlane (*U. Paris-Sud*), G. Morris (*UBC-TRIUMF*), Y.J. Uemura (*Columbia U.*), M. Verdager (*CNRS*), I. Yamada (*Chiba U.*)
845. μ SR studies of vortex phases in (Ba,K)BiO₃ [completed], G.M. Luke, M.A. Lumsden (*McMaster U.*), Y. Fudamoto, M.I. Larkin, Y.J. Uemura (*Columbia U.*), K.M. Kojima (*U. Tokyo*), M. Gingras (*U. Waterloo*), I. Jourard, T. Klein, J. Marcus (*U. Grenoble*)
846. Complex order parameter symmetry in YB₂Cu₃O_{7- δ} at low T and high magnetic field [completed], D.A. Bonn, J.H. Brewer, W.N. Hardy, R.F. Kiefl, R.X. Liang, J.-M. Ménard, R.I. Miller (*UBC*), D. Babineau, K.F. Poon, J.E. Sonier (*SFU*), C.E. Stronach (*Virginia State U.*)
847. Electron-doped high- T_c superconductors [active], P. Fournier (*U. Sherbrooke*), F.D. Callaghan, C.V. Kaiser, M. Laulajainen, J.E. Sonier (*SFU*), R.L. Greene (*U. Maryland*)
848. μ SR investigation of the vortex state of YBa₂Cu₃O_{6+x} [completed data-taking], D.A. Bonn, J.C. Chakhalian, K. Chow, W.N. Hardy, R.X. Liang, R. Miller, A.N. Price (*UBC*), J.H. Brewer, R.F. Kiefl (*UBC-TRIUMF*), J. Sonier (*SFU*)
849. Spin structure and magnetic volume fraction of La₂₁₄ systems: revisiting “1/8”, “stripes”, “spin glass”, and “swiss cheese” [completed], K.M. Kojima (*U. Tokyo*), Y. Fudamoto, I.M. Gat, M.I. Larkin, A.T. Savici, Y.J. Uemura (*Columbia U.*), G.M. Luke (*McMaster U.*), M.A. Kastner, Y.S. Lee (*MIT*), R.J. Birgeneau (*MIT-U. Toronto*), K. Yamada (*Kyoto U.*)
850. Effects of dilute (Cu,Zn) substitution in spin gap systems SrCu₂O₃ and CuGeO₃ [completed], Y. Fudamoto, I. Gat, M.I. Larkin, Y.J. Uemura (*Columbia U.*), K.M. Kojima, K. Manabe, K. Uchinokura (*U. Tokyo*), G.M. Luke (*McMaster U.*), M. Azuma, M. Takano (*Kyoto U.*)
851. μ SR in ruthenate and cuprate high- T compounds [active], D.R. Harshman (*Physikon Research Corp.*), M.K. Wu (*Nat. Tsing Hua U.*), F.Z. Chien (*Tamkang U.*), J.D. Dow (*Arizona State U.*), A.J. Greer (*Gonzaga U.*), A. Goonewardene, W.J. Kossler, X. Wan (*Coll. of William & Mary*), E. Koster, D.Ll. Williams (*UBC*), D.R. Noakes, C.E. Stronach (*Virginia State U.*), A.T. Fiory (*New Jersey Inst. Tech.*), A. Erb (*Walther-Meissner-Inst. Tieftemperaturforschung, Garching*), J.P. Franck, I. Issac (*U. Alberta*), Z.F. Ren, D.Z. Wang (*Boston College*), R.N. Kleiman (*Bell Labs*), R.C. Haddon (*U. California, Riverside*), W. Kang (*U. Chicago*)
852. Magnetic phases in geometrically frustrated rare earth pyrochlores [active], R. Kiefl (*UBC-TRIUMF*), S. Dunsiger, B.D. Gaulin, (*McMaster U.*), M.J.P. Gingras (*U. Waterloo*), G.D. Morris, J.M. Roper (*Los Alamos Nat. Lab.*), R. Miller (*U. Pennsylvania*), A.N. Price (*U. Erlangen-Nuernberg*), J.S. Gardner (*NIST*), S.T. Bramwell (*U. College London*), K. Chow (*U. Alberta*), J. Chakhalian (*MPI, Stuttgart*)
856. μ SR study on CuO [active], W. Higemoto, K. Nishiyama, K. Shimomura (*KEK*), M. Suzuki, S. Tanaka, N. Tsutsumi, X.G. Zheng (*Saga U.*)
857. Investigation of the magnetic properties of the cerium compound probed by negative muon [active], W. Higemoto, K. Nagamine, K. Nishiyama, K. Shimomura (*KEK*), V.V. Krishnamurthy (*RIKEN*)
858. Repolarization of muonic atom in semiconductors by laser optical pumping in solids [active], W. Higemoto, R. Kadono, K. Nagamine, K. Nishiyama K. Shimomura (*KEK*)

859. A search for non-Markovian μ^+ diffusion in solids: μ^+ spectral spin hopping in high transverse field [inactive], G. Alexandrowicz, A. Grayevsky, N. Kaplan, T. Tashma (*Racah Inst. Physics*), A. Schenck (*ETH Zürich*)
860. Mass and charge transport in disordered media: orientational glasses [completed], J.H. Brewer, A. Izadi, D.M.C. Liu, K.M. Nichol, S. Sivanandam, A.T. Warkentin (*UBC*), G.D. Morris (*TRIUMF*), V.G. Storchak (*Kurchatov Inst.*), D.G. Eshchenko (*INR, Moscow*), J.D. Brewer (*SFU*)
862. Polarization observables in the $\bar{p}(\pi^\pm, \pi^+, \pi^\pm)$ reactions: a test of chiral perturbation theory [completed data-taking], K. Craig, G. Hofman, M.M. Pavan, R. Tacik (*Regina-TRIUMF*), E. Mathie (*U. Regina*), J. Breitschopf, H. Denz, R. Meier, G. Wagner (*U. Tübingen*), E. Gibson (*California State U. Sacramento*), C.M. Riedel (*Montana State U. Bozeman*)
863. Magnetic dipole moments measurements of $^{75,77,79}\text{Ga}$ using low temperature nuclear orientation and β -NMR [completed data-taking], A.D. Davies, P.F. Mantica, T.J. Mertzimekis (*Michigan State U.*), C.A. Davis, P.P.J. Delheij (*TRIUMF*), B. Turrell (*UBC-TRIUMF*)
864. Measurement of the two-photon capture mode of the pionic deuterium atom [completed data-taking], S. Arole, T. Gorringer, C. Nenkov, S. Tripathi, P. Żohierczuk (*U. Kentucky*), D. Armstrong, J. Clark (*Coll. of William & Mary*), M. Hasinoff (*UBC*), D. Wright (*TRIUMF*)
865. Electronic structure and diffusion kinetics of muonium in group III nitrides [active], W. Higemoto, R. Kadono, K. Nishiyama, K. Shimomura (*KEK-IMSS*), M. Mizuta (*NEC Corp.*), M. Saito (*NEC Inf. Syst. Ltd.*)
866. $S = 0$ doping to the $1d$ spin chain: comparison between the $S = 1/2$ and $S = 1$ chains [active], I. Eisaki, K.M. Kojima, T. Masuda, S. Uchida, K. Uchinokura (*U. Tokyo*), Y. Fudamoto, I. Gat, M.I. Larkin, Y.J. Uemura (*Columbia U.*), G.M. Luke (*McMaster U.*)
867. μSR studies of magnetic properties of strontium/calcium ruthenates [active], Y. Fudamoto, I. Gat, M. Larkin, A. Savici, Y.J. Uemura (*Columbia U.*), G.M. Luke (*McMaster U.*), K. Kojima (*U. Tokyo*), S. Ikeda, Y. Maeno (*Kyoto U.*)
868. Magnetic correlations in impurity doped one dimensional spin systems [active], D. Baabe, H.-H. Klauss, W. Kopmann, F.J. Litterst, D. Mienert (*Tech. U. Braunschweig*), U. Ammerahl, B. Büchner (*U. Köln*), C. Geibel (*MPI Dresden*)
869. Measurement of the $^1\text{H}(\pi^-, \pi^0)n$ differential cross section at 100–140 MeV/ c and forward angles [completed data-taking], S. Arole, T. Gorringer, M. Kovash, S. Tripathi, P. Żohierczuk (*U. Kentucky*), M. Hasinoff (*UBC*), D. Armstrong (*Coll. of William & Mary*), M. Pavan (*TRIUMF*)
870. Breakout from the hot CNO cycle via the $^{18}\text{Ne}(\alpha, p)^{21}\text{Na}$ reaction [active], T. Davinson, A. Ostrowski, F. Sarazin, A. Shotter, P. Woods (*U. Edinburgh*), L. Buchmann, J. D’Auria (*TRIUMF*), J. Daly, J. Görres, M. Wiescher (*U. Notre Dame*), P. Leleux (*U. Catholique de Louvain*)
871. Meson and quark effects in nuclear β -decay of ^{20}Na [active], H. Fujiwara, M. Fukuda, K. Matsuta, M. Mihara, T. Minamisono, T. Nagatomo, M. Ogura, T. Sumikama (*Osaka U.*), R. Baartman, J. Behr, P. Bricault, M. Dombisky, K.P. Jackson, P. Levy (*TRIUMF*), R. Kiefl (*UBC*), K. Koshigiri (*Osaka Kyoiku U.*), M. Morita (*Josai Int. U.*), K. Minamisono (*JSPS-TRIUMF*)
872. Weak interaction studies with trapped radioactive ions [active], J. Dilling, D. Melconian (*SFU*), G. Savard (*Argonne Nat. Lab-U. Chicago*), G.C. Ball, J.A. Behr, P. Bricault, K.P. Jackson (*TRIUMF*), F. Buchinger, J.E. Crawford, J.K.P. Lee, R.B. Moore (*McGill U.*), K.S. Sharma (*U. Manitoba*)
874. Study of ^{19}Ne α -decay properties related to the hot-CNO breakout reaction $^{15}\text{O}(\alpha, \gamma)^{19}\text{Ne}$ [active], T. Davinson, D. Groombridge, A.M. Laird, A.N. Ostrowski, F. Sarazin, K. Schmidt, A.C. Shotter, P.J. Woods (*U. Edinburgh*), L. Buchmann (*TRIUMF*), S. Cherubini, P. Leleux (*U. Catholique de Louvain*), J. Hinnefeld (*U. South Bend*)
875. Muon scattering in low Z materials for muon cooling studies [active], M. Curtis-Rouse, T.R. Edgecock, M. Ellis, J. Lidbury, W. Murray, P.R. Norton, K.J. Peach (*Rutherford Appleton Lab*), K. Ishida, Y. Matsuda (*RIKEN*), T. McMahon, J.A. Wilson (*U. Birmingham*), G. Barber, A. Jamdagni, K. Long, E. McKigney (*Imp. Coll., London*), W. Allison, S. Holmes (*U. Oxford*), S. Benveniste, D. Cline, Y. Fukui, K. Lee, Y. Pischalnikov (*UCLA*), R. Fernow (*Brookhaven Nat. Lab*), P. Gruber, A. Lombardi (*CERN*), S.N. Nakamura (*U. Tohoku*), G. Marshall (*TRIUMF*), A. Bogacz (*Jefferson Lab*)
876. Disordered magnetism near magnetic instabilities in f -electron materials [completed], D.R. Noakes, C.E. Stronach (*Virginia State U.*), G.M. Kalvius (*Tech. U. Munich*), A. Loidl (*Augsburg U.*), H. Nakotte (*New Mexico State U.*), R. Wäppling (*Uppsala U.*), A.V. Andreev (*Charles U.*)
877. μSR studies of strongly correlated electron systems under a high pressure [active], W. Higemoto, R. Kadono, A. Koda, K. Nishiyama (*KEK-MSL*), K. Satoh (*Saitama U.*), Y. Kitaoka, K. Ishida (*Osaka U.*), K. Nagamine (*RIKEN-KEK-MSL*)

878. μ^+ SR studies on magnetism of layered compounds $\text{Cu}_2(\text{OH})_3\text{X}$ ($\text{X}=\text{Cl}, \text{Br}, \text{I}$) [active], G. Maruta, K. Nishiyama (*KEK-MSL*), S. Takeda (*Gunma U.*)
879. Proton- ^{21}Na elastic scattering at astrophysical energies [completed data-taking], L. Buchmann (*TRIUMF*), T. Davinson, A. Ostrowski, F. Sarazin, A. Shotter, P. Woods (*U. Edinburgh*), R.E. Azuma, J.D. King (*U. Toronto*), A. Chen (*TRIUMF-SFU*), J. Daly, J. Görres, M. Wiescher (*U. Notre Dame*), J. D'Auria (*SFU*), E.S. Konobeevsky, M.V. Mordovskoy, V.A. Simonov, A.V. Stepanov, V.P. Zavarzina (*INR, Moscow*)
880. Ortho-para effect of muon catalyzed fusion in solid deuterium [completed], K. Ishida, Y. Matsuda (*RIKEN*), K. Nagamine, K. Shimomura, A. Toyoda (*KEK*), S.N. Nakamura (*Tohoku U.*)
881. Magnetism of Ce-based heavy fermion superconductor [active], W. Higemoto, R. Kadono, A. Koda, K. Ohishi (*KEK-IMSS*), K. Ishida, Y. Kawasaki, Y. Kitaoka (*Osaka U.*), C. Geibel, F. Steglich (*Max-Planck Inst.*)
882. μ SR studies of unconventional superconductivity in an organic superconductor $(\text{TMTSF})_2\text{ClO}_4$ [active], I.M. Gat, M.I. Larkin, A. Savici, Y.J. Uemura (*Columbia U.*), T. Ito (*Columbia U.-ETL*), P. Kyriakou, G.M. Luke, M. Rovers (*McMaster U.*), K.M. Kojima (*U. Tokyo*), P.M. Chaikin, I.J. Lee (*Princeton U.*), M.J. Naughton (*Boston Coll.*)
883. Muonium-substituted methyl and associated free radicals [active], J.-C. Brodovitch, B. McCollum, P.W. Percival (*SFU*), K. Ghandi (*UBC-TRIUMF*), I. McKenzie (*U. Stuttgart*)
884. μ SR studies on magnetic ground state of $S = 1/2$ kagomé spin system $\text{Cu}_3\text{V}_2\text{O}_7(\text{OH})\cdot 2\text{H}_2\text{O}$ [active], A. Fukaya, I.M. Gat, M.I. Larkin, A. Savici, Y.J. Uemura (*Columbia U.*), T. Ito (*CERC-AIST*), A. Keren (*Technion-Israel Inst. of Tech.*), P.P. Kyriakou, G.M. Luke, M.T. Rovers (*McMaster U.*), Z. Hiroi (*U. Tokyo*)
885. High-TF line-shape measurement of impurity-doped high- T_c cuprates [active], K.M. Kojima, Y. Kojima, Y. Maeda, T. Okamura, S. Uchida (*U. Tokyo*), I. Gat, T. Itoh, A. Kinkhabwala, M.I. Larkin, Y.J. Uemura (*Columbia U.*), G.M. Luke (*McMaster U.*), S.R. Dunsiger, R.F. Kiefl, R. Miller (*UBC*), J.E. Sonier (*Los Alamos Nat. Lab*)
886. Study of field dependent T_1 relaxation and coexistence of order parameters in the (anti)ferromagnetic ruthenate-cuprate superconductors $\text{RuSr}_2(\text{Gd}, \text{Eu}, \text{Y})\text{Cu}_2\text{O}_8$ [active], C. Bernhard (*Max Planck Inst.*), C. Niedermayer, V. Oehmichen (*U. Konstanz*), E.J. Ansaldo (*U. Saskatoon*), J.L. Tallon (*NZIRD*)
887. Search for broken time reversal symmetry in high temperature superconductors [active], P. Kyriakou, G.M. Luke, M. Rovers (*McMaster U.*), R.H. Heffner (*Los Alamos Nat. Lab*), M.I. Larkin, Y.J. Uemura (*Columbia U.*), J. Sonier (*SFU*), K.M. Kojima (*U. Tokyo*)
888. Test of delayed-muonium model for hydrocarbon liquids [completed], D.C. Walker (*UBC-TRIUMF*), H.A. Gillis (*St. Francis Xavier U.*), G.B. Porter (*UBC*), S. Karolczak (*Politechnika, Poland*)
889. Study of field induced gap in Cu benzoate [active], Y. Ajiro, T. Asano, Y. Inagaki (*Kyushu U.*), H. Nojiri (*Tohoku U.*), W. Higemoto, R. Kadono, A. Koda (*KEK-IMSS*)
890. Anisotropic Kondo effect in $\text{Ce}_{0.8}\text{La}_{0.2}\text{Al}_3$? [completed], D.E. MacLaughlin (*U. California, Riverside*), O.O. Bernal (*Cal. State U., Los Angeles*), R.H. Heffner (*Los Alamos Nat. Lab*), G.M. Luke (*McMaster U.*), G.J. Nieuwenhuys (*U. Leiden*), J.E. Sonier (*SFU*), B. Andraka (*U. Florida*)
891. Superconductivity and magnetism in $\text{Ce}_n\text{T}_m\text{In}_{3n+2m}$ [active], R.H. Heffner, G.D. Morris, J. Sarrao (*Los Alamos Nat. Lab*), J.E. Sonier (*SFU*), D.E. MacLaughlin (*U. California, Riverside*), G.J. Nieuwenhuys (*U. Leiden*), O.O. Bernal (*Cal. State U., Los Angeles*)
892. Resonance ionization spectroscopy of stable and radioactive nuclides at TISOL [deferred] F. Buchinger, J.E. Crawford, S. Gulick, J.K.P. Lee (*McGill U.*), K. Sharma (*U. Manitoba*), J. Pinard (*Lab Aimé Cotton, Orsay*)
893. Hyperfine field of Rb in the ferromagnets Fe, Ni, Co [active], P. Bricault, C.A. Davis, P.P.J. Delheij, B. Roberts, (*TRIUMF*), K. Nishimura (*Toyoma U.*), S. Ohya (*Niigata U.*), E. Rezaie (*UBC*)
894. Muonium kinetics and free radical formation in solutions of fullerenes [active], B. Addison-Jones (*Douglas College*), J.-C. Brodovitch, S. Kecman, I. McKenzie, P.W. Percival (*SFU*)
895. The vortex structure and magnetism of electron-doped cuprate superconductors [active], K.M. Kojima, S. Uchida (*U. Tokyo*), W. Higemoto, R. Kadono, A. Koda (*KEK*), M. Azuma, M. Fujita, M. Takano, K. Yamada (*Kyoto U.*), K. Ishida, Y. Kawasaki, Y. Kitaoka (*Osaka U.*), M.I. Larkin, Y.J. Uemura (*Columbia U.*)
896. Investigation of spin liquid behaviour in chromium and manganese spinels [completed], H. Dabkowska, J. Greedan, P.P. Kyriakou, G.M. Luke, M.T. Rovers (*McMaster U.*), I.M. Gat, M.I. Larkin, A.T. Savici, Y.J. Uemura (*Columbia U.*), K.M. Kojima (*U. Tokyo*)

897. Absolute magnetic penetration depth in the Meissner state of superconductors measured with low frequency beta-NMR [active], D. Bonn, J.H. Brewer, K.H. Chow, W. Hardy, R. Liang, R. Miller, G. Morris (*UBC*), S. Dunsiger, B. Heffner (*Los Alamos Nat. Lab*), R.F. Kiefl (*UBC-TRIUMF*), S. Kreitzman, P. Levy (*TRIUMF*), G. Luke (*McMaster U.*), J. Sonier (*SFU*), C. Stronach (*Virginia State U.*)
898. MULTI development with applications in superconductors and semiconductors [completed], P. Amadruz, D. Arseneau, S. Chan, K.H. Chow, B. Hitti, G. Morris, R. Poutissou (*TRIUMF*), J. Chakhalian, S. Dunsiger, R.F. Kiefl, R. Miller (*UBC*)
900. A determination of the $\alpha+^{15}\text{O}$ radiative capture rate by a measurement of the $^{15}\text{O}(^6\text{Li},d)^{19}\text{Ne}$ reaction [active], B.R. Fulton, B. Greenhalgh, J. Pearson, D.L. Watson (*U. York*), N.M. Clarke (*U. Birmingham*), T. Davinson, N. Farrington, P. Monroe, C. Ruiz, F. Sarazin, K. Schmidt, A.C. Shotter, P.J. Woods (*U. Edinburgh*), L. Buchmann, P. Walden (*TRIUMF*), J. D'Auria (*SFU*)
902. Muon capture on ^{45}Sc , ^{51}V , ^{55}Mn and ^{59}Co [active], D.F. Measday (*UBC*), T.P. Gorringer (*U. Kentucky*)
903. Spectroscopic study of ^{11}Be with polarized ^{11}Li beam [active], A. Hatakeyama, Y. Hirayama, H. Izumi, T. Shimoda, M. Yagi, H. Yano (*Osaka U.*), H. Miyatake (*IPNS, KEK*), K.P. Jackson, C.D.P. Levy (*TRIUMF*)
907. Improving $S_{E1}(300)$: the $\beta - \alpha$ branching ratio of ^{16}N [deferred] R.E. Azuma, J.D. King (*U. Toronto*), L. Buchmann (*TRIUMF*)
909. Isospin symmetry breaking in superallowed Fermi beta decays [active], C. Andreoiu, D. Bandyopadhyay, P. Finlay, P.E. Garrett, G.F. Grinyer, B.H. Hyland, A.A. Phillips, M.A. Schumaker, C.E. Svensson, J.J. Valiente-Dobón (*U. Guelph*), J.A. Cameron, J.C. Waddington (*McMaster U.*), A. Andreyev, G.C. Ball, P. Bricault, R.S. Chakrawarthy, G. Hackman, A.C. Morton, C.J. Pearson, M.B. Smith (*TRIUMF*), R.A.E. Austin (*St. Mary's U.*), J.C. Hardy, V.E. Jacob (*Texas A&M U.*), J.R. Leslie (*Queen's U.*), J.L. Woods, W.D. Kulp (*U. Georgia*), A. Piechaczek, E.F. Zganjar (*Louisiana State U.*), P.M. Walker (*U. Surrey*), F. Sarazin (*U. Colorado*), H.C. Scraggs (*U. Liverpool*), J. von Schwarzenberg (*U. Vienna*)
910. Study of the ground state proton emitter ^{73}Rb and implications for the astrophysical rp-process [active], A. Piechaczek, E.F. Zganjar (*Louisiana State U.*), G.C. Ball (*TRIUMF*), J.C. Batchelder (*Oak Ridge Assoc. U.*), D. Kulp, B.D. MacDonald, J.L. Wood (*Georgia Inst. Tech.*)
911. Test of aerogel proto-type detector for $G\theta$ phase II [active], J. Birchall, W. Falk, L. Lee, S. Page, W.D. Ramsay, A. Rauf, G. Rutledge, W.T.H. van Oers (*U. Manitoba*), C. Davis (*TRIUMF*), L. Hannelius, J. Martin (*Caltech*), E. Korkmaz, T. Porcelli (*UNBC*), S. Kox, G. Quemener, R. Tieulent (*ISN Grenoble*), D. Beck (*U. Illinois, Urbana*)
912. Formation, structure, and dynamics of muonium in GaAs studied by EF-ALC-RF $\mu^+\text{SR}$ [active], B. Hitti, S.R. Kreitzman (*TRIUMF*), K.H. Chow (*U. Alberta*), J.H. Brewer (*UBC*), D.G. Eshchenko (*U. Zurich-PSI*), V.G. Storchak (*Kurchatov Inst.*)
913. Photo-induced dynamics and reactivity of spin polarized ^8Li in semiconductors [active], K.H. Chow (*U. Alberta*), T. Beals, R.F. Kiefl, R.I. Miller (*UBC*), P. Amadruz, D. Arseneau, S. Daviel, B. Hitti, S.R. Kreitzman, P. Levy, R. Poutissou (*TRIUMF*), R.L. Lichti (*Texas Tech. U.*), G.D. Morris (*Los Alamos Nat. Lab*), C. Bommas (*U. Bonn*)
914. Zero-field μSR in Bi2212 and Bi2201 searching for effects related to the pseudo-gap [active], M. Greven, N. Kaneko, (*Stanford U.*), I.M. Gat, M.I. Larkin, P.L. Russo, A. Savici, Y.J. Uemura, emph(Columbia U.), G.M. Luke, G.J. MacDougall, C.R. Wiebe (*McMaster U.*), Y. Ando (*U. Tokyo*)
915. Muonium in semiconductor alloys [completed data-taking], R.L. Lichti (*Texas Tech. U.*), P.J.C. King (*Rutherford Appleton Lab*), I. Yonenaga (*Tohoku U.*)
916. QLCR of diamagnetic states in GaP [completed], R.L. Lichti, W. Nusbaum (*Texas Tech. U.*), K.H. Chow (*U. Alberta*), S.F.J. Cox (*Rutherford Appleton Lab*), B. Hitti (*TRIUMF*)
917. Correlation between magnetism and transport properties of thermoelectric oxides [active], H. Itahara, H. Nozaki (*Toyota Central R&D Labs Inc.*), E.J. Ansaldo (*TRIUMF*), H. Ikuta, U. Mizutani, T. Takami (*Nagoya U.*)
918. High field study of La_2CuO_4 based superconductors [active], I.M. Gat, M.I. Larkin, P.L. Russo, A. Savici, Y.J. Uemura (*Columbia U.*), G.M. Luke, G.J. MacDougall, C.R. Wiebe (*McMaster U.*), K.M. Kojima, S. Uchida (*U. Tokyo*), T. Ito (*AIST, Tsukuba*), Y.S. Lee (*Nat. Inst. Standards Technology*), K. Yamada (*Kyoto U.*), M. Greven, M. Kaneko (*Stanford U.*), M.A. Kastner (*MIT*), R.J. Birgeneau (*U. Toronto*), R. Kadono (*KEK*), S. Tajima (*ISTEC*)
919. Proton irradiation effects in SOI devices [active], P. Dodd, G. Hash, R. Loemker, J. Schwank, M. Shaneyfelt (*Sandia Nat. Lab*), V. Ferlet-Cavrois, P. Paillet (*CEA, France*)

65

41

65

71

920. Nuclear charge radii and moments of short lived neutron deficient Lanthanum isotopes [active], H.A. Schuessler (*Texas A&M U.*), P. Levy (*TRIUMF*), H. Iimura (*Japan Atomic Energy Res. Inst.*), F. Buchinger, J. Crawford, J. Lee (*McGill U.*), R.I. Thompson (*U. Calgary*)
921. High-K isomers in neutron-rich $A = 170\text{--}190$ nuclei [active], S. Ashley, G.A. Jones, P.M. Walker, S.J. Williams, (*U. Surrey*), A. Andreyev, G.C. Ball, P. Bricault, R.S. Chakrawarthy, E. Cunningham, J. Daoud, G. Hackman, C. Morton, C. Pearson, M.B. Smith (*TRIUMF*), C.E. Svensson (*U. Guelph*), P.E. Garrett (*U. Guelph-TRIUMF*), R. Austin (*St. Mary's U.*), J.C. Waddington (*McMaster U.*), E.F. Zganjar (*Louisiana State U.*), J. Becker (*Lawrence Livermore Nat. Lab*), F. Sarazin (*Colorado School of Mines*)
922. On the production of ^{26}Al in novae: measurement of the $^{25}\text{Al}(p,\gamma)^{26}\text{Si}$ reaction rate [pending], S. Bishop, A.A. Chen, J.M. D'Auria, D. Hunter, M. Lamey, C. Wrede (*SFU*), L. Buchmann, D.A. Hutcheon, K.P. Jackson, A. Olin, J. Rogers (*TRIUMF*), S. Engel (*Ruhr-U. Bochum*), C.S. Galovich (*U. Northern Colorado*), D. Gigliotti, A. Hussein (*UNBC*), U. Greife, C.C. Jewett (*Colorado School of Mines*), J. José (*UPC/IEEC Barcelona*), P.D. Parker (*Yale U.*)
923. Measurement of $^{25}\text{Al} + p$ resonances through elastic scattering [active], A.A. Chen, J.M. D'Auria (*SFU*), L. Buchmann, F. Sarazin, A. Shotter, P. Walden (*TRIUMF*), T. Davinson, A. Murphy, I. Roberts, A. Robinson, C. Ruiz, P. Woods (*U. Edinburgh*), B. Fulton, D. Groombridge, J. Pearson (*U. York*), P.D. Parker (*Yale U.*)
924. The hot CNO cycle and the $^{14}\text{O}(\alpha,p)^{17}\text{F}$ reaction [active], M. Aliotta, T. Davinson, A. Murphy, I. Roberts, A. Robinson, P.J. Woods (*U. Edinburgh*), L. Buchmann, A. Chen, P. Walden (*TRIUMF*), B. Fulton, D. Groombridge, J. Pearson (*U. York*), P. Leleux (*U. Catholique de Louvain*), R. Azuma (*U. Toronto*)
925. Isospin mixing in ^{36}Ar via spin-polarized observables in $^{36}\text{K} \beta^+$ decay [active], J.M. D'Auria, D. Melconian (*SFU*), G.C. Ball, J.A. Behr, P. Bricault, M. Dombisky, K.P. Jackson (*TRIUMF*), S. Gu, M. Pearson (*UBC*), W.P. Alford (*U. Western Ontario*), D.A. Ashery, O. Aviv (*Tel Aviv U.*), I.A. Towner (*Queen's U.*), S. Karataglidis (*Los Alamos Nat. Lab*), B.A. Brown (*Michigan State U.*)
926. Measurement of charge radius and β^+ -decay Q-value of laser-trapped ^{74}Rb [active], S. Gu, M. Pearson (*UBC*), J.A. Behr, P. Bricault, M. Dombisky, K.P. Jackson (*TRIUMF*), D. Melconian (*SFU*), D.A. Ashery, O. Aviv (*Tel Aviv U.*)
927. Using ($^3\text{He},p$): spectroscopy of proton unbound ^{19}Na [active], G.C. Ball, L. Buchmann, G. Hackman, A. Laird, F. Sarazin, A. Shotter, P. Walden (*TRIUMF*), A.A. Chen (*SFU*), T. Davinson, I. Roberts, A. Robinson, C. Ruiz, P. Woods (*U. Edinburgh*), B. Fulton, D. Groombridge, J. Pearson (*U. York*), C.E. Svensson (*U. Guelph*), J. Waddington (*McMaster U.*)
928. Level structure of ^{21}Mg : nuclear and astrophysical implications [active], M. Aliotta, T. Davinson, A.St.J. Murphy, A. Robinson, P.J. Woods (*U. Edinburgh*), J.M. D'Auria (*SFU*), R. Azuma (*U. Toronto*), R. Boyd (*Ohio State U.*), L. Buchmann, A. Chen, D. Hutcheon, A. Laird, P. Walden (*TRIUMF*), B. Fulton (*U. York*)
929. Octupole deformation and spin-exchange polarization of odd- A radon isotopes: toward radon electric dipole moment measurements at ISAC [active], P. Finlay, B. Hyland, A.A. Phillips, M.A. Schumaker, C.E. Svensson (*U. Guelph*), T.E. Chupp, K.P. Coulter, S.R. Nuss-Warren, E.R. Tardiff (*U. Michigan*), G.C. Ball, J.A. Behr, G.S. Hackman, M.R. Pearson, M.B. Smith (*TRIUMF*), M.E. Hayden, T. Warner (*SFU*)
930. Measurement of π^- absorption in water [completed data-taking], T. Awes, V. Cianciolo, G. Young (*Oak Ridge Nat. Lab*), S. Berridge, W. Bugg, Yu. Efremenko, R. Gearhart, Yu. Kamyshev, S. Ovchinnikov (*U. Tennessee*), Yu. Davydov, T. Numao, J.-M. Poutissou (*TRIUMF*)
931. Magnetic properties of multinuclear, open-shell coordination complexes and polymers probed by μSR [active], F.D. Callaghan, N. Draper, C.V. Kaiser, M. Laulajainen, J. LeFebvre, D.B. Leznoff, C. Shorrock, J.E. Sonier (*SFU*)
932. Improving μ^- SR performance [active], J.H. Brewer, A.M. Froese, R. Moldovan (*UBC*), K. Ghandi (*UBC-TRIUMF*), B.A. Fryer (*Sechelt Secondary School*),
933. Effects of nonlocality in superconductors [completed data-taking], R. Miller, R. Kiefl (*UBC-TRIUMF*), S.L. Bud'ko, P. Canfield, V. Kogan (*Iowa State U.*), P. Poon, J.E. Sonier (*SFU*)
934. μSR study of polymerized C_{60} [active], A. Fukaya, I.M. Gat, P.L. Russo, A.T. Savici, Y.J. Uemura (*Columbia U.*), P. Kyriakou, G.M. Luke (*McMaster U.*), T. Makarova, B. Sundqvist (*Umea U. Sweden*), V.A. Davydov (*Moscow Inst. High Pressure*), T. Ito (*AIST, Tsukuba*)
935. High pressure study of URu_2Si_2 [active], J. Garrett, P. Kyriakou, G.M. Luke, C. Wiebe (*McMaster U.*), I.M. Gat, A. Savici, Y.J. Uemura (*Columbia U.*), Y. Sushko (*U. Kentucky*), K.M. Kojima (*U. Tokyo*)

936. Magnetic dynamics in spin ice systems [active], S.T. Bramwell, J. Lago (*U. College London*), S.R. Dunsiger (*Los Alamos Nat. Lab*), J.S. Gardner (*NRC*), M.J.P. Gingras (*U. Waterloo*), R. Kiefl (*UBC-TRIUMF*), G.M. Luke (*McMaster U.*)
937. Muonium in hexagonal semiconductors [active], R.L. Lichti (*Texas Tech. U.*), K.H. Chow (*U. Alberta*), S.F.J. Cox (*Rutherford Appleton Lab*), B. Hitti (*TRIUMF*)
938. Muonium formation and ionization in semiconductors and insulators [active], J.H. Brewer, A.M. Froese, R. Moldovan, S.L. Stubbs, A.G. Uy (*UBC*), B. Hitti (*TRIUMF*), Z.M. Salman (*TRIUMF-UBC*), R. Lichti (*Texas Tech. U.*), D.G. Eshchenko (*PSI*), B.A. Aronzon, V.G. Storchak (*Kurchatov Inst.*), S.P. Cottrell (*Rutherford Appleton Lab*) 78
939. Guest-host interactions and Hfcs of mu-radicals in zeolites [active], M. Bridges, D.G. Fleming, C. Fyfe, G. Patey, A. Wang (*UBC*), D. Arseneau (*TRIUMF*), K. Ghandi (*TRIUMF-UBC*), E. Roduner (*U. Stuttgart*), M. Senba (*Dalhousie U.*)
940. Thermoelectrics II: μ SR in layered manganese oxides [completed data-taking], K. Dohmae, H. Itahara, Y. Seno, J. Sugiyama, T. Tani, C. Xia (*Toyota Central R&D Labs Inc.*), J.H. Brewer (*UBC*), E.J. Ansaldo (*U. Saskatchewan*), B. Hitti (*TRIUMF*)
941. Investigation of spin dynamics in geometrically frustrated transition metal oxides [active], J.E. Greedan, G.M. Luke, G. MacDougall, C.R. Wiebe (*McMaster U.*), P. Russo, A. Savici, Y.J. Uemura (*Columbia U.*)
942. Magnetic fluctuations near metal insulator transitions in ruthenate pyrochlores [active], N. Hur, K.H. Kim, J. Thompson (*Los Alamos Nat. Lab*), S.R. Dunsiger (*McMaster U.*), R.F. Kiefl (*UBC-TRIUMF*), K.H. Chow (*U. Alberta*), M.J.P. Gingras (*U. Waterloo*), Z. Salman (*UBC*), F. Callaghan (*SFU*), S.W. Cheong, (*Rutgers U.-Lucent Tech.*), G.D. Morris (*TRIUMF*) 80
943. Muonium and muoniated free radical formation and reactivity in sub- and supercritical carbon dioxide [active], D.J. Arseneau (*TRIUMF*), M. Bridges (*UBC-TRIUMF*), D.G. Fleming, K. Ghandi, G. Patey, A. Wang (*UBC*), M. Pinto (*SFU*)
944. Muonium sites and dynamics in silicon carbide [active], H. Bani-Salameh, B.R. Carroll, B. Coss, R.L. Lichti, D.L. Stripe (*Texas Tech. U.*), K.H. Chow, (*U. Alberta*), S.F.J. Cox (*Rutherford Appleton Lab*) 81
945. Muoniated radicals formed from carbenes and carbene analogues [active], J.-C. Brodovitch, J.A.C. Clyburne, D. Dickie, B. McCollum, P.W. Percival, T. Ramnial (*SFU*), I. McKenzie (*U. Stuttgart*), K. Ghandi (*UBC-TRIUMF*) 82
946. Energy generation and nucleosynthesis in the HotCNO cycles: measurement of the $^{17}\text{F}(p, \gamma)^{18}\text{Ne}$ reaction rate [active], A.A. Chen (*McMaster U.-TRIUMF*), S. Bishop, J.M. D'Auria, M. Lamey, C. Wrede (*SFU*), L. Buchmann, D.A. Hutcheon, A. Olin, D. Ottewell, J. Rogers (*TRIUMF*), S. Engel (*Ruhr-Universität Bochum*), D. Gigliotti, A. Hussein (*UNBC*), U. Greife, C.C. Jewett (*Colorado School of Mines*), J. José (*UPC/IEEC Barcelona*), P.D. Parker (*Yale U.*)
947. Evaluation of the competition between single-step and multi-step γ decay in the $^{12}\text{C}(^{12}\text{C}, \gamma)$ reaction [active], T. Brown, S.P. Fox, B.R. Fulton, D. Groombridge, D.G. Jenkins, J. Pearson, R. Wadsworth, D.L. Watson (*U. York*), L. Buchmann, C. Davis, D. Hutcheon, S. Park, J. Rogers (*TRIUMF*), J.M. D'Auria (*SFU*), U. Greife (*Colorado School of Mines*), M.P. Carpenter, R.V.F. Janssens, T.L. Khoo, C.J. Lister, A.H. Wuosmaa (*Argonne Nat. Lab*), M. Freer (*U. Birmingham*), F. Azaiez, C. Beck, F. Haas, P. Papka, A. Sanchez (*IREs Strasbourg*), C. Andreoiu, M. Chartier, R.-D. Herzberg (*U. Liverpool*)
948. Proton radiation effects in silicon-on-insulator and bulk-silicon devices [active], P. Dodd, G. Hash, R. Jones, J. Schwank, M. Shaneyfelt (*Sandia Nat. Labs*), V. Ferlet-Cavroi, C. D'Hose, P. Paillet, J.-E. Sauvestre (*CEA, France*), E. Blackmore (*TRIUMF*)
949. μ SR study of magnetic order in high- T_c superconductor under high pressure [active], J. Arai, T. Goko, K. Sato, S. Takeshita (*Tokyo U. of Science*), W. Higemoto, K. Nagamine, K. Nishiyama (*KEK-MSL*) 85
950. High field study of Zn doped/Eu doped/overdoped systems [active], I.M. Gat, M.I. Larkin, P.L. Russo, A. Savici, Y.J. Uemura (*Columbia U.*), G.M. Luke, G.J. MacDougall, C.R. Wiebe (*McMaster U.*), K.M. Kojima, S. Uchida (*U. Tokyo*), T. Ito (*AIST, Tsukuba*), Y.S. Lee (*Nat. Inst. Standards Technology*), K. Yamada (*Kyoto U.*), M. Greven, M. Kaneko (*Stanford U.*), M.A. Kastner (*MIT*), R.J. Birgeneau (*U. Toronto*), R. Kadono (*KEK*), S. Tajima (*ISTEC*)
951. Magnetism and flux line lattice structure of oxychloride superconductors [active], W. Higemoto, R. Kadono, A. Koda, K. Ohishi (*KEK-IMSS*), M. Azuma, M. Takano, I. Yamada (*Kyoto U.*), K.M. Kojima (*U. Tokyo*) 87

952. $^{12}\text{C}(\alpha, \gamma)^{16}\text{O}$ at DRAGON [active], C. Barbieri, L. Buchmann, D. Hutcheon, A.M. Laird, A. Olin, M. Pavan, J. Rogers, C. Ruiz, F. Sarazin, J.M. Sparenberg (*TRIUMF*), C.R. Brune (*U. Ohio*), A. Chen (*McMaster U.*), J.M. D'Auria (*SFU*), J. Görres, M. Wiescher (*U. Notre Dame*), U. Greife (*Colorado School of Mines*), A. Hussein (*UNBC*), Z. Li, W. Liu (*Chinese Inst. of Atomic Energy*), A. Murphy (*U. Edinburgh*), S. Woosley (*U. California, Santa Cruz*), H.O. Meyer (*IUCF*)
953. Spin dynamics and quantum coherence in molecular magnets [active], Z. Salman (*TRIUMF*), A. MacFarlane, R. Kiefl (*UBC-TRIUMF*), K. Chow (*U. Alberta*), S. Dunsiger (*Los Alamos Nat. Lab*), B. Barbara (*Lab de Magnetisme Louis Néel*)
954. Half-lives of long-lived isotopes/chronology and environment [active] R.A.E. Austin, A. Chen, K.A. Koopmans, M. Lee, N. Novo, B. Singh, J.C. Waddington (*McMaster U.*), G.C. Ball, G. Hackman, F. Sarazin, H. Scraggs, M.B. Smith (*TRIUMF*), P.E. Garrett (*Lawrence Livermore Nat. Lab*), G. Grinyer, C.E. Svensson (*U. Guelph*)
955. Probing shell structure with β - and β -*n*-delayed γ spectroscopy [active], G.C. Ball, P. Bricault, M. Dombisky, G. Hackman, J. MacDonald, F. Sarazin, H. Scraggs, M.B. Smith (*TRIUMF*), G. Grinyer, C.E. Svensson (*U. Guelph*), J.C. Waddington (*McMaster U.*), E. Zganjar (*Louisiana State U.*), W.D. Kulp, J. Wood (*Georgia Inst. Tech.*), P.E. Garrett (*Lawrence Livermore Nat. Lab*), P. Walker (*U. Surrey-TRIUMF*)
956. Search for tensor interactions in recoil nucleus singles in decay of polarized ^{80}Rb [active], J.A. Behr, P. Bricault, M. Dombisky, K.P. Jackson, M.R. Pearson (*TRIUMF*), A. Gorelov, D. Melconian (*SFU*), D. Ashery (*Tel Aviv U.*), R. Pitcairn, E. Prime, D. Roberge (*UBC*), G. Gwinner (*U. Manitoba*) 44
957. Search for high-spin isomeric states in the vicinity of double-magic $N = Z$ ^{100}Sn [active], G.C. Ball, G.S. Hackman, F. Sarazin, H.C. Scraggs, M.B. Smith (*TRIUMF*), P.M. Walker (*U. Surrey*), C.E. Svensson (*U. Guelph*), J.C. Waddington (*McMaster U.*), E. Zganjar (*Louisiana State U.*), P.E. Garrett (*Lawrence Livermore Nat. Lab*), J.L. Wood (*Georgia Inst. Tech.*)
958. HTF- μ^+ SR lineshapes in overdoped high- T_c superconductors [active], D.A. Bonn, J.H. Brewer, M. Franz, W.N. Hardy, R.F. Kiefl, R.X. Liang, W.A. MacFarlane (*UBC*), F. Callaghan, K.F. Poon, J.E. Sonier (*SFU*), J. Chakhalian, Z. Salman (*TRIUMF*), S. Kim, G.M. Luke (*McMaster U.*), N.N. Kolesnikov (*Russian Acad. of Science*), C.E. Stronach (*Virginia State U.*)
959. New low field integral method for studies of diamagnetic muonium centers in group IV and II-VI semiconductors [active], K.H. Chow, K. Hoffman (*U. Alberta*), B. Hitti (*TRIUMF*), J.M. Gil (*U. Coimbra*), R.F. Kiefl (*UBC*)
960. Hydrogen (μ) defect level in II-VI chalcogenides [active], H.V. Alberto, N. Ayres de Campos, J.P. Duarte, J.M. Gil, R.C. Vilao (*U. Coimbra*), K.H. Chow (*U. Alberta*), S.F.J. Cox (*Rutherford Appleton Lab*), B. Hitti (*TRIUMF*), R.L. Lichti (*Texas Tech. U.*), A. Weidinger (*HMI/Berlin*) 88
961. $A \geq 62$ super-allowed Fermi β decays: constraining unknown corrections with ^{66}As and ^{70}Br decay [active], P.E. Garrett, W.E. Ormand, A. Schiller (*Lawrence Livermore Nat. Lab*), G.F. Grinyer, C.E. Svensson (*U. Guelph*), R.A.E. Austin, J.C. Waddington (*McMaster U.*), G.C. Ball, G. Hackman, F. Sarazin, H.C. Scraggs, M.B. Smith (*TRIUMF*), J. Allmond, W.D. Kulp, J.L. Wood (*Georgia Inst. Tech.*), A. Piechaczek, E. Zganjar (*Louisiana State U.*)
962. μ SR study on $\text{Na}_{0.33}\text{V}_2\text{O}_5$ [active], P.L. Russo, A.T. Savici, Y.J. Uemura (*Columbia U.*), G.M. Luke, C.R. Wiebe (*McMaster U.*), Y. Ueda, T. Yamauchi (*ISSP U. Tokyo*)
963. Underdoped/undoped cuprate single crystals [active], D.A. Bonn, J.H. Brewer, W.N. Hardy, R.F. Kiefl, R.X. Liang (*UBC*), F. Callaghan, K.F. Poon, J.E. Sonier (*SFU*), G.M. Luke (*McMaster U.*), R.L. Greene (*Maryland U.*), P. Fournier (*U. Sherbrooke*), C.E. Stronach (*Virginia State U.*), R.I. Miller (*Pennsylvania State U.*)
964. A study of the partial and total cross sections of the $^8\text{Li}(\alpha, n)^{11}\text{B}$ reaction at astrophysically relevant energies [deferred], L. Buchmann, A.C. Shotter, P. Walden (*TRIUMF*), R. Boyd, D. Reitzner (*Ohio State U.*), A.A. Chen (*McMaster U.*), J.M. D'Auria (*SFU*), B. Fulton, A.M. Laird (*U. York*), U. Greife, F. Sarazin (*Colorado School of Mines*) D. Hutcheon (*TRIUMF-U. Alberta*), Z. Li (*Chinese Inst. of Atomic Energy*), A. Murphy (*U. Edinburgh*), S. Nishimura (*RIKEN*), 47
965. Investigation of spin statics and dynamics in the new dipolar spin ice $\text{Ho}_2\text{Ru}_2\text{O}_7$ [active], J.E. Greedan, S.J. Kim, G.M. Luke, G. MacDougall, C.R. Wiebe (*McMaster U.*), M.J.P. Gingras (*U. Waterloo*), P. Russo, A. Savici, Y.J. Uemura (*Columbia U.*)
966. High precision mass determination for CVC tests [active], P. Bricault, J. Dilling, J. Vaz (*TRIUMF*), K. Sharma (*U. Manitoba*), M. Trinczek (*MPI-K-TRIUMF*), M. Smith (*UBC-TRIUMF*), F. Buchinger, J. Crawford, J. Lee, R.B. Moore (*McGill U.*)
967. Beta decay branching ratio of ^{21}Na [active], S.J. Freedman (*UC Berkeley-LBNL*), P.A. Vetter (*Lawrence Berkeley Nat. Lab*), A.A. Kwiatkowski, R. Maruyama (*U. California, Berkeley*)

968. Ortho-para effect of muon catalyzed fusion in liquid deuterium [active], N. Kawamura, K. Nagamine, A. Toyoda (*KEK*), H. Imao (*U. Tokyo-KEK*), K. Ishida, T. Matsuzaki (*RIKEN*)
969. Metamagnetic transitions and quantum critical behavior [active], S.R. Dunsiger, R.H. Heffner, G.D. Morris (*Los Alamos Nat. Lab*), D.E. MacLaughlin (*U. California, Riverside*), O.O. Bernal (*California State U.*), G.J. Nieuwenhuys (*U. Leiden*)
971. Precise measurement of the quadrupole moments of $^{20,21,25}\text{Na}$ [active], R. Baartman, J. Behr, P. Bricault, M. Dombbsky, P. Jackson, P. Levy, M. Pearson (*TRIUMF*), M. Fukuda, K. Matsuta, M. Mihara, T. Minamisono, T. Nagatomo, M. Ogura, T. Sumikama (*Osaka U.*), R. Kiefl (*UBC*), K. Koshigiri (*Osaka Kyoiku U.*), K. Minamisono (*JSPS-TRIUMF*), M. Morita (*Josai Int. U.*)
972. Meson and quark effects in the nuclear β decay of ^{20}F [active], R. Baartman, J. Behr, P. Bricault, M. Dombbsky, P. Jackson, P. Levy, M. Pearson (*TRIUMF*), M. Fukuda, K. Matsuta, M. Mihara, T. Minamisono, T. Nagatomo, M. Ogura, T. Sumikama (*Osaka U.*), R. Kiefl (*UBC*), K. Koshigiri (*Osaka Kyoiku U.*), K. Minamisono (*JSPS-TRIUMF*), M. Morita (*Josai Int. U.*)
973. Study of coexisting collective phases far from stability: systematic decay spectroscopy of the $N = 90$ isotones [active], W.D. Kulp, J.L. Wood (*Georgia Inst. Tech.*), E. Zganjar (*Louisiana State U.*), J. von Schwarzenberg (*U. Vienna*), D.J. Rowe (*U. Toronto*), P.E. Garrett (*U. Guelph-TRIUMF*), K.S. Krane (*U. Oregon*), C.E. Svensson (*U. Guelph*), R.A.E. Austin (*St. Mary's U.*), A. Andreyev, G.C. Ball, P. Bricault, R.S. Chakrawarthy, E. Cunningham, J. Daoud, G. Hackman, C. Morton, C. Pearson, M.B. Smith (*TRIUMF*), J. Becker (*Lawrence Livermore Nat. Lab*), C. Mattoon, F. Sarazin (*Colorado School of Mines*), J. Ressler (*SFU*)
974. μSR experiments on superconductivity and magnetism in the new layered oxide $\text{Na}_{0.35}\text{CoO}_2 \cdot y\text{H}_2\text{O}$ [active], C.R. Wiebe (*McMaster U.-Columbia U.*), S.J. Kim, G.M. Luke, G. MacDougall (*McMaster U.*), P. Russo, A. Savici, Y.J. Uemura (*Columbia U.*), J.E. Sonier (*SFU*)
975. Magnetism and superconductivity in $\text{Na}_x\text{CoO}_2 \cdot y\text{H}_2\text{O}$ and related cobalt oxides [active], W. Higemoto, R. Kadono, A. Koda, K. Ohishi (*KEK-IMSS*), S.R. Saha, H. Sakurai, K. Takada, E. Takayama-Muromachi (*NIMS, Japan*)
976. μSR study of strongly correlated electron behavior in filled skutterudite compounds [active], W. Higemoto, R. Kadono, A. Koda, K. Ohishi (*KEK-IMSS*), Y. Aoki, S.R. Saha, H. Sato, H. Sugawara (*Tokyo Metropolitan U.*)
977. Magnetism and superconductivity in spinel oxides [active], W. Higemoto, R. Kadono, A. Koda, K. Ohishi (*KEK-IMSS*), M. Isobe, Y. Ueda (*ISSP U. Tokyo*)
978. Magnetism in organic chiral compounds [active], W. Higemoto, R. Kadono, A. Koda, K. Ohishi (*KEK-IMSS*), H. Imai, K. Inoue (*IMS Okazaki Nat. Res. Inst.*)
979. Magnetism of equiatomic ternary uranium compounds [active], G.M. Kalvius (*Tech. U. Munich*), H. Nakotte (*New Mexico State U.*), D.R. Noakes, C.E. Stronach (*Virginia State U.*), R. Wäppling (*Uppsala U.*)
980. Quantum impurities in spin ladder compounds [active], I. Affleck (*Boston U.*), J. Brewer, R.F. Kiefl, W.A. MacFarlane (*UBC*), J. Chakhalian, Z. Salman (*TRIUMF*), S. Eggert (*Chalmers U.*), K. Kojima (*Tokyo U.*), Y.J. Uemura (*Columbia U.*)
981. Photoinduced magnetism in Prussian blue analogs [active], J. Chakhalian, Z. Salman (*TRIUMF*), R. Kiefl, A. MacFarlane, T. Parolin, D. Wang (*UBC*), K. Chow (*U. Alberta*), D. Leznoff, J. Sonier (*SFU*)
982. μSR study of the superferromagnetic transition in clinoptacumite [active], T. Mori, X.G. Zheng (*Saga U.*), W. Higemoto, K. Nishiyama (*KEK-MSL*)
983. Direct measurement of astrophysical $^{11}\text{C}(p, \gamma)^{12}\text{N}$ reaction at DRAGON [active], Z.H. Li, W.P. Liu (*China Inst. of Atomic Energy*), J.M. D'Auria (*SFU*), L. Buchmann, D. Hutcheon, A. Laird, A. Olin, J. Rogers, C. Ruiz (*TRIUMF*), A.A. Chen (*McMaster U.*), J. Caggiano, A. Parikh, P. Parker (*Yale U.*), X.D. Tang (*Argonne Nat. Lab*)
984. Fast lifetime measurements with the 8π spectrometer and nuclear structure below $N = 82$ [active], J.A. Becker (*Lawrence Livermore Nat. Lab*), H. Mach (*Uppsala U.*), C. Andreoiu, D. Bandyopadhyay, P.E. Garrett, G.F. Grinyer, B. Hyland, A. Phillips, M. Schumaker, C.E. Svensson (*U. Guelph*), J.C. Waddington (*McMaster U.*), G.C. Ball, R.S. Chakrawarthy, G. Hackman, A.C. Morton, C.J. Pearson (*TRIUMF*), W.D. Kulp, J.L. Wood (*Georgia Inst. Tech.*), E. Zganjar (*Louisiana State U.*), J. von Schwarzenberg (*U. Vienna*), F. Sarazin (*Colorado School of Mines*), J. Ressler (*SFU*), P.M. Jenneson, P.H. Regan, S.J. Williams (*U. Surrey*), R.A.E. Austin (*St. Mary's U.*)
985. Half-life and branching-ratio measurement of ^{18}Ne superallowed fermi β decay [active], A.N. Andreyev, G.C. Ball, P. Bricault, R.S. Chakrawarthy, G. Hackman, A.C. Morton, C.J. Pearson, M.B. Smith (*TRIUMF*), R.A.E. Austin (*St. Mary's U.*), J.R. Leslie (*Queen's U.*), F. Sarazin (*Colorado School of Mines*), C. Andreoiu, P. Finlay,

48

49

51

- P.E. Garrett, G.F. Grinyer, B. Hyland, A.A. Phillips, M.A. Schumaker, C.E. Svensson, J.J. Valiente-Dobón (*U. Guelph*), J.L. Wood (*Georgia Inst. Tech*), E.F. Zganjar (*Louisiana State U.*), J.J. Daoud, S.J. Williams (*U. Surrey*) 52
986. Proton irradiation effects in advanced semiconductor technologies [active], P. Dodd, G. Hash, J. Schwank, M. Shaneyfelt (*Sandia Nat. Lab*), C. D'Hose, V. Ferlet-Cavroi, P. Paillet, J.-E. Sauvestre (*CEA, France*), E. Blackmore (*TRIUMF*)
987. Collinear resonant ionization spectroscopy near proton drip line [deferred], L. Blomeley, F. Buchinger, T. Cocolios, J.E. Crawford, S. Gulick, J.K.P. Lee, R.B. Moore (*McGill U.*), J. Dilling, P. Levy, M. Pearson (*TRIUMF*), G. Gwinner, K. Sharma (*U. Manitoba*), R. Thompson (*U. Calgary*), H. Schuessler (*TAMU, Texas*), J. Billowes, P. Campbell, B.W. Tordoff (*U. Manchester*), F. Ibrahim, F. Le Blanc, J. Sauvage, R. Sifi (*IPN Orsay*), J. Pinarid (*LAC Orsay*)
988. Lifetime measurements in the rare-earth neutron-rich region using FEST [active], J.J. Ressler (*Yale U.-SFU*), R.F. Casten, E.A. McCutchan, N.V. Zamfir (*Yale U.*), D.S. Brenner (*Clark U.*), J.M. D'Auria (*SFU*), G. Ball, G. Hackman (*TRIUMF*), P.E. Garrett (*Lawrence Livermore Nat. Lab*), J.L. Wood (*Georgia Inst. Tech.*), R.E.A. Austin, J. Waddington (*McMaster U.*), C. Svensson (*U. Guelph*), E.F. Zganjar (*U. Louisiana*), A.A. Hecht (*Argonne Nat. Lab*)
989. Astrophysical studies using ^{26}Al ground-state and isomeric beams [active], C. Ruiz (*SFU-TRIUMF*), C. Angulo (*CRC Louvain-la-Neuve*), R.E. Azuma, J.D. King (*U. Toronto*), L. Buchmann, J. Caggiano, B. Davids, D.A. Hutcheon, A. Olin, J. Rogers (*TRIUMF*), A. Chen, C. Van Ouellet (*McMaster U.*), J.M. D'Auria (*SFU*), U. Greife, C.C. Jewett, F. Sarazin (*Colorado School of Mines*), A. Hussein, C. Iliadis (*UNBC*), J. Jose (*UPC/IEEC Barcelona*), A.M. Laird (*U. York*), A.S. Murphy (*U. Edinburgh*), P. Parker (*Yale U.*), A. Shotter (*TRIUMF-U. Alberta*) 53
990. Resonant elastic scattering of isomeric ^{26}Al on protons [active], C. Ruiz (*SFU-TRIUMF*), C. Angulo (*CRC Louvain-la-Neuve*), M. Aliotta, T. Davinson, A.S. Murphy, P.J. Woods (*U. Edinburgh*), R.E. Azuma, J.D. King (*U. Toronto*), L. Buchmann, B. Davids, P. Walden (*TRIUMF*), A. Chen, J. Pearson, C. Van Ouellet (*McMaster U.*), J.M. D'Auria (*SFU*), B.R. Fulton, D. Groombridge, A.M. Laird (*U. York*), F. Sarazin (*Colorado School of Mines*), A. Shotter (*TRIUMF-U. Alberta*)
991. Laser spectroscopic determination of the ^{11}Li charge radius [active], B. Bushaw (*Pacific Northwest Nat. Lab*), A. Dax (*PSI*), G.W.F. Drake (*U. Windsor*), G. Ewald, R. Kirchner, H.-J. Kluge, Th. Kuhl (*GSI Darmstadt*), A. Gluzicka (*Warsaw U.*), P. Bricault, J. Dilling, M. Domsbky, J. Lassen, P. Levy, M. Pearson (*TRIUMF*), W. Nörtershäuser, C. Zimmermann (*U. Tübingen*), G. Gwinner (*U. Manitoba*)
992. Lifetime of the 4.033 MeV state in ^{19}Ne [active], G.C. Ball, R.S. Chakrawarthy, B. Davids, G. Hackman, R. Kanungo, P. Walden (*TRIUMF*), J.S. Forster (*U. Montréal*), A.M. Laird (*U. York*), H. Leslie (*Queen's U.*), C. Ruiz (*TRIUMF-SFU*), A. Shotter (*TRIUMF-U. Alberta*), M. Subramanian (*UBC*) 54
993. Coulomb excitation of neutron rich beams with TIGRESS and the Si array [active], R.A.E. Austin, A.A. Chen, J.C. Waddington (*McMaster U.*), F. Sarazin (*Colorado School of Mines*), C. Andreoiu, G.F. Grinyer, C.E. Svensson (*U. Guelph*), G.C. Ball, G.S. Hackman, M.B. Smith (*TRIUMF*), T. Drake (*U. Toronto*), P. Garrett (*Lawrence Livermore Nat. Lab*), J.J. Ressler (*SFU*), P.M. Walker (*U. Surrey*)
994. On the rp-process bottleneck at $A = 56$: Coulomb excitation of ^{58}Zn at ISAC-II [active], R.A.E. Austin, A.A. Chen, J.C. Waddington (*McMaster U.*), C. Andreoiu, C.E. Svensson (*U. Guelph*), G.C. Ball, B. Davids, G. Hackman (*TRIUMF*), J.J. Ressler (*SFU*), F. Sarazin (*Colorado School of Mines*)
995. An alternate approach to radioactive beam production for volatile elements: proof-of-principle [active], J.M. D'Auria, S. Lapi (*SFU*), K. Buckley, K. Jayamanna, T.J. Ruth (*TRIUMF*), C. Ruiz, M. Trinczek (*TRIUMF-SFU*) 56
996. Nova observables – ^{18}F abundance and the $^{18}\text{F}(p, \alpha)^{15}\text{O}$ reaction [active], T. Brown, S. Fox, B. Fulton, D. Groombridge, A.M. Laird (*U. York*), M. Aliotta, P. Davinson, A. Murphy, P. Woods (*U. Edinburgh*), C. Angulo (*CRC Louvain-la-Neuve*), L. Buchmann, B. Davids, C. Ruiz, A. Shotter, P. Walden (*TRIUMF*), J. Jose (*UPC/IEEC Barcelona*), F. Sarazin (*Colorado School of Mines*)
997. μSR study on the magnetic structures in $\text{Cu}_{1-x}\text{Li}_x\text{O}$ [active], T. Mori, X.G. Zheng (*Saga U.*), W. Higemoto, K. Nishiyama (*KEK-MSL*)
998. Muon spin relaxation and dynamic scaling in novel magnetic materials [active], J.E. Anderson, D.E. MacLaughlin, L. Shu (*U. California, Riverside*), R.H. Heffner, T. Kimura, G.D. Morris, J.L. Sarrao (*Los Alamos Nat. Lab*), F. Callaghan, J.E. Sonier (*SFU*), O.O. Bernal (*Cal. State U., Los Angeles*), J.S. Kim, G.R. Stewart (*U. Florida*), N. Frederick, M.B. Maple, W.M. Yuhasz, (*U. California, San Diego*) 89

999. Local magnetic properties in Pu and Pu-based alloys [active], B. Chung, M. Fluss (*Lawrence Livermore Nat. Lab*), R. Heffner, J. Lashley, G.D. Morris, J. Sarrao (*Los Alamos Nat. Lab*), D. MacLaughlin (*U. California, Riverside*)
1000. Measurements of the vortex core size in type-II superconductors [active], F.D. Callaghan, C. Kaiser, M. Laulajainen, J.E. Sonier (*SFU*), D. Bonn, J.H. Brewer, W.N. Hardy, R. Liang (*UBC*), G.M. Luke (*McMaster U.*), R.I. Miller (*TRIUMF*), 90
1001. Defect levels and μ^0 dynamics in III-V semiconductors [active], H.V. Alberto, J.M. Gil, J.P. Duarte, R.C. Vilao (*U. Coimbra*), K.H. Chow (*U. Alberta*), S.F.J. Cox (*Rutherford Appleton Lab*), H. Bani-Salameh, B. Coss, B.R. Carroll, R.L. Lichti, D. Stripe (*Texas Tech. U.*) 92
1002. Knight shift measurements of dynamic spin systems [active], C.R. Wiebe (*McMaster U.–Columbia U.*), S.J. Kim, G.M. Luke, G. MacDougall, J. Rodriguez (*McMaster U.*), P. Russo, A.T. Savici, Y.J. Uemura (*Columbia U.*)
1003. μ SR in pure and diluted spin ice pyrochlore systems [active], I.M. Gat, P.L. Russo, A. Savici, Y.J. Uemura (*Columbia U.*), H. Dabkowska, G.M. Luke (*McMaster U.*), C.R. Wiebe (*Columbia U.–McMaster U.*), K. Ishida, Y. Maeno, S. Nakatsuji (*Kyoto U.*), P. Schiffer (*Pennsylvania State U.*), R.J. Cava (*Princeton U.*)
1004. Nuclear hyperfine interactions of the shallow muonium center in GaN [active], K.H. Chow, A.N. MacDonald, B. Schultz (*U. Alberta*), R. Kadono, K. Shimomura (*KEK*), K. Mizuta, K. Ohishi (*NEC Corp.*), R.L. Lichti (*Texas Tech. U.*), B. Hitti (*TRIUMF*), R.F. Kiefl (*UBC*)
1005. Optically induced dynamics and site changes in group IV semiconductors [active], K.H. Chow, A.N. MacDonald, B. Schultz (*U. Alberta*), B. Hitti, Z. Salman (*TRIUMF*), R.F. Kiefl, W.A. MacFarlane (*UBC*)
1006. Magnetic properties of $RECrSb_3$ ($RE = La, Gd$) [active], K.H. Chow, A. Mar, A. Tkachuk (*U. Alberta*), W.A. MacFarlane (*UBC*), B. Hitti, Z. Salman (*TRIUMF*)
1007. Equilibrium of $^{115}Cd^g$ and $^{115}Cd^m$ during the s -process [active], R.M. Clark, M. Cromaz, M.A. Deleplanque, M. Descovich, R.M. Diamond, P. Fallon, I.Y. Lee, A.O. Macchiavelli, E. Norman, E. Rodriguez-Vieitez, F.S. Stephens, D. Ward (*Lawrence Berkeley Nat. Lab*), A. Andreyev, G.C. Ball, R. Chakrawarthy, G. Hackman, A.C. Morton, C. Pearson, M. Smith (*TRIUMF*), C. Svensson, J.J. Valiente-Dobon (*U. Guelph*), P.E. Garrett (*Lawrence Livermore Nat. Lab*)
1008. Halo neutrons and the β -decay of ^{11}Li [active], J. Al-Khalili, P. Walker (*U. Surrey*), A. Andreyev, G. Ball, G. Hackman, D. Melconian, C. Morton, C. Pearson, R.S. Chakrawarthy, M. Smith (*TRIUMF*), P. Garrett (*Lawrence Livermore Nat. Lab*), C. Andreoiu, G. Grinyer, C. Svensson (*U. Guelph*), D. Kulp, J. Wood (*Georgia Inst. Tech.*), J. Leslie (*Queen's U.*), C. Mattoon, F. Sarazin (*Colorado School of Mines*), J. Waddington (*McMaster U.*), E. Zganjar (*Louisiana State U.*) 97
1009. Towards ^{100}Sn : Coulomb excitation of neutron-deficient Sn isotopes at ISAC-II [deferred], C. Andreoiu, P. Finlay, G.F. Grinyer, B. Hyland, A. Phillips, M. Schumaker, C.E. Svensson, J.J. Valiente-Dobón (*U. Guelph*), T. Drake (*U. Toronto*), P.E. Garrett (*Lawrence Livermore Nat. Lab*), A.N. Andreyev, G.C. Ball, G. Hackman, A.C. Morton, C.J. Pearson, M.B. Smith (*TRIUMF*), R.A.E. Austin (*St. Mary's U.*), A.A. Chen, J. Waddington (*McMaster U.*), C. Plettner (*Yale U.*), F. Sarazin (*Colorado School of Mines*)
1010. Hyperfine anomaly measurements in neutron deficient Francium isotopes [deferred], J.A. Behr, P. Bricault, M. Dombosky, K.P. Jackson, J. Lassen, P. Levy (*TRIUMF*), M.R. Pearson (*UBC–TRIUMF*), G. Gwinner (*U. Manitoba*), G.D. Sprouse (*SUNY Stony Brook*), B.A. Brown (*NSCL Michigan State*)
1011. μ SR study of $LiHo_xY_{1-x}F_4$ [active], S.J. Kim, G.M. Luke, G. MacDougall, J. Rodriguez, C. Wiebe (*McMaster U.*), P. Russo, A. Savici, Y.J. Uemura (*Columbia U.*), M.J.P. Gingras, J. Kycia, J. Quilliam (*U. Waterloo*)
1012. Organic free radicals under hydrothermal conditions [active], J.-C. Brodovitch, B. McCollum, P.W. Percival (*SFU*), K. Ghandi (*UBC–TRIUMF*), I. McKenzie (*U. Stuttgart*) 93
1013. Superconductivity of β -pyrochlore oxides [active], R. Kadono, A. Koda, K. Ohishi, S.R. Saha (*KEK-IMSS*), W. Higemoto (*JAERI*), Z. Hiroi, Y. Muraoka, S. Yonezawa (*U. Tokyo*) 95
1014. Magnetism of oxygen adsorbed in carbon nanotubes [deferred], R. Kadono, A. Koda, K. Ohishi, S.R. Saha (*KEK-IMSS*), W. Higemoto (*JAERI*), Y. Maniwa, K. Matsuda (*Tokyo Metropolitan U.*)
1015. Unconventional behavior of field-induced quasiparticle excitation in novel superconductors [active], J. Akimitsu, S. Kuroiwa, H. Takagiwa, Y. Tomita, M. Yamazawa (*Aoyama Gakuin U.*), R. Kadono, A. Koda, K. Ohishi, S.R. Saha (*KEK-IMSS*), W. Higemoto (*JAERI*)
1016. Studies of muonium in isotopically enriched Si and Ge [active], K.H. Chow, A.N. MacDonald, B. Schultz (*U. Alberta*), P.J.C. King (*Rutherford Appleton Lab*), B. Hitti (*TRIUMF*), R.F. Kiefl (*UBC*), K. Itoh (*Keio U.*)

1017. Quasicrystals [active], R. Asahi, H. Nozaki, J. Sugiyama (*Toyota Central R&D Labs Inc.*), T.J. Sato (*ISSP U. Tokyo*), U. Mizutani (*Nagoya U.*), E.J. Ansaldi (*TRIUMF*), J.H. Brewer (*UBC*), D.R. Noakes (*Virginia State U.*)
1018. Investigations of superconductivity in the ultra-2D limit [active], C.R. Wiebe (*McMaster U.–Columbia U.–NSEC*), P.L. Russo, Y.J. Uemura (*Columbia U.–NSEC*), G.M. Luke, G.J. MacDougall, J. Rodriguez, Z. Tang (*McMaster U.*), A.T. Savici (*Columbia U.*)
1019. High-field μ SR measurements of superconductivity in Hg-1201 [active], P.L. Russo, A.T. Savici, Y.J. Uemura (*Columbia U.*), C.R. Wiebe (*McMaster U.–Columbia U.*), G.M. Luke, G.J. MacDougall, J. Rodriguez, Z. Tang (*McMaster U.*), M. Greven (*Stanford U.*)
1020. Muonium reaction with halogen molecules, and consequent unconventional bound states [deferred], D.J. Arsenneau (*TRIUMF*), S. Cottrell, S.F.J. Cox, C. Johnson (*Rutherford Appleton Lab*), D.G. Fleming, K. Ghandi, J. Valiani (*UBC*), U.A. Jayasooriya (*U. East Anglia*)
1021. Proton irradiation effects in advanced semiconductor technologies [active], P. Dodd, J. Felix, G. Hash, J. Schwank, M. Shaneyfelt (*Sandia Nat. Lab*), J. Baggio, C. D'Hose, V. Ferlet-Cavrois, P. Paillet (*CEA, France*), E. Blackmore (*TRIUMF*)
1022. The resonant radiative capture $^{12}\text{C}(^{16}\text{O},\gamma)^{28}\text{Si}$ reaction [active], C. Beck, S. Courtin, F. Haas, M. Rousseau, M.-D. Salsac, A. Sanchez (*IReS Strasbourg*), D.A. Hutcheon (*TRIUMF*), J. D'Auria (*SFU*), B.R. Fulton, R.G. Glover, D.G. Jenkins, P. Papka (*U. York*), C.J. Lister (*Argonne Nat. Lab*)
1023. A pilot study of fusion of halo nuclei: $^{11}\text{Li} + ^{70}\text{Zn}$ [active], Z. Huang, W. Loveland, B. Matteson, R. Naik, P. Sprunger, A.M. Vinodkumar (*Oregon State U.*), F. Liang, D. Shapira (*Oak Ridge Nat. Lab*), G. Ball, M. Dombisky, M. Trinczek (*TRIUMF*), J. D'Auria, J. Ressler, T. Ruth (*SFU*)
1024. $^{40}\text{Ca}(\alpha,\gamma)^{44}\text{Ti}$ for astrophysics [active], L. Buchmann, J. Caggiano, B. Davids, D.A. Hutcheon, A. Olin, J. Pearson, C. Ruiz, G. Ruprecht, M. Trinczek, C. Vockenhuber (*TRIUMF*), A. Chen (*McMaster U.*), J.M. D'Auria (*SFU*), D.G. Gigliotti, A. Hussein (*UNBC*), U. Greife (*Colorado School of Mines*), M. Hass (*Weizmann Inst.*), J. José (*UPC/IEEC Barcelona*), A.M. Laird (*U. York*), H. Nassar, M. Paul (*Hebrew U.*), P. Parker (*Yale U.*)
1025. $^7\text{Be}+p$: elastic scattering [deferred], L. Buchmann, J. Caggiano, B. Davids, M. Pavan, G. Ruprecht, P. Walden (*TRIUMF*), D. Gigliotti (*UNBC*), A. Laird (*U. York*), J. Pearson (*McMaster U.*), C. Ruiz (*SFU*), J.M. Sparenberg (*U. Libre de Bruxelles*)
1026. Projectile fragmentation of Na isotopes on light targets: isotopic enhancement by N/Z [deferred], F. Gagnon-Moisan, J. Gauthier, F. Grenier, J. Moisan, R. Roy, C. St-Pierre, D. Thériault, A. Valée (*Laval U.*), A. Chbihi, J.P. Wieleczko (*GANIL*), M. Samri (*Kénitra, Ibn Tofail U.*)
1027. Measurement of the $^{22}\text{Na}(p,\gamma)$ reaction rate [active], L. Buchmann, J. Caggiano, D.A. Hutcheon, J. Pearson, C. Ruiz, M. Trinczek, C. Vockenhuber (*TRIUMF*), J.M. D'Auria, J.J. Ressler (*SFU*), M. Wiescher (*U. Notre Dame*), K. Snover (*U. Washington*), J. José (*Barcelona*)
1028. Ultra-high precision decay measurements of the superallowed β -emitter ^{26m}Al [active], A. Andreyev, G.C. Ball, P. Bricault, R.S. Chakrawarthy, G. Hackman, A.C. Morton, C. Pearson, M.B. Smith (*TRIUMF*), J.R. Leslie (*Queens U.*), R.A.E. Austin (*St. Mary's U.*), J. Ressler (*SFU*), C. Andreoiu, P.E. Garrett, G.F. Grinyer, B. Hyland, A.A. Phillips, M.A. Schumaker, C.E. Svensson, J.J. Valiente-Dobon (*U. Guelph*), D. Melconian (*U. Washington*)
1030. Charged-particle channels in the β -decay of ^{11}Li [active], A. Andreyev, L. Buchmann, R. Chakrawarthy, A.C. Morton, C. Pearson, M.B. Smith, P. Walden (*TRIUMF*), M.J.G. Borge, O. Tengblad (*Ist. Estructura de la Materia, CSIC, Madrid*), C.A. Diget, K. Rüsager (*U. Aarhus*), M. Huyse, I. Mukha, J. Ponsaers, R. Raabe, P. Van Duppen (*Katholieke U. Leuven*), J. Pearson (*McMaster U.*), C. Ruiz (*SFU*), F. Sarazin (*Colorado School of Mines*)
1031. Charged-particle exit channels from the $^{12}\text{C}+^{12}\text{C}$ fusion reaction at astrophysical energies [active], M. Aliotta, T. Davinson, A. Murphy (*U. Edinburgh*), C.J. Barton, S.P. Fox, B.R. Fulton, A.M. Laird, P. Mumby-Croft, K. Vaughan, D. Watson (*U. York*), L. Buchmann, G. Ruprecht, A.C. Shotter, P. Walden (*TRIUMF*), J. José (*UPC/IEEC Barcelona*)
1032. Penetration depth and time reversal symmetry breaking in filled-skutterudite $\text{Pr}(\text{Os}_{1-x}\text{Ru}_x)_4\text{Sb}_{12}$ [active], J.E. Anderson, D.E. MacLaughlin, L. Shu (*U. California, Riverside*), R.H. Heffner (*Los Alamos Nat. Lab*), J.E. Sonier (*SFU*), O.O. Bernal (*U. California, Los Angeles*), G.D. Morris (*TRIUMF*), M.B. Maple (*U. California, San Diego*)

1033. Phase separation in the A-site ordered perovskite manganites [active], Y. Kawasaki, Y. Kishimoto, T. Ohno (*Tokushima U.*), R. Kadono, A. Koda, K. Ohishi, S.R. Saha (*KEK-MSL*), W. Higemoto (*JAERI*), T. Nakajima, Y. Ueda (*U. Tokyo*)
1034. One-dimensional cobalt oxide BaCoO₃ [active], H. Nozaki, J. Sugiyama (*Toyota Central R&D Labs. Inc.*), H. Ikuta, U. Mizutani, T. Takami (*Nagoya U.*), E.J. Ansaldo (*TRIUMF*), J.H. Brewer (*UBC*)
1035. μ SR measurements of magnetism in (Ca,Sr)₂RuO₄ in ambient and applied pressure [active], I. Gat-Malureanu, P.L. Russo, Y.J. Uemura (*Columbia U.*), A.T. Savici (*Brookhaven Nat. Lab*), C.R. Wiebe (*Brock U.*), G.M. Luke, G.J. MacDougall, J. Rodriguez, Z. Tang (*McMaster U.*), Y.V. Sushko (*U. Kentucky*), S.R. Julian (*U. Toronto*), E. Baggio-Saitovitch, H. Saitovitch (*CBPF, Rio*), J. Sereni (*CAB Bariloche, Argentina*), K. Ishida, Y. Maeno, S. Nakatsuji (*Kyoto U.*), F. Nakamura (*Hiroshima U.*), J. Arai, T. Goko (*Tokyo-Science U.*)
1036. β -NMR study of single molecule magnets films [active], R. Miller, Z. Salman (*TRIUMF*), R. Kiefl, A. MacFarlane (*UBC-TRIUMF*), M.D. Hussain, T. Keeler, A. Morello, T. Parolin, D. Wang (*UBC*), K. Chow (*U. Alberta*), D. Gatteschi, R. Sessoli (*U. Florence*)
1038. A μ SR study of orbitally ordered La₄Ru₂O₁₀ [active], R. Kiefl, R. Miller, Z. Salman (*TRIUMF*), P. Khalifah (*U. Massachusetts*), M.D. Hussain, T.A. Keeler, A. MacFarlane, T. Parolin, H. Saadaoui, D. Wang (*UBC*)
1039. A μ SR study of ferromagnetic superconductors at low temperatures [active], R. Kiefl, R. Miller, Z. Salman (*TRIUMF*), M.D. Hussain, T.A. Keeler, A. MacFarlane, T. Parolin, H. Saadaoui, D. Wang (*UBC*)
1040. Light-induced magnetism in manganite thin films studied with β -NMR [active], R. Kiefl, R. Miller, Z. Salman (*TRIUMF*), M.D. Hussain, T.A. Keeler, A. MacFarlane, T. Parolin, H. Saadaoui, D. Wang (*UBC*)
1041. β NMR search for spontaneous magnetism near the surface of unconventional superconductors [active], J.H. Brewer, M.D. Hossain, R.F. Kiefl, W.A. MacFarlane, T.J. Parolin, H.X. Saadaoui, D. Wang (*UBC*), R.I. Miller, G.D. Morris, Z. Salman (*TRIUMF*), K.H. Chow (*U. Alberta*), R.H. Heffner (*Los Alamos Nat. Lab*), L.H. Greene (*U. Illinois*), G.M. Luke (*McMaster U.*), Y. Maeno (*Kyoto U.*), Z. Yamani (*AECL Chalk River*)
1042. β NMR investigation of finite size effects in metallic thin films and nanoparticle arrays [active], M.D. Hossain, T. Keeler, R.F. Kiefl, W.A. MacFarlane, T.J. Parolin, H.X. Saadaoui, D. Wang (*UBC*), R.I. Miller, G.D. Morris, Z. Salman (*TRIUMF*), J. Buriak, K.H. Chow (*U. Alberta*), S. Hak (*Groningen U.*), J. Chakhalian (*Max Planck Inst.*)

*deceased

LIFE SCIENCES PROJECT PROPOSALS

The following lists life sciences project proposals received up to the end of 2004 (missing numbers cover proposals that have been withdrawn or replaced by later versions, rejected, or combined with another proposal). Page numbers are given for those experiments which are included in this Annual Report.

Page

- LS0. PET facilities [active], K.R. Buckley, E.T. Hurtado, P. Piccioni, W. Sievers (*TRIUMF*), M.-L. Camborde, C. English, S. Jivan, S. Shah, C. Williams (*UBC-TRIUMF*), S. McCormick (*Pacific Parkinson's Research Centre*), J. Publicover (*U. Victoria*), S. Lapi (*SFU*) 97
- LS1. Attenuation maps for quantitative SPECT [completed], A. Celler (*UBC-VH&HSC*), S. McFarland (*UBC*), S. Barney, M. Limber (*SFU*)
- LS2. Synthesis of ^{18}F -glycosides as potential imaging agents for the study of glycosidase activity in the brain [completed], M.J. Adam (*TRIUMF*), D. Lyster (*VH&HSC*), G. Matte (*Halifax H.*)
- LS3. Synthesis of radiopharmaceuticals for positron emission tomography [active], M.J. Adam, K.R. Buckley, E.T. Hurtado, J. Huser, S. Jivan, J.-M. Lu, T.J. Ruth (*TRIUMF*) 99
- LS4. TR13 targets for PET radioisotope production [active], K. Buckley, T. Hurtado, T.J. Ruth, S.K. Zeisler (*TRIUMF*) 99
- LS5. Production and on-line separation of ^{124}I from enriched tellurium [inactive], W.Z. Gelbart, E.T. Hurtado, T.J. Ruth, N.R. Stevenson, S.K. Zeisler (*TRIUMF*), R.R. Johnson (*UBC*)
- LS6. Bone calcium resorption studies in pre- and peri-menopausal women using accelerator mass spectrometry [completed], R.R. Johnson, A. Priestman, J.C. Prior (*UBC*), A. Altman, W.Z. Gelbart, V. Sossi (*TRIUMF*), D. Berkovits, S. Ghelberg, M. Paul (*Racah Inst., Hebrew U. Jerusalem*), L.M. Shulman (*Chaim Sheba Med. Centre*), R. Chechik (*Weizmann Inst.*), E. Venzel (*SFU*)
- LS7. PET 3D data quantification and integration into a research clinical environment [completed], K.S. Morrison, T.J. Ruth, V. Sossi, M.W. Stazyk (*UBC-TRIUMF*), K.R. Buckley (*TRIUMF*), J.S. Barney (*VH&HSC*), D. Sirota, B.J. Snow (*UBC*)
- LS8. Radiotracers for the physical and biosciences [active], L. Buchmann, T.J. Ruth, S.K. Zeisler (*TRIUMF*), A.D.M. Glass, R.R. Johnson, M. Lowe, C.E.R. Orvig (*UBC*), T.F. Budinger (*Lawrence Berkeley National Lab*) 101
- LS10. Biological evaluation of radiohalogenated DNA aptamers [completed], H. Dougan (*TRIUMF*), J.B. Hobbs, D.M. Lyster (*UBC*), J.I. Weitz (*McMaster U.*)
- LS11. Development of single photon imaging agents [inactive], D. Lyster (*UBC-VH&HSC*), L. Alcorn, M. Hampong, T. Lutz, C. Vo (*UBC*)
- LS12. A simulation platform for the design of position encoding multicrystal detectors [completed], A. Altman, C. Moisan, J.G. Rogers (*TRIUMF*), E. Hoskinson, G. Tsang (*UBC*)
- LS13. Utility of 2-[F-18]-fluoro-2-deoxy-d-glucose SPECT imaging in the evaluation of patients with solitary pulmonary nodules [completed], A. Celler, D. Lyster, D. Worsley (*UBC*), M. Adam (*TRIUMF*)
- LS14. Production of ^{127}Xe from cesium with 90–110 MeV protons [inactive], D. Pearce, J. Vincent (*TRIUMF*)
- LS15. Investigation of frame realignment on the reproducibility of ^{18}F -6-fluorodopa positron emission tomography [inactive], K.S. Morrison, T.J. Ruth (*UBC-TRIUMF*), B.J. Snow (*UBC*)
- LS17. Table-top radiocarbon facility [inactive], W. Gelbart, R.B. Schubank (*TRIUMF*), E. Venzel (*UBC-SFU*), S. Calvert, R.R. Johnson, J. Nagel, T. Peterson, V. Sossi (*UBC*), D.E. Nelson (*SFU*), J. Prior, K. Schoenholzer, R. Sutton, V. Walker (*UBC-VH&HSC*), R. Middleton (*U. Pennsylvania*), M. Paul (*Hebrew U. Jerusalem*), J. Clague, L. Jackson, J. Lutenuer, D. Templeman-Kluit (*Geological Survey of Canada*), R.N. McNeely, J.-S. Vincent (*GSC Ottawa*), V. Barrie (*Pacific Geoscience Center*), D. Prior, K.R. Robertson, G. Vilks (*Bedford Inst. Oceanography*), R. Brown, S. Wang (*Elemental Research Inc.*), J. Vogel (*Lawrence Livermore National Lab*), A.E. Litherland (*U. Toronto*), S. Dias, S. Sood (*Ontario Hydro*), H.R. Andrews, R.M. Brown, R.J. Cornett (*AECL*), D.B. Carlisle (*Environment Canada*), J. Carron, A. Kabir, R.C.J. Wilkinson (*Canadian Centre for Inland Waters*), R. Gephart, P. Molton, D. Robertson (*Batelle Pacific Northwest Labs*)
- LS18. Cooperative development of ^{82}Sr -Rb generators for human use in Canada [completed], J. Vincent (*TRIUMF*), R. Beanlands (*U. Ottawa Heart Inst.*), B. Bowen (*McMaster U.*), W. Dickie (*Nordion Int.*)
- LS19. An ^{15}O -water generator: a feasibility study [inactive], K.R. Buckley, T.J. Ruth (*TRIUMF*)

- LS20. Prototype heat-pipe water target for ^{18}F -production [inactive], K.R. Buckley, E.T. Hurtado, T.J. Ruth (*TRIUMF*), J.W. Lenz (*private consultant*)
- LS21. Aluminum kinetics in plants [inactive], A. Glass, R.R. Johnson, L. Oliveira (*UBC*), K. Buckley, Z. Gelbart (*TRIUMF*), D. Berkovitz, M. Paul (*Hebrew U. Jerusalem*), E. Venczel (*SFU*)
- LS22. Virtual national biomedical tracer facility [inactive], T.J. Ruth, J.S. Vincent (*TRIUMF*), E.J. Peterson, D. Phillips (*Los Alamos National Lab*)
- LS24. Scanning for early detection and staging of breast cancer: a comparative study using FDG PET and MIBI SPECT [inactive], P.F. Cohen, P. Klimo (*Lions Gate H.-UBC*), M. Cackette (*EBCO Industries Ltd.*), J. Whiffen (*JALORN*), V. Sossi (*TRIUMF-UBC*), J. Porter (*Nordion Int.*), R.R. Johnson (*UBC*)
- LS25. 3D PET in human neuroreceptor studies: quantification and reconstruction [completed], K.S. Morrison, T. Oakes, T.J. Ruth, V. Sossi (*UBC-TRIUMF*), K.R. Buckley (*TRIUMF*), M. Krzywinski, M. Schulzer, J. Stoessl (*UBC*)
- LS26. A gaseous planar positron source for routine 3D PET normalization [completed], T. Oakes, T.J. Ruth, V. Sossi (*UBC-TRIUMF*), K. Buckley, S. Jivan, R. MacDonald (*TRIUMF*)
- LS27. The feasibility and efficacy of using 2-(F-18)-fluoro-2-deoxy-D-glucose (18-FDG) to evaluate children with musculoskeletal neoplasm [deferred], R. Anderson, J. Davis, D. Lyster, H.R. Nadel, T.J. Ruth, M. Stilwell, D. Worsley (*UBC*)
- LS28. Evaluation of potentially viable myocardium with dobutamine myocardial SPECT imaging [completed], H. Abbey, A.-Y. Fung, L. Hook, D.M. Lyster, D.F. Worsley (*VH&HSC*), M. Adam, S. Jivan (*TRIUMF*)
- LS29. Production and distribution of FDG for clinical studies [completed], D. Lyster, D. Worsley (*VH&HSC*), P. Cohen (*Lions Gate H.*), H. Nadel (*Children's H.*), M.J. Adam, S. Jivan, T.J. Ruth, V. Sossi (*TRIUMF*)
- LS31. Auger electron emitters for therapy-physics and chemistry [inactive], D. Pearce, T.J. Ruth, J. Vincent, A. Zyuzin (*TRIUMF*), V. Kokhanyuk, V. Kravchuk, B.L. Zhuikov (*INR Moscow*)
- LS32. $^{18}\text{F}\text{-H}_2^{18}\text{O}$ supply to the University of Alberta [completed], S.A. McQuarrie, J.R. Mercer (*U. Alberta*), A.J.B. McEwan (*CCI*), R.R. Johnson (*UBC-EBCO*), T.J. Ruth (*UBC-TRIUMF*)
- LS33. Evaluation and improvement of a dual head coincidence camera [completed], K.S. Morrison, T.J. Ruth, V. Sossi (*UBC-TRIUMF*), M. Krzywinski (*UBC*), P. Cohen (*Lions Gate H.*), P. Klimo (*Lions Gate H.-UBC*), T.K. Lewellen, D.A. Mankoff (*U. Washington*)
- LS34. Production of ^{103}Pd [inactive], R.R. Johnson, R. Pavan (*UBC*), M. Cackette, K.L. Erdman (*EBCO Industries Ltd.*), Z. Gelbart (*TRIUMF*)
- LS35. Development of F-18 labelled nitroimidazole PET imaging agents for tissue hypoxia [completed], M.J. Adam (*TRIUMF*), K. Skov (*BCCRC-UBC*), S. Evans, C. Koch, A. Kachera (*U. Pennsylvania*), I. Baird, B. James (*UBC*)
- LS37. Feasibility of ^{125}Xe implantation as a ^{125}I brachytherapy source [completed], D. Ottewell, T. Ruth, J. Vincent, A. Zyuzin (*TRIUMF*)
- LS38. Dopaminergic tracers kinetic modeling with minimally invasive scanning procedures [completed], G. Chan, M. Krzywinski, T.J. Ruth, V. Sossi (*UBC-TRIUMF*), J. Holden (*U. Wisconsin*), D. Doudet, J. Stoessl (*UBC*)
- LS39. Positron emission profiling (PEP) for pulp and paper fluid dynamic studies [active], M. Martinez, J. Olson (*UBC*), M.J. Adam, K. Buckley, S. Jivan, T.J. Ruth, V. Sossi (*TRIUMF*)
- LS40. F-18 FDG cardiac PET scans using a coincidence PET/SPECT camera to assess myocardial viability in patients with fixed abnormalities and low ejection fractions on gated sestamibi stress tests [completed], P.F. Cohen, J. Imrie, K. Woo (*Lions Gate H.*), D. Worsley (*Vancouver General H.*), V. Sossi (*TRIUMF-UBC*), T. Ruth (*UBC-TRIUMF*), R.R. Johnson (*UBC*)
- LS41. Impact of the ADAC coincidence PET camera in the management of selected cancer patients [completed], P.F. Cohen, J. Imrie, K. Woo (*Lions Gate H.*), J. Powe (*Vancouver General H.*), V. Sossi (*TRIUMF-UBC*), T. Ruth (*UBC-TRIUMF*), R.R. Johnson (*UBC*)
- LS42. Configuration modeling and image reconstruction studies on a depth encoding research tomograph [active], T. Ruth, V. Sossi (*UBC-TRIUMF*), V. Astakhov (*UBC*), K. Buckley (*TRIUMF*), S. Houle (*Centre Addiction & Mental Health, Toronto*), C. Moisan (*U. Laval*)
- LS43. Positron emission mammography system (PEM) [deferred], K. Buckley, S. Jivan, T.J. Ruth, V. Sossi (*TRIUMF*), M. Stilwell (*B.C. Women's H.*), P. Gordon (*UBC*), H. Nadel (*Children's H.*)
- LS44. Development of a high-speed formation (areal density) measurement system for paper [active], M. Avikainen, S. Heath, M. Martinez, J. Olson (*UBC*), K. Buckley, T.J. Ruth, M. Salomon (*TRIUMF*)

101

102

- LS45. Modelling genetic risk for ionizing radiation exposure in space [deferred], J.G. de Boer, J. Holcroft, S. Zhang (*U. Victoria*)
- LS46. Modelling of the dopaminergic system in more severely affected PD patients [completed], T.J. Ruth, V. Sossi (*UBC-TRIUMF*), J. Holden (*U. Wisconsin*), R. de la Fuente-Fernandez, D. Doudet, C.S. Lee, M. Schulzer, J. Stoessl (*UBC*)
- LS47. PET imaging of recurrent prostate cancer with 2-F-18-fluoromethyl-2-hydroxyethylammonia (FCH), [deferred], M. Gleave, D. Lyster, J. Powe, D. Worsley (*Vancouver General H.-UBC*), M. Adam (*TRIUMF*), H. Abbey (*Vancouver General H.*)
- LS48. Anorexia nervosa: autonomic dysfunction, the brain and the heart [completed], A.S. Belzberg, C.L. Birmingham, C. Kerr, G.P. Sexsmith, M. Stilwell (*St. Paul's H.*), M.J. Stock (*St. George's H.*), P. Beumont (*U. Sydney, Aust.*), V. Sossi (*UBC-TRIUMF*)
- LS49. ¹⁸F FDG cardiac PET scans using a third generation coincidence camera to assess myocardial viability in patients who are candidates for cardiac transplantation [inactive], A.S. Belzberg, S. Chan, A. Ignaszewski, M. Kiess, G. Sexsmith, M. Stilwell (*St. Paul's H.*), V. Sossi (*TRIUMF-UBC*)
- LS50. Antisense imaging nucleic acids for Parkinson's disease [active], M. Adam, H. Dougan, T.J. Ruth (*TRIUMF*), J.B. Hobbs, D.M. Lyster, J. Stoessl (*UBC*), A.I. Kassis (*Harvard U.*) 102
- LS51. Auger therapy for prostate cancer [active], H. Dougan, T.J. Ruth, J.S. Vincent (*TRIUMF*), C.C. Nelson, P.S. Rennie (*Prostate Centre*), C.M. Ludgate (*UBC-U. Victoria*), D.M. Lyster (*UBC*) 103
- LS52. Comparison of commercial FDG synthesis systems [completed], T.J. Ruth (*UBC/TRIUMF*), M. Adam, K. Buckley, S. Jivan (*TRIUMF*), D. Lyster (*UBC*), R. McDonald (*IPET*)
- LS53. Synthesis of ^{99m}Tc and ^{186,188}Re sugar derivatives [active], M.J. Adam (*TRIUMF*), C. Orvig (*UBC*), S. Bayly, C. Fisher (*TRIUMF/UBC*), M. Abrams (*AnorMED*) 103
- LS54. Wavelet reconstruction for high resolution three-dimensional positron emission tomography [deferred], C.-H. Chen, A. Rahmim, K. Raywood (*UBC*), T.J. Ruth, V. Sossi (*UBC/TRIUMF*)
- LS55. Detection of metastases in intermediate thickness melanoma with ¹⁸FDG and a coincidence hybrid scanner [inactive], A. Belzberg, G. Sexsmith, M. Stilwell (*St. Paul's H./UBC*), A. Lee (*Surrey Memorial H.*), T.J. Ruth (*UBC/TRIUMF*)
- LS56. Synthesis of radiolabelled nucleotides and oligonucleotides [active], M.J. Adam, H. Dougan, A. Studenov (*TRIUMF*), J. Wilson (*Cross Cancer, Edmonton*), J. Hobbs (*UBC*) 104
- LS57. Quantitative imaging with the Concorde MicroPET [active], A. Rahmin, V. Sossi (*UBC*), K. Raywood, T.J. Ruth (*UBC-TRIUMF*), K. Buckley, P. Piccioni (*TRIUMF*), C. Thompson (*Montreal Neurological Inst.*), S. Lapi (*SFU*) 104
- LS58. Production and distribution of FDG for clinical studies [deferred], D. Lyster (*UBC*), J. Powe, D. Worsley (*VH&HSC*), P. Cohen (*Lions Gate Hospital*), H. Nadel (*Children's Hospital*), M. Stilwell (*BC Women's Hospital*), A. Belzberg (*St. Paul's Hospital*), K. Buckley, T. Hurtado, S. Jivan, P. Piccioni, T.J. Ruth (*TRIUMF*), M. Kovacs (*EBCO Tech.*)
- LS59. Mechanisms underlying therapeutic benefit from retinal pigmented epithelial cell implantation for Parkinson's disease [active], I. Cepeda, D.J. Doudet, J. Grant, N. Monasterio, P. Rosa-Neto (*UBC*)
- LS60. The physiological role of copper in marine phytoplankton [active], S. Harris, M.T. Maldonado (*UBC*), S. Lapi (*SFU*), T.J. Ruth (*TRIUMF*) 105
- LS61. In vivo PET study of the effect of striatal implantation of retinal pigment epithelial cells in a primate model of Parkinson's disease [active], D.J. Doudet, J. Flores, J. Grant, P. Rosa-Neto (*UBC*)
- LS62. The effects of electroconvulsive therapy in an animal model of Parkinson's disease: mechanisms of a potential adjunct treatment [active], D.J. Doudet, J. Grant, E. Strome (*UBC*)
- LS63. Non-invasive monitoring of tumour progression in the Shionogi tumour model for prostate cancer [active], D. Yapp (*BC Cancer Agency*), M. Gleave, P. Kozlowski (*The Prostate Centre*), M. Adam, T. Ruth (*TRIUMF*) 105
- LS64. Development of radiotracers based on oligonucleotides [active], M.J. Adam, A.H. Dougan, T.J. Ruth (*TRIUMF*), A.J. Stoessl (*Pacific Parkinson's Research Centre*), D. Perrin (*UBC*)
- LS65. In vivo study of the direct and indirect striatal output pathways in mild and severe primate models of Parkinson's disease [active], D.J. Doudet, J. Grant, P. Rosa-Neto (*UBC*)
- LS66. MicroPET tracking of pancreatic islets following transplantation [active], S.-J. Kim, C. McIntosh, M. Speck (*UBC*)

- LS67. Function imaging of human tumours before and during therapy [deferred], C. Aquino-Parsons, M. Bally, R. Durand, A. Minchinton, P. Olive, T. Pickles, M. Sadar, K. Skov, D. Wilson, D. Yapp (*BC Cancer Agency*)
- LS68. Neural mechanisms underlying response changes to levodopa in Parkinson's disease [deferred], S. Ahn, C. Cheng, D. Doudet, C.S. Lee, A. Phillips (*UBC*)
- LS69. In vivo studies on regulation of dopamine turnover using a Parkinson's disease rat model and a microPET [active], D. Doudet, C. Lee, A. Phillips, V. Sossi, E. Vandervoort (*UBC*), M.-L. Camborde, R. Koernelson, S. McCormick (*UBC-TRIUMF*), T.J. Ruth (*TRIUMF*), J. Holden (*U. Wisconsin*) 106
- LS70. Quantification of high resolution brain imaging [active], K. Cheng, A. Rahmin, V. Sossi, E. Vandervoort (*UBC*), S. Blinder, M.-L. Camborde, K. Raywood, T. Ruth (*UBC-TRIUMF*), K. Buckley, P. Picciotto (*TRIUMF*), C. Thompson (*Montreal Neurological Inst.*), S. Lapi (*SFU*) 107
- LS71. Investigation of salt stress in rice plants [active], D.T. Britto, H.J. Kronzucker, S. Sieger, P. Tehrani (*U. Toronto*), T.J. Ruth (*TRIUMF*), S. Lapi (*SFU*)